Directionally Structured Dual Phase Steel Composites

A thesis submitted in fulfilment
of the requirements for the degree of
Doctor of Philosophy in Engineering

Shoujin Sun

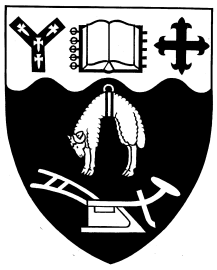

Department of Mechanical Engineering
University of Canterbury,
Christchurch, New Zealand

July 1998

Contents

Abstract

Manganese partitioning and mechanical properties of dual phase steels have been examined. The manganese partitioning coefficient increases to a limit with increasing isothermal holding time, and the final equilibrium partitioning coefficient decreases with increasing annealing temperature. The combination of diffusion equations in austenite and ferrite plus mass balance and austenite growth can give the manganese distribution in austenite and ferrite respectively, and the manganese partitioning coefficient at any isothermal holding time.

The introduction of rolling during annealing or at the end of annealing can strengthen dual phase steels by elongating austenite and introducing internal stresses and dislocations, the magnitude of which depends on finishing rolling temperature and the timing of rolling during annealing. The tensile properties of as-rolled dual phase steels are strongly influenced by finishing rolling temperature and martensite volume fraction because of internal stresses and dislocation density, whereas those of post-rolling annealed steels depend on only martensite volume percentage.

To model the heat-treatment for producing dual phase steels (“in-situ” dual phase steel), a steel-steel composite is produced by incorporating high strength steel-wires into ductile steel sheets through hot-rolling (“artificial” dual phase steel). The properties of the reinforcing wire, matrix steels, interfacial strength between wire and matrix steels and steel-steel composite are affected by the surface condition of wire, finishing rolling temperature, preform holding time at rolling temperature before rolling, and heat-treatment after fabrication of composites.

Mileiko’s theory can predict the relationship between the steel-steel composite strength and the volume fraction of wire. But for dual phase steels, Mileiko’s theory can be applied only when martensite volume fraction is over 30% because the residual stress, high dislocation density and carbide are produced at low temperature, at which low martensite volume fraction is obtained.

Continuous wire composites can simulate the as-rolled dual phase steel when the reinforcement content is over 30%, but discontinuous wire composites can not simulate the post-rolling annealed dual phase steel.

Acknowledgment

First of all, I wish to express my grateful thanks to my supervisors - Dr. M. D. Pugh and Professor L. A. Erasmus for their continual interest and supervision. Their time spent on this project and their invaluable advice have been much appreciated. Their friendship and encouragement enabled me to conduct this research.

Second of all, I thank Dr. J. S. Smaill, and Mr. M. Flaws for his help in SEM observation and element analysis, Mr. H. Mobbs for his help in preparation in metallography, and Mr. K. Stobbs and Mr. D Healy for their assistance in mechanical properties testing.

Further acknowledgment will be given to Mr. O. Bott, Mr. K. Brown, and Mr. S. Amies for their preparation of testing samples and guidance for use of machines in the workshop, Mr. G. Leathwick for ordering the materials used in this project and very kindly lending tools from store.

I also want to thank all staff in the Department of Mechanical Engineering who gave suggestions and help for this project. Special thanks are given to Prof. R. J. Astley, the Head of Department of Mechanical Engineering, for use of facilities within the department.

The University of Canterbury and the Department of Mechanical Engineering offered scholarships; their financial supports are appreciated.

BHP New Zealand Steel Ltd supplied steel sheets used in this project and their generous help is much appreciated.

Finally, I would like to thank my wife, Li Suo and my son, Michael Sun, without their understanding and encouragement, I couldn’t finish this thesis.

List of Figures

List of Tables

Table of Key Symbols

Pre-RA	Pre-rolling annealing
Post-RA	Post-rolling annealing (or annealed)
CH	Cold-Hot rolling
CHSPRS	Short Piano-wire Reinforced Steel made by CH method
CHCH	Cold rolling-Heating-Cold rolling-Hot rolling
CHCHSPRS	Short Piano-wire Reinforced Steel made by CHCH method
α	Ferrite
γ	Austenite or boundary energy
M	Martensite
σ_c, ε_c	Tensile strength and true uniform strain of composites
σ_{mu}, ε_m	Tensile strength and true uniform strain of matrix (ferrite for in-situ dual phase steel, and matrix steel for artificial dual phase steel)
σ_{fu}, ε_f	Tensile strength and true uniform strain of fibre (martensite for in-situ dual phase steel, wire for artificial dual phase steel)
V	Volume fraction of reinforcement (martensite or wire)
C_{Mn}^{0}	Manganese content in whole steel
$C_{Mn}^{\alpha,0}$	Manganese solubility in ferrite at a given temperature
C_{Mn}^{α}, $\overline{C_{Mn}^{\alpha}}$	Manganese content and the mean manganese content in ferrite
$C_{Mn}^{\gamma,0}$	Manganese solubility in austenite at a given temperature
C_{Mn}^{γ}, $\overline{C_{Mn}^{\gamma}}$	Manganese content and the mean manganese content in austenite
W	Work of fracture during wire pull-out
μ	Bond energy
C_{carbon}	Carbon content at the wire-matrix interface
$\left.\frac{dC_{carbon}}{dr}\right\|_{r=r_0}$	Carbon concentration gradient in the matrix side of the interface

Chapter 1 Introduction

Among the engineering materials, steel is the most widely used structural metal because of its high strength, availability and formability. More specifically, as strength is usually one of the most significant properties of structural materials, high strength material is desired for bearing load.

In addition to strength, high ductility is required for engineering materials in order to avoid brittle fracture, which can cause a disaster, and also to improve the formability. But strength and ductility of a material are a pair of uncompromising properties, the increase of one property will sacrifice the other. The optimum way is to increase strength as high as possible whilst maintaining sufficient ductility to meet requirements.

After the fuel crisis in the 1960s, United States Federal Regulations required automobile manufacturers to limit fuel consumption[(1)]. The best and simplest method to achieve this goal appears to be by the reduction of vehicle weight. By using high strength steel in automobiles, the weight can be decreased significantly with thinner components without sacrificing strength requirements. This provided a great challenge for scientists to develop high strength steel which also has high ductility.

In 1975, a Japanese scientist introduced a new alloy[(2)], which had low yield strength, high ultimate strength, high elongation and uniform strain. This kind of alloy, named duplex phase steel, two phase steel, or dual phase steel, has received great attention all over the world since then[(3-5)].

Dual phase steel, based on a low carbon, high ductility, ferrite matrix reinforced with high carbon, high strength, martensite islands, offers high strength combined with good ductility and successfully overcomes the disadvantage of conflicting requirement for high strength and improved formability[(6,7)]. The wonderful strength and ductility combination makes dual phase steel find application in the automobile industry[(8-10)] such as car body panels.

The typical tensile stress-strain curve of dual phase steel is shown in Figure 1.1: its 0.2% yield strength is lower than 380MPa, the tensile strength is 620MPa or higher, and the

total elongation is higher than 27%. The low yield strength and high ductility (in terms of uniform strain before plastic instability) make it suitable for cold deep-forming into complex shapes, while the high work hardening rate produces significant strengthening during cold deformation.

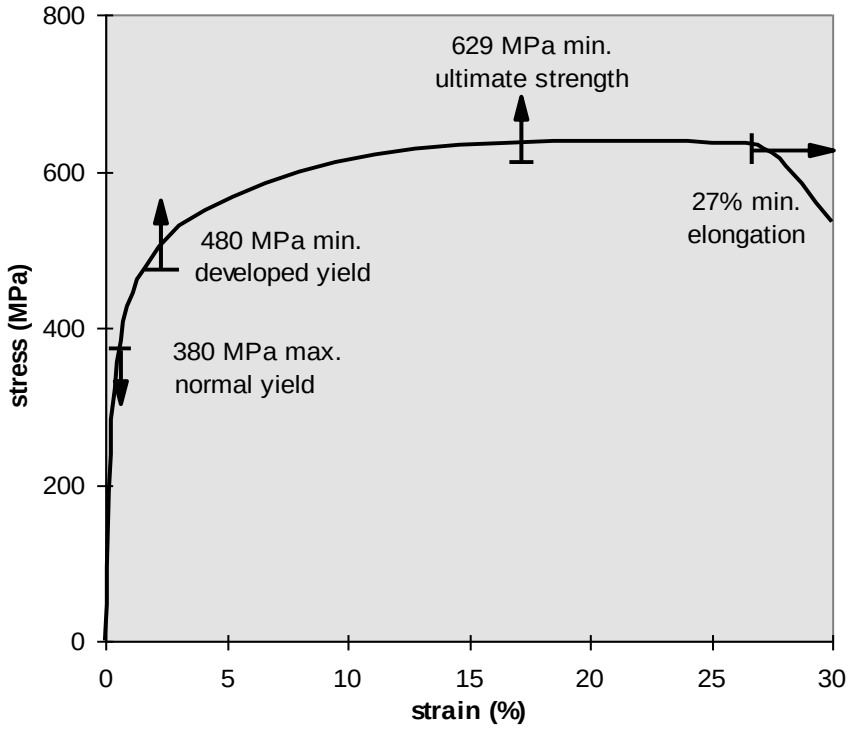

Figure 1.1 Typical stress-strain curve of dual phase steel [11]

1.1 Process routes

Dual phase steels can be made by several techniques in theory, but only two main methods, intercritical annealing and hot-rolling, are successful in commercial application because of their easy operations and low cost. These two principal methods will be described in the following sections.

1.1.1 Intercritical annealing.

When heated in the ferrite + austenite ($\alpha + \gamma$) region between Ac_1 (austenite-cementite transformation temperature during heating) and Ac_3 (austenite-ferrite transformation temperature during heating) and held for a while, the conventional high strength and low-alloy (HSLA) steels will comprise austenite and polygonal ferrite; dual phase steels will be produced with the austenite transforming to martensite during cooling[12-16]. In

order to prevent the transformation of austenite to pearlite, cooling must be rapid from the intercritical annealing temperature, the critical cooling rate being determined by the composition of the steel. The factors that affect the properties of intercritical annealed dual phase steel include annealing temperature, annealing time, the starting structure, and the prior cold deformation. These factors will be reviewed in section 1.3.

1.1.2 Hot rolling.

The steel is required to contain both strong ferrite formers, like silicon, and transformation-delaying elements such as Cr, Mn or Mo. The rolling and coiling temperature on the hot mill are adjusted so that no pearlite phase appears. When the low carbon steel is hot rolled at a temperature between Ac_1 and Ac_3, additional ferrite is formed on the water-cooled run-out table from the mill, and the transformation of austenite to martensite occurs in the following coiling process (below the pearlite-ferrite transformation temperature). The steel produced by this processing step is called *intercritically rolled dual phase steel*. If the steel is rolled in the austenitic temperature range followed by cooling into the ($\alpha + \gamma$) region before final quenching to martensite, the steel is termed *austenitic rolled dual phase steel* (as shown in Figure 1.2).

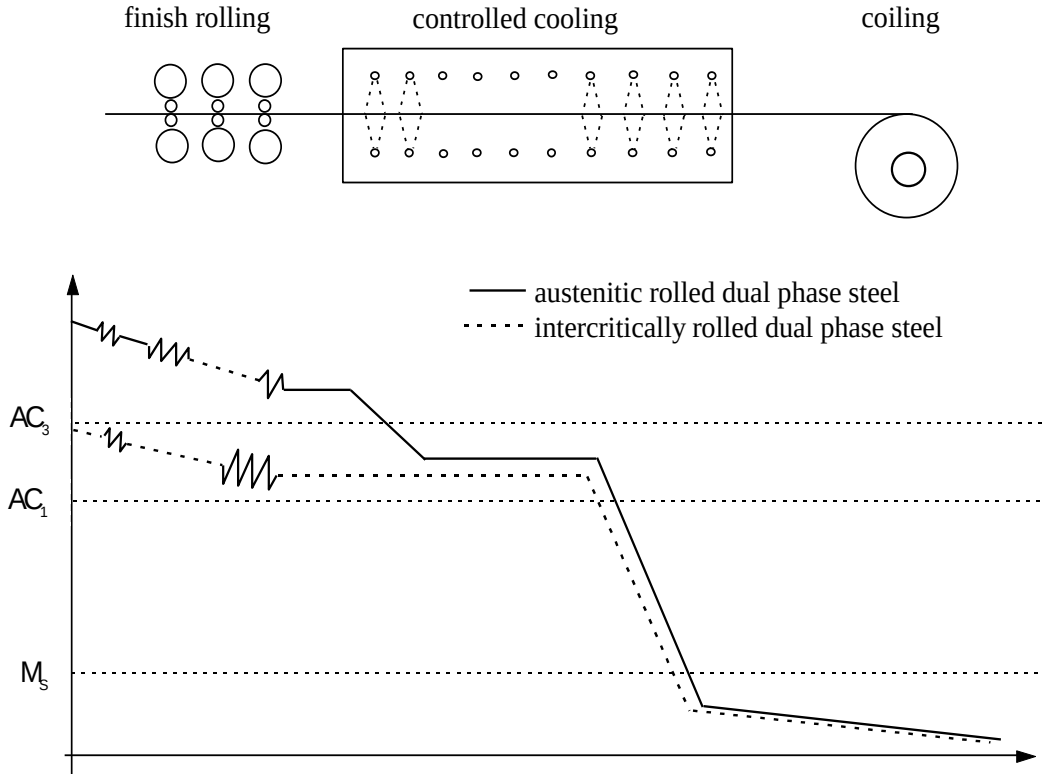

Figure 1.2 Illustration of the formation routes of hot-rolled dual phase steels [17]

The principal processing factors influencing the properties of dual phase steel through formation of the appropriate microstructure are: finishing rolling temperature, intermediate temperature, and coiling temperature. The finishing rolling temperature determines the volume fraction of martensite and the dislocation density.

The cooling rate for both the intercritical annealing and hot rolling processes must be higher than the critical cooling rate for the transformation of austenite to martensite. It is necessary to lower this critical cooling rate of the steel by adding some alloying elements so that conventional cooling techniques (water quenching, for example) can be used. These elements, which include Mn, V, Ti, Mo, Cr[3, 18-22], etc., must be austenite stablizers to promote austenite and retard the formation of ferrite, pearlite and bainite during cooling.

1.2 Formation of dual phase steel

The formation of intercritically annealed dual phase steel is dependent on the parent/starting microstructure of the steel[23-25] and can be classed in terms of intermediate quenching, intercritical annealing, and step quenching, as shown in Figure 1.3. The nucleation and growth of dual phase steel is different for each formation path (as illustrated in Figure 1.4).

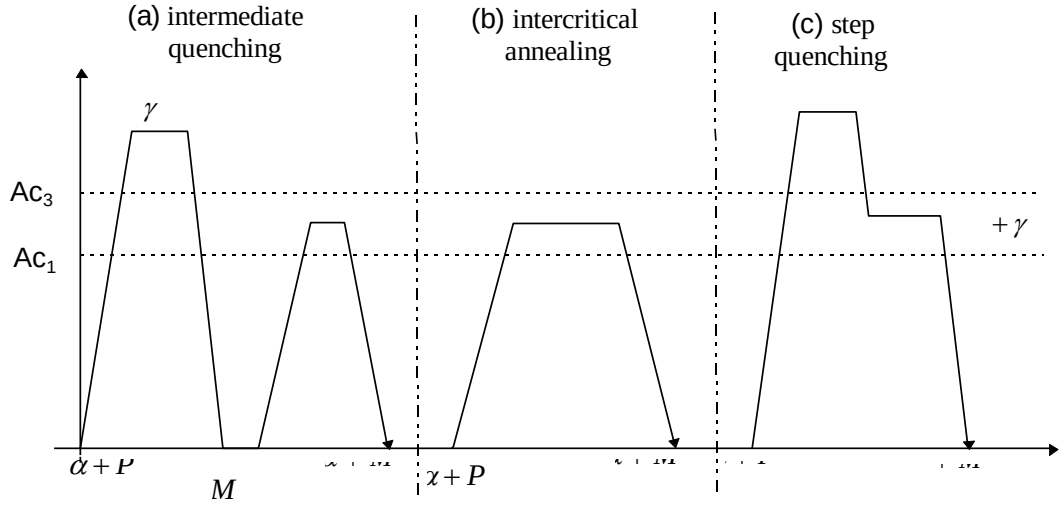

Figure1.3 Different process routes for formation of dual phase steels[23]

where, α = ferrite;
P = pearlite;
M = martensite;
γ = austenite.

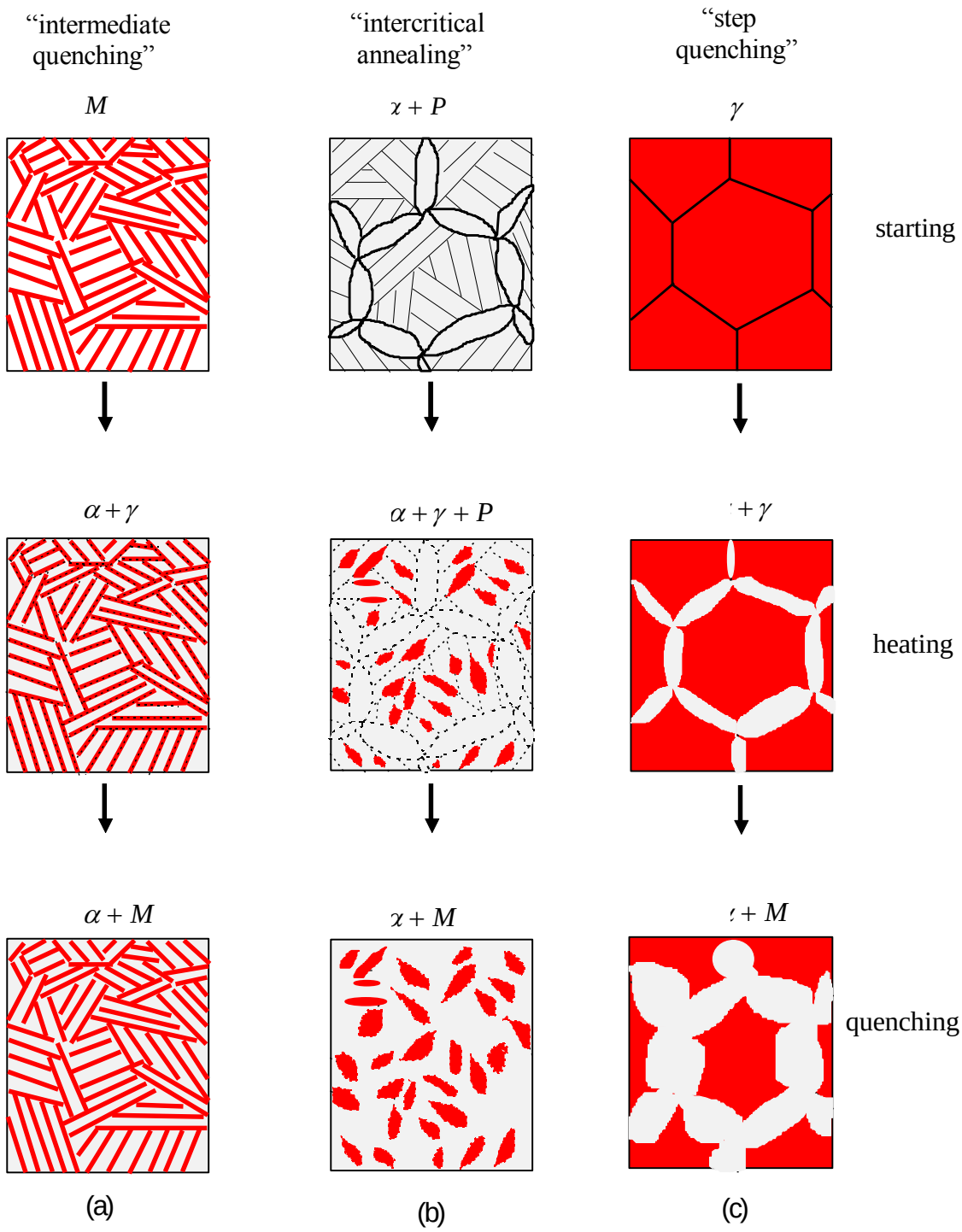

Figure 1.4 Illustration of nucleation and growth in dual phase steels through different formation paths

The "intermediate quenching" process starts with the production of martensite, which is then heated into the two-phase range. Austenite nucleates at the martensite lath boundaries and grows. As carbon diffuses to the austenite, the remainder of the prior

martensite transforms into ferrite. The final microstructure is needle-like martensite dispersed in ferrite (shown schematically in Figure 1.4 (a)).

The "intercritical annealing" process involves the annealing of ferrite and pearlite. When heated into the ($\alpha + \gamma$) region, austenite nucleates at the interface between ferrite and carbide inside the pearlite colonies (Figure 1.4 (b)), and grows into the carbide as the carbides dissolves. The resultant microstructure when the steel is quenched to room temperature is fine, globular martensite distributed along the ferrite boundaries.

The starting microstructure of "step quenching" is austenite. When the austenite is cooled to a temperature between Ar_1 and Ar_3 (critical phase transformation temperatures during cooling), ferrite nucleates at the prior austenite boundaries and grows into the austenite. The subsequent structure after quenching is coarse martensite surrounded by ferrite. The grains obtained from "step quenching" are larger and coarser than those obtained from the other two formation processes (shown in Figure 1.4(c)).

The annealing temperature of "step quenching" is lower than those of "intermediate quenching" and "intercritical annealing' for obtaining the same volume fraction of martensite because both Ac_1 and Ac_3 are higher than Ar_1 and Ae_3 for a given alloy.

1.3 Fe-C-Mn ternary phase diagram and Mn Partitioning

The Fe-C-Mn phase diagram at the iron-rich corner is schematically shown in Figure 1.5: the interface composition contour (IC contour) plot approximates the shape of a triangle because of a very large ratio of carbon diffusion coefficient to manganese diffusion coefficient (i.e. D_C / D_{Mn}). The equilibrium interface (i.e. ferrite and austenite) composition of an alloy A will be given by the tie-line that intersects the end points of the IC contour[26, 27]. Generally, the tie-line passes through the bulk composition of steel (point A) after equilibrium has been reached, but under LE (local equilibrium) condition, this tie-line will not necessarily pass through the bulk composition[28].

During the formation process of dual phase steel, carbon and manganese diffusion occurs because of the different solubility of these elements in ferrite and austenite in the two-phase temperature range (Figure1.5). This causes partitioning of the carbon and manganese in the ferrite and austenite.

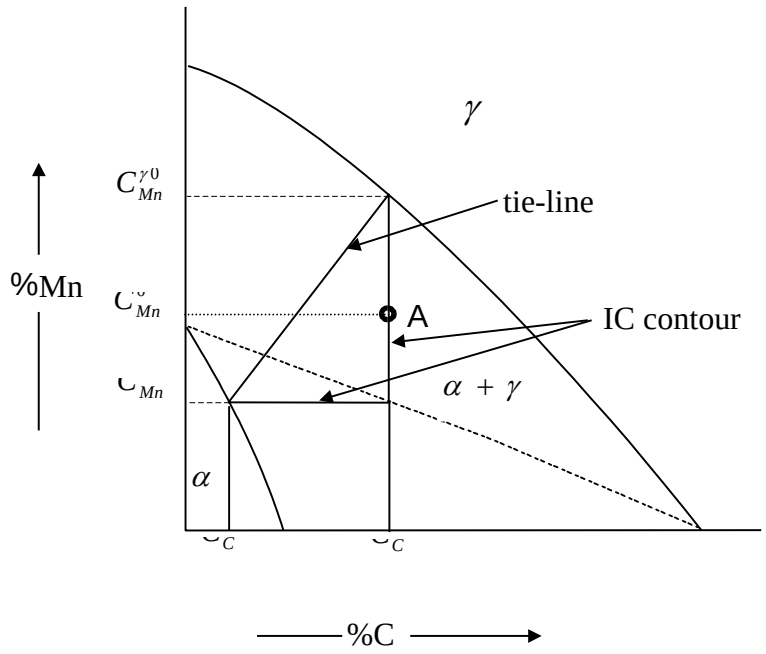

Figure 1.5 Determination of manganese contents in austenite and ferrite of alloy A in the iron-rich corner of Fe-Mn-C ternary phase diagram

The intercritical annealing process is used as an example to review the partitioning of carbon and manganese during transformation, as follows[12, 29, 30]:

(a) Transformation of pearlite to austenite (or dissolution of pearlite). This is controlled by carbon diffusion within the interlamellar spacing of pearlite (~0.2 um), and is very rapid occurring in a few second or less.

(b) The newly-formed austenite grains grow both into the ferrite and along the ferrite grain boundaries (in order to achieve partial equilibrium given by the lever rule in the two-phase region). This step is controlled by both carbon and manganese diffusion.

(c) Final equilibration within the austenite. The concentration gradients of the substitutional elements such as manganese will be eliminated by their diffusion through the austenite grains.

Because the diffusion rate of manganese in austenite is three orders of magnitude slower than in ferrite and because of the large size of the austenite grains, a long time (longer than ten hours) is needed to finish the 2nd and 3rd steps (shown in Figure1.6)

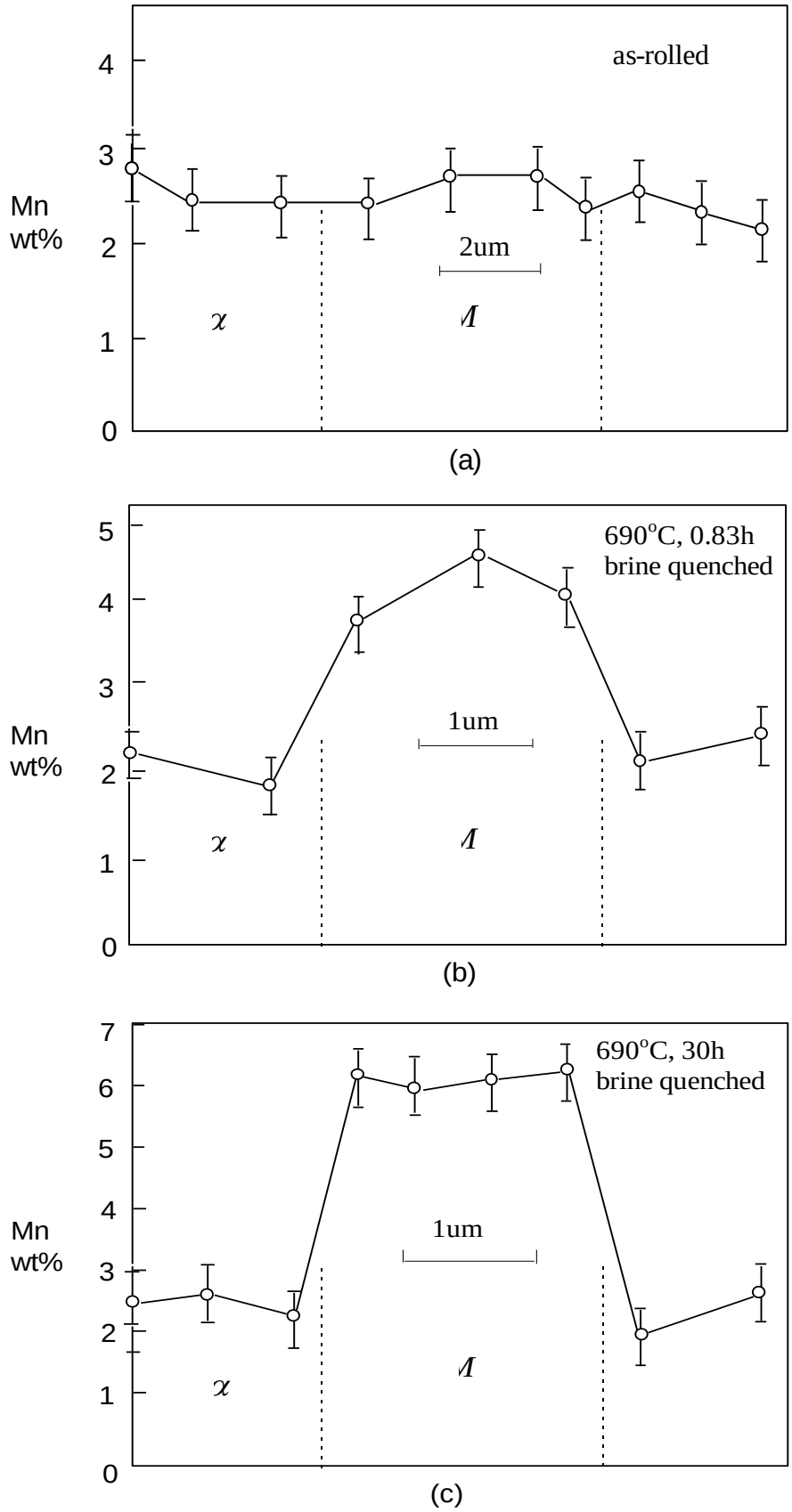

Figure 1.6 Variation of Mn distribution in ferrite and martensite with annealing time[29]

An example of carbon diffusion and manganese diffusion controlling processes in austenite formation during intercritical annealing of 0.12C-1.5Mn steel is shown in Figure 1.7. By using this diagram, one can easily find the austenite amount and the controlling kinetic process of austenite formation for a given annealing temperature, associated with isothermal holding time.

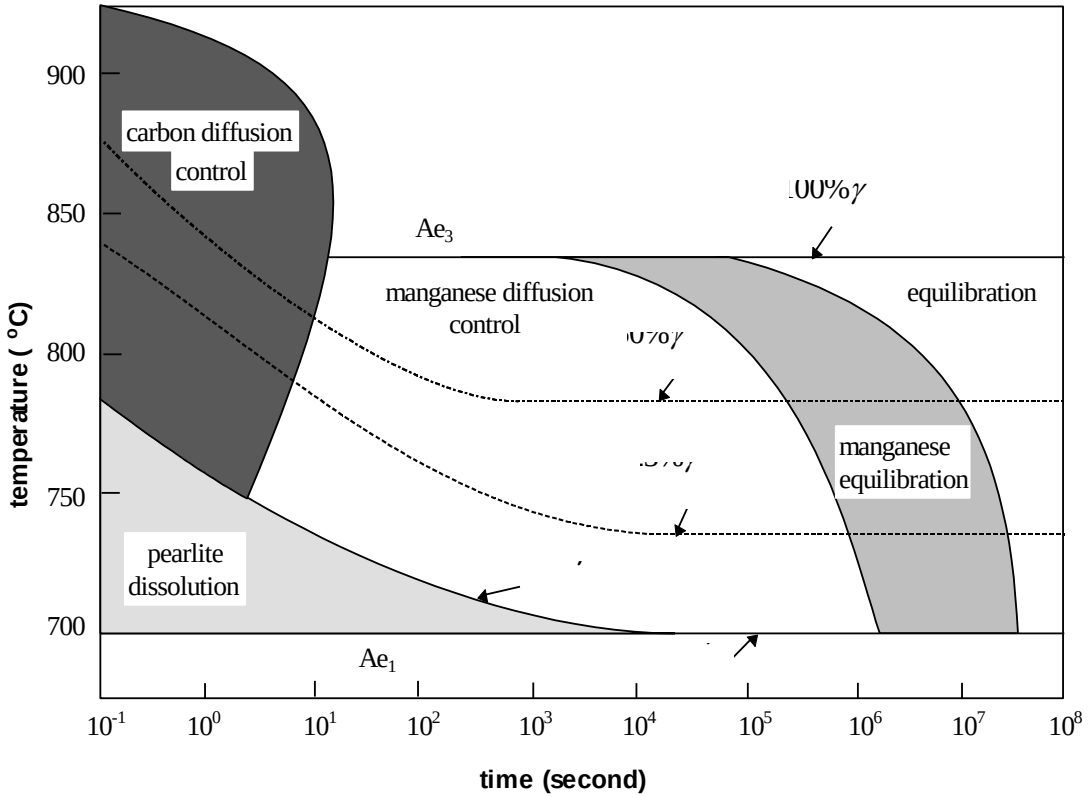

Figure 1.7 Austenite formation diagram for 0.12C-1.5Mn steel[12]

As it is an austenite stabilizer, the manganese concentrated in the austenite will strengthen the austenite and its successor phase (martensite). It also suppresses the martensite formation temperature allowing the austenite to transform to martensite at relatively low cooling rates.

The partitioning of interstitial elements in dual phase steels during annealing makes most alloying element contents increase in the austenite and decrease in the ferrite, which gives ferrite high ductility, and hence the superior ductility of the low alloy ferrite will give the dual phase steel high ductility[31].

In addition to the manganese and carbon partitioning, other austenite stabilizing alloy elements will also concentrate in the austenite; among them nitrogen is the most important.

The partitioning of nitrogen is found to be retarded by the manganese, probably because the nitrogen diffusion is controlled by the diffusion of Mn-N clusters as opposed to interstitial diffusion of nitrogen, and thus it takes a similar time as the manganese partitioning to reach the final equilibrium. The concentration of nitrogen in austenite is probably the main reason for the absence of a discontinuous yield point in dual phase steels, "since the removal of nitrogen from the ferrite matrix prevents ambient temperature ageing"[32, 33].

1.4 Characteristics

The second phase in dual phase steels is either a lath or twinned martensite or a combination of the two, inevitably with varying amounts of retained austenite, which appears to increase the ductility at a particular strength level. The retained austenite has only moderate stability and thus transforms to martensite during straining, which produces increased uniform elongation, strength and work-hardening rate. This increased work-hardening arises from the gradual strain-induced transformation of $\gamma_R \rightarrow M$ over a large strain range.

Generally, a high dislocation density due to the volume and shape change associated with the austenite-to-martensite transformation is observed in the ferrite grains contiguous with the martensite. That is, the dislocation density is high adjacent to the martensite and low in the interior of the ferrite grains, which is the reason that dual phase steels have low yield strength and show a continuous yielding behaviour with a high initial work hardening rate[34-37]. In addition, they posses greater resistance to the onset of necking (i.e., plastic instability) in uniaxial tensile tests and multiaxial sheet metal forming processes to give large uniform strain.

Dual phase steels can also be strengthened significantly by static or dynamic strain ageing[38]. Additionally, those steels containing low carbon content have been shown to exhibit excellent resistance to fatigue crack propagation[39] and improved toughness[40].

As discussed in section 1.2, the morphology of the martensite is due to the formation procedure and affects the strength and ductility of the dual phase steel. Kim et al [24] found that the DBTT (the ductile-to-brittle transition temperature) of the fine, fibrous martensite dual-phase steel produced by intermediate quenching is much higher than

that of the fine, globular martensite dual-phase structure obtained from intercritical annealing, regardless of volume fraction of martensite. The DBTT-controlling effective grain size of dual phase steels is the same as that of the starting structure prior to two-phase annealing, i.e. the austenite grain size for intermediate quenching and ferrite grain size/mean free path for intercritical annealing.

The coarse martensite dual-phase steel has a much lower ductility, but a higher strength than the fine fibrous and globular structures. The failure of coarse martensite dual-phase steel is caused by the initiation of cleavage cracks in the ferrite whereas that of the fine fibrous/globular martensite dual phase steel is by void nucleation and coalescence[23].

The relationship between grain size/mean free path of ferrite, d_f, and the yield strength and tensile strength of dual phase steels agrees with the Hall-Petch equation, i.e. $\sigma = \sigma_0 + k d_f^{-\frac{1}{2}}$. The slope k increases with increasing volume fraction of martensite (V_m) in dual phase steels for both yield strength and tensile strength, and the σ_0 is independent of V_m for yield strength, but increases with V_m for tensile strength[41].

The grain size of dual phase steel can be refined by adding nitrogen. There seems to be a correlation between the microstructure and the resulting increased strength levels and work hardening rates obtained at high nitrogen contents, which may be due to: (1) the increased nucleation rate of austenite through a nucleating effect of increased amounts of nitride precipitates; (2) the increased pinning effect of nitride precipitates on the $\alpha - \gamma$ interface to retard the growth of austenite during intercritical annealing[34]. The addition of V, and Nb can refine the grain size, but V addition does not improve the mechanical properties of low carbon dual phase steels when they are rapidly quenched or air cooled[21, 42].

The grains of dual-phase steels can also be refined by deformation before intercritical annealing[43-46]. The pearlitic cementite is fragmented and the dislocation structure is introduced into the pearlitic ferrite by cold deformation. During intercritical annealing, the recrystallization of ferrite and spheroidization of the cementite are accelerated, and the growth of ferrite after recrystallization is restricted by the pinning action of the austenite grains which have nucleated in the boundaries between deformed and unrecrystallised ferrite grains and in spheroidal cementite particles in recrystallised

ferrite grains. Thus the finer ferrite+martensite structure can be obtained after quenching and the austenite not only locates in ferrite grain boundaries, but also distributes intragranularly in ferrite. The ferrite recrystallization proceeds austenite formation[13].

The predeformation also increases the amount of twinned martensite for the steels with lower volume fraction of martensite, and increases the tensile strength and yield strength as well. Ductility is reduced because of the banded distribution of martensite islands and the amount of twinned martensite[45].

In addition to the morphology, grain size, and distribution of ferrite and martensite, the volume fraction of martensite (which is determined by annealing temperature and carbon content) has a distinctive influence on the properties of dual phase steel[47]. Jena's equation[48]:

$$\sigma = \sigma_f + \left(\sigma_m^0 - \sigma_f\right) \cdot V_m + K_m \left(g C_0 V_m\right)^{\frac{1}{2}} \qquad (1.1)$$

where, g and K_m are constants, and Mileiko's equation (details discussed later) shows that the tensile strength increases non-linearly with the volume fraction of martensite. Jena's equation also shows that the carbon content in steel, C_0, increases the strength of dual phase steel as one would expect.

But Davies[49] has concluded that the strength of dual phase steel is dependent only on the volume fraction of martensite and the ferrite grain size, and is not dependent on the strength and carbon content of the martensite phase. This appears simplistic as the strength of a composite material is a function of the constituent phases' strengths; in this case, the martensite strength is primarily dependent on its carbon content.

Similarly to tensile strength, the ductility of dual phase steel is directly dominated by the volume fraction of martensite. In addition to volume percentage of martensite, the ductility of the ferrite also influences that of the dual phase steel. High ductility of the ferrite can be obtained through a fine grain size and a low interstitial content (reducing the solid solution hardening).

The research conducted by Marder[18] shows that the relationship between the strength and ductility of dual-phase steels is independent of the alloy addition at a low strength level (700MPa); above this strength level, the increasing effect of Mo on ductility is higher that that of V for an equivalent strength level. The small additions of Mo and/or

V are thought to remove interstitial atoms from the ferrite solution and increase the ductility of the ferrite.

The total elongation of dual-phase steel is comprised of two parts: uniform elongation and post-uniform elongation. The uniform elongation increases slightly with increasing strain rate, whereas post-uniform elongation increases significantly with increasing strain rate. Decreased uniform elongation at low strain rates is attributed to a decrease in strain-hardening rates near instability, whereas increased post-uniform elongation is correlated with the increase in strain rate sensitivity with increased strain rate.

Mileiko's theory which is derived for describing relationship between tensile properties and volume fraction of ductile fibre reinforced metal matrix composite[50] has been introduced to describe dual phase steels even though the second phase (martensite) is not exactly in a continuous fibre form[1, 51].

The conclusions that can be drawn are that fine grain size, high strength (more alloying element content partitioning), high carbon content and a high volume fraction of martensite will increase the tensile strength of a dual phase steel, but a high volume fraction of martensite combined with carbide precipitation reduces ductility. The amount and carbon content of the martensite phase are primarily dependent on the intercritical annealing temperature and the overall carbon content of the steel, but are also affected by manganese partitioning.

In addition to the yield strength, tensile strength and ductility, the work-hardening behaviour of dual phase steel is another important research topic[52-59]. The deformation of dual phase steel is a complex and combined process of deformation of ferrite and martensite. The strain distribution between ferrite and martensite is dependent on the carbon content in the martensite and the volume fraction of martensite[60]. For low martensite volumes and/or a low carbon content in the martensite, the strain-hardening behavior of dual-phase steel can be described by a single work-hardening rate, n, because both the martensite and ferrite are deformed plastically. For high volume fractions of martensite and/or high carbon contents in martensite, the dual phase steel exhibits two distinct stages of work-hardening in the range of plastic deformation; the work-hardening rate for the first stage (where ferrite deforms plastically, and martensite elastically) is higher than that of second stage (where both ferrite and martensite deforms plastically)[52, 61].

Chapter 2 Objectives

As reviewed in Chapter 1, dual phase steel is a structure of hard martensite dispersed in soft ferrite, which can be viewed as a metal matrix composite (MMC), so composite theory may be applied to model the dual phase steels.

The distribution of reinforcement is random in the intercritical annealed dual phase steels, which is of limited reinforcing effect compared with a preferred orientation distribution of reinforcement according to the theory and practice of composite materials. A thermomechanical treatment will be introduced to the dual phase steel formation process to obtain a preferred orientation distribution of fibrous martensite dual phase steel - one kind of ductile short fibre reinforced metal matrix composite.

2.1 In-situ dual phase steels

The dual phase steels obtained by intercritical annealing are hereinafter referred to as "in-situ" dual phase steels in order to differentiate these from the "artificial" dual phase steels which will be introduced later.

During intercritical annealing manganese partitioning takes place. The variation of the partitioning coefficient with annealing time at a given temperature has been examined[29, 32], but the effect of annealing temperature on manganese partitioning has not been investigated yet.

The effect of change in morphology of micro-constituents of in-situ dual phase steels due to thermomechanical treatment on tensile properties has been studied[62]. Warm rolling in the two-phase temperature range causes an increased strength in the rolling direction probably due to (1) flattening and consequent fibering of the martensite particles in the rolling direction, (2) absence of epitaxial ferrite. But the residual stresses which were introduced during warm rolling because of the different deformabilities of austenite and ferrite are of concern.

Cold drawing of dual phase steel is an effective way to produce high strength steel wire, the deformation during cold drawing can strengthen the dual phase steels[63, 64].

There are some limits to modelling dual phase steel with current composite mechanics because of:

(1) the variation of chemical composition (especially carbon content) in martensite with volume fraction of martensite for a given steel. The carbon content in martensite, which determines the strength and hardness of martensite, decreases with increasing volume fraction of martensite (ie, increasing annealing temperature);

(2) the variation of grain size of martensite with volume fraction of martensite for a given steel. The grain size of martensite increases with volume fraction of martensite (ie, increasing annealing temperature and time).

To obtain a constant chemical content and size of reinforcement with different volume fraction, the concept of an artificial dual phase steel will be introduced in the following section.

2.2 Artificial dual phase steels - steel/steel composites

Because of the limitations of in-situ dual phase steels, an artificial dual phase steel, which actually is an eutectoid-steel-wire reinforced ferrite composite, can be made to model dual phase steel with a high volume fraction of second phase and constant carbon content in the second phase.

Composites are combinations of two or more materials made by mixing or bonding them in such a way that each maintains its integrity. One part generally acts as a matrix and the other as the reinforcement. The constituents that are mutually insoluble and different in form or composition on a macroscale can be physically identified and exhibit an interface between one another. Composite materials' tailored properties are achieved by the systematic combination of constituents and certain properties will be superior to those of the separate components.

In composites, the component materials generally are not merely different at the molecular level but often have distinctive component properties and they are generally mechanically separable. The important factors related with composites are reviewed in the following sections.

2.2.1 Fibre/wire

Fibres/wires are materials that have one very long axis compared to the other two; the cross section often being circular or nearly circular. These fibres/wires can often have significantly higher strength in their long direction than in the transverse directions except glass fibre (the longitudinal and transversal mechanical properties for glass fibres are nearly equal). The fibres often used in composites are glass, carbon, silicon carbide and boron fibres.

In addition to carbon and ceramic fibres, metallic fibres/wires[65-69] also have the potential to be used as reinforcements for composites. The great advantage of metallic wire is that it has a more consistent strength and a higher ductility than any ceramic fibre.

The reinforcement used in the current project is eutectoid steel (0.8%C) wire (also known as piano wire), which is made by cold drawing fine eutectoid pearlitic steel. The high strength of this steel wire is obtained from heavy cold deformation and elongation of the pearlite[70], but most of the strengthening contribution of the cold drawing will be lost when the steel wire is introduced into the steel matrix at elevated temperature. This is the primary disadvantage of using steel wire. The variation in tensile properties of the steel wire with composite fabrication conditions will be examined in Chapter 5.

2.2.2 The interface

The interface between the reinforcement and matrix in a composite is a bonding surface where discontinuity of some kind occurs. This discontinuity may be sharp or gradual. Through the interface region, material parameters, such as concentration of an element, crystal structure, atomic registry, elastic modulus and coefficient of thermal expansion, change from the values of one material (eg. the matrix) at one side to those of the other material (the reinforcement, for example) at the other side. The differences in these parameters between reinforcement and matrix may produce residual stresses after composite fabrication.

Different interfaces are desired for different composites. For ceramic matrix composites, an increased toughness is the primary requirement. The interface must be weak so that it will debond leading to crack deflection and fibre pullout thus promoting energy dissipation at the interface so as to raise the toughness. The fibre works as a toughening agent rather than as a strengthening or stiffening reinforcement[71,72].

High strength and stiffness are usually the most important factors required for fibre reinforced metal matrix composites. So when a crack propagates to the interface, the interface must be strong enough to resist the crack propagating along the interface (ie. debonding)[73-75]. Thus, the stress concentration caused by the crack can be carried by the high strength of the fibre until the fibre is eventually broken (as shown in Figure 2.1).

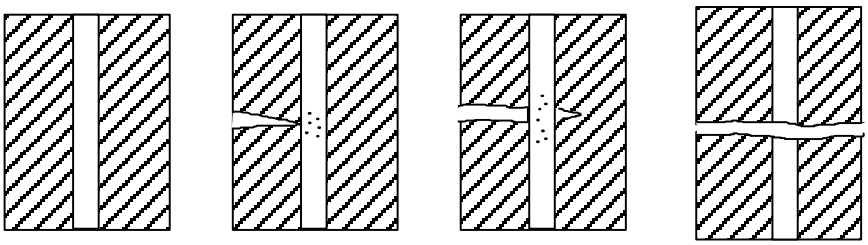

Figure 2.1 The process of crack propagation in fibre reinforced metal composites

To obtain desirable characteristics in composite materials, one should be careful that the fibres are not weakened and that the applied load is effectively transferred from the matrix to the fibre through the interface. It can be seen that the interface is so important that it plays the controlling part in the interaction and load-transfer between fibre and matrix. It becomes extremely important to understand what exactly is going on in the interface region of any given composite system under a given set of conditions. Wettability of the fibre by the matrix and the type of bonding between reinforcement and matrix are the primary considerations. The characteristics of the interface and how they are affected by temperature, diffusion, residual stress, etc. are important in understanding a composite system.

2.2.2.1 Wettability[76-79]

Wettability is used to describe the extent to which a liquid would spread on a solid surface. A liquid drop on the surface of solid is shown in Figure 2.2. In order to obtain complete wettability, the following condition must be satisfied:

$$\gamma_{LS} + \gamma_{LV} < \gamma_{SV} \qquad (2.1)$$

where, γ is the specific surface energy, and the subscripts S, L, and V represent solid, liquid, and vapor phase involved in the equilibrium system, respectively. From Figure 2.1, the equation of force equilibrium can be written as[80]:

$$\gamma_{LS} + \gamma_{LV} \cdot \cos\theta = \gamma_{SV} \tag{2.2}$$

or

$$\theta = \cos^{-1}\left(\frac{\gamma_{SV} - \gamma_{LS}}{\gamma_{LV}}\right) \tag{2.3}$$

θ , the angle that the liquid drop makes with the solid surface, is called the contact angle , and can be used to describe the wettability between two materials (ie., matrix and reinforcement in composites). Good wettability can be obtained when θ is lower than 90°. θ depends on the nature of the surface and the structure of the components. The wettability between components of similar structure (such as metal-metal) is better than that between different structure components (such as metal-ceramics).

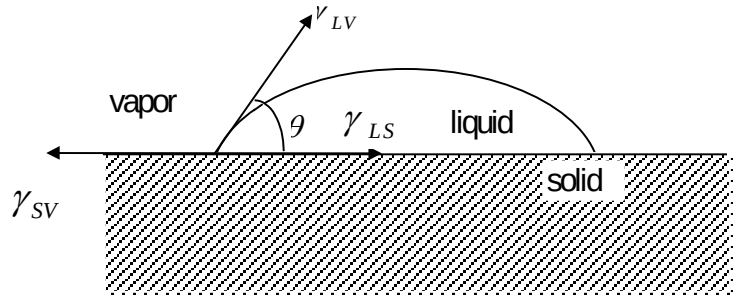

Figure 2.2 Schematic showing contact angle formed between solid, liquid and vapor phases

From the discussion above, it can be seen that wettability is very important for liquid metal infiltration into a reinforcement preform and good wettability must be achieved for composites made using molten metals.

2.2.2.2 Types of interfacial bonding

The bonding between fibre and matrix can be classified as:

(1).Mechanical bonding;

(2).Chemical bonding

(a) Dissolution bonding;

(b) Reaction bonding.

Mechanical bonding: In this case, there is no reaction at the interface. Simple mechanical keying effects between two surfaces can lead to a considerable degree of bonding. The interfacial strength is governed by Van der Waals forces between fibre and matrix; any contraction of the matrix onto a central fibre would result in a gripping of the latter by the former. The bonding strength can be increased by introducing a rough interface, which improves the keying between components. Vennett[81] and Schoene[82] have made metallic wire reinforced metal composites and confirmed that in the presence of an internal compressive force, a wetting or metallurgical bond is not necessary because the mechanical gripping of the fibre by the matrix is sufficient to cause an effective reinforcement as indicated by the occurrence of multiple necking in the fibre. But pure mechanical bonding alone will not be sufficient in most cases, In carbon fibre-metal systems, this weak interface will allow fibre pull-out during failure, but high strengths can not be obtained with this kind of interface. A good example of this type of behavior is carbon fibre reinforced copper.

Chemical bonding:

(a) Dissolution bonding. In this situation, the reinforcement dissolves into the matrix at the interface with a gradual distribution of the solute element. The interfacial dissolution reduces the fibre diameter but increases the interfacial strength, as in carbon fibre-nickel composites. The extensive formation of the solution degrades the fibres and is detrimental to the strength of the composite.

(b) Chemical reaction bonding: the reinforcement reacts with the matrix to form a compound (a brittle phase in most cases) at the interface. The reaction strengthens the interface but also causes embrittlement, for example; carbon fibre reacts with aluminium to produce Al_4C_3 at the interface in carbon/aluminium composites, which reduces the strength and impact properties of the composite.

In metal-metal systems, not only solid solution but also intermetallic compounds form (shown in Figure 2.3), due to the diffusion between fibre and matrix. In addition, the reaction products and reaction rates may vary depending on the composition of the components, reaction time and temperature.

Only under careful control, can dissolution and reaction bonding be used to strengthen composites.

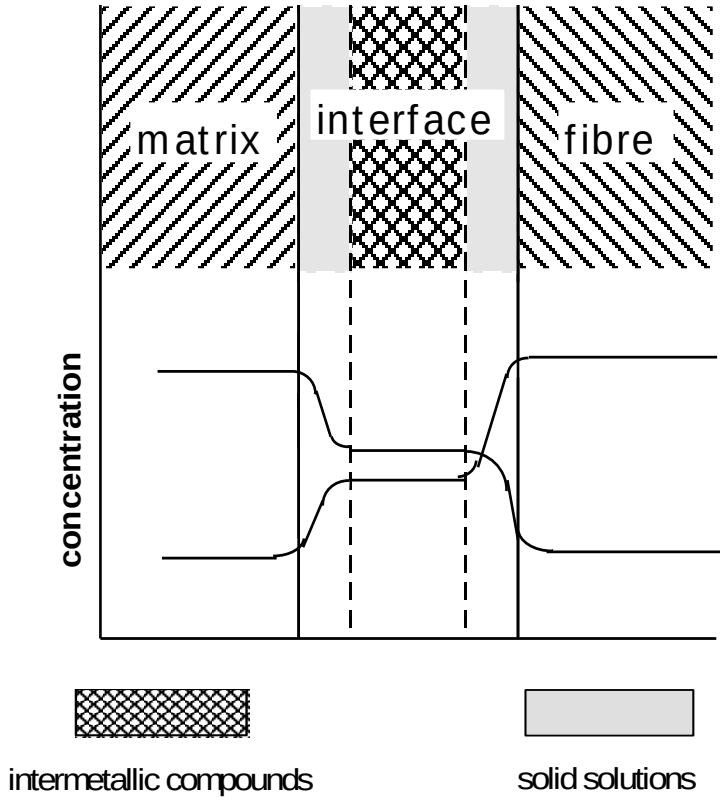

Figure 2.3 The interfacial reaction and element distribution in the reaction bonding interface region

The microstructure and element distribution at the interface of a fibre composite with three different types of interfacial bondings are shown schematically in Figure 2.4; distinct interface and sharp variation of elements for mechanical bonding; a smooth interface and gradual change of concentration of elements for dissolution bonding, and thirdly, reaction-produced grains in reaction bonding which exhibit the step change of element concentration.

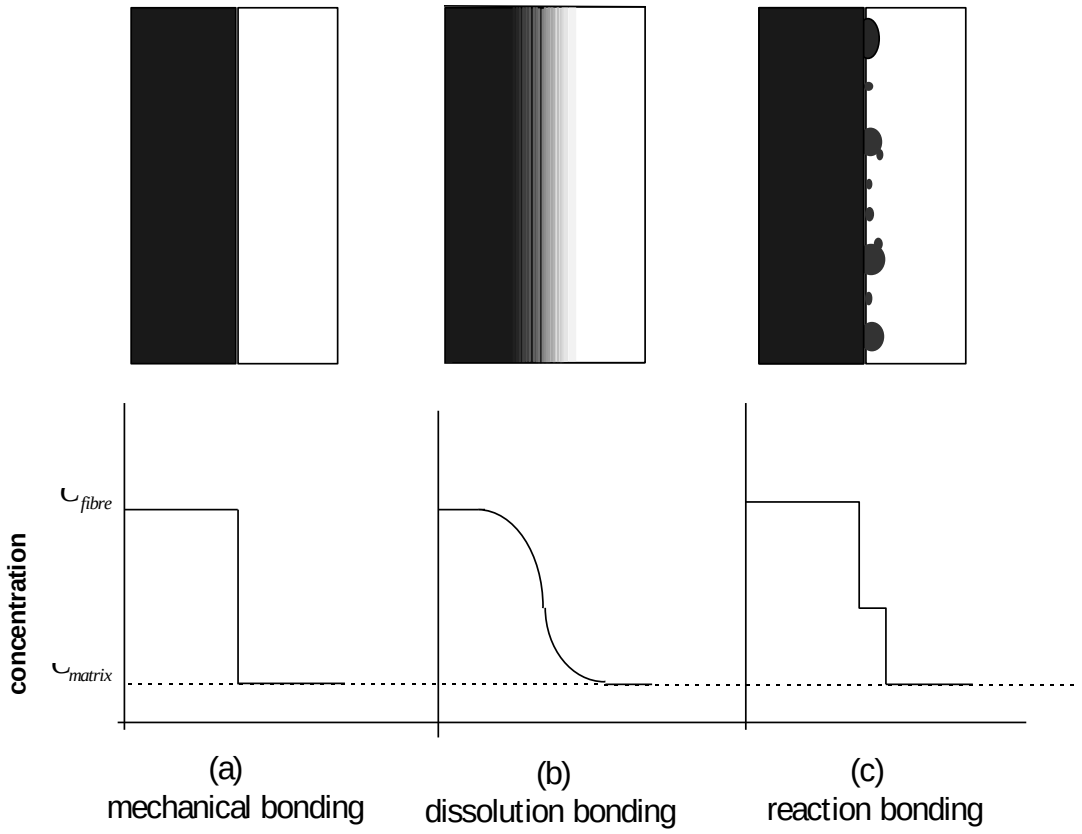

Figure 2.4 Element distribution through interfaces with 3 different interface bondings

2.2.2.3 Interfaces introduced by fibre coatings

A new interface between fibre and matrix will form when a coating is introduced onto the fibre surface. The coating is employed to (a) resist diffusion and reaction to protect the reinforcement from chemical attack, (b) promote wetting, and (c) increase interfacial bonding by introducing dissolution and/or reaction for extremely weak bonding interfaces.

Generally, the materials used for barrier coatings must meet the requirement that they will not react with matrix or reinforcement, ie. the coating materials are thermodynamically stable at the manufacturing or utilisation temperature. In fact, many barrier coatings have been explored to slow down interfacial reaction to a suitable degree, rather than to completely stop the reaction because the coating techniques are very limited for thermodynamically stable materials.

Duplex metal coating has been proposed to improve the interfacial strength of weak-bonding composites (carbon fibre reinforced copper composites, for example): the duplex coating was designed as “inert metal-active metal” (as shown in Figure 2.5). The

inert metal (internal coating) will neither react with nor dissolve the fibre; the active metal (external layer) must have a certain solubility in the inert metal but does not react with the inert metal to form a brittle intermetallic compound and is able to diffuse through the inert metal to the surface of fibre in order to react with or dissolve the fibre. On the other hand, the thickness of the inert metal layer is able to adjust the concentration of the active metal on the surface of fibre to control the extent of the reaction or dissolution at the interface. The application of duplex coatings in C/Cu composites has been successful in increasing strength[83].

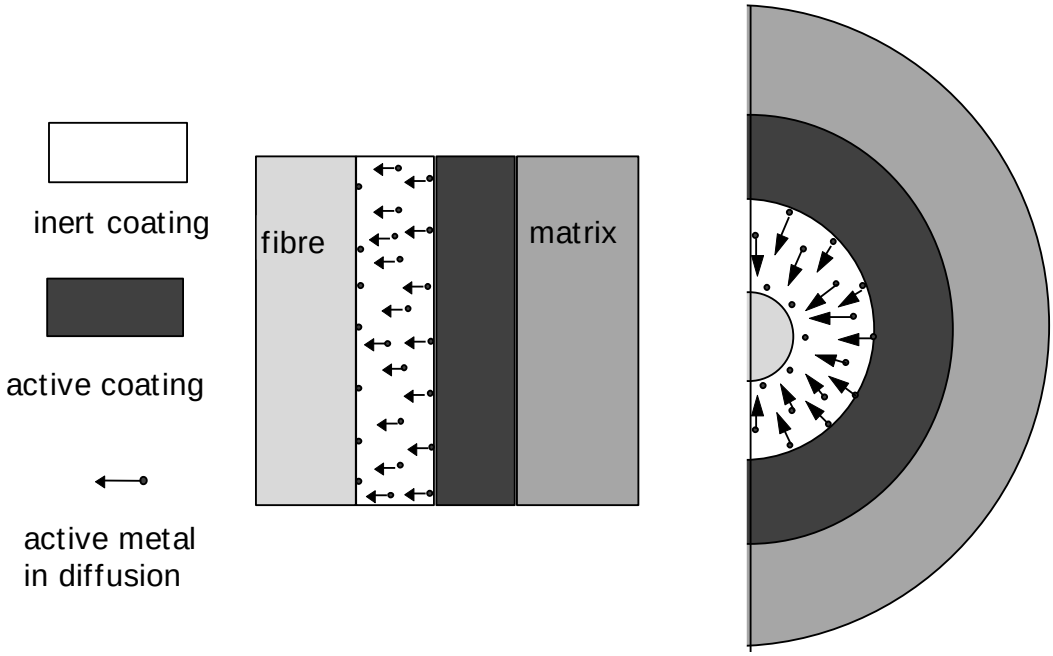

Figure 2.5 Schematic illustration of duplex metal coating in fibre composites

The most often used coating methods are chemical vapor deposition, physical vapor deposition, electroplating, and electroless plating.

2.2.2.4 Methods for characterising interfacial strength

A variety of tests have been developed to test the interfacial bonding strength between fibre and matrix; the most commonly used are single fibre tests.

Fibre pull-out[84-89]/fibre push-out[89-92] test. In these cases, a portion of fibre is embedded within a matrix, an axial tensile load is required to pull/push out the fibre from the surrounding matrix (shown in Figure 2.6). The interfacial strength is the maximum shear stress around the fibre which causes fibre debonding or frictional sliding.

The fibre push-out test has an advantage over fibre pull-out test, because the fibre is not as likely to break as under the tensile stress applied in the latter test. The applied load does change the normal stress on the interface, the differential Poisson expansion tending to increase the radial compressive stress. Once the debonding occurs, it will propagate along the length of the fibre and subsequent motion will occur purely by frictional sliding at the interface[93].

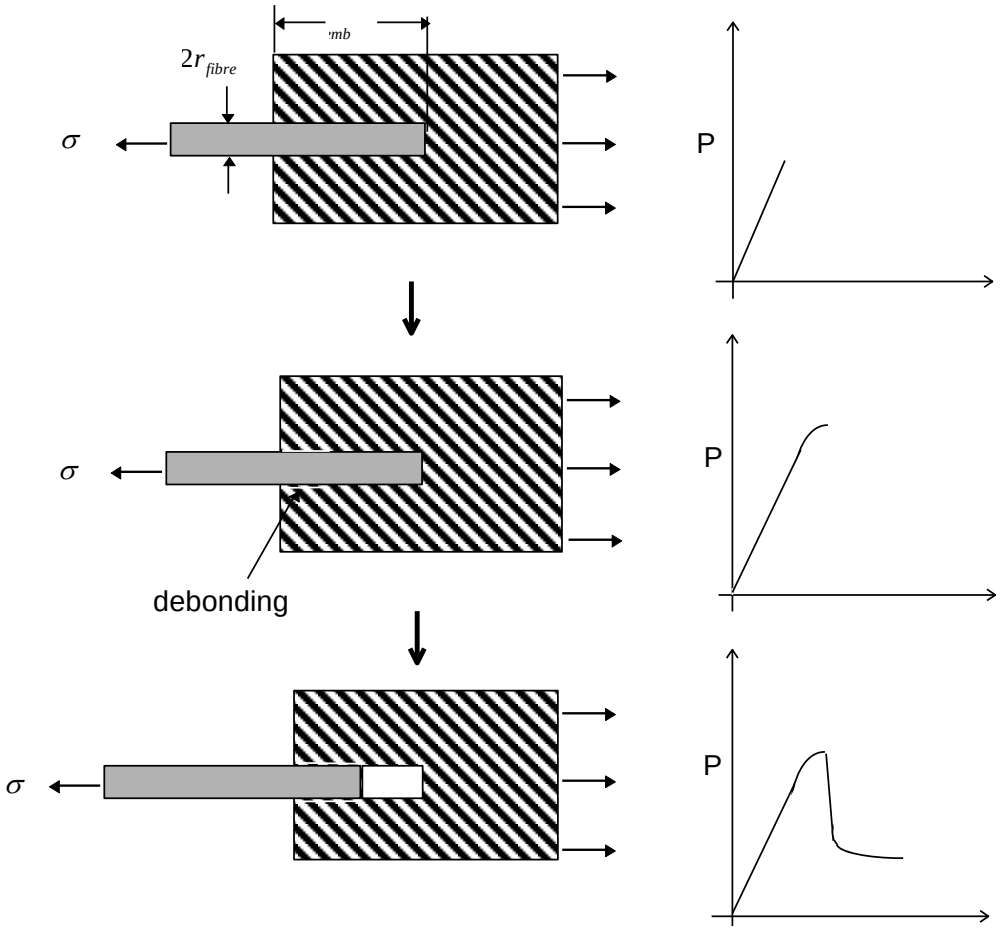

Figure 2.6 Schematic illustration of the fibre pull-out process and load-displacement plot for single fibre pull-out testing

The interfacial strength can be calculated by using the maximum load measured from fibre pull-out (tensile) and fibre push-out tests (compressive), as:

$$\tau = {2P_{\max}}/{\pi \cdot l_{emb} \cdot r_{fibre}} \qquad (2.4)$$

where, $P_{\max}$ is the maximum load to pull/push fibre out, l_{emb} is the embedded fibre length, and r_{fibre} is the radius of fibre.

The single fibre pull/push-out test have been used to test the interfacial shear strength of metal rods, carbon filaments, glass fibres, polymer fibres in concrete, epoxy, metals.

In addition to the fibre pull-out and push-out methods, the 4-point bend test also can be use to test the interface bonding.

2.2.2.5 Relationship between interfacial condition and composite properties

The role of the interface is crucial in composites: stiffening and strengthening depend on load transfer across the interface (high interfacial strength is desired), toughness is affected by crack deflection/fibre pull-out (medium/weak interface bonding is necessary), and ductility is influenced by relaxation of peak stress near the interface (medium interfacial strength is required).

An example of the influence of interfacial condition (bonding strength and chemical reaction) on the strength and fracture behavior of B/Al composites is shown in Figure 2.7. With increasing pressing time, t, and pressing temperature, T, the tensile strength initially increases due to increase in interfacial bonding strength but then decreases due to degradation of the fibre by an interfacial chemical reaction, (length of fibre pull-out decreases).

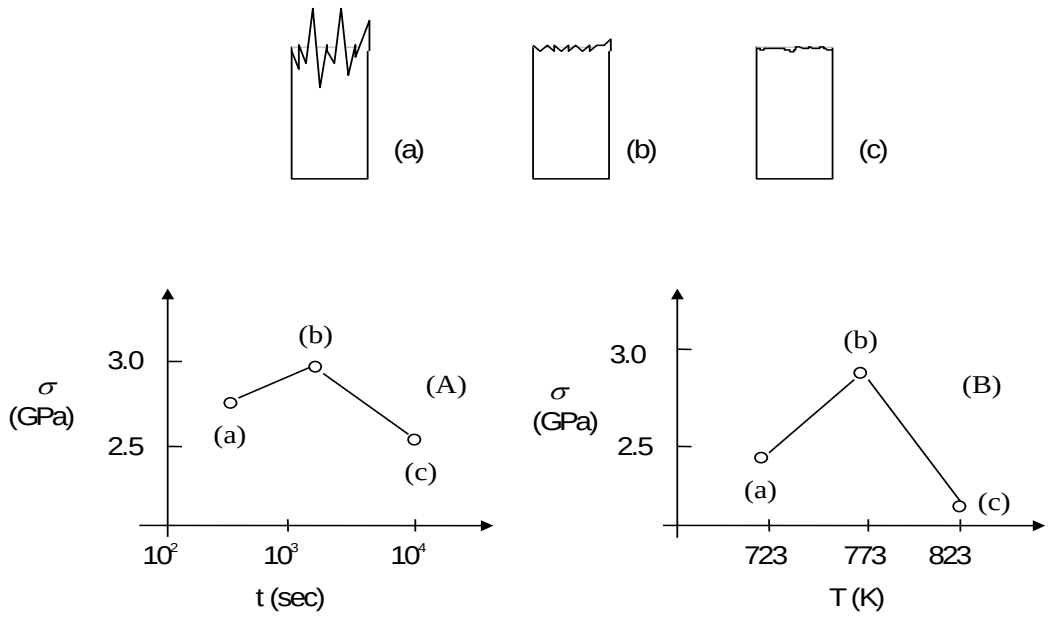

Figure 2.7 Schematic of fracture surface and variation of tensile strength of boron fibre/aluminum composites (A) as a function of hot pressing time at 773K under a given pressure of 50MPa and (B) as a function of pressing temperature for a given pressing time of 1.2ks [(94)]

Without any interfacial reaction, the strength of the fibre does not change, and the tensile strength of the composite increases with interfacial bonding strength, which is shown in Figure 2.8. The important characteristics are as follows:

(a) When the interfacial strength is lower than the matrix yield shear stress, the composite tensile strength increases slightly with increasing interfacial strength.

(b) When the interfacial strength is higher than the matrix yield stress but is not high enough to suppress interfacial debonding, the strength of composite increases sharply with the interfacial strength.

(c) The tensile strength of the composite keeps nearly constant when the interfacial strength is high enough to suppress debonding.

(d) The more uniform the strength of the fibres (ie., the smaller the CV), the less sensitive the composite strength is to interfacial strength.

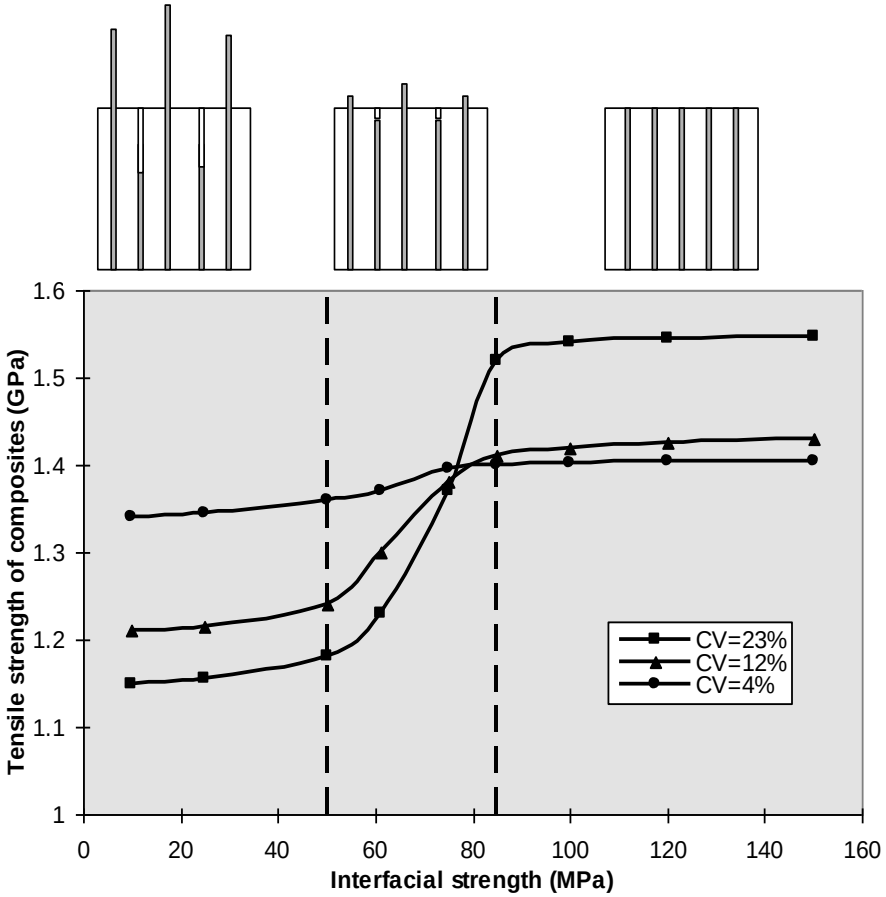

Figure 2.8 The influence of interfacial strength on strength of composites without reaction occurring at interface, obtained by computer simulation (yield shear strength of matrix is 50MPa)[94]

If the reaction takes place at the interface, not only the interfacial strength but also the fibre strength will vary with reaction layer thickness, as shown schematically in Figure 2.9. The interfacial strength increases with increasing reaction layer thickness, but the strengths of both fibre and composite decrease rapidly when the reaction layer exceeds a critical thickness.

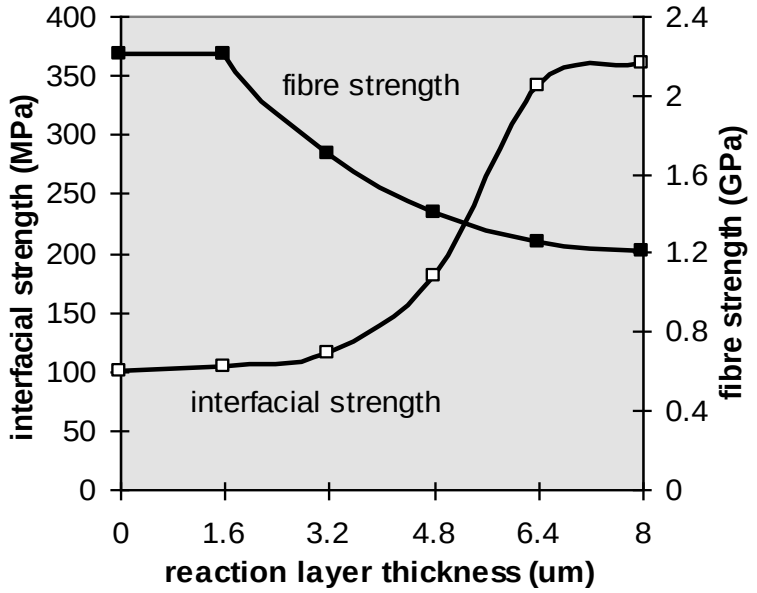

(a)

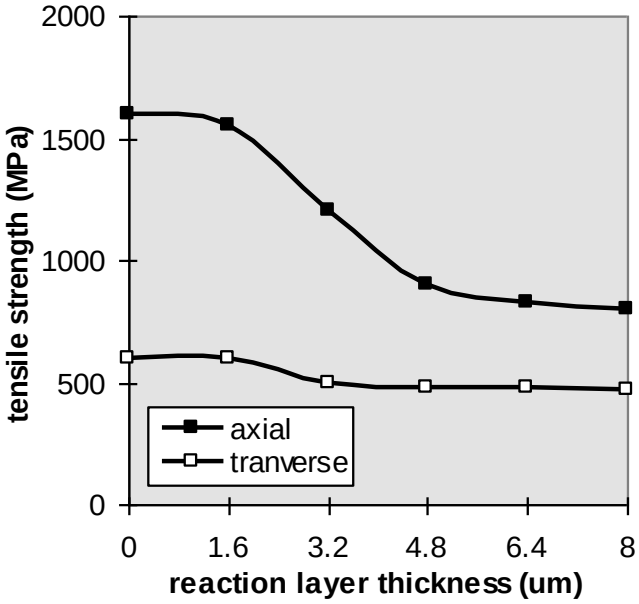

(b)

Figure 2.9 The variation of strength of interfacial bonding, fibre (a), and of SiC/Ti composites (b) as a function of chemical reaction layer thickness[93]

2.2.3 Residual stress and its effect on composites

Residual stresses are commonly present in composites because of the difference in the mechanical-thermal elastic properties of reinforcement and matrix. The residual stress can be generated from either thermal change (thermal residual stress) or applied external load.

Thermal residual stress normally exists in metal matrix composites, since the temperature at which the composite is made is higher than that at which it is used. The residual stress due to thermo-mechanical effects is important for the overall (engineering) properties and performance of those composites.

Normally in metal matrix composites, the ceramic reinforcement's thermal expansion coefficient is smaller and its elastic stiffness is greater than those of the matrix. This indicates that the residual stress is compressive for the fibre and tensile for the matrix during cooling after fabrication of continuous fibre composite, as given by:

$$\langle\sigma\rangle_m = \frac{V_f E_f E_m}{E_c}\left(\alpha_f - \alpha_m\right)\Delta T \qquad (2.5)$$

$$\langle\sigma\rangle_f = -\frac{V_m E_m E_f}{E_c}\left(\alpha_f - \alpha_m\right)\Delta T \qquad (2.6)$$

where, $\langle\sigma\rangle_m$ and $\langle\sigma\rangle_f$ are mean residual stresses in matrix and fibre respectively,

α_f and α_m are the thermal expansion coefficients of fibre and matrix respectively,

ΔT is the temperature change in composites.

A calculated example in the Al+Al_2O_3 system is shown in Figure 2.10, $\Delta T = -600°C$ means that there is no relaxation during cooling from the liquid state for an Al+Al_2O_3 composite, ie. water quenching after fabrication. And in the situation of air-cooling after fabrication with partial relaxtion (at high temperature), the effective temperature change which gives residual stress is set as $\Delta T = -250°C$. Figure 2.10 shows that the residual stress depends on the cooling condition, thermo-mechanical properties of components and volume fraction of reinforcement[95].

As the thermo-elastic properties determine the residual stress, the mechano-elastic properties govern the stress distribution between reinforcement and matrix. Both experimental test and theoretical analysis show that the residual stresses is concentrated near the interface and depend strongly on the properties of interfacial region (i.e. an interface coating or a reaction product)[96].

The existence of residual stresses in reinforcement and matrix can strengthen both reinforcement and matrix (if they can be strengthened by strain hardening). In continuous fibre composites under tensile loading parallel to fibre, the axial compressive residual stress in the fibres indicates that an extra tensile load equivalent to the residual stress is required to break the fibre, therefore, onset of fibre fracture is delayed, failure strain/strength of the composite increase; the tensile residual stress in the matrix means that the matrix near the interface region yields at a lower applied load than the matrix far away from the interface area. The residual stress changes the stress-strain curve, especially during the early stages of deformation[97].

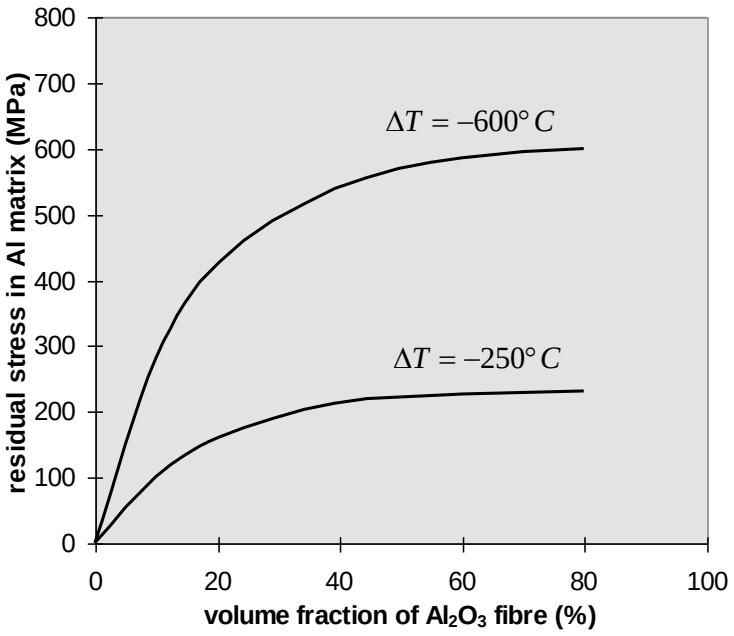

Figure 2.10 Calculated maximum residual stress in matrix of $Al+Al_2O_3$ composite as a function of fibre volume fraction[95]

Residual stress at the fibre-matrix interface in metal composites can be measured experimentally: an X-ray diffraction technique[98-102] has been used to measure the residual stress by measuring the change of diffraction angle, which is generally limited to near-surface region (within ~10 μm); but neutron scattering[103-105] has been used to

detect the main fibre stress throughout the composite because neutron beam can penetrate through much thicker sections of materials than X-ray (by factors of ~10^3); a method based on optical fluorescence has been adopted for measuring the residual stress in sapphire-reinforced MMCs utilising the stress dependent optical fluorescence from chromium impurities in the reinforcement[(106)].

2.2.4 The performance of metal matrix composites

Besides the interfacial strength, there are many other factors that influence the properties of metal matrix composites, including volume fraction, alignment, size/aspect ratio, strength distribution of reinforcement, mechanical behavior of components, and so on.

Figures 2.11 and 2.12 [(93)] show the effect of particle size and fibre aspect ratio on the strength of composites. The effective particle should be as fine as 0.01 to 0.6 μm and the aspect ratio should be high enough to bear the load. The critical fibre aspect ratio is dependent on the fibre's strength and the interfacial strength (the $\frac{\sigma_{YC}}{\sigma_{YM}}$ in Figures 2.11 and 2.12 is the ratio of composite yield strength to the matrix yield strength, showing the effect of reinforcement on the composite).

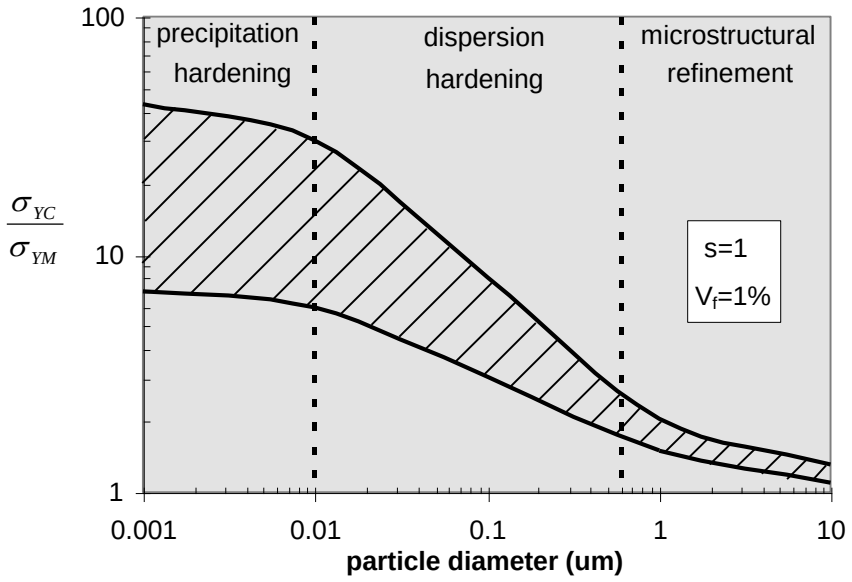

Figure 2.11 Strengthening effect as a function of particle size

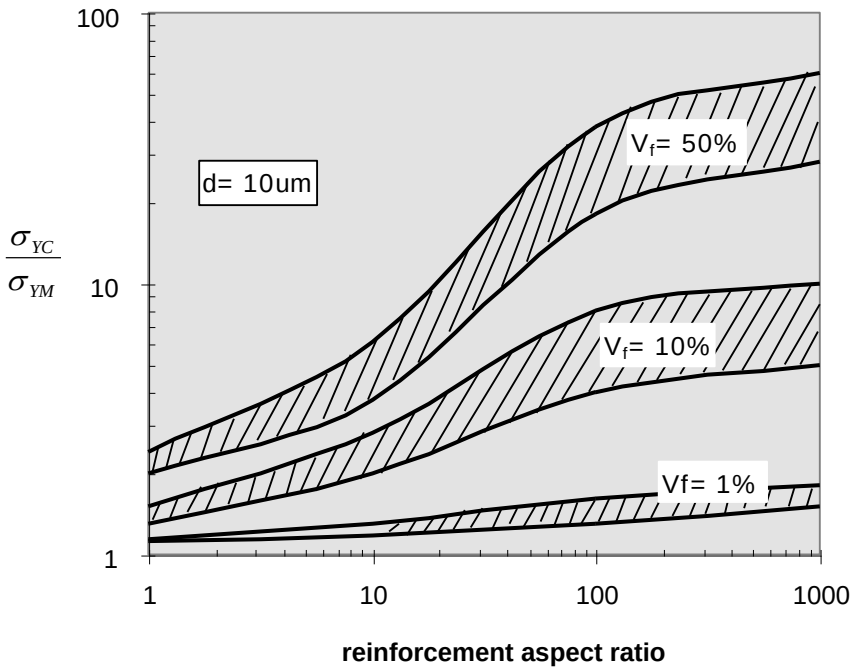

Figure 2.12 Schematic illustration of strength of composite against fibre aspect ratio

The effect of fibre volume fraction on the strength of the composite depends on the ductility of fibre. The following two theories are most often used to analyze the brittle and ductile fibre composites.

Rule-of-Mixture (ROM)[(107)]:

For brittle fibres, the strength of composites is given by:

$$\sigma_c = \sigma_{fu} V_f + \sigma_m^* V_m \quad \text{When } V_f > V_{\min} \tag{2.7}$$

and

$$\sigma_c = \sigma_{mu} V_m \quad \text{when } V_f < V_{\min} \tag{2.8}$$

where, σ_{fu} and σ_{mu} are the tensile strengths of fibre and matrix respectively,

V_f and V_m are the volume fraction of fibre and matrix, respectively (they satisfy $V_f + V_m = 1$),

σ_m^* is the stress in the matrix at the fracture strain

$V_{\min}$ is the minimum volume fraction of fibres required for strengthening the composite, defined by:

$$V_{\min} = \frac{\sigma_{mu} - \sigma_m^*}{\sigma_{fu} + \sigma_{mu} - \sigma_m^*} \tag{2.9}$$

Mileiko's theory[50]:

The relationship between strength of composites and volume fraction of ductile fibre has been proposed by Mileiko, that is:

$$V = \frac{1}{1 + \beta \frac{\varepsilon_c - \varepsilon_f}{\varepsilon_m - \varepsilon_c} \varepsilon_c^{\varepsilon_f - \varepsilon_m}} \tag{2.10}$$

where

$$\beta = \frac{\sigma_{fu} \cdot \varepsilon_m^{\varepsilon_m} \cdot \exp \varepsilon_f}{\sigma_{mu} \cdot \varepsilon_f^{\varepsilon_f} \cdot \exp \varepsilon_m} \tag{2.11}$$

and for the tensile stress at ε:

$$\sigma = V \cdot \lambda' \cdot \sigma_{fu} + (1 - V) \cdot \lambda'' \cdot \sigma_{mu} \tag{2.12}$$

where

$$\lambda' = (\frac{\varepsilon}{\varepsilon_f})^{\varepsilon_f} \cdot \exp(\varepsilon_f - \varepsilon) \tag{2.13}$$

and

$$\lambda'' = (\frac{\varepsilon}{\varepsilon_m})^{\varepsilon_m} \cdot \exp(\varepsilon_m - \varepsilon) \tag{2.14}$$

where, σ_c and ε_c are the tensile strength and the true uniform strain respectively of composites;

σ_{mu} and ε_m are the tensile strength and the true uniform strain respectively of matrix;

σ_{fu} and ε_f are the tensile strength and the true uniform strain respectively of fibre.

V is the volume fraction of fibre in composites.

Figure 2.13 shows a comparison of composites when reinforced with brittle and ductile fibres.

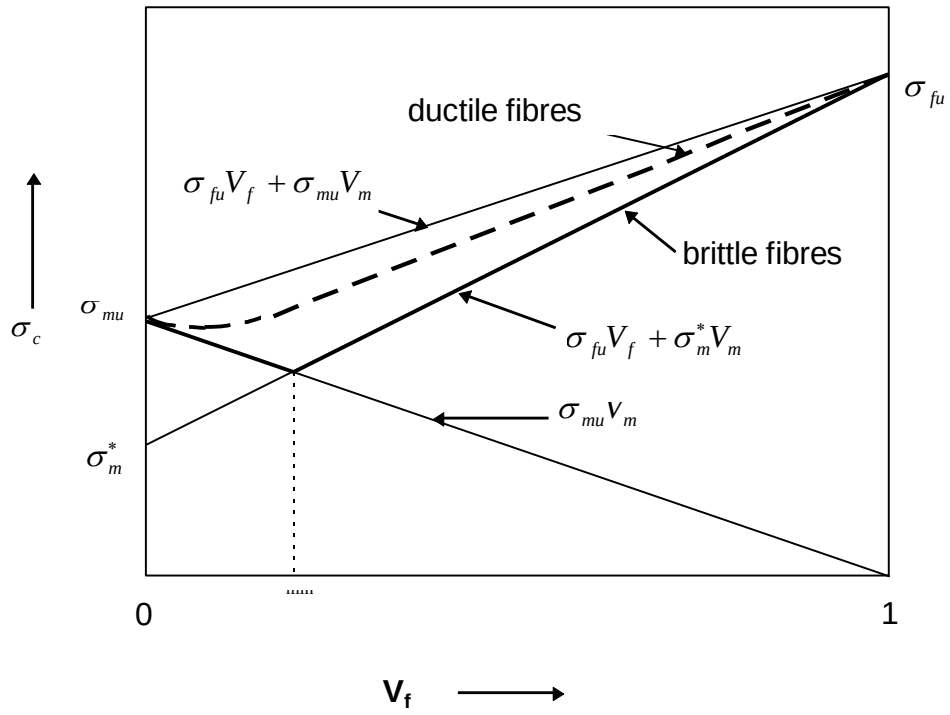

Figure 2.13 The strength of ductile fibre and brittle fibre reinforced composites as a function of volume fraction of fibre

2.2.5 Fabrication considerations

In order to make the proposed artificial dual phase steels (steel-wire reinforced steel composites) by conventional metal forming process, it is necessary to review the mechanism of sheet bonding techniques, and the factors influencing the formability and structure of sheet materials.

The conventional sheet-metal bonding processes include thermomechanical treatment - hot rolling, hot pressing - diffusion bonding, and explosive welding, etc. The mechanisms of these techniques and the factors influencing the products made by these processes are reviewed in the following section.

2.2.5.1 Thermomechanical treatment

Thermomechanical treatment or thermomechanical processing involves a combination of thermal treatment, plastic deformation and phase transformation within a single heat treatment cycle to control the structure, morphology, and grain size of the parent phase (e.g., austenite) and subsequent grain and subgrain structure in the transformation product phases (such as ferrite) and/or interaction between dislocations and fine precipitates (e.g., alloy carbides and/or carbo-nitrides). Its main objective is to obtain

ultra-high strength, improved ductility, greater toughness, higher resistance to brittle cleavage and low-energy ductile fracture, and lower impact-transition temperature in a wide variety of finished and semi-finished steel products. It is necessary to review thermomechanical treatment because it has been used to make the dual phase steel and composites studied in the present work.

In the steel industry, hot rolling is one of the most important thermomechanical treatment techniques and is widely used to produce steel sheet and strip because of its high productivity. The mechanical properties of rolled product are strongly related to the microstructure and grain size which are controlled by the rolling parameters[108]. Therefore, the relationships between rolling parameters: microstructure/grain size and mechanical properties are very important.

It is well known that the critical factors in controlling the microstructure, grain size and properties of steels are the strain rate, accumulated strain, temperature during rolling, and cooling path subsequent to rolling for a given composition of steel.

The classification of hot-rolling[109-111]

Hot rolling processes can be classified based on where the deformation occurs relative to the phase transformation, as in the following four major groups (schematically shown in Figure 2.14):

(1) Conventional hot rolling: During this process, the rolling of steel is conducted continuously and is usually finished at a temperature higher than the upper cooling transformation temperature, i.e. Ac_3. That is, the steel is deformed in the gamma phase.

(2) Controlled rolling: This process of steel rolling is interrupted by one or two delays which allow one to deform the steel first in the gamma-region and then in the (gamma+alpha)-region.

(3) Low finishing temperature rolling: in this process, the finishing rolling passes are conducted below the lower cooling transformation temperature, Ac_1, i.e., in the alpha-region.

(4) Continuum rolling: This process produces deformation in the gamma-, (gamma+alpha)-, and alpha-regions.

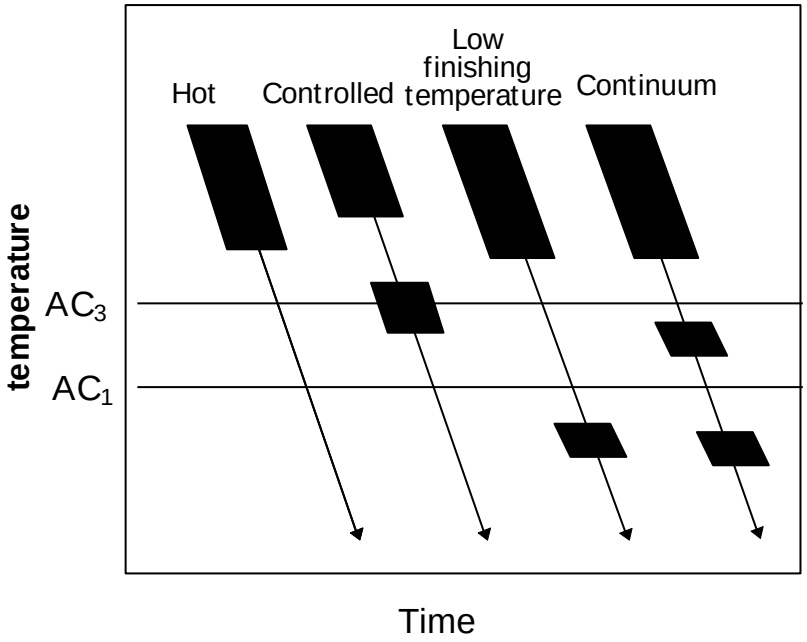

Figure 2.14 Schematic illustration of four major hot rolling processes

Residual stress arising from rolling [112]

Residual stresses can be generated in rolled sheets and plates due to inhomogeneous plastic deformation in the roll gap. The stress status is dependent on the diameter of the rolls and the rolling reduction (Figure 2.15). Large-diameter rolls and high reductions tend to deform the bulk to a greater extent than the surface. This is due to the frictional constraint at the surface along the arc of the contact. This situation generates residual stresses that are tensile on the surface and compressive in the bulk. On the other hand, small-diameter rolls or small rolling reductions allow plastic deformation to take place at the surface of the workpiece, therefore a compressive residual stresses on the surface and tensile stresses in the bulk will be generated.

The residual stress distribution in the section is not uniform, ie, a stress gradient exists in the workpiece, that will affect the fracture of the rolled sheet.

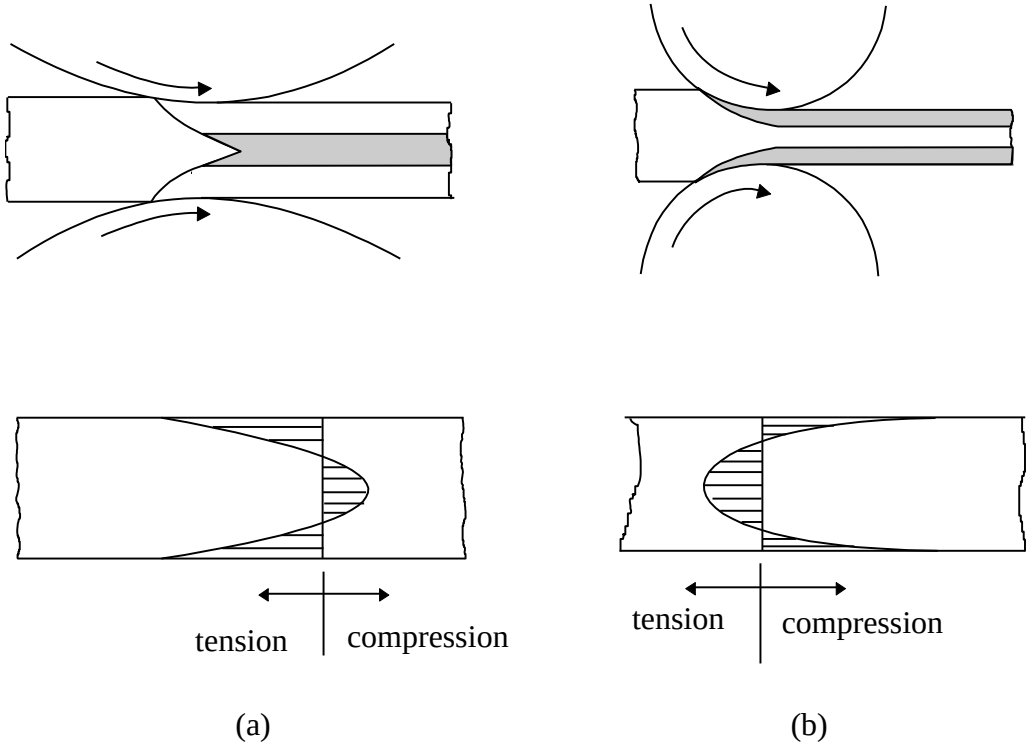

Figure 2.15 The effect of roll radius on the residual stresses developed in flat rolling (a) large roll, or large reduction in thickness, (b) small roll, or small reduction[112]

The main parameters of hot rolling

The high temperature workpiece will lose some heat when it is subjected to rolling due to heat transfer to its surroundings. The finishing rolling temperature is one of main factors which decides the internal stresses due to rolling, the structure, the strength and the ductility of products.

When the heated workpiece is rolled, the austenite is elongated; its deformation is a function of both rolling temperature and rolling reduction. The structural changes of the elongated grains after rolling depend on the finishing rolling temperature and cooling rate. If the finishing rolling temperature is higher than the eutectioid transformation temperature, Ac_1, recrystallization and phase transformation will occur during cooling; if the finishing rolling temperature is lower than the Ac_1, phase transformation will not occur but recrystallization and recovery of the deformed grains may take place, which can influence the residual stresses of the rolled workpiece.

There are some inevitable defects that may occur in the rolled workpiece, such as alligatoring, wavy edges, zipper cracks in the centre of strip, and edge cracks.

Hot rolling is an effective means to produce metal matrix composite sheets, but the high elongation of the workpiece during rolling limits the use of brittle fibre.

2.2.5.2 Diffusion bonding

Diffusion bonding is a solid state welding process that produces a weld by the application of pressure at elevated temperature without macroscopic deformation or relative motion of the workpieces (as takes place in the rolling process). In this way, two similar or dissimilar metals, or even a metal and ceramic can be joined. Diffusion bonding is often used for producing composites.

***Fundamentals*[113]**

The process of diffusion bonding includes the following three stages:

(1) Deformation of the contacting asperities occurs primarily by yielding and by creep deformation mechanisms to produce intimate contact over a large fraction of the interfacial area, with some voids present.

(2) Diffusion becomes more important than deformation, and many of the voids disappear as grain boundary diffusion of atoms continues. Simultaneously, interfacial grain boundaries migrate to an equilibrium configuration away from the original welding interface, leaving many of the remaining voids within the grain.

(3) The remaining voids in grains are eliminated by volume diffusion of atoms to the void surface (equivalent to diffusion of vacancies away from the void).

Parameters determining the diffusion bonding are temperature, time and pressure, and initial surface finishes; these are interrelated for many cases. The functions of these parameters are:

(1) Temperature is the most influential variable since it, together with pressure, determines the extent of contact area during stage one and it alone determines the rate of diffusion that governs void elimination during the second and third stages. The temperature for diffusion bonding is generally set at $0.5\sim0.8T_m$ (T_m is the melting temperature of the metal).

(2) Pressure is necessary only during the first stage to produce a large area of contact at the welding temperature. Removal of pressure after first stage does not significantly

affect joint formation. The pressure is usually kept slightly below the yield stress at the welding temperature.

(3) The time require to form a joint depends on the temperature and pressure. Because diffusion reactions progress with the square root of time, longer times become less and less effective.

(4) Rough initial surface finishes generally adversely affect bonding by impeding the first stage and leaving large voids that must be eliminated.

The strength of properly made diffusion bonds between similar metals usually is equal to that of the base metal. Heat-affected zones, with their attendant residual stress and heterogeneous properties, are not present in a diffusion bonded assembly because the entire unit is heated to a uniform temperature during process.

Application to composite fabrication

The fabrication of long-fibre reinforced metal matrix composites by diffusion bonding is schematically shown in Figure 2.16. This process includes (1) aligning of fibre on matrix foils; (2) evacuating a box in which a fibre-foil preform is sealed; (3) heating and pressing.

Because there is no relative motion between the matrix foil and fibre, the diffusion bonding process does not damage the fibre. No limitation on fibre type for diffusion bonding.

Many works[114-116] have focused on the fabrication of metal matrix composites by diffusion bonding. Chang and Scala[117] showed that the pressure required for consolidation is independent of the fibre volume fraction, but rises with increasing coefficient of friction between the contacting surfaces. The matrix creep characteristics and the factors affecting surface oxide film durability are also important.

The disadvantages of diffusion bonding for producing composites are:

(1) a long time heating is required to obtain the perfect consolidation and may cause a significant interfacial reaction/diffusion layer to form which will degrade the fibre;

(2) it is difficult to produce very high fibre volume fractions and homogeneous fibre distribution.

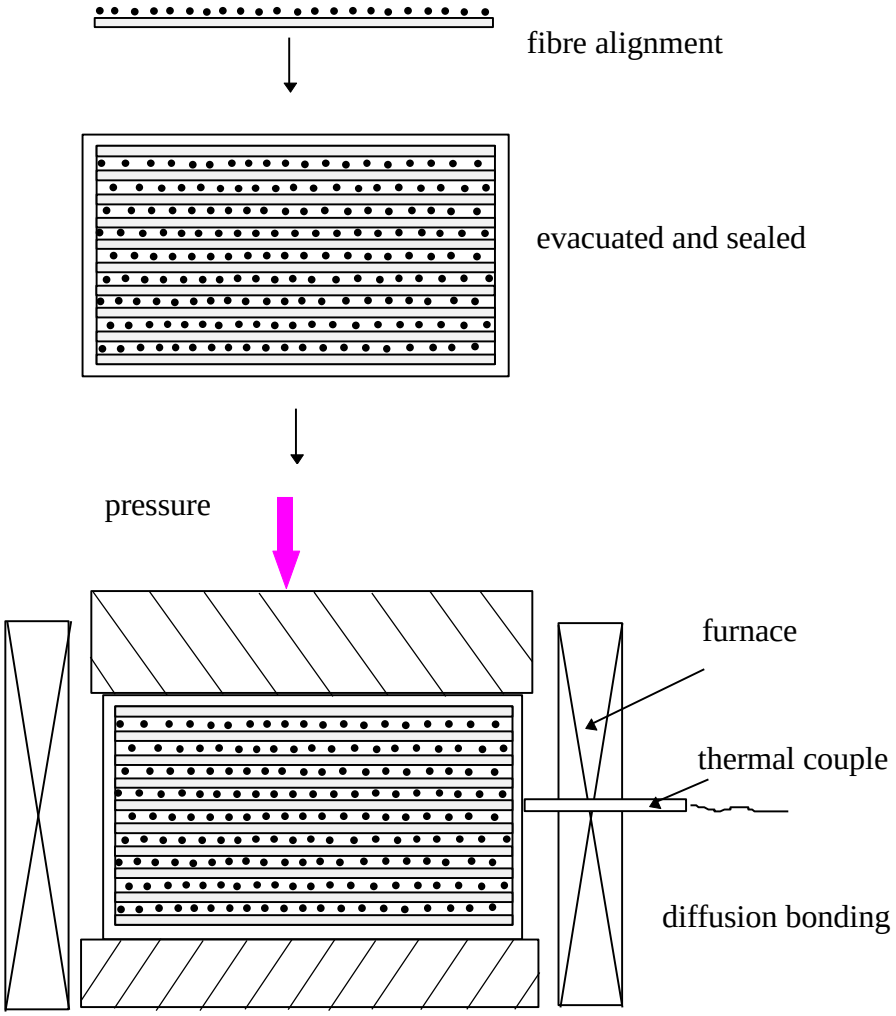

Figure 2.16 Schematic process of composite fabrication by diffusion bonding

2.2.5.3 Explosive bonding

Mechanism[118-121]

Explosive bonding is a solid-state welding process that produces a weld by high velocity impact of the workpieces as a result of controlled detonation. The explosion accelerates the metal to a speed at which a metallic bond will form between them when they collide. Different from hot-rolling and diffusion bonding, the process of explosive bonding does not involve an external heating process: the force to make two metals join comes from the high energy of the explosion although the bonding surfaces are heated to some extent by the energy of the collision. Bonding is accomplished through plastic flow of the metal on these surfaces.

Fundamentally, explosive bonding requires three components, they are base metal, facing metal (the thickness of facing metal is limited), and explosive. The typical set-up

for explosive bonding is shown in Figure 2.17. The two metal sheets may be parallel to each other with a separation of about 0.63mm (Figure 2.17 (a)), or may be arranged at a small angle of about 1 to 10 degree (as shown in Figure 2.17 (b)). A sheet of explosive is placed on the facing sheet, and is detonated at one end. As detonation progresses along the sheet of explosive, a shock-wave front forces the facing sheet down onto the base metal in a shearing action. The detonation velocity of the explosives used is usually in the order of 6400 m/s. The pressure produced at the interface may be in the order of 0.7 to 7GPa[118].

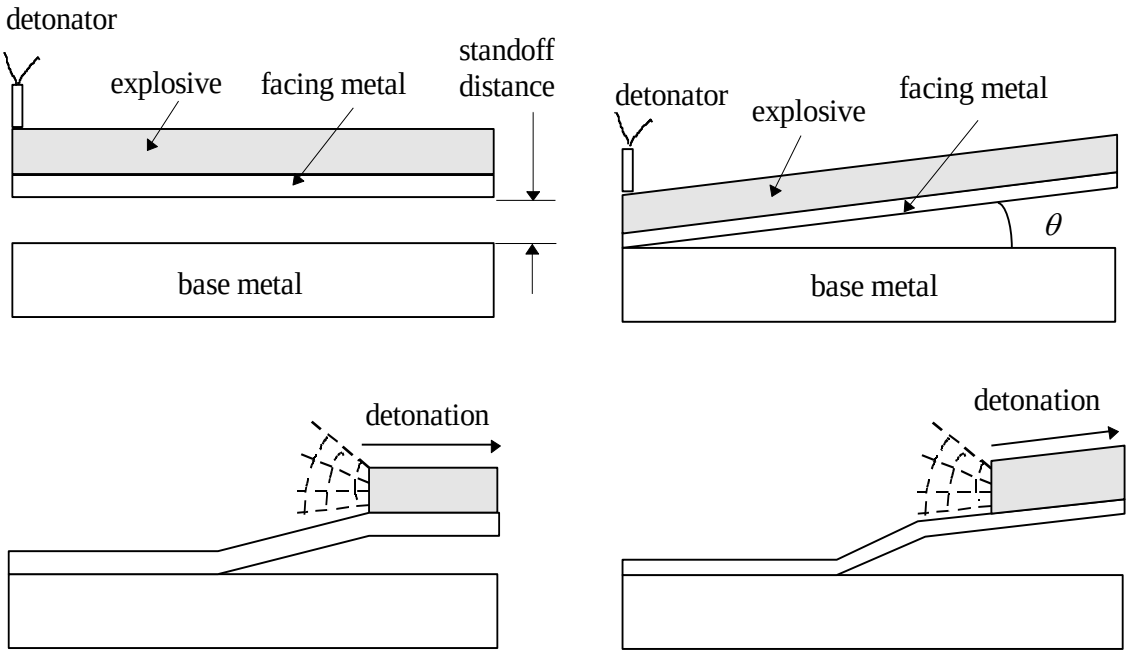

(a) parallel setting (b) angle setting

Figure 2.17 Two typical component arrangements for explosive bonding

The heat generated by the high energy impact between the two metals and the shearing at the interface is sufficient to cause bilateral melting across the interface and produce bonding. The thin molten layer at the interface forms an amorphous layer within the bonding zone, which gives high bonding strength.

Use in producing composite

The application of explosive bonding to produce fibre-reinforced metal matrix composites has been restricted to those employing relatively ductile metal wire of only moderately high specific strength and modulus (such as tungsten and steel wire).

Explosive bonding has been used to produced composites from stacks consisting of alternate layers of wires and foils (as shown in Figure 2.18); the wires can be laid unidirectionally or in planar mesh form[122-124].

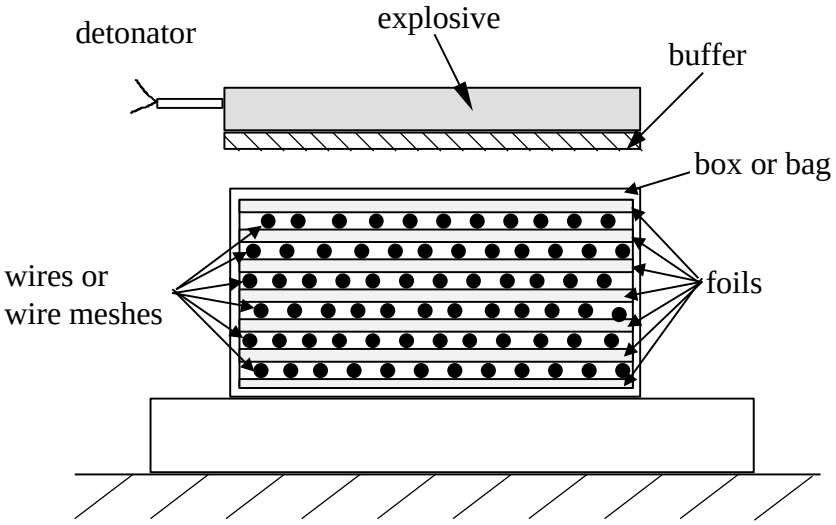

Figure 2.18 Geometries for explosive welding foils to wires or wire meshes[125]

Placing the stack of foils and wires in a plastic bag and evacuating prior to compaction avoid the risk of delamination or blister formation from trapped air pockets. Under optimum conditions, densities approaching theoretical rule-of-mixtures values have been achieved, with the residual porosity confined to the interstices between the mating foils and wires.

Explosive bonding offers an interesting alternative means of consolidating composites consisting of alternate layers of metal wires and foils. The main advantages of explosive bonding over other fabrication methods is the absence of wire/matrix thermal degradation effects and the potential for producing large areas of composites. However, the achievable wire volume fraction appears to be limited since the highest reported was 40%[125].

2.3 Summary

Considering the operation safety and apparatus availability in the Department of Mechanical Engineering at the University of Canterbury, hot rolling was chosen to produce steel-wire reinforced steel composite.

Chapter 3 Experimental

3.1 In-situ dual phase steels

3.1.1 Materials

The steels used to examine the partitioning and mechanical properties of dual phase steels were in the form of 40x40 mm^2 billets in the as-forged condition. The chemical compositions are given in Table 3.1.

Steels A and B were chosen with similar carbon contents and varying manganese contents in order to investigate manganese effect. Steels C and D, with nearly the same manganese contents but different carbon contents, were used to study the effect of carbon content.

As an austenite stabilizer, manganese can reduce the Ac_1, Ac_3 and M_s temperatures as follows[111]:

Ac_1=723-10.7Mn-16.9Ni+29.1Si+16.9Cr +290As+6.38W

Ac_3=910-203$C^{0.5}$-15.2Ni+44.7Si+104V+31.5Mo+13.1W-30Mn-11Cr-20Cu

+700P+120As

M_s =539-42.3C-30.4Mn-17.7Ni-12.1Cr-7.5Mo+10Co-7.5Si

The contents of all elements in the above three empirical equations are represented by their percentages, the Ac_1, Ac_3 and M_s are represented by degrees.

The change of the Fe-Fe_3C phase diagram at the iron-rich corner caused by adding 2.5% manganese is shown in Figure 3.1.

As a substitutional alloying element in iron, manganese prefers to concentrate in austenite. The solid solution formed with manganese will strengthen austenite and its successor phase - martensite - after transformation. Manganese also increases the yield strength of carbon steel by refining the ferrite grain and pearlite nodule sizes.

Table 3.1 Chemical compositions of experimental dual phase steels

Code	C	Mn	Si	S	P	Al	Ni	Cr	Mo	Cu	Sn	V	Ti
A	0.11	2.67	0.020	0.015	0.016	0.0008	0.046	0.046	0.013	0.034	0.003	0.008	0.003
B	0.13	1.52	0.08	0.019	0.019	0.002	0.14	0.40	0.005	0.11	0.007	0.056	0.002
C	0.07	1.71	0.12	0.022	0.022	0.002	0.22	0.40	0.007	0.07	0.006	0.049	0.003
D	0.17	1.77	0.25	0.019	0.020	0.002	0.19	0.57	0.006	0.07	0.005	0.063	0.003

Manganese can react with sulfur in steel to form manganese sulphide inclusions. These inclusions are randomly distributed in the steel and can be elongated and produce cracks after hot-rolling as shown in Figure 3.2. These cracks will, of course, be detrimental to the tensile properties of the steel.

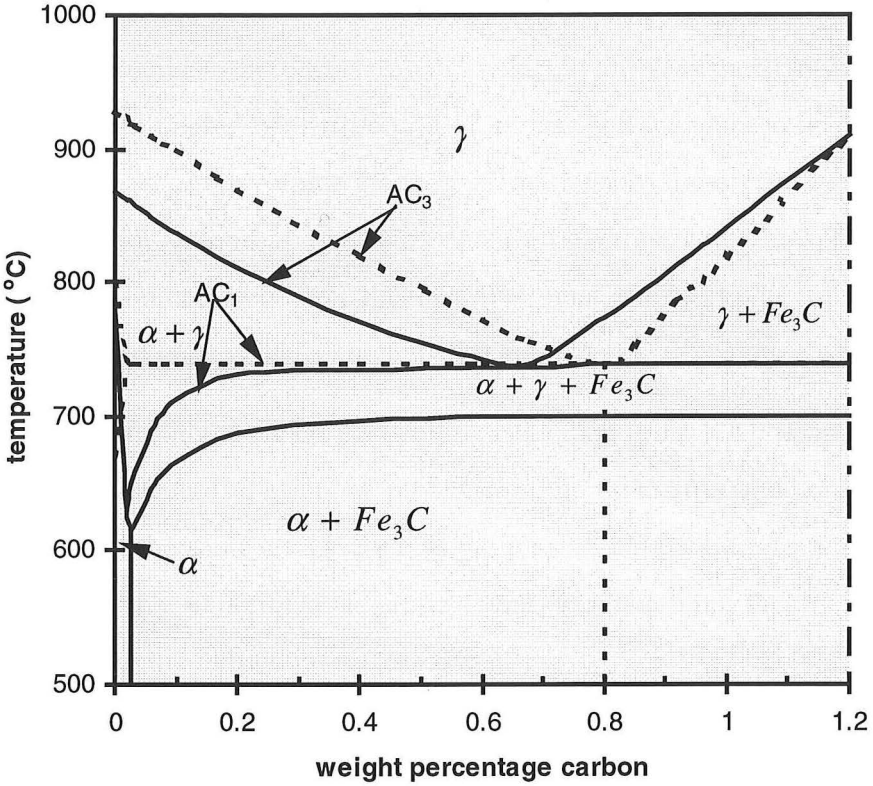

Figure 3.1 The change of Fe-Fe_3C phase diagram by adding 2.5%Mn. (···· for C-Fe, and —— for C-Fe-2.5% Mn)

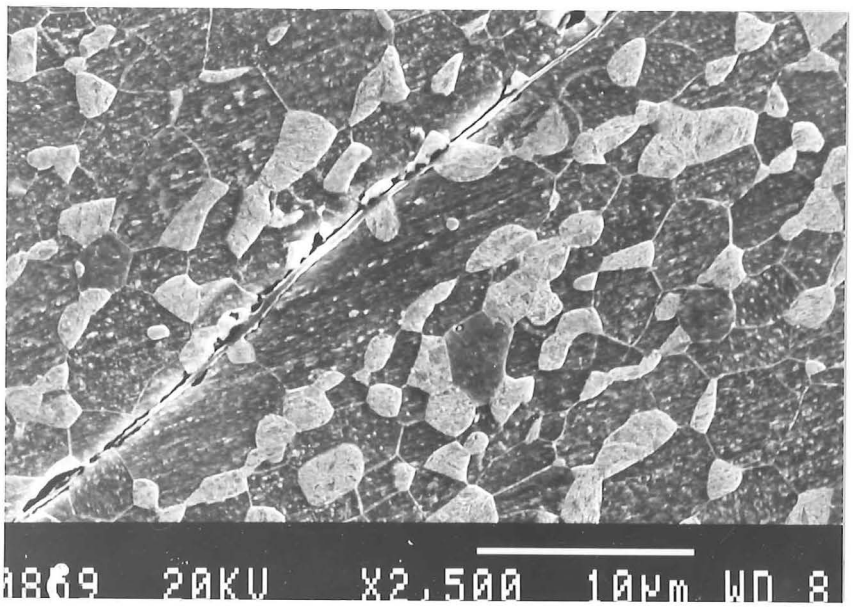

Figure 3.2 The manganese sulphide inclusion after rolling

3.1.2 Annealing and rolling

The heat-treatment for the forged steel before rolling is hereafter referred to as pre-rolling annealing (pre-RA), the steel after pre-RA is named as-rolled steel. The intercritical pre-RA temperature of this treatment determines the volume fraction of martensite in the steel (20-30%). The optimum pre-annealing temperatures for steels A, B, C, and D were found to be 680°C, 710°C, 720°C, 730°C respectively. In order to reach the equilibrium degree of partitioning of carbon and manganese in the austenite and ferrite and the required volume fraction of martensite, the steels were heated at these temperatures for as long as 144 hours under a flowing argon atmosphere in order to avoid oxidation. Immediately after this heat treatment, the steel was rolled, the final thickness of the rolled plate is approximately 2.0 mm.

The annealing after rolling is called post-rolling annealing (post-RA), and its product is marked as post-RA steel. The effect of post-RA on the microstructure was determined by annealing steel at the same temperature as the pre-RA temperature for various times. Figure 3.3 shows the experimental process and the potential factors influencing properties of steels in the individual stages.

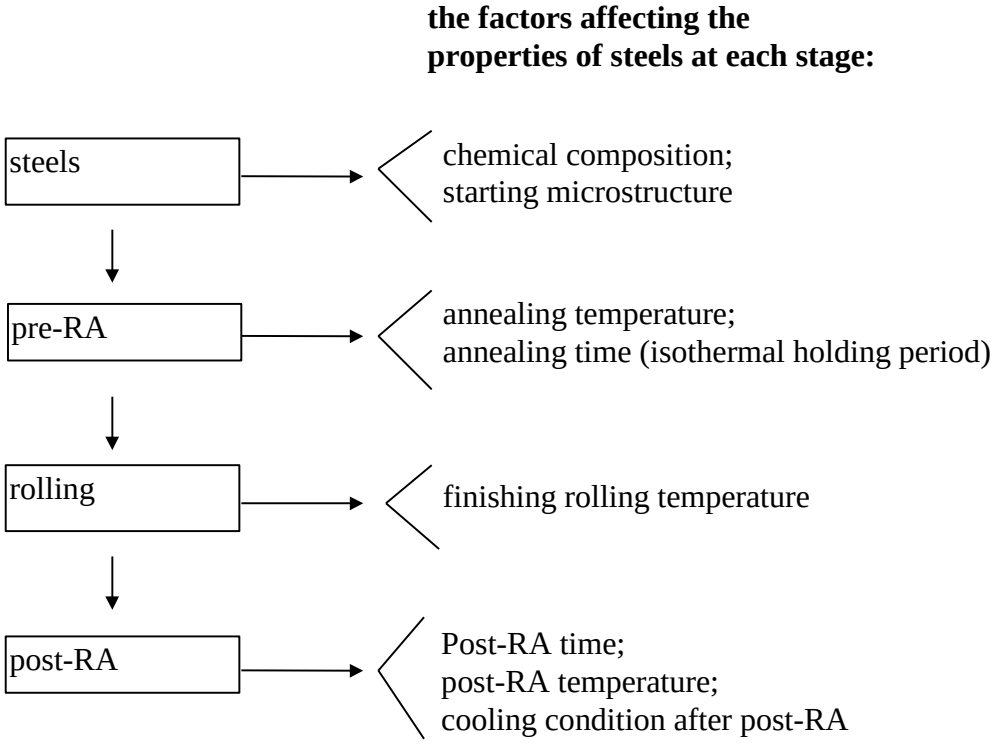

Figure 3.3 Flow chart for production and examination of dual phase steels

The rolling was carried out in both quasi-isothermal and variable temperature conditions (i.e. continuous rolling). In the continuous rolling process, the rolling began at the pre-rolling annealing temperature but no more heat was supplied during rolling. The final thickness was achieved in several passes. The quasi-isothermal rolling process involved quenching the steel from the pre-rolling annealing temperature and reheating it to the finishing rolling temperature (chosen as some temperature between the two-phase region and room temperature). It was then rolled at the set finishing rolling temperature for one pass, and then reheated, rolled another pass, and reheated until reaching the final thickness after several cycles; the interval between two passes was set at 10min to reheat the steel. Illustrations of continuous and quasi-isothermal rolling are shown in Figure 3.4.

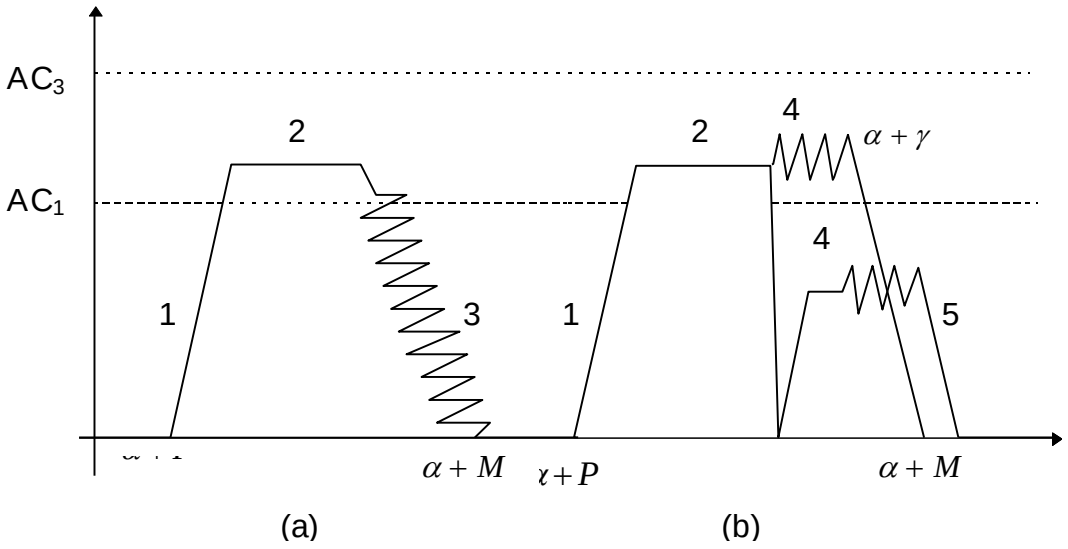

Figure 3.4 Schematical illustration of the pre-RA and rolling process, (a) continuous rolling, (b) quasi-isothermal rolling processes. 1: heating, 2: pre-rolling annealing, 3: rolling and air cooling, 4: quasi-isothermal rolling, 5: water quenching

The effect of cooling conditions on the tensile properties of post-RA steel A was examined by using water-quenching (heating at 680°C for 10-60min. then water quench), austempering (heating at 680°C for 10-60min. then quenching in 260°C oil and holding for 360min followed by air cooling) and martempering (heating at 680°C for 10-60min. then quenching in 260°C oil and holding for 5min and then air cooling); a schematic of these cooling processes for post-RA is shown in Figure 3.5.

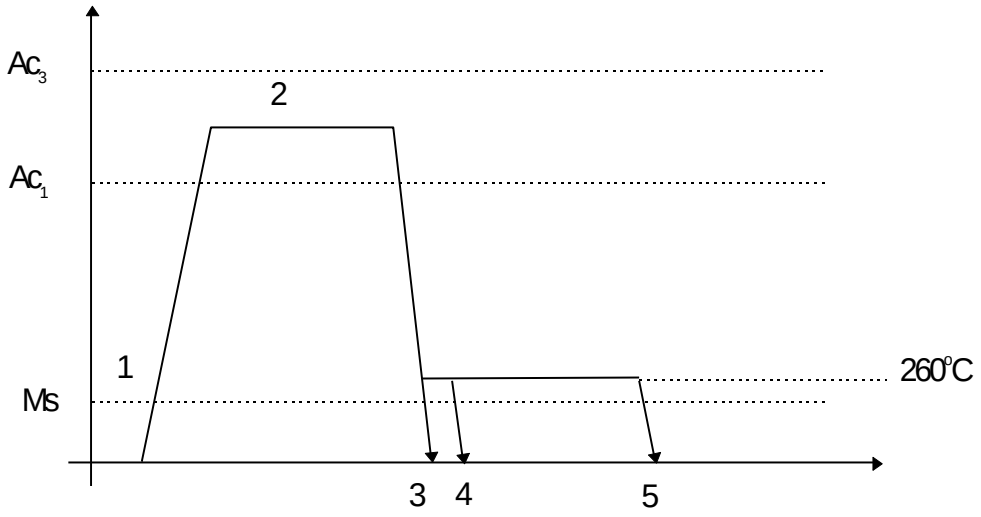

Figure 3.5 Illustration of cooling conditions on the dual phase steel after post-RA. (1) heating; (2) post-rolling annealing at 680℃;(3) water-quenching; (4) martempering; (5) austempering

3.1.3 Tensile testing

Tensile testing samples were machined from the rolled strips as shown in Figure 3.6. The tests were carried out at ambient temperature with a crosshead speed of 0.2mm/s. In each case the value plotted is the average of 3 or 5 individual tests. The fracture surfaces obtained were examined by SEM.

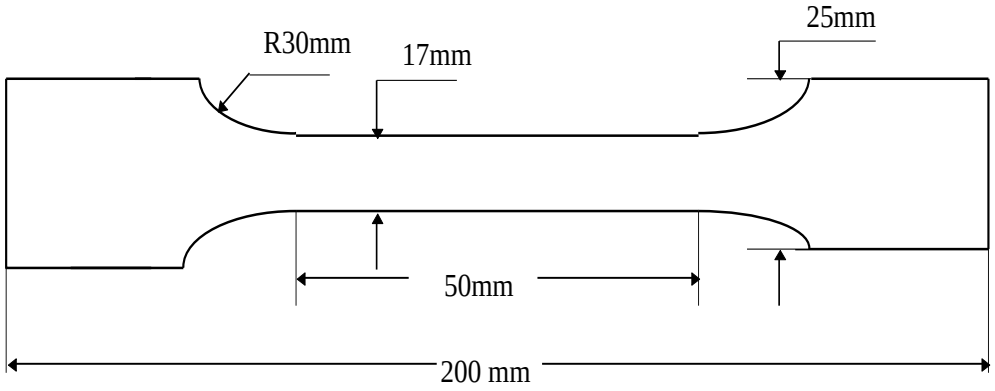

Figure 3.6 Illustration and dimension of tensile test sample

3.1.4. Metallography and elemental analysis

Scanning Electron Microscopy (SEM) was used to observe the microstructure of the steel after polishing and etching in 2% nital. Elemental analysis in the martensite and

ferrite was determined with an energy dispersive X-ray analyzer attached to the SEM, and the manganese partitioning coefficients shown in the result plots are mean values of 10 testing data. The volume fraction of martensite was measured using the point-counting method on selected micrographs.

3.2 Artificial dual phase steels

3.2.1 Materials

High carbon (0.8 wt%) steel wire (also called piano wire) was used as the reinforcement for producing steel-steel composites; the diameter of wire ranged from 0.3 to 1.6 mm.

The principal matrix steel was a low carbon, commercial, cold-rolled product (supplied by BHP New Zealand Steel Ltd) that will be referred to hereafter as steel No.1. The composition of this steel and those of two others with different carbon contents that were used to investigate the influence of matrix on interfacial strength and properties of composites are given in the following Table 3.2.

3.2.2 Protection and testing of wire.

During fabrication of composites, the steel wire will be exposed to high temperatures. Diffusion of carbon between wire and matrix will take place because of the large difference in carbon content between them. It may be necessary to protect the steel wire with a coating to control carbon diffusion.

3.2.2.1 Surface treatment for steel wire

Copper and nickel were used as protective coatings because of their zero or low carbon solubility. Continuous electroplating was used to plate a uniform copper coating on the wire (shown in Figure 3.7). Nickel coating was plated by using an electroless coating technique. The solutions used for copper and nickel coatings are listed in Table 3.3 and Table 3.4, respectively.

Table 3.2 Chemical composition of steel matrices for steel-steel composites

	C	Mn	Si	Al	N	P	Cr	V	S	Sn	Cu	Ni
No.1	0.044	0.196	0.003	0.054	0.005	0.016	0.031	0.08	0.024	0.002	0.012	0.015
No.2	0.06	0.32	0.0005	0.039	0.0041							
No.3	0.14	0.58	0.002	<0.008	0.0139							

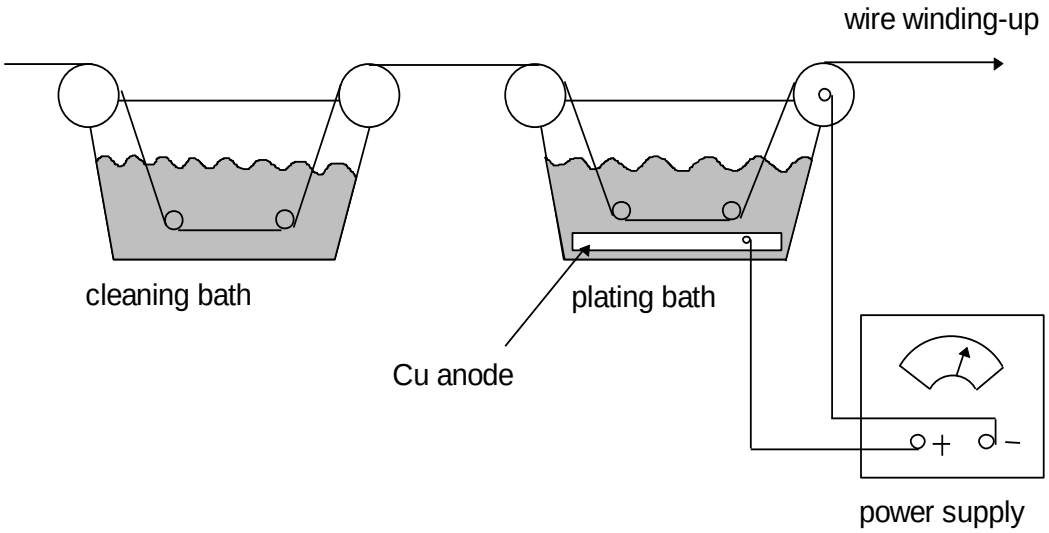

Figure 3.7 Continuous electroplating of copper on wire

Table 3.3 Solution for copper electroplating

	concentration (g/l)	current density (A/dm^2)	voltage (volt)
		1-20	**3**
$CuSO_4 5H_2O$	**200**		
H_2SO_4	**50**		
phenol*	**1**		

* the phenol is sulphonated by heating with it own weight of sulphuric acid to 120°C for 1 hr before use

Table 3.4 Electroless nickel coating solution

nickel sulphate	37g
sodium hypophosphite	26g
sodium acetate	6g
sulfuric acid	60ml
distilled water	1000ml
temperature	82-88°C

3.2.2.2 Preparation of sample for single wire tensile testing

Because of the brittleness of the rolled steel wire, ordinary testing methods for the wire cannot be applied. A test sample was designed as shown in Figure 3.8 to simulate the

situation of the wire during composite fabrication. The steel wire was laid between two steel plates (the surfaces of the plates were oxidized to resist bonding between the wire and steel plates) to form a preform. After being rolled under different conditions and following different heat-treatments, the two steel plates of preform were detached and the part with the oxide was cut off. A hole was drilled on the centre line of wire.

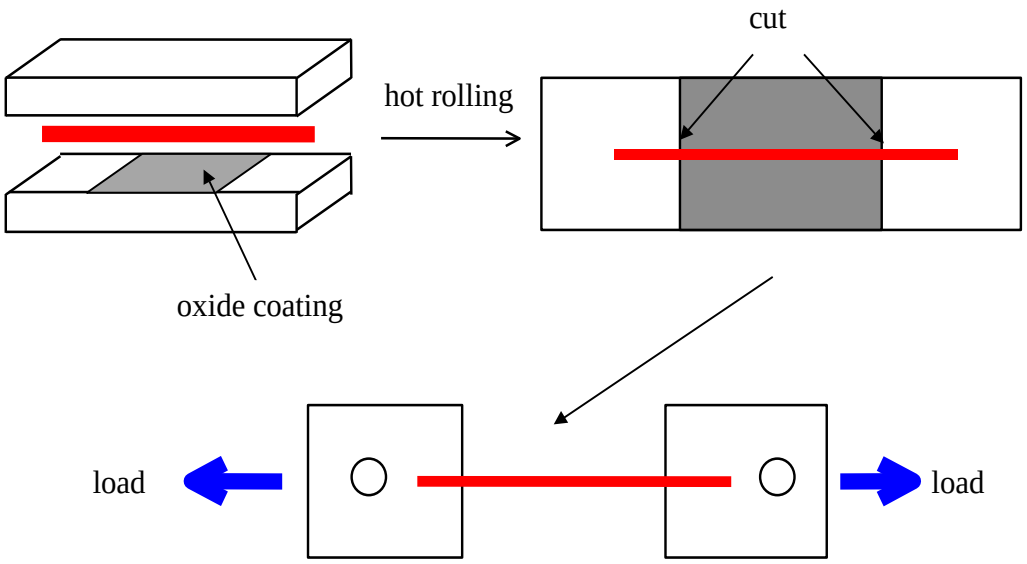

Figure 3.8 Illustration of sample preparation and testing of wire

The tensile testing of the wire was carried out in the Hounsfield Extensometer testing machine, the load and displacement were recorded during testing. The fracture surface was observed by SEM.

3.2.2.3 Thermomechanical treatment of wire

The release of work-hardening of the cold drawn steel wire is a function of annealing time and temperature. The variation of tensile strength and elongation of steel wires with isothermal holding time was investigated by heating the wire at 950°C for 3, 5, 10, 15, 20, 25, 30 min followed by air-cooling.

The properties of the wire depend on the phase composition. The rolled wires were transformed into pearlite, martensite, and bainite by reheating the rolled wires to 800°C for 2 min followed by air-cooling , water-quenching, and oil-quenching into 260°C oil and isothermally holding for 5min (martempering) or 300min then air cooling (austempering), respectively. Bainite was chosen as the final phase for the reinforcing

wire. The property relationship between the as-rolled pearlitic wire and the subsequent bainitic wire was established.

The effects of rolling parameters (such as finishing rolling temperature, holding time before rolling, rolling reduction) on the properties of the bainitic wire have been investigated.

After rolling, the section of wire will be deformed to an oval shape (see Figure 3.9). As tensile strength is calculated by:

$$\sigma = \frac{P}{S_1} \tag{3.1}$$

in which, P is the maximum load the wire carried, and S is the sectional area of the rolled wire, for the oval wire the new cross sectional area is given by:

$$S_1 = \frac{1}{6h}\langle (b^2 + 4h^2)^{\frac{3}{2}} - b \cdot (b^2 + 4h^2) \rangle + b \cdot h \tag{3.2}$$

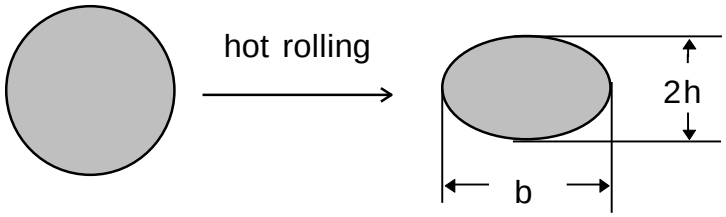

Figure 3.9 Illustration of change of wire section due to rolling

3.2.3 Interfacial strength testing

3.2.3.1 Sample preparation

Fabrication of interfacial strength testing samples is shown schematically in Figure 3.10. The lower surface of the top steel plate is coated with a layer of refractory to allow easy separation of the two plates after rolling (the interface is so strong that the wire cannot be pulled out when the whole wire surface is embedded in the matrix).

Rolling temperatures were varied from 850ºC to 1100ºC and heat treatment times from 3 to 30 minutes in order to investigate the effect on interfacial strength. In addition, the effects of % reduction on interfacial strength was also examined.

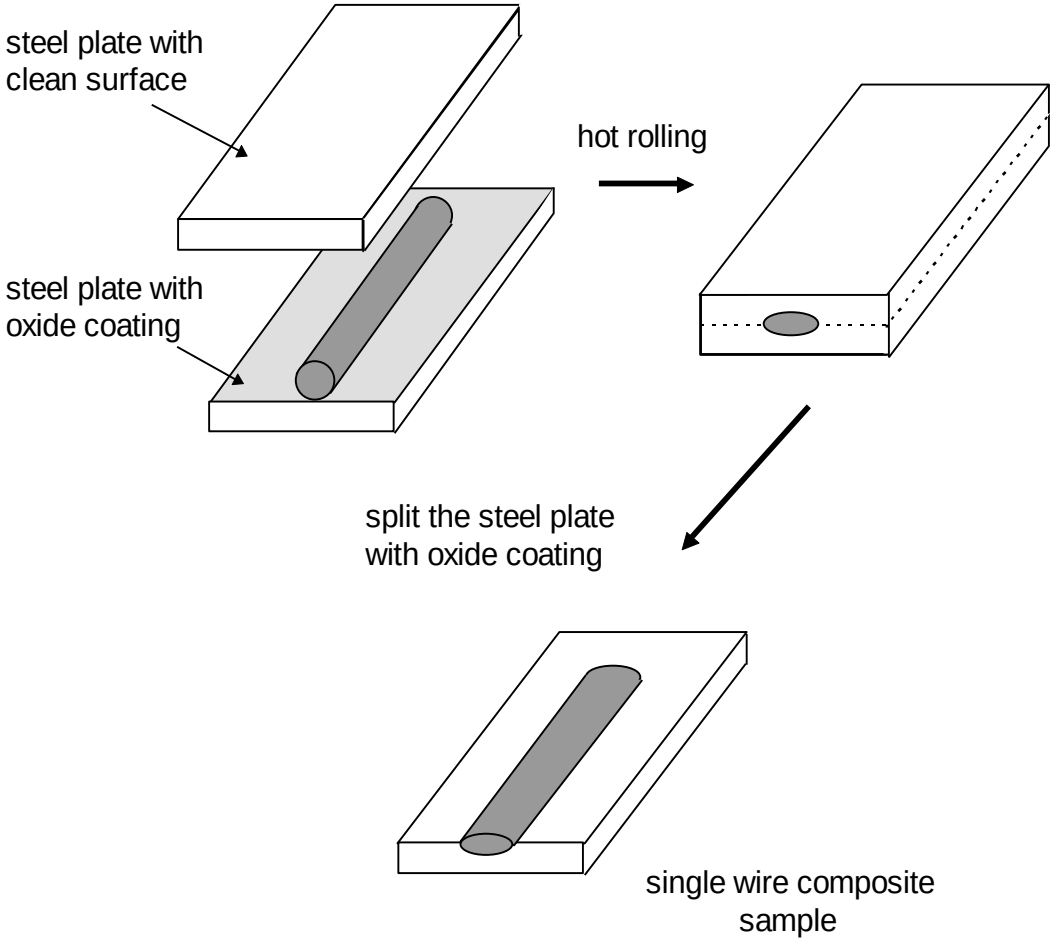

Figure 3.10 Fabrication of single wire composites for interfacial testing

The steels and wire plies were cold rolled by differing reductions to make some preforms, which were then rolled at 950ºC after heating for 3, 7, 10, 15, 20, 25 or 30 min, following by air cooling to look at the effect of cold rolling reduction on the interfacial strength.

3.2.3.2 Interfacial strength testing

The test sample is schematically shown in Figure 3.11. The test point for pullout of the wire was varied along the wire by cutting the wire at different distances from the end of the as-fabricated wire to investigate the variation of interfacial strength with the distance from the end of wire.

The interfacial testing was carried out in a Hounsfield Extensometer with load parallel to the wire, and load-displacement plots were recorded.

The interfacial area between wire and matrix after rolling is as follows:

$$S_2 = \frac{1}{3}(4\sqrt{b^2 + 4h^2} - b) * L_0 \qquad (3.3)$$

in which, L_0 is the length of wire pullout, and b and h are the dimensions of the section of the rolled wire (shown in Figure 3.9). The interfacial strength is calculated by:

$$\tau = F / S_2 \qquad (3.4)$$

in which , F is the maximum load at wire pullout.

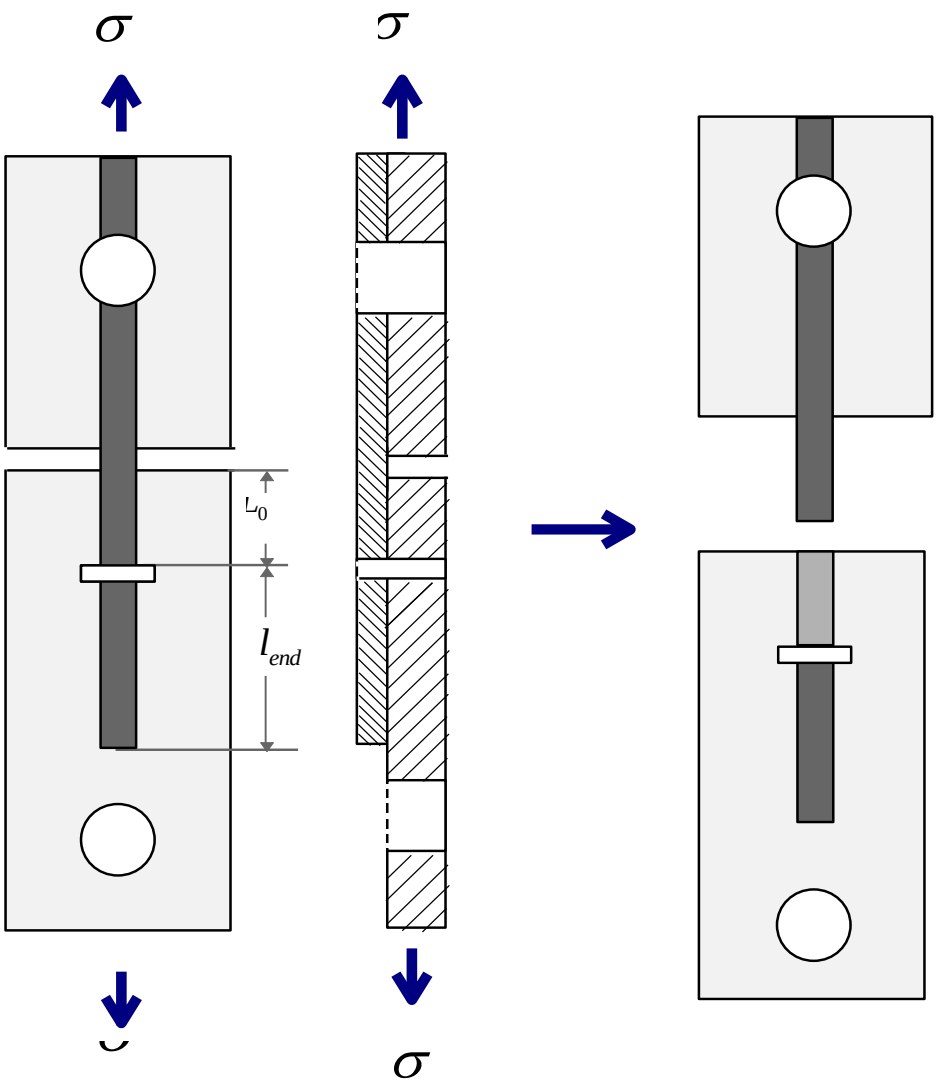

Figure 3.11 Schematic illustration of interface testing

The surfaces of both pullout wire and matrix were observed by SEM.

3.2.4 Artificial dual phase steels - steel/steel composites

3.2.4.1 Fabrication of the artificial dual phase steels

Illustrations of the fabrication of both continuous and discontinuous steel wire reinforced unidirectional composites are shown in Figures 3.12-3.14. The potential factors affecting the properties of the composites at each stage are listed on the right-hand side of the Figures.

The surfaces of both wire and matrix steels were cleaned by grinding and ultrasonic cleaning. The preform of the plies of unidirectional wire and matrix steel was sealed in a steel box and cold rolled to remove the air from the preform and then rolled after heating at the chosen temperature for a certain time. The final thickness of the rolled composites is about 1 mm.

Because decarburization of the high carbon wire will take place at high temperature during composite fabrication, some steel wires were coated with copper and nickel by electoplating and electroless plating respectively (refer to the section 3.2.2). The unidirectional composites were reinforced by plain wire, copper-coated and nickel-coated wires to study the influence of coating on the composites.

The fabrications of unidirectional discontinuous wire composites was achieved in two ways:

(1) the wires were chopped into the required length and put into the grooves on the matrix steel sheets to make a preform, which was heated at 950°C for 5min and then rolled (as shown in Figure 3.14). This approach is called CH (Cold-Hot rolled) method.

(2) the cold-rolled continuous unidirectional preform was heated to 800°C for 3min and quenched into water to allow the wire to transform to martensite. This was followed with cold rolling, during which the quenched martensitic wire was broken into short wire; the lengths of the broken wires depend upon the reduction during cold rolling. The short wire composite was made by heating this short wire preform at 950°C for 5min followed with hot rolling. This method is called the CHCH (Cold rolled-Heated-Cold rolled-Hot rolled) approach (details are shown in Figure 3.15).

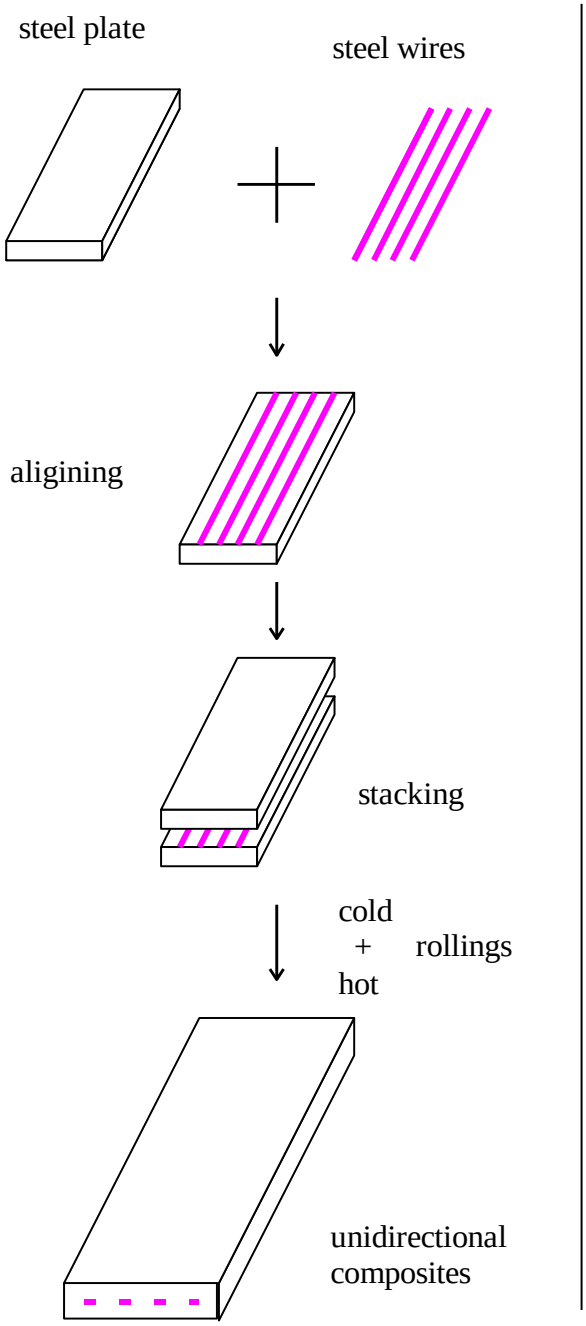

The factors that affect the properties of the composites:

wire size;
coating on wire;
volume of wire.

starting rolling temperature;
heating time;
finishing rolling temperature;
cooling condition after rolling;
rolling reduction.

Figure 3.12 Illustration of fabrication of continuous wire reinforced steel composites and the factors that influence properties

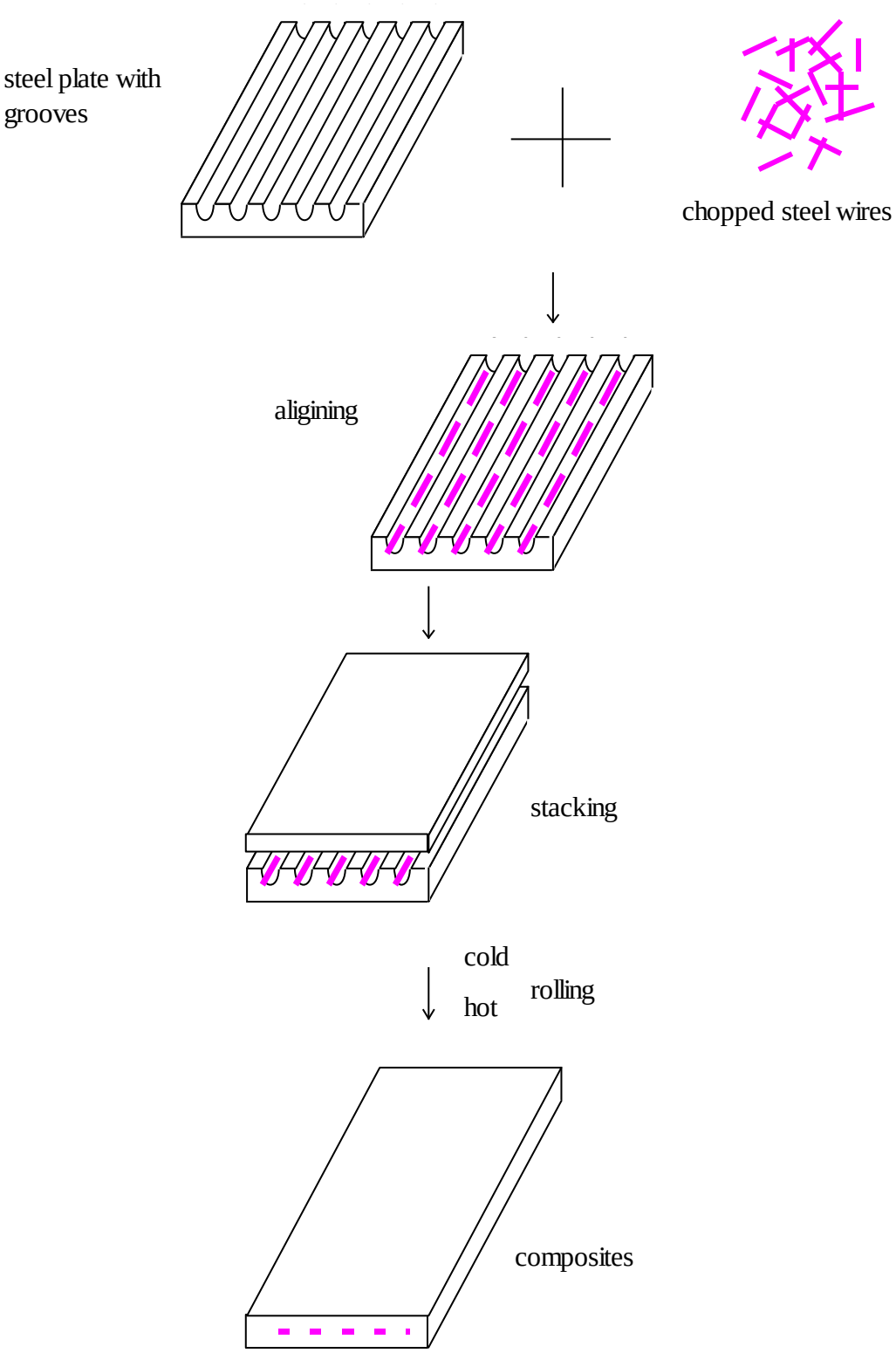

Figure 3.13 Fabrication of orientated discontinuous steel/steel composites known as CHSPRS (Cold-Hot rolled Short Piano-wire Reinforced Steel)

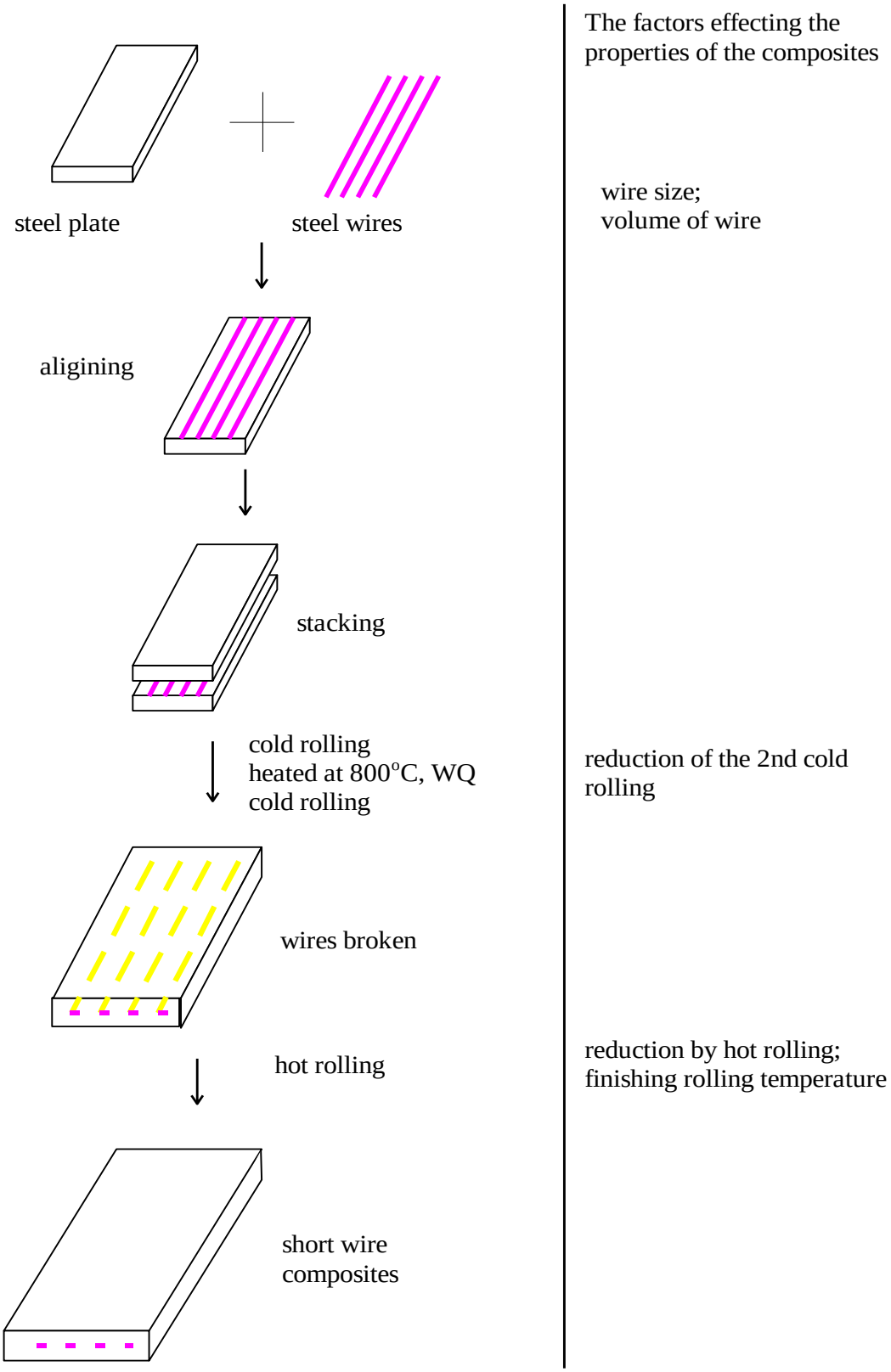

Figure 3.14. Fabrication of short wire composites, known as CHCHSPRS (Cold rolled-Heated-Cold rolled-Hot rolled Short Piano-wire Reinforced Steel)

3.2.4.2 Heat-treatment employed for composites after fabrication

Figure 3.15 is an illustration of the heat-treatment employed for the as-rolled steel-steel composites. All samples were heated at 800°C for 2min in order to make the temperature uniform in the samples. The cooling paths are:

path 1: quenching into water - water quench;

path 2: air cooling - normalizing;

path 3: quenching into oil at temperature T (ranges between 180~340°C) and holding for certain time t (varies from 5 to 305min), then air cooling - martempering.

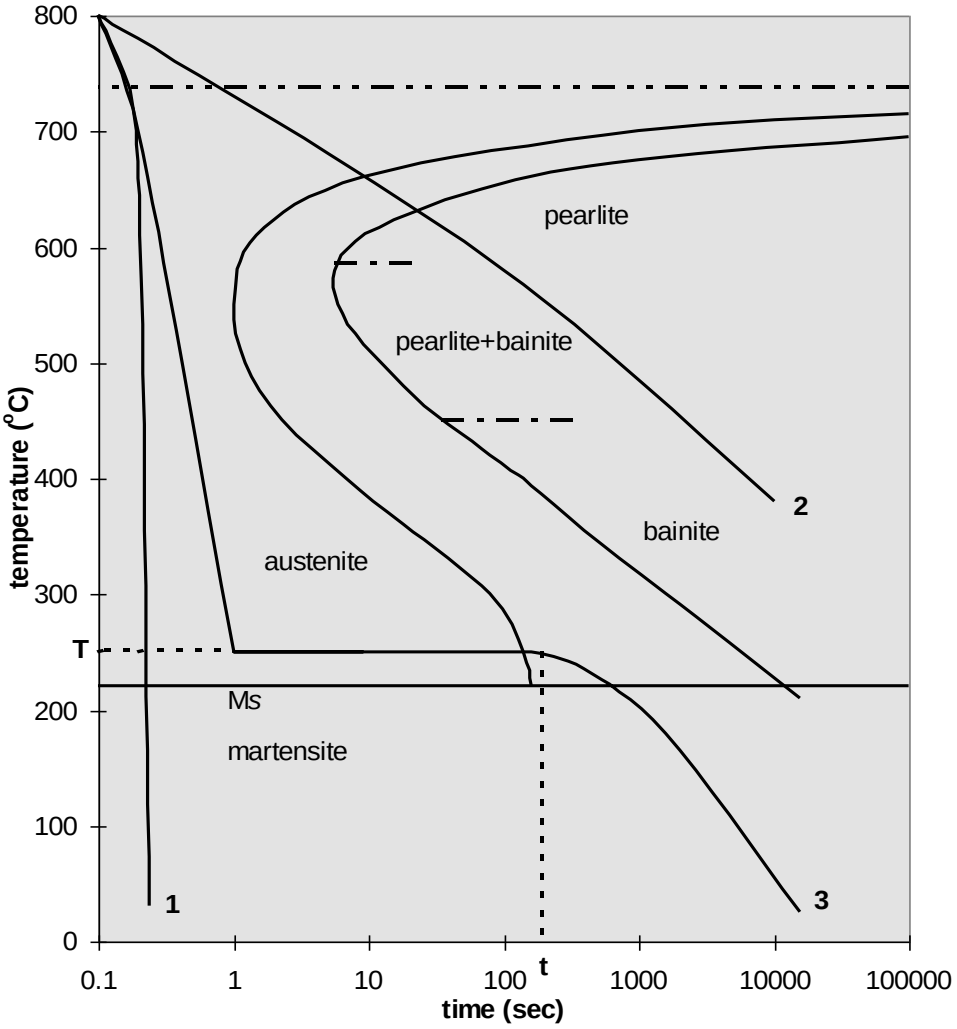

Figure 3.15 Illustration of heat-treatment paths of rolled steel-steel composite on the time-temperature-transformation (T-T-T) diagram of 0.8 wt% carbon steel[126]

The general flow chart of experiments on steel wire, interface, and steel-steel composite is shown in Figure 3.16, for some cases, the routes may change.

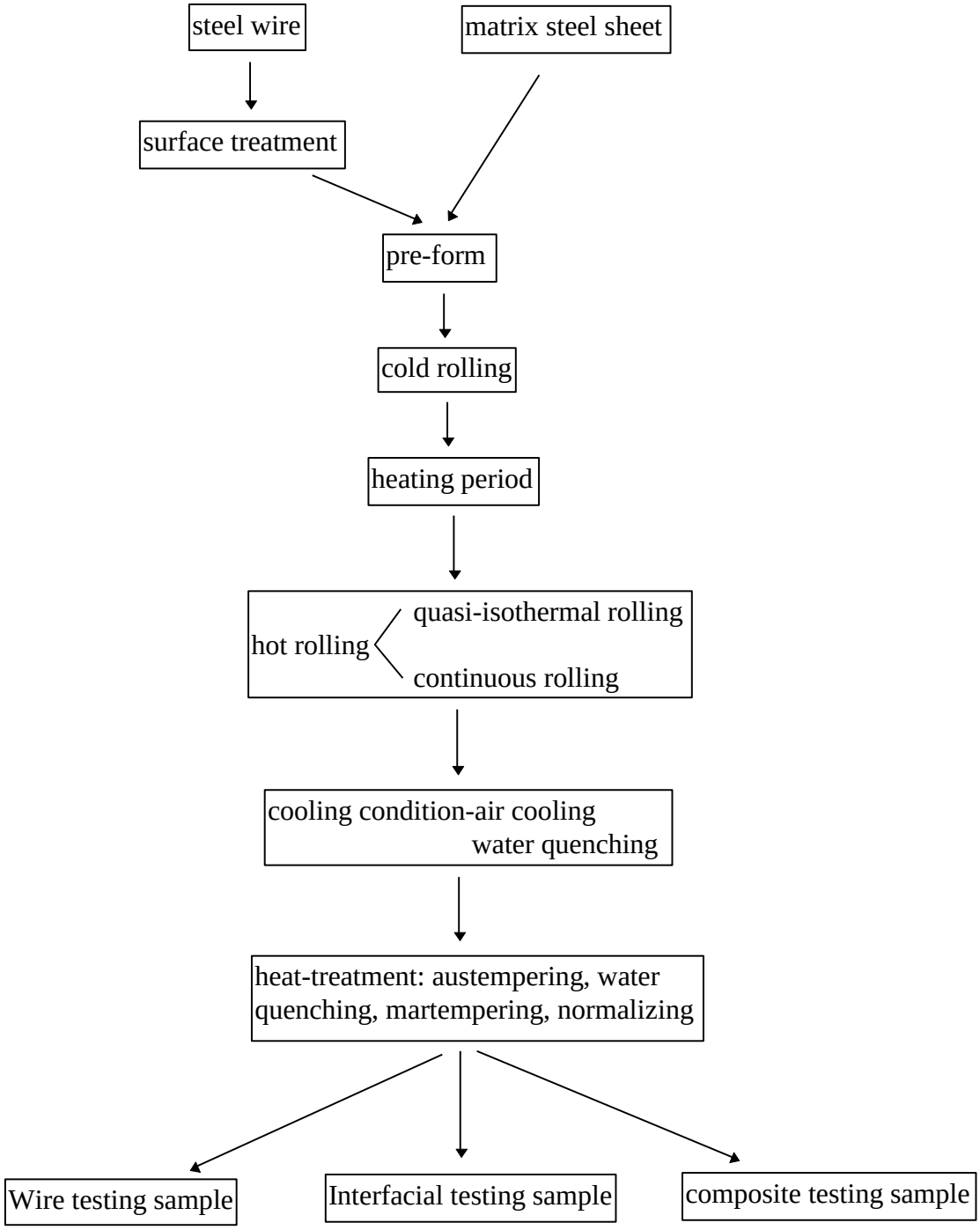

Figure 3.16 General flow chart of wire, interface, and composite testing samples preparation

3.2.4.3 Tensile testing

The tensile tests were carried out in the Hounsfield Extensometer testing machine, the load-displacement relationship was recorded. The result is the average of 3 tests for

each condition. The sample used for testing is shown in Figure 3.17. The fracture surfaces of composites were observed by SEM.

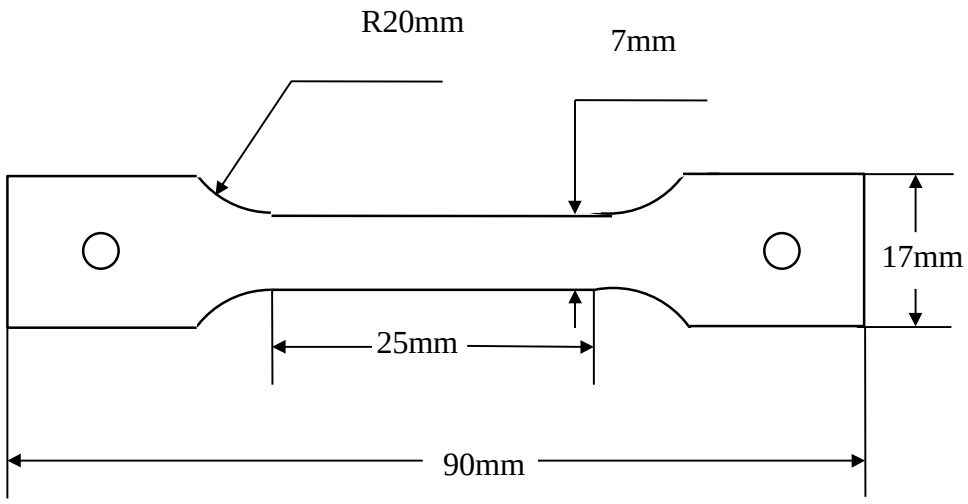

Figure 3.17 Illustration of tensile testing sample

Chapter 4

Results and Discussion, In-Situ Dual Phase Steels

As discussed in Chapter 1, alloying elements redistribute between austenite and ferrite during annealing of dual phase steels. The increase of austenite stablizing alloy content in austenite can strengthen and harden the austenite and the transformed martensite, whereas the decrease of this element in ferrite will give the ferrite higher ductility by reducing solid solution hardening in ferrite.

The morphology of martensite has an effect on the properties of dual phase steel; the obtained morphologies of martensite are fibrous, granular, and coarse grain. A fine size martensite is good for strength, ductility and toughness in dual phase steels. The martensite obtained by “intermediate quenching” is short and random fibrous, which does not appear superior to the granular martensite dual phase steel. Long, and preferred orientation, martensite is required for producing high strength dual phase steel because it has a significant reinforcing effect.

The manganese partitioning between austenite and ferrite during annealing and the variation of partitioning with annealing temperature and isothermal holding time will be studied in this section. A model will be developed to analyse the manganese partitioning and a comparison made with experimental data. The long fibrous martensite can be obtained by rolling steel in the austenite + ferrite region after annealing followed by water-quenching. This long fibrous martensite can then be shortened to a granular form by a following long post-RA (post-rolling annealing) time. The tensile properties and work hardening behavior of both long fibrous martensite and granular martensite dual phase steels will be examined.

4.1 Partitioning of manganese and microstructure

4.1.1 The influence of pre-rolling annealing (pre-RA)

The microstructure of dual phase steel A after pre-RA treatment for 48 hours is shown in Figure 4.1. Austenite is nucleated in the ferrite grain boundaries and grows both into the ferrite matrix and along the ferrite grain boundaries only in the case of intercritical annealing (shown in Figure 4.2).

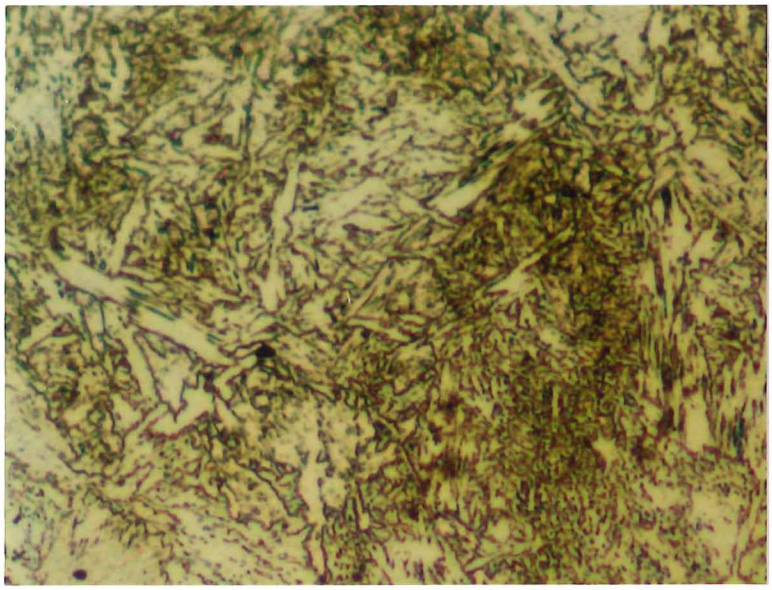

(a) intermediate quenching

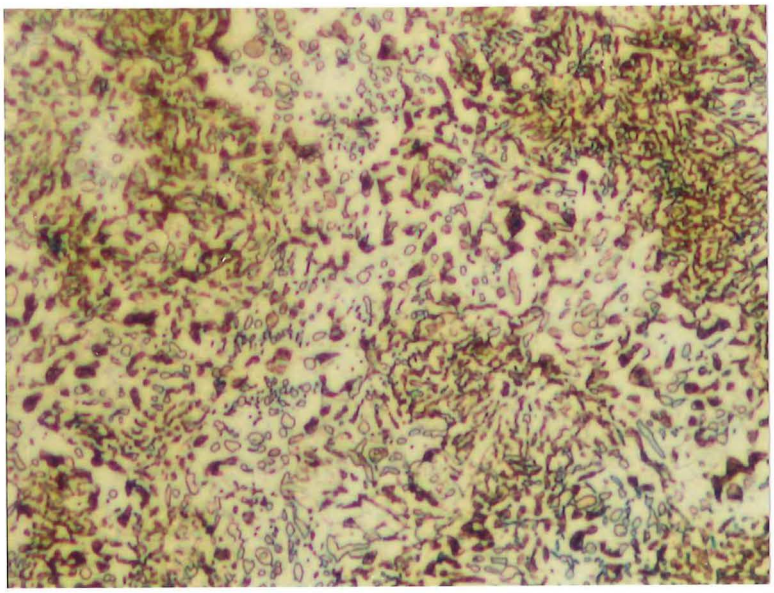

(b) intercritical annealing

Figure 4.1 Optical microstructure of pre-RA dual phase steel A after 48 hour annealing at 680℃ (×230)

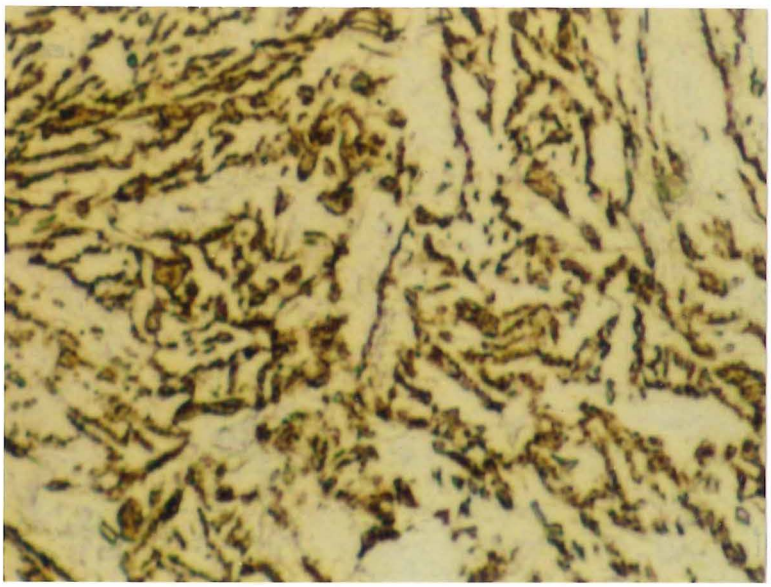

(a) intermediate quenching

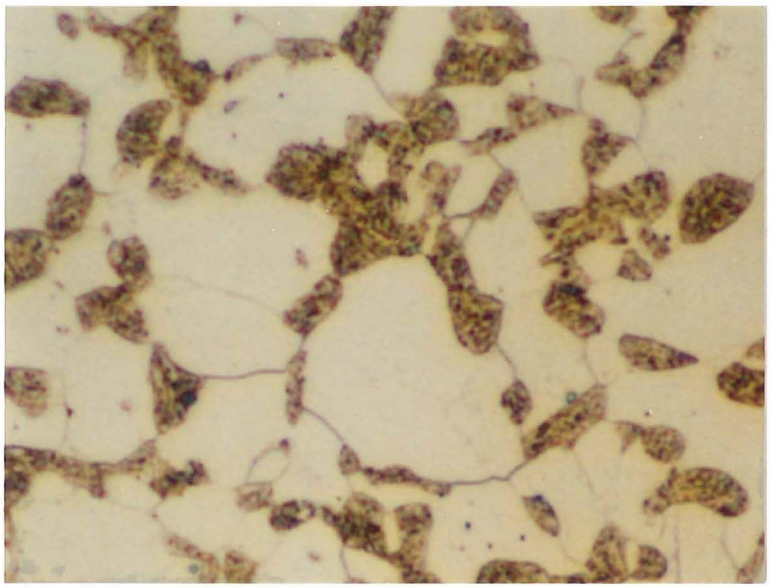

(b) intercritical annealing

Figure 4.2 Optical microstructure of pre-RA dual phase steel B after 48 hour annealing at 720℃ (× 575)

The needle-liked martensite produced by intermediate quenching is much finer than the granular martensite obtained by intercritical annealing.

The volume fraction of martensite of all four steels increases with increasing annealing temperature (shown in Figure 4.3); the martensite volume fraction in the higher alloy steel is higher than that in lower alloy steel at the same annealing temperature. Generally, 10-30% martensite is required to give a good combination of strength and ductility. Therefore, 680°C, 710°C, 720°C and 730°C were chosen for steels A, D, B,

and C respectively as these are the temperatures at which 30% martensite is produced. These will be referred to as the intercritical annealing temperatures.

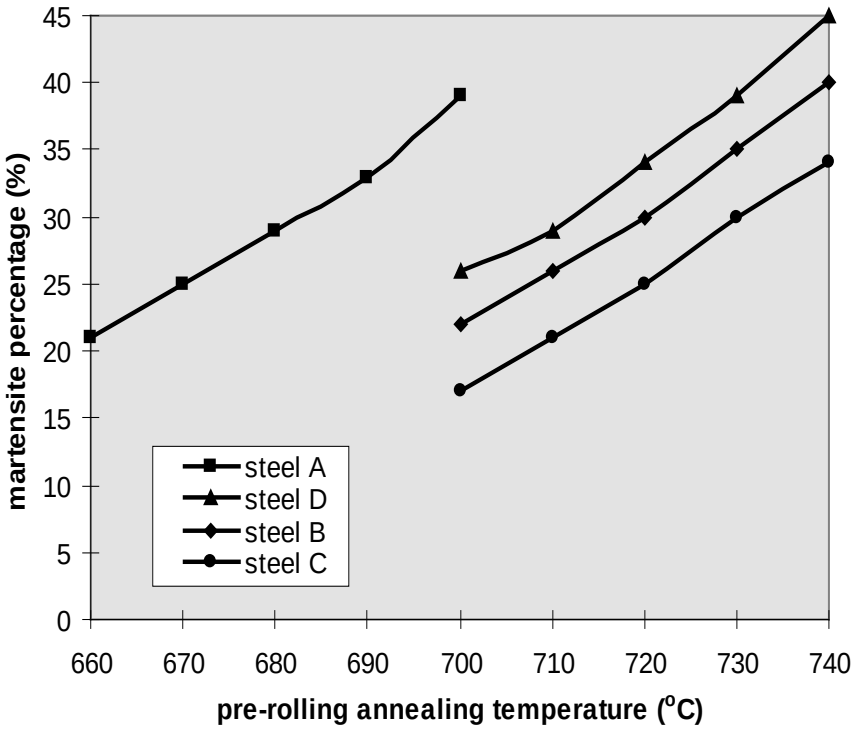

Figure 4.3 The influence of pre-RA temperature on the martensite content of four steels (for 48 hours)

The effect of annealing temperature on the manganese partitioning in the martensite and ferrite is shown in Figures 4.4 (a, b, c, and d). The term “partitioning coefficient”, which describes the degree of manganese partitioning, is defined as the ratio of average manganese content in martensite grains to that in the adjacent ferrite matrix.

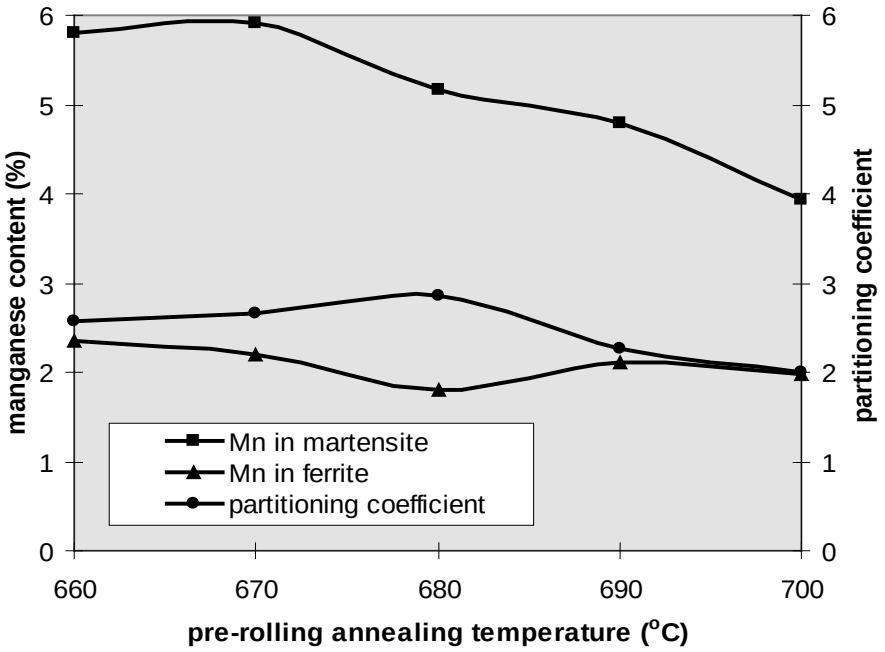

(a) steel A

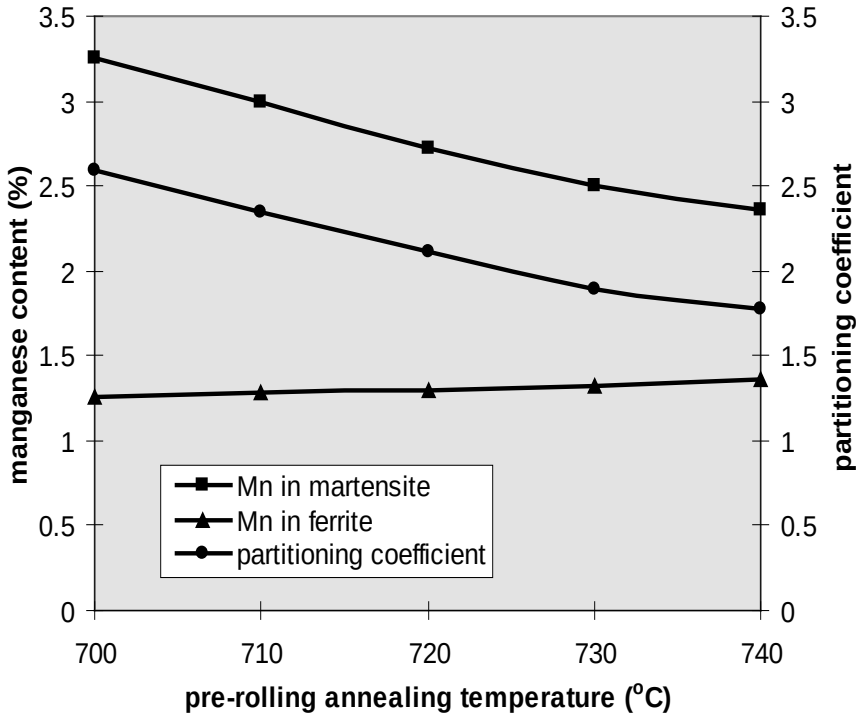

(b) steel B

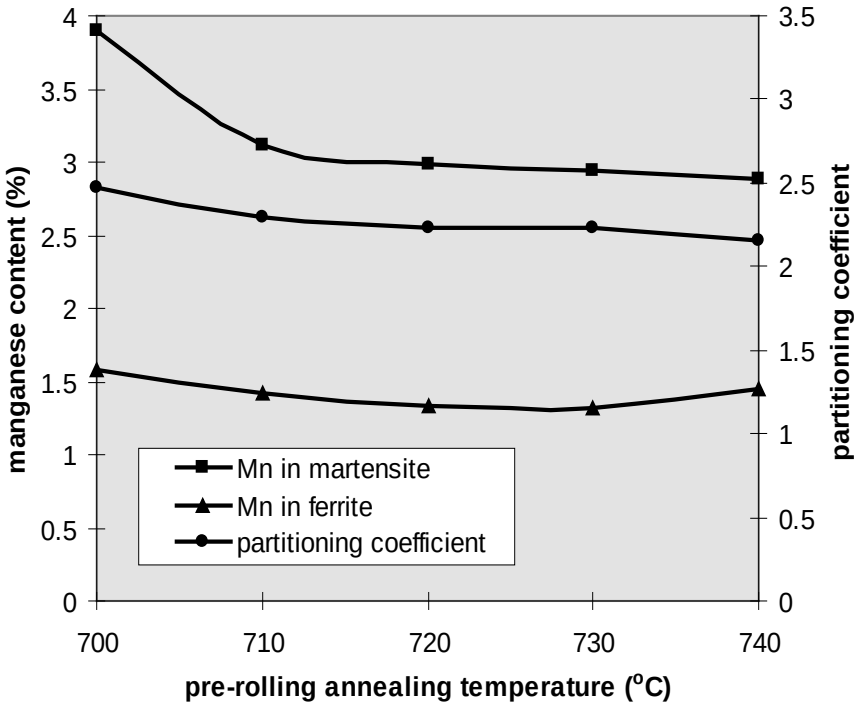

(c) steel C

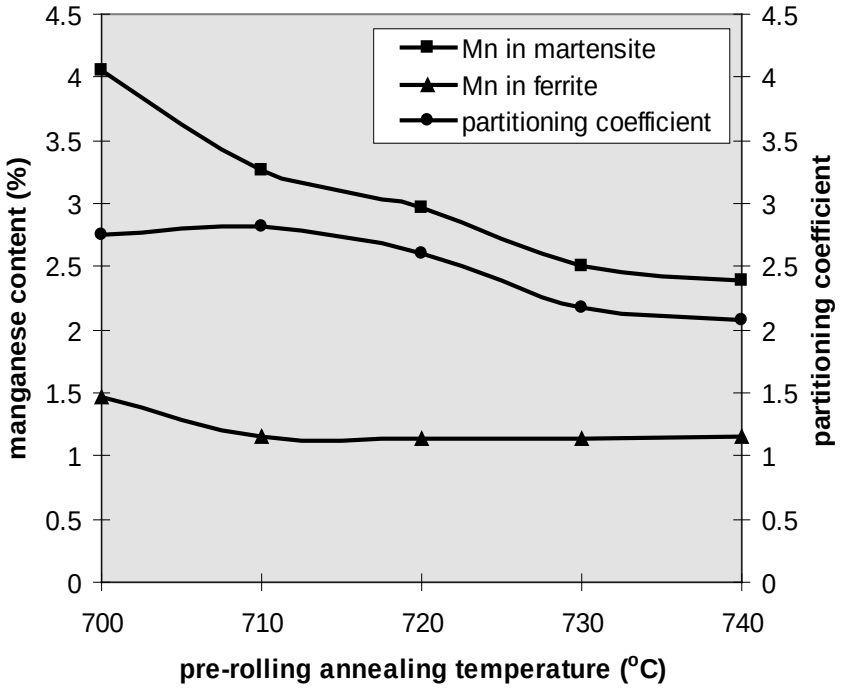

(d) steel D

Figure 4.4 The influence of pre-RA temperature on Mn partitioning (48hrs)

The partitioning coefficients of all steels except steel A decreases with increasing annealing temperature after annealing for 48 hours. The partitioning coefficient of steel A reaches a maximum at 680°C.

According to thermodynamics, the manganese will redistribute in the austenite and ferrite because of the difference in heats of solution (ΔH) of manganese in these phases during heat-treatment. Andrews[127] proposed that the final equilibrium value of the partitioning coefficient is:

$$\frac{C_{Mn}^{\gamma}}{C_{Mn}^{\alpha}} = \exp(-\frac{\Delta H}{R \cdot T}) \qquad (4.1)$$

This indicates that the final equilibrium partitioning coefficient decreases with increasing annealing temperature.

From the Fe-C-Mn ternary phase diagram, increasing annealing temperature decreases the solubility of manganese in austenite sharply, with a corresponding slight decrease in the ferrite manganese content. The variation of solubility of manganese makes the partitioning coefficient decrease with increasing temperature, ie. the equilibrium partitioning coefficient is dependent on annealing temperature and initial bulk composition of steel. On the other hand, the manganese partitioning process is controlled by diffusion rate - the time needed for reaching equilibrium partitioning at low temperature is much longer than that at high temperature (shown Figure 4.5). After annealing for a limited time (here it is 48 hrs), the partitioning at high annealing temperature reaches equilibrium, but at low temperature it does not, so that the partitioning coefficient of steel A is at a maximum at 680°C when annealed for 48 hours.

Another reason for the low partitioning coefficient of steel A annealed at 660°C for 48 hours is the low volume fraction of martensite. The lower the volume fraction of martensite in steel, the longer the path need to transport manganese from ferrite, increasing the time required to reach final equilibrium partitioning.

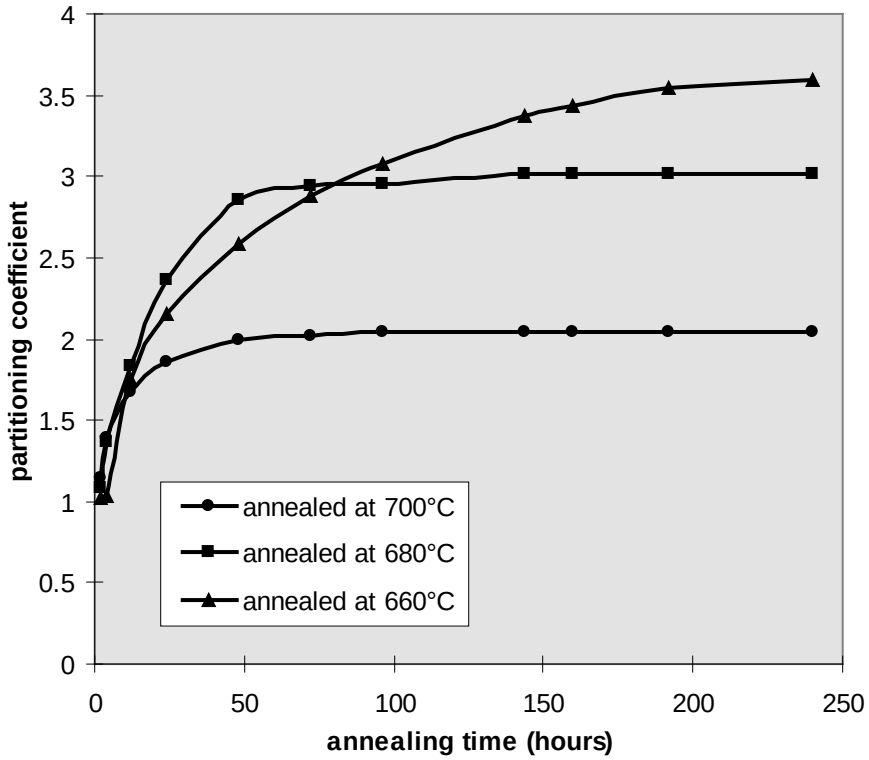

Figure 4.5 The partitioning coefficient as a function of annealing time and temperature in steel A

The influence of pre-RA time on the volume fraction of martensite is shown in Figure 4.6; the volume fraction of martensite increases with time at the intercritical annealing temperature, and reaches the equilibrium value after about 150 hours. The time needed to reach equilibrium for lower carbon steel (such as steel C) is less than that for higher carbon steel (steel D, for example), because:

(1) the intercritical annealing temperature for lower carbon/alloy steel is higher than that of higher carbon/alloy steel. The growth of grains and element diffusion are faster at higher annealing temperatures;

(2) the high volume fraction of carbide particles in higher carbon/alloy steel has more retarding force on grain growth.

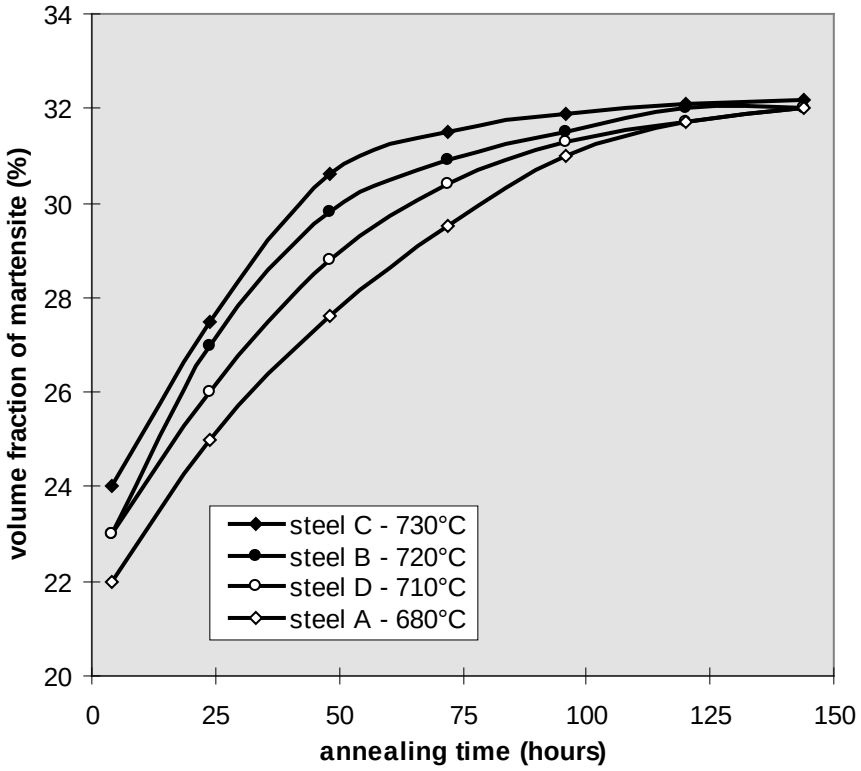

Figure 4.6 The influence of pre-RA time on the martensite contents of four steels at the intercritical annealing temperatures

When dual phase steels are held for long times at the intercritical annealing temperature, not only the volume fraction of austenite but also the morphology of austenite will vary with annealing time. Figures 4.7 and 4.8 show how the microstructures of intercritical annealed and intermediate quenched steels vary with annealing time (see Figure 1.3 for description and structure of various processes).

There are new austenite grains nucleating while the initial nucleated austenite grains grow, ie. the nucleation of austenite continuously takes place throughout the whole isothermal annealing process. Both the growth of prior austenite grains and the continuous nucleation of austenite contribute to the increase of volume fraction of austenite with annealing time.

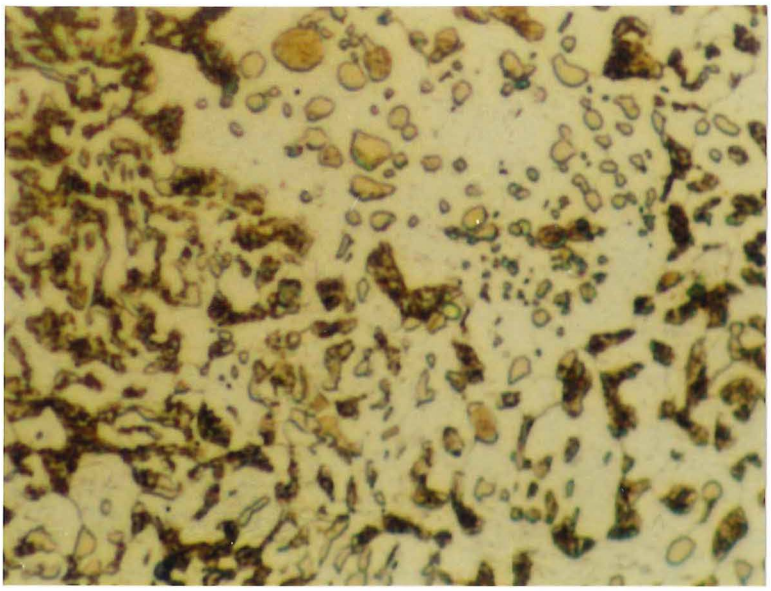

(a) intercritical annealing at 680°C for 2 hours

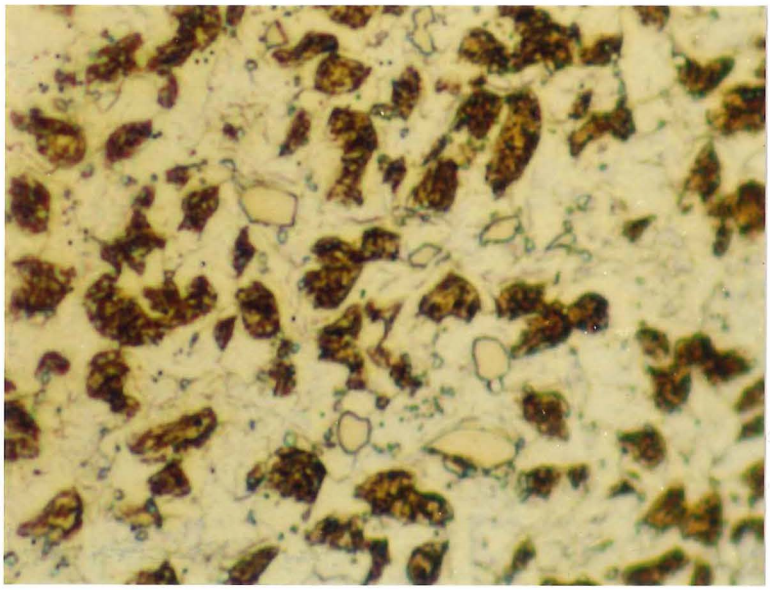

(b) intercritical annealing at 680°C for 96 hours

Figure 4.7 The effect of annealing time on the microstructure of intercritical annealed steel A (× 575)

The microstructure formed by intermediate quenching is a needle-like austenite in the beginning. By increasing annealing time, the initial needle-liked austenite grains grow slowly in both radial and axial directions, whilst the austenite nucleated later is granular, which grows faster. That means the nucleation of austenite from martensite lath (intermediate quenching) is much faster than that in ferrite boundaries (intercritical annealing).

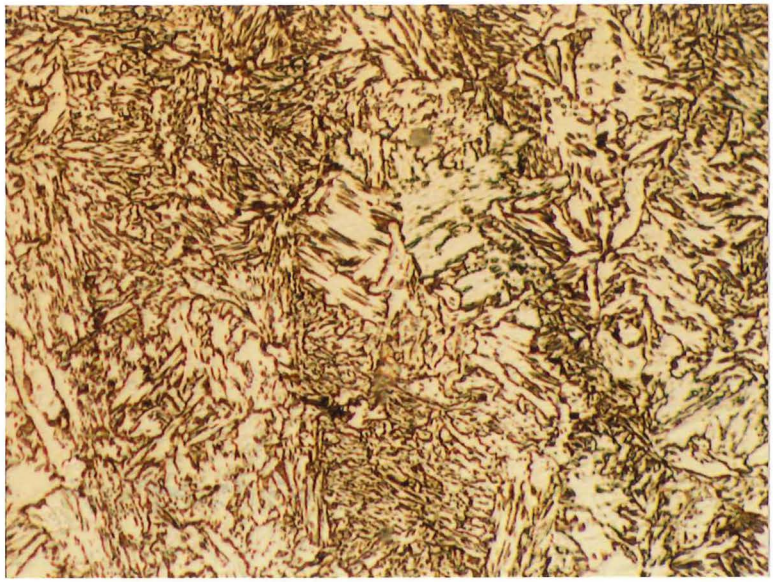

(a) intermediate quenching at 680°C for 2 hours

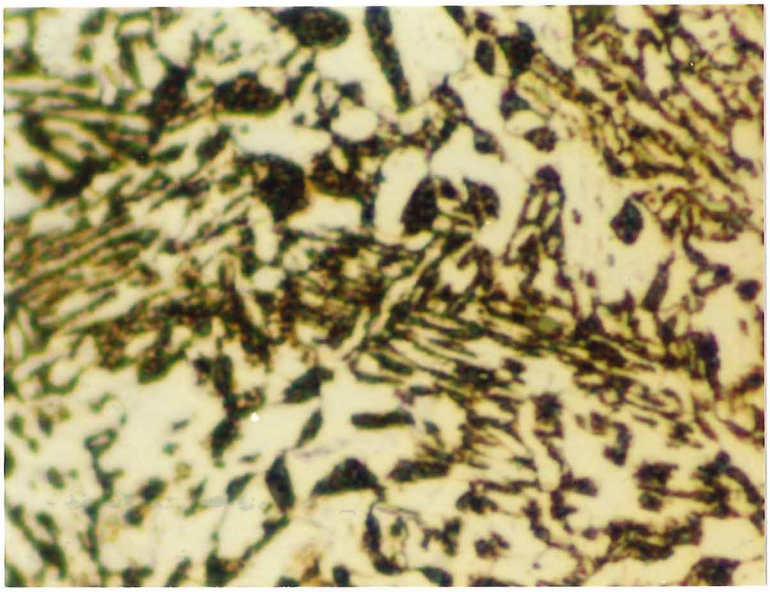

(b) intermediate quenching at 680°C for 96 hours

Figure 4.8 The effect of annealing time on the microstructure of intermediate quenched steel A (× 575)

The influence of pre-RA time on the partitioning coefficient of four dual phase steels is shown in Figures 4.9 (a, b, c, and d) at their intercritical annealing temperatures; the partitioning coefficient increases with intercritical annealing time. This effect diminishes at longer pre-annealing times and finally, the partitioning coefficient will reach the equilibrium values.

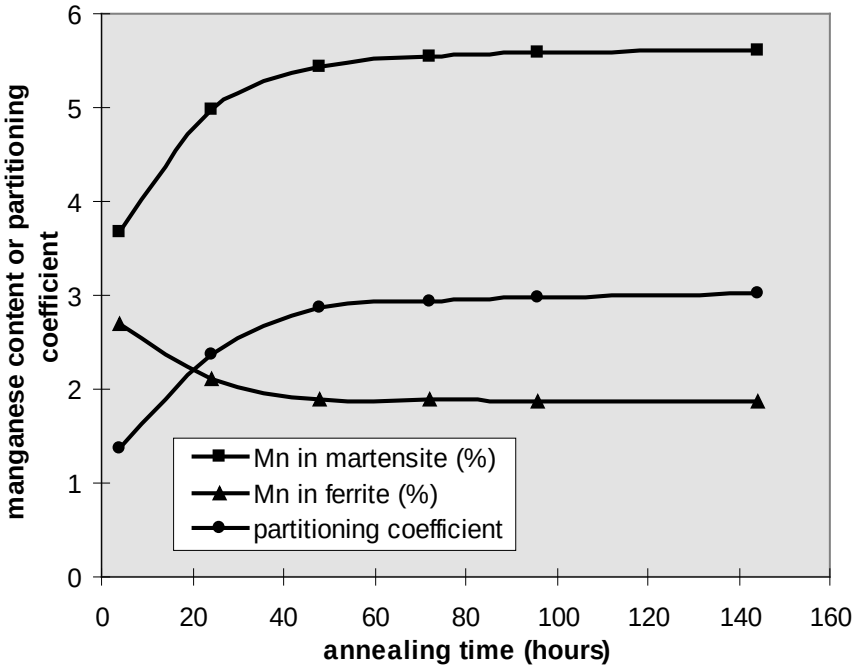

(a) steel A at 680°C

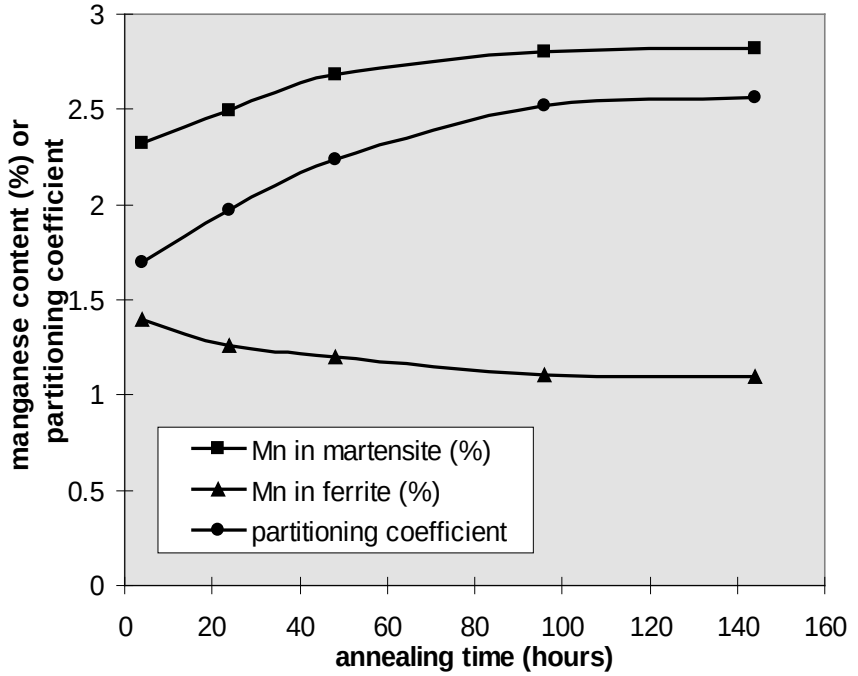

(b) steel B at 720°C

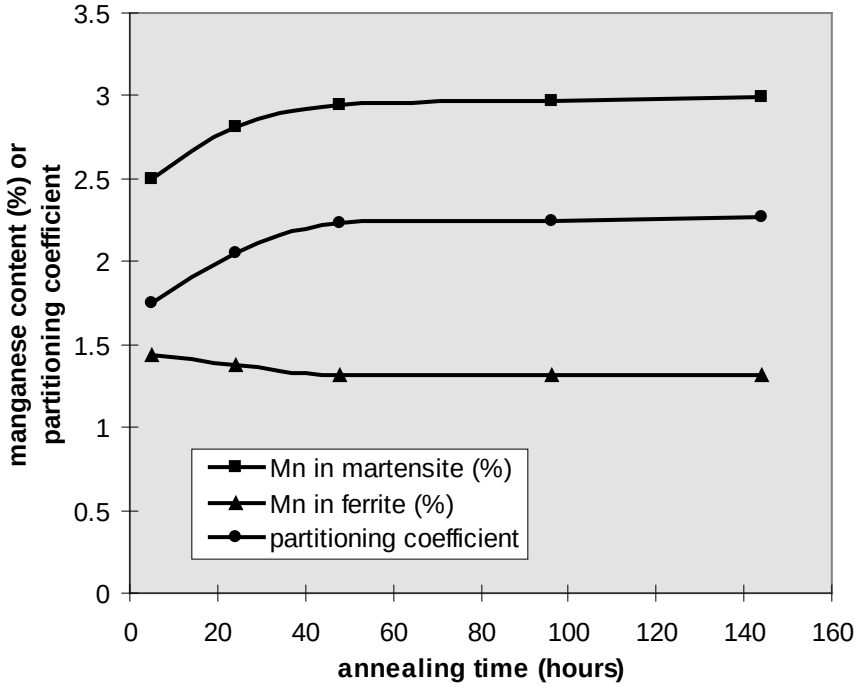

(c) steel C at 730°C

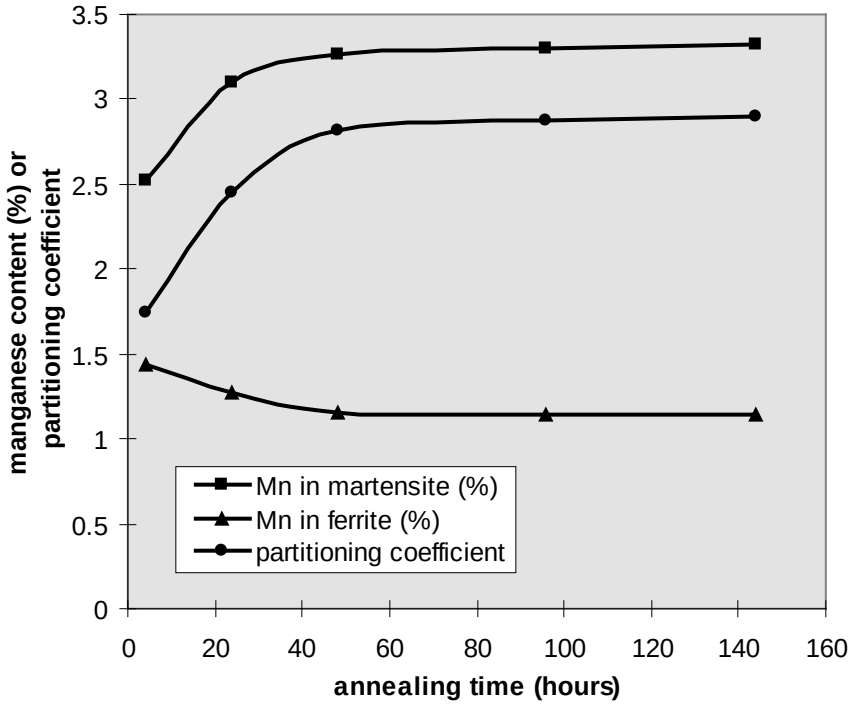

(d) steel D at 710°C

Figure 4.9 The effect of pre-RA time on Mn partitioning

4.1.2 Hot rolling

Hot rolling involves mechanical processing in the ($\alpha + \gamma$) region, which changes the morphology of both the ferrite and the austenite (which will transform to martensite after cooling); the rolling process is illustrated in Figure 4.10. The deformation by thermomechanical treatment has little effect on the volume fraction of martensite[128] and the manganese partitioning at any given temperature.

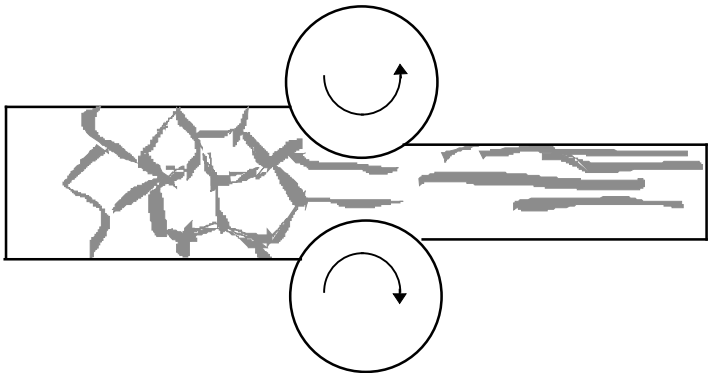

Figure 4.10 Schematic of microstructure of dual phase steel due to hot rolling (the ferrite is white and the austenite is dark)

During hot rolling, the austenite grain islands are flattened and elongated. In addition, with rolling, the temperature of the sample decreases into the alpha-region, which will produce a desirable combination of increased strength and toughness in extra-low-carbon steel because of[111]:

"(1) grain refinement of both gamma and alpha structure by repeated heavy deformation,

(2) dynamic recovery that produces a fine polygonal α-Fe substructure, and

(3) cube-on-corner crystallographic texturing that results from the deformation process."

The final microstructures, both parallel and perpendicular to the rolling direction, for steel A after pre-rolling annealing for 48 hours and with rolling commenced at 680°C are shown in Figure 4.11. The martensite phase exists in the form of fibres and ribbons instead of islands as is normally the case; the higher aspect ratio of this martensite phase leads to a reinforcing effect (in the fibre/rolling direction) as would be expected from composite theory.

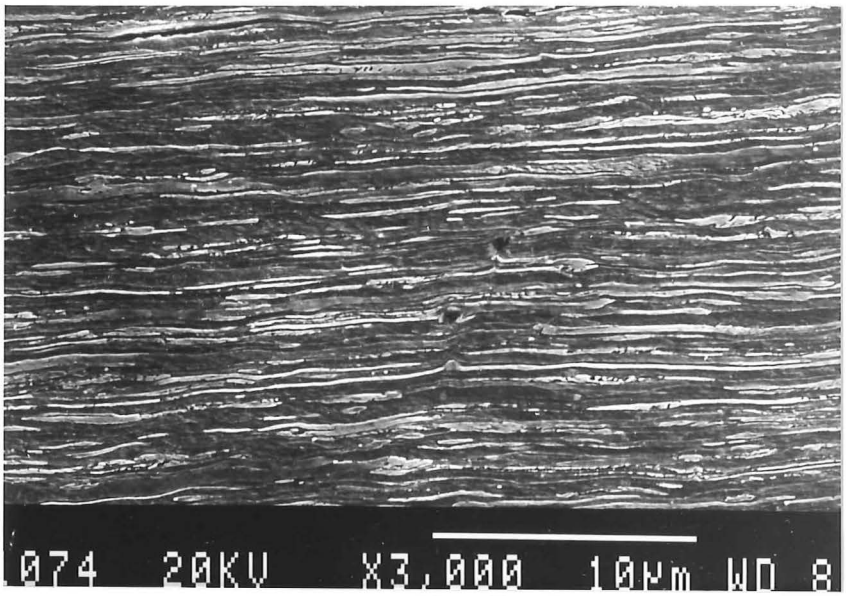

(a) parallel to rolling direction

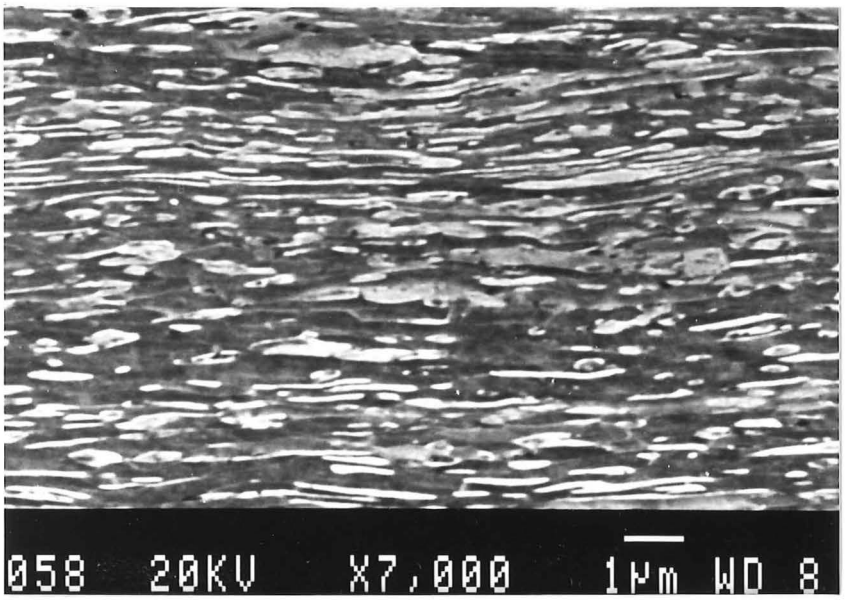

(b) perpendicular to rolling direction

Figure 4.11 The microstructure of steel A after pre-rolling annealing at 680℃ and continuous rolling commencing at 680℃

4.1.3 The effect of post-rolling annealing (post-RA)

Post-RA effects the microstructure of the as-rolled dual phase steel. After post-RA, the release of the high energy imparted by the rolling tends to shorten the long, fibrous martensite with a resultant decrease in aspect ratio (the more equiaxed structure being more thermodynamically stable under these conditions). This change in morphology with post-RA time is shown in Figure 4.12 (a, b, c and d).

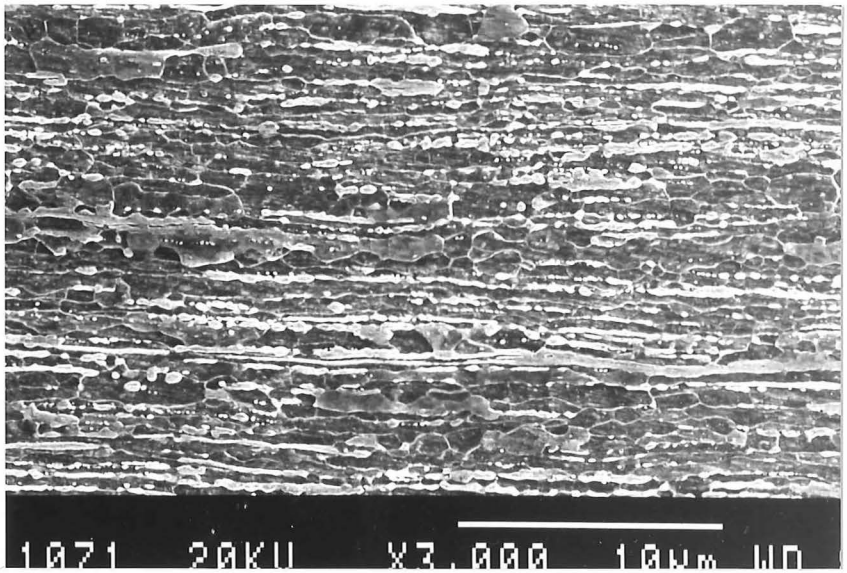

(a) annealing for 10 min

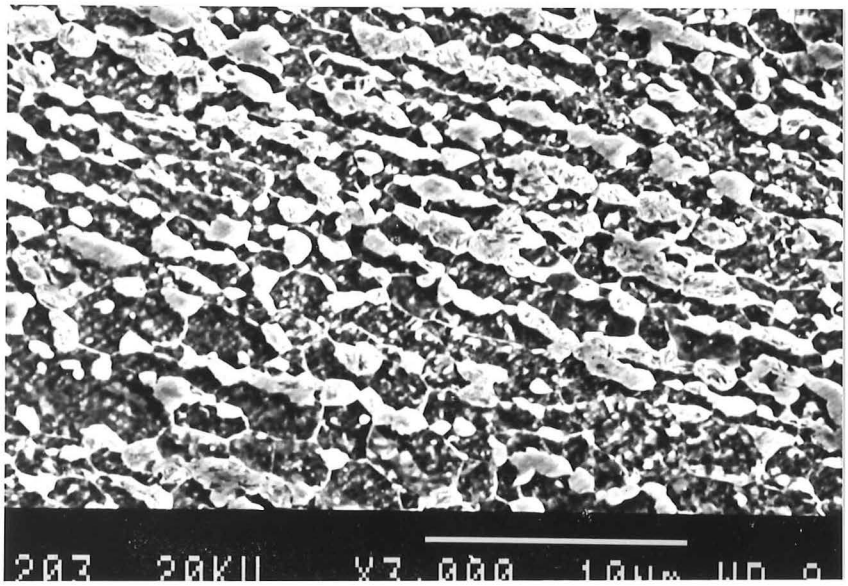

(b) annealing for 60 min

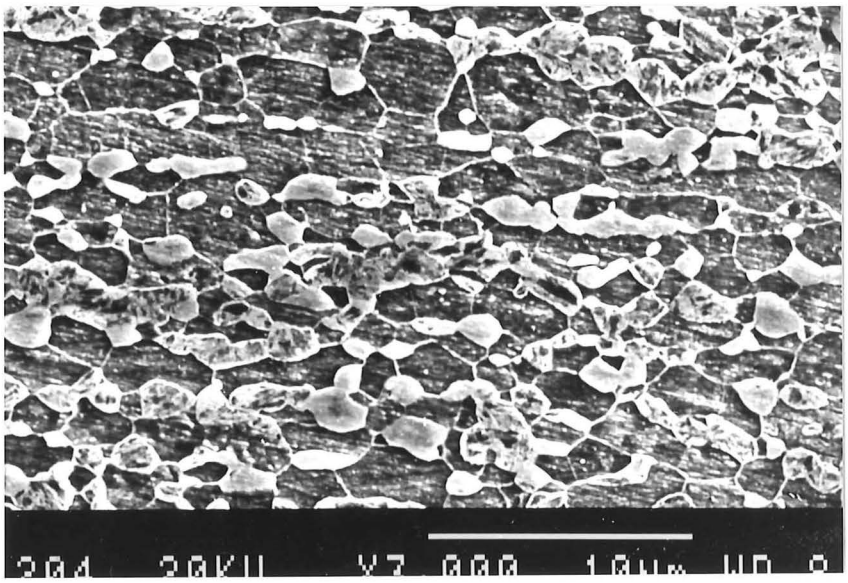

(c) annealing for 240 min

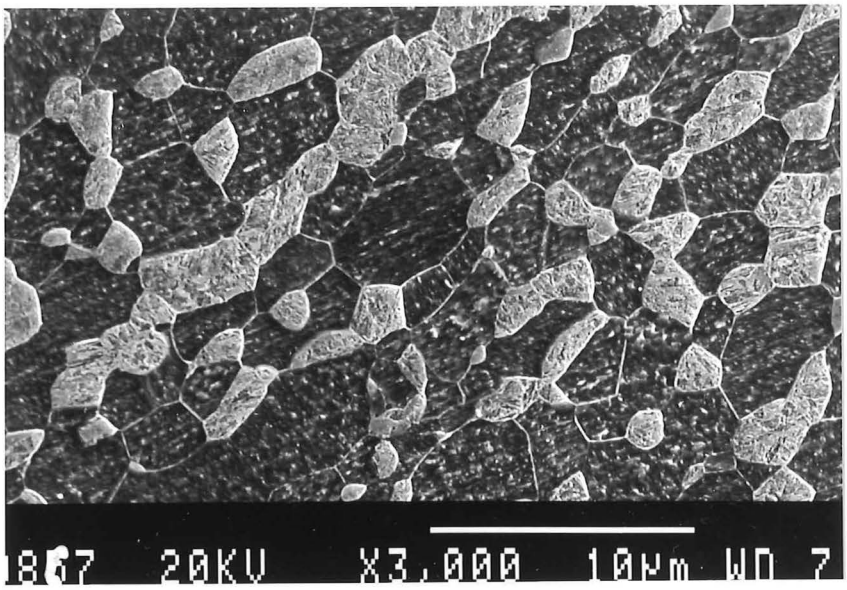

(d) annealing for 48 hrs

Figure 4.12 The change of martensite morphology of steel A after post-RA at 680°C

When the thin rolled steel sheet is exposed at high temperature for long time, decarburization will take place and cause the volume fraction of martensite to decrease with temperature and time of post-RA (shown in Figures 4.13 and 4.14).

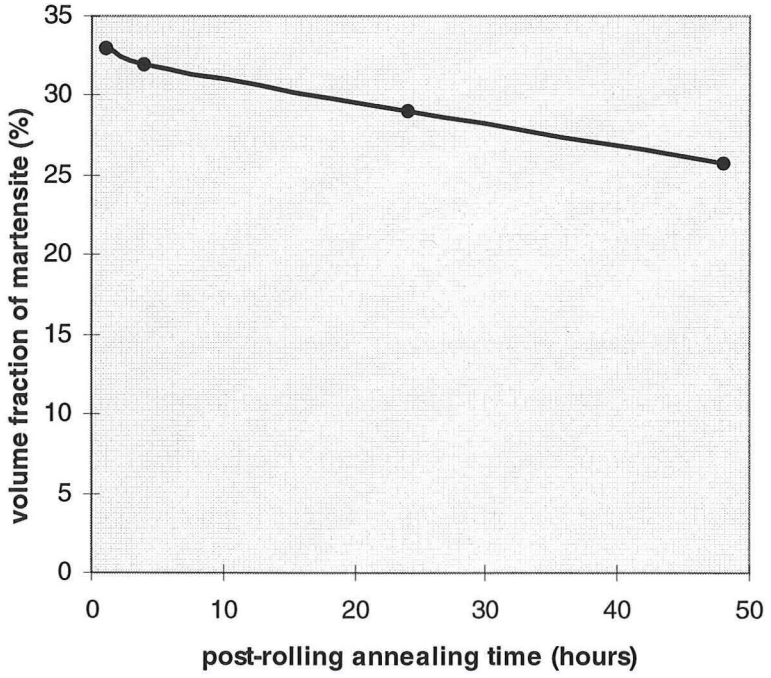

Figure 4.13 The effect of post-RA time on martensite volume fraction of steel A at 690°C

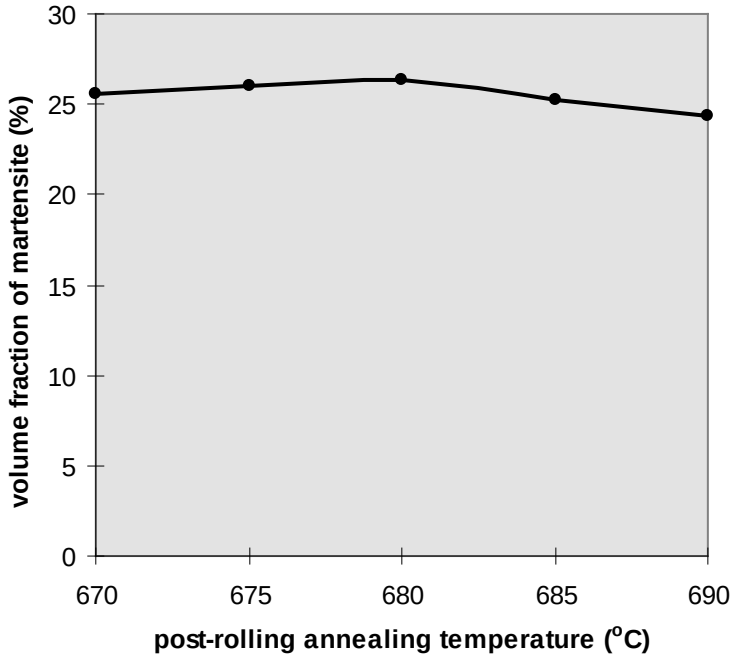

Figure 4.14 The influence of post-RA temperature on martensite fraction of steel A (48 hours)

The effect of post-RA on the manganese partitioning of as-rolled steels depends on the pre-RA history of the steels. If the temperature of post-RA is different from that of pre-RA or the partitioning didn't reach equilibrium after pre-RA, manganese redistribution in the austenite and ferrite will occur during post-RA, otherwise, the manganese contents in austenite and ferrite will keep constant.

4.2. Modelling and analysis for manganese partitioning

Because of the importance of manganese partitioning between austenite and ferrite of dual phase steels during annealing[129,130], a lot of work has concentrated on both the experimental and theoretical analysis of manganese partitioning[12, 29,32,33]. A new model will be established to analyse the manganese diffusion process, calculate the partitioning coefficient, and examine the effect of austenite grain size on manganese partitioning. The predicted values will be compared with experimental data in this section.

4.2.1 Modelling

Consider the intermediate quenched dual phase steel; the needle-like austenite is surrounded by ferrite, but the austenite will appear circular in cross-section (introduced

in section 1.3 and shown in Figure 4.15). A polygonal unit with the austenite needle in its centre is selected as an analysis unit (shown in Figure 4.15). For the simplification of analysis, both the unit and austenite are considered as concentric cylinders (as shown in Figure 4.16).

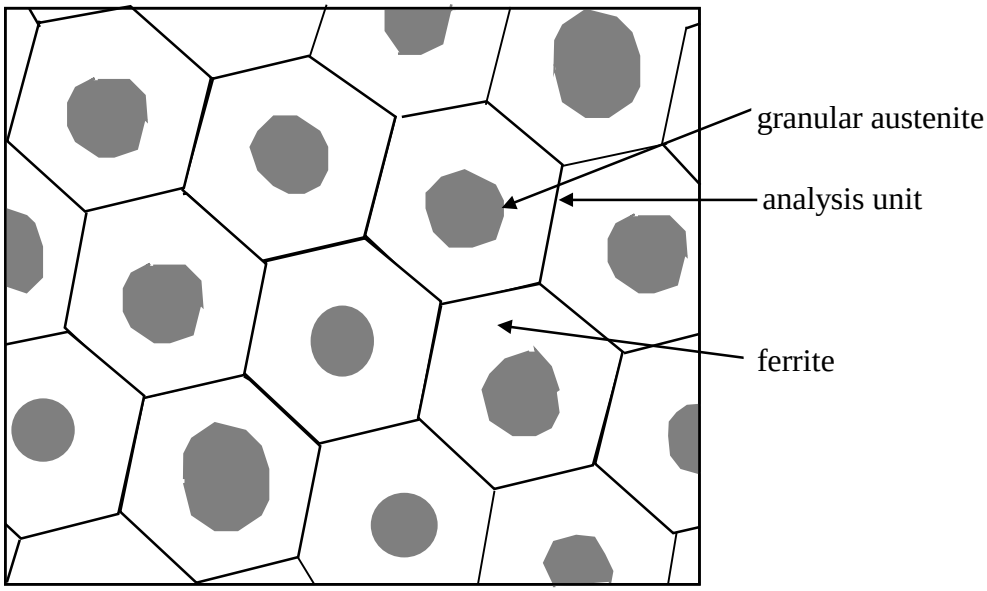

Figure 4.15 Illustration of intermediate quenched dual phase steel microstructure

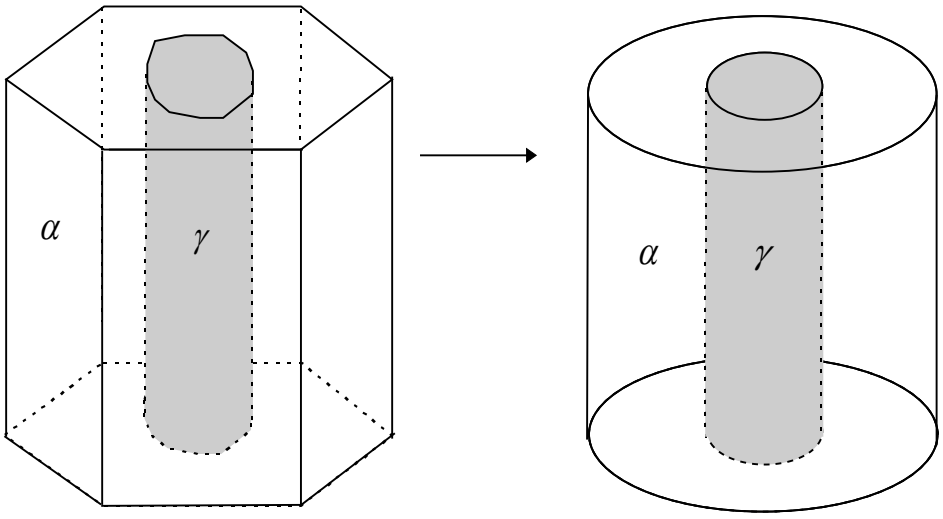

Figure 4.16 The simplification of analysis unit for dual phase steel

Owing to the high aspect ratio of the needle austenite, the manganese diffusion between austenite and ferrite in the axial direction of the austenite “fibre” can be ignored when

compared with the diffusion in the radial direction. The analysis of manganese diffusion in this section is based on the diffusion in the radial direction.

Take the X-axis as the distance from the centre of austenite cylinder in the radial direction, and Y-axis as the concentration of manganese. The coordinate set-up is shown in Figure 4.17.

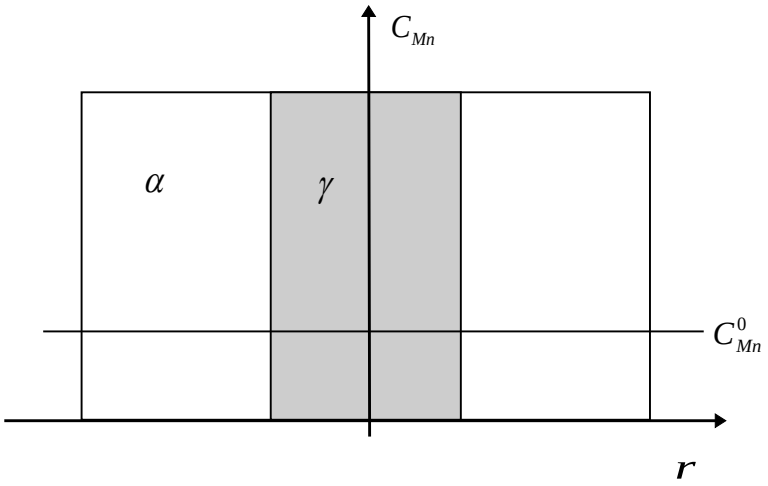

Figure 4.17 Set-up of the coordinates for analysis of manganese between austenite and ferrite during intercritical annealing

When the dual phase steel with manganese content C_{Mn}^{0} is heated at a temperature T between AC_1 and AC_3, the nucleation and growth of austenite is controlled by carbon diffusion in the first two stages and is completed in several seconds (refer to section 1.3). As discussed in Chapter 1, after the transformation controlled by carbon diffusion has been completed, manganese diffusion starts to dominate the transformation. The manganese diffusion process is analysed from the end of the first two stages controlled by carbon diffusion (ie., several seconds after annealing).

At the beginning of the manganese diffusion, the ferrite is supersaturated with manganese. The supersaturated manganese will precipitate at the boundary between austenite and ferrite and form a low manganese rim on the edge of the ferrite grain (manganese content is $C_{Mn}^{\alpha 0}$, the equilibrium manganese solubility in ferrite at temperature T), whilst the precipitated manganese will dissolve in austenite and form a high manganese rim at the boundary of the austenite (manganese content is $C_{Mn}^{\gamma 0}$, the maximum manganese solubility in austenite at temperature T).

Because the diffusion rate of manganese in ferrite is three orders higher than in austenite, the precipitated manganese from the ferrite will form a manganese-rich rim (The manganese concentration is marked as C_{Mn}^{i}, which is variable) at the interface between ferrite and austenite, in addition to dissolving in the austenite. The inner dimension of this manganese-rich rim is the grain size of austenite and the outer dimension is the inner size of the ferrite. A manganese gradient exists in the regions within the austenite ($<r_{\gamma}$) and ferrite ($>r_{\alpha}$). The dimension relationship is shown in Figure 4.18 as:

$$r_{\gamma} + \Delta r = r_{\alpha} \tag{4.2}$$

where Δr is the thickness of the manganese-rich rim in the interface, which is at the scale of grain boundary and the manganese-rich rim is thought of as an interphase, which is neither austenite or ferrite. Both r_{γ} and r_{α} increase with annealing time at a given temperature, which means that the boundary between austenite and ferrite is moving during annealing.

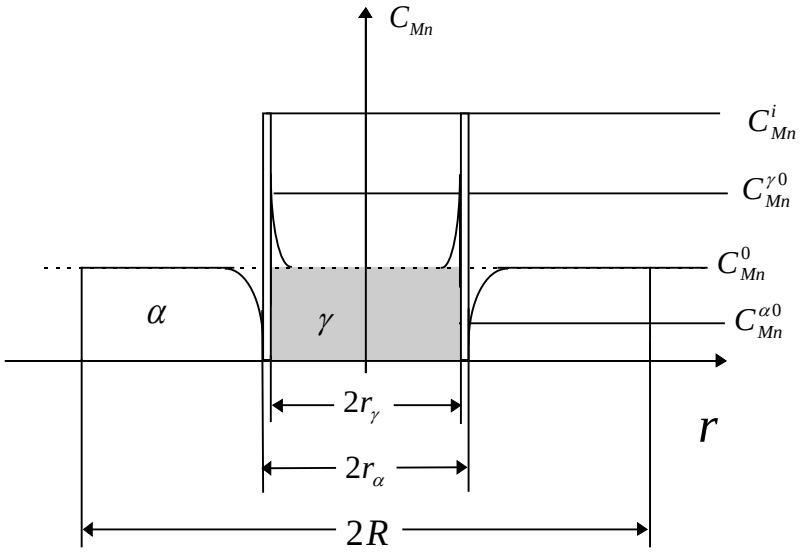

Figure 4.18 Illustration of manganese distribution in austenite and ferrite during intercritical annealing

According to the growth kinetics of austenite, the grain size of austenite at a given temperature T is:

$$r_{\gamma} = k_0 t^n \cdot \exp(-\frac{Q}{2RT}) \tag{4.3}$$

where, Q is the empirical heat of activation for the austenite growth process, k_0 and n are constants for a given alloy at the given temperature - generally the exponent n increases with increasing temperature and reaches the value of $1/2$ [131]. Equation (4.3) differentiated with respect to time, t, gives the moving velocity of the austenite-ferrite boundary.

While annealing is in progress, the supersaturated manganese in the ferrite will transport to the boundary to form the manganese-rich rim, which is then the manganese source for diffusion into the austenite. The manganese in this rim will diffuse into the austenite until the manganese gradient in austenite is eliminated. The distribution of manganese in the ferrite and austenite can be obtained by solving Fick's second law at the proper boundary conditions.

Fick's second law for manganese diffusion is written as:

$$\frac{\partial C_{Mn}}{\partial t} = -\nabla J_{Mn} \tag{4.4}$$

where, ∇ means the grad operation. In a ternary system, the manganese diffusion flux J_{Mn} depends on the concentration gradient of both carbon and manganese; it is expressed phenomenologically with self-diffusion and inter-diffusion coefficients as:

$$J_{Mn} = -D_{Mn}^{inter} \nabla C_C - D_{Mn} \nabla C_{Mn} \tag{4.5}$$

where D_{Mn}^{inter} is the inter-diffusion coefficient, and D_{Mn} is the self-diffusion coefficient. The inter-diffusion coefficient, D_{Mn}^{inter}, gives a quantitative measure of the effect of a concentration gradient of carbon on the flux of the manganese. In Fe-C-Mn ternary alloys, the effect of carbon gradient on the flux of Mn is generally negligible, so Fick's second law on Mn diffusion is written as follows when D_{Mn} is independent of manganese content:

$$\frac{\partial C_{Mn}}{\partial t} = -D_{Mn} \nabla^2 C_{Mn} \tag{4.6}$$

The boundary conditions for Mn diffusion in ferrite are:

$$\begin{cases} C_{Mn}^{\alpha} = C_{Mn}^{0} & when \quad t = 0 \\ C_{Mn}^{\alpha} = C_{Mn}^{\alpha 0} & when \quad r = r_{\alpha} \end{cases} \tag{4.7}$$

The solution to Fick's second law in ferrite can be written as:

$$C_{Mn}^{\alpha} = C_{Mn}^{0} - \left(C_{Mn}^{0} - C_{Mn}^{\alpha 0}\right) \cdot \left[1 - erf\left(\frac{r - r_{\alpha}}{2\sqrt{D_{Mn}^{\alpha} t}}\right)\right] \text{ when } r_{\alpha} \le r \le R \tag{4.8}$$

$$\text{and } D_{Mn}^{\alpha} = D_{Mn}^{\alpha 0} \exp\left(-\frac{Q_{Mn}^{\alpha}}{R \cdot T}\right) \tag{4.9}$$

The boundary conditions for manganese diffusion from the Mn-rich rim in austenite are set as:

$$\begin{cases} C_{Mn}^{\gamma} = C_{Mn}^{0} & when \quad t = 0 \\ C_{Mn}^{\gamma} = C_{Mn}^{\gamma 0} & when \quad r = r_{\gamma} \end{cases} \tag{4.10}$$

The equation for manganese distribution in austenite is:

$$C_{Mn}^{\gamma} = C_{Mn}^{0} - \left(C_{Mn}^{0} - C_{Mn}^{\gamma 0}\right) \cdot \left(1 - erf\left(\frac{r_{\gamma} - r}{2\sqrt{D_{Mn}^{\gamma} t}}\right)\right) \text{ when } 0 \le r \le r_{\gamma} \tag{4.11}$$

$$\text{and } D_{Mn}^{\gamma} = D_{Mn}^{\gamma 0} \exp\left(-\frac{Q_{Mn}^{\gamma}}{R \cdot T}\right) \tag{4.12}$$

Regardless of the manganese compound, the manganese is still thought to dissolve as a solute, so the mass balance equation should be applicable:

$$\frac{\int_{S_{\alpha}} C_{Mn}^{\alpha} dS_{\alpha}}{S_{\alpha} + S_{\gamma} + S^{i}} + \frac{\int_{S_{\gamma}} C_{Mn}^{\gamma} dS_{\gamma}}{S_{\alpha} + S_{\gamma} + S^{i}} + \frac{S^{i} C_{Mn}^{i}}{S_{\alpha} + S_{\gamma} + S^{i}} = C_{Mn}^{0} \tag{4.1.13}$$

where S_{α}, S_{γ} and S^{i} are the areas occupied by ferrite, austenite and the manganese-rich rim (interphase) and the following relationships apply:

$\frac{S_{\gamma}}{S_{\alpha} + S_{\gamma} + S^{i}} = V_{\gamma}$, the volume fraction of austenite, increasing with annealing;

$S_{\gamma} = \pi \cdot r_{\gamma}^{2}$ (the area of austenite, which increases with annealing);

$S_\alpha = \pi \cdot \left(R^2 - r_\alpha^2\right)$ (the area of ferrite, which decreases with annealing);

$S^i = \pi \cdot \left(r_\alpha^2 - r_\gamma{}^2\right)$ (the area of manganese-rich rim at interface; final value is 0).

The equilibrium manganese contents in ferrite and austenite at temperature T, $C_{Mn}^{\alpha 0}$ and $C_{Mn}^{\gamma 0}$ also meet the balance requirement:

$$C_{Mn}^{\alpha 0} \cdot (1 - V_\gamma^{final}) + C_{Mn}^{\gamma 0} \cdot V_\gamma^{final} = C_{Mn}^0 \tag{4.14}$$

where, V_γ^{final} is the equilibrium volume fraction of austenite.

The equilibrium manganese contents in ferrite and austenite, $C_{Mn}^{\alpha 0}$, $C_{Mn}^{\gamma 0}$, can be found from:

(a) thermodynamics: equation (4.1) can predict the equilibrium concentration of manganese in ferrite and martensite, associated with equation (4.14).

$$\frac{C_{Mn}^{\gamma 0}}{C_{Mn}^{\alpha 0}} = \exp(-\frac{\Delta H}{R \cdot T}) \tag{4.1}$$

where ΔH is the difference in heats of solution of manganese in austenite and ferrite phases; or:

(b) the Fe-C-Mn ternary phase diagram (refer to section 1.3).

When dual phase steel is annealed at temperature T for annealing time t, the variation of manganese contents in ferrite and austenite can be obtained through solving equations (4.8) and (4.11), the mean manganese contents in ferrite and austenite, $\overline{C_{Mn}^{\alpha}}$ and $\overline{C_{Mn}^{\gamma}}$, can be obtained by integrating equations (4.8) and (4.11) with the ferrite and austenite areas respectively, and the partitioning coefficient can be written as:

$$\frac{\overline{C_{Mn}^{\gamma}}}{\overline{C_{Mn}^{\alpha}}} = \frac{\dfrac{\int_{S_\gamma} C_{Mn}^{\gamma} dS_\gamma}{S_\gamma}}{\dfrac{\int_{S_\alpha} C_{Mn}^{\alpha} dS_\alpha}{S_\alpha}} = \frac{S_\alpha}{S_\gamma} \cdot \frac{\int_{S_\gamma} C_{Mn}^{\gamma} dS_\gamma}{\int_{S_\alpha^0} C_{Mn}^{\alpha} dS_\alpha} \tag{4.15}$$

4.2.2 Example

Take steel A with $C_{Mn}^{0} = 2.67\%$ as an example; the annealing temperature is 680°C, and the parameters are set as:

the final grain size of austenite/martensite $r_f = 0.56\mu m$;

the grain size of unit $R = 1.0\mu m$;

the final volume fraction of austenite/martensite $V_{\gamma}^{final} = 31.5\%$;

the dimension of the manganese-rich rim is at the boundary scale as $\Delta r = 0.001\mu m$

the maximum solubility of manganese in austenite at 680°C is taken as $C_{Mn}^{\gamma 0} = 5.0\%$;

and the maximum content of manganese in ferrite is set as $C_{Mn}^{\alpha 0} = 1.6\%$.

The distribution of manganese in ferrite is:

$$C_{Mn}^{\alpha} = 2.67 - 1.07\left(1 - erf\left(\frac{r - r_{\gamma} - \Delta r}{2\sqrt{D_{Mn}^{\alpha} t}}\right)\right) = 1.6 + 1.07 erf\left(\frac{r - r_{\gamma} - \Delta r}{2\sqrt{D_{Mn}^{\alpha} t}}\right)$$

$$\text{when } r_{\gamma} + \Delta r \le r \le 1 \times 10^{-4}$$

$$D_{Mn}^{\alpha} = 1.49 \exp\left(-\frac{233600}{8.31 \times 953}\right) = 2.31 \times 10^{-13}\ cm^2/s$$

The variation of manganese in austenite is:

$$C_{Mn}^{\gamma} = 2.67 + 2.33\left(1 - erf\left(\frac{r_{\gamma} - r}{2\sqrt{D_{Mn}^{\gamma} t}}\right)\right) = 5.0 - 2.33 erf\left(\frac{r_{\gamma} - r}{2\sqrt{D_{Mn}^{\gamma} t}}\right) \quad \text{when } 0 \le r \le r_{\gamma}.$$

$$D_{Mn}^{\gamma} = 0.16 \exp\left(-\frac{261700}{8.31 \times 953}\right) = 7.12 \times 10^{-16}\ cm^2/s$$

but Pussengoda[29] suggested that the diffusion rate of manganese in austenite may increase with increasing Mn levels to a maximum at ~3 pct Mn, so the diffusion rate of manganese in austenite at 680°C will be set instead as:

$$D_{Mn}^{\gamma} = 7.12 \times 10^{-15}\ cm^2/s$$

And the partitioning coefficient is given as:

$$\frac{\overline{C_{Mn}^{\gamma}}}{C_{Mn}^{\alpha}} = \frac{\dfrac{1}{\pi \cdot r_{\gamma}^{2}}}{\dfrac{1}{\pi \cdot \left((1\times10^{-4})^{2} - (r_{\gamma} + \Delta r)^{2}\right)}} \cdot \frac{\displaystyle\int_{0}^{r_{\gamma}} \left(5.0 - 2.33 erf\left(\frac{r_{\gamma} - r}{2\sqrt{7.12\times10^{-15} t}}\right)\right) \cdot r dr}{\displaystyle\int_{r_{\gamma}+\Delta r}^{1\times10^{-4}} \left(1.6 + 1.07 erf\left(\frac{r - r_{\gamma} - \Delta r}{2\sqrt{2.13\times10^{-13} t}}\right)\right) \cdot r dr}$$

The predicted manganese distribution across austenite and ferrite and the partitioning coefficient are shown in Figures 4.19 and 4.20.

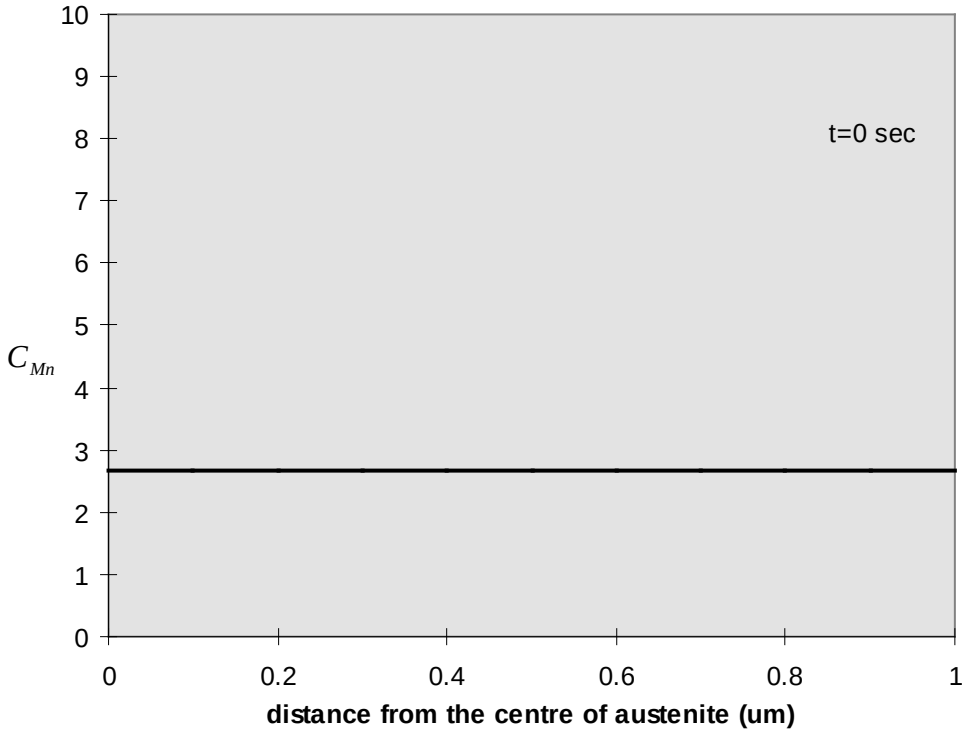

(a)

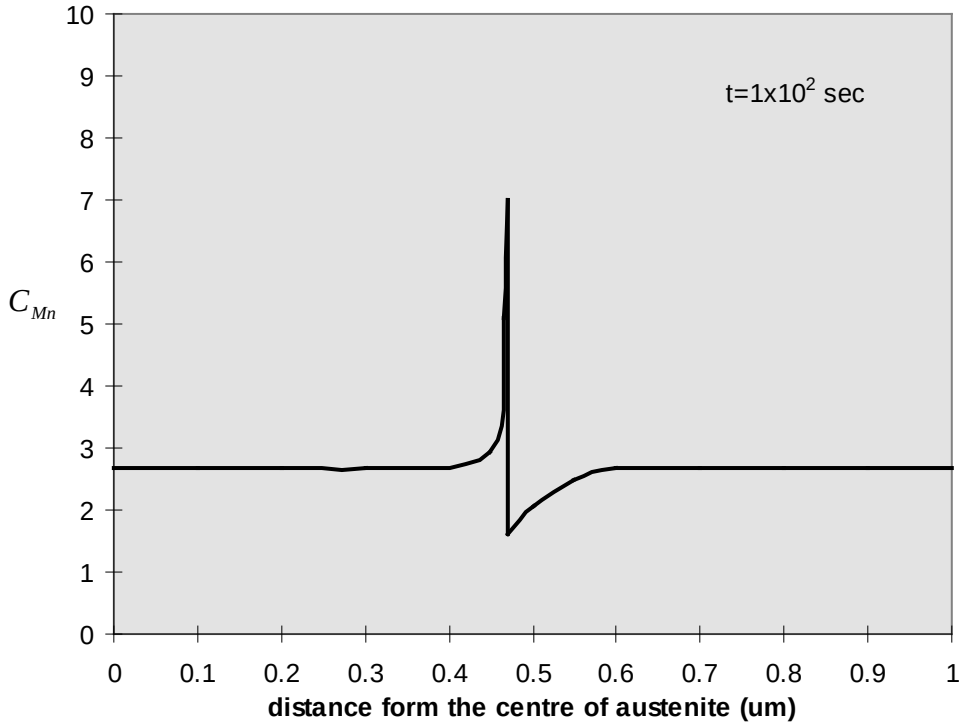
t=1x10^2 sec
C_{Mn}
10
9
8
7
6
5
4
3
2
1
0
0
0.1
0.2
0.3
0.4
0.5
0.6
0.7
0.8
0.9
1
distance form the centre of austenite (um)

(b)

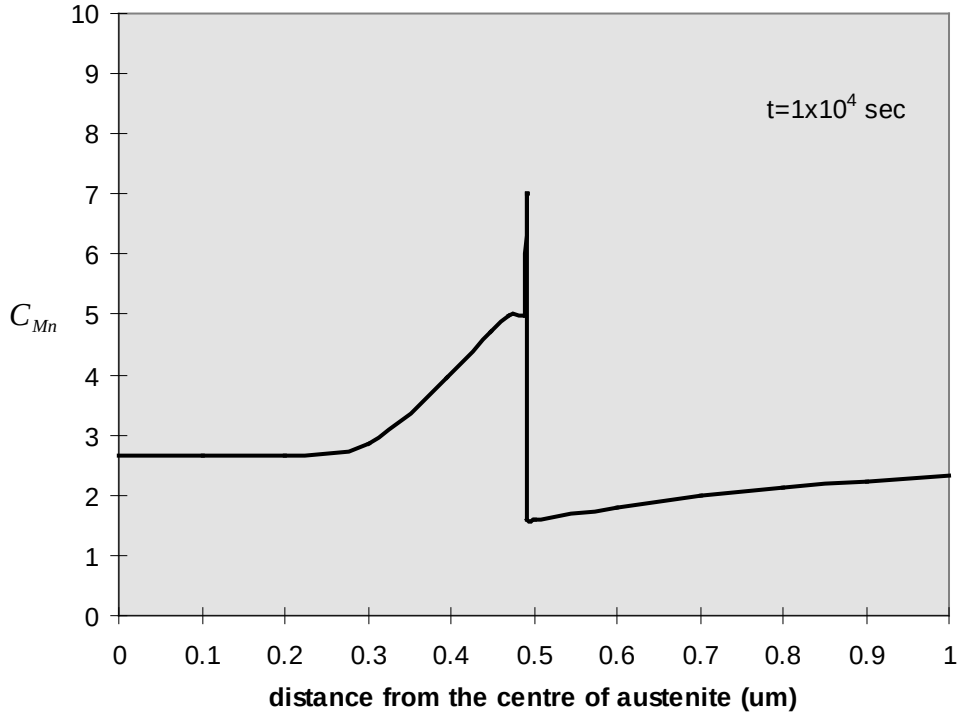
t=1x10^4 sec
C_{Mn}
10
9
8
7
6
5
4
3
2
1
0
0
0.1
0.2
0.3
0.4
0.5
0.6
0.7
0.8
0.9
1
distance from the centre of austenite (um)

(c)

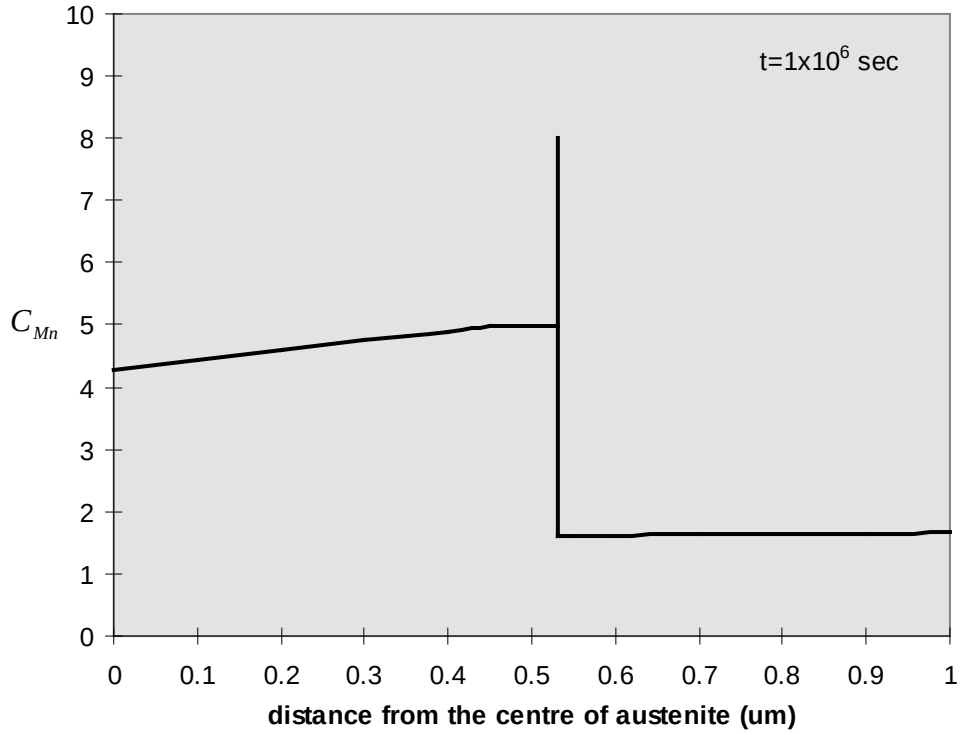

(d)

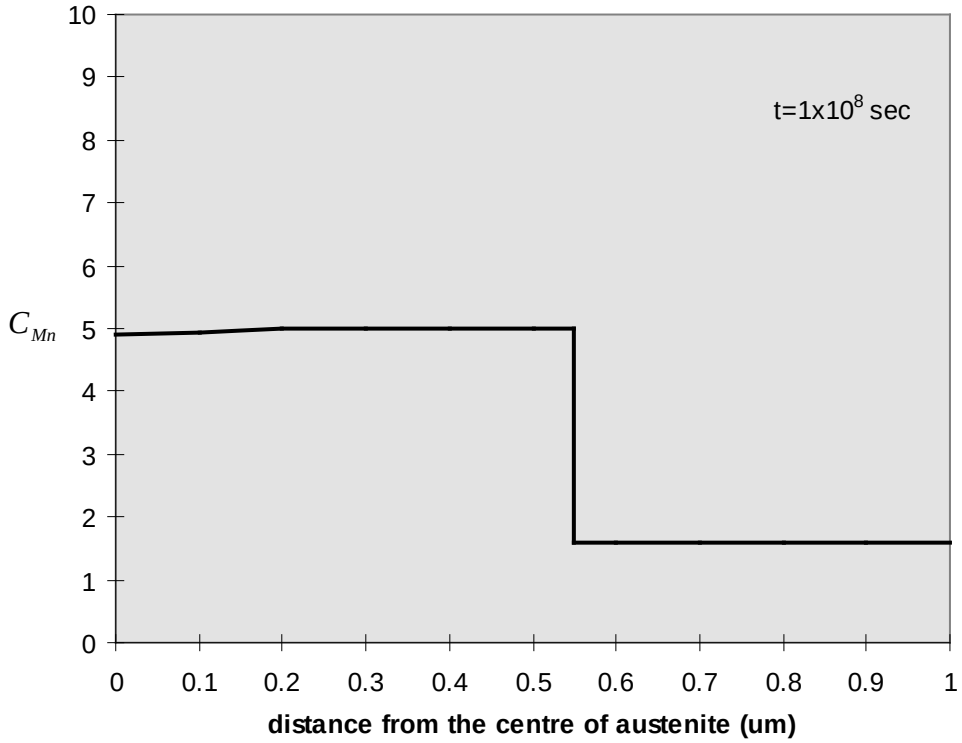

(e)

Figure 4.19 Prediction of manganese distribution as a function of annealing time at 680℃ for steel A

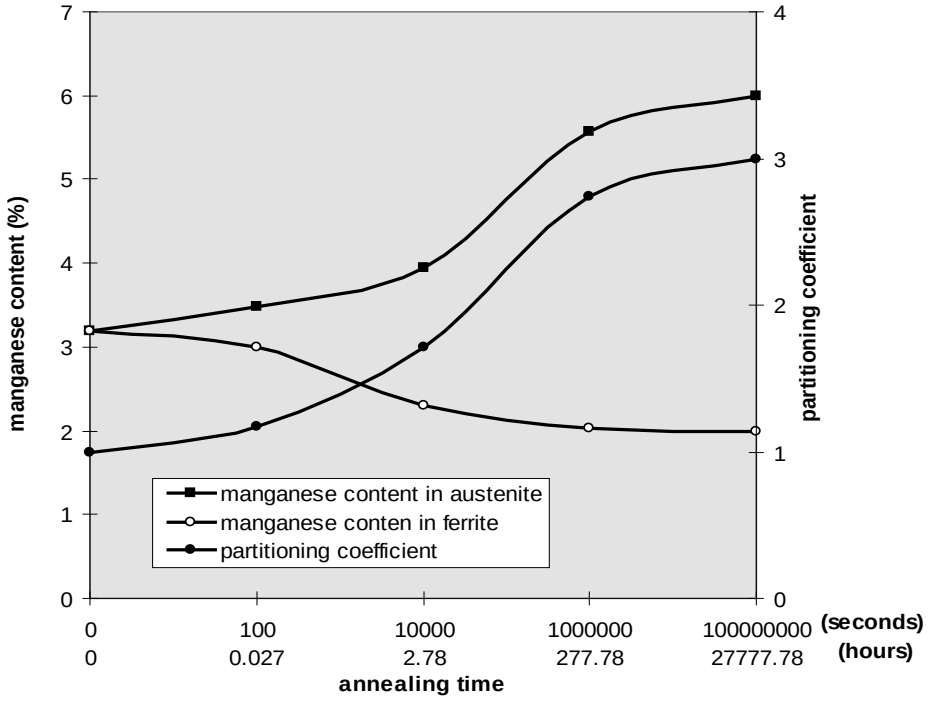

Figure 4.20 The predicted variation of manganese contents in austenite and ferrite and partitioning coefficient with annealing time (steel A)

The predicted effect of austenite grain size (diameter of fibre) on the partitioning is shown in Figure 4.21, the smaller the austenite grain size, the less time is needed to reach final equilibrium partitioning. The partitioning coefficient with small austenite grains is higher than that for large grains before reaching equilibrium.

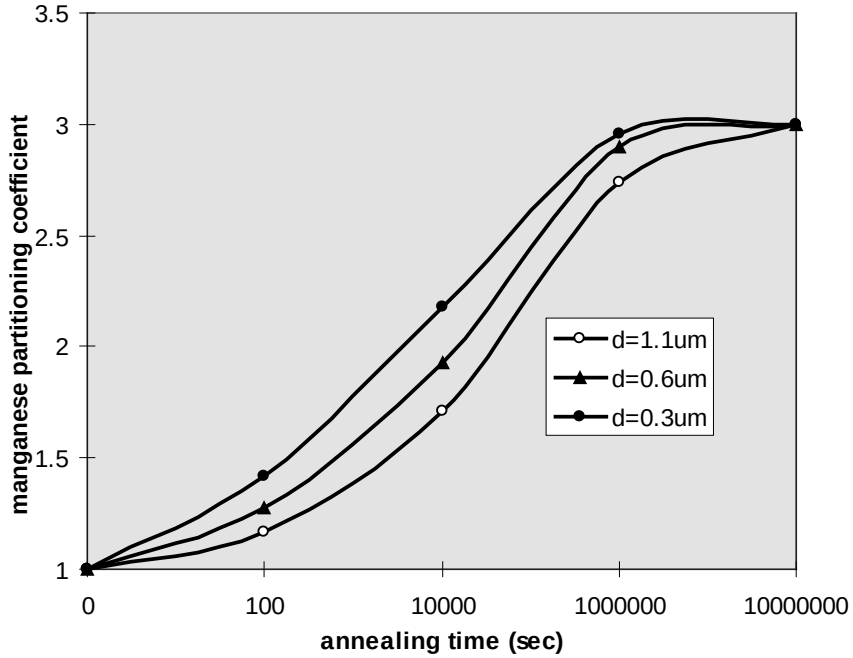

Figure 4.21 Predicted effect of diameter of austenite "fibre" on the Mn partitioning

4.2.3 Comparison with experiments

The comparison between theoretical and experimental data for steel A is shown in Figure 4.22. The predicted data (with $D^{\gamma}_{Mn} = 7.12 \times 10^{-15}\ cm^2/s$) are lower than the experimental data. This may be because the selected diffusion rate of Mn in austenite is lower than the true one. If instead, $D^{\gamma}_{Mn} = 7.12 \times 10^{-14}\ cm^2/s$, the predicted manganese partitioning is much closer to the experimental results, and supports the suggestion that the Mn diffusion rate in austenite increases with Mn[29].

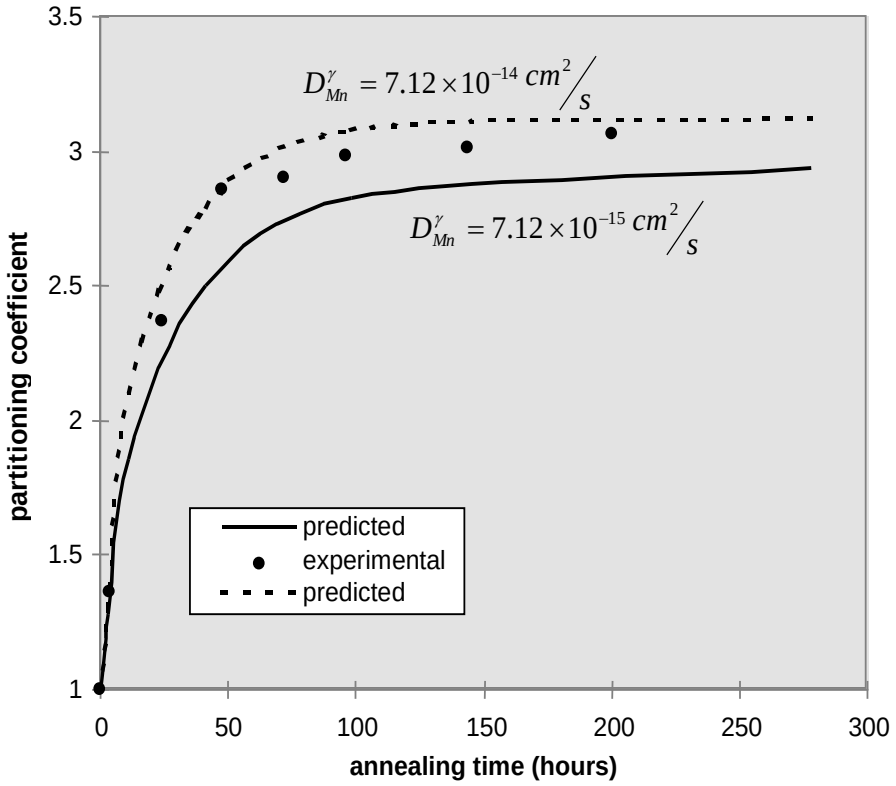

Figure 4.22 The comparison of partitioning coefficient between theoretical prediction and experimental data for steel A at 680℃

4.3. Mechanical properties of dual phase steels

The steels used for experiments are in the form of 40x40 mm^2 billets, which must be rolled into steel sheets to obtain elongated martensite and for testing. The rolling methods employed after pre-RA have an influence on the mechanical properties of as-rolled steel. This will be examined in the following section.

4.3.1 The effect of rolling

The rolling involved in the formation of dual phase steel not only changes the morphology of phases but can also introduce internal stress, both of which depend on the finishing rolling temperature and volume fraction of the second phase. In the case of quasi-isothermal rolling (see Figure 3.4), the phase composition during rolling is dependent on the rolling temperature. When rolling is carried out between Ac_3 and Ac_1 temperatures, both austenite and ferrite can be deformed and a fibrous martensite microstructure and low residual stress status are obtained. If the annealed steels were rolled below the Ac_1 temperature, the previously obtained martensite cannot be deformed and remains granular; high residual stresses are obtained. The reheating before rolling can also temper the martensite and make it more ductile, which depends on the reheating/rolling temperature. The residual stress and martensite hardness decrease with increasing rolling temperature due to tempering. The effect of quasi-isothermal rolling temperature on the tensile strength of as-rolled steel A is shown in Figure 4.23.

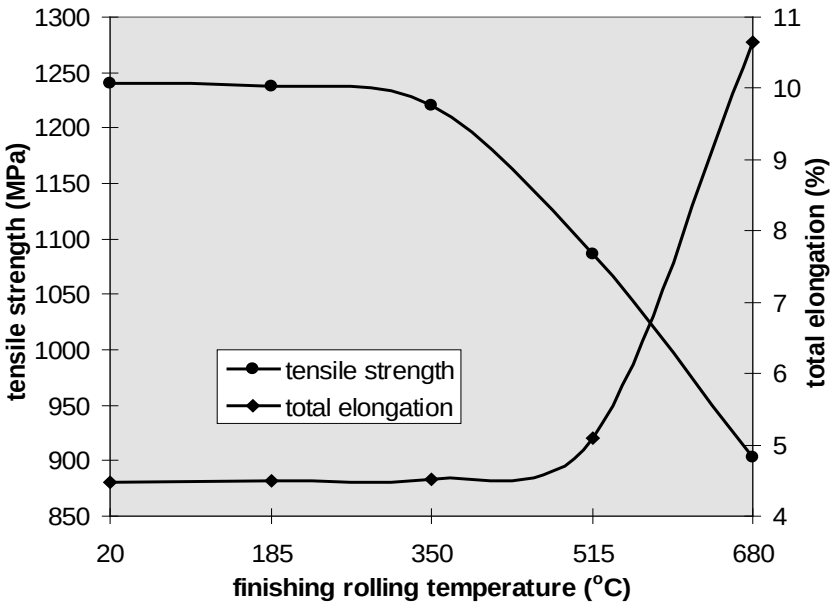

Figure 4.23 The effect of finishing rolling temperature of quasi-isothermal rolling on the tensile properties of steel A

The as-rolled steel has a high strength and low elongation when rolled at lower than 350°C because the steel received more cold deformation and minimal tempering resulting in high residual stresses. With increasing rolling temperature (ie. residual

stress decreasing and tempering effect increasing), the strength decreases and elongation increases. This decrease of strength and increase of elongation becomes sharp when the steel is rolled in the two-phase region, so the residual stress/martensite tempering during reheating and the phase composition during rolling are the primary factors for controlling the as-rolled dual phase steel properties.

Although there is not a big difference in the martensite morphology of dual phase steels which were continuously rolled (starting in austenite plus ferrite two phase region and cooling to room temperature, see Figure 3.4) or quasi-isothermally rolled in the two-phase region, the residual stresses in each rolling process are different, which results in the large difference in properties of as-rolled steel A (shown in Figure 4.24). The strengths of the continuously rolled steels are much higher than those of the quasi-isothermally rolled steels and the elongations much lower at the same volume fraction of martensite because of the higher work hardening of continuous rolling.

The effect of rolling on the strengths of ferrite and martensite can be evaluated by extrapolating from Figure 4.24(a). The finishing rolling temperatures for all percentage of martensite steels drop to room temperature for the continuous rolling so the strengthening of ferrite and martensite throughout the martensite content range can be thought to be the same, so the strengths of martensite and ferrite for continuous rolling steel can be extrapolated linearly as 2400 and 830MPa respectively.

But for quasi-isothermal rolling, the rolling temperature is different for different martensite fractions; the lower austenite fraction is obtained at lower rolling temperature, under which higher residual stresses are produced, so the strengthening of ferrite and martensite is different for different percentage of martensite (obtained under different rolling temperature). The strengths of martensite and ferrite can be extrapolated for quasi-isothermal rolling steels roughly as 2400 and 345MPa respectively for more than 30% martensite (ie higher rolling temperature). But for steel with 25% or less martensite, it is rolled at very different finishing rolling temperature for the different volume fractions of martensite. In this case, the strength of ferrite has been extrapolated individually using the martensite strength and the particular V_f datum point (light broken line for 20% martensite, as shown in Figure 4.24(a)).

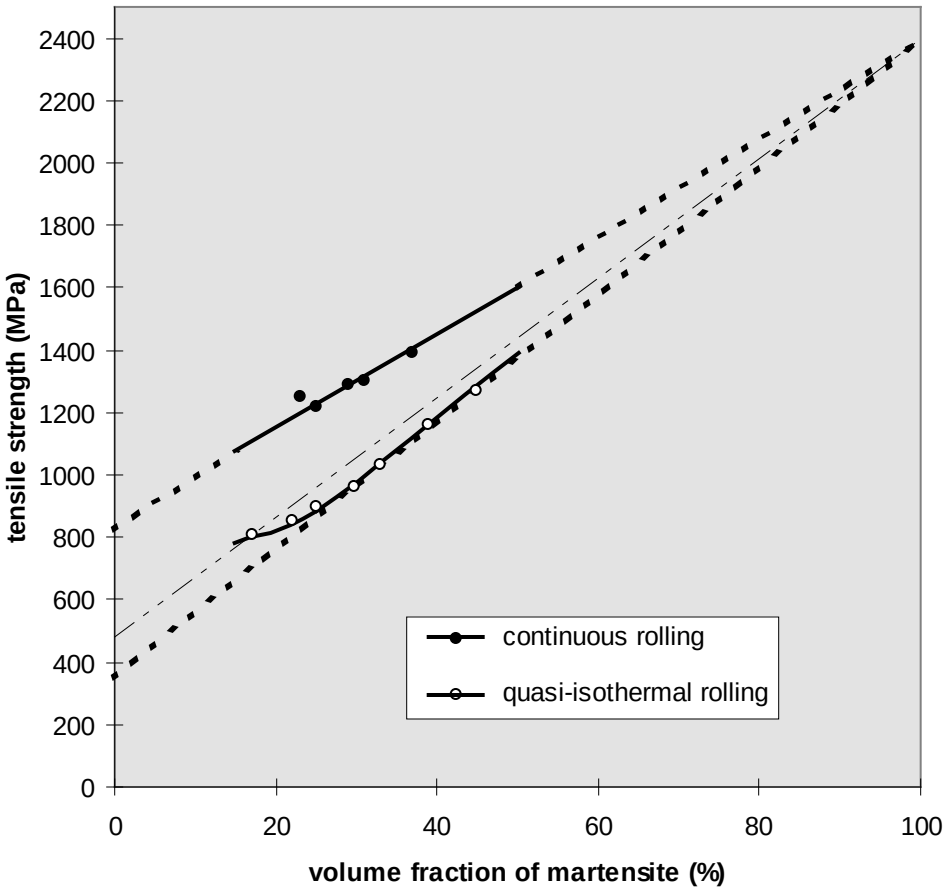

(a) tensile strength

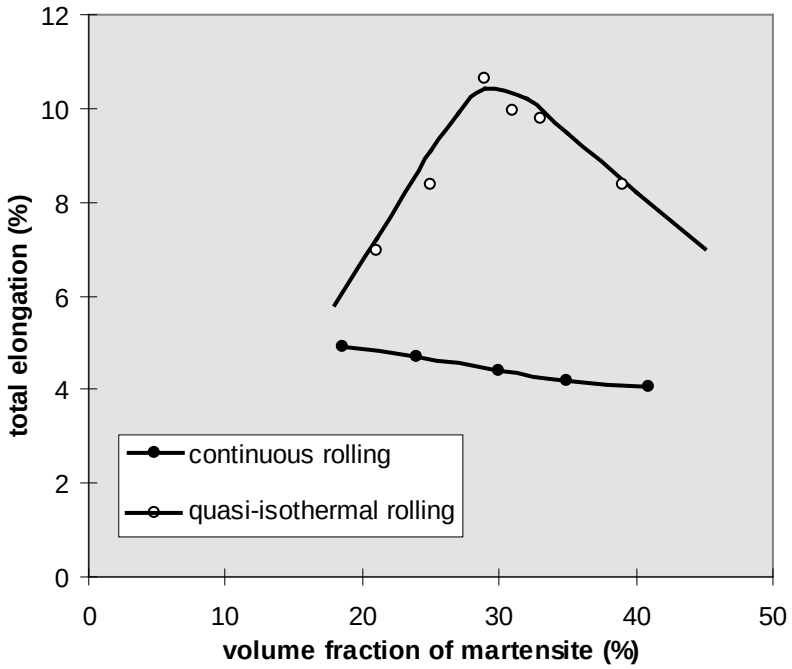

(b) total elongation

Figure 4.24 Properties of continuously rolled and quasi-isothermally rolled steels A as a function of volume fraction of martensite (varied with pre-RA temperature)

The strengthening of dual phase steel during rolling may thus be due to any of the follows: (1) deformation of ferrite grain (absence of polygonal ferrite); (2) increase of dislocation density (work-hardening, mostly in ferrite); (3) change in the shape, size of martensite; (4) strain-induced interphase precipitation[128].

4.3.2 The influence of pre-RA

Dual phase steels were quasi-isothermally rolled after pre-RA at the annealing temperature. The partitioning and stress status in steels are governed by the pre-RA temperature and time, so the mechanical properties of as-rolled dual phase steels are also influenced by pre-RA.

The influence of pre-RA temperature on the mechanical properties of as-rolled dual phase steel is shown in Figure 4.25. All tensile tests were carried out on samples cut parallel to the rolling direction.

The tensile strength of as-rolled steel A is at its lowest at 680°C and strengths of the other steels increase with increasing annealing temperature. The % elongations are highest at 680°C for steel A, 720°C for steel B, 730°C for steel C, and 710°C for steel D respectively.

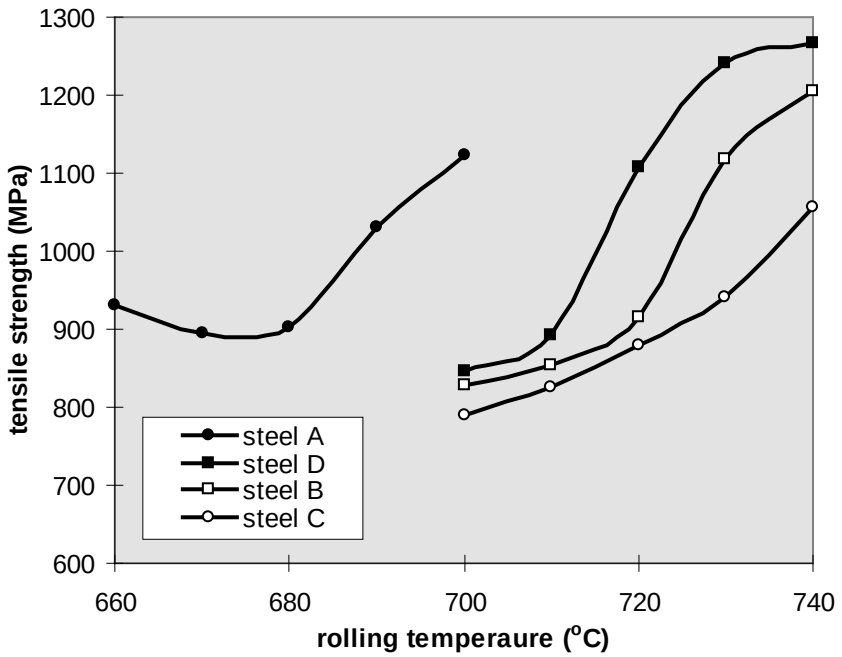

(a) tensile strength

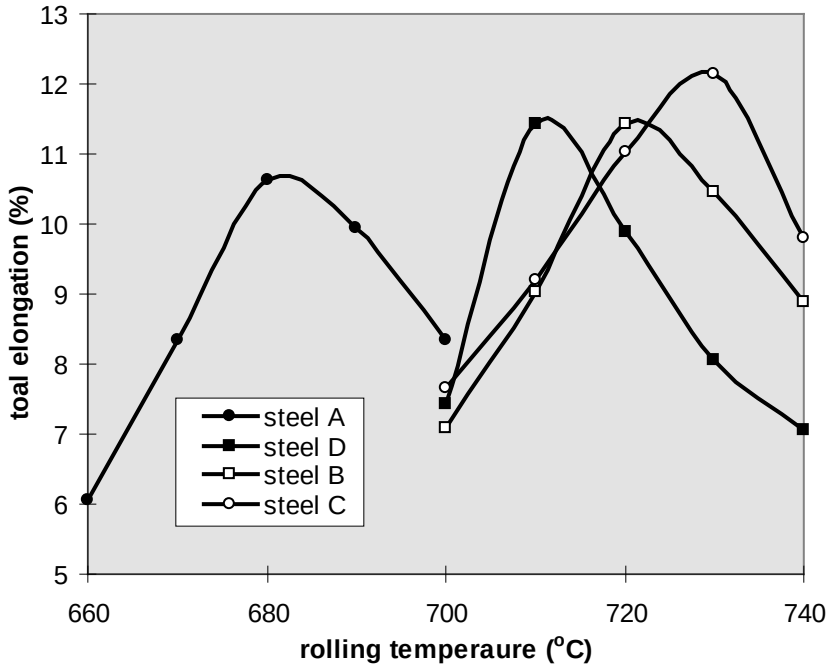

(b) total elongation

Figure 4.25 The effect of pre-RA/rolling temperature on the tensile properties of as-rolled dual phase steels

The effect of pre-RA temperature on the properties of as-rolled dual phase steels works through the three following aspects:

(1) Residual stresses are produced by thermomechanical treatment (rolling), which enhance the strength and lower the ductility of steel. The lower the rolling temperature, the higher the residual stresses.

(2) Carbide precipitation takes place at low temperature, which hardens steel with a loss of elongation. The volume fraction of carbide decreases with increasing temperature.

(3) Volume fraction of martensite is a function of temperature, the volume fraction of martensite increases with increasing temperature.

The residual stresses and carbide precipitation at the lower annealing temperature and the higher volume fraction of martensite at the higher temperature lead to an increase in the tensile strength and a decrease in the elongation to fracture. The contribution of the above three factors results in a maximum elongation and minimum strength of as-rolled steels with variation of annealing temperature. The best combination of tensile strength and elongation was thus obtained by annealing and rolling the dual phase steels at their

intercritical annealing temperatures because no carbides and appropriate amounts of martensite are formed at these temperature.

At the intercritical annealing temperature, the properties of as-rolled dual phase steels are a function of annealing time, as shown in Figure 4.26. As discussed in section 4.1, the volume fraction of martensite and manganese partitioning increase and reach the final equilibrium values with increasing annealing time. The strengths of steels do increase with increasing annealing time with the same trend as martensite content and manganese partitioning. The final strengths of all steels are very close regardless of the difference in their chemical compositions. That suggests that the strength of dual phase steels primarily depends on the volume fraction of martensite as originally stated by Davies[49].

The variation of elongation with annealing time is different to that of strength: the elongations of the four steels increase in the initial 48 hours and then decrease with further annealing time. The contribution of martensite content and manganese partitioning to the ductility of the steel is different. The ductility increases with increasing partitioning and decreasing martensite volume fraction. The combination of increase of partitioning and % martensite with annealing time produces the maximum elongation after 48 hours annealing.

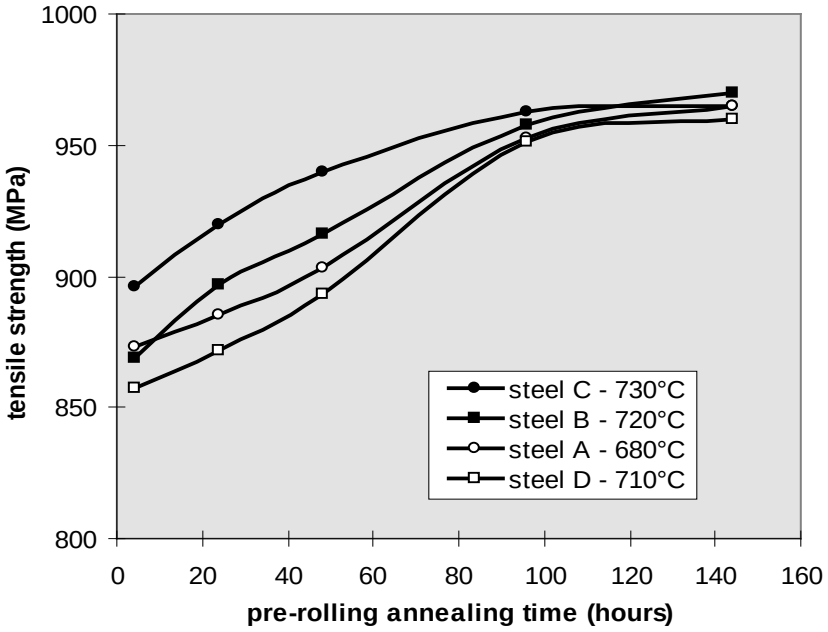

(a) tensile strength

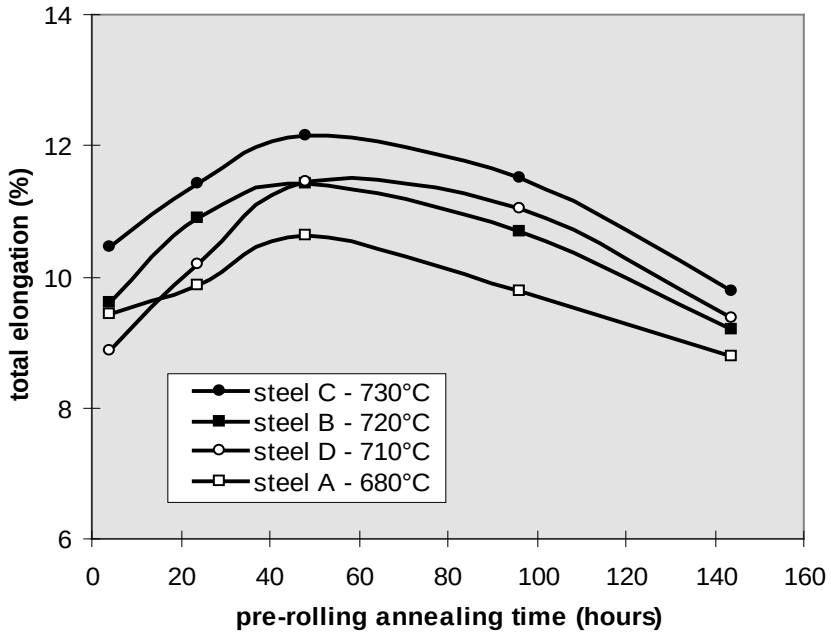

(b) total elongation

Figure 4.26 The tensile properties of as-rolled dual phase steels as a function of annealing time

The elongation of higher carbon and manganese steels (such as steel A) is lower than that of lower carbon and manganese steel (steel C for example) when the steels are rolled at their intercritical annealing temperature. That is because the intercritical annealing temperature for the higher carbon and manganese steel (680°C for steel A) is lower than that for the lower carbon and manganese steel (730°C for steel C), therefore, the residual stress in the as-rolled higher carbon and manganese steel is a little higher than that in the as-rolled lower carbon and manganese steel because of the small difference in their rolling temperatures. The elongation of as-rolled steel is much more sensitive to residual stress than the strength.

4.3.3.The influence of cooling condition after post-RA

The tensile properties of steel A are also functions of post-RA time and cooling condition after post-RA at 680°C (same as the intercritical temperature). Water-quenched steel has the highest tensile strength and lowest elongation, the martempering produces the lowest strength and highest elongation and the strengths of steels decrease and elongations increase with annealing time for all three cooling conditions (shown in Figures 4.27).

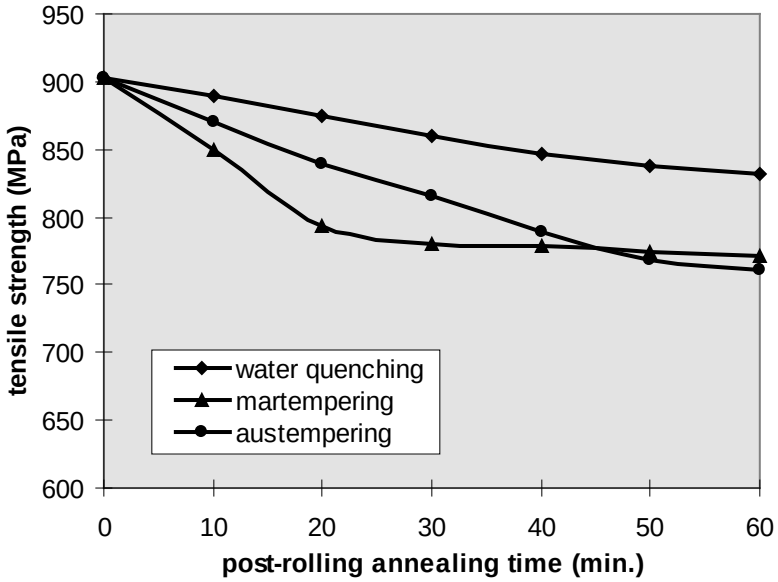

(a) tensile strength

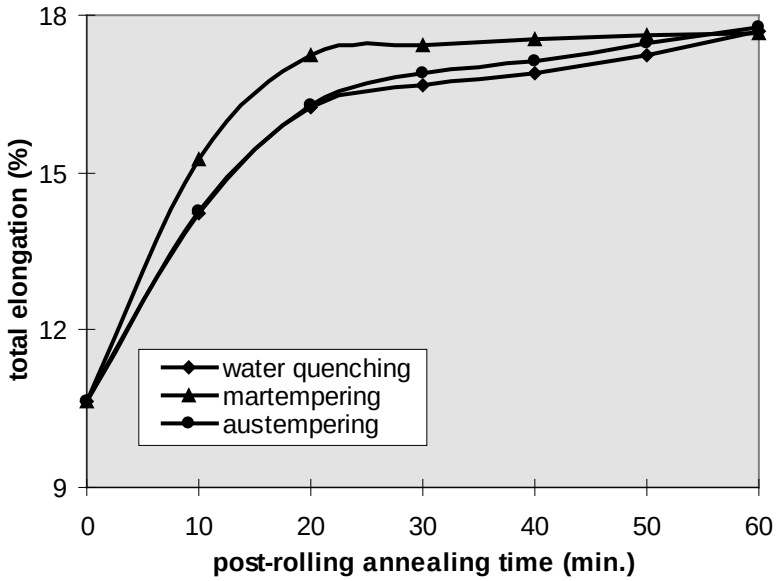

(b) total elongation

Figure 4.27 The influence of cooling condition and post-RA time on the tensile properties of post-RA dual phase steel A

The strength and ductility of dual phase steel depends on the hardness of the second phase for a given volume fraction. The hardness of the reinforcing phase (martensite or bainite) is a function of cooling condition - the water-quenched martensite is harder than both the martempered martensite and austempered bainite, so the water-quenched dual phase steel is the strongest and most brittle.

According to the above results, the post-RA for as-rolled dual phase steels is chosen as annealing at their pre-RA temperature (to keep the same volume fraction of martensite and manganese partitioning as the as-rolled steels) for 30min and then water quenching.

The sharp decrease of strength and increase of elongation in the initial post-RA are probably caused by the release of residual stresses and elimination of dislocations due to tempering and recrystallization of the deformed grains, and the further smooth decrease of strength and increase of elongation are due to the morphology change of martensite from “long fibres” to granules.

4.3.4 The influence of post-RA

As discussed in 4.3.2, the internal residual stress can be thought to be eliminated by the post-RA due to the tempering and recrystallization of deformed grains, so the contribution of residual stress to tensile strength is reduced to zero. The manganese partitioning after post-RA can be thought to stay the same with that after pre-RA because of the relatively short post-RA time (30min. comparing with 4-144 hour pre-RA). The properties of post-RA steels are mainly controlled by the volume fraction of martensite (the morphology of martensite can be thought to be the same after the same time of post-RA).

The variations of the tensile properties of the post-RA dual phase steels with pre-RA temperature (same as the post-RA temperature) are shown in Figures 4.28. With increasing post-RA temperature, the tensile strengths of all dual phase steels linearly increase (meanwhile total elongations decrease), except steel A below 670°C. The strengths of post-RA steels are much lower and elongations much higher than those of as-rolled dual phase steels because of the release of residual stresses due to tempering and recrystallization.

Steel A is exceptional because that there are some carbides formed below 670°C; which makes the strength of the steel higher and the elongation lower.

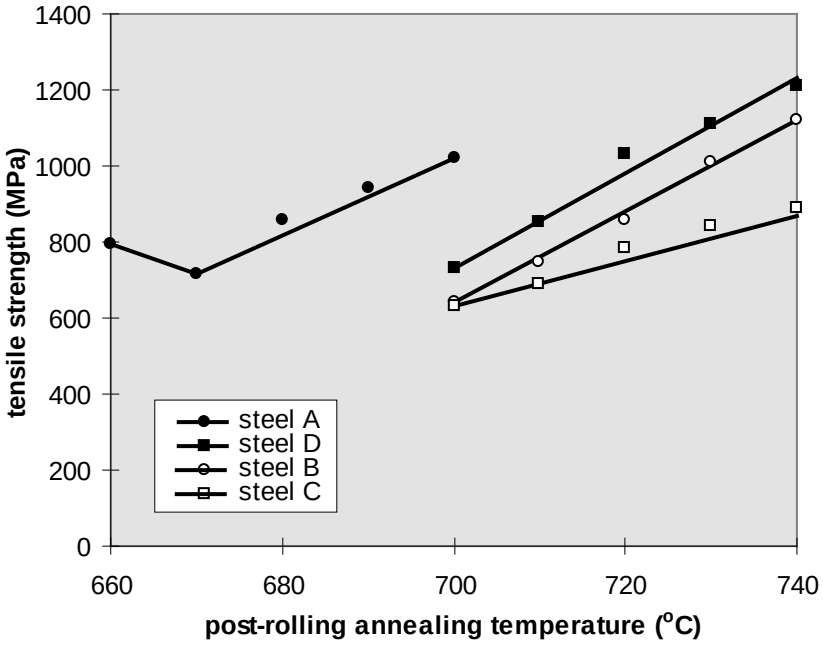

(a) tensile strength

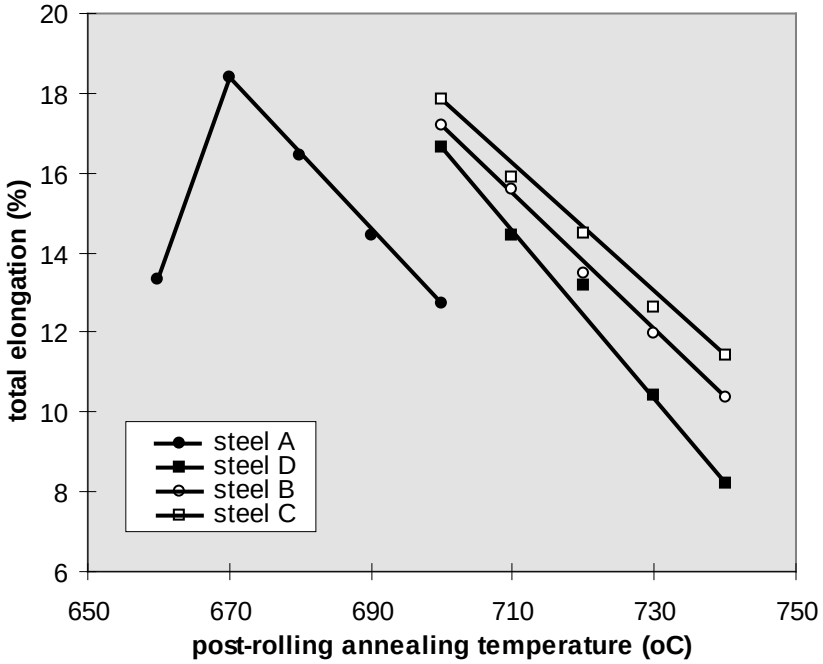

(b) total elongation

Figure 4.28 The tensile properties of post-RA dual phase steel as a function of annealing temperature

The variation of properties of post-RA steels with pre-RA time is similar to that of as-rolled steels (shown in Figure 4.29). The difference is that the elongation of higher carbon and alloy steel (steel A) is higher than that of lower carbon steel (steel B), which is probably because the martensite grain size of higher carbon steel is smaller owing to

the higher retarding effect of more carbides during annealing and lower intercritical annealing temperature of higher carbon steel (the microstructures of steels A and B are shown in Figure 4.30).

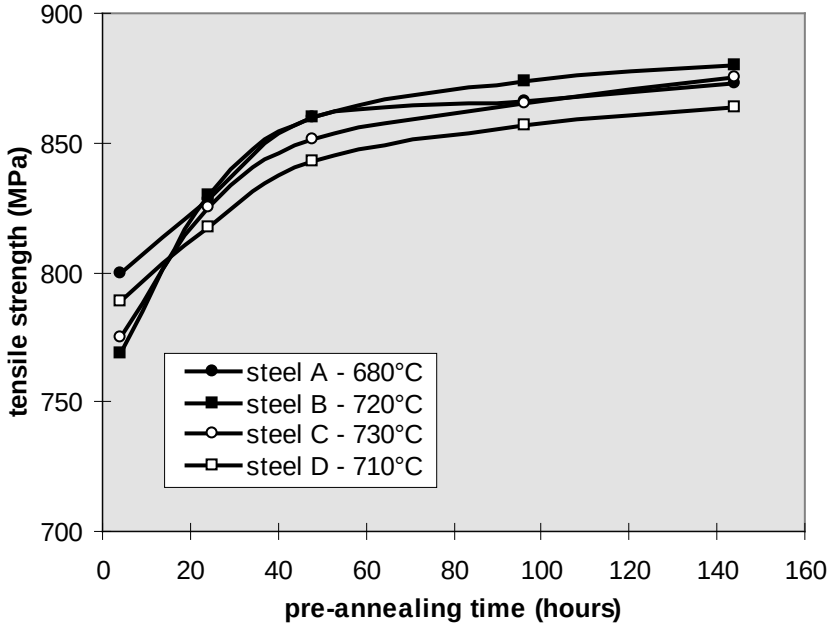

(a) tensile strength

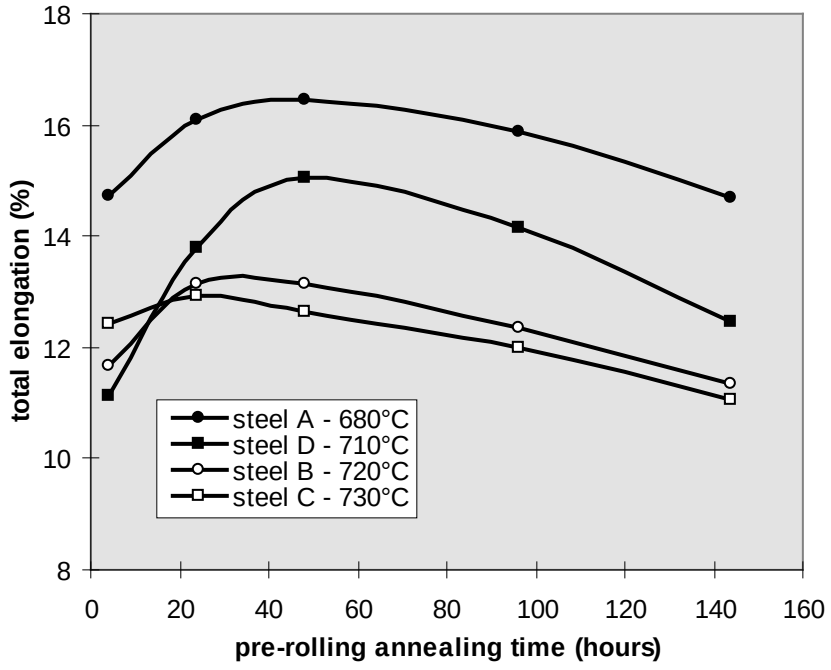

(b) total elongation

Figure 4.29 Variation of properties of post-RA steels (30 min) with pre-RA time

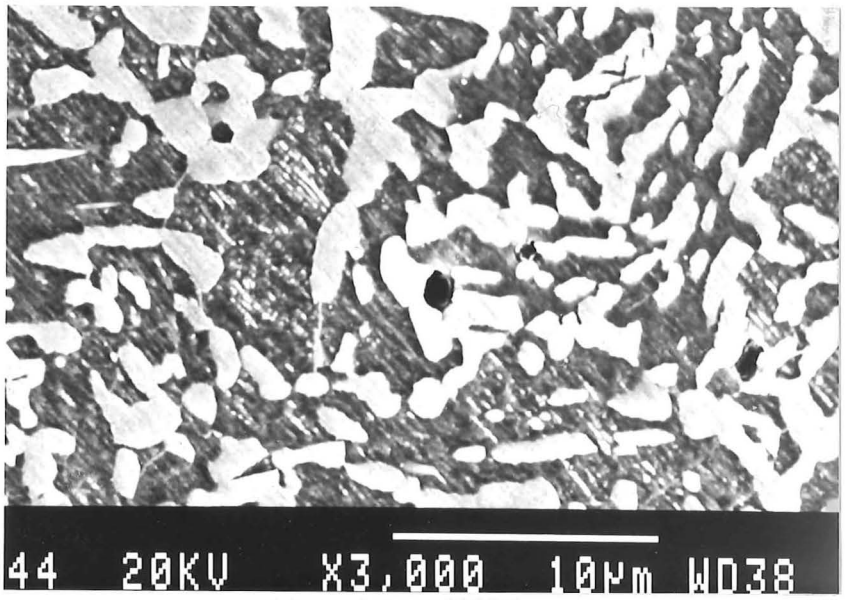

(a) steel A at 680°C

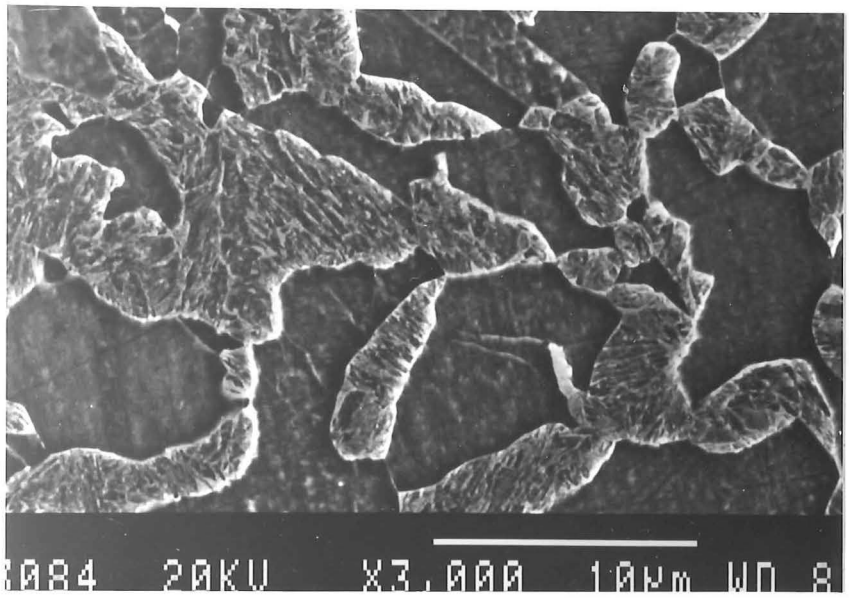

(b) steel B at 720°C

Figure 4.30 SEM microstructure of post-RA steels

The true stress-true strain curve is usually used to analyse the work-hardening behavior and the material fracture process. The recorded engineering stress-engineering strain curves have been replotted as true stress-true strain relationships for steel A both in the as-rolled and post-RA states (shown in Figure 4.31). Also shown is the true stress-strain curve based on Mileiko's theory (refer to Chapter 2 for details). This has been generated using values for the true strength and true uniform strain for the martensite and ferrite phases from the literature[51].

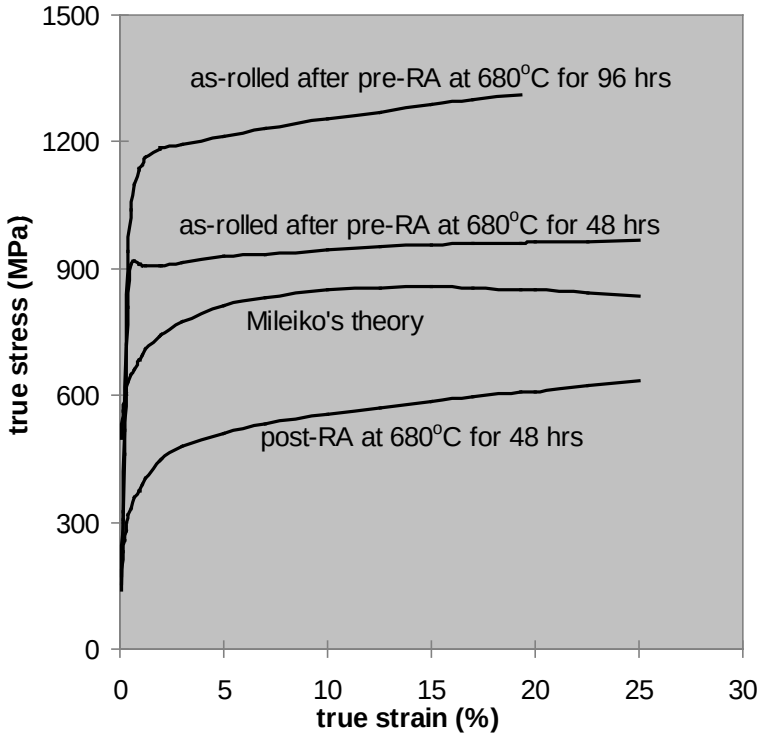

Figure 4.31 True stress-true strain curves for steel A under different conditions

4.3.5 Fractography

The fracture of the as-rolled steel has the appearance of delamination (Figure 4.32). Whilst the material is not fabricated from individual laminae, the hot-rolling process has produced ribbons of martensite oriented in the rolling plane of the steel sheet. Due to the combination of these very strong aligned ribbons and the ductile ferrite matrix the fracture has occurred preferentially along the axis of the ribbon orientation. The fracture in fibrous dual phase steels has been shown to be by void nucleation at the martensite-ferrite interface[23] and in this case, the majority of this interface is in the plane of rolling and hence the jagged fracture surface.

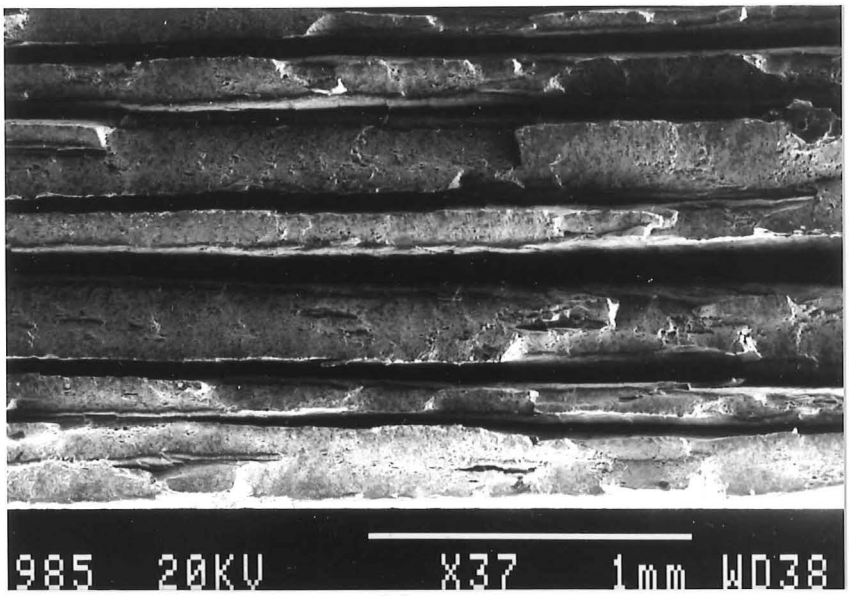
985 20KV X37 1mm WD38

(a)

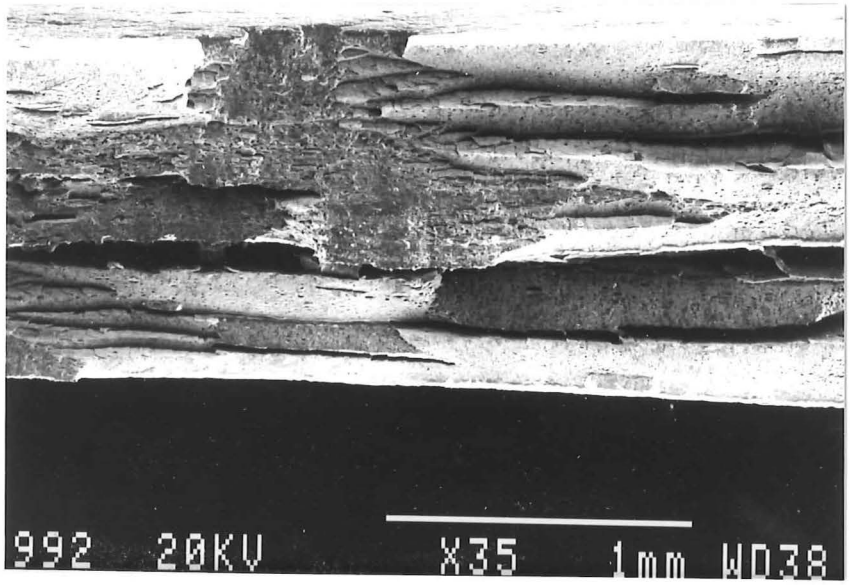
992 20KV X35 1mm WD38

(b)

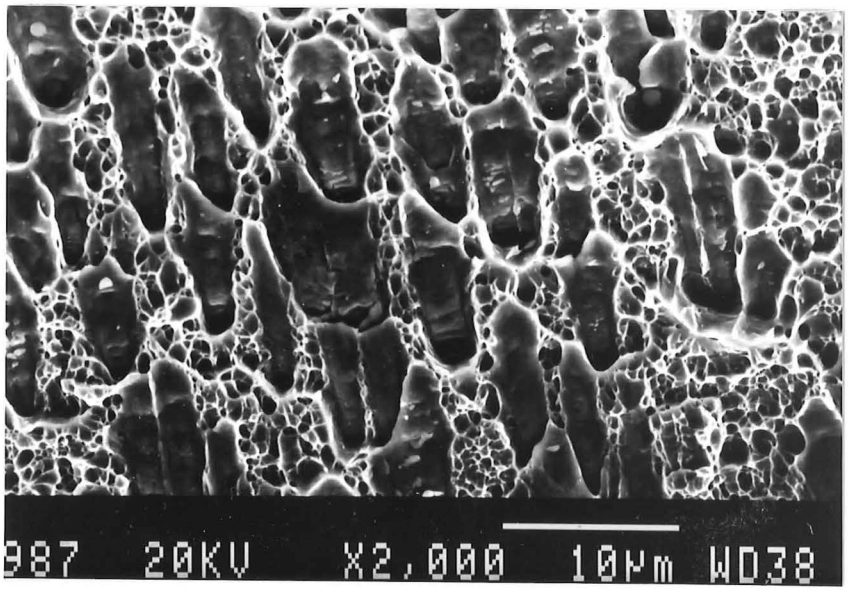
987 20KV X2,000 10µm WD38

(c)

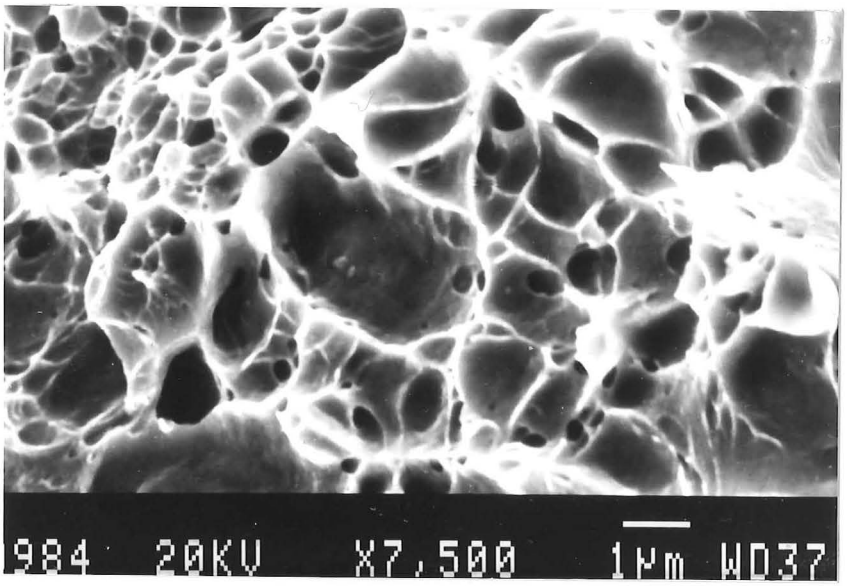

(d)

Figure 4.32 Fracture surfaces of as-rolled steel A

As the strength of the dual phase steel decreases (due to a decrease in the aspect ratio), this "laminar type" failure decreases. For example, the tensile strength and elongation of steel with pre-annealing at 680°C for 96 hours are 1312 MPa and 19.3% respectively, and eight "layers" can be seen in the fracture surface (see Figure 4.32(a)). In contrast, for the same steel and conditions but with only 48 hrs pre-annealing, the tensile strength was 968 MPa with an elongation of 24%, and the laminar nature of the fracture is reduced showing 5 apparent layers (Figure 4.32(b)). Figures 4.32(c) and (d) show the ductile failure in the ferrite regions of these layers.

The fracture surface of steel after post-RA at 680°C for 48 hours is different from that in the as-rolled state. From Figure 4.33, it can be seen that there is no "delamination" taking place and no martensite pull-out, the plastic deformation takes place on the whole fracture surface and the ductility is higher than that of the as-rolled steel. This is due to the change in the martensite morphology and volume fraction.

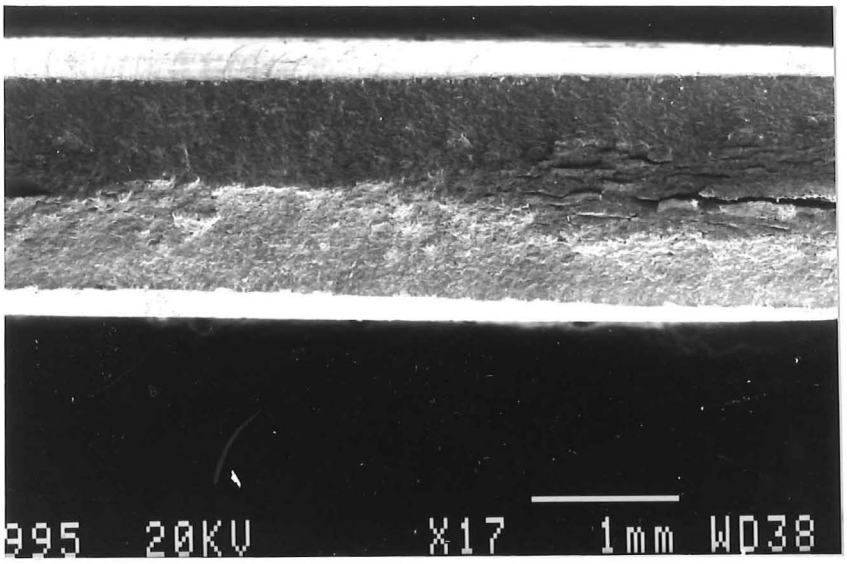

(a)

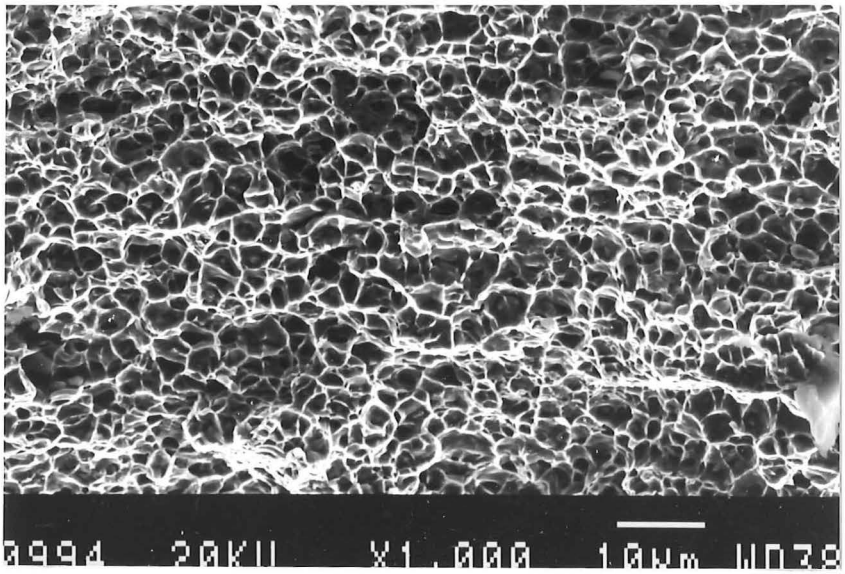

(b)

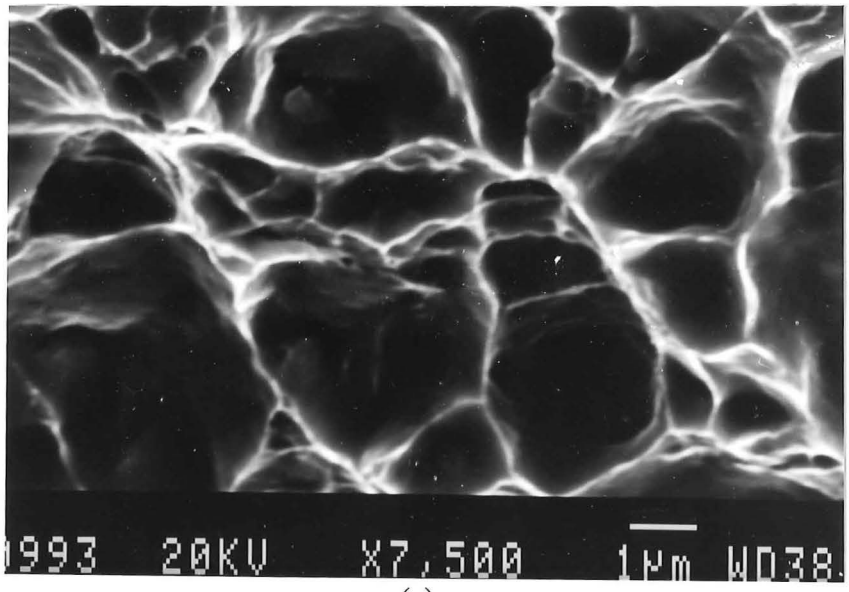

(c)

Figure 4.33 Fracture surfaces of steel A after post-RA

Two different ways of void nucleation in dual phase steels have been observed; these are decohesion at ferrite-martensite interfaces and fracture of martensite[62]. The crack initiation of elongated martensite dual phase steels are shown in the longitudinal microstructures of dual phase steels near the fracture surface (Figure 4.34). For long martensite (as-rolled) dual phase steel, cracks initiate in the martensite-ferrite interface and propagate along the axial direction of martensite "fibre" and eventually result in martensite break (Figure 4.34(a)), which gives the steel high strength and low elongation; with short post-RA time, the martensite shrinks into short "fibres" and voids form at the martensite-ferrite interface at the end of these short "fibres", the effective stress tranfer between martensite and ferrite makes the martensite break under applied tensile load (Figure 4.34(b)). For the granular martensite steel obtained from long post-RA, cracks form at the martensite-ferrite interface and grow around the martensite and into the ferrite matrix during tensile test - high elongations can be obtained, no fracture of martensite has been observed (Figure 4.34(c)). All the three crack locations correspond to the crack initiation in continuous fibre, short fibre, and particle reinforced metal composites.

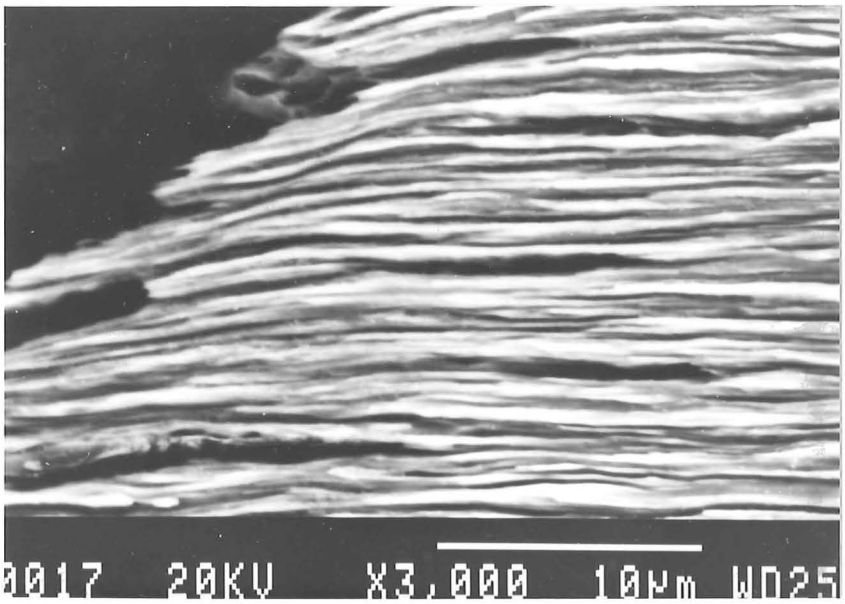

(a) as-rolled, long martensite "fibre"

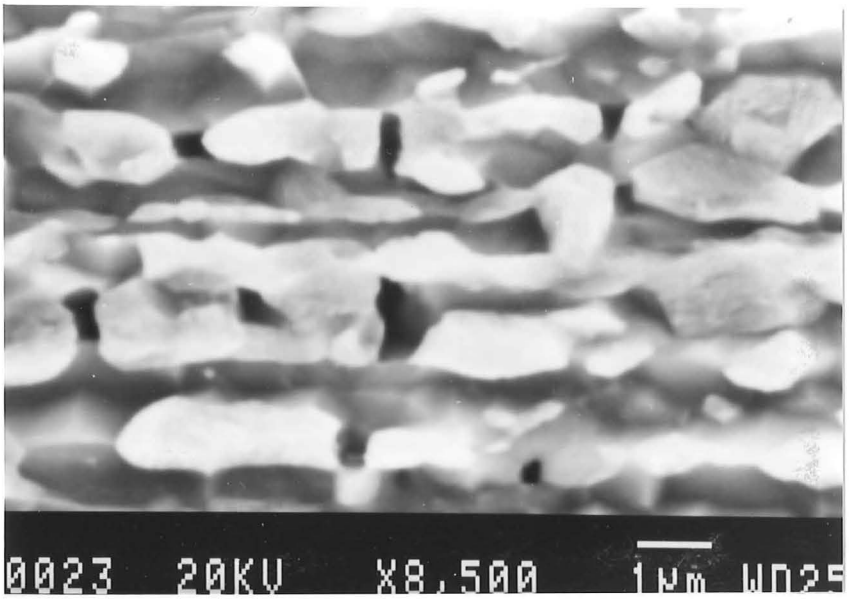

(b) post-RA at 680°C for 30min, short martensite "fibre"

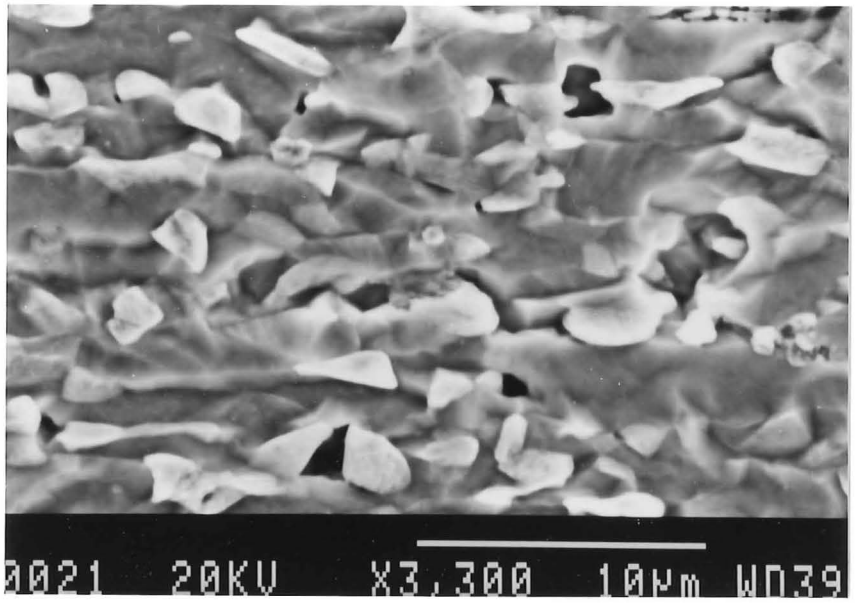

(c) post-RA at 680°C for 48hours, granular martensite

Figure 4.34 Longitudinal cross-section near the fracture surfaces of steel A

4.3.6 Work-hardening behaviour

The strain hardening behavior of dual phase steel has been related to the dislocation density in the ferrite phase[35]. The distribution of dislocation tends to be non-uniform with regions of high dislocation density in the ferrite adjacent to the transformed martensite grains and a low density in the interior of the ferrite grains. The plastic strain behaviour of dual phase steel consists of several processes[52-56], and cannot always be described by a single n value over the whole plastic strain range.

The following stress-strain equation is often used to analyse the deformation behavior of steel:

$$\sigma = k \cdot \varepsilon^n \tag{4.16}$$

where, σ is the true stress, ε is the true plastic strain, k and n are constants, in which n is the work-hardening exponent of the steel.

Thus, n can be calculated from the plot of $\lg\sigma$ versus $\lg\varepsilon$,

$$n = \frac{\Delta \lg \sigma}{\Delta \lg \varepsilon} \tag{4.17}$$

or $$n = \varepsilon_c \tag{4.18}$$

where, ε_c is the true uniform strain, The plots of σ *vs* ε on a logarithmic scale are shown in Figure 4.35 for steel A under different conditions.

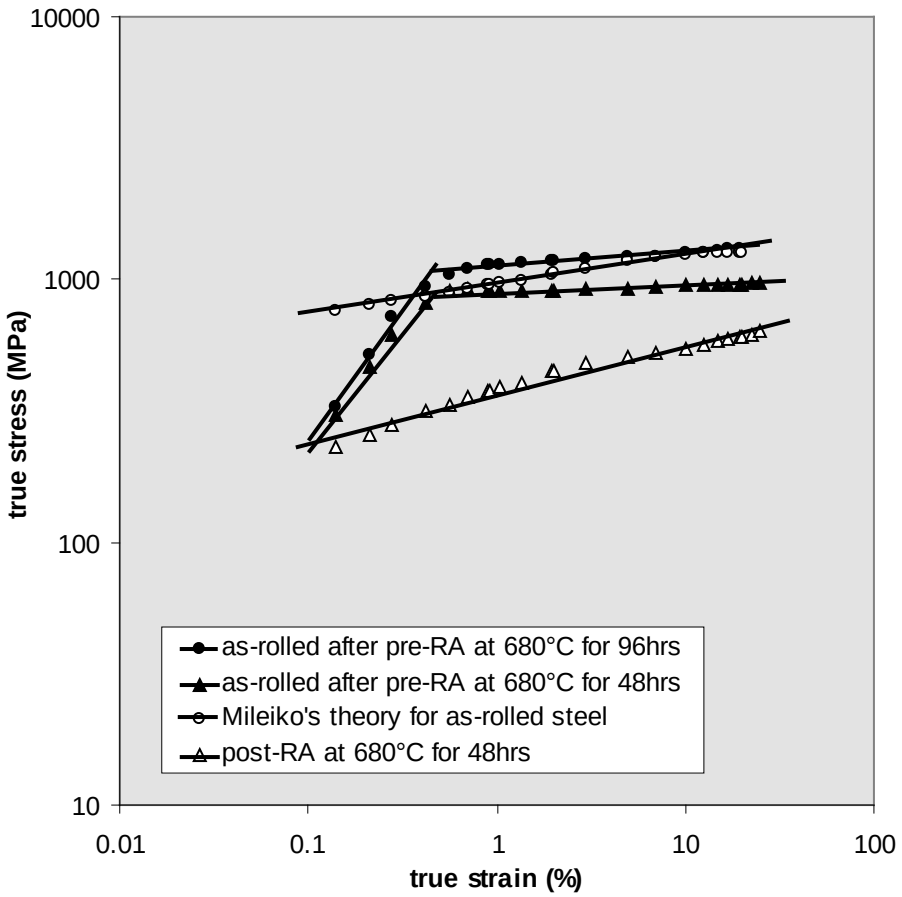

Figure 4.35 The log-log plot of σ # ε curves for dual phase steel A (transformed from Figure 4.31)

It is apparent that the as-rolled steel contains two distinct work-hardening processes with the exponent, n, for the initial strain-hardening process being much higher than for the second process. The first work-hardening stage occurs at low plastic strain where the ferrite phase deforms plastically and the martensite elastically; the work hardening in this stage is primarily controlled by the dislocation distribution and density in the ferrite[(55)]. The second stage (in the high strain range) is associated with the plastic deformation of both ferrite and martensite. Because of the high degree of "fibering" induced by the rolling process, not only is the martensite phase in the form of thin ribbons, but the ferrite matrix is sandwiched between these ribbons in a similar way to the ferrite in pearlite colonies. This could explain the rapid work-hardening seen in the early stages in the as-rolled material (a similar behavior is also observed in pearlite).

In contrast with as-rolled steel, the post-RA material's behavior shows a similar trend to that predicted by Mileiko's theory although there is a slight indication of a bimodal distribution but the magnitude is considerably lower than in the case of the as-rolled steel and the transition is more gradual.

4.4. Summary

During annealing, the elements of dual phase steel will distribute in austenite and ferrite depending on their characters. Manganese, the austenite stabiliser, concentrates in austenite; the force to drive the manganese diffusion between austenite and ferrite is the difference in heats of solution of manganese in these two phases.

The volume fraction of austenite increases with annealing temperature but the manganese partitioning decreases. Both austenite volume fraction and manganese partitioning increase with annealing time at a certain temperature until reaching equilibrium values.

The intercritical annealing temperature is set as the temperature at which about 30% martensite was obtained. The intercritical annealing temperature, determined by the steel composition, decreases with increasing carbon content.

Nucleation of austenite during annealing takes place throughout the whole isothermal holding period and the continuous nucleation combined with austenite growth contributes to the increase of austenite volume fraction. With increasing annealing time,

the needle-like austenite formed initially from intermediate quenching retains its "fibrous" morphology, and the continuously formed austenite is granular, similar to that formed in the intercritical annealing process and grows much faster than the "fibrous" austenite.

The redistribution of manganese in ferrite and austenite during annealing takes place as follows:

(1) manganese diffuses from ferrite to the ferrite-austenite boundary and precipitates; a manganese-rich rim is formed at the boundary;

(2) manganese diffuses from the manganese-rich rim at the ferrite-austenite boundary to austenite.

The diffusion of manganese in austenite is the dominant process because of the much lower diffusion rate of manganese in austenite. The modelling analysis results agree well with the trend of the experimental data but are lower in values, which is thought to be due to the increase of the manganese diffusion rate in high manganese steel.

The model established predicts that the grain size of austenite affects the manganese partitioning; the time needed to reach final equilibrium partitioning in finer grained material is less than that in coarse grained material.

The rolling after annealing makes the austenite elongated and introduces internal residual stresses and dislocations (ie. work-hardening); all of which can be eliminated by post-RA due to the tempering and recrystallization. The residual stresses and dislocation are produced mainly in the ferrite and decrease with increasing rolling temperature (same as the pre-RA temperature).

Tensile strength and elongation of as-rolled dual phase steels depend on the internal residual stress and martensite volume fraction. The optimum combination of tensile strength and elongation of as-rolled steels can be achieved by rolling at their intercritical annealing temperature; lower temperature will promote carbide precipitation/introduce high residual stress and higher temperature increases the volume fraction of martensite, both of which will degrade the ductility of the steel.

The strength of post-RA dual phase steels is strongly dependent not only on the volume fraction of martensite but on the morphology of the second phase; a high aspect ratio martensite "fibre" increases the strength of the material but lowers the ductility.

Decrease in strength and increase in elongation of post-RA steel with increasing post-RA time are the results of residual stress relief, martensite morphology change and presence of the polygonal ferrite due to tempering and recrystallization during post-RA. The estimated strength of post-RA in ferrite obtained from extrapolating is much lower than that of as-rolled steel.

Work-hardening of as-rolled dual phase steels comprises two stages with different exponents. The higher exponent in the first stage is primarily controlled by the dislocation distribution and extra high density in the ferrite caused by the rolling, and the lower one in the second stage is associated with the plastic deformation of the both ferrite and martensite. However, the work-hardening behaviour of post-RA dual phase steels can be expressed by a single exponent.

Chapter 5

Results and Discussion, Artificial Dual Phase Steel

5.1 Components for artificial dual phase steel

5.1.1 Reinforcing wire

To simulate the dual phase steels with "fibrous" martensite, eutectoid steel wire with 0.8% carbon was selected to produce an artificial dual phase steel. The phase transformation and tensile properties of steel wire under the fabrication conditions are examined in this section to ascertain the "fibre" properties of the composite. It is also necessary to see how the fabrication procedure affects these properties.

5.1.1.1 The tensile properties of as-received wire

The reinforcing wire is made in eutectoid steel, which is approximately 100% pearlite, by extensive cold drawing. During wire drawing the ferrite is elongated; the microstructural scale of the phases decreases commensurately with the wire diameter. The cell structure, formed at a relatively low strain, controls the strength of the steel wire and the key to the high strengths developed lies in the extremely fine ferrite cell size generated during wire drawing. The cell size in steel wire scales approximately with the wire diameter d, which is related to the initial wire diameter d_0 and the true drawing strain ε_T, that is:

$$\varepsilon_T = 2\ln(\frac{d_0}{d}) \qquad (5.1.1)$$

The strength of the wire (assumed to be proportional to the square root of cell diameter) varies with d_0 and ε_T as[(132)]:

$$\sigma \sim \frac{\exp(\varepsilon_T / 4)}{d_0^{1/2}} \qquad (5.1.2)$$

The relationship between strength and the diameter of the drawn wire is shown in Figure 5.1.1. High strength wire can be obtained with finer initial eutectoid pearlite and larger drawing strain (i.e. strain hardening).

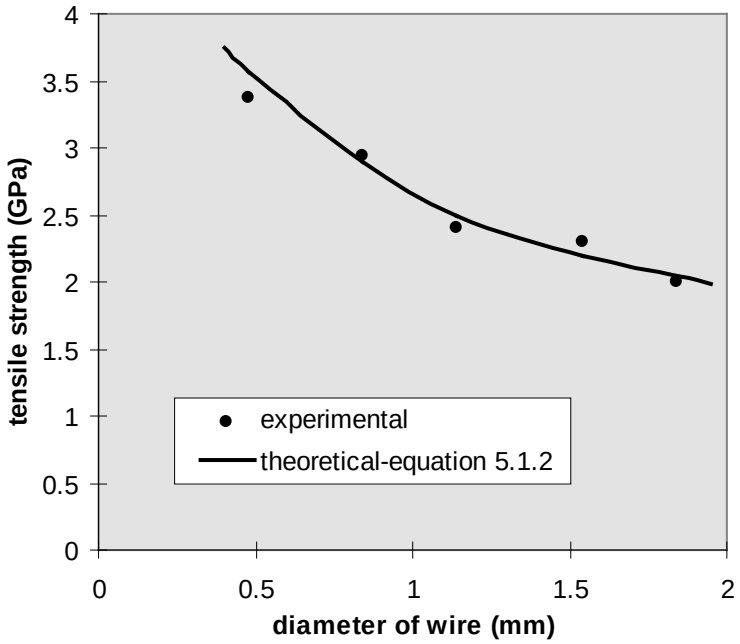

Figure 5.1.1 The influence of diameter on the tensile strength of as-received wire

5.1.1.2 The effect of heat-treatment on the wire

As we know, the high strength of the steel wire arises in part from the heavy deformation during cold drawing, but this work-hardening is affected by the following heat-treatment (as shown in Figure 5.1.2). Tensile strength decreases and total elongation increases for both plain wire and copper coated wire within an annealing time of 200sec. Furthermore, the tensile strength and elongation of plain wire slowly decreases and increases respectively with longer annealing times, whereas, those of copper coated wire keep constant.

The sharp changes of strength and elongation of wires are due to the phase transformation as the oriented pearlite transforms into austenite at the high temperature and equiaxed pearlite will form during air cooling. The microstructure change due to this heat-treatment is shown in Figure 5.1.3. The further smooth decrease in tensile strength and increase in elongation of plain wire for longer times is caused by decarburisation; a further thirty minutes of heat-treatment at 950°C reduces the strength by about 50MPa.

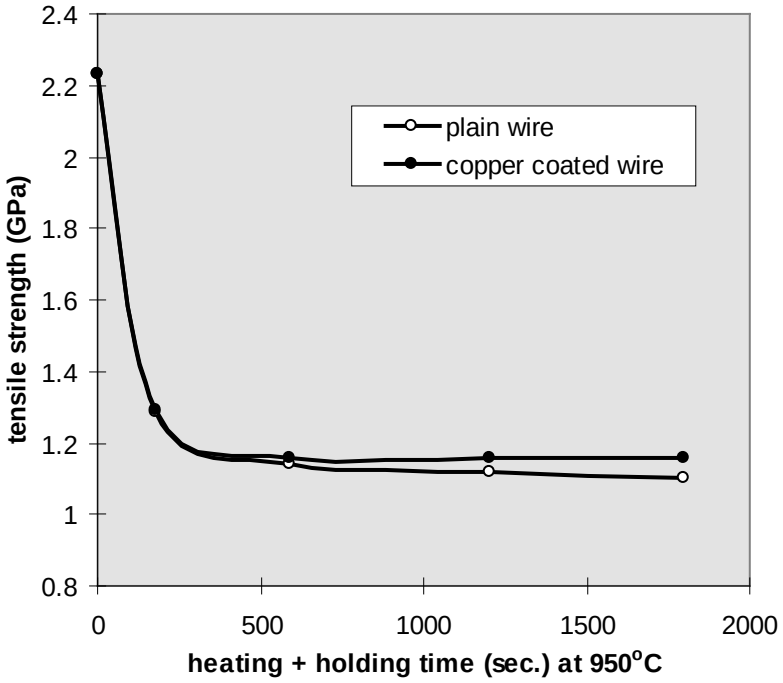

(a) tensile strength

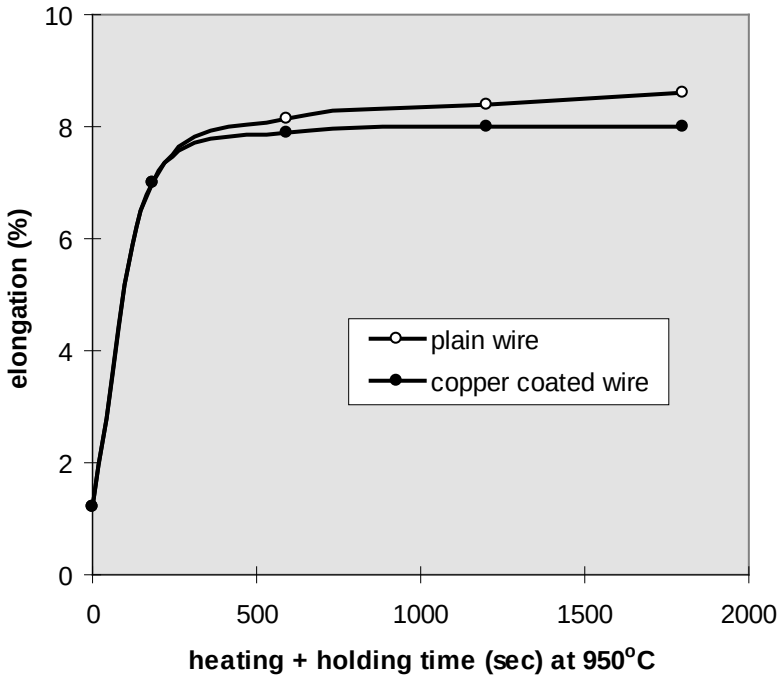

(b) total elongation

Figure 5.1.2 Effect of heat-treatment (heating and holding at 950°C, then air cooling) on tensile properties of wire (a) tensile strength, and (b) total elongation

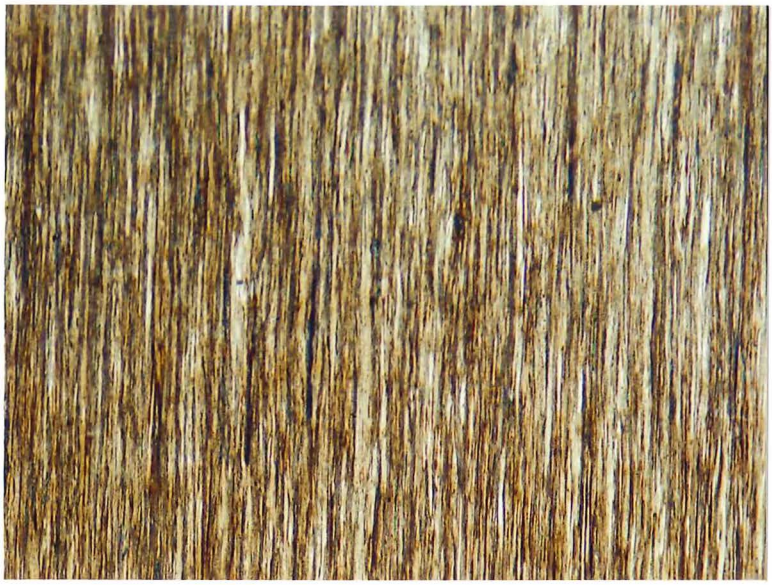

(a) as-received plain wire

(b) center of wire heated at 950°C for 30min

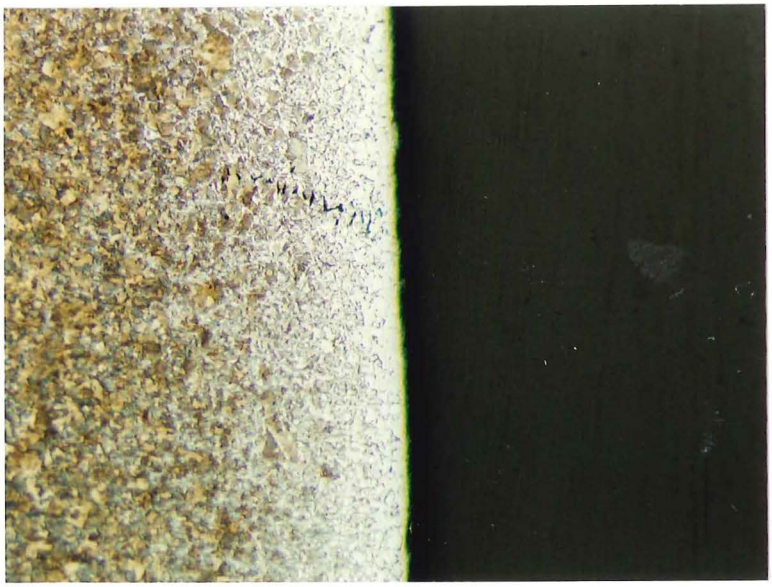

(c) surface of plain wire heated at 950°C for 30min

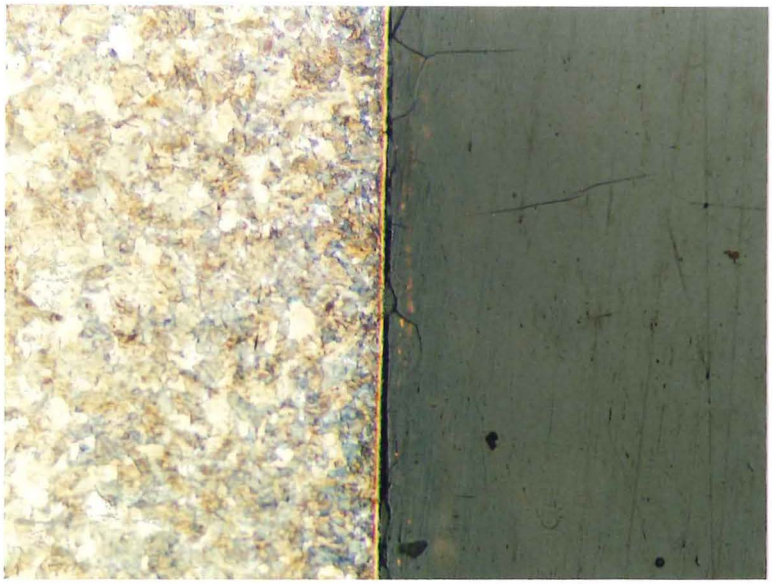

(d) surface of copper-coated wire heated at 950°C for 30min

Figure 5.1.3 The microstructure change due to heat-treatment (a,) (b) and (c) plain wire, (d) copper-coated wire (× 115)

5.1.1.3 Phase transformation of steel-wire

The structure in the as-received wire is strained pearlite, which is relatively brittle but can easily be subjected to heat-treatment. Normally, the hard phases such as martensite and bainite are desirable to achieve significant reinforcing effect in dual phase steels.

In order to check the effect of phase transformation on the properties of wire, the as-received wire was heated and held at 950°C for different times followed by air-cooling (this is to simulate the fabrication process of the composite), then was heated at 800°C for 2min and quenched into water or 260°C oil (water quenching, or austempering) to obtain martensite or bainite (as shown in Figure 5.1.4 (a)). The results are shown in Figures 5.1.4 (b) and (c). Both the tensile strength and elongation of water-quenched martensitic wire are the lowest.

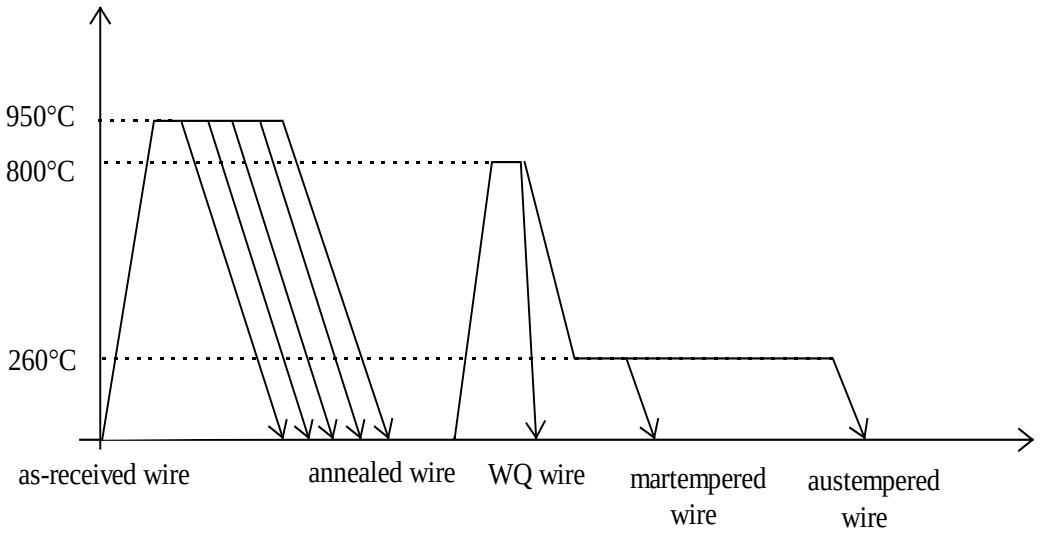

(a) experimental procedures

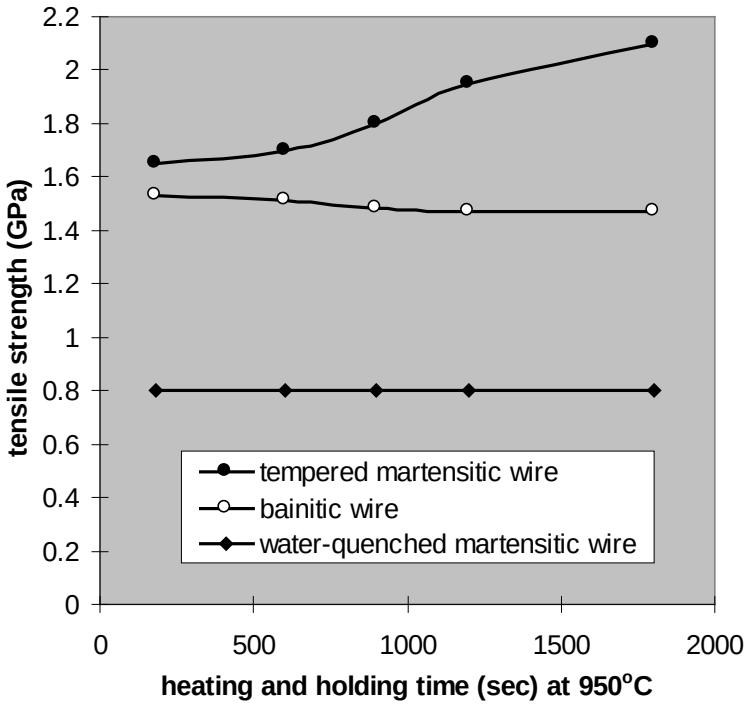

(b) tensile strength

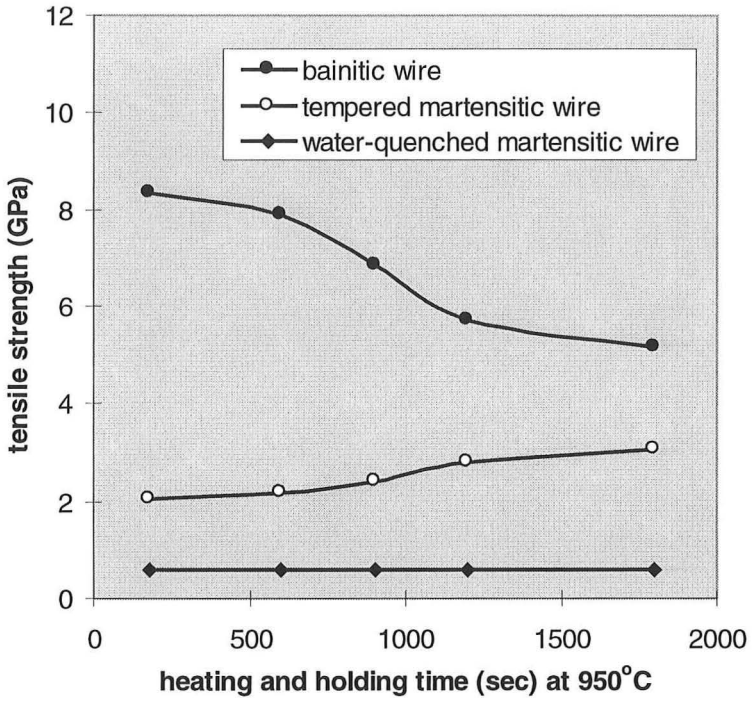

(c) total elongation

Figure 5.1.4 Effect of heating and holding time (at 950℃) on the tensile properties of martensitic and bainitic wires

Internal stresses are produced during transformation of austenite to martensite by water-quenching, which will produce micro-cracks in the boundaries of the prior austenite grains[133]. The existence of these cracks results in intergranular fracture of water-quenched martensitic wire under tensile load (the fracture surface is shown in Figure 5.1.5); this is why the low strength and elongation were obtained for as-quenched martensitic wire.

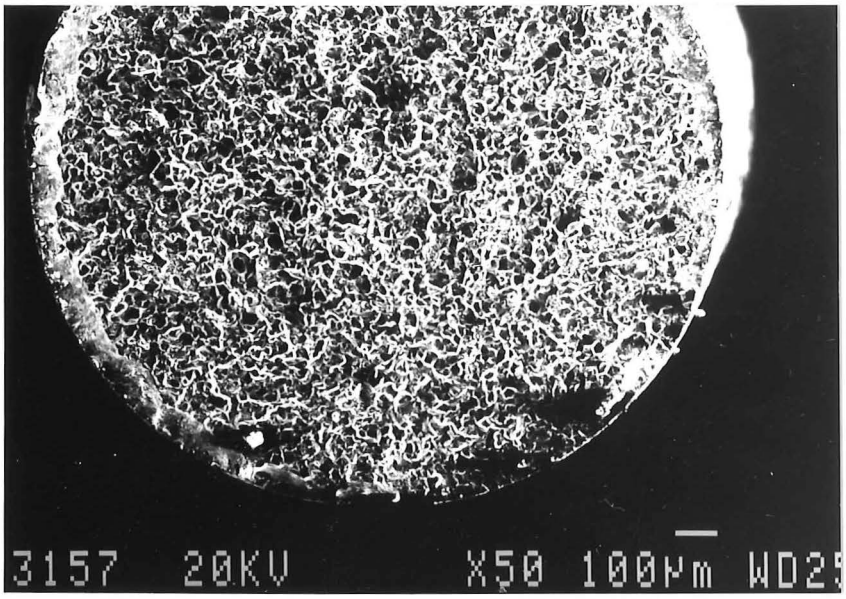

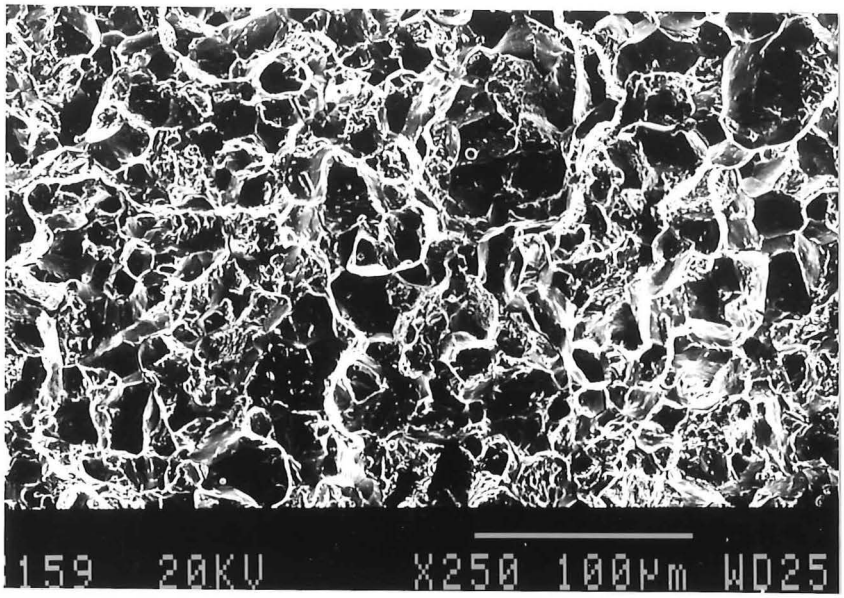

Figure 5.1.5 Fracture surfaces of as-quenched martensitic wire

The tempering followed water-quenching makes the martensite transform to ferrite plus carbide (tempered martensite), which can release internal stress and minimize the effect of the micro-cracks, both of these effects will increase tensile strength and elongation. Bainite obtained by austempering is a crack-free structure with less internal stresses because of the moderate transformation. Owing to the best combination of strength and elongation, bainite was selected as the final phase for wire in the artificial dual phase steels. The fracture surfaces of tempered martensitic and bainitic wires both show plastic deformation (shown in Figure 5.1.6).

When eutectoid steel wire is heated above the Ac_1 temperature, the grain size of the austenite increases with the annealing temperature and isothermal holding time. On cooling, grain size of the prior austenite determines the packet diameter of the transformed bainitic lath size. The bainite strength decreases with increasing lath size, as described by the following equations[134]:

$$\sigma_y{}^B = \sigma_0^B + k^B \cdot d^{-1/2} + p \cdot n^{1/4} \qquad (5.1.3)$$

where, σ_0^B and k^B are constants, d is prior austenite grain size, p is the dislocation density and n is the number of carbides per mm^2. The equation shows that the strength of bainite decreases with increasing prior austenite grain size, ie. the bainite lath size (increasing isothermal holding time).

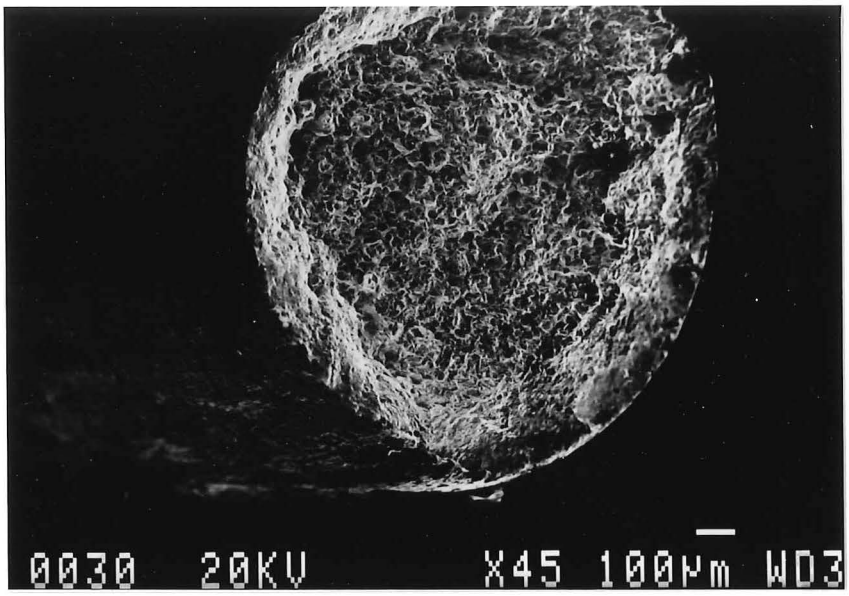
0030 20KV X45 100µm WD3

(a)

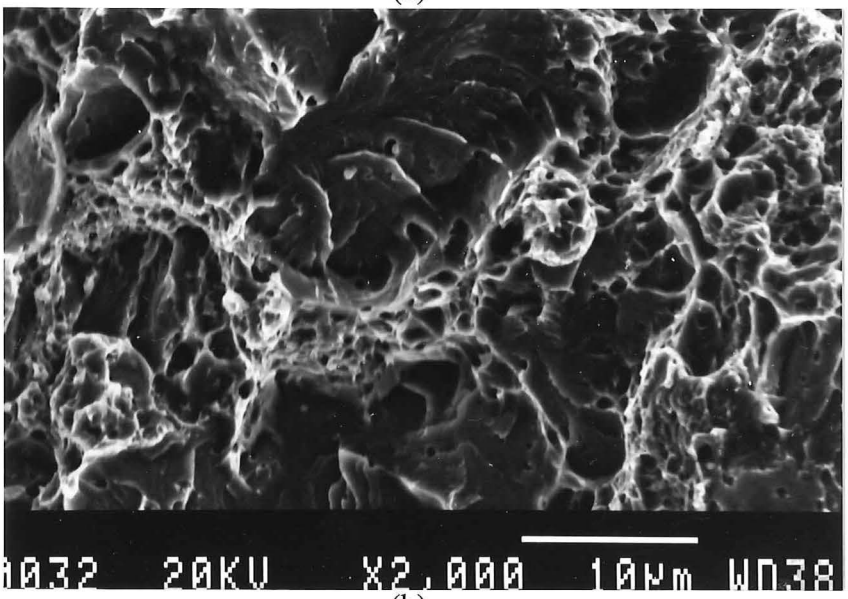
0032 20KV X2,000 10µm WD38

(b)

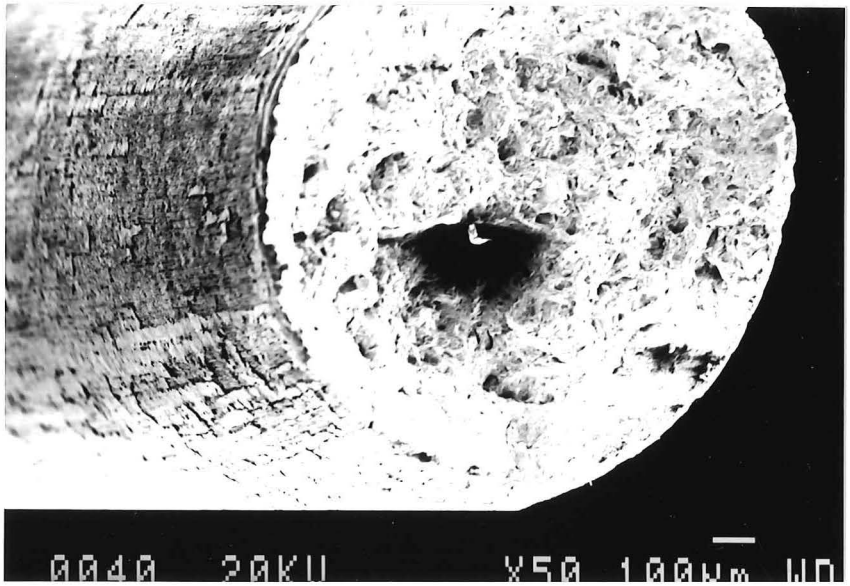
0040 20KV X50 100µm WD

(c)

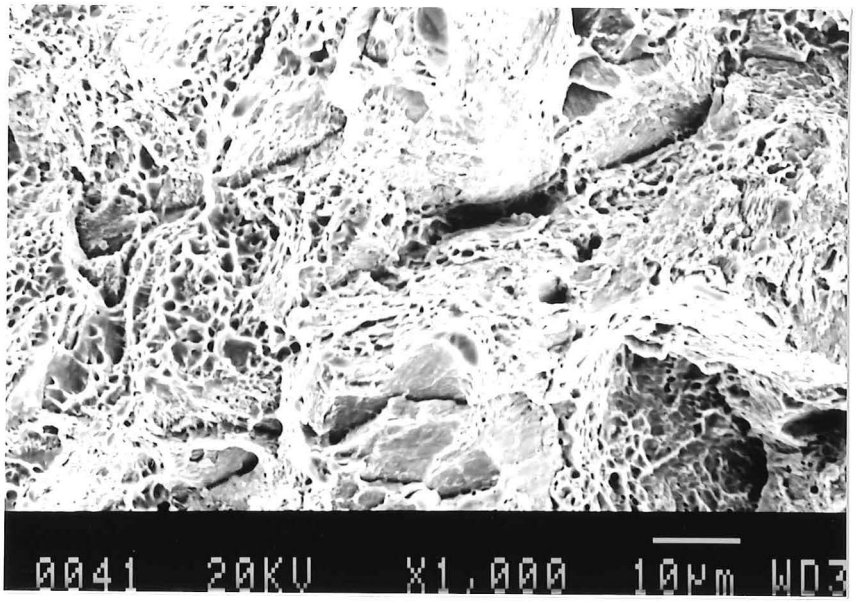

(d)

Figure 5.1.6 Fracture surfaces of (a) and (b) tempered martensitic, (c) and (d) baintic wire

The strength relationship between bainitic wire and its parent wire (the pearlitic wire) is investigated by rolling the pearlitic wire at different temperatures followed by austempering (shown schematically in Figure 5.17 (a)). The results are shown in Figures 5.1.7 (b) and (c). The strength and elongation of bainitic wire increase with increasing strength and elongation of pearlitic wire, but the strength of bainite is higher than that of the pearlite, whereas the bainite elongation is lower.

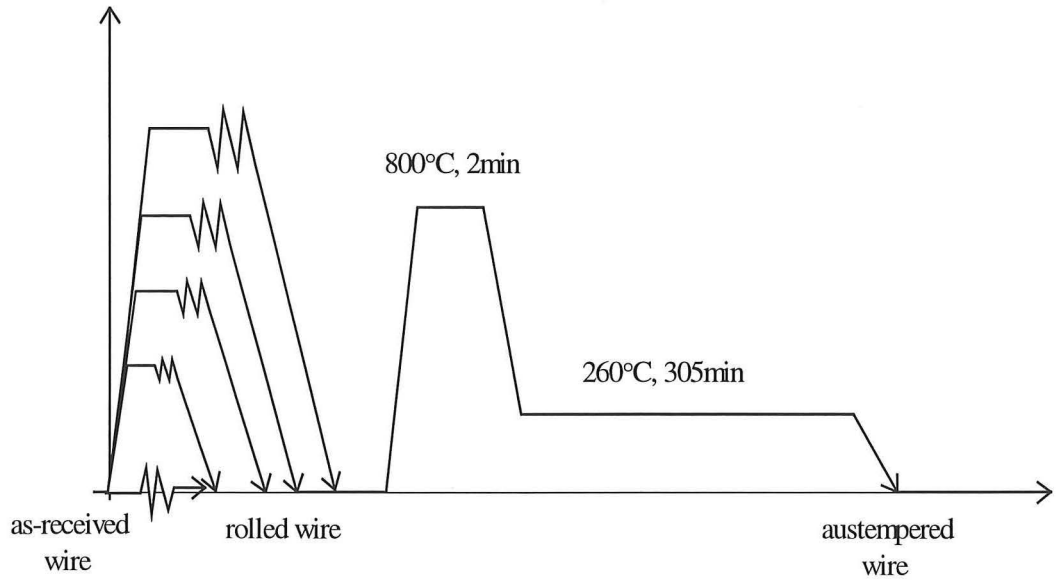

(a) experimental procedures

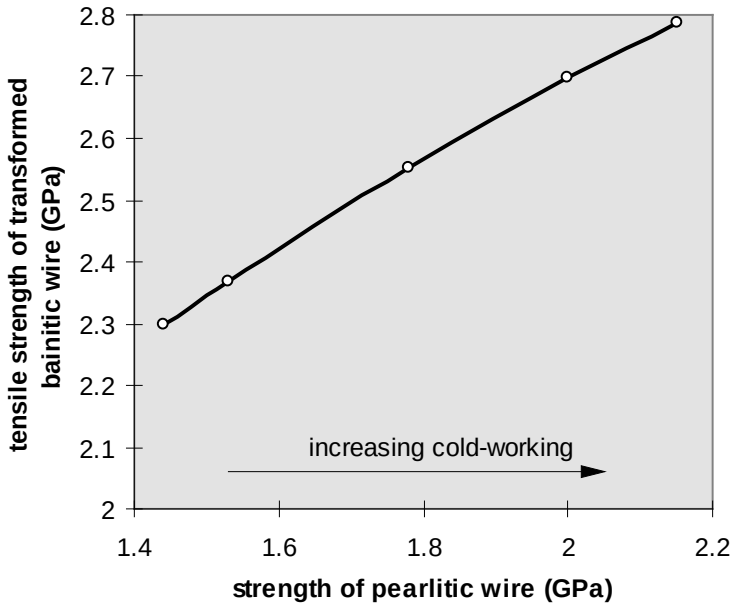

(a) tensile strength

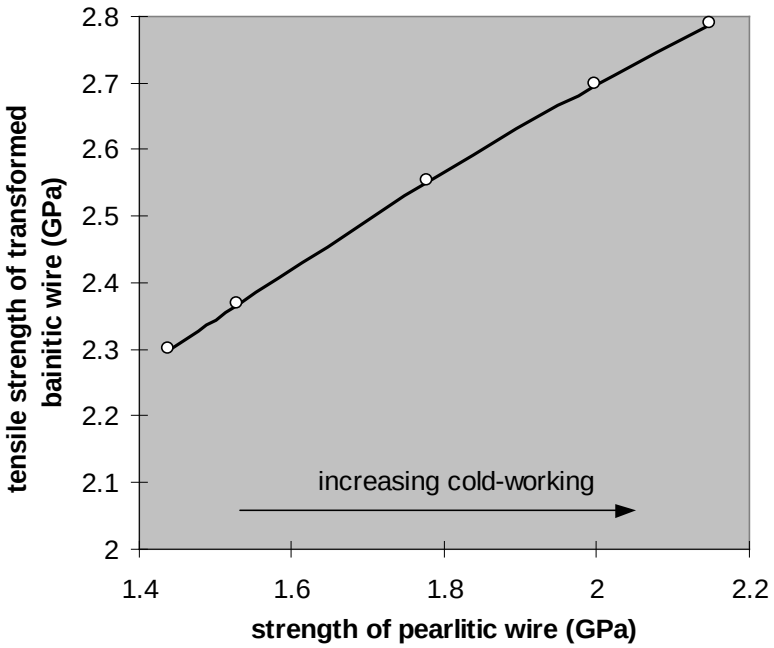

Figure 5.1.7 The relationship of tensile properties between transformed bainitic and pre-transformed pearlitic wires

The high strength of the rolled pearlitic wire is due to the heavy deformation, i.e. the high dislocation density and residual stress, which is dependent on the deformation temperature, and deformation reduction. The high dislocation density and residual stress produced at low rolling temperature and with high reduction give the pearlitic wire high strength and low elongation. In addition, higher cold-working also produces finer pearlite grain size, which can give high strength.

During the heating and holding period of transformation of pearlite to bainite at high temperature, all dislocations and residual stresses in the as-rolled pearlitic wire are released, and the strength of the bainite is dependent on the transformation and factors affecting the transformation, such as prior cold-working, composition etc.

5.1.1.4 Properties of steel-wire under the composite fabrication conditions

Finishing rolling temperature

The effects of finishing rolling temperature on the tensile properties of as-rolled (pearlitic) and transformed (bainitic) wire are shown in Figure 5.1.8. The strengths of both pearlitic and bainitic wires decrease with increasing finishing rolling temperature, whereas elongation increases with increasing finishing rolling temperature.

Finishing rolling temperature determines the internal residual stresses and density of dislocations in the as-rolled wire, which determines the strength and elongation of the wire. Owing to the decrease in flow stress with increasing temperature, the internal stresses and dislocations generated at low temperature are much higher than those at high temperature and the internal stresses and dislocations generated at high temperature may be partially released by recovery during air cooling. The low internal stresses and dislocation density in the wire rolled at high temperature result in lower strength and higher elongation.

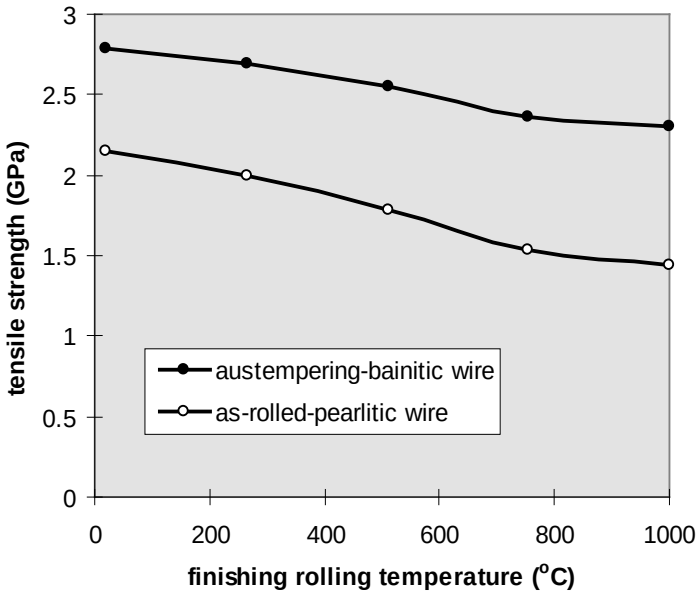

(a)tensile strength

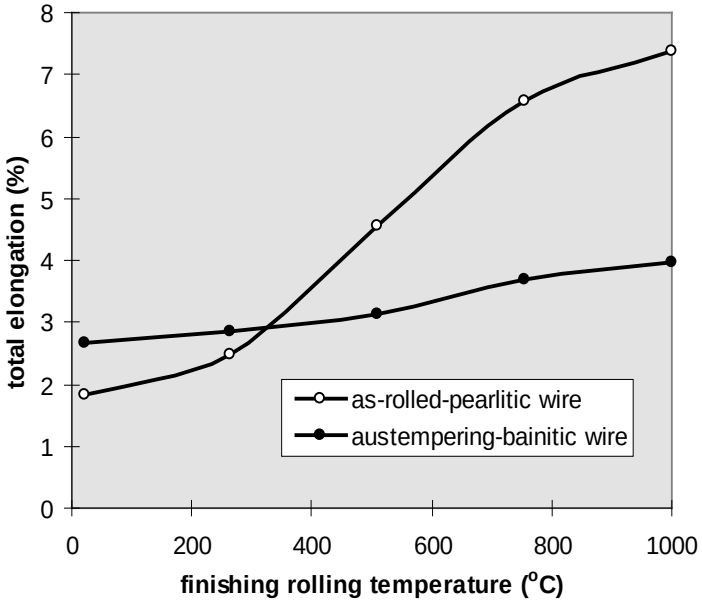

(b) total elongation

Figure 5.1.8 Effect of finishing rolling temperature on tensile properties of both as-rolled wire and austempered wire

Elongation of pearlitic wire rolled below 300°C is lower than that of bainitic wire but increases to higher than for bainitic wire when rolled above 300°C.

Starting rolling temperature (isothermal holding temperature)

The starting rolling temperature is the temperature at which the wire had been isothermally held for a while to make the temperature distribution uniform in the composites and produce a good bond between wire and matrix.

The tensile properties of plain wire, copper-coated wire and nickel-coated wire after rolling at various temperature are shown in Figure 5.1.9. The strength of plain wire decreases and elongation increases a little with increasing starting rolling temperature; the tensile strength and elongation of copper-coated wire remains constant, whereas those of nickel-coated wire decrease with increasing starting rolling temperature.

Decarburiztion in plain wire increases with temperature, which makes the strength of plain wire decrease and elongation increase with increasing temperature.

Copper coating stops the decarburiztion of steel-wire at high temperature and does not react with iron, thus the strength and elongation of the copper-coated wire do not change with increasing temperature.

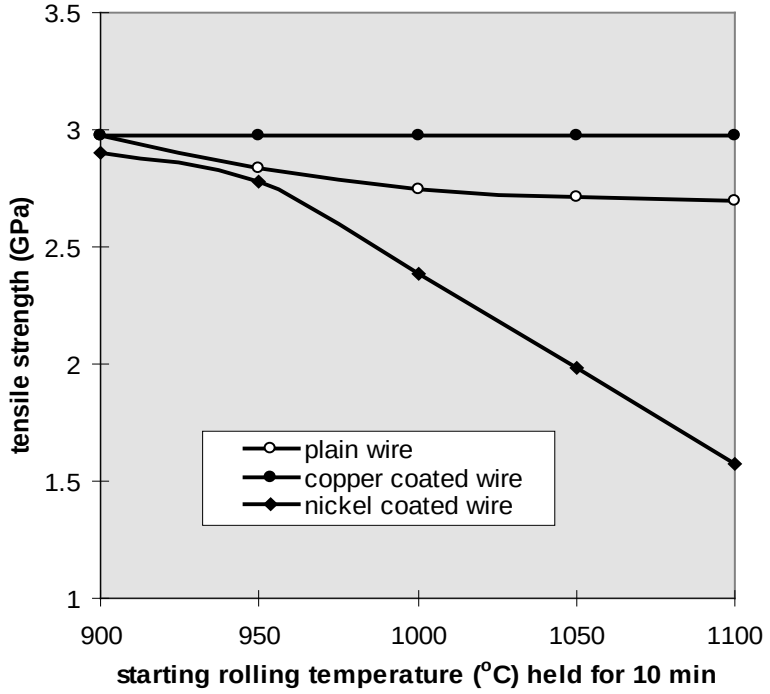

(a) tensile strength

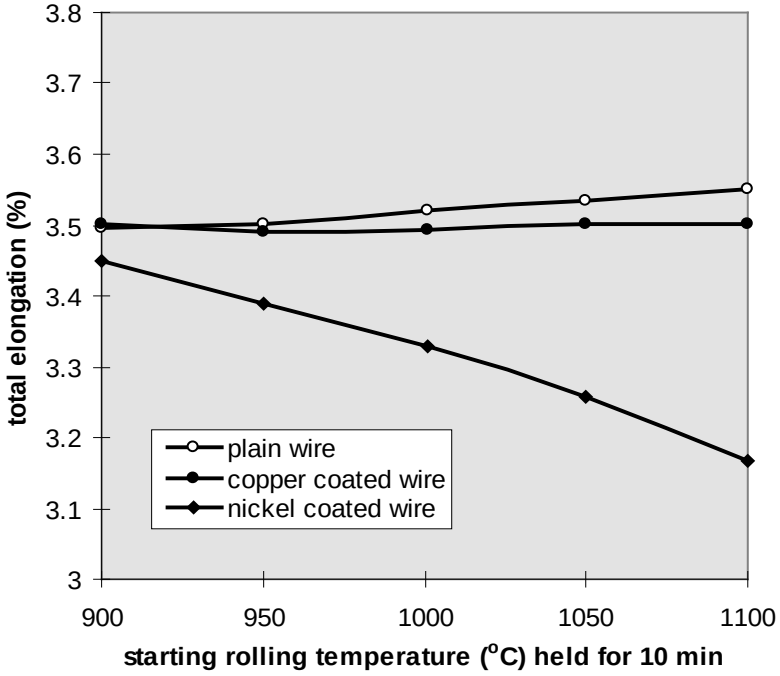

(b) total elongation

Figure 5.1.9 The properties of bainitic wire as a function of starting rolling temperature with water-quenching after rolling

The nickel coating is different to copper: it can reduce decarburization of wire but can also react with iron to form the intermetallic compound $FeNi_3$. The interfacial reaction

may strengthen interfacial bonding (this will be investigated in section 5.2), and may affect the tensile properties of the wire.

The effect of this interfacial reaction on the properties of the wire is dependent on the extent of reaction. When the reaction layer is brittle and fractures at small strain, a notch is formed first in the reaction layer on the wire surface during the fracture process. The formed notch hastens fracture of the wire due to stress concentration, resulting in loss of composite strength.

A model of the effect of interfacial reactions on the strength of reinforcements and composites was developed by Ochia[94 ,135, 136] (schematically shown in Figure 5.1.10). The strength of the reacted fibre is a function of the thickness of the reaction layer and also depends on the interfacial bonding.

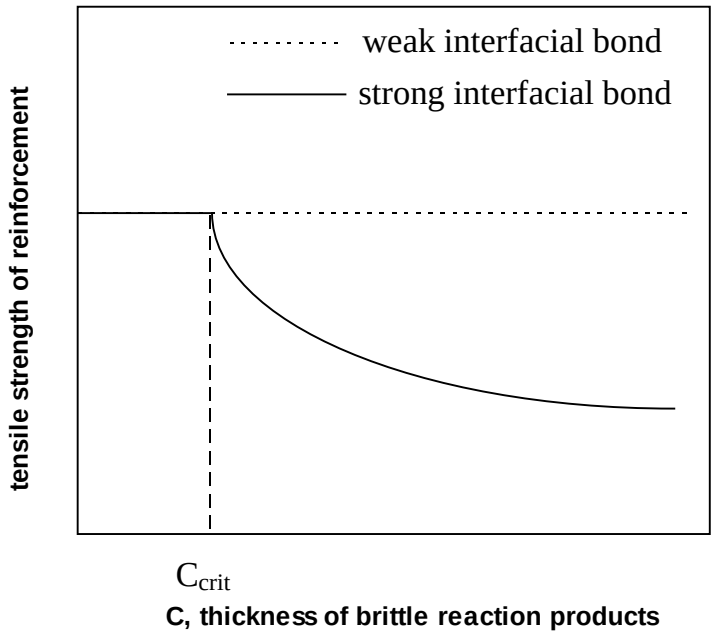

Figure 5.1.10 Effect of thickness of reaction layer on strength of reinforcement

For weak interfacial bonding, the reaction does not affect the strength of fibre. When the bonding is strong, the strength of the reacted fibre is reduced and decreases with increasing thickness of reaction zone when C is larger than a critical thickness of layer, C_{crit}, that is:

$$\sigma_{fu} = \frac{1}{F}\left(\frac{E_f G_c^*}{\pi C}\right) \qquad (5.1.3)$$

where G_c^* is the critical strain energy release rate (i.e.fracture toughness value) and F is the finite width correction factor (1.12 for $C << d_f$, the fibre diameter).

For the nickel-coated wire, in addition to decarburization, the chemical reaction between nickel and iron to form an intermetallic compound $FeNi_3$ decreases the elongation and strength. The thickness of reaction products increases with increasing isothermal holding temperature and time, so the strength and elongation of nickel-coated wire decreases with increasing the thickness of the reaction zone.

The effect of heating and holding time before rolling

The variation of wire properties with heating and holding time at 950°C is similar to those with starting rolling temperature (shown in Figure 5.1.11). The decrease in strength and increase in elongation of plain wire with increasing heating and holding time are attributed to decarburization; the decreases in strength and elongation of nickel-coated wire are caused by both the decarburization and the chemical reaction. The increase of reaction extent with increasing holding time is much lower than that with increasing temperature. The strength and elongation of copper coated wire do not change with isothermal holding time.

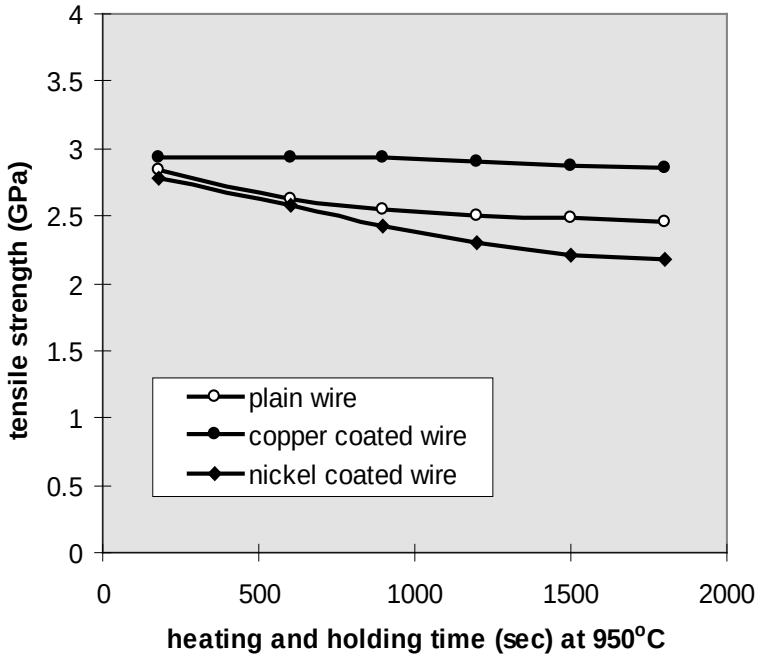

(a) tensile strength

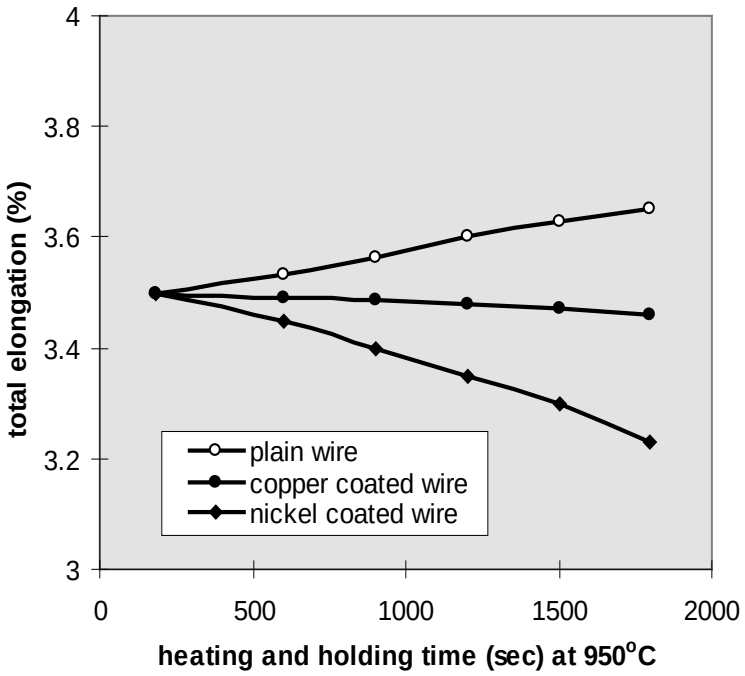

(b) total elongation

Figure 5.1.11 The properties of bainitic wire as a function of heating and holding time at 950℃ before rolling (water quenching after rolling)

The grain size of the austenite increases during isothermal holding. The large lath size of bainite produced from the larger austenite size with longer holding time gives lower strength and lower elongation.

The variation of wire properties with isothermal holding time is due to the combined effect of grain size change, decarburization (not in the copper-coated wire), and chemical reaction (only in the nickel-coated wire).

5.1.2 Matrix steels

The matrix has to bind and transfer stress to the reinforcement. Generally, the matrix is required to have good ductility for metal matrix composites. If we are considering the composite steel as an “artificial” dual phase steel, the matrix should be predominantly a low carbon ferrite matrix. Three steels with 0.044, 0.06, and 0.14% carbon contents were chosen as matrices to investigate the effect of matrix characteristics on the composites. The variation of tensile properties of these three steels with rolling parameters is studied in this section.

The microstructures of the three kinds of steel under fully annealed condition are shown in Figure 5.1.12. The phase compositions are 98% ferrite+2% pearlite for No.1 steel, 95%ferrite+5% pearlite for steel No.2, and 85% ferrite+15% pearlite for steel No.3. The properties of these steels are functions of the rolling reduction and rolling temperature, which will be discussed in the following section.

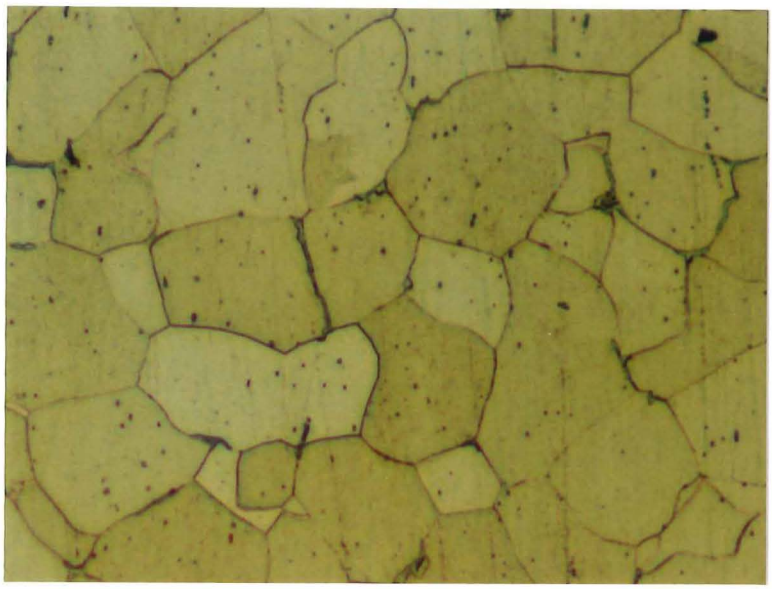

No.1

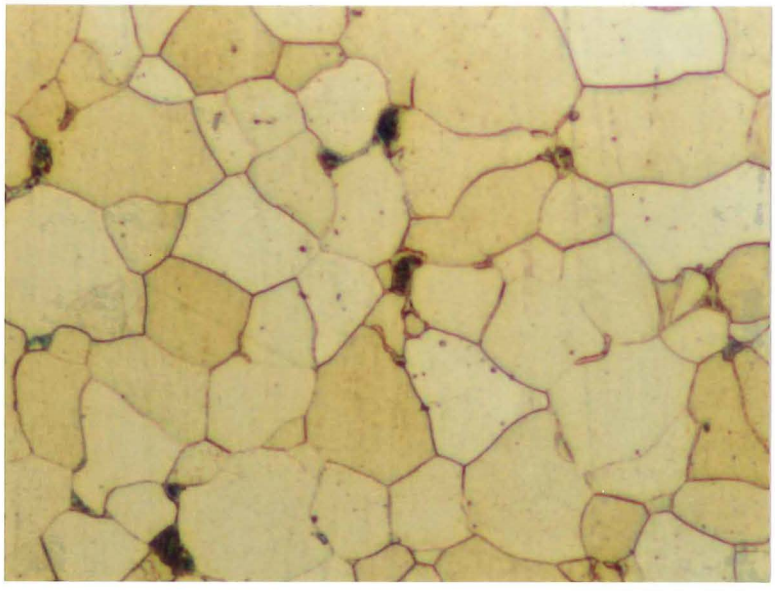

steel No.2

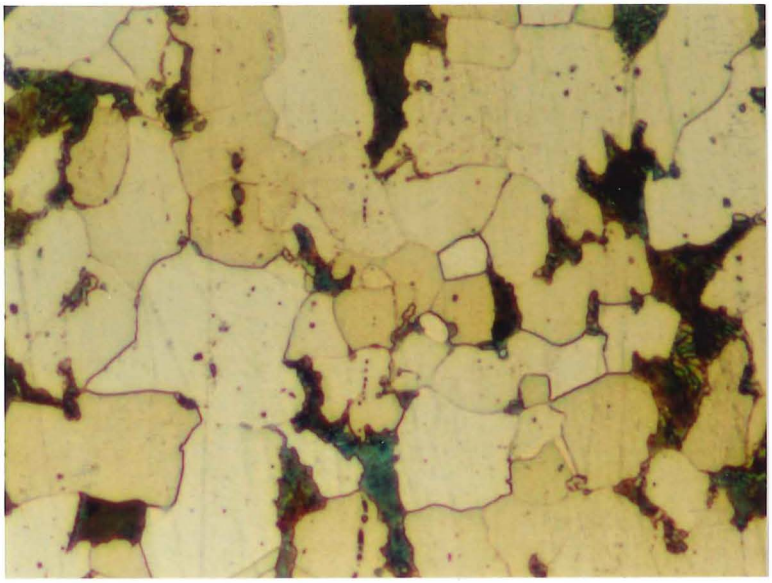

steel No.3

Figure 5.1.12 Microstructures of annealed matrix steels (× 575)

Because austempering was chosen to heat treat the steel wire to obtain a bainitic structure, the deformed matrix steels are tested after the same austempering treatment.

5.1.2.1 Effect of finishing rolling temperature

Similar to the steel-wire, the strengths of the matrix steels increase with decreasing finishing rolling temperature and the elongation decreases owing to the effect of work-hardening (shown in Figure 5.1.13). The tensile strengths of the as-rolled steels decrease smoothly with increasing rolling temperature when the rolling temperature is below 750°C, and then decrease sharply when rolling temperature is over 750°C as expected; the tensile strengths and elongation of the austempered steels vary only slightly with increasing rolling temperature.

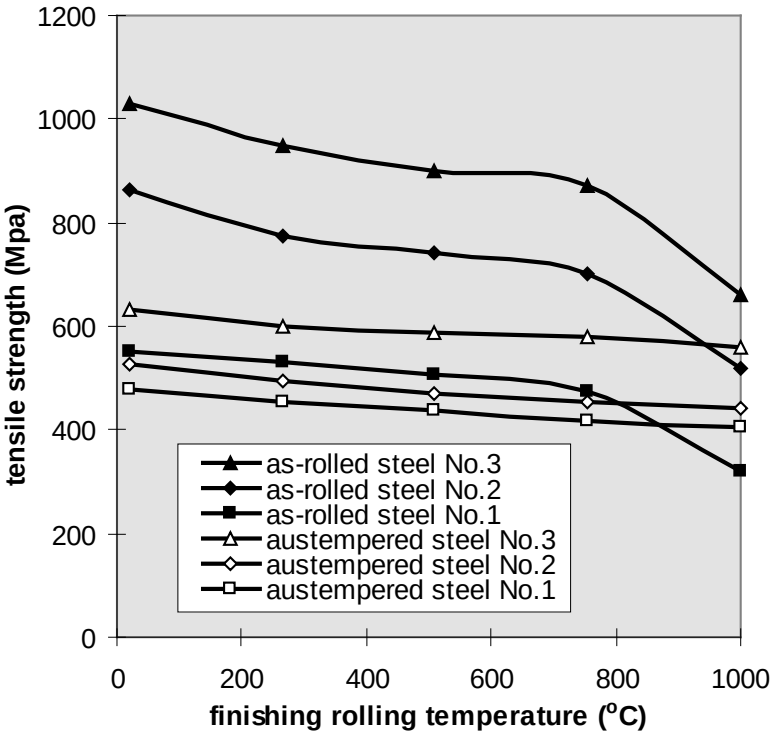

(a) tensile strength

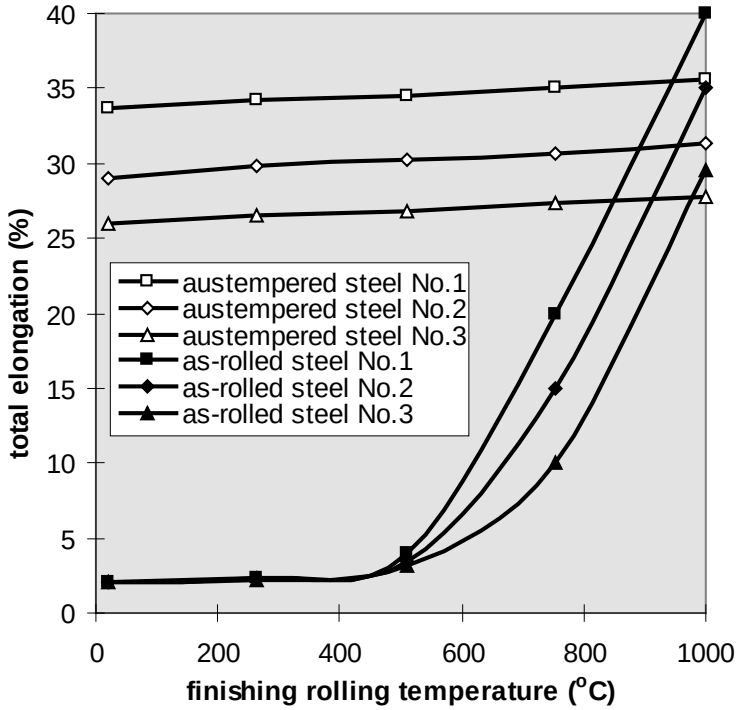

(b) total elongation

Figure 5.1.13 The properties of matrix steels as a function of finishing rolling temperature

Variation of the tensile properties of pre-deformed steels is caused by the change of dislocation density in the deformed steels. The effect of dislocation hardening can be

eliminated by recrystallization during reheating as in austempering hence the tensile properties of austempered steels change little with prior rolling temperature.

5.1.2.2 Rolling reduction

The tensile properties of these three matrix steels rolled at 580°C as a function of rolling reduction is shown in Figure 5.1.14. The tensile strength increases with increasing rolling reduction for both as-rolled and austempered steels but the strengths of austempered steels are lower than those of as-rolled steels; the elongation decreases with increasing rolling reduction, the elongation of the austempered steels being higher than that of as-rolled steels.

The rolling reduction, associated with the rolling temperature decides the dislocation density in the as-rolled steels, which also is affected by the flow strength of the steel (related to the carbon and alloy contents). At the same rolling temperature, the dislocation density in the as-rolled steels increases with % reduction; the higher dislocation density increases tensile strength and decreases elongation. At the same rolling reduction and temperature, the dislocation density generated in the higher alloy steel is higher than that in lower alloy steel because of the difference in flow stress, This is the reason that the tensile strength of steel No.3 is higher than those of steels No1 and 2 for both austempered and as-rolled.

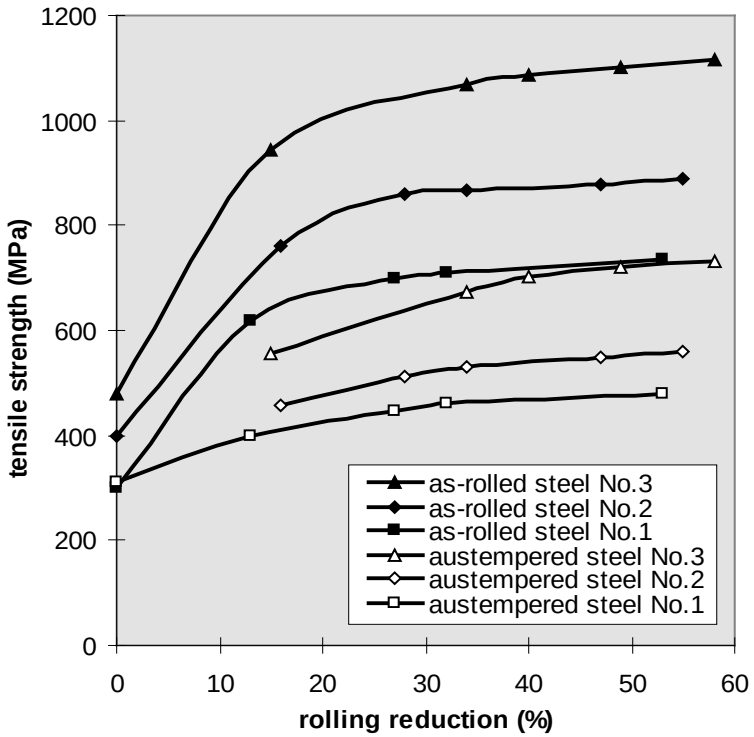

(a) tensile strength

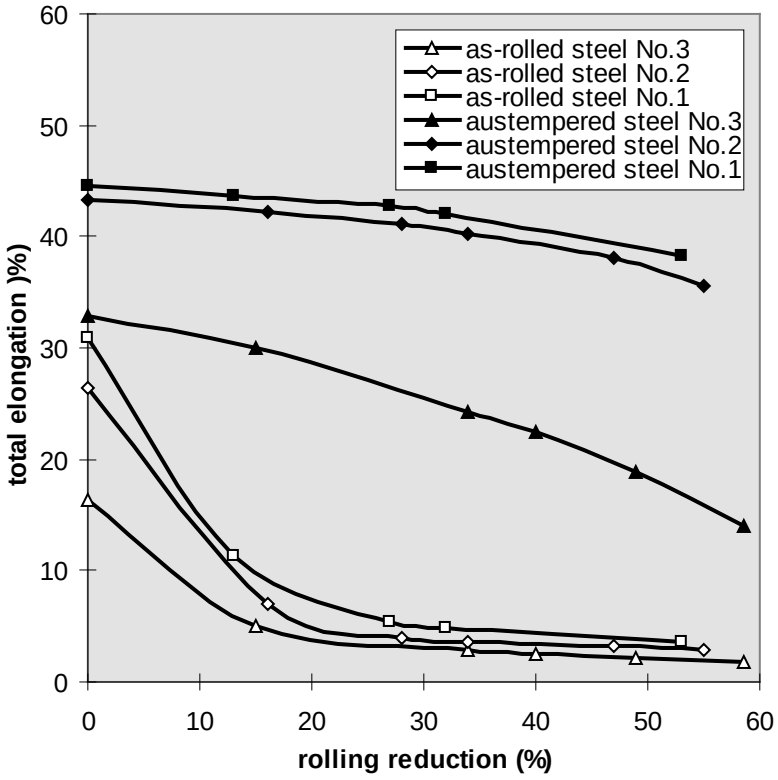

(b) elongation

Figure 5.1.14 The properties of matrix steels (rolled at 580℃) as a function of rolling reduction

5.1.3 Summary

The high strength of eutectoid steel-wire is derived from its high carbon content and work hardening during cold-drawing. With the dislocation density in wire decreasing after annealing, the strength of the wire drops to a constant (elongation increases to a constant), which is determined by carbon content. An extra decrease in strength is caused by decarburization.

For the eutectoid steel wire, martensite and bainite were produced by martempering and austempering respectively; the bainitic wire is superior to martensitic wire because of its higher ductility at equivalent strength with martensitic wire.

Tensile properties of transformed bainitic wire depend on its parent, i.e. the pearlitic wire. Both strength and elongation of the bainitic wire increase as those of the pre-deformed pearlitic wire but are superior to those of the pearlitic wire.

The tensile properties of both pearlitic and bainitic wire are affected by the rolling process parameters, especially by finishing rolling temperature. Rolling at low

temperature increases the tensile strength and reduces ductility of both the bainitic and pearlitic wires.

The temperature and time of the isothermal holding period before rolling determine the decarburization, grain size of wire, and chemical reaction between wire and coating, all of which increase with increasing isothermal holding temperature and time. These effects on the properties of wire are described as follows:

Decarburization, which can take place in plain wire and nickel-coated wire, decreases strength and increases elongation.

Grain growth reduces both elongation and strength and can happen in plain wire, copper-coated wire, and nickel-coated wire.

Chemical reaction, which happened only in the nickel-coated wire, will reduce strength and elongation when the thickness of the brittle reaction product, $FeNi_3$, is over a critical value.

The combined effects of these factors make:

the strength of plain wire decrease, and elongation of plain wire increase with increasing isothermal holding temperature and time;

both the strength and elongation of copper coated wire decrease a little with increasing isothermal holding temperature and time;

both the strength and elongation of nickel coated wire decrease a little at low temperature and initial isothermal holding time, and decrease quickly at high temperature and longer holding time.

The strength increases and elongation decreases with increasing rolling reduction and decreasing rolling temperature for both as-rolled and austempered matrix steels.

5.2. Interface of steel-steel composites

The interface of plain steel-wire reinforced steel composites is simple compared with that of either ceramic-metal composites or ceramic-ceramic composites because no foreign chemical reaction takes place in this system (Fe-C/Fe-C). The fabrication process of steel-steel composites is quite similar to a solid diffusion bonding process; the carbon diffusion between wire and matrix plays an important role in the interfacial bonding. The diffusion is a function of rolling temperature and isothermal holding time.

However if some metals are introduced as barrier coatings to stop or reduce carbon diffusion, the metals may react with the steel to form intermetallic compounds, depending on the reactivity between the coating metals and steel. The interfacial reactions do enhance the interfacial bonding, but may degrade the high strength and ductility of the wire if the reaction exceeds a critical level.

Besides carbon diffusion, another factor that influences the interface is residual stress produced during rolling due to the different deformation resistivity (ie. flow stress) of the low carbon matrix and the high carbon wire. The residual stress is related to the fabrication parameters, including rolling temperature, finishing rolling temperature, rolling reduction, and any following heat-treatment.

The factors influencing interfacial strength will be examined in this section and models will be established to analyse the interfacial strength due to internal stress and carbon diffusion, and a comparison between the modelling analysis and experimental results will be made.

5.2.1 Analysis of residual internal stress at interface due to rolling

Residual internal stress is a common phenomenon in mechanically and thermally inhomogeneous materials, especially in composites. Usually, the residual stress in composites is generated from differential thermal expansion coefficients after the composites are fabricated at an elevated temperature. The well-known Eshelby approach[93, 137] can be used to analyse this type of internal stress.

Owing to the similar thermal properties of the wire and matrix steels, the internal stresses in steel-steel composites arise due to the difference in flow stresses of the wire

and matrix (the wire tends to deform less than the surrounding matrix during fabrication rolling). The magnitude of this internal stress varies according to the rolling temperature and the thermal and mechanical properties of wire and matrix. The analysis of the internal stress in the steel-wire composite by the Eshelby method is shown in Figure 5.2.1.

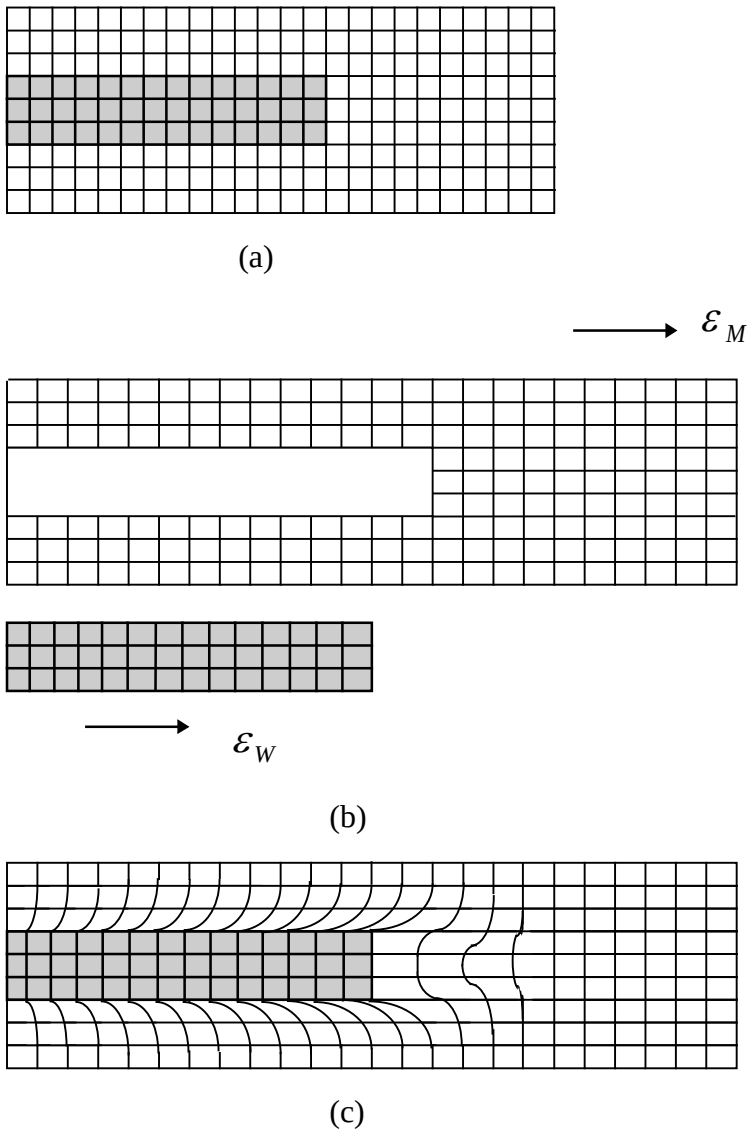

Figure 5.2.1 Illustration of Eshelby method to analyse the internal stress due to hot rolling (a) initially (b) separately rolled (c) rolled together

In the model shown in Figure 5.2.1, the steel-wire aligned inside the matrix is rolled to a certain reduction after heating. The strains of the separate wire and matrix are ε_W and ε_M respectively without any internal stresses in either the wire or matrix. If the strained wire and matrix are brought together without any defects (shown in Figure 5.2.1 (c)),

and the wire is thought to be strained uniformly throughout, the internal stress in the wire can be written as:

$$\sigma_W = C_W(\varepsilon_M - \varepsilon_W) \tag{5.2.1}$$

where, C_W is the stiffness tensor of the wire.

Because the strain in the matrix, $\varepsilon_M(x)$, is not uniform, it varies with the distance from the interface, the residual stress in the matrix is a function of distance from the interface, as:

$$\sigma_M(x) = C_M \varepsilon_M(x) \tag{5.2.2}$$

The term $(\varepsilon_M - \varepsilon_W)$ reflects the deformability difference between wire and matrix; it increases with decreasing deformation temperature and increasing reduction, so the internal stress also increases with decreasing deformation temperature and increasing reduction.

The illustration of internal residual stress is shown in Figure 5.2.2; there are high stresses in the interface zone.

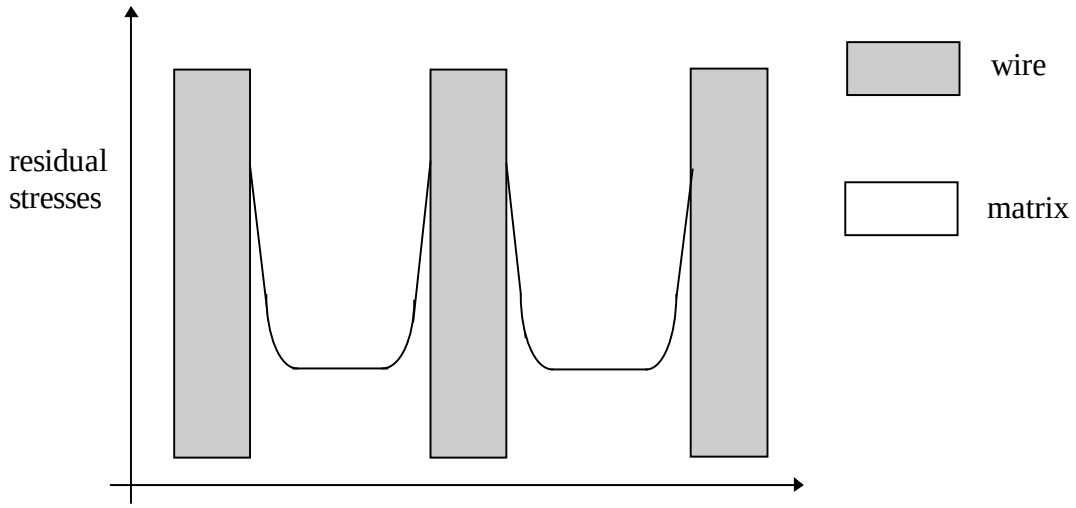

Figure 5.2.2 Illustration of internal stress distribution in steel-steel composite due to rolling

The effect of residual internal stress at the interface on the interfacial strength is dependent on the level of internal stress and interface bonding:

(a) If the internal stress is lower than t
at the interface and the internal stress may
hardening.

(b) If however, the internal stress is al
matrix, interfacial debonding or sliding wil
decrease.

The relationship between interfacial strengt
testing the variation of interfacial strength as
quasi-isothermal rolling (for nearly the san
procedures are shown in Figure 5.2.3. All pref
rolled by one pass with 20% reduction follov
then reheated to 20, 265, 510, 755, and 1(
isothermally rolled at these temperature with
followed by air-cooling (stage 2).

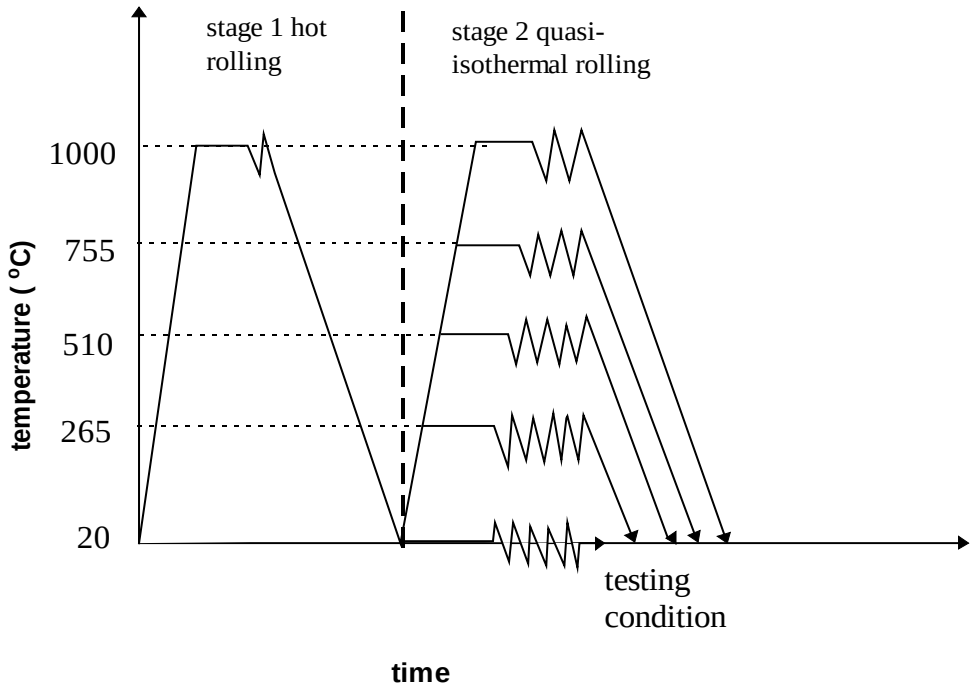

Figure 5.2.3 Quasi-isothermal rolling approach for testing the effect of finishing rolling temperature on the interfacial strength

In stage 1, both the matrix and wire are rolled as austenite with the same deformation so internal stresses can be ignored, and the interfacial strength is about 210MPa (see the

broken line in Figure 5.2.4). The variation of interfacial strength after stage 2 is caused by the internal stresses due to the quasi-isothermal rolling at different temperatures.

It is common knowledge that the internal stress and dislocation density increase with (a) decreasing deforming temperature (the finishing rolling temperature in this case) and (b) increasing deformation. The results (shown in Figure 5.2.4) show that the interfacial strength increases with increasing finishing rolling temperature to $\cong 450°C$, and then decreases with increasing finishing rolling temperature over 500°C.

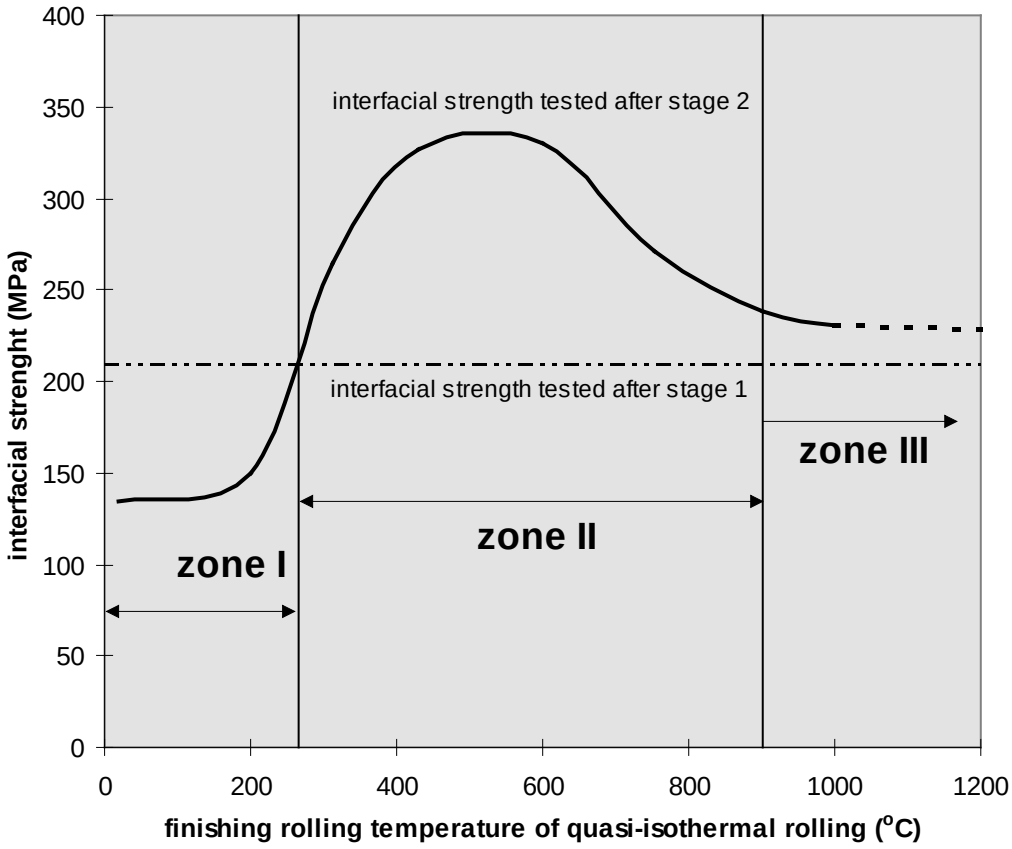

Figure 5.2.4 Interfacial strength as a function of finish rolling temperature shows the effect of internal stress on the interface

When the well bonded wire and matrix were rolled at low temperature, the high internal stresses were produced because of the high flow stress difference between the pearlitic wire and the ferritic matrix; these high internal stresses will produce some voids to relax the internal stress concentration at interface if the internal stresses at the interface are over the interfacial strength (shown in Figure 5.2.5 a). The lower the rolling temperature, the more voids were produced; these voids at the interface reduce the

bonding (the interfacial strength after stage 2 is lower than that after stage 1, as shown in zone I in Figure 5.2.4).

In zone II of Figure 5.2.4, the effect of internal stress makes the interfacial strength higher than that for stage 1 because the internal stress is not high enough to break the interface bonding achieved in stage 1. The interfacial strength reaches its maximum value at a finishing rolling temperature of 500°C. When the finishing rolling temperature is over 500°C, the internal stresses decrease with increasing finishing rolling temperature and so does the interfacial strength (shown in zone II of Figure 5.2.4). Above 910°C, both the wire and matrix are in the austenite region so there are no internal stresses produced during rolling and the interfacial strength keeps a constant value, which is a little higher than the interfacial strength tested after stage 1 because of carbon diffusion during reheating in stage 2.

The microstructures of the interface zones (shown in Figure 5.2.5) show the heavy deformation of grains and voids in the interface zone rolled at low temperature, large grains at the interface rolled at high temperature.

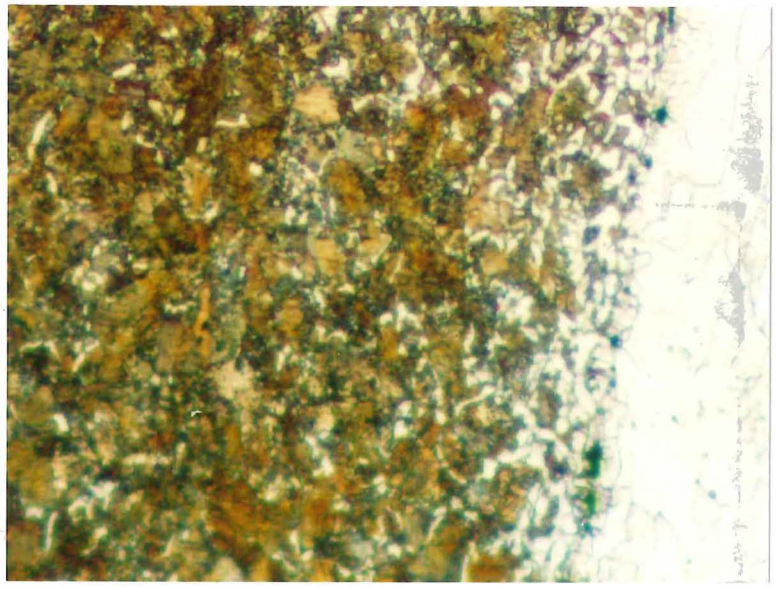

(a) rolled at 20°C

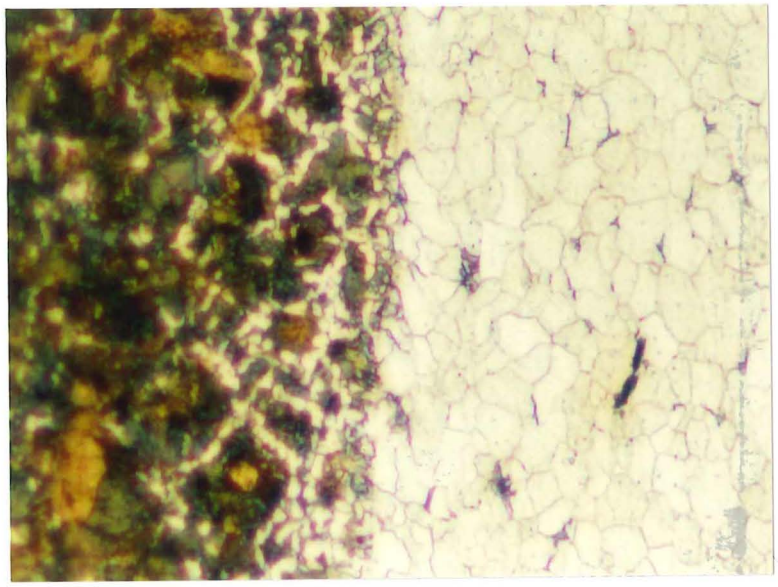

(b) rolled at 510°C

Figure 5.2.5 Microstructures of interface between wire and matrix with various finishing rolling temperatures (×230)

5.2.2 Interface relaxation by heat-treatment

If the previous analysis of interfacial strength due to internal stress at the same thermal environment is true, the interfacial strength achieved due to the internal stresses will be reduced by a following heat-treatment that relieves the internal stresses because of tempering and recrystallization. Figure 5.2.6 is the variation of interfacial strength with heat-treatment time. The interfacial strength decreases with increasing heat-treatment time until reaching a minimum value.

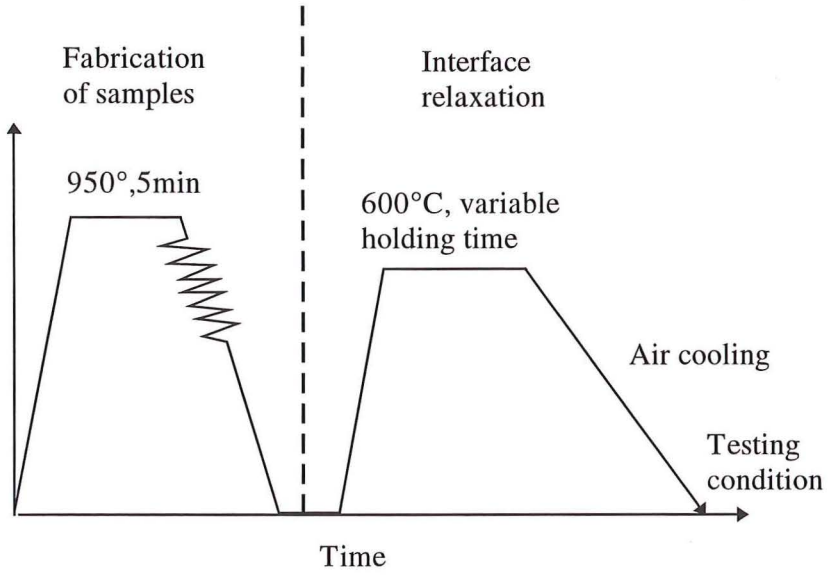

(a) experimental procedures

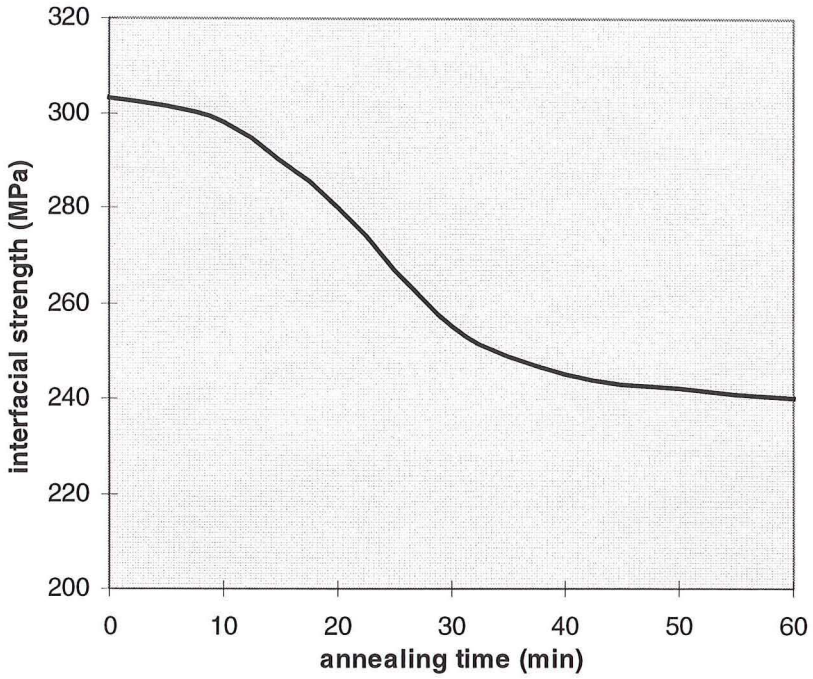

(b) testing result

Figure 5.2.6 Interfacial strength as a function of heat-treatment time (at 600 ℃)

During the heat-treatment of the deformed samples, relief of internal stresses due to recovery of deformed grains and recrystallization occurs at the interface, which decreases the interfacial strength, and the final constant strength is given by the diffusion bonding presumably where all internal stresses have been relieved.

Figure 5.2.7 shows that the elongated interfacial grains disappear and instead form large equiaxed ferrite after heat treatment.

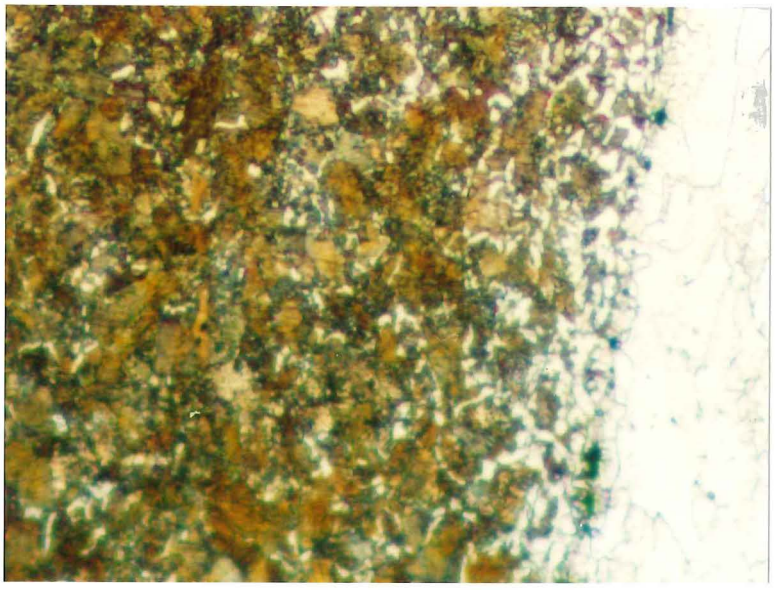

(a) as rolled interface

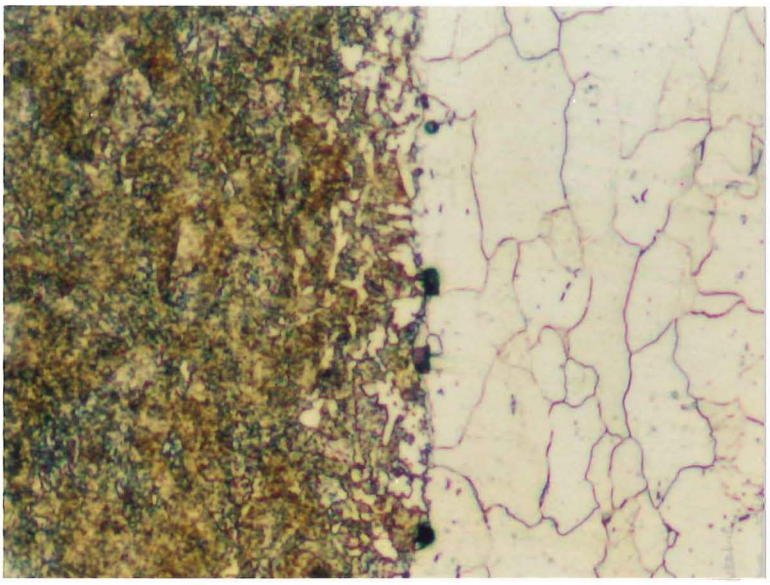

(b)annealed at 600°C for 60 min

Figure 5.2.7 Effect of heat-treatment on relaxation of interfacial deformation (× 230)

The interface softening at high temperature may take place through the following mechanisms:

(a) relief of internal stresses - the internal stresses produced during rolling are released at high temperature.

(b) motion and rearrangement of dislocation - transportation of dislocations from the interface to matrix reduces misfit between wire and matrix (recovery).

(c) recrystallization - the heavy deformation at the interfacial region accelerates the recrystallization of the deformed matrix grain, which removes the effect of work-hardening. This only happens at a temperature higher than the recrystallization starting temperature.

5.2.3 The end effect of wire

The variation of interfacial strength with the distance of testing point from the end of wire, l_{end} (refer to Figure 3.11), is shown in Figure 5.2.8. The interfacial strength increases with the distance l_{end}, and reaches the final constant value at distances greater than 30mm from the end of the wire.

A serious problem with rolling is "alligatoring" caused by inhomogeneous deformation of material during rolling. This problem is more serious during rolling plied sheets (as

illustrated in Figure 5.2.9). The alligatoring means that there is a stress managing to split the plies of sheets and wire, which weakens the bonding between the wires and the matrix at the "enter" end. With increasing distance from the enter end, the stress trying to split the plied sheets decreases and reaches zero, so the interfacial strength increases and reaches its equilibrium value. Owing to this end effect, all the interfacial testing will be carried out at a point which is $\geq$30mm from the wire end.

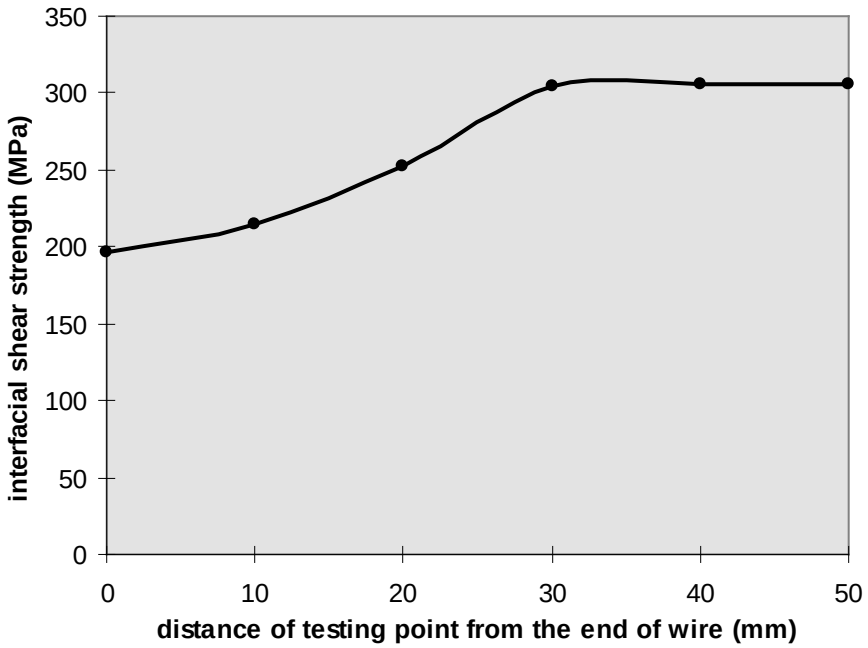

Figure 5.2.8 Variation of interfacial strength with the testing point for the steel wire reinforced steel rolled at 950ºC after heating for 3min.

As shown in Figure 5.2.1, the internal stresses at the interface reach their maximum values at the end of the wire and may be sufficient to break the bonding between wire and matrix at the wire end.

The SEM photos of the surface of pulled-out wire shows that the bonding at the centre of the wire is better than that at the end of the wire (Figure 5.2.10); the interface at the wire centre slides during pull-out of the wire.

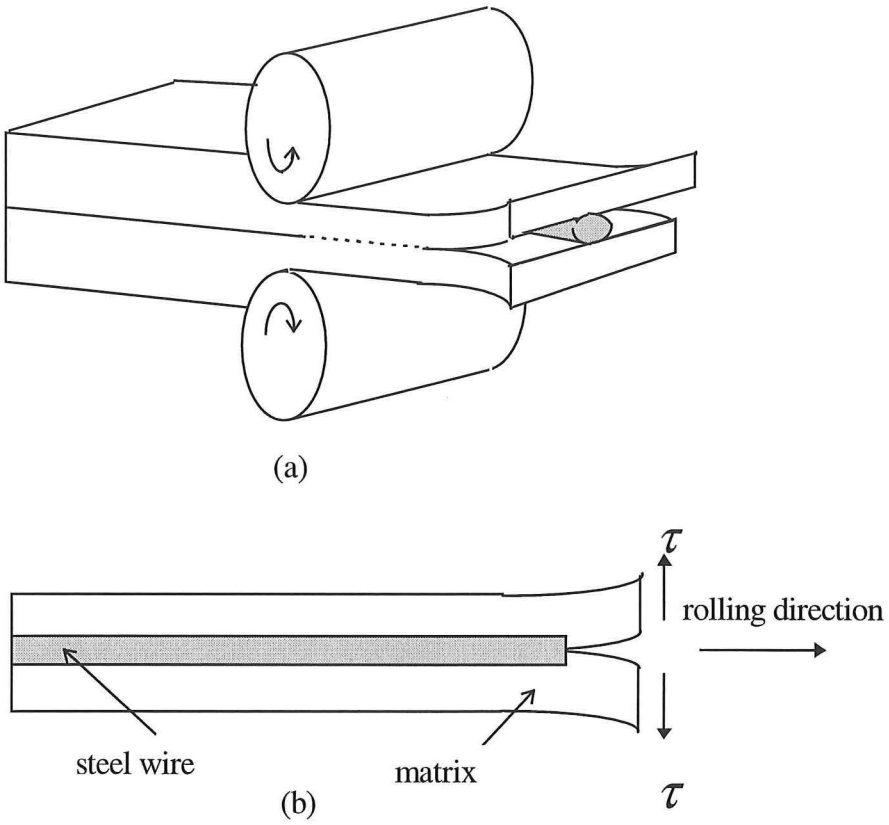

Figure 5.2.9 The illustration of alligatoring at the "enter" end of preform during rolling (a) and wire in the bent matrix (b)

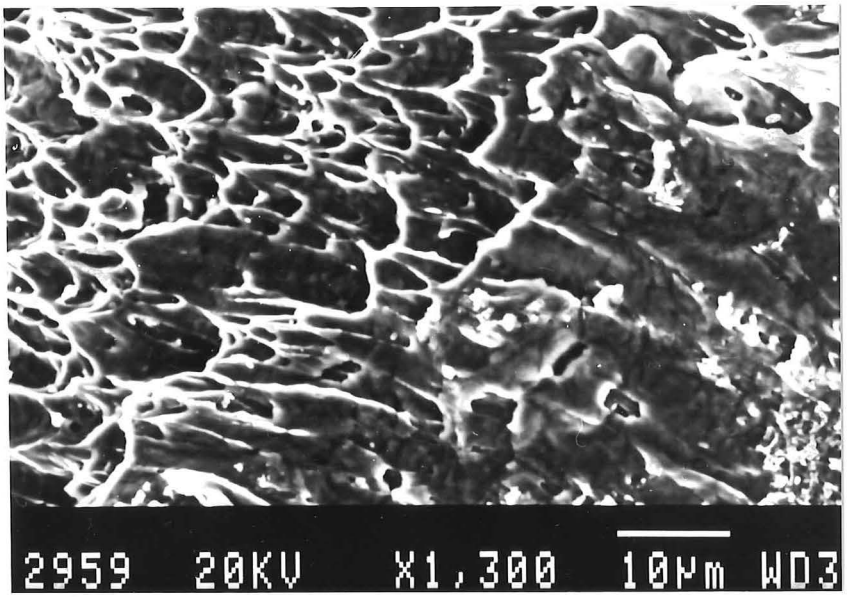

(a) at the center of the wire

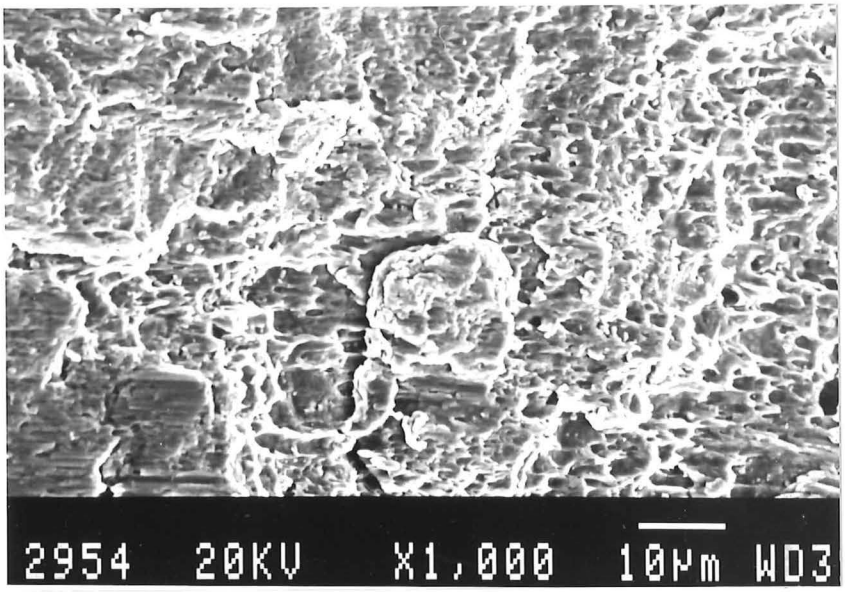

(b) at the end of the wire

Figure 5.2.10 The surface of pulled-out plain wire

5.2.4 The influence of rolling reduction of wire

After hot rolling and elongating of the wire, the cross section of the wire will change shape from round to oval (shown in Figure 3.9). This reduction in height can be expressed by:

$$\%\Delta h = {}^{(D-2h)}\!/_{D} \times 100$$

The influence of wire reduction on the interfacial strength between plain wire and matrix (continuously rolled starting at 950°C) is shown in Figure.5.2.11. The interfacial strength increases with increasing rolling reduction at low reduction (<40%), and reaches a constant value after ≥40%.

For the same thermal history (ie. the same diffusion condition), the interfacial strength (ie. the shear strength at the interface between wire and matrix) is only affected by the stress status at the interface. Because of the similar lattice constants of wire and matrix, the interfacial bonding is thought to be strong enough to resist the formation of cracks at the interface when the finishing rolling temperature is above 500°C. The internal stresses generated from the deformation will strengthen the interface owing to the work hardening effect (as examined in section 5.2.1); The higher the rolling reduction, the higher the strengthening effect.

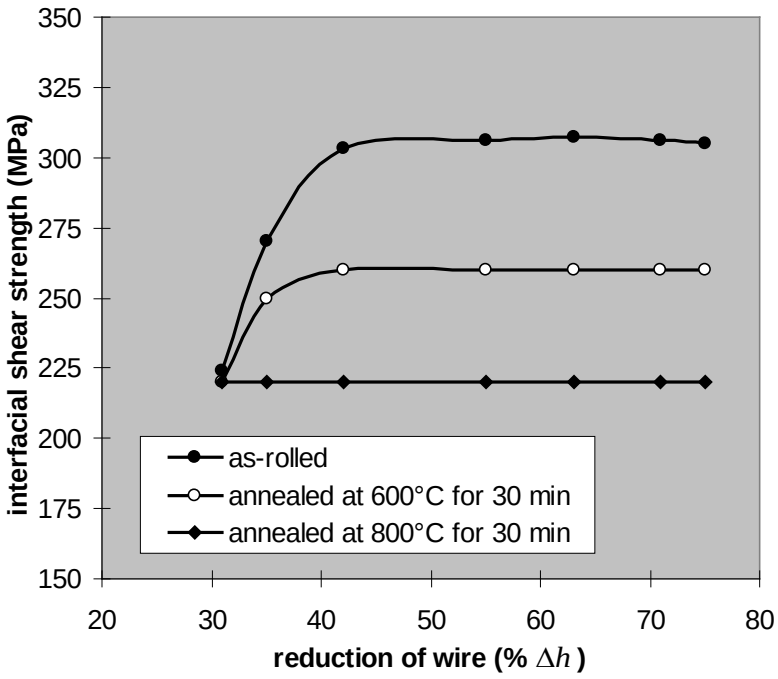

Figure 5.2.11 The effect of wire reduction on the interfacial strength

The internal stresses generated are not only due to the rolling reduction but also to the variation of finishing rolling temperature. In order to achieve higher reductions, more rolling passes are required so the finishing rolling temperature is lower for the higher reduction sample.

For the as-rolled sample, one may suppose that the lower interfacial strength at 30% reduction is caused by poor bonding. In order to check out this reasoning all the as-rolled samples with different reductions were reheated at 600°C and 800°C for 30min. 800°C is higher than the finishing rolling temperatures for all samples. At this temperature all internal stresses of the as-rolled samples can be relieved, so the interfacial strengths for all heat-treated samples reduce to the same values. 600°C is lower than the finishing rolling temperature of the 30% reduction sample but higher than the finishing rolling temperatures of higher reduction samples. After being heated for 30min, the interfacial strength of the sample rolled at 30% reduction doesn't change, but the interfacial strengths of the rest of the samples decrease (shown in Figure 5.2.11). The increase of interfacial strength with increasing rolling reduction is truly caused by the internal stresses. The effect of rolling reductions on grain deformation at the interface regions is shown in Figure 5.2.12.

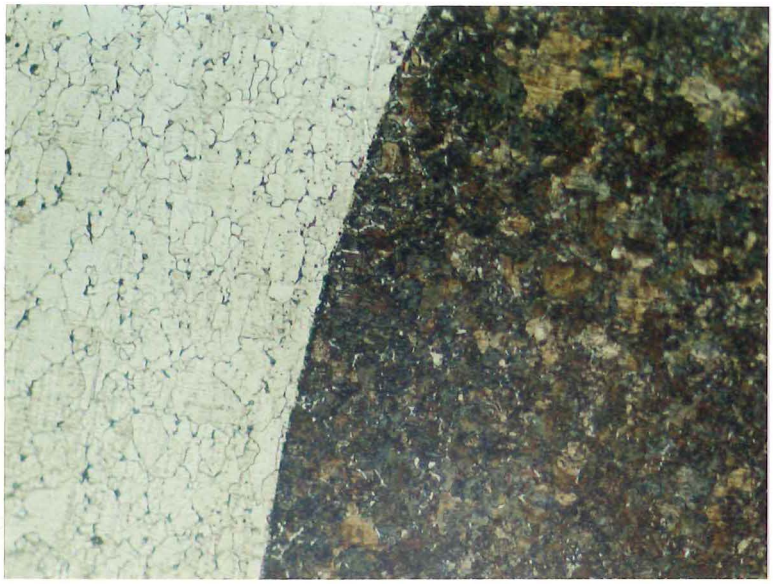

(a) 30% rolling reduction

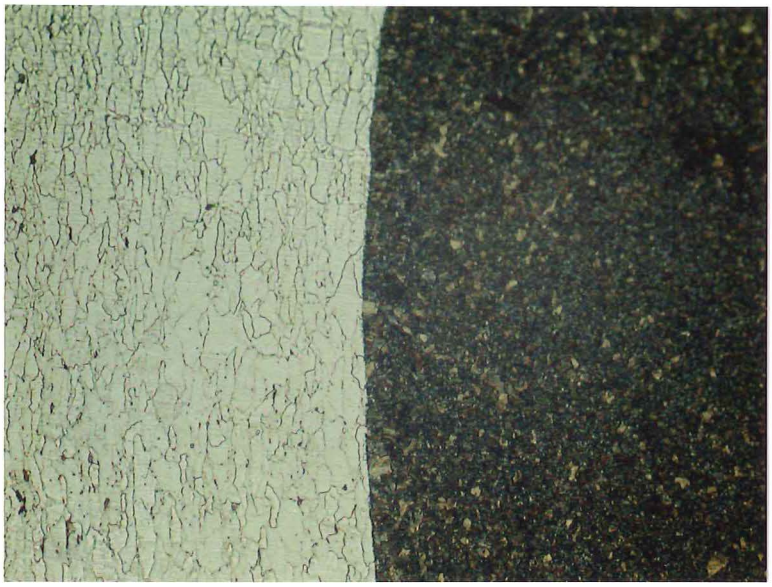

(b) 50% rolling reduction

Figure 5.2.12 The optical microstructure of interface zones with different rolling reductions (×230)

It is found that the specific surface area, which is defined as the ratio of surface area to the unit length (1mm, for example, shown in Figure 5.2.13) of deformed wire drops slowly and the total surface area increases due to extension of the wire after rolling (see Figure 5.2.14). The decrease of specific surface area is due to stretching and thinning of wire. The interfacial strength remains constant for reductions over 40%, which means that a higher load is needed to pull out the same length of wire with heavier

deformation, and a higher strength for the composites can be obtained from higher deformation reductions during the fabrication process as long as the high rolling reduction does not break the wire.

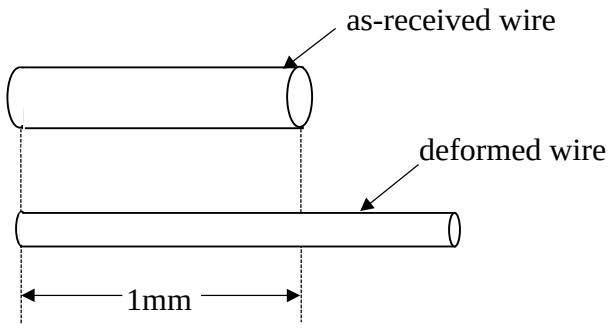

Figure 5.2.13 Definition of specific surface area of wire

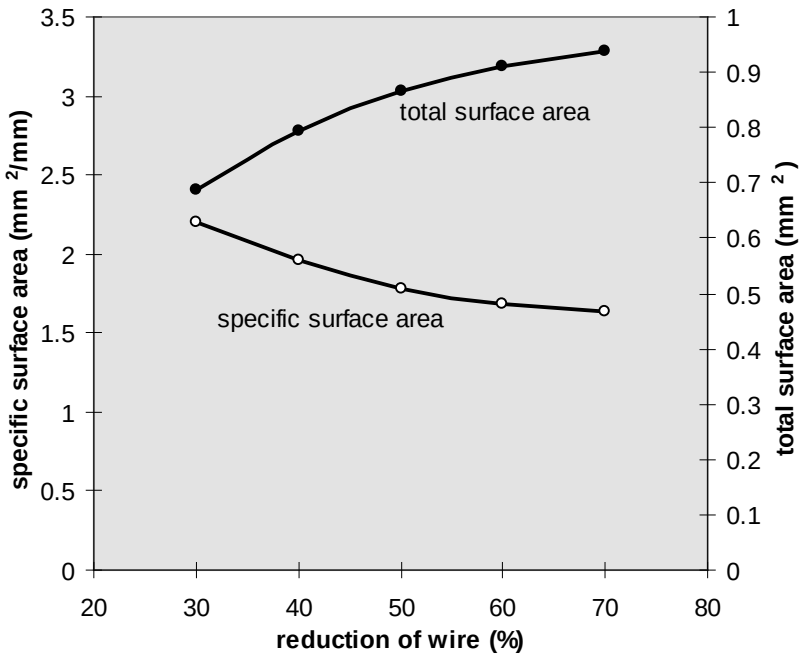

Figure 5.2.14 Variation of specific surface area and total surface of one wire with reduction

5.2.5 The effect of rolling temperature on the interfacial strength

Rolling temperature is the temperature at which the cold-rolled composite pre-form was heated, held and rolled. Because the final rolling temperature for all samples is nearly the same after 2 rolling passes (below Ac_1), the effect of internal stress/warm rolling (below Ac_1) on all samples is thought to be the same, so the main effect of rolling temperature on the interfacial strength is the effect it has on diffusion while the sample was heated and held at the rolling temperature.

The influence of rolling temperature on the interfacial strength between plain, copper coated and nickel coated wire and matrix is shown in Figure 5.2.15. The interfacial strengths for all samples increase with increasing rolling temperature, but the rolling temperature has a greater influence for the nickel-coated and plain wire than for copper-coated wire.

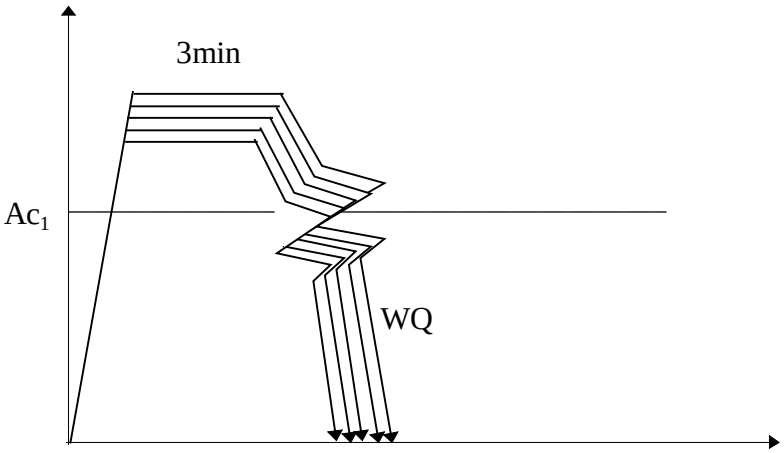

(a) experimental procedures

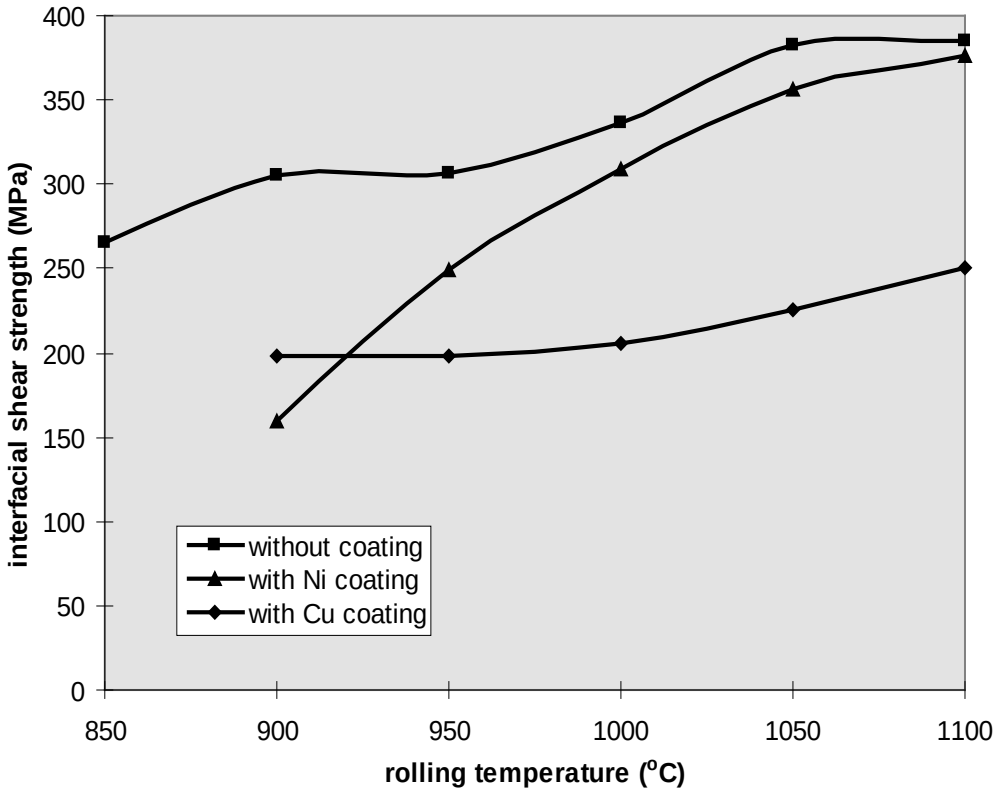

(b) testing results

Figure 5.2.15 Influence of rolling temperature (held for 3 min) on the interfacial strength between matrix steel and wire with different surfaces

During the heating of the sample, the redistribution of carbon will take place because of the large concentration difference between the matrix steel (0.04%) and the wire (0.8%). The diffusion of carbon across the interface will tend to reduce the abrupt nature of the interface resulting in a gradual strengthening of the matrix close to the interface (due to the higher carbon content) and a smoother transfer of load between the wire and matrix, thus increasing the interfacial strength.

The carbon diffusion depends primarily on temperature, time, and the lattice structure of the host material. In the uncoated material, there appears to be a slight dip in the trend around 900/950°C where we could expect the matrix to transform from ferrite to austenite, with the associated drop in diffusion rate, but otherwise the materials tend to increase in interfacial strength as rolling temperature increases.

For the composite reinforced with plain wire, the carbon diffuses from the high carbon wire to matrix with minimal resistance. However, for the copper-coated wire composites, carbon cannot dissolve in copper and the solubility of copper in iron is only about 7% at 1000°C, so carbon can diffuse into the matrix only through defects in the coating or after the copper-coating has fully dissolved in the matrix; the latter of which will need long time and high temperature. Thus the interfacial strength for copper-coated wire composite is fairly constant with a small increase above 1000°C.

Because carbon is soluble in nickel (the solubility of carbon in nickel is about 0.2% at 1000°C), carbon diffusion can occur through the nickel-coating to the matrix steel. The resistance of the nickel-coating to carbon diffusion is lower than that of the copper-coating but higher than that for plain wire, so the interfacial strength for nickel-coated wire composite is located between the others. With increasing rolling temperature, the solubility of carbon in nickel increases (from 0.2% in 1000°C to 0.3% in 1100°C), and the interfacial strengths in nickel-coated wire reinforced composites approaches that of the uncoated composites.

Another feature of nickel coating at high temperature is that nickel can react with iron to form the intermetallic compound $FeNi_3$ (see the phase diagram in Figure 5.2.16). The formation of this intermetallic compound at the interface not only strengthens the interfacial bonding but embrittles the wire (refer to section 5.1).

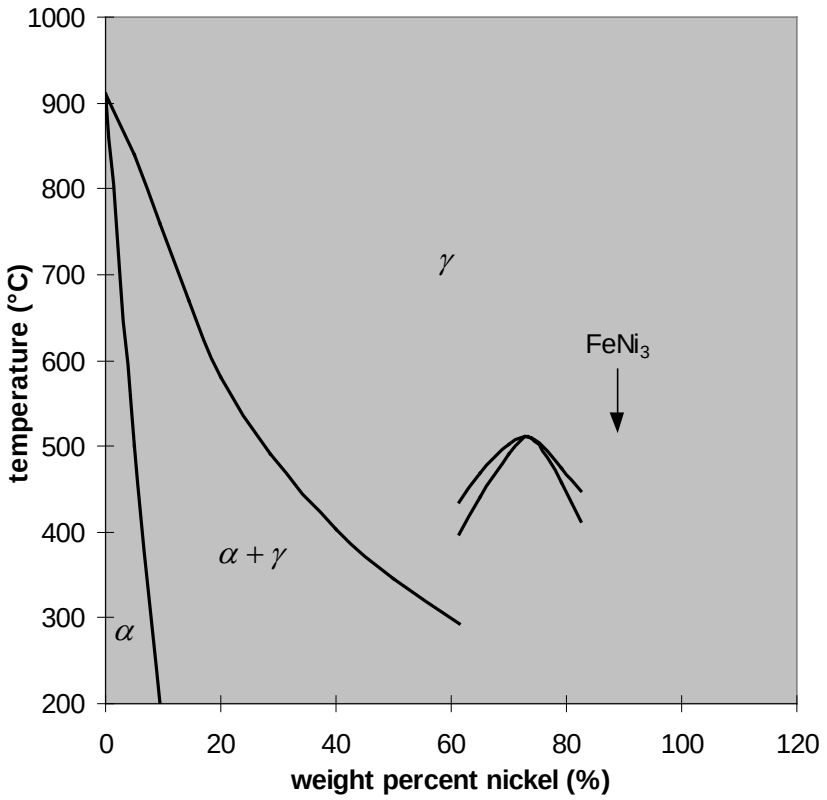

Figure 5.2.16 Phase diagram of iron-nickel showing the possible formation of $FeNi_3$ intermetallic compound[138]

The strengthening by the interfacial reaction results from the resistance of layer to the propagation of cracks along the interface. Because the reaction product is a hard phase, its strengthening effect is more effective than carbon diffusion and thus the increase of interfacial strength of nickel-coated wire composite with rolling temperature is more rapid than that of the plain wire composite.

Because the samples are heated in 3 mins, there are no large changes in microstructure (shown in Figure 5.2.17) as the carbon diffusion is limited to very short distances at the interface.

(a) plain wire heated at 950°C for 3 min

(b) plain wire heated at 1100°C for 3 min

(c) nickel-coated wire heated at 950°C for 3 min

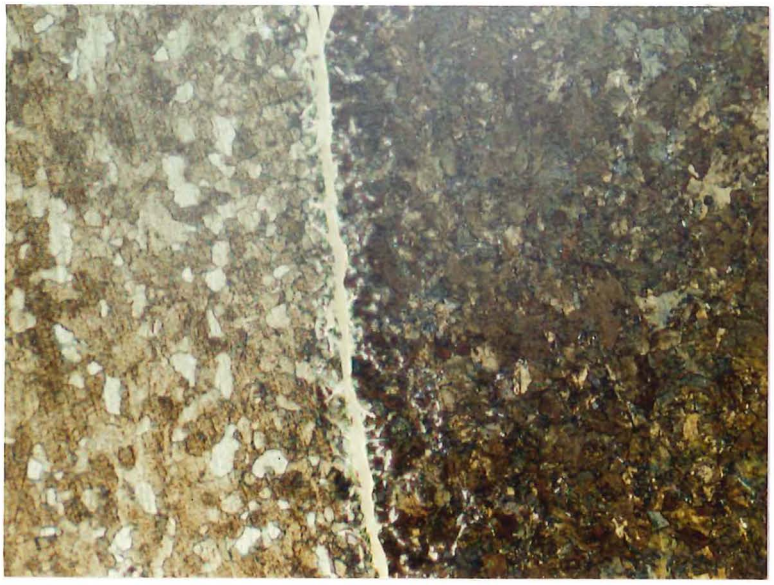

(d) nickel-coated wire heated at 1100°C for 3 min

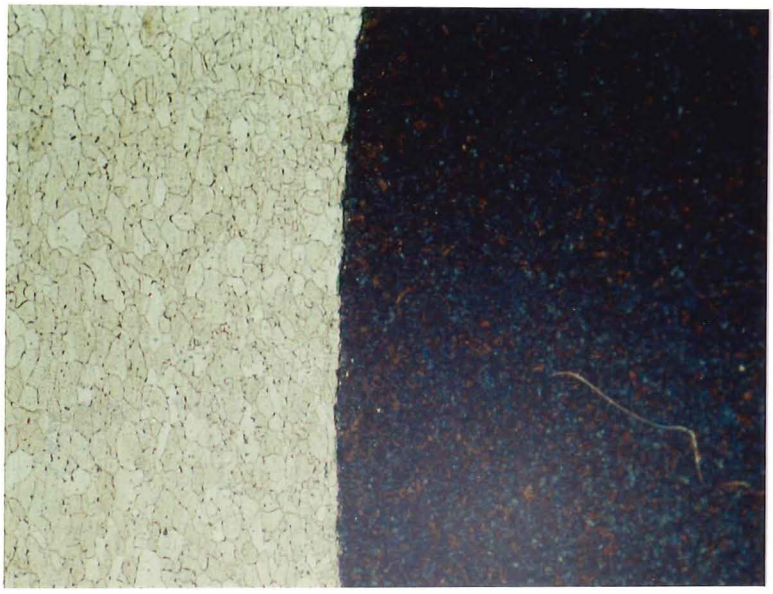

(e) copper-coated wire heated at 950°C for 3 min

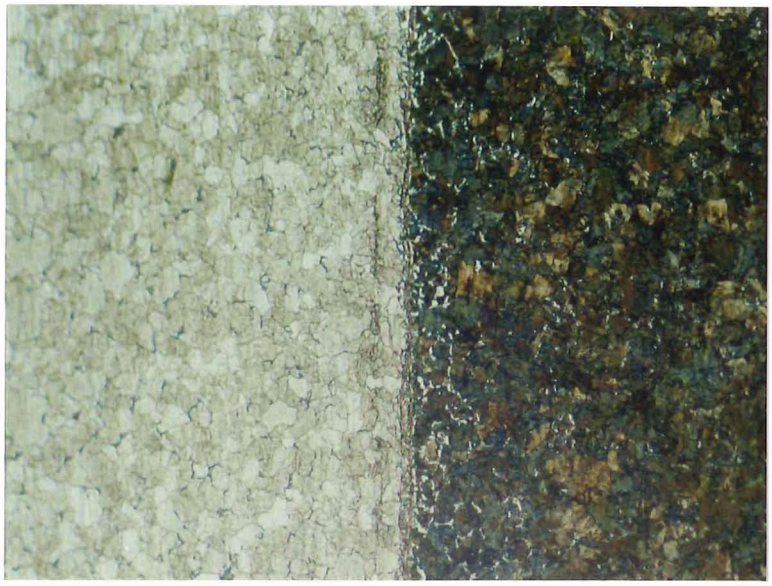

(f) copper-coated wire heated at 1100°C for 3 min

Figure 5.2.17 Variation in interfacial microstructure with rolling temperature and coatings (×230)

5.2.6 The influence of holding time on interfacial strength

As discussed above, in addition to rolling temperature, the holding time before rolling affects the interfacial strength through carbon diffusion and interfacial reaction respectively (shown in Figure 5.2.18). With increased holding time at a certain temperature, more carbon can diffuse through the interface if there is no barrier coating, more reaction product can form in nickel-coated wire composite, and thus the interfacial strengths of both uncoated and nickel-coated wire composites increase.

For copper-coated wire, the interfacial strength hardly changes even after 900 seconds at 950°C, whereas for both the uncoated and nickel coated wire, the interfacial strengths rise quite quickly with increasing time before reaching a plateau at about 360MPa (>700 seconds).

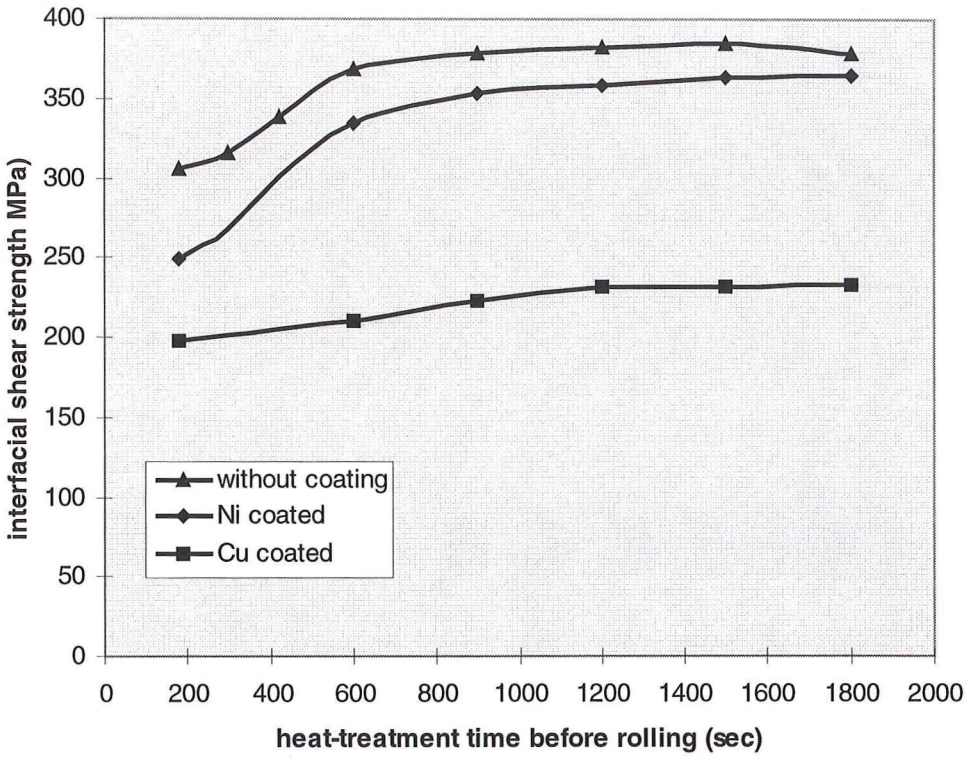

Figure 5.2.18 Influence of heat-treatment time at 950℃ before rolling on interfacial strength

The interface microstructure due to carbon diffusion is shown in Figure 5.2.19, with longer holding times more carbon has diffused into the matrix in plain wire, and nickel-coated wire composites.

(a) plain wire heated at 950°C for 3 min

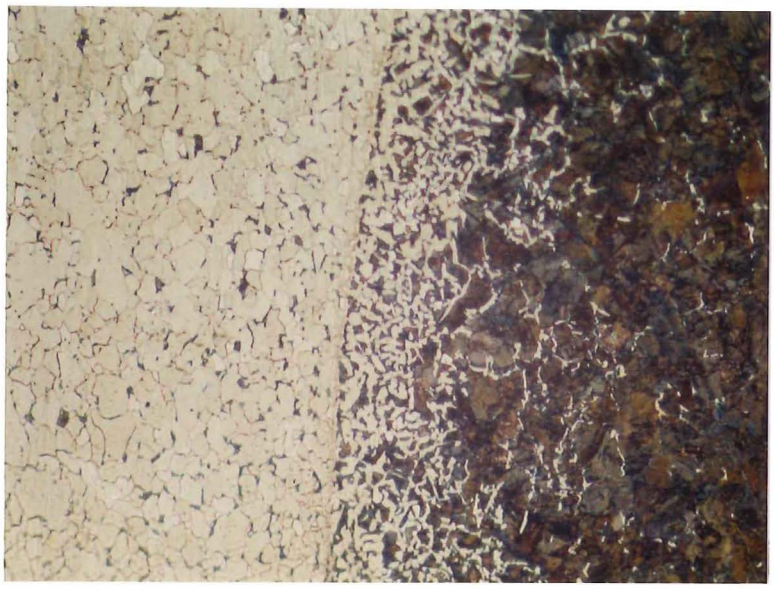

(b) plain wire heated at 950°C for 30 min

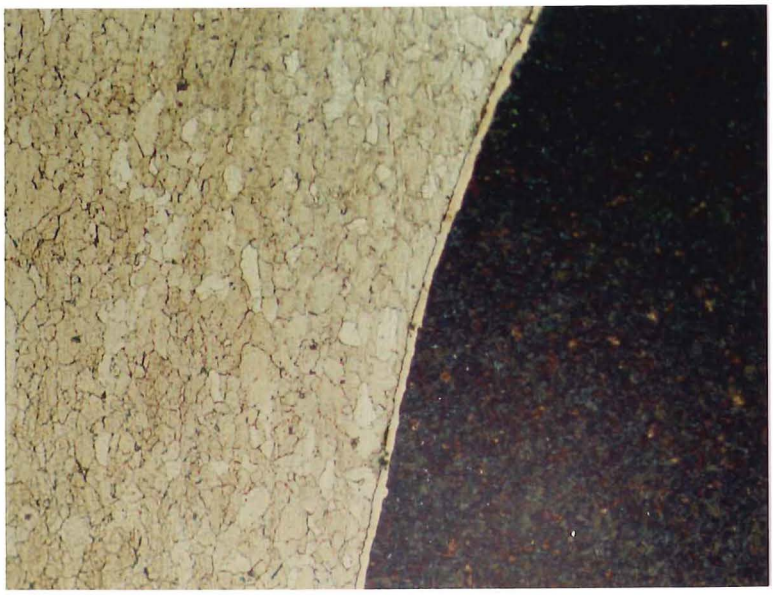

(c) nickel-coated wire heated at 950°C for 3 min

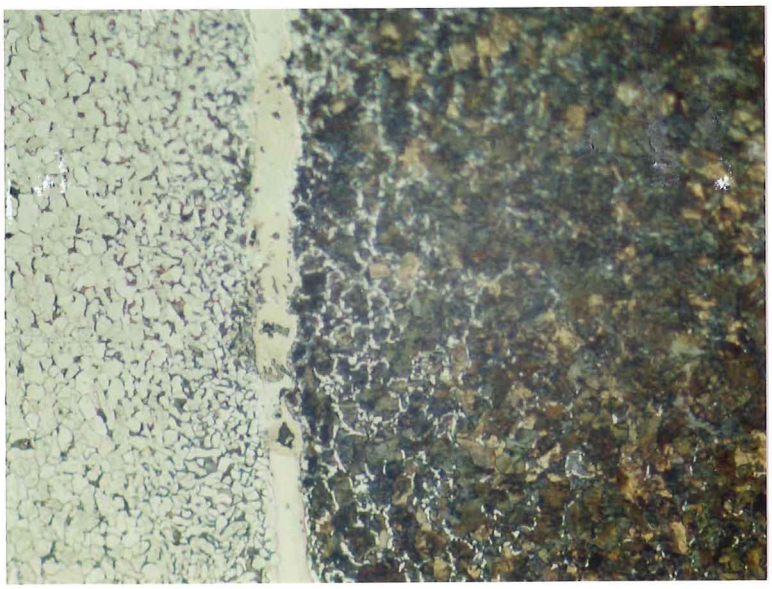

(d) nickel-coated wire heated at 950°C for 30 min

(e) copper-coated wire heated at 950°C for 3 min

(f) copper-coated wire heated at 950°C for 30 min

Figure 5.2.19 Microstructure of interface variation with holding time due to carbon diffusion (× 230)

5.2.7 Reduction by cold rolling prior to hot rolling

As can be seen in Figure 5.2.20, there is an improvement in interfacial strength if the specimen is subjected to a higher % reduction during the cold rolling stage before the holding period at elevated temperature.

The effect of cold rolling reduction could be due to a number of reasons:

(1) better bonding at the interface due to the increased forging at higher reductions.

(2) better protection of the wire surface from oxidation and thus more carbon diffusion into the matrix during the heating and holding period due to the flow of the matrix around the wire at higher reductions (see Figure 5.2.21). For small reductions, some of the wire surface is still exposed to oxidation, and less carbon diffusion occurs during the holding period before rolling. The wire has a high flow stress (because of its high carbon content and the strain hardening of cold drawing) and undergoes very little deformation during the cold rolling stage unlike the matrix steel.

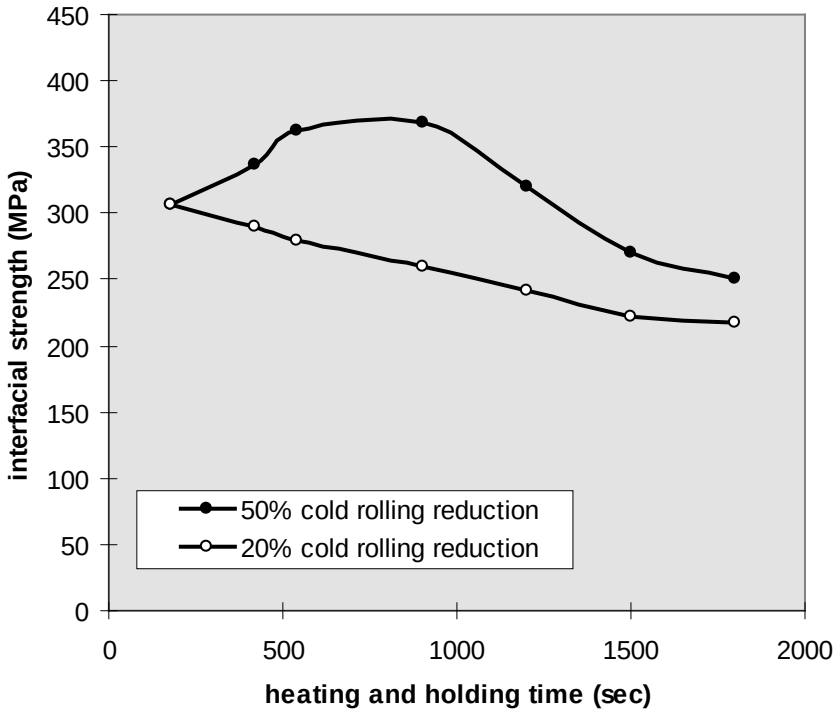

Figure 5.2.20. The effect of cold rolling before heating on the interfacial strength for plain wire reinforced matrix steel (air cooled after hot rolling)

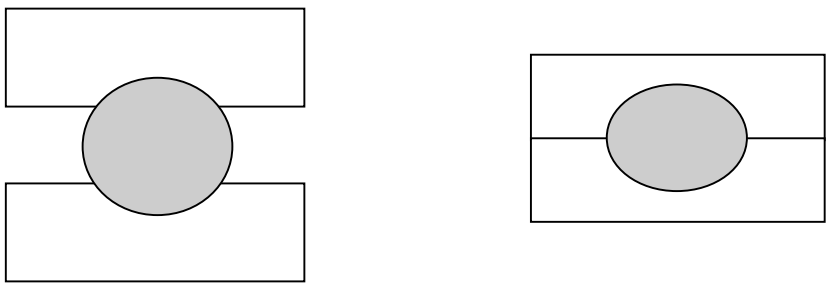

(a) 20% (b) 50%

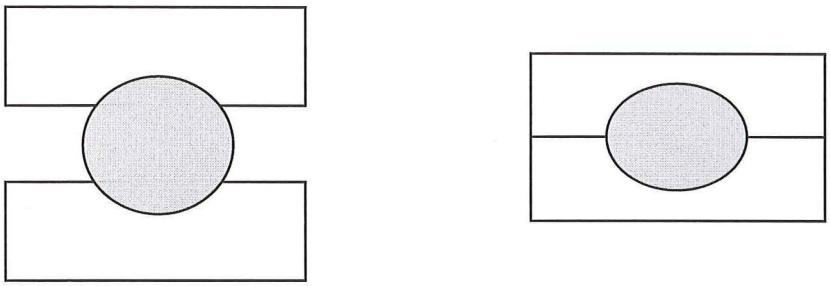

(a) 20% (b) 50%

Figure 5.2.21 Schematic section of different cold reductions before heating

As can be seen from Figure 5.2.22, there is very little pearlite in the interface of the 20% reduction sample compared to the heavily rolled material, and also there is an inclusion layer found at the interface, suggesting that there has been less carbon diffusion into matrix and that oxidation at the interface has occurred. This would support the oxidation mechanism proposed in (2) above.

The variation of interfacial strength with cold-rolling reduction suggests that cold rolling must be heavy enough to seal all the wire in the matrix in order to make good composites.

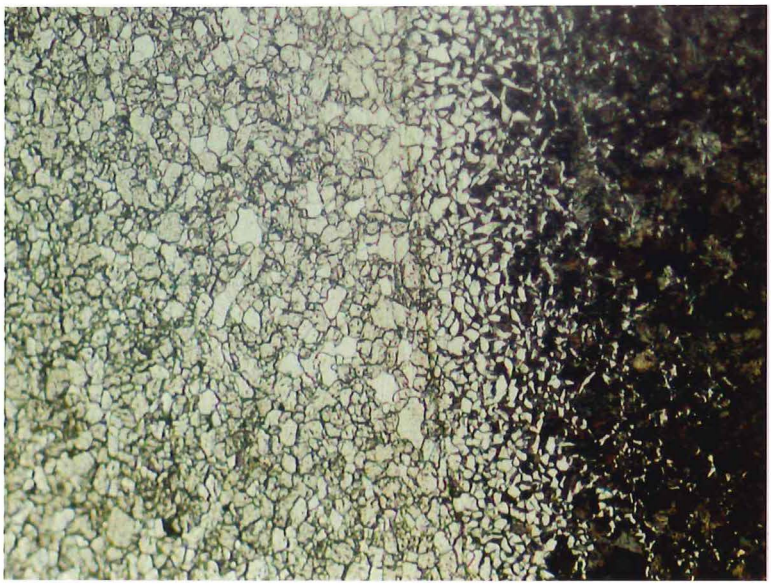

(a) 20 % cold rolling reduction

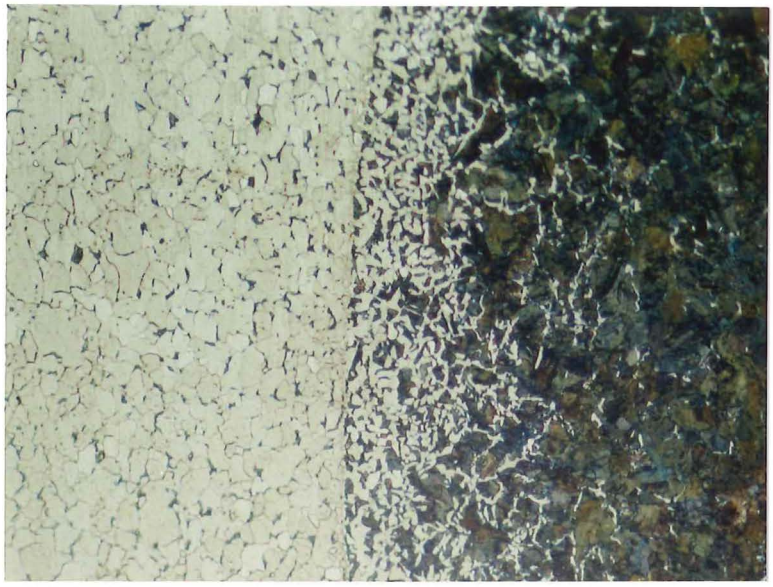

(b) 50% cold rolling reduction

Figure 5.2.22 The interface microstructure in composites with different cod rolling reductions (×230)

5.2.8 The effect of austempering on the interfacial strength

Owing to the high brittleness of the wire arising from cooling after rolling (as has been discussed in section 5.1), the as-rolled composites need an extra heat-treatment after fabrication to obtain the best combination of strength and ductility. Austempering was chosen for the high carbon material instead of water-quenching to prevent martensitic formation which has been shown to reduce wire strength dramatically due to premature fracture (refer to section 5.1). The effect of austempering on the interfacial strength has been examined in Figure 5.2.23.

Figures 5.2.23 (a) and (b) show a schematic of the austempering procedures and the interfacial strength relationship between as-rolled and austempered samples respectively. The variation in interfacial strengths of the as-rolled composites are due to their different fabrication parameters (ie. the rolling temperature, as shown in Figure 5.2.23 a). It can be seen that austempering lowers the interfacial strength of the as-rolled composites; the interfacial strength of austempered composite increased linearly with that of as-rolled composite.

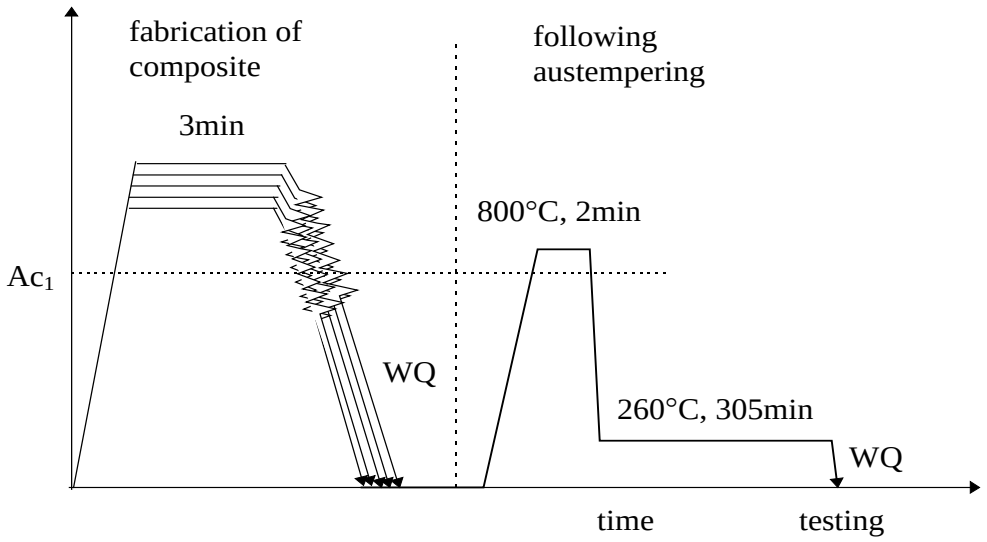

(a) experimental procedures

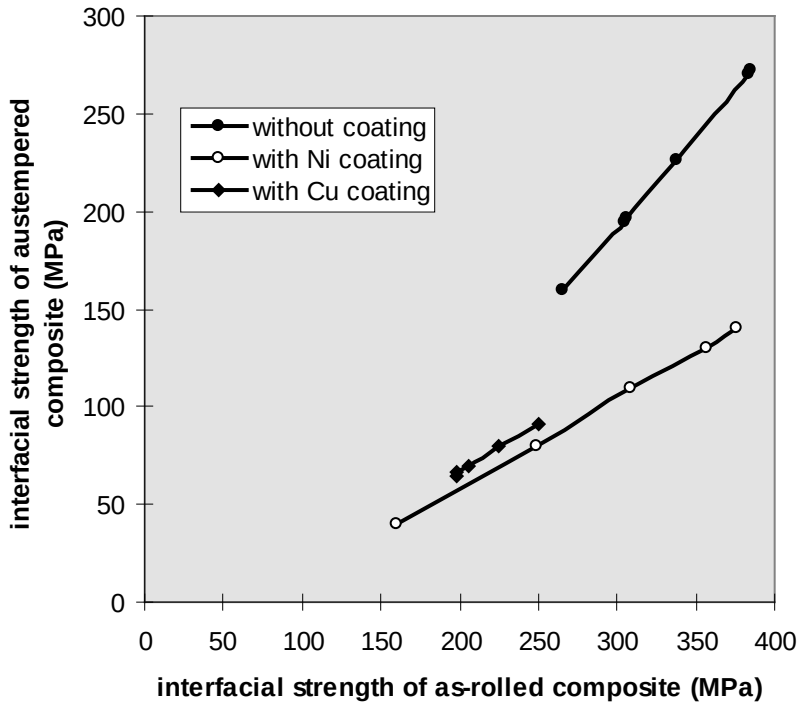

(b) testing results

Figure 5.2.23. Interfacial strength relationship between as-rolled and austempered composites

The austempering affects the interfacial strength through the follows:

(1) the relaxation of the deformed interface due to recrystallization during reheating for austempering, which decreases the internal stress and dislocation density, thus reducing the interfacial strength.

(2) phase transformation at the interface; the deformed interfacial phases of the water-quenched samples transform into pearlite or bainite, which reduce the interfacial strength. The transformed interface is shown in Figure 5.2.24.

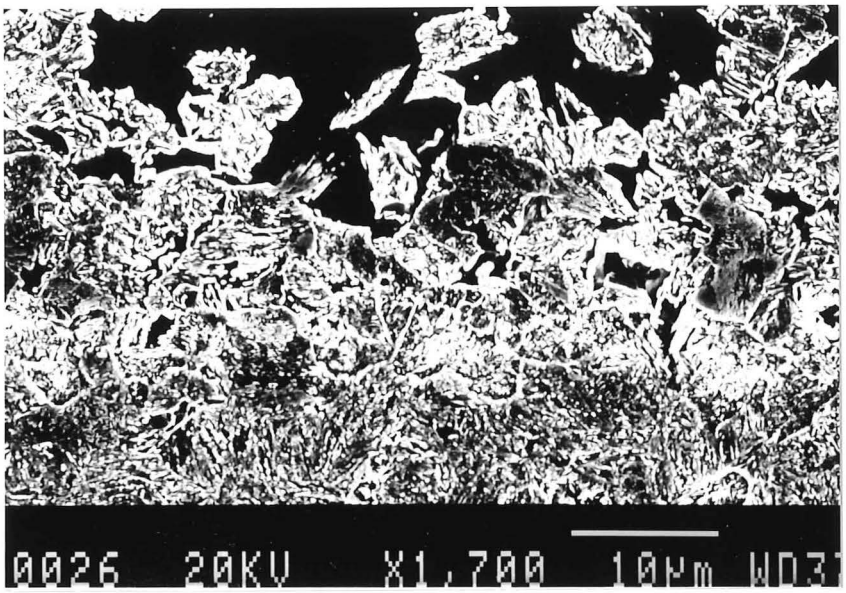

Figure 5.2.24 The microstructure of interface after austempering

The effect of austempering on interfacial bonding depends on the wire surface. The decrease of interfacial strength in nickel-coated and copper-coated wire composites is more pronounced than in uncoated wire composites.

5.2.9 Analysis of interface due to diffusion

At the isothermal holding period before rolling, carbon diffusion between wire and matrix takes place. The main difference in composition of the wire and matrix steel is in carbon content. The carbon diffusion between wire and matrix is thought to play an important role in strengthening the interface and the matrix near the interfacial region (in addition to that provided by internal stresses).

5.2.9.1 Carbon diffusion

Consider a single wire in the matrix steel (as shown in Figure 5.2.25) and take an element at a distance r from the centre of the wire (Figure 5.2.26).

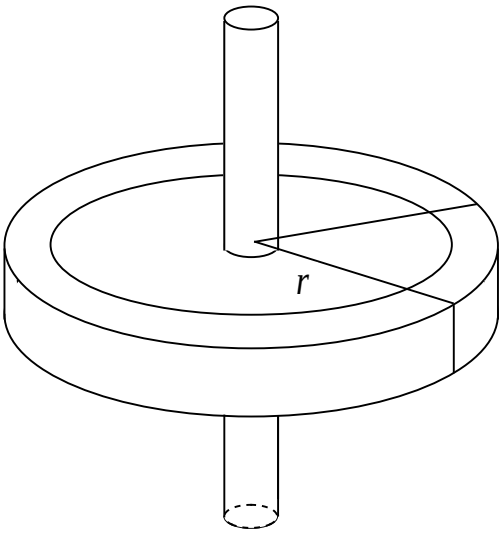

Figure 5.2.25 The single-wire reinforced composite model

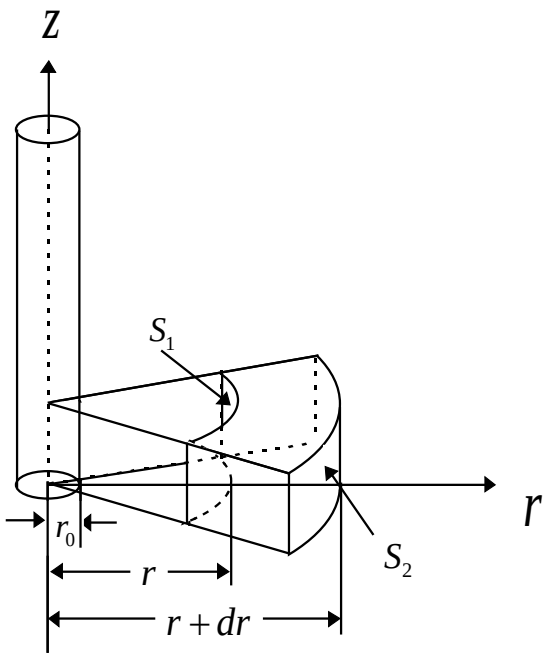

(a) analysis model

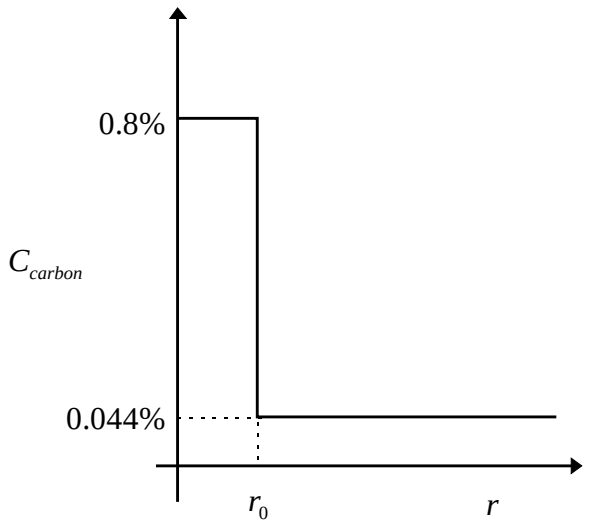

(b) initial carbon profile

Figure 5.2.26 Diffusion analysis on an element at distance r from the centre of the wire

According to Fick's first law, the carbon diffusion flux J_1^c across the first reference plane S_1 is:

$$J_1^c = -D\frac{dC}{dr} \tag{5.2.3}$$

where, C is the carbon content, and D is the diffusion coefficient of carbon in iron, which varies with temperature according to:

$$D = D_0 \exp(-\frac{Q}{RT}) \tag{5.2.4}$$

where, T is the isothermal holding temperature, R is the gas constant ($8.31\ J/mol \cdot K$), D_0 is the frequency factor, and Q is the activation energy of diffusion of carbon in iron. The values of D_0 and Q of carbon in austenite can be found in several sources as follows:

Table 5.2.1 Diffusion constants of carbon in iron (austenite)

Reference sources	D_0 (m^2/s)	Q (kJ/mol)
Smithells metals reference book[139]	2.34×10^{-5}	147.81
CRC Materials science and engineering handbook[140]	1.5×10^{-5}	142.35
Foundations of materials science and engineering[141]	1×10^{-5}	136

The diffusion flux J_2^c across the second reference plane S_2 is:

$$J_2^c = J_1^c + \frac{dJ_1^c}{dr} dr \tag{5.2.5}$$

The carbon concentration in the element is changing with time; its rate ($\frac{\partial C}{\partial t}$) is the difference in diffusion flux between S_1 and S_2, ie,

$$\frac{\partial C}{\partial t} = \frac{J_2^c - J_1^c}{dr} = \frac{\partial}{\partial r}(D\frac{\partial C}{\partial r}) \tag{5.2.6}$$

Because the diffusion coefficient of carbon in iron, D, can be considered constant, the equation (5.2.6) can be changed to:

$$\frac{\partial C}{\partial t} = D\frac{\partial^2 C}{\partial r^2} \tag{5.2.7}$$

The solution to equation (5.2.7) can be obtained with different boundary conditions for the different surface characteristics of the wire.

Carbon diffusion in uncoated wire reinforced composites

In this case, the boundary conditions for carbon diffusion are:

$$\begin{cases} C = C_m & at \quad t = 0 \\ C = \frac{1}{2}(C_w + C_m) & at \quad r = r_0 \end{cases} \tag{5.2.8}$$

where, C_m and C_w are the carbon contents in matrix and wire respectively before heating, t is the isothermal holding time at a given temperature, r_0 is the radius of wire. The solution to equation (5.2.7) is given as:

$$C = C_m - \frac{C_w - C_m}{2}(1 - erf\ \frac{r - r_0}{2\sqrt{Dt}}) \tag{5.2.9}$$

Replacing Q and D_0 by 2.34×10^{-5} m^2/sec and 147.81KJ/mol[(140)] respectively in equation (5.2.4) and C_m, C_w and r_0 by 0.044%, 0.8% and 8×10^{-4} m, respectively in equation (5.2.9), we can get the following equations:

$$C = 0.422 - 0.378 erf\left(\frac{r - 8 \times 10^{-4}}{2\sqrt{Dt}}\right) \qquad (5.2.10)$$

$$D = 2.34 \exp\left(-\frac{147810}{8.31 \times T}\right) \times 10^{-5} m^2 / \sec \qquad (5.2.11)$$

to solve the carbon diffusion in plain wire reinforced matrix composites.

The carbon content distributions across the interface according to equations (5.2.10) and (5.2.11) and are shown in Figures 5.2.27 (for a certain holding time, 3min) and 5.2.28 (at a given temperature, 950°C). The carbon content at the surface of the wire tends to 0.422%, and there is an increasingly thicker band of matrix with a higher carbon content as both temperature and isothermal holding time are increased.

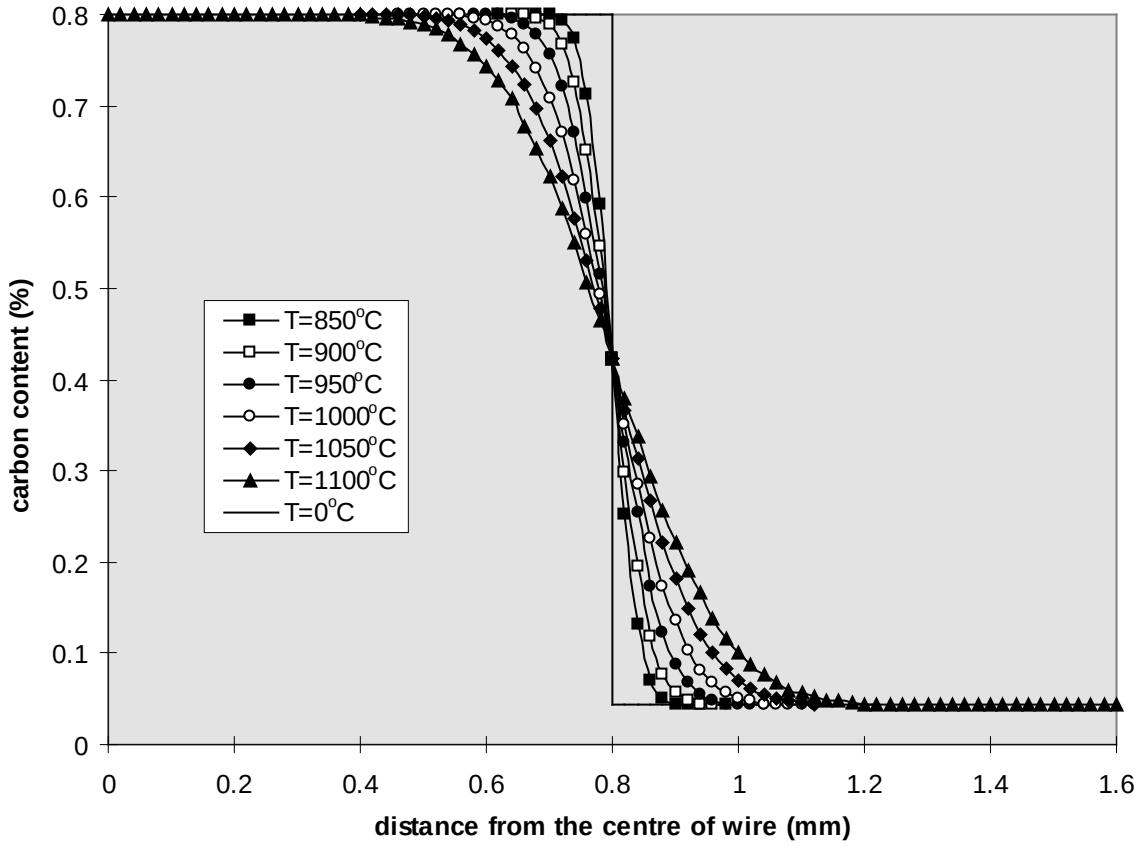

Figure 5.2.27 The influence of rolling temperature on the carbon diffusion between steel No.1 and plain wire (isothermal held for 3 min.)

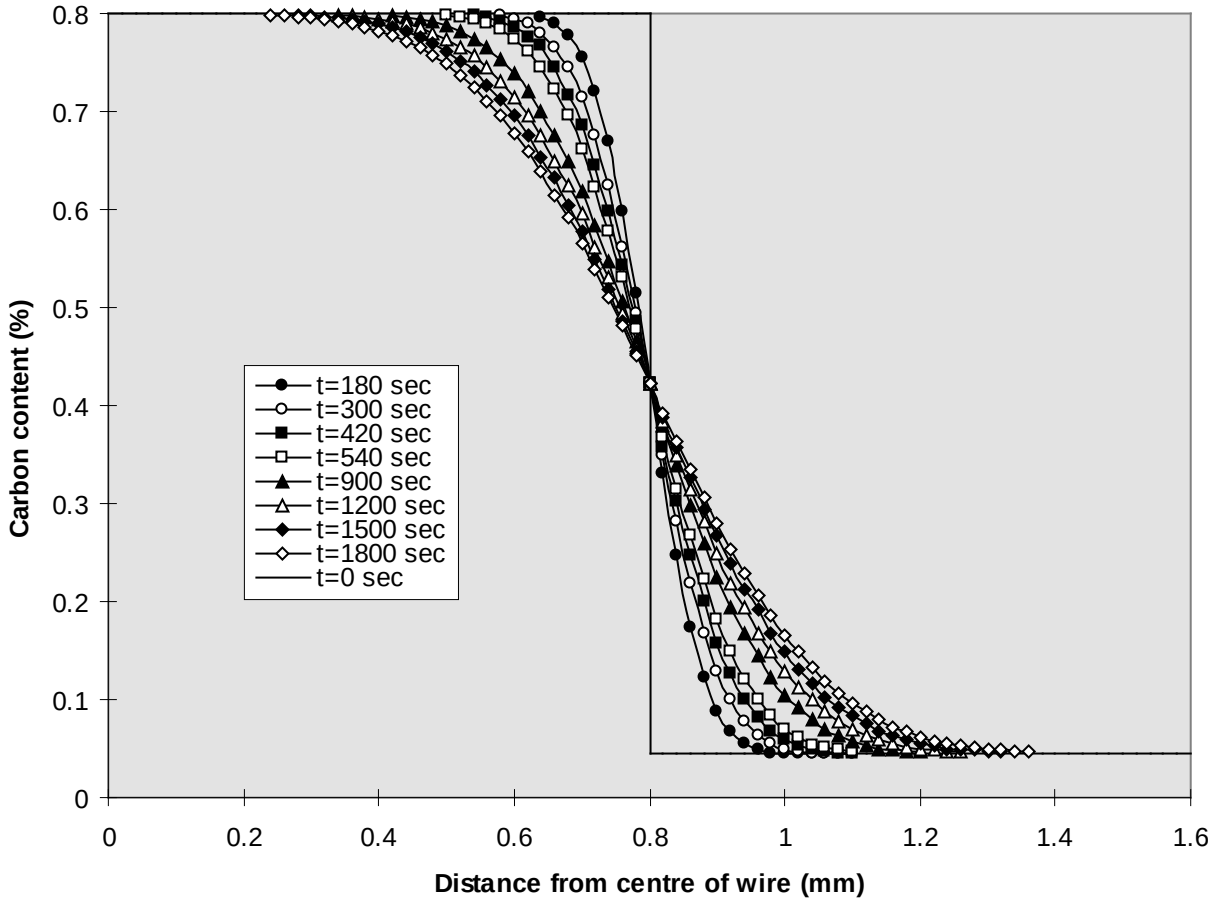

Figure 5.2.28 The effect of isothermal holding time on the carbon diffusion between 0.044%C matrix steel and plain wire (at 950^{o}C)

Carbon diffusion in coated wire composites

For nickel-coated wire reinforced composites, there are three different diffusion processes take place during heating:

(1) nickel diffusing into the wire and the matrix;

(2) carbon diffusing into the nickel coating from the wire;

(3) carbon in the nickel coating diffusing into the matrix.

In the first process, the diffusion coefficient of nickel in iron at 950°C is given by[139]:

$$D_{Ni}^{Fe} = 7.7\exp(-\frac{280500}{8.31*1223})\times 10^{-5} = 7.9*10^{-17} m^2 / \sec$$

which is much lower than that of carbon in iron by a factor of $\cong 10^6$, so the nickel diffusion into the steel can be ignored.

Because the maximum solubility of carbon in nickel is about 0.18% at 950°C, the carbon diffusion through the interface will be limited. The boundary condition for nickel coating is:

$$\begin{cases} C_C^{Ni} = 0 & at \quad t = 0 \\ C_C^{Ni} = C_{\max}^{Ni} & at \quad r = r_0 \end{cases} \tag{5.2.12}$$

where C_C^{Ni} is the carbon content in nickel coating, and $C_{\max}^{Ni}$ is the maximum solubility of carbon in nickel, which varies with temperature. The carbon content in the nickel coating is obtained by applying the above boundary condition to equation (5.2.7), as:

$$C_C^{Ni} = C_{\max}^{Ni}(1 - erf\ \frac{r - 8\times 10^{-4}}{2\sqrt{Dt}}) \tag{5.2.13}$$

$$D = 1.2\exp(-\frac{137300}{8.31*T})\times 10^{-5} m^2 / \sec \tag{5.2.14}$$

The boundary condition for the carbon diffusion in the matrix is:

$$\begin{cases} C_C^{Fe} = \frac{1}{2}\left(C_{C,surface}^{Ni} + C_m\right) & r = r_0 + h_{Ni} \\ C_C^{Fe} = C_m & t = 0 \end{cases} \tag{5.2.15}$$

where, C_C^{Fe} is the carbon content in the matrix steel that has diffused through the nickel coating, $C_{C,surface}^{Ni}$ is the carbon content in the surface of the nickel coating obtained from equation (5.2.14) at $r = r_0 + h_{Ni}$, and h_{Ni} is the thickness of the coating, so the carbon content variation is:

$$C_C^{Fe} = C_m + \frac{C_{C,surface}^{Ni} - C_m}{2}(1 - erf\ \frac{r - 8\times10^{-4} - h_{Ni}}{2\sqrt{Dt}}) \qquad (5.2.16)$$

$$D = 2.34\exp(-\frac{147810}{8.31\times T})\times10^{-5} m^2\ /\ \sec \qquad (5.2.17)$$

The carbon content at the interface between the nickel-coated wire and the steel matrix as a function of rolling temperature and isothermal holding time is shown in Figures 5.2.29 and 5.2.30, which show that the carbon content at the interface between nickel-coated wire and matrix is much smaller than that for the uncoated wire composites (refer to Figures 5.2.17 and 5.2.19).

For copper-coated wire reinforced composites, carbon diffusion can take place only after the copper-coating has diffused into the surrounding steel wire and matrix because the solubility of carbon in copper is 0%. The diffusion coefficient of copper in iron at 950°C is given by[140]:

$$D_{Cu}^{Fe} = 2.86\exp\left(-\frac{306700}{8.31\times1223}\right)\times10^{-4} m^2\ /\ \sec = 2.22\times10^{-17} m^2\ /\ \sec$$

The time needed to diffuse a 0.07mm thick layer of copper into steel is:

$$t = \frac{h_{Cu}{}^2}{D_{Cu}^{Fe}} = 6.13\times10^4\ hours$$

so in the limited isothermal holding time used, the carbon is thought to diffuse from wire into matrix only through defects in the copper coating; it's hard to find pearlite at the interface between copper-coated wire and matrix (verified in Figure 5.2.19).

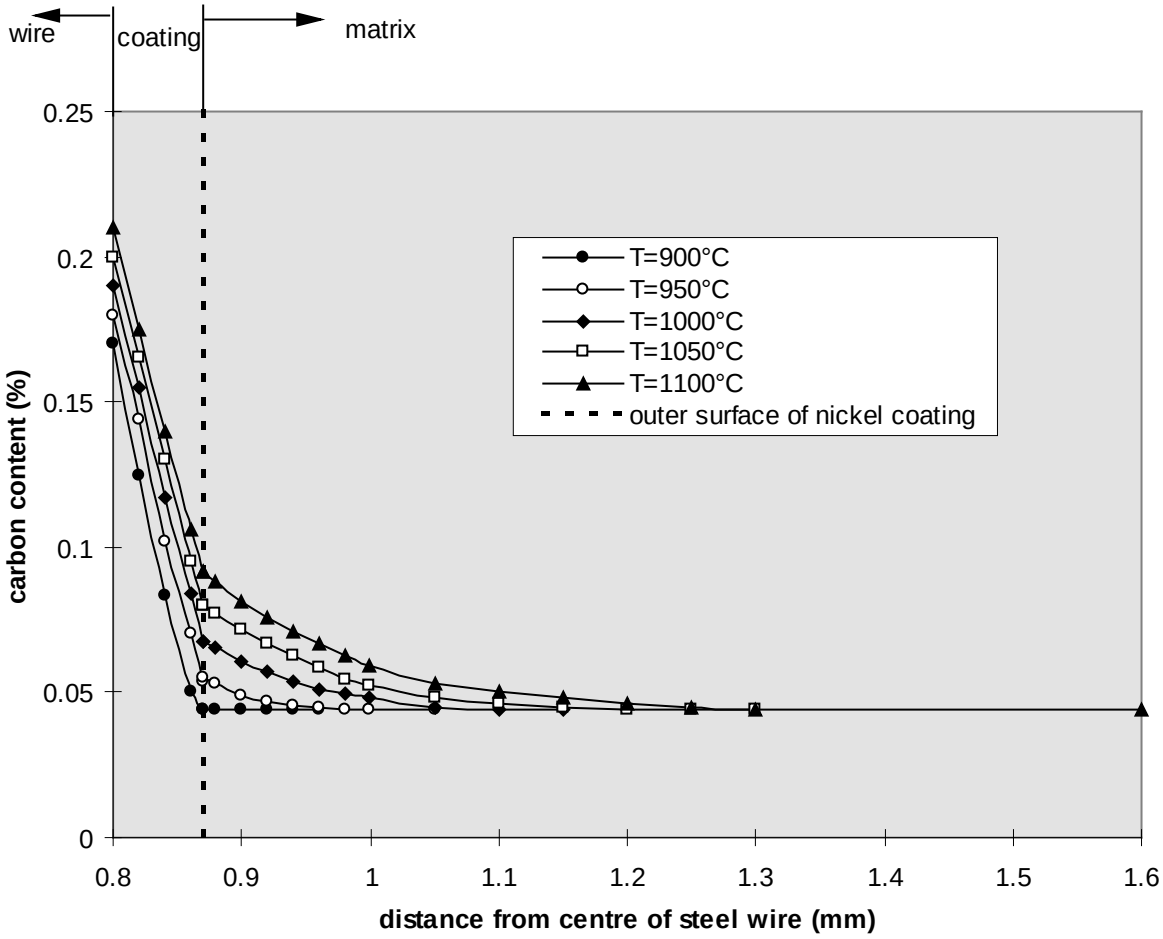

Figure 5.2.29 The influence of temperature on the carbon diffusion to the matrix from the nicked-coated wire (for 180 sec)

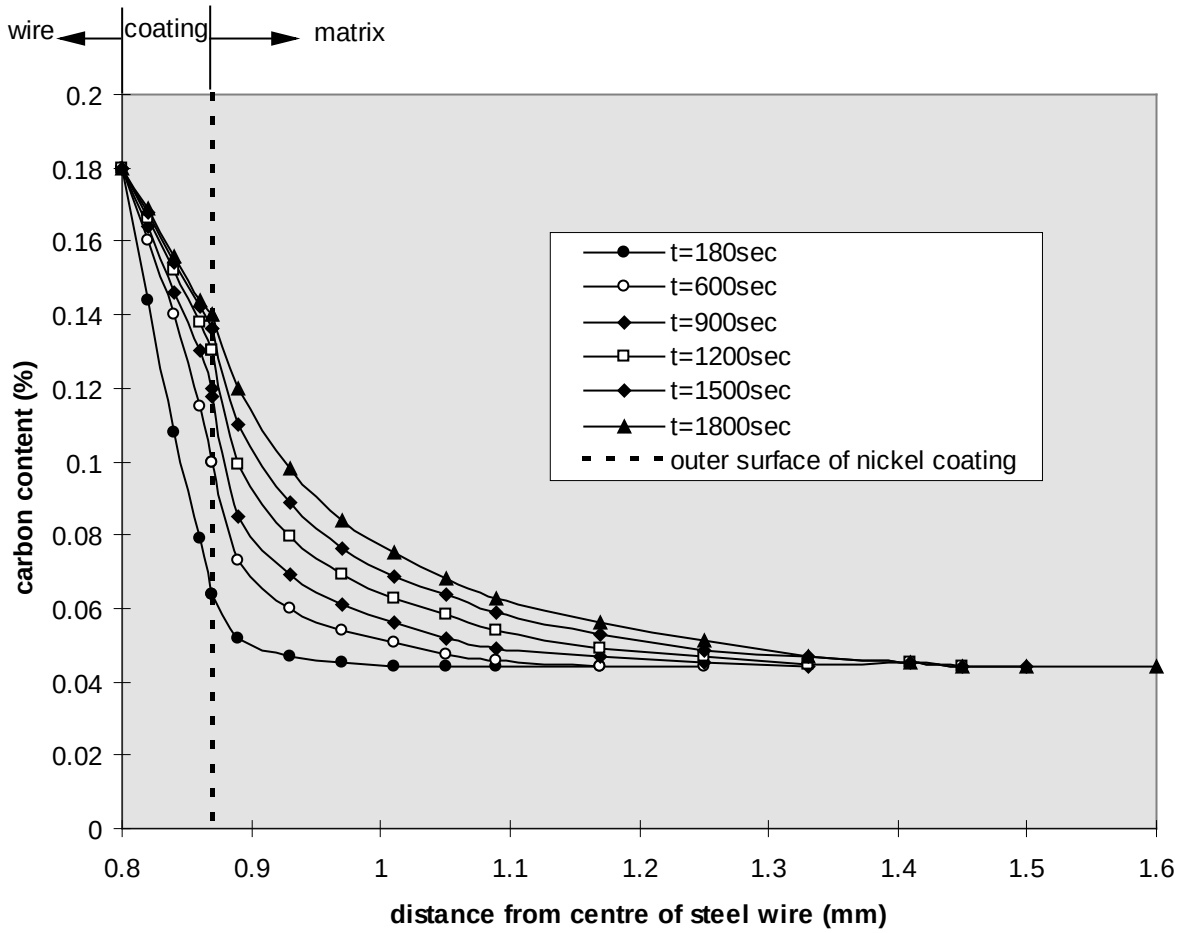

Figure 5.2.30 Variation of carbon content across the interface of nickel coated wire as a function of isothermal holding time (950℃)

5.2.9.2 Interfacial strength

The interfacial shear strength is in fact the shear strength of the matrix steel near the interface, the process of interface fracture involves breaking atomic bonds at the interface. This can be viewed from fracture energy equilibrium considerations.

Energy equilibrium theory

The interfacial energy is a very important parameter for a grain boundary when nucleation, and growth (grain boundary movement) are investigated. The interfacial energy in composite materials is also important for understanding interface debonding and crack propagation along the interface during composite fracture.

A brief introduction to the following three analysis methods which are used to treat the grain boundary energy will be helpful for studying the interfacial energy in steel-steel composite materials.

(a) *The Nearest Neighbor Broken Bond Model*: This model was developed by Becker[142] and was used to investigate the coherent interphase boundary energy, under the assumption that both phases are homogeneous up to their common interface, the coherent boundary energy is expressed as:

$$\gamma = n_s Z_s (x_\alpha^{\alpha\beta} - x_\beta^{\beta\alpha})^2 \cdot \Delta E \qquad (5.2.18)$$

where n_s is the number of atoms per unit area at the interface, Z_s the coordination number across the interface, $x_\alpha^{\alpha\beta}$ and $x_\beta^{\beta\alpha}$ are the equilibrium atom fractions of solute in the α and β phases, and ΔE is defined by:

$$\Delta E = \mu_{AB} - (\mu_{AA} + \mu_{BB})/2 \qquad (5.2.19)$$

where, the μ's are the enthalpies of single A-B, A-A and B-B bonds, respectively. Usually, Becker's prediction is inaccurate because it is based on a very restrictive assumption that both phases are homogeneous up to their common interface but the fact is, there is a width of the composition-altered region in the vicinity of the boundary.

(b) *Continuum Model*: Cahn and Hilliard[143] developed a continuum description of coherent interphase boundary energy, which was based on integration of a multi-

variable Taylor's Series expansion of the free energy of an inhomogeneous solid solution:

$$\gamma = 2n_v \lambda kT_c \int_{x_\alpha^{\alpha\beta}}^{x_\beta^{\beta\alpha}} (\Delta f \ / \ kT_c)^{1/2} dx \qquad (5.2.20)$$

where n_v is the number of atoms per unit volume, λ is an interaction distance which is very sensitive to the details of the interatomic potential function, k is Boltzman's constant, T_c is the critical temperature of the miscibility gap for a regular solution, and Δf is free energy difference between an atom at a given concentration in the inhomogeneous zone and an atom in an equilibrium mixture of the two phases. Using the regular solution model, and supplementary approximations to circumvent a numerical integration, the coherent boundary energy was obtained:

$$\gamma = 2n_v \lambda [kT_c]^{1/2} [\pi \cdot \Delta x_e (\Delta f_{\max})^{1/2} \ / \ 2][1 - (\pi / 2 - 4/3)(T / T_c)] \qquad (5.2.21)$$

where $\Delta x_e = 0.5 - x_\alpha^{\alpha\beta}$ and

$$\Delta f_{\max} = -2kT_c (0.5 - x_\alpha^{\alpha\beta})^2 + kT[0.5 \ln 0.5 / x_\alpha^{\alpha\beta} + 0.5 \ln 0.5 / (1 - x_\alpha^{\alpha\beta})]$$

The coherent boundary energy obtained from continuum theory is independent of boundary orientation as shown above.

(c) *Discrete Lattice Model*: Different from the continuum treatment introduced above, a discrete lattice plane model has been put forward to calculate the equilibrium concentration profile and chemical interfacial energy of fully coherent f.c.c.:f.c.c., b.c.c.:b.c.c. and h.c.p.:f.c.c. interphase boundaries[(144)]. By using statistical thermodynamics, the interfacial energy is:

$$\gamma \ = \Delta H - T\Delta S$$

where ΔH and ΔS are the total bond enthalpy and entropy changes between the initial state and equilibrium state respectively, and T is the temperature. By calculating the enthalpy and entropy changes, the coherent boundary energy is obtained:

$$\gamma = n_s \sum_i [-\Delta E (x_i - x_\alpha^{\alpha\beta})^2 Z + \Delta E \sum_j (x_i - x_{i+j})^2 Z_j + kT \left\{ x_i \ln \frac{x_i}{x_\alpha^{\alpha\beta}} + (1 - x_i) \ln \frac{1 - x_i}{1 - x_\alpha^{\alpha\beta}} \right\}]$$

where x_i is the atom fraction of solute in the i'th boundary layer, Z and Z_j are total

coordination number and coordination number to the nearest neighboring atoms in the j'th boundary layer.

From the three models reviewed above, the boundary energy is dependent on the energy of a single bond at the boundary and the number of bonds near the boundary; these concepts will be used in the following analysis.

Analysis of work of fracture

When the wire is pulled out from the matrix and the interface is sheared, the work performed (work of fracture) breaks the atomic bonds between the matrix and the reinforcement. According to energy equilibrium theory, this work of fracture must equal the total bond energy of the broken bonds.

The work of fracture is the area under the load/displacement curve (shown in Figure 5.2.31) and is given by:

$$W = \int_{\Delta} PdL \tag{5.2.22}$$

where, P is the load, and Δ is displacement.

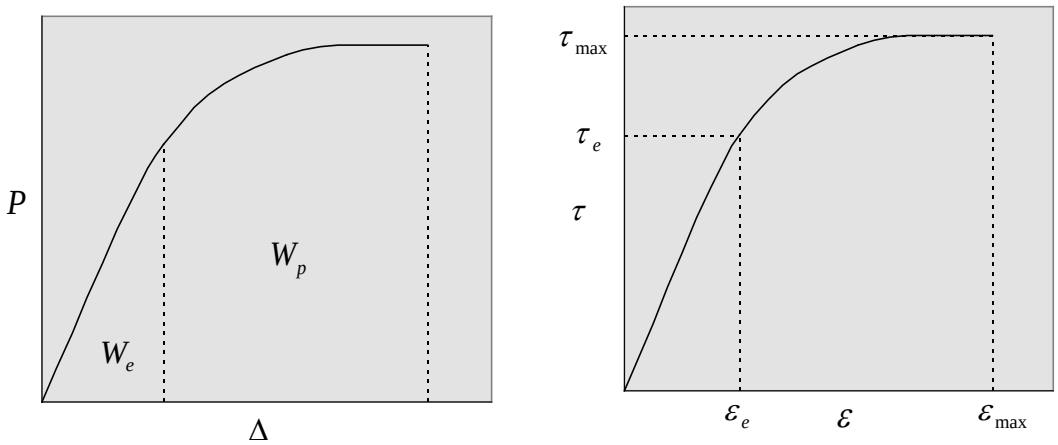

Figure 5.2.31 Illustration of (a) load-displacement and (b) shear stress-strain plots

If the fracture is within the elastic limit, ie. the interfacial strength is not high enough to cause plastic deformation at interface, the work of fracture will be

$$W = \frac{1}{2} P \cdot \Delta = \frac{1}{2} \tau \cdot \varepsilon \cdot S_0 \cdot L_0 \tag{5.2.23}$$

where, S_0 and L_0 are the initial surface area and length respectively, τ and ε are the interfacial shear strength and shear strain and their relationship obeys Hooke's law:

$$\tau = G\varepsilon$$

where, G is shear modulus, so the work of fracture is:

$$W = k\tau^2 \tag{5.2.24}$$

where, $k = S_0 \cdot L_0 / 2G$.

If the fracture is beyond the elastic limit, the work of fracture is comprised of elastic deformation work, W_e, and plastic deformation work, W_p (see Figure 5.2.31), ie,

$$W = W_e + W_p \tag{5.2.25}$$

in which, $W_e = k\tau_e^2$, where τ_e is the maximum elastic shear stress, which is a constant for the same steel-wire and steel matrix system.

$$W_p = S_0 \cdot L_0 \int_{\varepsilon_e}^{\varepsilon_{\max}} \tau d\varepsilon \tag{5.2.26}$$

where $\varepsilon_{\max}$ is the maximum shear strain, and ε_e is the maximum elastic shear strain. According to the Swift equation, the relationship between plastic stress and strain is as follows:

$$\varepsilon = \varepsilon_0 + m\tau^n \tag{5.2.27}$$

where, ε_0, m, n are constants, so the plastic work can be written as:

$$\begin{aligned} W_p &= S_0 \cdot \Delta_0 \cdot m \cdot n \int_{\tau_e}^{\tau_{\max}} \tau^n d\tau \\ &= S_0 \cdot \Delta_0 \cdot m \cdot n\left(\tau_{\max}^{n+1} - \tau_e^{n+1}\right) / (n+1) \\ &= A\tau_{\max}^{n+1} + B \end{aligned} \tag{5.2.28}$$

where, $A = \dfrac{S_0 \cdot \Delta_0 \cdot m \cdot n}{n+1}$, and $B = \dfrac{S_0 \cdot \Delta_0 \cdot m \cdot n}{n+1}\tau_e^{n+1}$.

The complete work of fracture is:

$$W = A\tau_{\max}^{n+1} + C \tag{5.2.29}$$

where, $C = W_e + B$.

Interfacial bond energy

Consider the atomic array in the interface layer (shown in Figure 5.2.32). Because the diffusion rate of copper and nickel in steel is several orders lower than that of carbon in steel, only the carbon diffusion will be taken into account when calculating the bond energy at the interface.

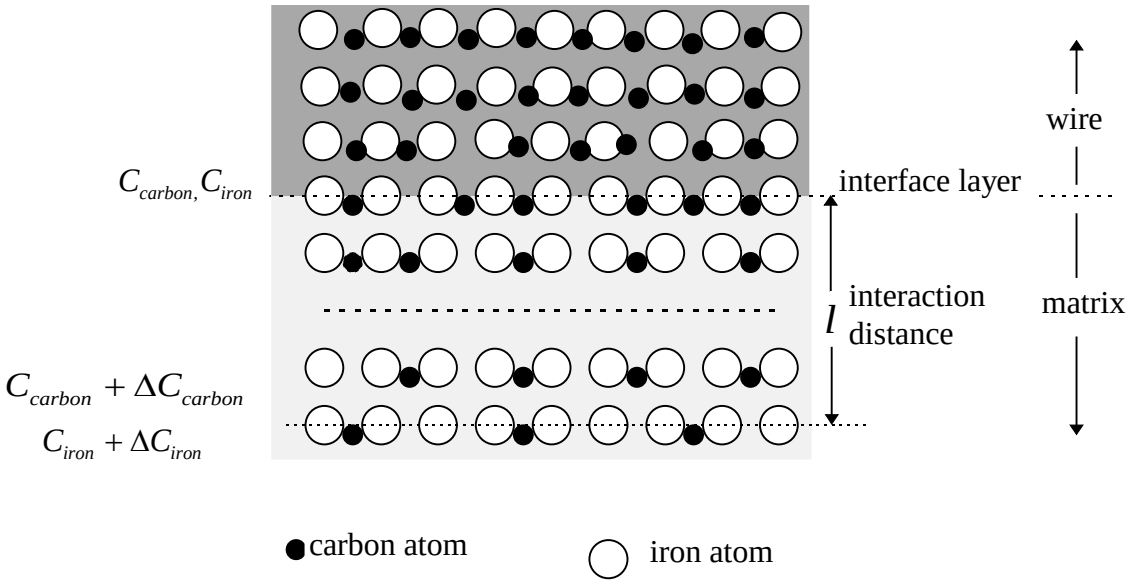

Figure 5.2.32 Illustration of atomic array in the interfacial zone

We will analyse the interfacial bond energy with plain steel wire under the following two assumptions:

(1) all the carbon atoms dissolve in the steel, ie. no carbides form at the interface;

(2) the interface is clean enough that no inclusions or oxides form at the interface.

According to interfacial energy theory, the total bond energy at the interface is the sum of energies of carbon-carbon bonds, carbon-iron bonds, and iron-iron bonds within interaction distance, l. The interaction distance, l, is defined as a distance from the interface only within which the atom bonds can contribute to the interface bonding, so the total bond energy at the interface, γ , can be given as:

$$\gamma = \text{volume fraction of carbon-carbon bonds} \times \mu_{carbon-carbon}$$

+ volume fraction of iron-iron bonds $\times$ $\mu_{iron-iron}$

+ volume fraction of iron-carbon bonds $\times$ $\mu_{carbon-iron}$ (5.2.30)

where, $\mu_{carbon-carbon}$, $\mu_{iron-iron}$ and $\mu_{carbon-iron}$ are the bond energy per unit volume of carbon-carbon bond, iron-iron bond, and carbon-iron bond respectively, they are constants at a given temperature and under same stress status.

The volume fraction of carbon-carbon bonds within l is:

$$C_{carbon} \times (C_{carbon} + \Delta C_{carbon})$$

the volume fraction of iron-iron bonds within l is:

$$C_{iron} \times (C_{iron} + \Delta C_{iron})$$

and the volume fraction of iron-carbon bonds within l is:

$$C_{carbon} \times (C_{iron} + \Delta C_{iron}) + C_{iron} \times (C_{carbon} + \Delta C_{carbon})$$

where, C_{carbon} and C_{iron} are the carbon and iron contents at the interface respectively, and ΔC_{carbon} and ΔC_{iron} are the changes of carbon and iron contents, respectively, from the interface within the interaction distance. Because of the short interaction distance l, the carbon and iron concentration gradients in the matrix side of the interface, $\left.\frac{dC_{carbon}}{dr}\right|_{r=r_0}$ and $\left.\frac{dC_{iron}}{dr}\right|_{r=r_0}$ $(= -\left.\frac{dC_{carbon}}{dr}\right|_{r=r_0})$ can be thought of as constants within the interaction distance, so the element change at the interaction distance is:

$$\Delta C_{carbon} = l \left.\frac{dC_{carbon}}{dr}\right|_{r=r_0}$$

$$\Delta C_{iron} = l \left.\frac{dC_{iron}}{dr}\right|_{r=r_0} = -l \left.\frac{dC_{carbon}}{dr}\right|_{r=r_0}$$

The interfacial bond energy is written as:

$$
\begin{aligned}
\gamma \; &= C_{carbon}(C_{carbon} + l\frac{dC_{carbon}}{dr}\Big|_{r=r_0})\mu_{carbon-carbon} \\
&+ C_{iron}(C_{iron} + l\frac{dC_{iron}}{dr}\Big|_{r=r_0}) \cdot \mu_{iron-iron} \\
&+ \left[C_{carbon}(C_{iron} + l\frac{dC_{iron}}{dr}\Big|_{r=r_0}) + C_{iron}(C_{carbon} + l\frac{dC_{carbon}}{dr}\Big|_{r=r_0}) \right] \cdot \mu_{carbon-iron} \\
&= C^2{}_{carbon} \cdot \mu_{carbon-carbon} + C^2_{iron} \cdot \mu_{iron-iron} + 2C_{carbon} \cdot C_{iron} \cdot \mu_{carbon-iron} \\
&+ \left[C_{carbon} \cdot \mu_{carbon-carbon} - C_{iron} \cdot \mu_{iron-iron} + (C_{iron} - C_{carbon})\mu_{carbon-iron} \right] \frac{dC_{carbon}}{dr}\Big|_{r=r_0}
\end{aligned}
\tag{5.2.31}
$$

From the carbon diffusion analysis in section 5.2.9.1, the carbon content and iron content are constants in the interface, the interfacial bond energy can be written as:

$$
\gamma = B' + A' \frac{dC_{carbon}}{dr}\Big|_{r=r_0} \tag{5.2.32}
$$

the carbon concentration gradient in the matrix side of interface, $\frac{dC_{carbon}}{dr}\Big|_{r=r_0}$, varies only with the heat-treatment history, and is a parameter to describe the carbon diffusion. The effects of rolling temperature and isothermal holding time on $\frac{dC_{carbon}}{dr}\Big|_{r=r_0}$ can be obtained by differentiating equations (5.2.10) with respect to r at a given holding time or temperature, and are shown in Figures 5.2.33. With increasing rolling temperature and holding time, the carbon concentration gradient tends to zero, ie. with increasing carbon diffusion, $\frac{dC_{carbon}}{dr}\Big|_{r=r_0}$ varies to a certain limit, zero.

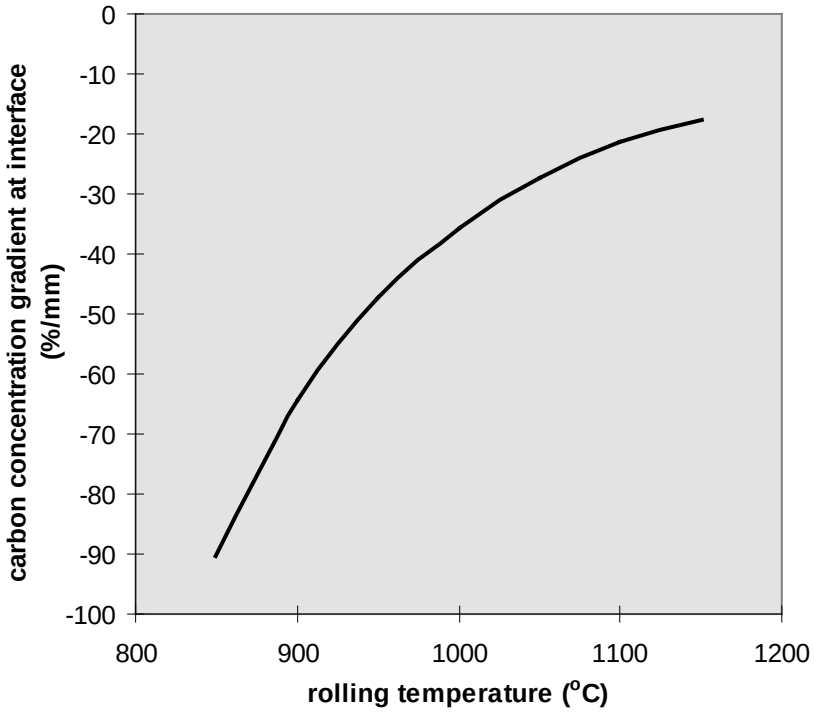

(a)

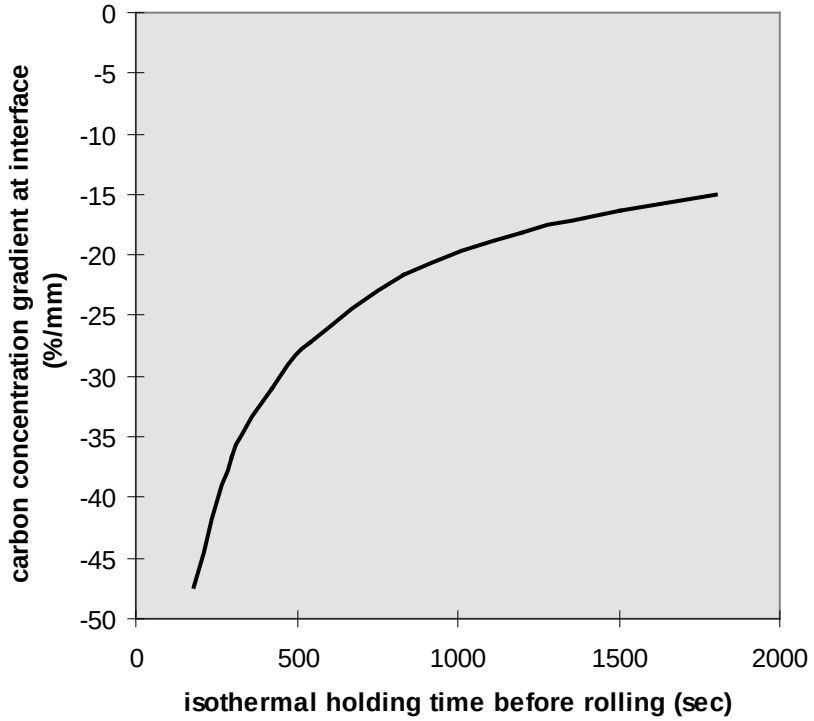

(b)

Figure 5.2.33 Predicted variation of carbon concentration gradient in the matrix side of interface with (a) rolling temperature and (b) isothermal holding time before rolling

Relationship between interfacial strength and diffusion

According to energy equilibrium theory, the work of fracture during wire pull-out equals to the total energy of broken bonds, this will be applied in the following two situations:

(a) For elastic deformation, the energy equilibrium equation is formed by equating the equations (5.2.24) and (5.2.32) ie:

$$k\tau_{\max}^2 = B' + A' \left. \frac{dC_{carbon}}{dr} \right|_{r=r_0}$$

Let $g = \left. \frac{dC_{carbon}}{dr} \right|_{r=r_0}$, so we have:

$$g = \frac{k}{A'} \tau_{\max}^2 - B' \qquad (5.2.33)$$

In its logarithmic form and differentiated with respect to $\tau_{\max}$ gives:

$$\lg \frac{dg}{d\tau_{\max}} = \lg \frac{2k}{A'} + \lg \tau_{\max}$$

Let $p = \lg \frac{2k}{A'}$, then we have:

$$\lg \frac{dg}{d\tau_{\max}} = \lg \tau_{\max} + p \qquad (5.2.34)$$

(b) If plastic deformation occurs during wire pullout process, the energy equilibrium equation is obtained by equating equations (5.2.29) and (5.2.32) as follows:

$$C + A\tau_{\max}^{n+1} = B' + A' \left. \frac{dC_{carbon}}{dr} \right|_{r=r_0}$$

$$g = \frac{A}{A'} \tau_{\max}^{n+1} + \frac{C - B'}{A'} \qquad (5.2.35)$$

which in its logarithmic form and differentiated with respect to $\tau_{\max}$ is :

$$\lg \frac{dg}{d\tau_{\max}} = \lg \frac{A(n+1)}{A'} + n \lg \tau_{\max}$$

Let $q = \lg \frac{A(n+1)}{A'}$, then we have:

$$\lg \frac{dg}{d\tau_{\max}} = n \lg \tau_{\max} + c$$

The relationship between interfacial strength and c
interface is shown in Figure 5.2.34, in which the
equations (5.2.33) and (5.2.35). The interfacia
concentration gradient. It also can be seen that the
interfacial strength with carbon concentration gradi
deformation). The transition between elastic and pla

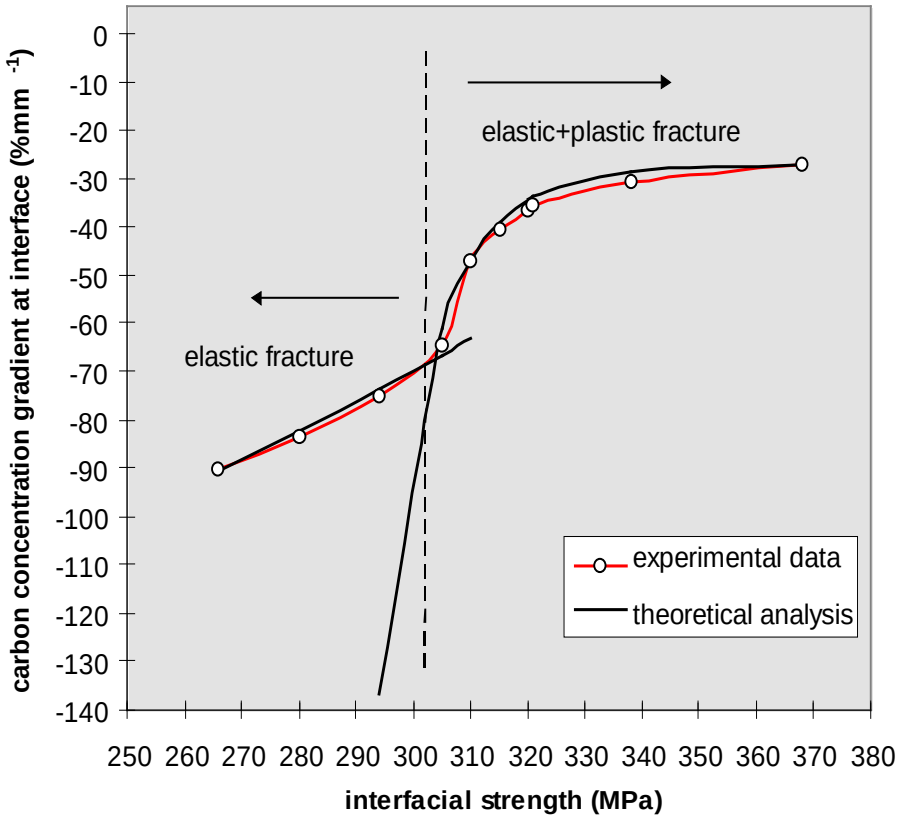

Figure 5.2.34 The relationship between interfacial strength and carbon concentration gradient in interface between plain wire and matrix

From equations (5.2.34) and (5.2.36), the big difference between elastic and plastic fractures is that the slope of $\lg \frac{dg}{d\tau_{\max}}$ against $\lg \tau_{\max}$ for elastic fracture (n=1) is higher than that for plastic fracture ($n < 0$), as is shown in Figure 5.2.35. The theoretical

analysis agrees with experimental values very well except for the transition zone between elastic and plastic processes.

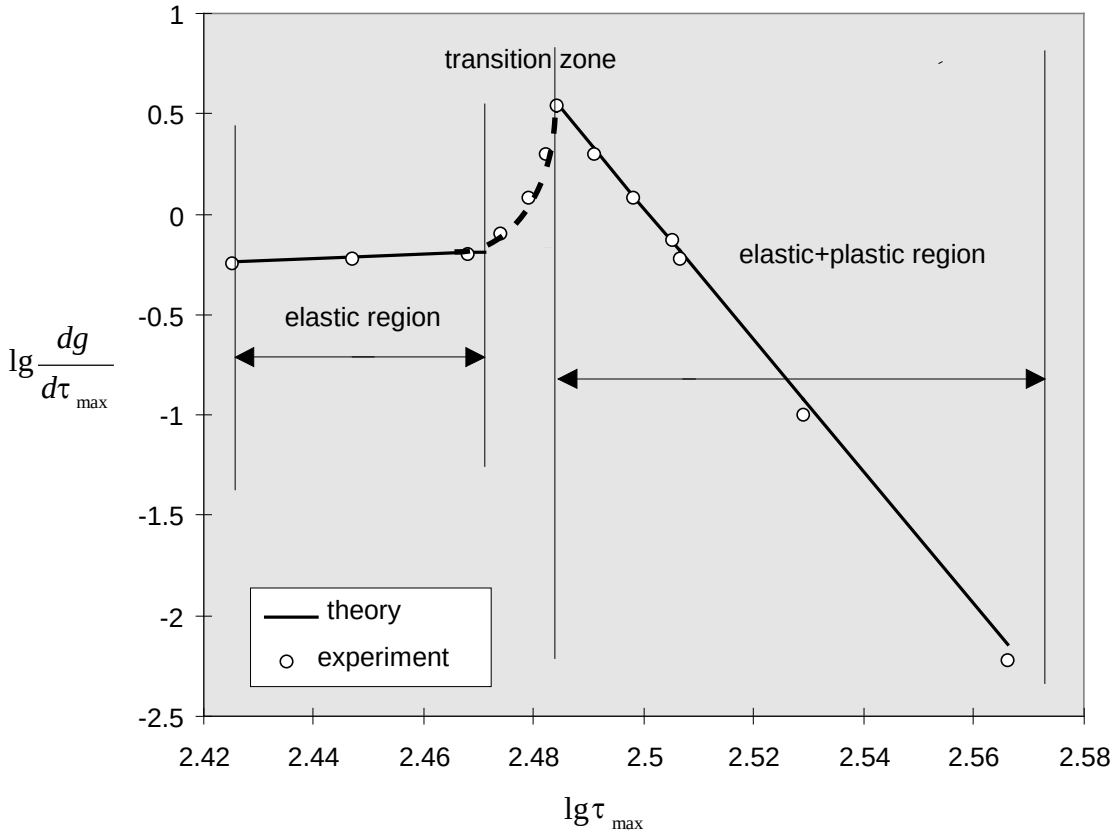

Figure 5.2.35 The relationship between $\lg\frac{dg}{d\tau_{\max}}$ *and* $\lg\tau_{\max}$

5.2.10 Summary

The interfacial strength between steel-wire and steel matrix was examined and the testing approach put forward is proved to be practical.

The interfacial strength of steel-steel composites is determined by the internal residual stress at the interface, work-hardening during rolling, the status of the steel-wire surface, and diffusion during fabrication.

The residual stress is generated from the flow stress difference between wire and matrix during rolling, and is concentrated at the interface. The residual stress at the interface depends on the finishing rolling temperature and the rolling reduction.

The effect of residual stress on the interfacial strength is decided by the level of residual stress: the residual stress may increase the interfacial strength if it does not break the interface.

Heavy deformation at the interface increases the interfacial strength by work-hardening. Both the residual stress and work-hardening can be released by annealing, so the interfacial strength decreases with annealing.

Besides work-hardening during rolling, the carbon diffusion between wire and matrix plays an important role in strengthening of the interface. The carbon diffusion, determined by the coating on the wire, is a function of temperature and holding time before rolling of the composites and can be described by the carbon concentration gradient at the interface.

Carbon diffusion between plain wire and matrix increases with increasing temperature and holding time, which makes the interfacial strength increase with temperature and holding time.

Because a perfect copper coating on the wire can stop the diffusion of carbon from wire to matrix, the interfacial strength between copper coated wire and matrix increases only a little with both temperature and time by the solid diffusion between copper and iron and carbon diffusion from wire to matrix through defects of copper coating.

Chemical reaction between wire and coating occurred in the nickel-coated wire, which strengthened the interface. The interfacial strength increases very quickly with increasing temperature and time.

The austempering after fabrication of the composite lowers the interfacial strength by two possible causes: (1) recovery and recrystallization of the deformed grain at interface during reheating; (2) phase transformation of the interface. The decreases of interfacial strengths in nickel and copper coated composites by austempering are much more than that of uncoated wire composite.

The interfacial strength is thought to be the stress that breaks the bonds at the interface during the wire pull-out process. The work of fracture that the applied stress has done to pull the wire out is equal to the total bond energy at the interface according to energy equilibrium theory.

The bond energy at the interface of plain wire and matrix is the sum of the bond energies between carbon-carbon, carbon-iron, and iron-iron within the interaction distance. The single bond energy can be affected by work-hardening and residual stress.

Under the similar work-hardening and residual stress, the interface is a function of carbon concentration gradient at the interface. The modelling analysis agrees with experimental data very well in both the elastic and plastic fracture processes.

5.3 Artificial dual phase steel composite materials

As dual phase steels with elongated martensite show an excellent combination of strength and ductility (section 4.1.3), an attempt to make an "artificial" dual phase steel reinforced with continuous, or discontinuous martensitic or bainitic wire was made as part of the effort to develop a model system for studying dual phase steels.

From sections 5.1, and 5.2, it was seen that the eutectoid steel wire exhibited variable tensile properties under different rolling parameters, surface conditions, and the heat-treatment after fabrication. Those factors also affected the interfacial strength between the wire and matrix. The effect of these factors on the tensile properties of the steel-steel composite will be examined in this section.

Finally, properties of short wire reinforced composites made by two approaches will be examined and compared with those of the long wire reinforced composites.

5.3.1 The structure of as-rolled composites

Figures 5.3.1 (a, and b) show 3-dimensional views of the as-rolled steel composites in which the wires are distributed uniformly.

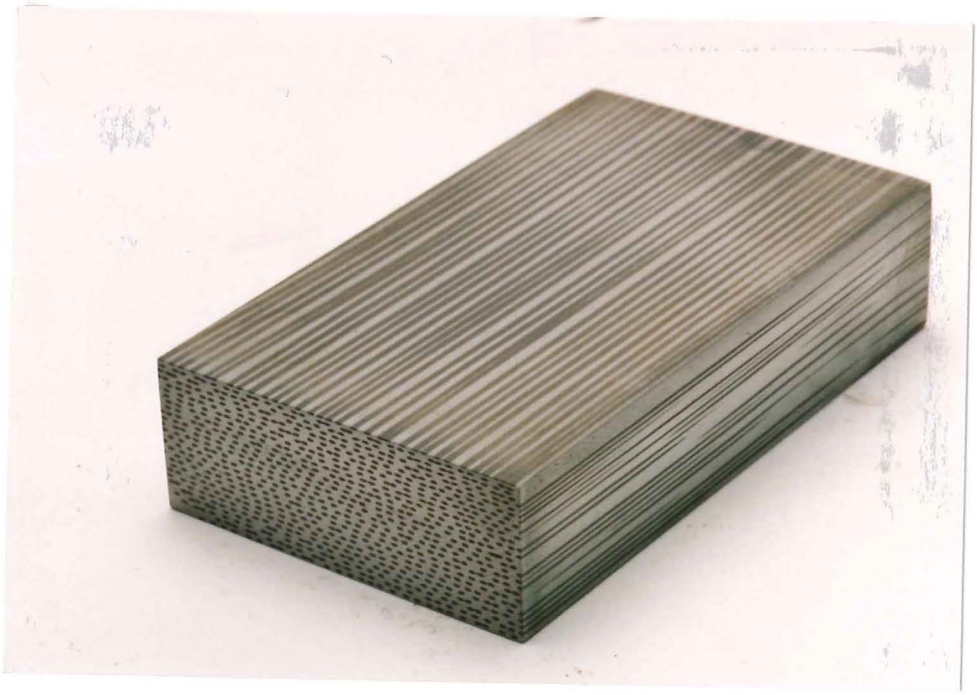

(a) continuous wires

(b) short wires

Figure 5.3.1 Structure of unidirectional artificial dual phase steels (× 0.5)

The microstructure of the cross-section is shown in Figure 5.3.2 at higher magnification. The cross-section of the wire changes from round to oval during rolling, and the matrix around the wire (ie. the interfacial zone) is heavily deformed. There will be residual stresses generated in this region owing to the different deformability between wire and matrix during rolling (as discussed in section 5.2). The matrix is polygonal ferrite and the wire is very fine pearlite after heavy rolling.

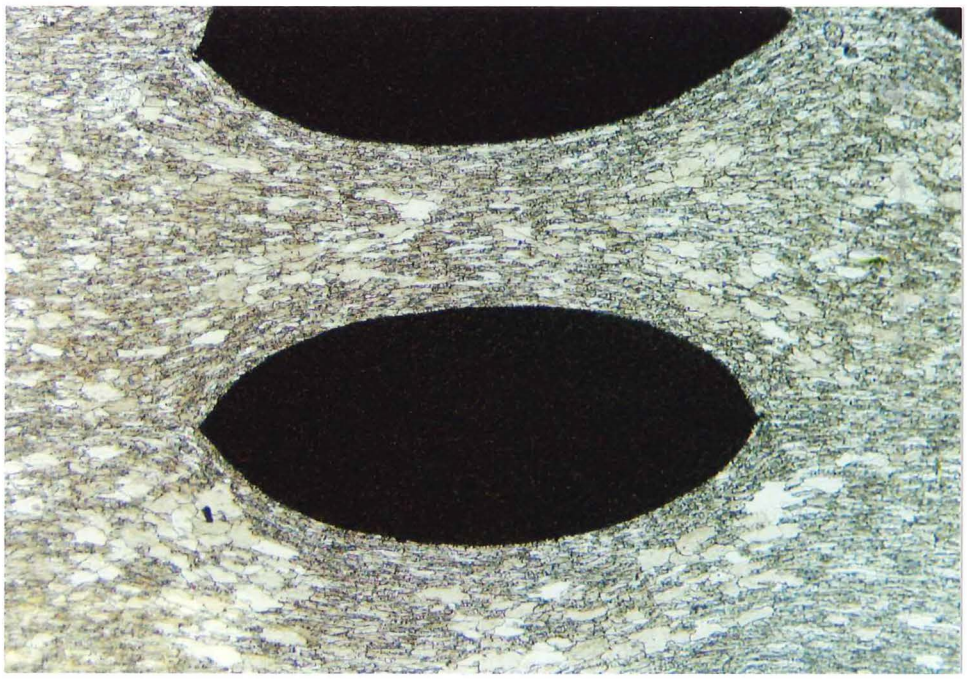

Figure 5.3.2 Cross-section of artificial dual phase steel after fabrication (x115), dark ovals are deformed wire and white area is matrix

5.3.2 The effect of heat-treatment after fabrication

As the properties of a metal are strongly dependent on phase composition and structure, which vary with the heat-treatment of the metal, this section details the different heat-treatments employed on as-rolled artificial dual phase steel to find an optimum heat-treatment. The steel-steel composite used here without special notation is obtained in the following manner:

0.04%C steel preform reinforced with 20% volume fraction of 0.8%C wire (1.6mm in diameter) was heated at 950°C for 5min and then continuously rolled (for two passes - about 60% reduction) and then water quenched.

5.3.2.1 General comparison

Table 5.3.1 and Figures 5.3.3 show the results of the tensile testing and fracture surfaces of the composites after water-quenching, oil-quenching (including martempering and austempering), normalizing etc (refer to Figure 3.17 for the heat-treatments adopted for the composite).

Table 5.3.1 The effect of heat-treatment on the tensile properties (parallel to wire) of steel wire-steel composites (V_w = 20%)

Heat treatment heated at 800°C for 2min then	Tensile strength (MPa)	Elongation (%)
air cooling — normalized	496	29.3
water-quenching	477	2.1
hold in 260°C oil for 1 min. and then air cooling — half martempering and half normalized	574	3.9
hold in 260°C oil for 5 min. and then air cooling — martempering	516	2.7
hold in 260°C oil for 105 min. and then air cooling — austempering	929	9.8

It was found that composites have lowest strength and ductility after water-quenching because micro-cracks, formed along prior austenite boundary during the martensitic transformation, cause the premature fracture of the martensitic wire under the high residual stresses produced during transformation (see Figure 5.3.3(a) and refer to

Chapter 6 for detailed analysis). The normalizing gives composites with the highest elongation and low tensile strength owing to the steel wire being transformed to pearlite which is more ductile and weaker than martensite or bainite. Oil-quenching gives the composites with a better strength and ductility combination than either water quenching or normalizing. The properties of the oil-quenched composites are dependent on the oil temperature and the isothermal holding time in oil, which will be examined later (the microstructure is shown in Figures 5.3.3(c) and (d)).

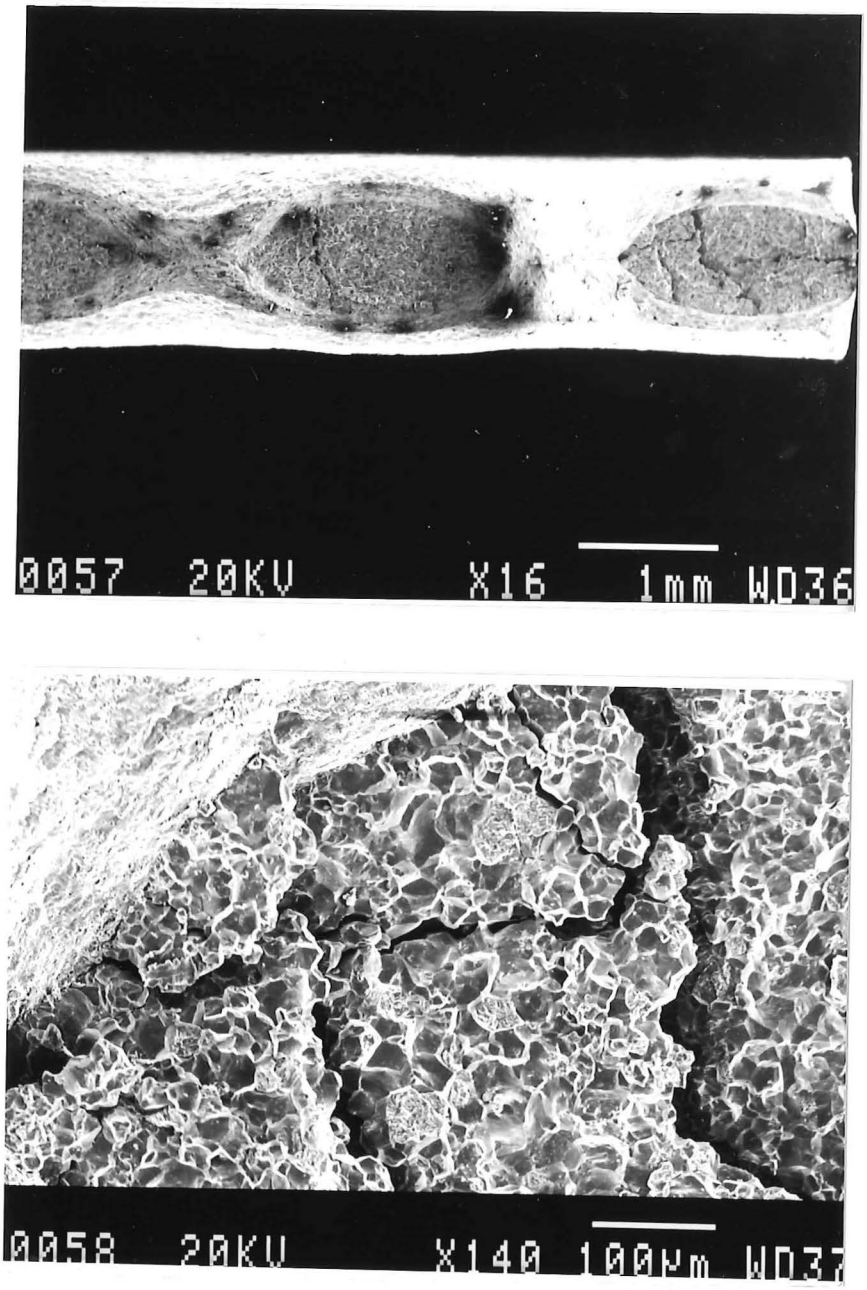

(a) water quench

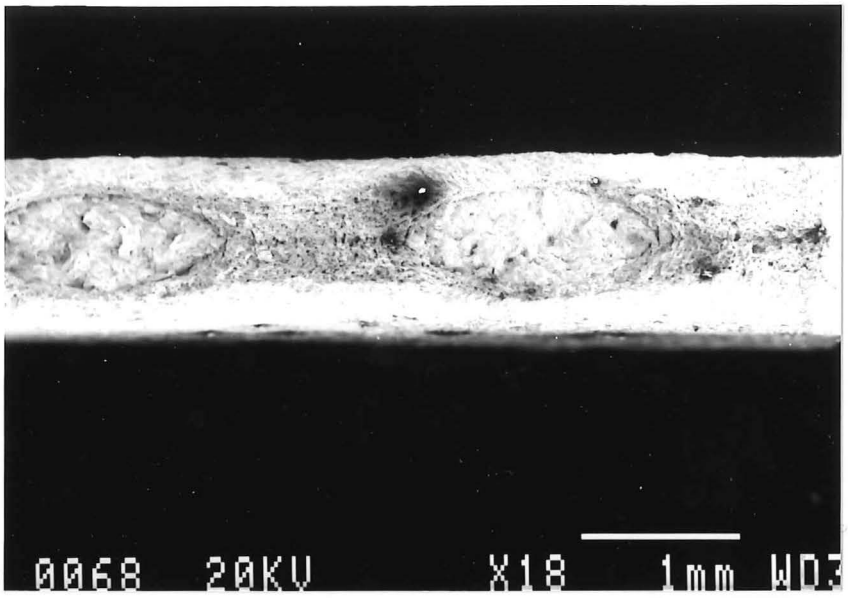

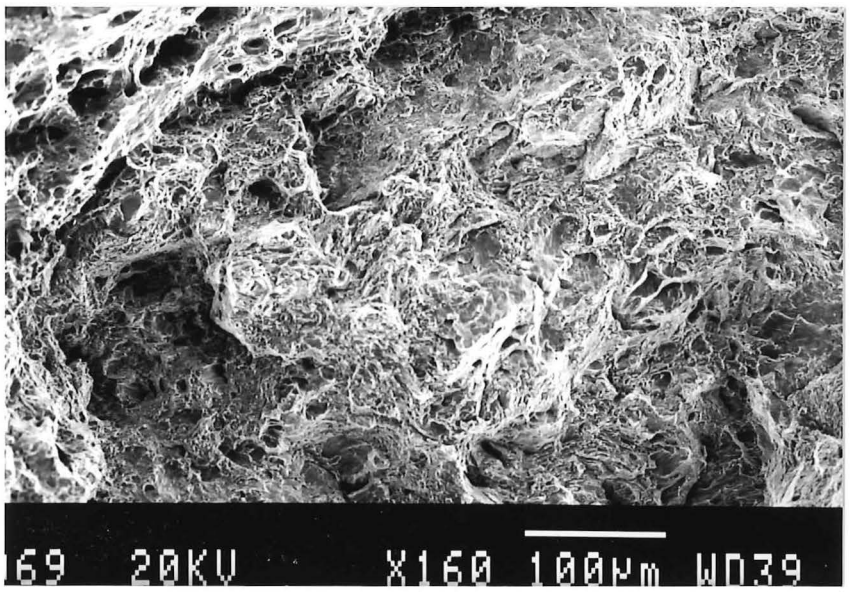

(b) normalizing

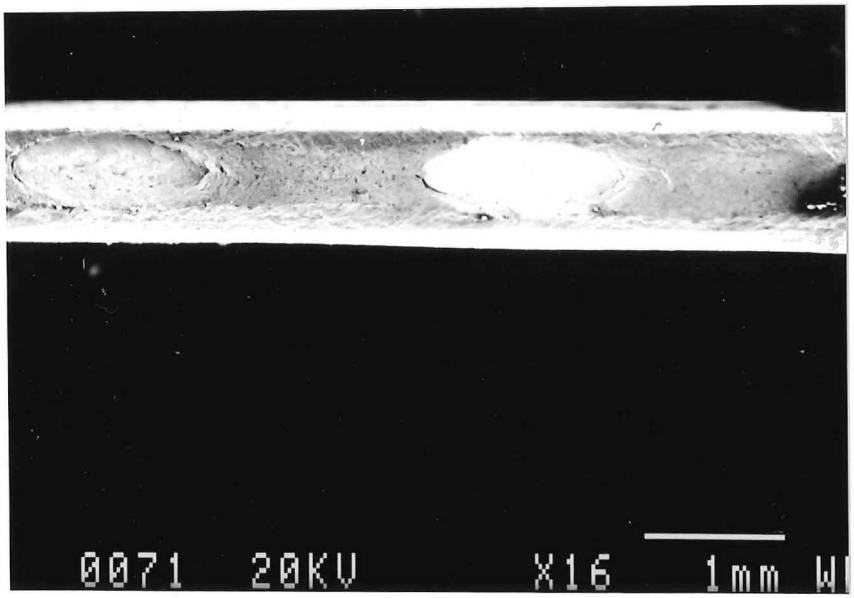

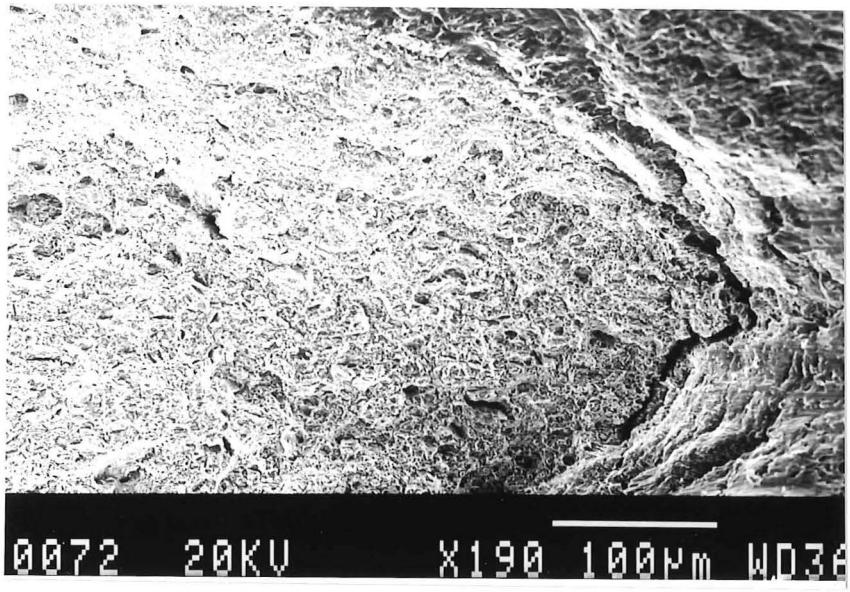

(c) austempering

Figure 5.3.3 Fracture surfaces of composites after different heat-treatment

The tensile stress-strain curves for composites after different heat-treatments are shown in Figure 5.3.4; the large difference in behavior of the composites after different heat-treatments is quite obvious.

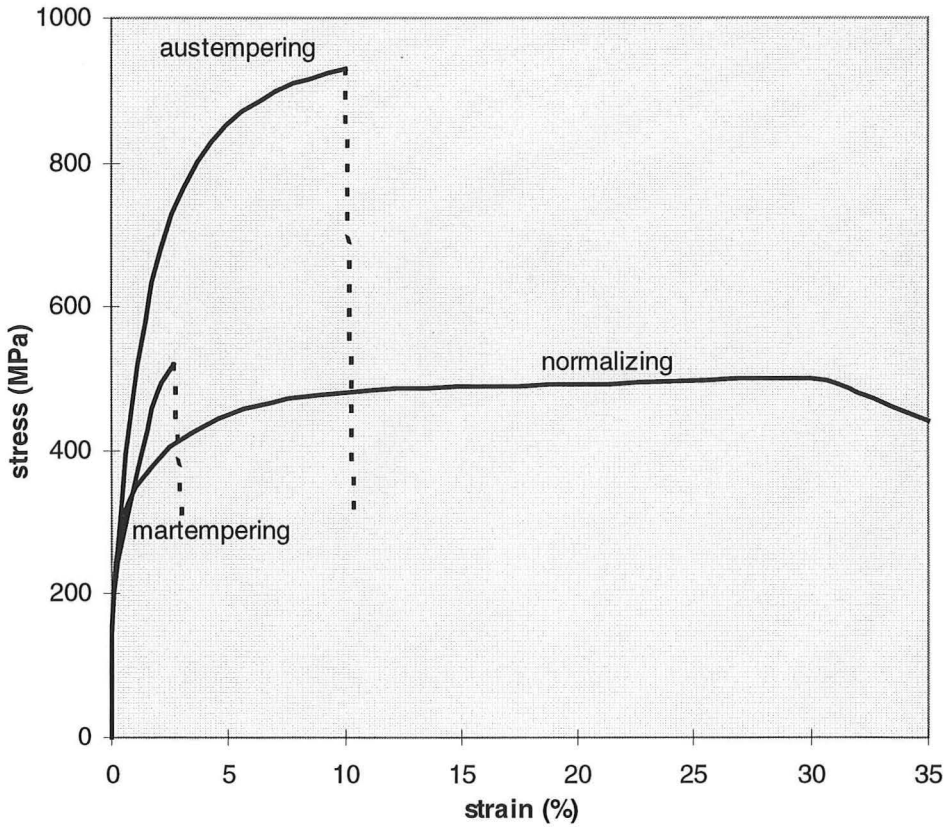

Figure 5.3.4 The stress-strain curves for steel-steel composites

As has been discussed in section 5.1, the formation of martensitic wire has not led to very good strength properties and as can be seen from Table 5.3.1, the water-quenched composite has a low strength and elongation. This problem means that it will be difficult to model dual phase steels in this quenched condition. Therefore the heat-treatment which avoids such brittle failure behavior has been used - austempering.

5.3.2.2 Isothermal holding time in 260℃ oil after heating at 800℃

The period when the sample is in hot oil (above the martensitic start temperature Ms) decides the microstructure of the wire (shown in Figure 5.3.5) and its tensile properties (as shown in Figure 5.3.6). When the sample, heated at 800°C, is quenched into 260°C oil, the distribution of temperature in the whole sample is not uniform initially; it needs time to reach the thermal equilibrium. After a short time (such as 1 min.), the temperature in the centre of the sample is within the pearlite transformation range and that at the surface of the sample bypasses pearlite and bainite transformation, so martensite with a fraction of pearlite will be obtained after air cooling from the short oil treatment (shown in Figure 5.3.5 a).

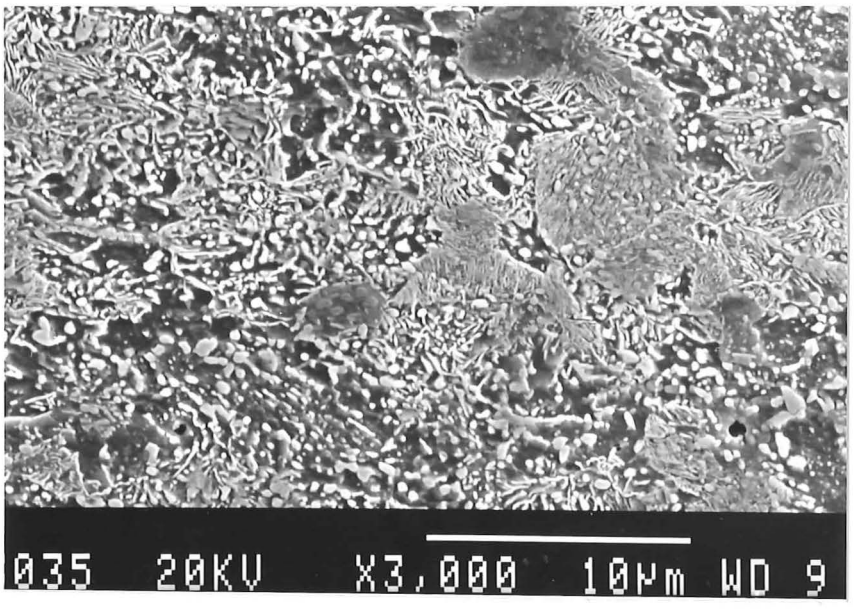

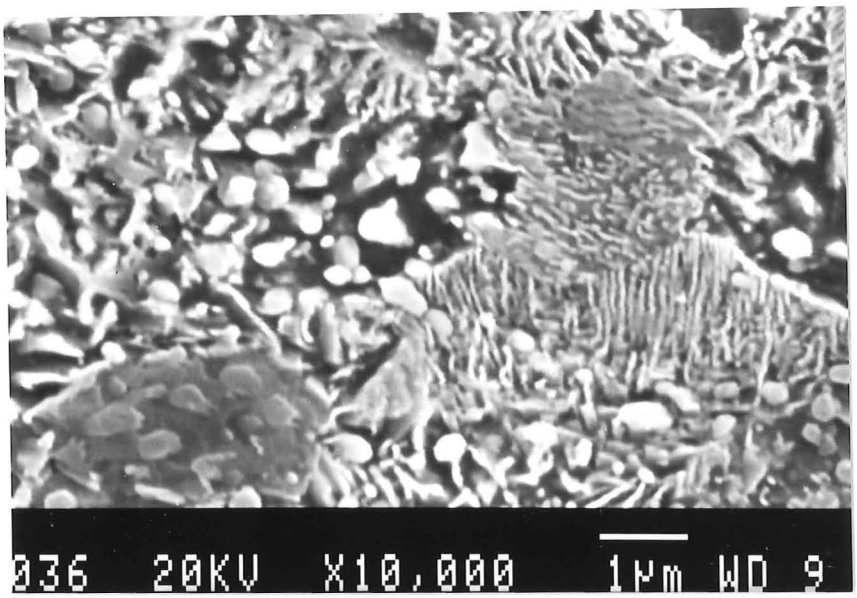

(a) 1 min in oil

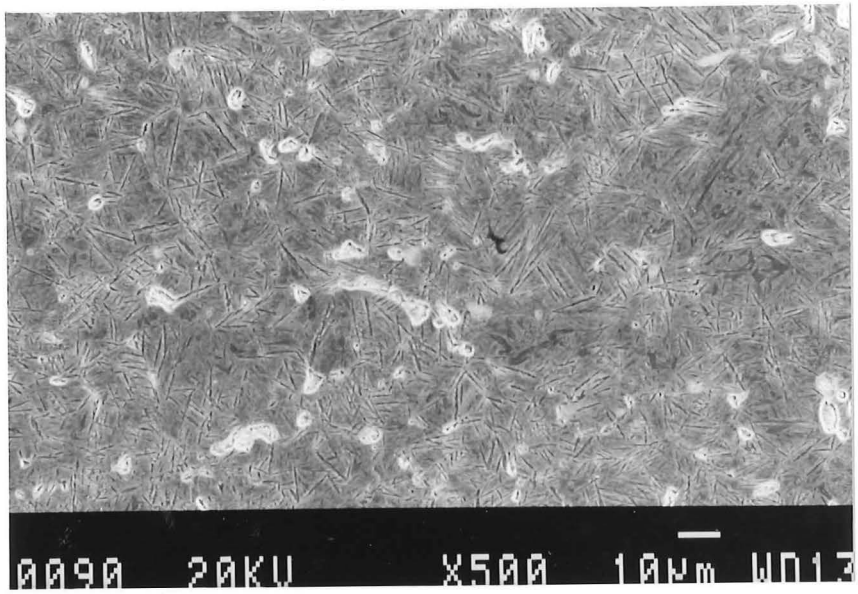

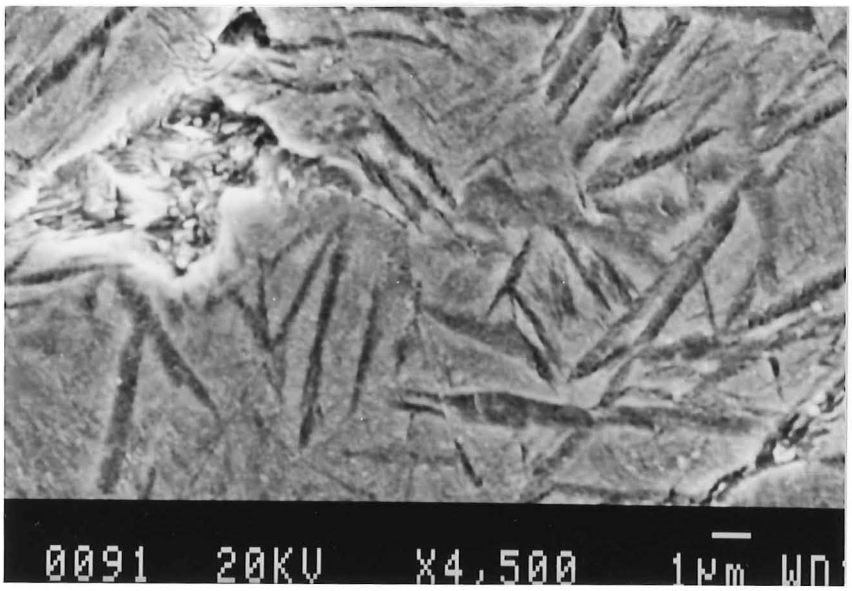

(b) 5 min in oil

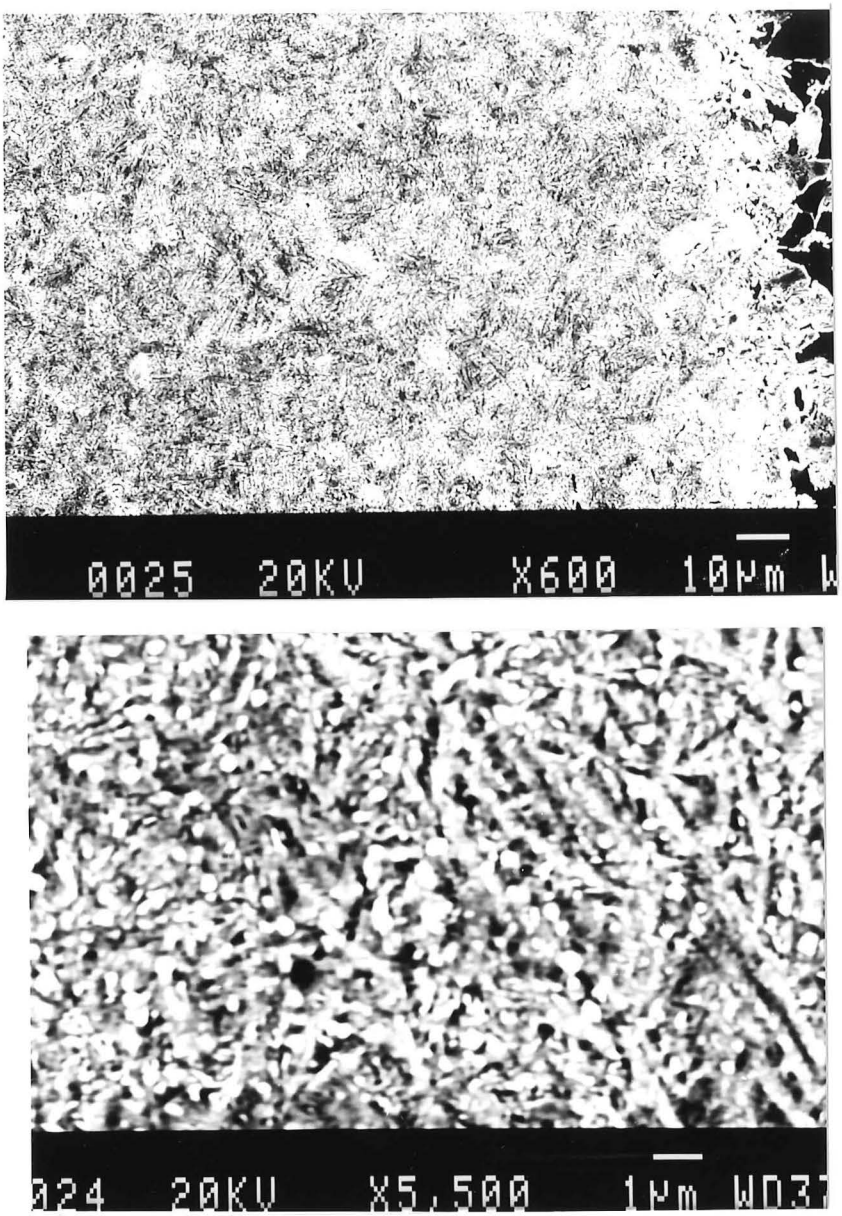

(c) 305min in oil

Figure 5.3.5 Influence of holding time in oil on microstructure

With increased holding time in 260°C oil, thermal equilibrium has been achieved, and the microstructure of wire is determined by the holding time as follows:

(a) if the sample cools to room temperature before the reaction of austenite → bainite starts, the phase composition in the wire is martensite (as shown in Figure 5.3.5 b);

(b) if the sample cools to room temperature after completion of the bainite transformation, the wire is bainitic (see Figure 5.3.5 c);

(c) the microstructure of the wire is martensite plus bainite for the sample held in oil for a period that is longer than (a) and shorter than (b).

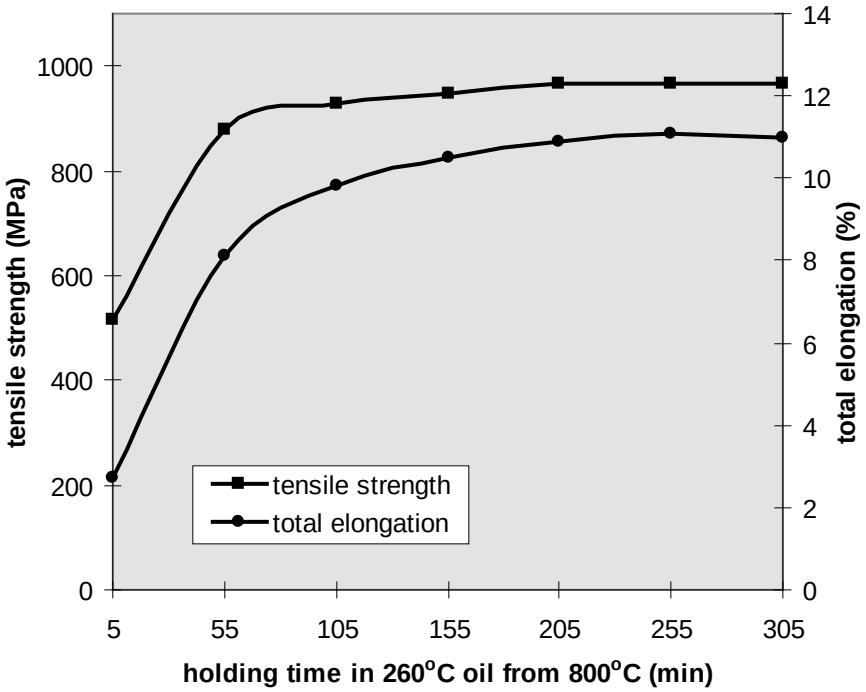

Figure 5.3.6 The variation of tensile properties with the holding time in 260℃ oil after 800℃ heat-treatment

From the Figure 5.3.6, it can be found that both tensile strength and elongation of composites increase with increasing holding time in oil. When eutectoid steel wire is quenched from the austenite region to a temperature above Ms and held at this temperature for a while, the decomposition of austenite will take place and bainite will form isothermally. The phase composition is martensite and bainite, and the volume fraction of bainite increases to 100% with increasing holding time. As discussed in section 5.1, bainite has superior ductility to martensite at the equivalent level of strength because the bainite is crack-free. The strength and elongation of the wire will increase with increasing volume fraction of bainite in the wire (ie. the holding time in oil), thus so will the strength and elongation of the composites.

5.3.2.3 Effect of oil quenching temperature

The temperature of oil into which the hot steel composites are quenched decides the phase of the wire. Figure 5.3.7 shows the effect of oil temperature on the tensile properties of composites; the total elongation increases with increasing oil temperature,

and the tensile strength reaches its maximum value at 260°C and decreases with further increases in oil temperature.

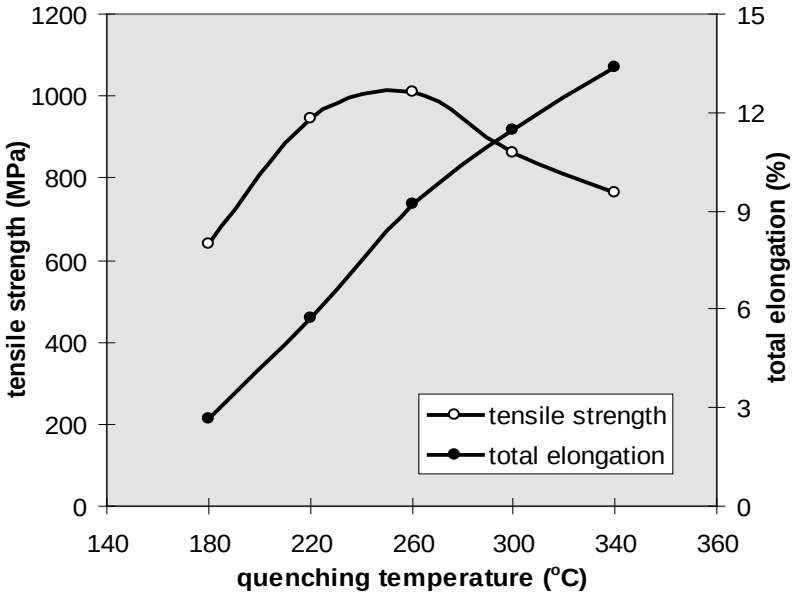

Figure 5.3.7 The effect of quenching oil temperature on the tensile properties of composites after heating at 800℃ (held for 305 min.)

The martensite starting temperature, Ms, of the steel-wire is determined by its composition as:

M_s = 539-423C-30.4Mn-17.7Ni-12.1Cr-7.5Mo+10Co-7.5Si ≅ 220°C

For a long enough holding time, the wire will transform to bainite if the oil temperature is over 220°C, or isothermally transform to martensite if the temperature is lower than 220°C (the variation of microstructure of wire with oil temperature is shown in Figure 5.3.8). Similar to the water-quenched samples, the sample transformed below 220°C is brittle but has higher strength and ductility than the water-quenched one: this is because there are fewer transformation defects and lower stresses in the isothermally transformed sample than those in the water-quenched sample. The brittleness of the isothermally transformed martensite makes the wire fracture at lower strain so that a lower strength is obtained.

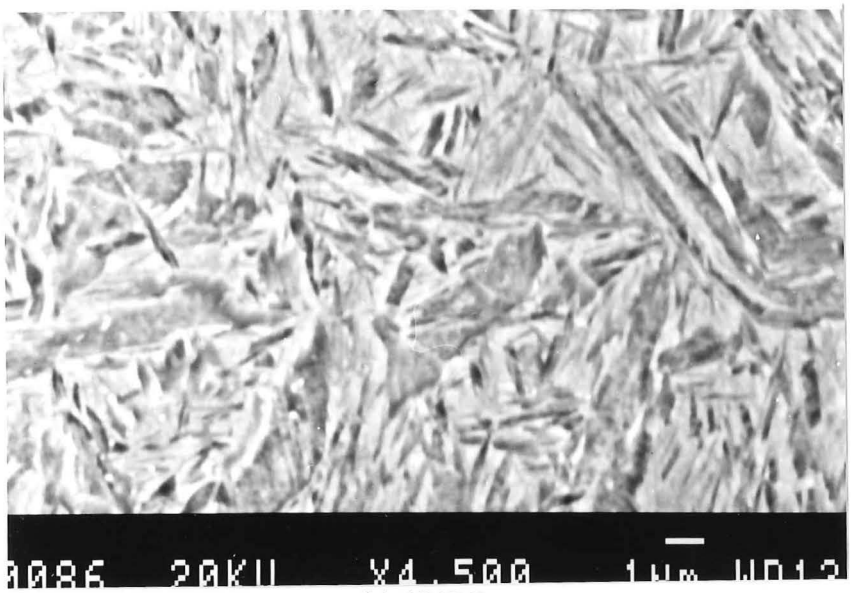

(a) 180°C

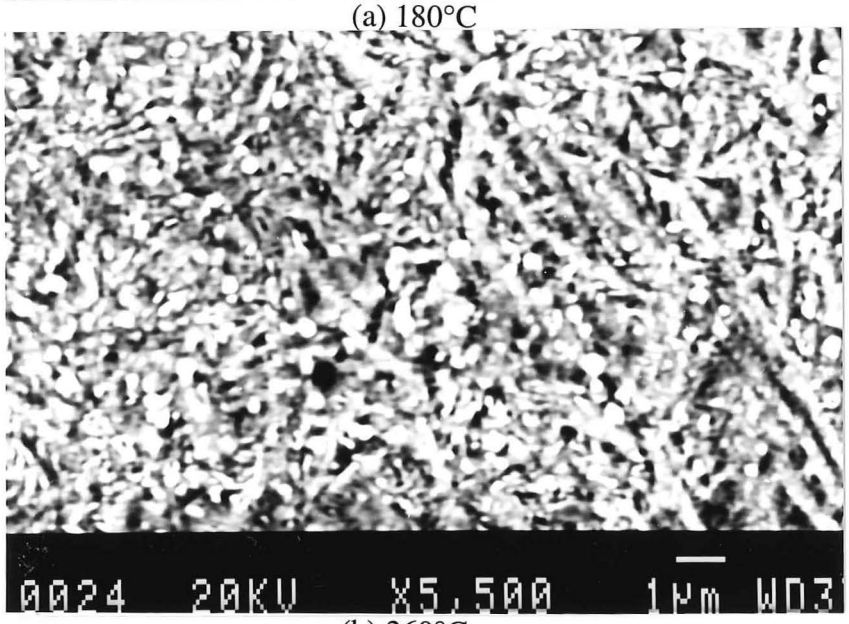

(b) 260°C

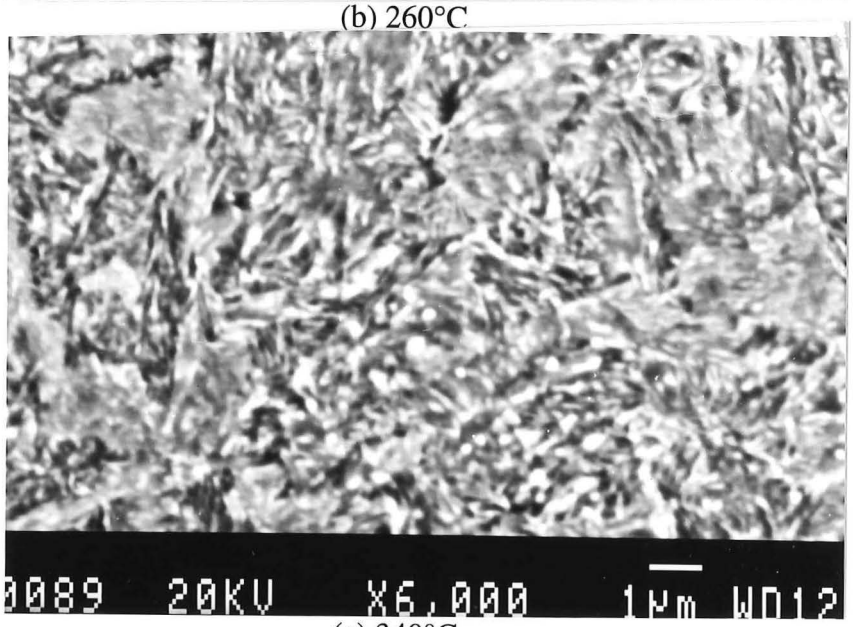

(c) 340°C

Figure 5.3.8 SEM microstructures of oil-quenched wire at different temperatures

At high temperatures, above 320°C, the reinforcing wire may transform to upper bainite, which will increase ductility and decrease strength. The temperature for the best combination of strength and ductility seems to be 260°C.

5.3.2.4 Tempering

It is well known that residual stress, distortion, and crack-formation can occur during phase transformations, especially for the water-quenching martensitic transformation. Residual stresses and crack effect are usually minimized by a following tempering. The effect of tempering time on the properties of martempered composites is shown in Figure 5.3.9. Both strength and elongation increase initially on tempering (about 2 hours) and then remain constant up to about 7 hours then the strength decreases and elongation increases.

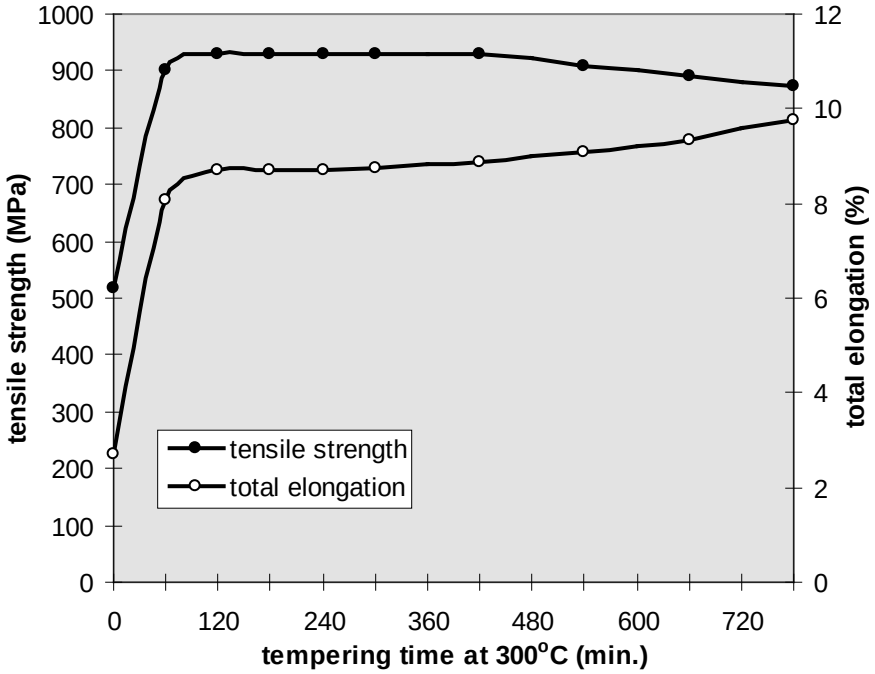

Figure 5.3.9 The effect of tempering time (at 300℃) on the tensile properties of composites which have been held at 260℃ oil for 5 min after 2min at 800℃

As is well known, the brittleness of martensite results from the combination of its very high hardness, cracks, and residual stresses. Under the internal residual stresses, cracks produced during the martensitic transformation can easily propagate at low applied loads and result in intergranular fracture with low strength and ductility. If the martensite has been tempered, the residual stresses around cracks are partially or totally

released depending on the temperature and tempering time. The relief of residual stresses will ensure that cracks will only propagate at higher applied loads.

Not only are residual stresses released during tempering, but phase transformation occurs; the very hard martensite transforms to hard carbide plus soft ferrite, which avoids the probability of premature fracture of quenched martensite. Both the relief of residual stresses and phase transformation in wire during tempering result in an increase in strength and ductility of the wire and composites as well.

The tempering temperature also affects the properties of the composites (shown in Figure 5.3.10). The tensile strengths of all the composites increase with tempering temperature below 300°C (except the austempering sample which is shown for comparison), and decrease with increasing tempering temperature over 300°C. The total elongations of all samples increase with tempering temperature (the elongation of the austempered composite increases with tempering temperature over 300°C).

Comparing comprehensively the strength and elongation behavior of these different heat-treatments, austempering was chosen as the final heat-treatment after fabrication of composites. The procedure for austempering is: heated at 800°C for 2 min., quenched into oil at 260°C and held for 305min, then air cooled to room temperature.

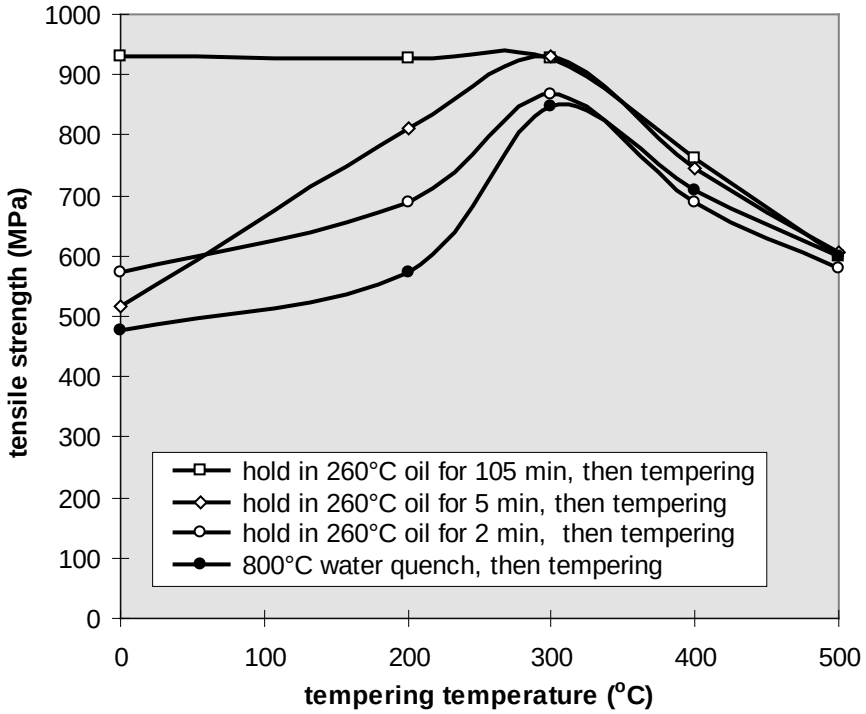

(a) tensile strength

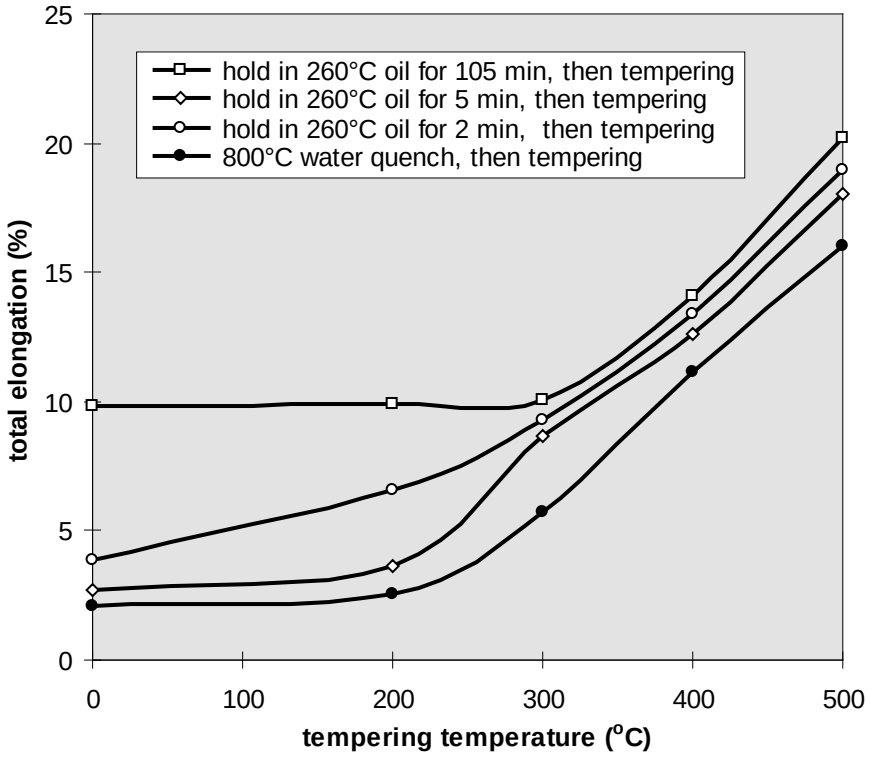

(b) total elongation

Figure 5.3.10 The influence of tempering temperature (for 3 hours) on tensile properties of composites under different treatment conditions

5.3.3 The effect of wire size on the tensile properties

The variation of properties of the composites with diameter of wire was examined and is shown in Figure 5.3.11. The strength and elongation increase with diameter of wire.

Compared with large diameter wires, the small wires have larger total surface areas for the same volume fraction of wire. The effect of this will be to make the interface more sensitive to oxidation and bring more wires into mutual contact. This, in turn, will make the composite more brittle and preclude the effective transfer of the load from matrix to wire.

The end result is a decrease in both tensile strength and elongation of the composites as wire diameter decreases. From now on, all samples are made with 1.6mm wires.

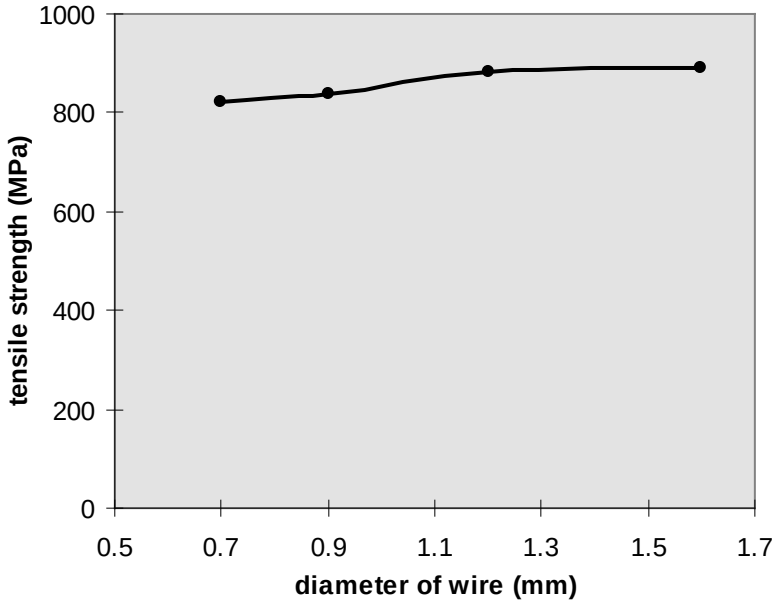

(a) tensile strength

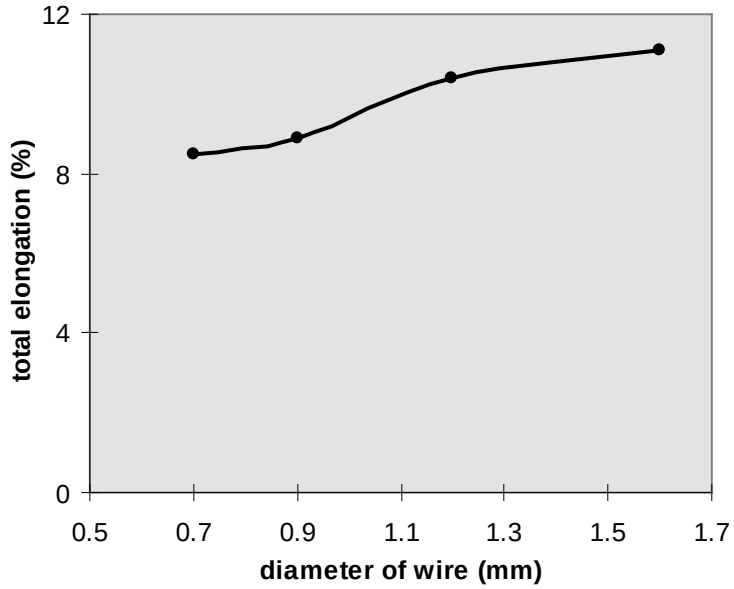

(b) total elongation

Figure 5.3.11 Variation of composite tensile strength (a) and elongation (b) with wire size

5.3.4 Effect of fabrication process

From section 5.1, it is known that the properties of both the wire and matrix steel are affected by fabrication process. The variables in the rolling process include finishing rolling temperature, rolling reduction, preform heating temperature, heating time before rolling, etc., all of which influence the properties of the wire, and the interfacial strength

(discussed in section 5.1 and 5.2 respectively). The effect of these factors on the tensile properties of the composites will be examined in this section.

5.3.4.1 Finishing rolling temperature

The experimental procedures and results of the effect of finishing rolling temperature on tensile properties of both as-rolled and austempered composites are shown in Figures 5.3.12 and 5.3.13. Because interfacial strength decreases at the lower finishing rolling temperature required for higher reductions, the rolling procedures are: 40% reduction rolling at 950°C, and then 30% reduction for the following quasi-isothermal rolling. In this case, the interfacial strength is high enough to resist debonding during testing, and no wire pullout is observed in all tensile testing samples. All strengths decrease with increasing finishing rolling temperature, and elongations increase.

The finishing rolling temperature decides the internal residual stress of the as-rolled composites. The residual stress produced will be higher at lower finishing rolling temperatures than that at higher temperatures. The residual stress and work hardening effect increase the strength of both the wire and matrix, and reduce the elongation of both matrix and wire, which makes the strength increase and elongation decrease with decreasing finishing rolling temperature of as-rolled composites.

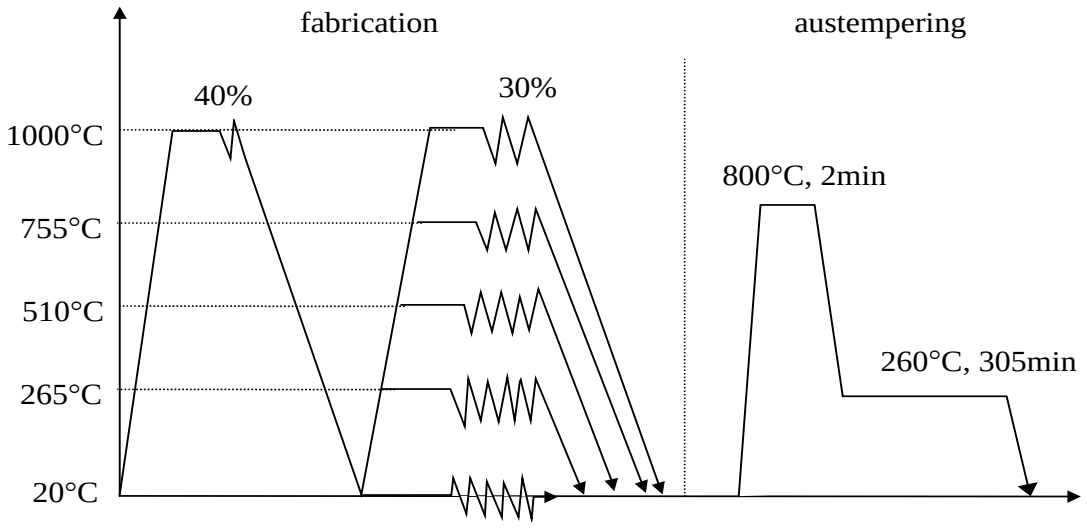

Figure 5.3.12 Experimental procedures for effect of finishing rolling temperature

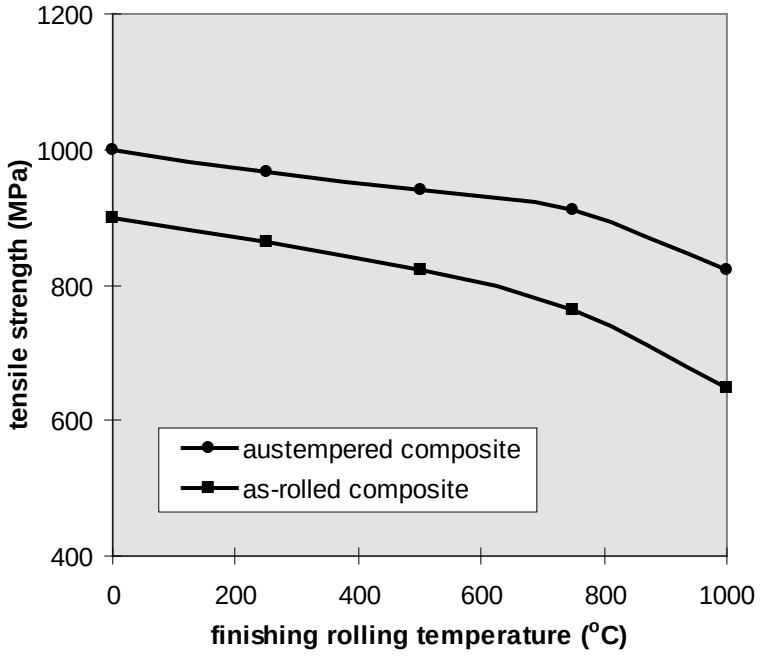

(a) tensile strength

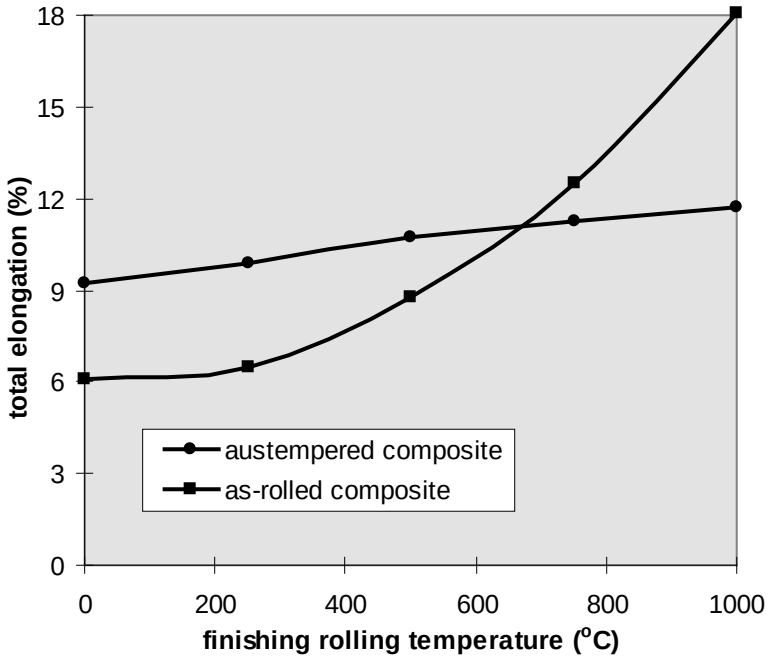

(b) elongation

Figure 5.3.13 The effect of finishing rolling temperature on the strength and total elongation of as-rolled and austempered composites

During heating at 800°C for the austempering heat-treatment, the residual stresses produced during rolling in both the wire and matrix are released, but the austenite grain size (bainite lath size after austempering) of the wire which has been rolled at lower finishing rolling temperature is finer than those which have been rolled at higher finishing rolling temperature. This is the reason for the increasing strength and

decreasing elongation of austempered composites with decreasing finishing rolling temperature.

The austempered composites are stronger than the as-rolled ones within the examined temperature range, which means that the strength of bainite wire is higher than that of the as-rolled pearlite wire (verified in section 5.1). The ductility of the as-rolled composites is higher than that of austempered composites when the finishing rolling temperature is over the austenite transformation temperature, because there is not much residual stress produced in the as-rolled composite when rolling in the austenite region.

5.3.4.2 Rolling reduction

In addition to the finishing rolling temperature, the amount of reduction associated with the rolling temperature can affect the work-hardening and residual stress produced. The effect of rolling reduction on the properties of composites was investigated through continuous and cold rolling (schematically shown in Figure 5.3.14).

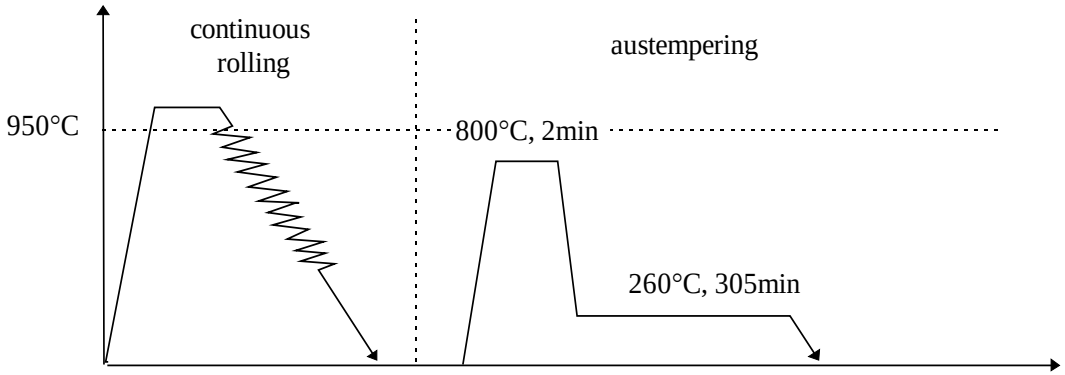

(a) continuous rolling

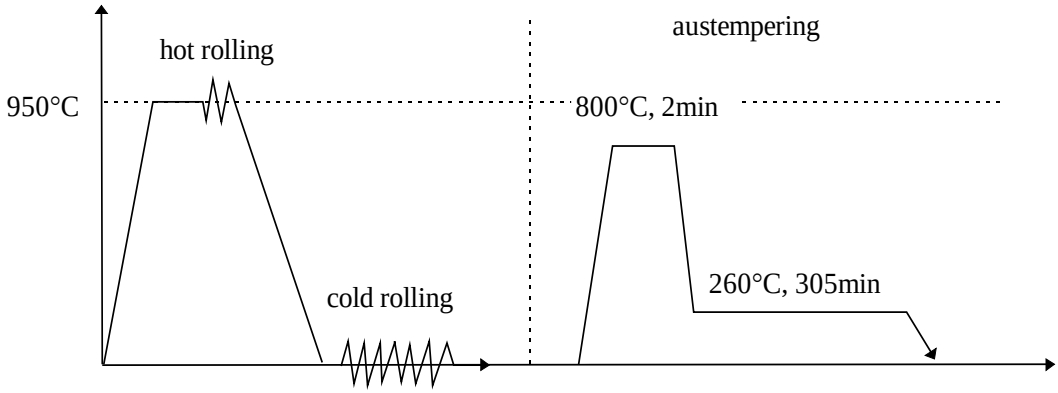

(b) cold rolling

Figure 5.3.14 Schematic of rolling procedures

Continuous rolling starting at 950°C

The effect of reduction by continuous rolling is related to the finishing rolling temperature; the temperature is lower when more rolling passes are used in order to achieve higher reductions. Thus, the variation of tensile properties of composites with increasing % reduction is similar to that with decreasing finishing rolling temperature (comparing Figures 5.3.13 and 5.3.15).

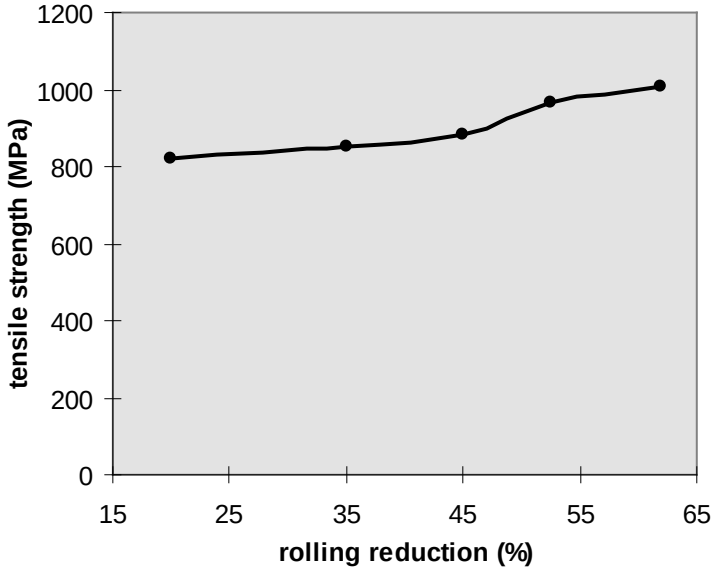

(a) tensile strength

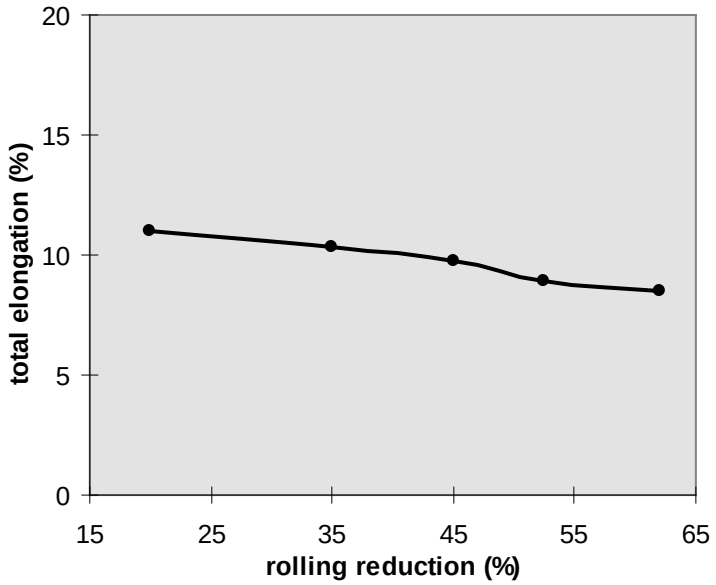

(b) total elongation

Figure 5.3.15 Effect of continuous rolling reduction on the tensile properties of artificial dual phase steel

Cold rolling

The effect of reduction by cold rolling on the properties of composites is shown in Figure 5.3.16. Strengths of both as-rolled and austempered composites increase with increasing reduction as expected, but the strength of the as-rolled composite decreases when the rolling reduction is 45% or higher, and elongation sharply decreases at this stage.

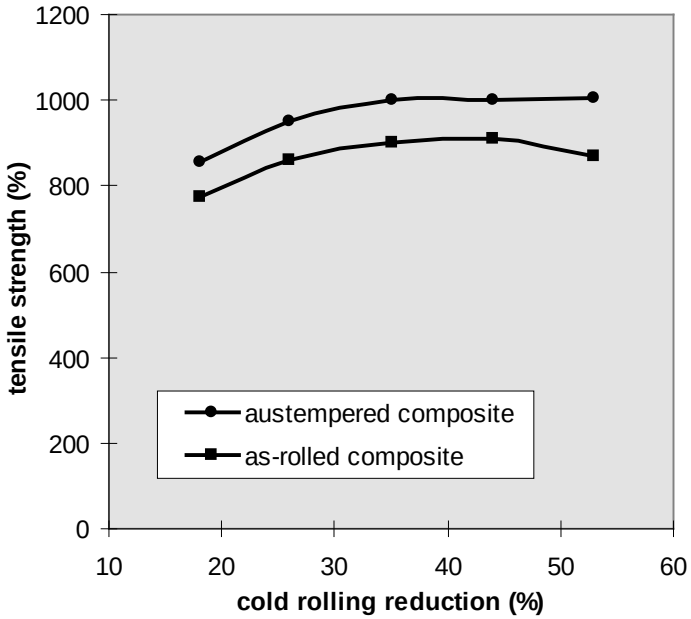

(a) tensile strength

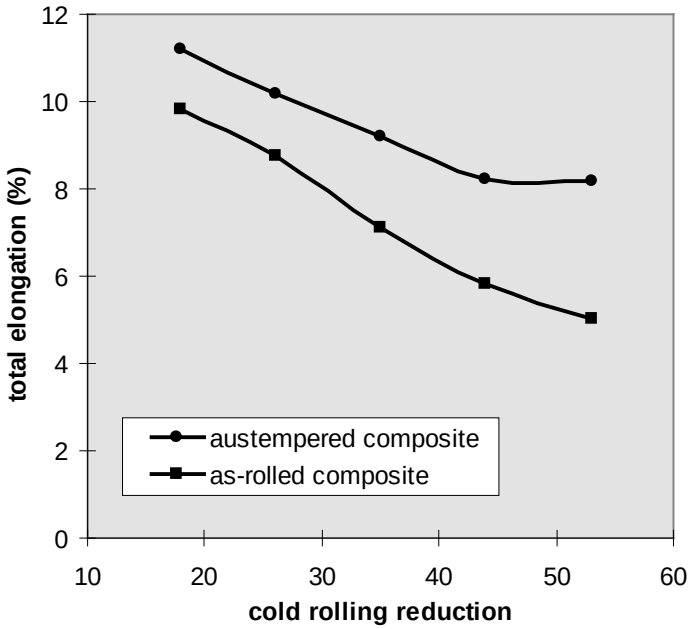

(b) total elongation

Figure 5.3.16 The variation of tensile properties with cold rolling reduction

The cold rolling reduction is a parameter that reflects the degree of work-hardening during rolling - the higher the cold reduction, the higher the work-hardening. The strength of as-rolled composites increases with work-hardening (ie. reduction) before reaching a constant.

As discussed in section 5.2, the heavy cold rolling (higher than 45% reduction) will affect the interfacial strength because the internal stresses at the interface break the bonding. The poor interfacial bonding results in a lower tensile strength and elongation for the as-rolled composites.

5.3.4.3 Starting rolling temperature of continuous rolling

As shown in section 5.1 and 5.2, both the properties of the wire and the interfacial strength are dependent on the starting rolling temperature, and this must also affect the properties of composites (shown in Figure 5.3.17).

In the plain wire reinforced composites, the interfacial strength is strong enough to resist crack propagation during loading. The key factors influencing the properties of the composite are the properties of the wire. Because of the small drop in strength of the wire caused by decarburization, the tensile strength of the plain wire reinforced composites decreases slowly with increasing temperature; the elongation does not change with rolling temperature.

The strength and elongation of the copper-coated wire composites increase with increasing rolling temperature as a better bond is formed between the coated-wire and matrix at higher temperature. The interfacial strength of copper-coated wire reinforced composites rolled under 1050°C is not strong enough for transferring the maximum stress during tensile testing; the crack initiates at the interface and propagates along the interface.

As shown in section 5.1 and 5.2, the interfacial reaction between the nickel coating and the wire increases the interfacial strength and also reduces the strength of wire with increasing temperature. The increase in interfacial strength increases the tensile strength with increasing temperature from 900 to 950°C by resisting debonding. The degradation of the wire by reaction makes the strength and elongation decrease with increasing temperature above 950°C. The primary factor affecting the composites in nickel-coated

wire reinforced composites is this reaction, which must be carefully controlled if we want to improve the properties of the composites.

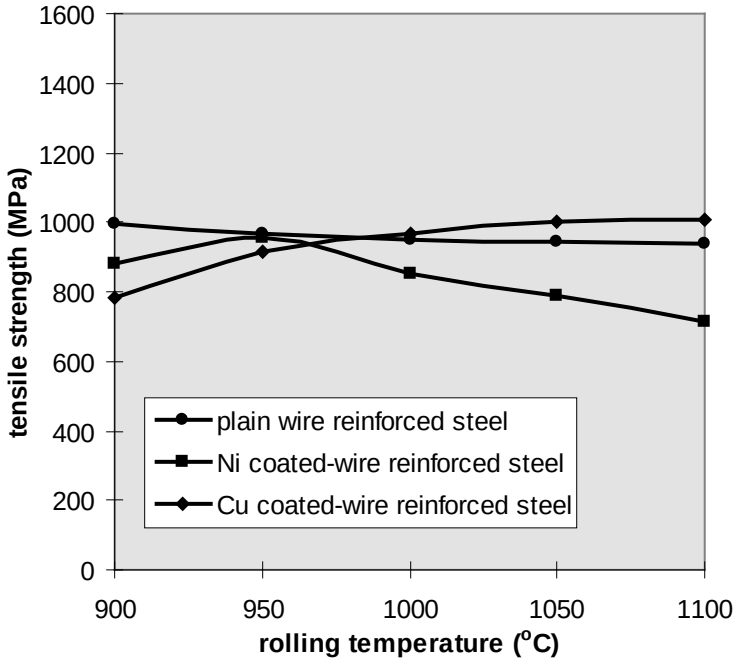

(a) tensile strength

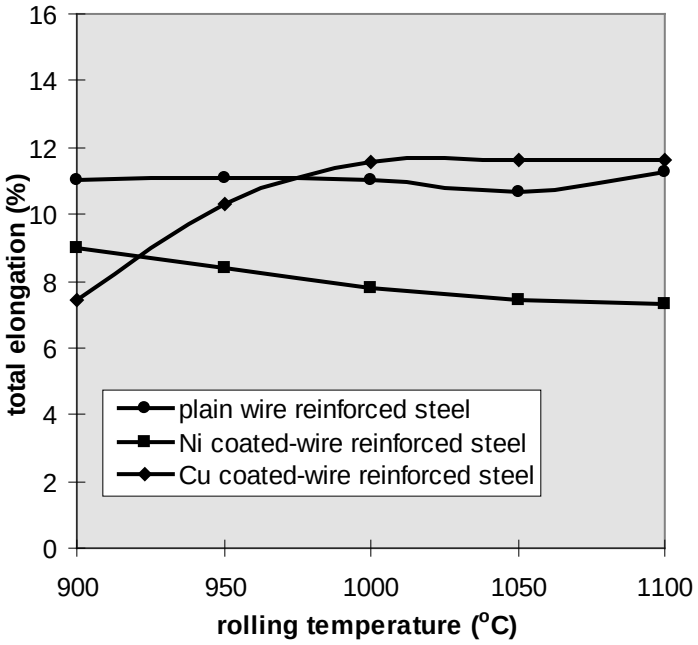

(b) total elongation

Figure 5.3.17 Variation of properties of composites with rolling temperature

The effect of interfacial reaction on the properties of composites is dependent on the extent of reaction. Excess chemical reaction degrades the properties of reinforcements and composites by the following mechanisms:

(1) When the reaction layer is brittle and fractures at small strain, a circumferential notch is thus formed on the fibre surface. The formed notch hastens fracture of the wire, resulting in loss of composite strength.

(2) When the wire surface is roughened during reaction, a high stress concentration arises at the irregularities.

(3) The intrinsic properties of the wires are degraded during reaction, and the composites strength is, of course reduced.

(4) The diameter of the wire decreases due to the reaction, and so the effective volume fraction of fibre is reduced.

The fracture surfaces of tensile fractures of plain, copper-coated, and nickel-coated wire reinforced composites are shown in Figure 5.3.18.

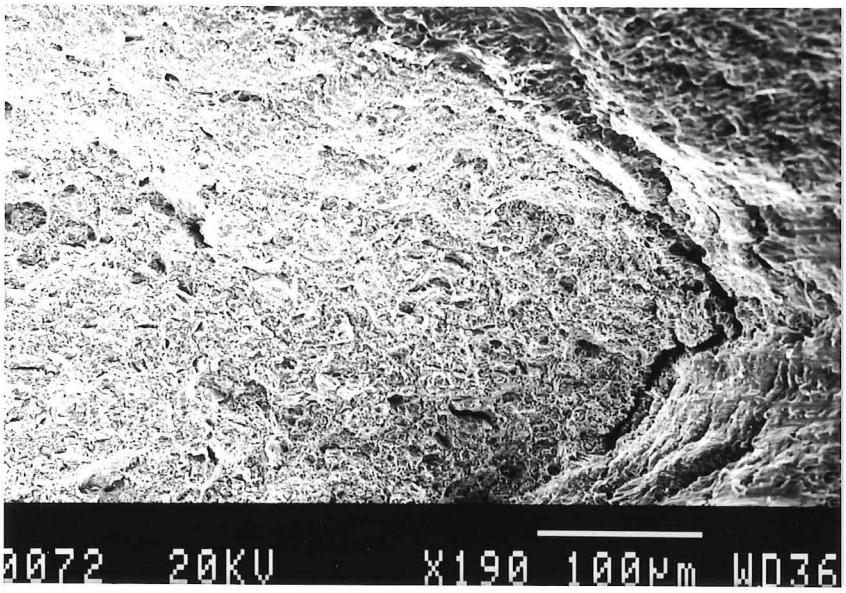

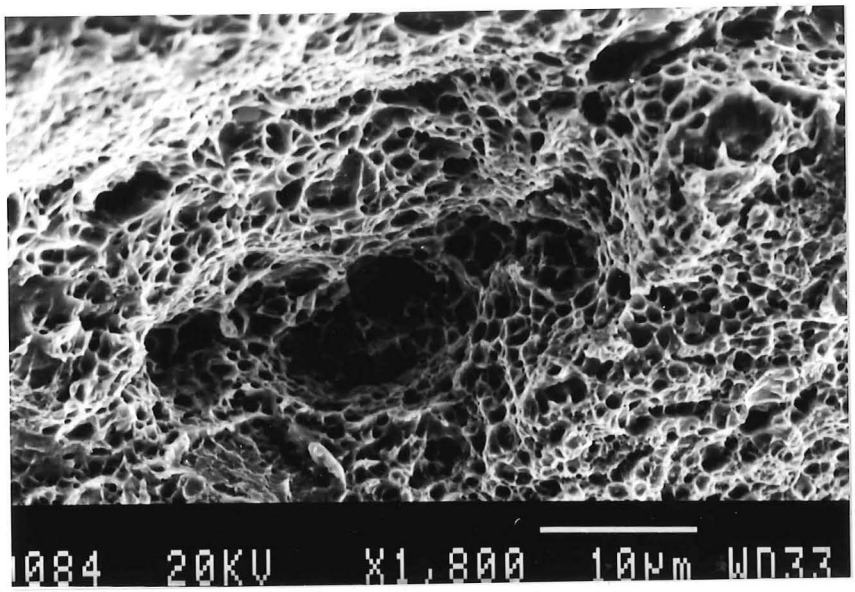

plain wire composites

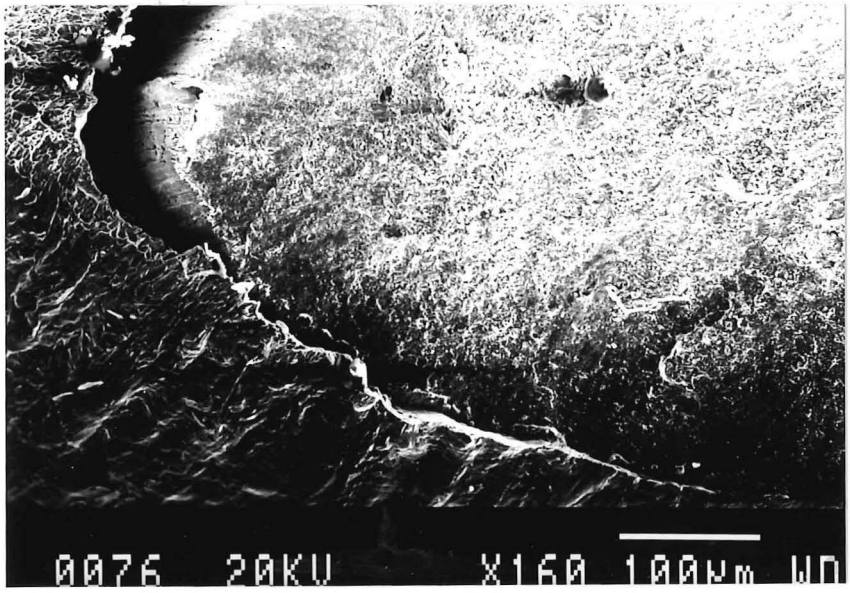

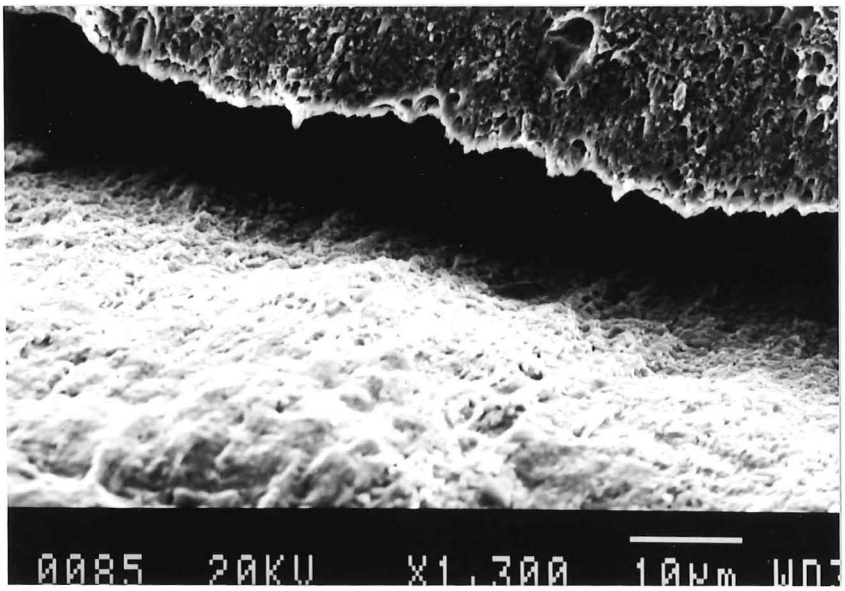

copper-coated wire composites

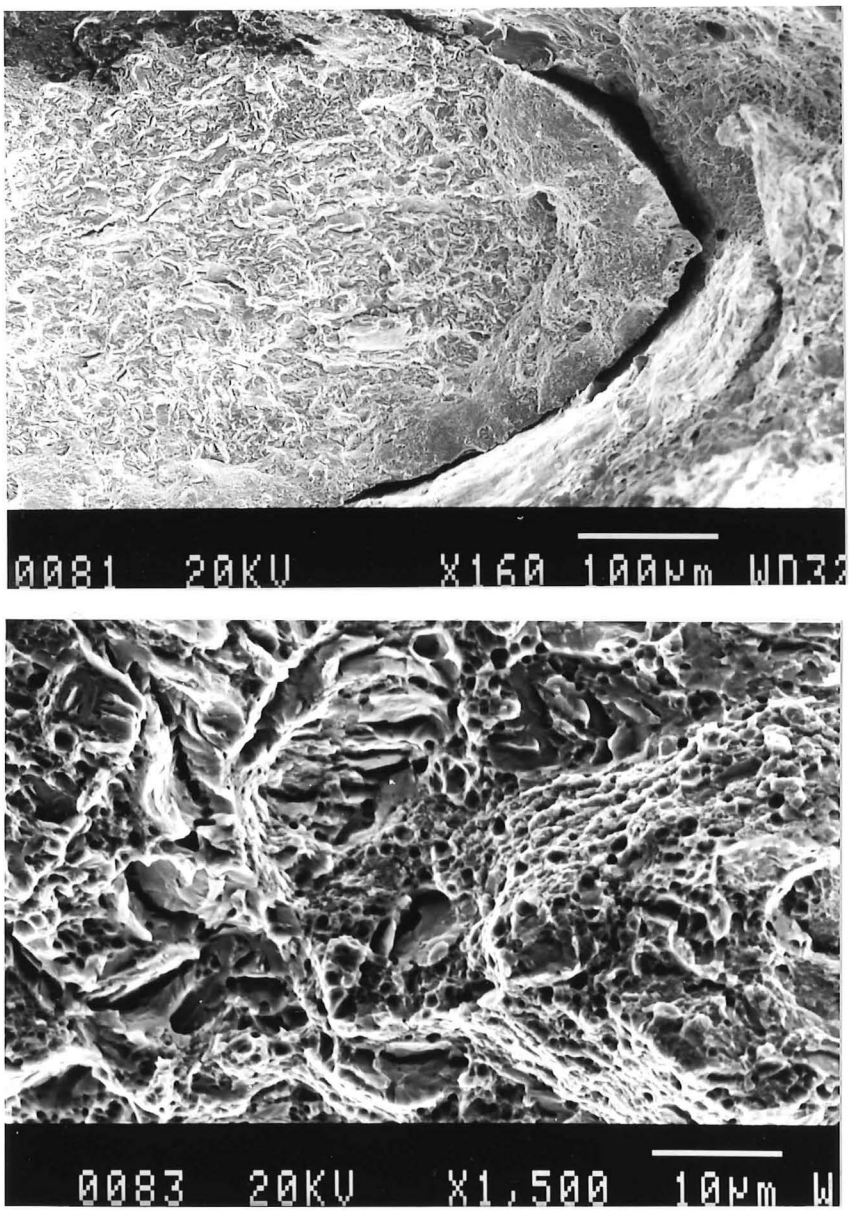

nickel-coated wire composites

Figure 5.3.18 Fracture surfaces of composites

5.3.4.4 Holding time before rolling

Similar to rolling temperature, the holding time at high temperature affects decarburization and chemical reaction. The effect of holding time on the tensile properties of composites (as shown in Figure 5.3.19) is similar to the effect of rolling temperature. The strengths of plain and nickel-coated wire composites decrease with holding time at 950°C by decarburization and reaction respectively, whereas that of copper-coated wire composites increases to a limit with time because of improvement of bonding.

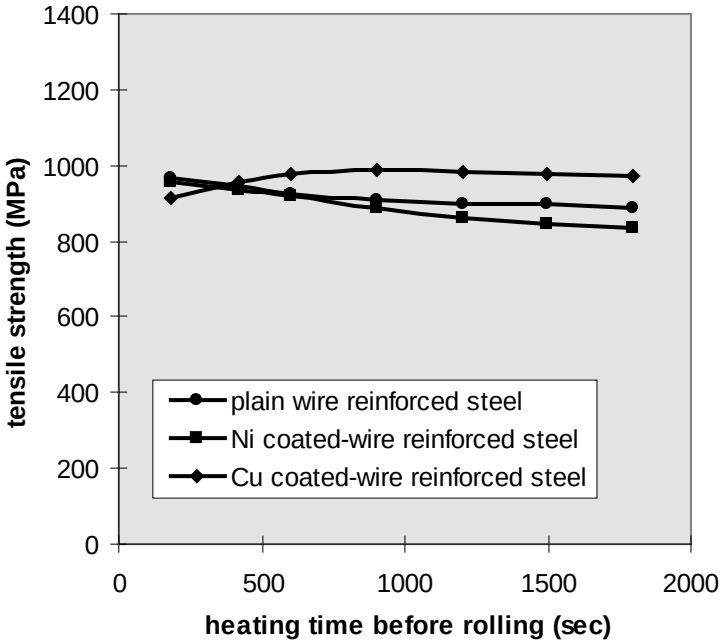

(a) tensile strength

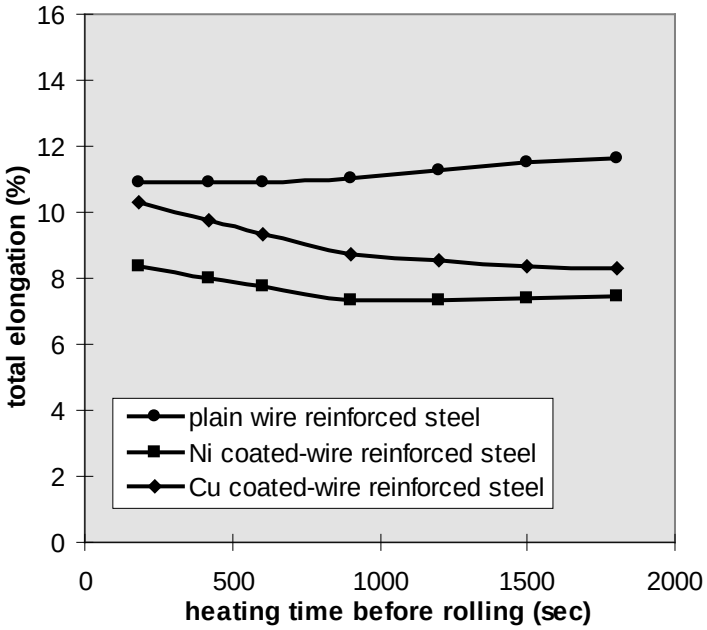

(b) total elongation

Figure 5.3.19 Plot of tensile properties of composite against heating time before rolling

The results of sections 5.3.4.3 and 5.3.4.4 show that the properties of composites are dependent not only on the properties of the wire but also on the interfacial strength. Only if the interfacial strength is high enough to resist debonding, can the high performance of the wire be taken advantage of.

5.3.5 The effect of steel matrix

The study above shows the effect of variation of wire strength due to thermomechanical treatment on the properties of composites. In addition to the wire, the matrix has a large influence on the properties of composites as expected. Figures 5.3.20 are the properties of the composites with different matrices as a function of holding time at 950°C before rolling; the higher strength matrix gives composites with higher strength and lower elongation.

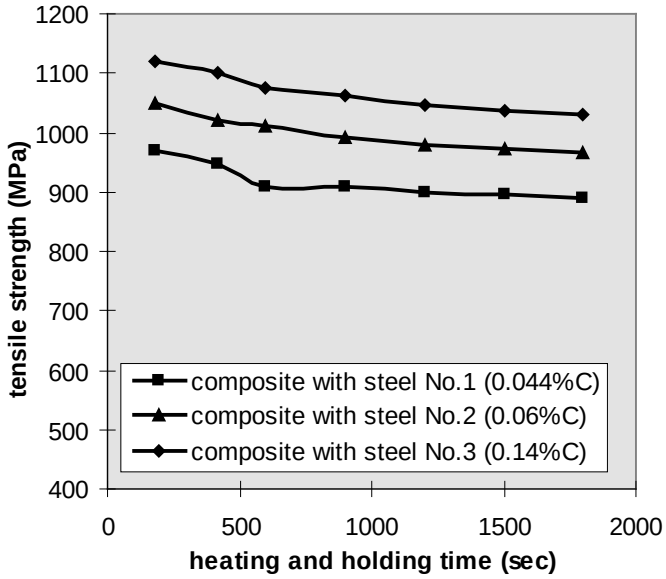

(a) tensile strength

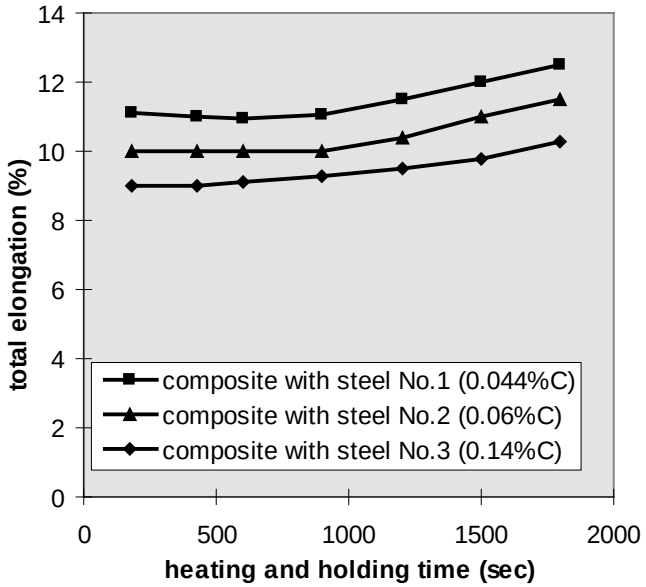

(b) total elongation

Figure 5.3.20 The tensile properties of composites with different matrices as a function of holding time at 950℃ before rolling

As discussed in section 5.2, the interfacial strength is different for a different matrix, but the interfacial strengths in all three matrix composites are high enough to resist the interfacial debonding during tensile testing.

5.3.6 Short wire composites

By using the CHCH (cold rolling-heating/quenching-cold rolling-hot rolling) approach to manufacture short-wire reinforced composites (as outlined in section 3.2.4), the length of the discontinuous wire is determined by the second cold rolling and the following hot rolling.

After the first cold rolling, the air between steel sheets and wires is evacuated to stop the oxidation of the steel in the following heating into the austenite region. When the heated pre-form is quenched into water, the wire is transformed into brittle martensite, which is easily broken by the applied deformation of the cold rolling. The average lengths of the broken wires are a function of the second cold rolling reduction (shown in Figure 5.3.21). The photographs in Figure 5.3.22 show the variation of wire length with rolling.

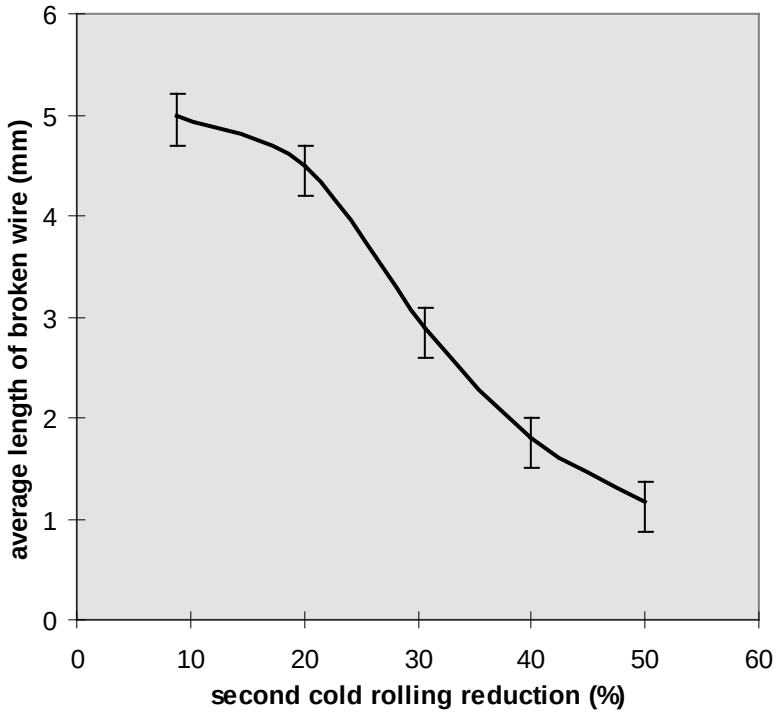

Figure 5.3.21 Average length of the broken wire as a function of the second cold-rolling reduction

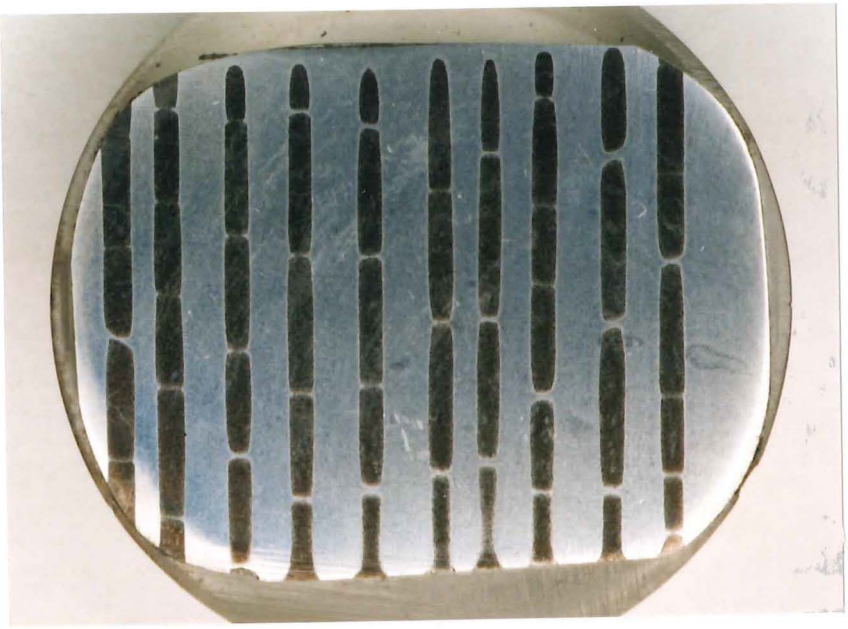

(a) 30% rolling reduction

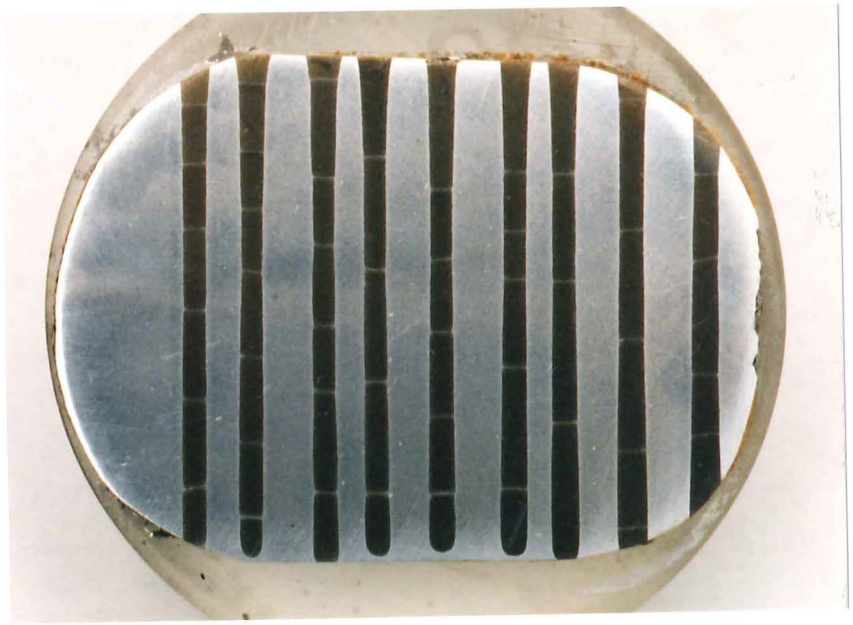

(b) 40% rolling reduction

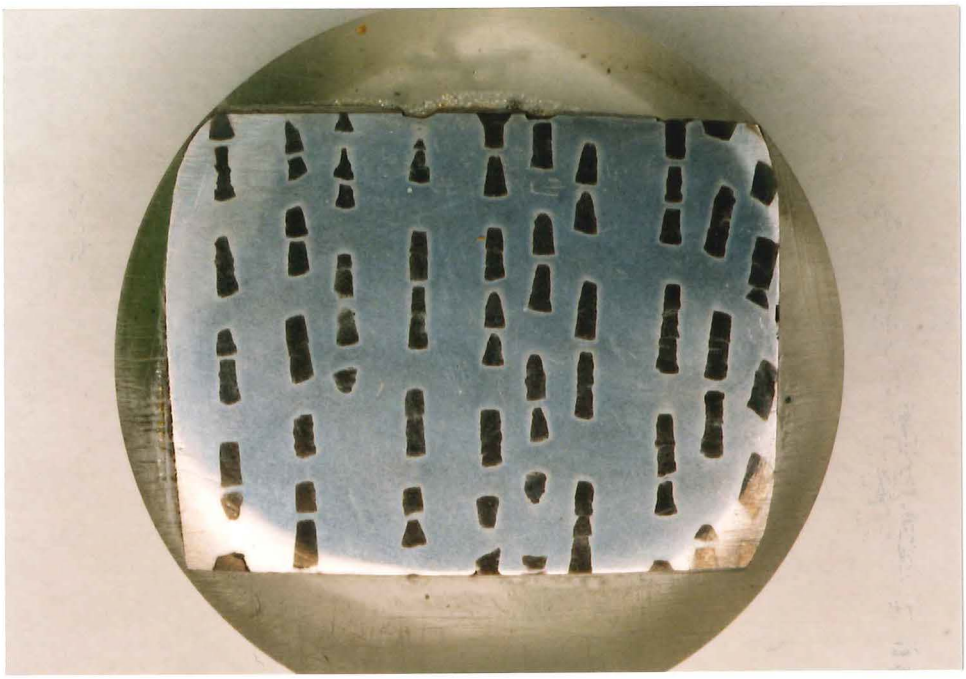

(c) 50% rolling reduction

Figure 5.3.22 Variation of wire length with the second cold-rolling reduction (× 4)

During the hot rolling, the broken wires are elongated again, and the final length of the wire pieces are dependent on the degree of hot rolling. The effect of hot rolling reduction on the tensile properties of short wire composites is shown in Figure 5.3.23. The combination of strength and elongation of short wire composites is superior to the continuous composites only when the rolling reduction is over 80%.

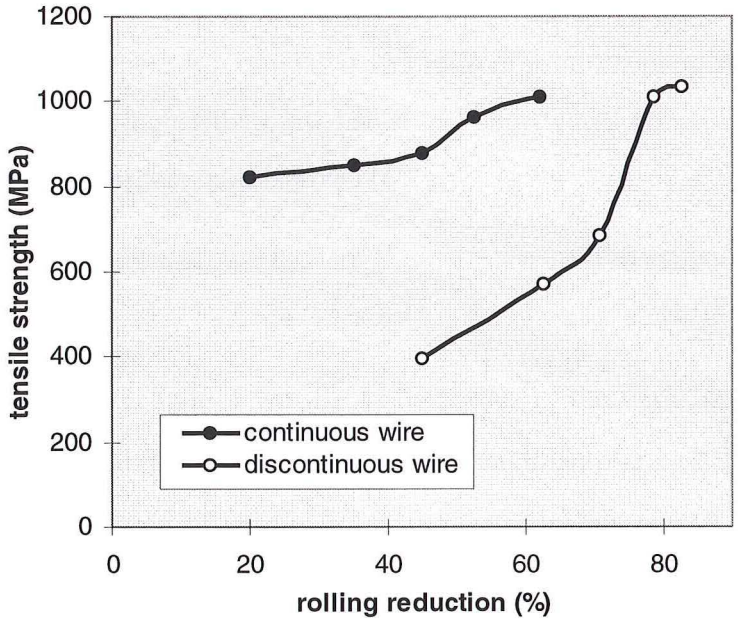

(a) tensile strength

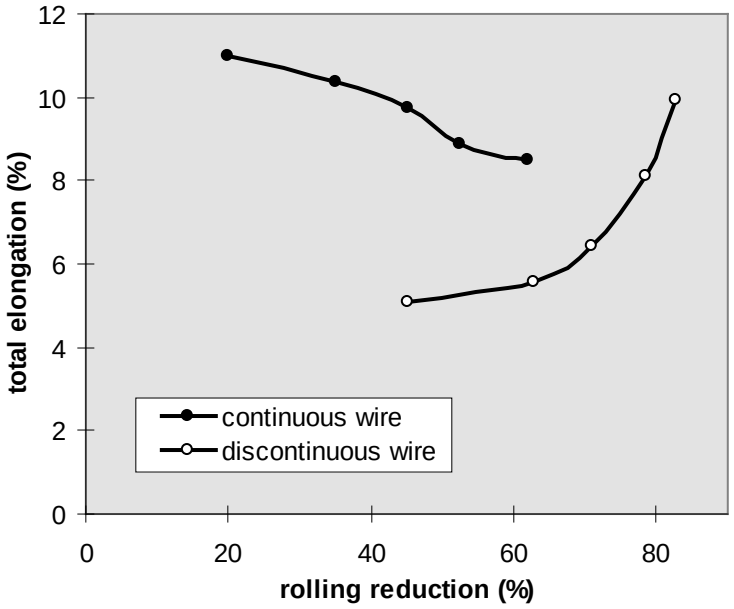

(b) total elongation

Figure 5.3.23 The effect of hot rolling reduction on (a) tensile strength and (b) elongation of CHCH short wire composite.

The most important factors dominating the mechanical properties of the discontinuous composites are wire distribution and aspect ratio. In the aligned condition where the short wires are aligned in one direction, the aspect ratio, which is defined as the ratio of length to radius of the wire, will control the properties of the composite.

According to Kelly[107] there is a critical aspect ratio of reinforcement for discontinuous composites; Only when higher than this value, can short wires effectively reinforce the composite. The critical aspect ratio is given by:

$$\frac{l_w^c}{r_w} = \frac{\sigma_w^{UTS}}{\tau_{\text{int}er}} \tag{5.3.1}$$

where, l_w^c is the critical length of wire, r_w is the radius of the wire, σ_w^{UTS} is the tensile strength of the wire, and $\tau_{\text{int}er}$ is the interfacial strength. In the case of the steel wire composite, the cross-section of wire is not round (refer to Figure 3.9). So the nominal radius, r_w , can be expressed as:

$$r_w = \frac{L_w}{2\pi} = \frac{1}{3\pi}\left(4\sqrt{b^2 + 4h^2} - b\right) \tag{5.3.2}$$

where L_w is the circumference of the cross-section of the deformed wire. Referring to section 5.1 and 5.2, the σ_w^{UTS} and $\tau_{\text{int}er}$ can be estimated as 2500MPa and 350MPa respectively, so the critical aspect ratio is about 7. The relationship between tensile strength of discontinuous composite and aspect ratio is shown in Figure 5.3.24 by replotting Figure 5.3.23(a).

When the aspect ratio is lower than the critical value, composite failure is determined by the matrix strength, and the strength of the composites is given by:

$$\sigma_c^{UTS} = \left(\frac{l_w \tau_{\text{int}er}}{2r_w} \right) \cdot V_w + \sigma_m^{UTS} \left(1 - V_w\right) \qquad (5.3.3)$$

where, V_w is volume fraction of wire, and σ_m^{UTS} is the tensile strength of the matrix. The crack initiates at the end of the wires and propagates into the matrix because of the weak bonding and voids between the wire and matrix at the end of the wire. There is no wire-breaking involved in this case. The fracture surfaces are shown in Figure 5.3.25 for low aspect ratio (obtained from the lowest rolling reduction).

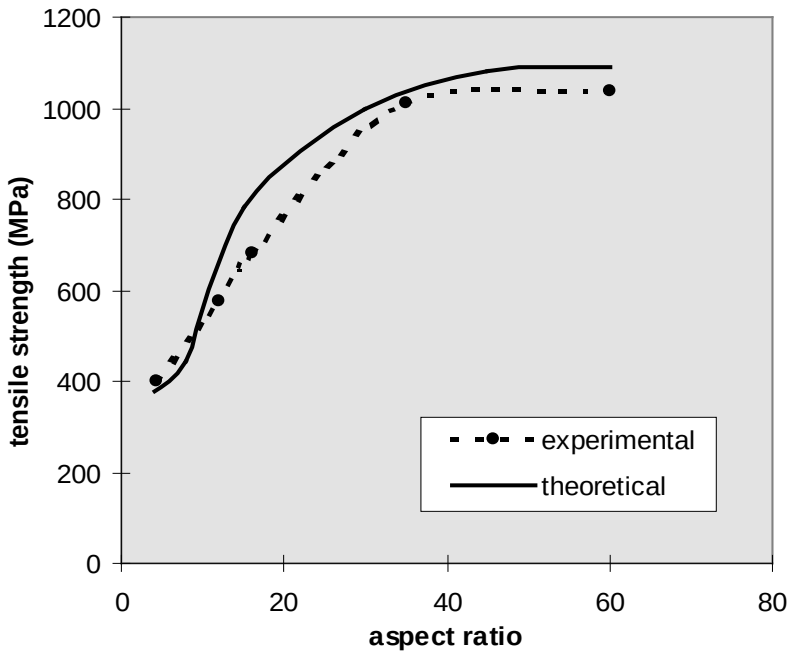

Figure 5.3.24 Tensile strength of discontinuous composite against aspect ratio of wire

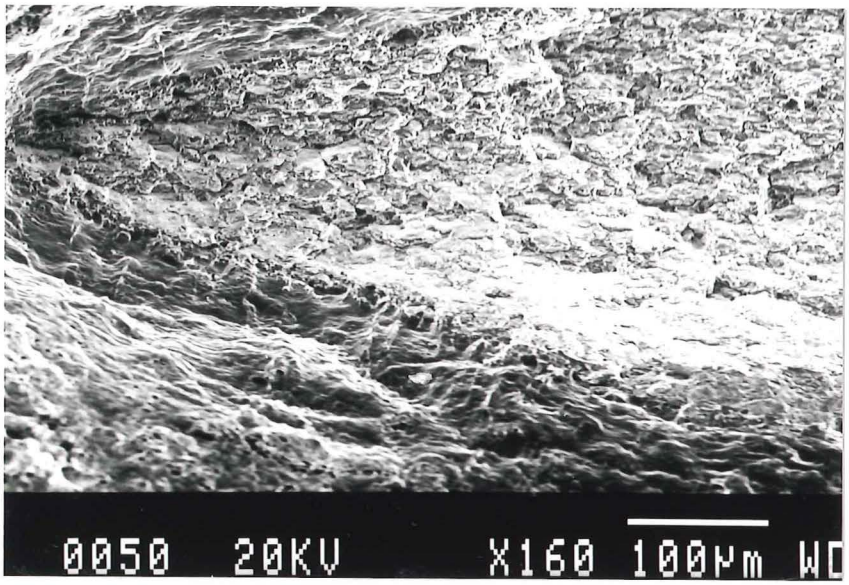

(a)

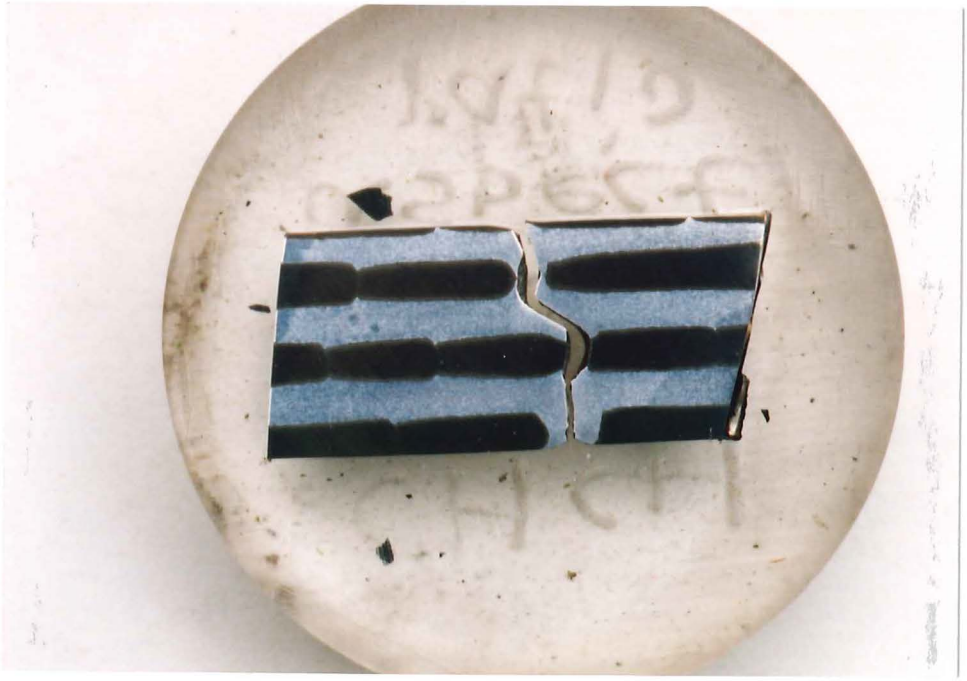

(b), ×2

Figure 5.3.25 Fracture surface (a) and longitudinal cross-section (b) of discontinuous composite with low aspect ratio (about 4)

When the aspect ratio is higher than its critical value, the load can be effectively transferred to wire to the extent that to break the composite one needs to be able to break the wire. The average stress, $\overline{\sigma}_w$, in the wire at failure is given by:

$$\overline{\sigma}_w = \left(1 - \frac{l_w^c}{2l_w}\right) \cdot \sigma_w^{UTS} \tag{5.3.4}$$

The strength of the composite can be obtained by replacing σ_{fu} in Mileiko's theory (equation (2.12)) by equation (5.3.4) as follows:

$$\begin{aligned} \sigma_c^{UTS} = V_w \left(\frac{\varepsilon_c^{NEC}}{\varepsilon_w^{NEC}}\right)^{\varepsilon_w^{NEC}} \exp(\varepsilon_w^{NEC} - \varepsilon_c^{NEC}) \left(1 - \frac{\sigma_w^{UTS} \cdot r_w}{2\tau_{inter} \cdot l_w}\right) \sigma_w^{UTS} \\ + (1 - V_w) \left(\frac{\varepsilon_c^{NEC}}{\varepsilon_m^{NEC}}\right)^{\varepsilon_m^{NEC}} \exp(\varepsilon_m^{NEC} - \varepsilon_c^{NEC}) \sigma_m^{UTS} \end{aligned} \tag{5.3.5}$$

where, $\varepsilon_c^{NEC}, \varepsilon_w^{NEC}, \varepsilon_m^{NEC}$ are true uniform strain of composite, wire, and matrix respectively, and roughly estimated as the elongations.

Fracture surfaces of high aspect ratio wire composites are shown in Figure 5.3.26, and show the fracture occurring in the wire.

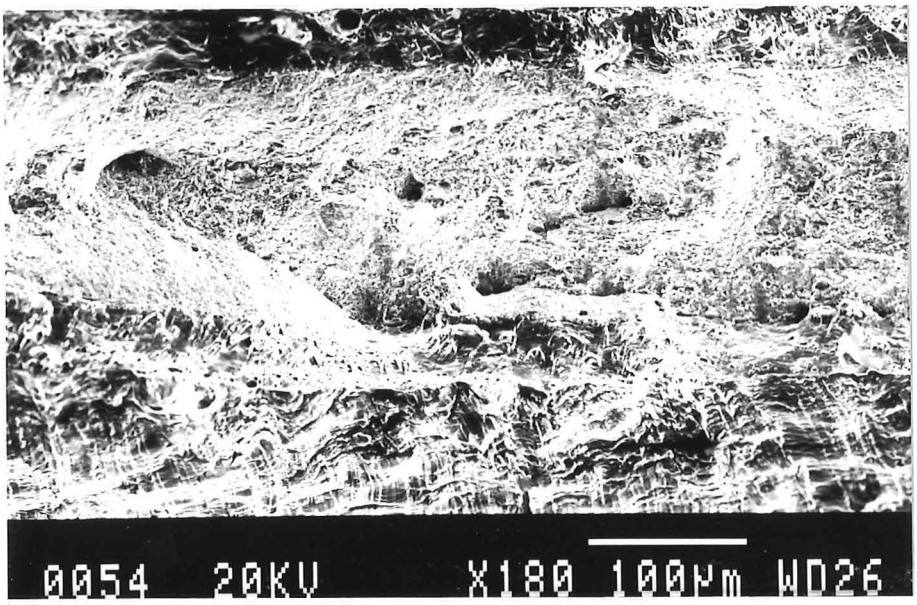

(a)

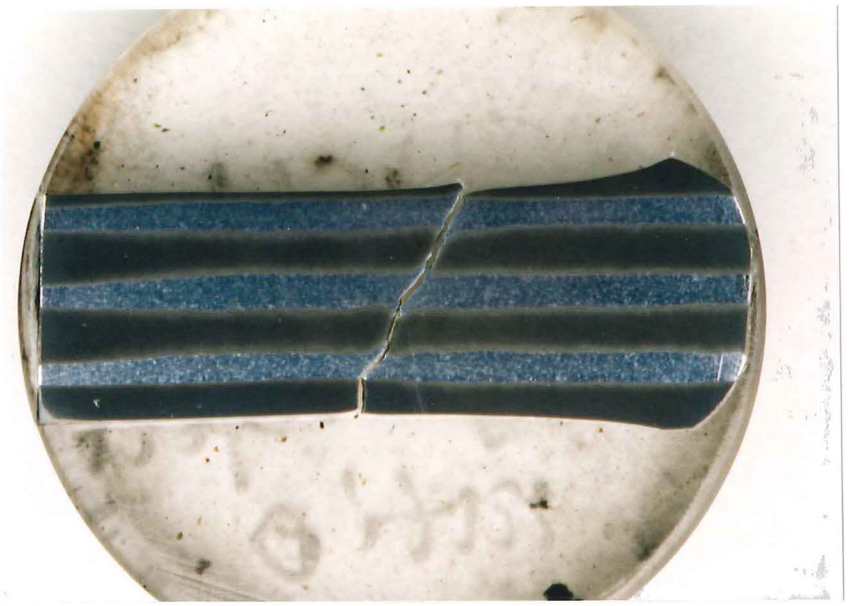

(b), $\times 2$

Figure 5.3.26 Fracture surface (a) and longitudinal cross-section (b) of short wire composite with high aspect ratio (about 50)

For comparison, the predicted relationships between strength and aspect ratio from equations (5.3.3) and (5.3.5) are shown in Figure 5.3.24. Both experimental data and theoretical prediction indicate that the strength of discontinuous composites increases with increasing wire aspect ratio and reach the strength of a continuous composite when the aspect ratio is about 5 times the critical aspect ratio.

The short-wire composite made by the CH approach (single cold + hot rolling) has a big shortcoming; this is the poor bonding between wire and matrix at the end of the wire, which is caused by the grooves in the matrix sheet and the flow stress difference between wire and matrix steel (the void at the end of wire is shown in Figure 5.3.27).

Compared with the CHCH short wire composite, the CH short wire composite has lower tensile strength and elongation (see Figure 5.3.28) because the defect at the end of the wire works as an initial crack, propagates along the matrix, and leads to the failure of the composite. The effect of this defect at the end of the wire on strength and ductility diminishes with increasing length of the wire, ie. the tensile strength and total elongation increase with increasing length of wire. The fracture surfaces are shown in Figure 5.3.29.

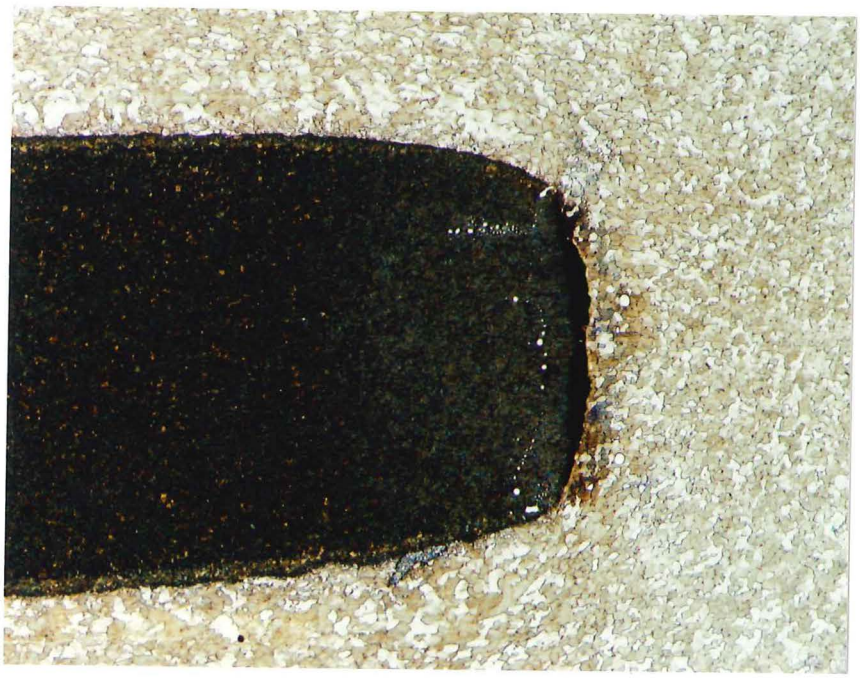

Figure 5.3.27 Defect at the end of a wire in a CH short-wire composite (× 57.5)

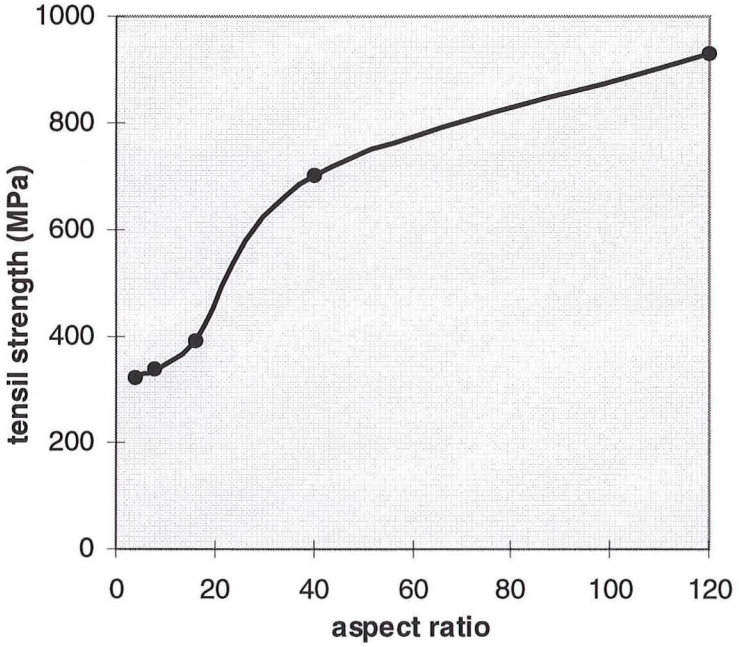

(a) tensile strength

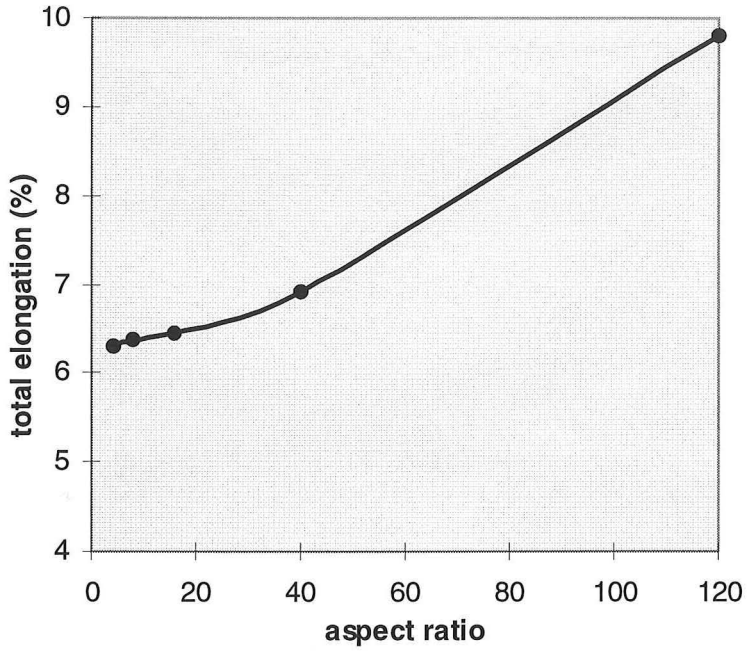

(b) elongation

Figure 5.3.28 The effect of initial length of wire on the tensile properties of CH short wire composite

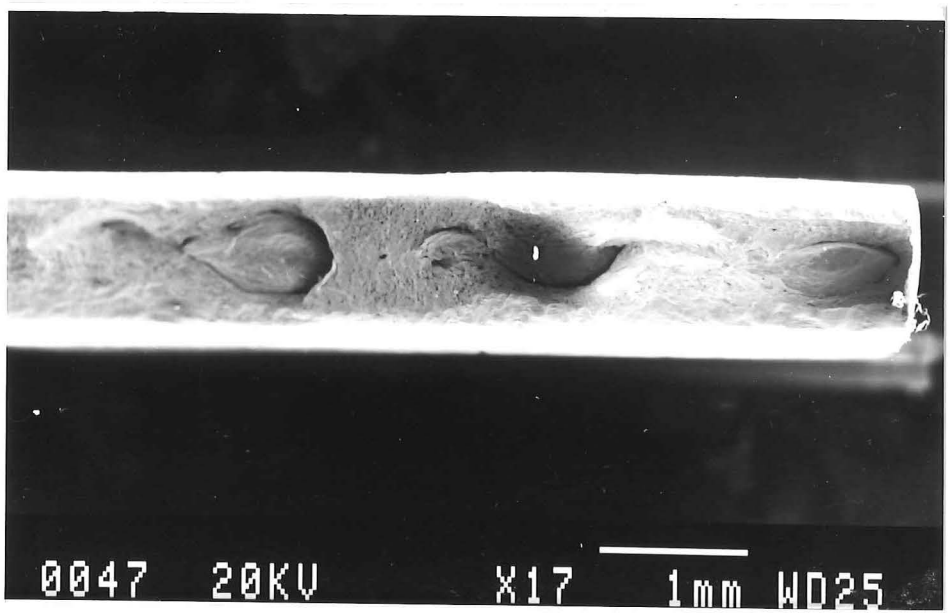

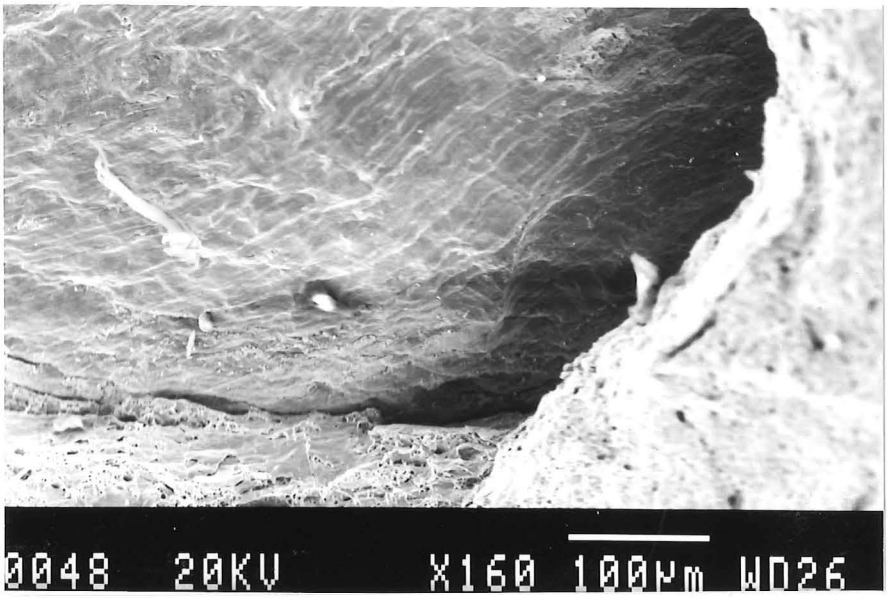

Figure 5.3.29 Fracture surface of CH discontinuous composites

5.3.7 Summary

Artificial dual phase steel has been made successfully by hot-rolling. Heat-treatment following fabrication is required in order to obtain a good combination of strength and ductility. Of the various heat treatments investigated, namely austempering, martempering, water-quenching and normalizing, austempering was chosen as the final treatment for the rolled steel-steel composites because it gives the best combination of strength and elongation. The condition of austempering is set as: heating at 800°C for 2min and quenching into oil at 260°C and isothermally holding at 260°C for 305min.

The tensile properties of the composites are functions of the properties of the components, and the interfacial strength. Any factors which can influence the strength of the wire (such as strain hardening or cold rolling, finishing rolling temperature, decarburization, rolling reduction) can also influence the strength of the composite.

High strength and elongation of composites can be obtained when there is strong interfacial bonding, and the fracture process of these composites is crack formation in the matrix and propagation through the interface, to the wire.

In the composites with weak interfacial bonding, the crack initiates at the interface and propagates along the interface, and the composites fracture without the wire being

broken. The reinforcing effect of the wire has not been taken advantage of, which makes the composites exhibit low strength and elongation.

The wire can be embrittled if a brittle intermetallic compound forms at the interface, which gives the composite low strength and elongation. In the case of nickel-coated wire composite, the amount of intermetallic compound ($FeNi_3$) at the interface increases with increasing temperature and holding time, so the tensile strength and elongation decrease with increasing temperature and holding time.

The tensile properties of the matrix steels can also affect tensile properties; A high strength/low ductility matrix steel gives a composite with high strength/low ductility.

The properties of the composite are influenced by the size of wire. Elongation and strength increase with increasing wire diameter, because the higher surface area of the finer wire makes the composite more brittle, and the finer wires more easily contact each other and break during fabrication rolling.

The CHCH (cold rolling-heating/quenching-cold rolling-hot rolling) approach was successful for fabricating unidirectional short wire composites. The aspect ratio of the short wires is dependent on the second cold rolling and the final hot rolling. The elongation of short wire composites is superior to continuous composites at an equivalent strength only when rolling reduction is over 80%.

Compared to the CHCH approach, the CH (cold rolling plus hot rolling) method was not successful for making short wire composites because not only is a lot of manual preparation work involved, but there are lower properties for the CH composite at an equivalent aspect ratio. The presence of voids at the end of the short wires is the main reason for the poorer properties of the CH composite.

Chapter 6 Overall

Following the discussions in Chapters 4 and 5, some key points related to the work in general are discussed in the following sections.

6.1 Superiority of the oriented DP-steel to the random DP-steel

As outlined in Chapter 2, one aim of the current research is to produce a dual phase steel with oriented martensite instead of random martensite. A comparison between three kinds of martensite morphology in steel A is shown in Figure 6.1. It can be seen that in the present range of martensite content, the long fibrous martensite steel has the highest strength and lowest ductility and the granular martensite steel has lowest strength and highest elongation. With increasing martensite volume fraction, the strengths of all steels linearly increase, and total elongations decrease except the as-rolled steels.

This exception by the as-rolled steels is caused by internal stresses. The lower martensite volume fractions were obtained by annealing and rolling the steel at lower temperature, which produced higher internal stresses. This effect resulted in a maximum elongation at about 30% martensite in the as-rolled steel.

The rolling carried out in the two-phase region causes flattening and elongation of the austenite islands and a consequent fibering of the resultant martensite in the rolling direction. In addition, it also introduces internal stresses and dislocations, especially in ferrite. Both the fibrous martensite and the internal stresses increase the strength and reduce the elongation of the as-rolled steel.

After a short annealing time, both the residual stress and dislocations in the as-rolled steel are reduced and the long martensite “fibres” shrink to short “fibres”. The deformation of ferrite due to the warm rolling accelerates recrystallization during post-RA and results in ferrite grain refinement. Both the shrinkage of martensite and recrystallization of ferrite due to short annealing times cause a decrease in strength and an increase in ductility.

The steels subjected to long post-rolling annealing time comprising of large granular martensite and growing epitaxial ferrite, exhibit the lowest strengths and highest

elongations. This is because of the presence of ductile epitaxial ferrite and the lower reinforcing effect of granular martensite compared to continuous or discontinuous martensite “fibres”.

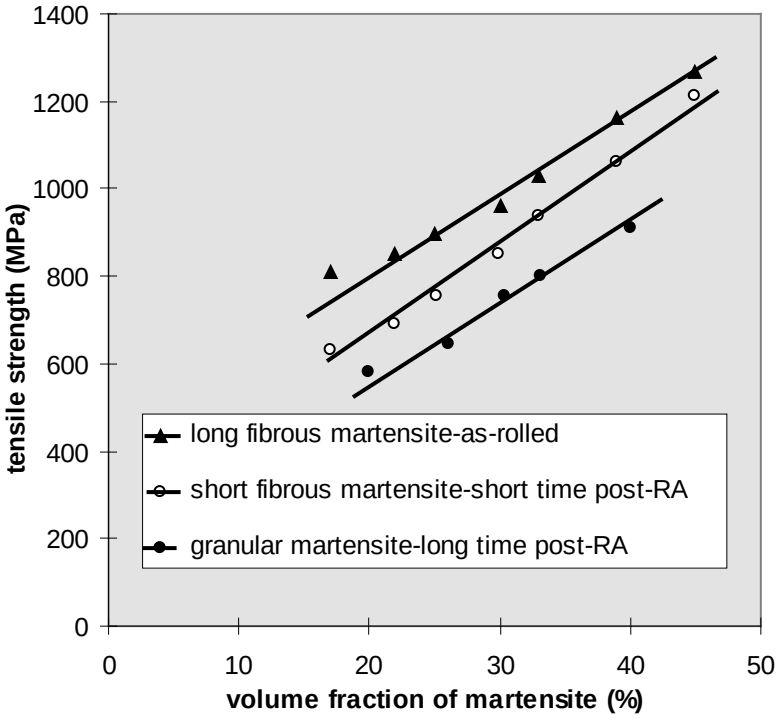

(a) tensile strength

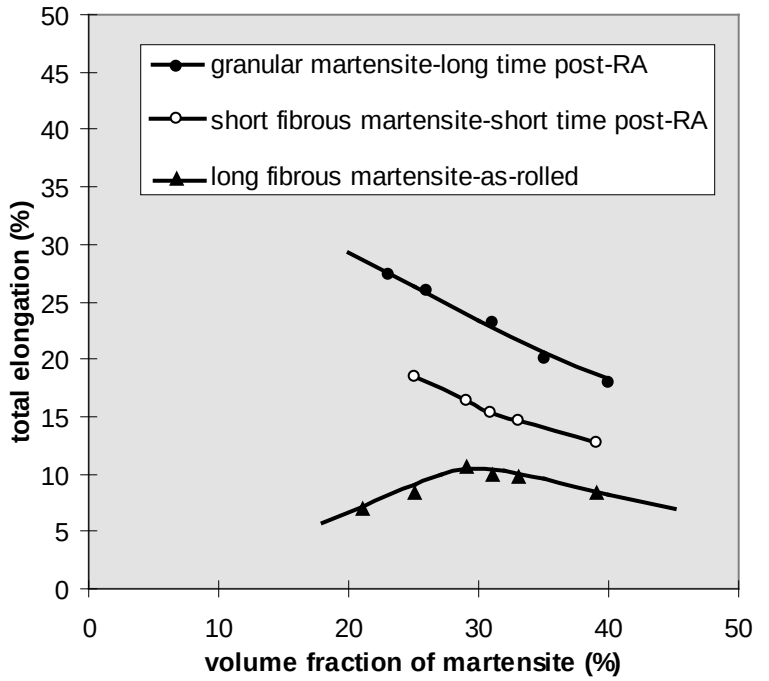

(b) total elongation

Figure 6.1 Variation of tensile properties with martensite morphology in steel A

The high ductility of granular martensite dual phase steel may also be caused by strain partitioning. Previous studies shows that the hard martensite phase carries a higher stress but undergoes a smaller strain than the softer ferrite phase during plastic deformation[60, 145]. Owing to the strain partitioning, dual phase steel can fracture at a strain higher than the failure strain of martensite which is the reason why dual phase steel has a higher elongation to fracture than HSLA steel of similar carbon content: the higher the strain partitioning, the higher the elongation of dual phase steel. Compared to the long "fibrous" martensite dual phase steel, the post-RA steel contains granular martensite and should therefore have higher strain partitioning, so exhibit higher elongation.

The stress ratio between martensite and ferrite during plastic deformation demonstrates the reinforcing effect of martensite. The higher aspect ratio of the martensite "fibres" should increase the stress ratio and improve the load transfer from ferrite matrix to martensite "fibre". The improved load transfer in the fibrous martensite steel during plastic deformation results in higher strength.

The comparison between the present research and the literature is shown in Table 6.1, it clearly shows that the strength of short martensite dual phase steels obtained by short annealing time after warm-rolling is superior to that of the granular martensite dual phase steels at the equivalent martensite volume fraction, but the as-rolled steels with long martensite "fibres" is the strongest and the most brittle.

Through the comparison, the best combination of strength and ductility of dual phase steel can be obtained by the following processing:

Intercritical annealing at the temperature under which 25-30% martensite is obtained for a certain time when equilibrium manganese partitioning is achieved, and quasi-isothermal rolling at the annealing temperature to the required reduction, and then annealing at the previous annealing temperature for 30min (eliminating internal stresses produced during rolling).

The effect of manganese partitioning can be clearly seen on the critical cooling rate. After annealing at 680°C for 48 hours, the manganese partitioning in steel A enable austenite to transform to martensite during air-cooling after rolling.

The effect of manganese partitioning on the mechanical properties of dual phase steels is hard to conclude because the variation of manganese partitioning with annealing temperature and time also results in the change of martensite volume fraction and ferrite grain size, but it is sure that manganese partitioning benefits the strength and ductility of dual phase steel.

Table 6.1 Comparison between current research and literature

sample	volume fraction of martensite (%)	the form of martensite	tensile strength (MPa)	total elongation (%)
current research	22	long fibre	850	7.0
current research	31	long fibre	960	10.2
current research	39	long fibre	1160	8.4
current research	25	short fibre	714	18.5
current research	31	short fibre	866	15.4
current research	39	short fibre	1020	12.7
current research	20	granular	580	28.5
current research	31	granular	754	23.2
current research	40	granular	910	18
reference[146]	19	granular	700	16.5
reference[146]	31	granular	800	14.5
reference[146]	42	granular	863	13
reference[4]	29.1	granular	771	17
reference[4]	35.5	granular	824	17.0
reference[4]	41.3	granular	924	14.5

6.2 Davies interpretation of Mileiko's theory

Davies[49] has described the relationship between strength/true uniform strain and volume fraction of martensite of intercritical annealed dual phase steels by using Mileiko's theory (refer to section 2.2.3). The application of Mileiko's theory in in-situ and artificial dual phase steels is investigated in the following sections.

6.2.1 In-situ dual phase steels

In the case of in-situ dual phase steels, ferrite works as the matrix, and martensite as the reinforcing fibre. By replacing σ_{mu}, σ_{fu}, ε_m and ε_f by 415MPa, 2000MPa, 0.31 and 0.07 (the values suggested by Davies) in equation (2.12), the relationship between strength and volume fraction of martensite for steel A can be plotted as shown in Figure 6.2. It can be seen that the experimental values for the as-rolled dual phase steel A are considerable higher than those predicted by Davies's interpretation, whereas those for the post-RA steel are much closer to the predicted values except at high volume fraction of martensite. This difference between the theoretical and experimental data for the as-rolled steel A is most likely due to the effect of rolling on the properties of martensite and ferrite.

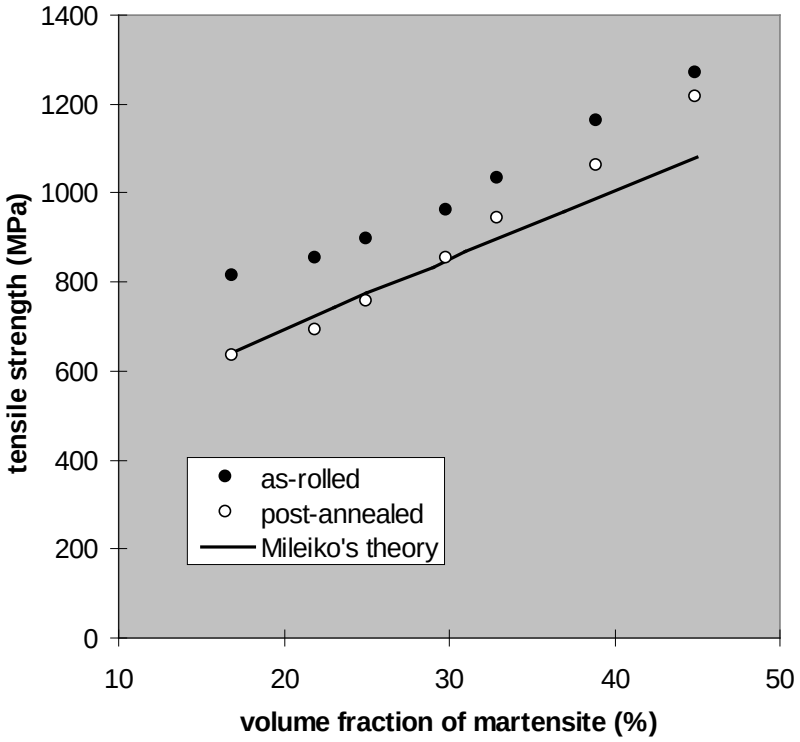

Figure 6.2 The comparison between present experiments and Davies's interpretation

When considering the effect of rolling on the strength of martensite and ferrite of the as-rolled steel A, the properties of the components should be revised, eg by using figures extrapolated from the data shown in Figure 4.24 for the continuous rolled steel A (σ_m=354MPa, σ_f=2400MPa). Equation (2.12) can then describe the relationship of strength and martensite volume fraction of as-rolled steel A when martensite is over 25%. By replacing σ_m, σ_f, with 211MPa, 2400MPa, a linear relationship can also be seen between strength and martensite volume fraction of post-RA steel A when martensite volume fraction is higher than 20% (as shown in Figure 6.3).

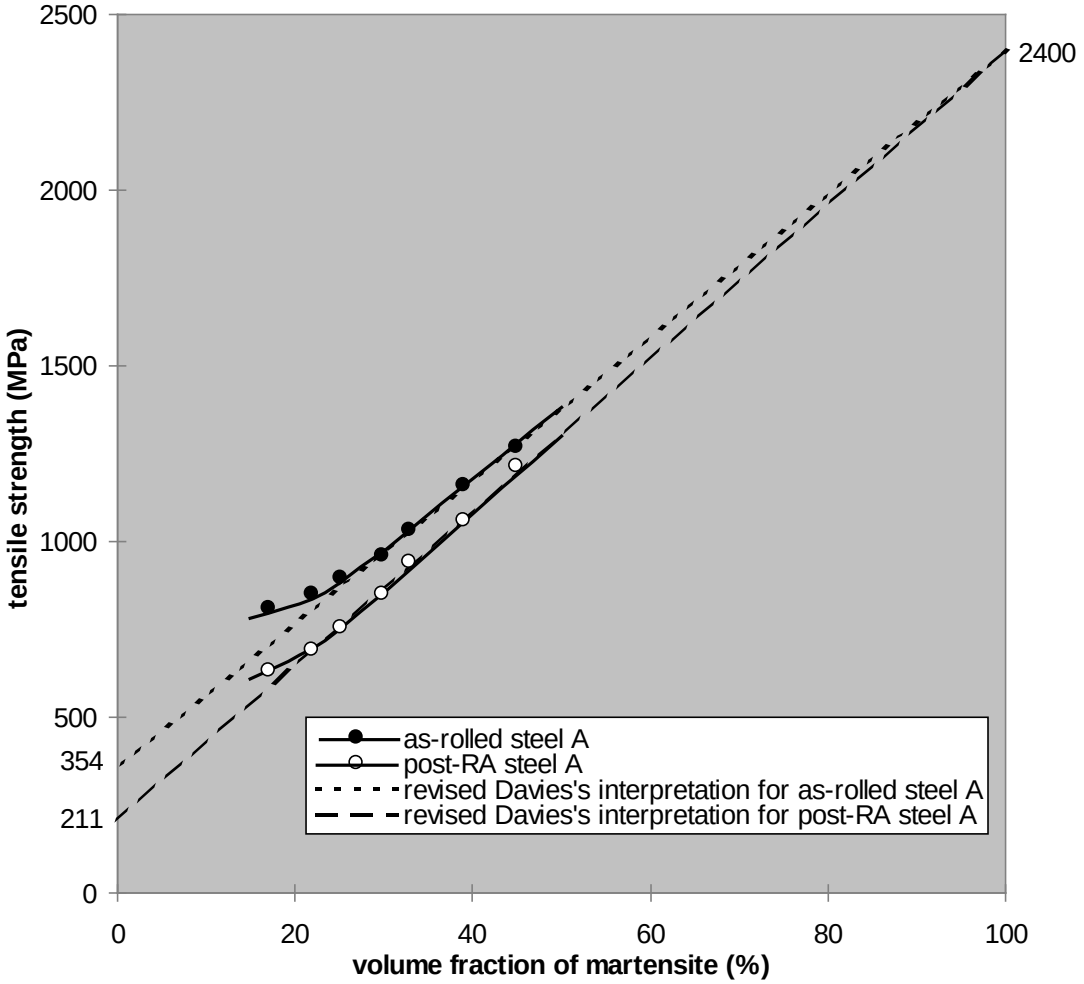

Figure 6.3 Comparison between the experiment and theory with revised components data

The same extrapolated martensite strength for both as-rolled steel A and post-RA steel A suggests that the rolling doesn't have much effect on the martensite strength but does apparently strengthen the ferrite. The lower the martensite volume fraction (ie. the lower the rolling temperature), the larger the strength difference between the as-rolled steel and post-RA steel.

The deviation of the experimental data with the revised Davies's interpretation at lower martensite volume fraction may caused by the following:

(1) Internal stress. The lower martensite volume fraction in the dual phase steels was obtained at lower temperature, at which higher internal stresses were produced during rolling;

(2) Work-hardening. Rolling at lower temperature primarily strengthens the ferrite; the lower the rolling temperature, the higher the ferrite strength;

(3) Carbide precipitation. Carbides can precipitate at lower temperature, which increases the strength of the dual phase steel;

(4) Ferrite refinement. Ferrite deformed at lower temperatures will recrystallize during post-RA, the heavier the deformation (lower deformation temperature), the finer the ferrite grain.

The above reasons (1), (2) and (3) are suitable for the as-rolled steel, and reasons (3) and (4) refer only to the post-RA steel.

This indicates that Davies's interpretation can apply for these dual phase steels only when the martensite volume fraction is over a critical value.

Owing to limitations in testing facilities, true uniform strain could not be obtained and the relationship between true uniform strain and martensite volume fraction could not be investigated and correlated with Davies's interpretation.

6.2.2 Artificial dual phase steels

In the continuous wire composites (artificial dual phase steels), the properties of the wire are strongly affected by the fabrication parameters and heat-treatment after fabrication. The variation of the composite strength with strength of the wire can be predicted by equation (2.12) (assuming σ_{mu}=450MPa, ε_m=0.31 and ε_f=0.07) and is shown in Figure 6.4. The strength of composites increases linearly with increasing wire strength, and the Mileiko's theory agrees with the experimental data very well. Owing to the lack of current ε_f and ε_m values, we will adopt the ε_f and ε_m values suggested by Davies[49] in this section.

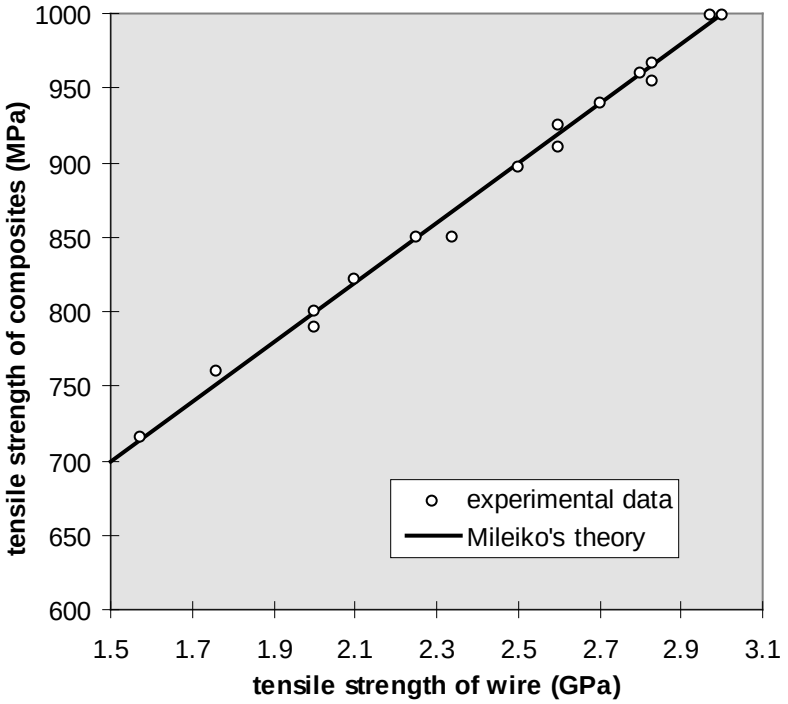

Figure 6.4 The comparison of tested tensile strength relationship between wire and composites (containing 20% wire) with theory

The effect of volume fraction of wire on the tensile strength of wire composites can be predicted by substituting 2500MPa, 450MPa (refer to sections 5.1.1.4 and 5.1.2.1), 0.31, and 0.07 for σ_{fu}, σ_{mu}, ε_m and ε_f respectively in equation (2.12), and is shown in Figure 6.5. The nearly linear increase of strength with volume fraction of wire corresponds to the prediction by Mileiko's theory.

Mileiko's theory agrees with the experimental data for the artificial dual phase steels for the whole range of wire volume fraction without the deviation seen in the in-situ dual phase steel at lower martensite volume fraction.

The comparison above shows that Mileiko's theory can predict the relationship between the tensile strength of ductile second phase reinforced composites and the volume fraction of the second phase as long as the right component properties are chosen, no matter what the scale of the reinforcement. If the properties of the components vary with volume fraction of the second phase, the values adopted in Mileiko's theory need to be revised.

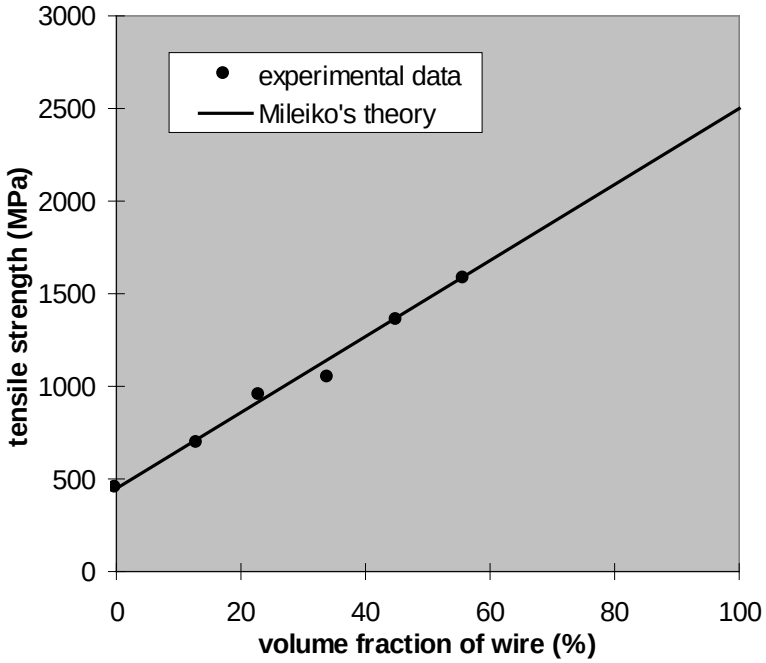

Figure 6.5 Variation of strength of artificial dual phase steels with volume % of wire

6.3 Advantage of Bainitic wire over martensitic wire in artificial DP steel

In section 5.3, bainite was chosen as the wire's final phase instead of martensite. Comparing the hardness of the wire with the tensile strengths of the wire and the wire reinforced composites (listed in Table 6.2), one may wonder why the hardest martensitic wires lead to the lowest strength of both the wire and composite.

Table 6.2 Comparison between hardness of wire and tensile properties of wire and composites with different wire

type of wire	*hardness of wire (Hv)*	*strength of wire (MPa)*	*elongation of wire (%)*	*strength of composites (MPa)*	*elongation of composite (%)*
martensitic	1100	800	0.6	477	2.1
bainitic	820	2500-3000	3.5	929	9.8
pearlitic	640	1100	8.2	496	29.3

The fracture surface of the martensitic wire after tensile failure shows intergranular failure has been found as shown in Figure 6.6. This intergranular fracture results in

premature failure of the martensitic wire and the lowest strength and elongation are obtained.

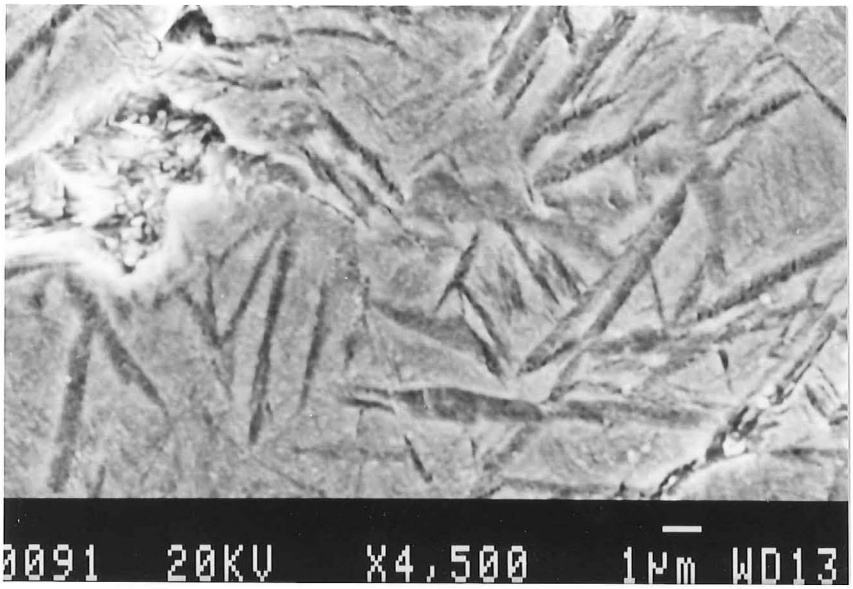

Figure 6.6 Polished cross section of martensitic wire showing intergranular fracture

The stresses produced during the water-quenching are attributable to thermally induced deformation and the volume expansion associated with the martensitic transformation. The combination of these two factors can often result in internal tensile stresses after quenching and in some cases, depending on quenching severity and composition, cracking in the component. These cracks usually follow prior austenite grain boundaries[134]. The residual stresses are tensile in the inside of a quenched cylinder and compressive in the outside.

As mentioned, the residual stresses and micro-cracks formed in martensite depend, in part, on the expansion during the martensitic transformation, which is a function of the carbon content in the steel. The higher the carbon content, the higher the expansion, and the higher the residual stresses and likelihood of cracking. These quench cracks were prevalent at a carbon equivalent value above 0.525[134], so the residual stresses and cracking problem are much more aggravated in the eutectoid martensite than in low carbon martensite, that is why intergranular fracture has not been observed in the low carbon martensite.

Under an applied tensile load, the propagation of the existing micro-cracks depends on the stress field at the crack tip. In the case of water-quenched wire, the stress at the end

of crack is caused by not only the applied stress but also any residual tensile stress produced during quenching. For the water-quenched martensite, the stress at the end of the micro-crack caused by the applies stress σ_{app}^{WQ} is given as[147]:

$$\sigma_{end}^{WQ} = 2\sigma_{app}^{WQ}\left(\frac{c}{\rho_{WQ}}\right)^{1/2} \qquad (6.1)$$

where, $2c$ is the length of the major axis of the elliptical crack, and ρ_{WQ} is the radius of the curvature at the end of the crack (see Figure 6.7).

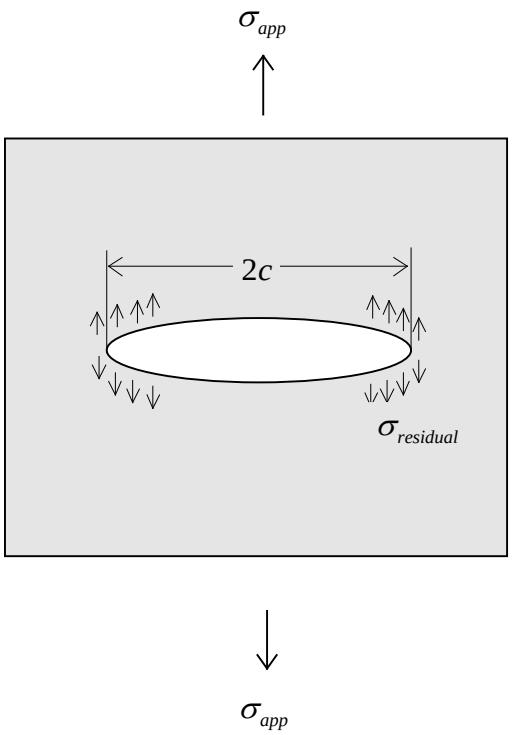

Figure 6.7 Crack in the material

Under the joint effects of applied stress σ_{app}^{WQ} and residual stress $\sigma_{residual}$, the crack will propagate when the stress at the end of crack reaches the critical stress, ie. the theoretical stress σ_{th}. The condition for propagation of the existing crack is:

$$\sigma_{end}^{WQ} + \sigma_{residual} = \sigma_{th} \qquad (6.2)$$

Substituting σ_{end}^{WQ} in equation (6.2) with equation (6.1), we have:

$$\sigma_{app}^{WQ} = \frac{1}{2}\left(\sigma_{th} - \sigma_{residual}\right)\left(\frac{\rho_{WQ}}{c}\right)^{1/2} \qquad (6.3)$$

Equation (6.3) shows that crack in martensitic wire can propagate at a stress lower than theoretical stress because of the residual stress; premature fracture takes place in the water-quenched eutectoid wire because of the existence of micro-cracks and high residual stresses.

In the tempered martensitic wire, owing to the elimination of residual stress due to tempering, the equation (6.3) should be changed to:

$$\sigma_{app}^{tem} = \frac{\sigma_{th}}{2}\left(\frac{\rho_{tem}}{c}\right)^{1/2} \qquad (6.4)$$

The tempering not only releases residual stress but makes the end of crack duller than the sharp crack in water-quenched wire, ie. $\rho_{tem} >> \rho_{WQ}$, so the strength of tempered wire is much higher than that of water-quenched wire, ie. $\sigma_{app}^{tem} >> \sigma_{app}^{WQ}$.

Compared to the water-quenched martensitic wire, bainitic wire comprises no residual stresses or micro-cracks because of its moderate transformation. The bainitic wire can thus reach a higher strength and for this reason bainite was chosen as the phase for the reinforced wire.

6.4 In-situ DP steel and artificial DP steel

Ignoring the difference in phase composition of the reinforcements in in-situ and artificial dual phase steels, a comparison of the tensile properties between in-situ and artificial continuous dual phase steels can still be made, and is shown in Figure 6.8. Higher strength/lower ductility is obtained in the artificial dual phase steel because of its higher strength components, and continuous reinforcing wire.

Both the strength and elongation of artificial continuous dual phase steel are very close to those of as-rolled in-situ dual phase steel A when the volume fraction of the reinforcement is higher than 30% because of their component's similar properties. Both the as-rolled in-situ and artificial continuous dual phase steel involve breaking of "fibres" during tensile fracture and it is believed that it is possible to use the artificial continuous dual phase steel to simulate the properties and fracture of the as-rolled dual phase steel.

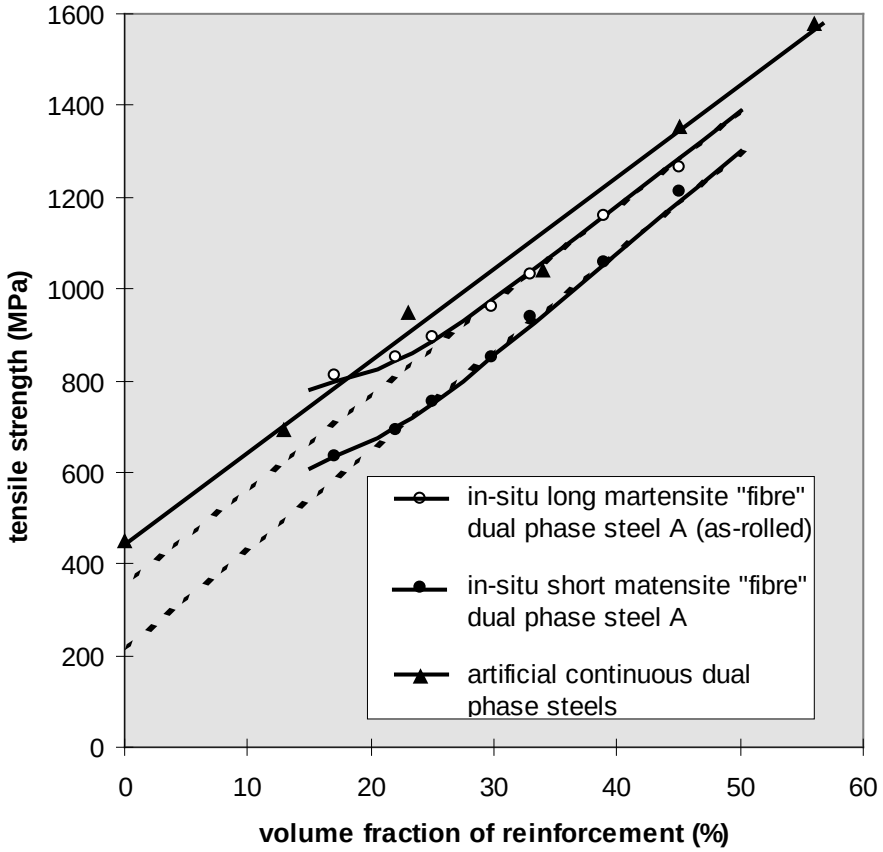

(a) tensile strength

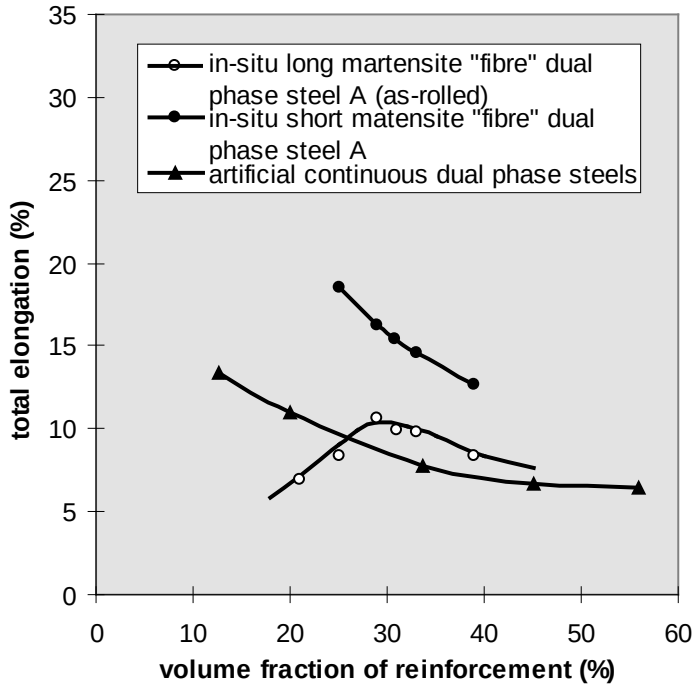

(b) total elongation

Figure 6.8 Comparison between in-situ and artificial continuous dual phase steels

Because there is no martensite fracture involved in the failure of the short martensite "fibre" dual phase steel (refer to section 4.3.5), the long wire artificial dual phase steel can not simulate the properties and fracture of this kind of steel.

The variation of tensile strengths of discontinuous artificial and in-situ dual phase steels with aspect ratio of reinforcement is shown in Figure 6.9. The strengths of both steels increase with increasing aspect ratio until reaching constants, which are the strengths of continuous composites.

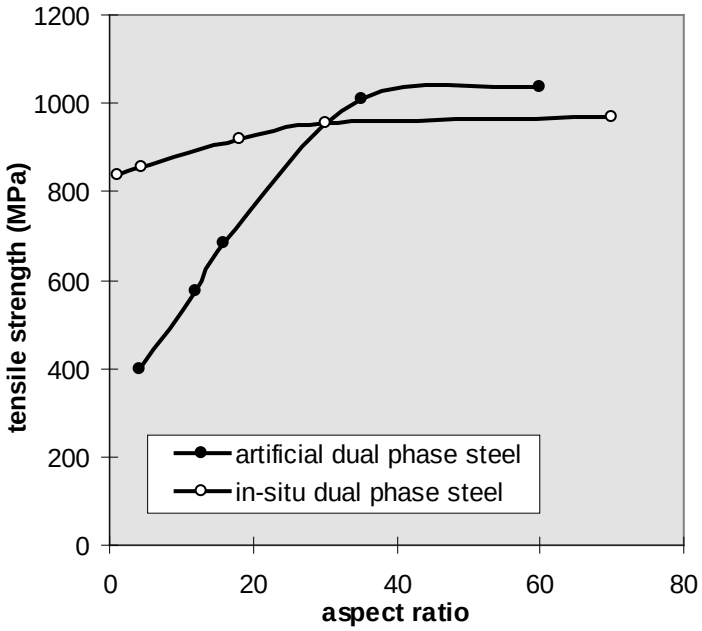

Figure 6.9 Variation of tensile strength of both in-situ and artificial dual phase steels with aspect ratio of reinforcement

The critical aspect ratio applies to artificial dual phase steels only. Below this aspect ratio, the stress cannot transfer to the wire effectively, the short wires act as a void rather than a reinforcement and so the strength of the discontinuous artificial dual phase steel is lower than the strength of the matrix steel when the wire is shorter than this critical length.

The good bond between martensite and ferrite in in-situ dual phase steel eliminates the end effect of the fibre. This effect is most severe when the reinforcement is shorter than its critical aspect ratio. The void initiated in the end of the martensite "ribbon/fibre" doesn't cause the in-situ dual phase steel to fracture at the end of the martensite because both the martensite "ribbon/fibre" and the void are micro-scale, which differs from the macro-scale of the wire and the void at the end of wire. This macro-scale void at the end

of wire causes the artificial dual phase steel to fracture at the end of wire (refer to section 5.3.6).

6.5 Summary

The oriented martensite dual phase steel is superior to the granular martensite dual phase steel because of the ferrite refinement and the high aspect ratio of the martensite. As-rolled dual phase steel with long martensite “fibres” has the lowest ductility and highest strength. The short martensite “fibre” dual phase steel has the best combination of strength and ductility.

Davies’s interpretation of Mileiko’s theory can describe the relationship between strength and volume fraction of martensite in dual phase steels when the martensite content is 30% or more, but can describe the steel-steel composite over the whole tested range of reinforcement. The scale and morphology of reinforcement does not affect the application of Mileiko’s theory as long as the parameters for the components are chosen properly. The deviation of the experiments with theory when the martensite volume fraction is less than 30% in in-situ dual phase steels due to internal stress and carbide.

Quenched wire shows interganular fracture, because of the micro-cracks formed during water-quenching. The micro-cracks propagate at lower applied stress due to the high residual stresses produced during quenching, which results in premature failure of martensitic wire and the martensitic wire composites, low strength and ductility are thus obtained. Bainite is the best phase for the wire in order to achieve a good combination of strength and ductility.

Long wire steel-steel composites can simulate the fracture and properties of as-rolled dual phase steel because in both cases the reinforcements are broken during tensile testing, but short wire composite can not simulate short martensite “fiber” dual phase steels.

Chapter 7 Conclusions

Manganese partitioning and mechanical properties of dual phase steels and the fabrication and mechanical properties of steel-steel composites have been studied in this thesis and the following conclusions have been drawn.

Manganese partitioning is affected by the temperature and isothermal holding time of annealing. The partitioning coefficient increases with decreasing annealing temperature for a long enough holding time, and increases to a limit with increasing isothermal holding time at a given temperature.

Decarburization occurs during annealing, which is serious for thin steel sheet. Decarburization reduces the volume fraction of austenite, and affects the manganese partitioning.

The analysis of the manganese redistribution in ferrite and austenite during annealing can be based on the following two processes:

(1) Manganese transports from ferrite to ferrite-austenite boundary and forms a manganese-rich rim in ferrite-austenite boundary, the manganese distribution in ferrite can be expressed as:

$$C_{Mn}^{\alpha} = C_{Mn}^{0} - \left(C_{Mn}^{0} - C_{Mn}^{\alpha 0}\right) \cdot \left(1 - erf\left(\frac{r - r_{\alpha}}{2\sqrt{D_{Mn}^{\alpha} t}}\right)\right) \quad \text{when } r_{\alpha} \le r \le R$$

(2) The manganese in the manganese-rich rim in the ferrite-austenite boundary diffuses into austenite until equilibration is reached and the manganese gradient in the austenite is eliminated. The following equation describes the manganese distribution in the austenite:

$$C_{Mn}^{\gamma} = C_{Mn}^{0} - \left(C_{Mn}^{0} - C_{Mn}^{\gamma 0}\right) \cdot \left(1 - erf\left(\frac{r_{\gamma} - r}{2\sqrt{D_{Mn}^{\gamma} t}}\right)\right) \quad \text{when } 0 \le r \le r_{\gamma}$$

The diffusion analysis for the above two processes combined with the mass balance and austenite grain growth can give the manganese distribution and partitioning coefficient

at any time during annealing. The predicted coefficient shows the same trend as the experimental data with isothermal holding time, but at slightly lower values, which may be the result of the manganese diffusion rate in these steels being higher than the literature value.

The rolling which is carried out either continuously, starting at the austenite+ferrite temperature, or quasi-isothermally in the two-phase region, can produce dual phase steels with elongated or “fibrous” martensite rather than granular martensite. Internal stresses exist in the as-rolled steels obtained by both continuous rolling and quasi-isothermal rolling and depend on finishing rolling temperature. The tensile properties of as-rolled (quasi-isothermal) steels are dependent on internal stresses and martensite volume fraction, both of which depend on isothermal holding temperature (ie the rolling temperature). The optimum properties of quasi-isothermally rolled steels can be obtained by annealing and rolling at their intercritical annealing temperature (at which ~30% martensite can be obtained). The strength [elongation] of continuously rolled steels is much higher [lower] than that of quasi-isothermally rolled steels because of its lower finishing rolling temperature (higher internal stresses can be obtained at lower finishing rolling temperature).

Post-rolling annealing (where the temperature is the same as that for pre-rolling annealing for the same steel) initially reduces the internal stresses and then the aspect ratio of the elongated martensite because of recrystallization; these two effects decrease strength and increase total elongation of post-rolling annealed steels.

Work-hardening behaviours for as-rolled steels and post-rolling annealed steels are quite different. The work-hardening behaviour of as-rolled steels shows two stages with different exponents; the higher exponent in the first stage is primarily controlled by dislocation distribution and the extra high dislocation density in ferrite caused by the rolling, and the lower one in the second stage is associated with the plastic deformation of both the ferrite and martensite. In contrast, the work-hardening behaviour of post-rolling annealed steels shows one stage with a single exponent, which means that the plastic deformation of martensite occurs simultaneously with that of the ferrite.

An attempt to make a high strength steel-steel composite with good ductility by introducing high strength steel wire into low carbon steel sheet was successful. The

performance of these steel-steel composites is dependent on the properties of the wire, matrix steel and the interfacial strength.

High strength of the eutectoid steel wire can be obtained when the phase composition of the wire is martensite or bainite, which can be secured by martempering and austempering respectively. The properties of the bainitic wire are superior to those of martensitic wire because of the high ductility of bainitic wire at equivalent strengths. Tensile properties of the transformed bainitic wire depend on its parent, ie. the as-rolled pearlitic wire; both strength and elongation of bainitic wire increase as these value increase for the pearlitic wire, but are superior to those of the pearlitic wire.

Tensile properties of both pearlitic and bainitic wire are effected by the rolling process parameters, especially by finishing rolling temperature. More dislocations and high internal stress can be generated by rolling at low temperature, which increase the tensile strength and reduce ductility.

The temperature of rolling and the time of isothermal holding before rolling determine the decarburization of wire, grain size of wire, and chemical reaction between wire and coating, all of which increase with increasing isothermal holding temperature and time. The strength of plain wire decreases and elongation increases with increasing isothermal holding temperature and time due to decarburization and grain growth; both the strength and elongation of copper-coated wire decrease a little with increasing isothermal holding temperature and time because of grain growth; and both the strength and elongation of nickel-coated wire decrease a little at low temperature and initial isothermal holding time, and decrease quickly at high temperature and longer holding time mainly due to chemical reaction between the nickel coating and iron.

The strength increases, and elongation decreases with increasing rolling reduction and decreasing rolling temperature for both as-rolled and austempered matrix steels.

Not only the properties of the wire but the interfacial strength between wire and matrix steel varies with rolling parameters.

The interfacial strength of steel-steel composites is comprehensively determined by the internal residual stress at the interface, work-hardening during rolling, the status of the steel-wire surface and diffusion during fabrication.

Residual stresses and dislocations are generated during inhomogeneous plastic deformation of wire and matrix during rolling because of the difference in flow stress between wire and matrix. The residual stresses and dislocation are concentrated at the interface and are affected by the finishing rolling temperature, isothermal holding time, starting rolling temperature and heat-treatment after fabrication of the composite.

The effects of residual stresses and dislocation hardening on the interfacial strength are decided by the level of residual stresses; the residual stresses and dislocations may increase the interfacial strength by work-hardening if the residual stresses are under the critical value and do not cause failure of the interface, but when over the interfacial shear strength the internal stresses will decrease the interfacial strength. In the latter situation, the interface bonding is broken by the extremely high residual stresses and heavy interfacial deformation. The effects of residual stresses and dislocations on interfacial strength can be eliminated by annealing.

In addition to residual stresses and work-hardening during rolling, carbon diffusion between wire and matrix plays an important role in strengthening of the interface. The carbon diffusion, determined by the coating on the wire, is a function of temperature and time of holding period before rolling and can be described by the carbon concentration gradient at the interface.

Carbon diffusion between plain wire and matrix increases with increasing temperature and time of isothermal holding which makes the interfacial strength increase with temperature and time.

Because a perfect copper coating on the wire can stop the diffusion of carbon from wire to matrix, the interfacial strength between copper-coated wire and matrix increases a little with both temperature and time by the solid diffusion between copper and iron and carbon diffusion from wire to matrix through defects in the copper coating.

Chemical reaction between wire and coating occurred in the nickel-coated wire. The reaction product, $FeNi_3$, can strengthen interface bonding and the interfacial strength increases very quickly with increasing temperature and time.

The austempering after fabrication of composite lowers the interfacial strength by: (1) relaxation of interface during reheating and isothermal holding; (2) phase transformation. The decreases of interfacial strengths in nickel and copper coated

composites by austempering are much more than that of uncoated wire composite; this suggests that the interfacial strength of copper-coated wire and nickel-coated wire are strongly controlled by residual stresses and work-hardening.

An analysis based on energy equilibrium theory for the work of fracture required to pull the wire out has been performed and under similar work-hardening and residual stress conditions, the interfacial strength is a function of the carbon concentration gradient at the interface as follows:

$$\tau^2 = B' + A' \left. \frac{dC_{carbon}}{dr} \right|_{r=r_0} \quad \text{for elastic deformation of interface;}$$

$$\tau^{n+1} = B'' + A'' \left. \frac{dC_{carbon}}{dr} \right|_{r=r_0} \quad \text{for elastic plus plastic deformation of interface.}$$

The modelling analysis agrees well with experimental data in both the elastic and plastic fracture processes.

Tensile properties of the artificial dual phase steel are strongly dependent on the heat-treatment after fabrication. Between austempering, martempering, water-quenching and normalizing, the austempering was chosen as the final treatment for the rolled steel-steel composites because the austempered composites have the best combination of strength and elongation, whereas the micro-cracks and high residual stresses formed during martensitic transformation cause premature failure of water-quenched wire. The optimum condition of austempering was: heat at 800°C for 2 min, quench into 260°C oil and hold isothermally in 260°C oil for 305min.

The tensile properties of the composites are functions of the properties of the components and the interfacial strength. Any factor which can influence the strength of wire and the interfacial strength (such as strain hardening during cold rolling, finishing rolling temperature, decarburization, rolling reduction) can also affect the strength of the composite. The tensile strength of composites increases nearly linearly with increasing strength of wire with good interfacial bonding.

High strength and elongation of composites can be obtained at strong interface bonding; the fracture process of composites with strong interfaces is crack formation in the matrix and propagation through the interface to the wire.

In the weak interfacial bonded composites reinforced with copper-coated wire, the crack is formed at the interface and propagates along the interface. The composites fracture without wire breakage and the reinforcing effect of the wire has not been taken advantage of, which makes the composites exhibit low strength and elongation.

The wire can be embrittled by intermetallic compounds formed at the interface, which gives low strength and elongation. In the case of nickel coated wire composite, the amount of intermetallic compound $FeNi_3$ at the interface increases with increasing temperature and holding time, so the tensile strength and elongation decrease with increasing temperature and holding time.

Tensile properties of matrix steels also affect tensile properties; high strength/low ductility matrix steel gives composites with high strength/low ductility.

The proposed CHCH (cold rolling-heating/quenching-cold rolling-hot rolling) approach was successful for fabricating the unidirectional short wire composites. The aspect ratio of these short wires is dependent on the second cold rolling and final hot rolling. The strength and total elongation of the CHCH short wire composite increase to limits (equal to those of a continuous wire composite) with increasing aspect ratio. The elongation of short wire composites is not superior to continuous composites at equivalent strength.

Compared to the CHCH approach, the CH (cold rolling plus hot rolling) method was not successful for making short wire composites because voids, formed at the end of the short wire, lowered the mechanical properties.

Davies's interpretation of Mileiko's theory can describe the relationship between strength and volume fraction of martensite in dual phase steels when the martensite content is 30% or more, but it can describe the steel-steel composite over the whole tested range of reinforcement. The scale and morphology of reinforcement does not affect the application of Davies's theory as long as the parameters for the components are chosen properly.

The long wire steel-steel composites can simulate the fracture and properties of as-rolled dual phase steels, but the short wire composites can not simulated post-rolling annealed dual phase steel because of the macro-scale of voids in the end of wire formed during testing.

Reference

(1) Erasmus, L. A. The Relationship between tensile strength and ductility of 3% manganese dual phase steels. In Proc. 33rd annual conf. Australasian institute of metals. 1980. P.33-40.

(2) Hayami, S. and Furukawa, T. In Microalloying 75' Conference Proceedings, Vol.1. New York, Union Carbide Corp, 1977. P.78.

(3) Davies, R. G. Deformation behavior of vanadium strengthened dual phase steels, Metall. Trans. 9A: 41-52, 1978.

(4) Speich, G. R. and Miller, R. L. Mechanical properties of ferrite-martensite steels. In Kot, R. A. and Morris, J. W. Structure and Properties of Dual Phase Steels. TMS-AIME, Warrendale PA, 1979. P.145-182.

(5) Shen Xianpu, The present condition and the prospect of dual phase steels, Journal of Mechanical Engineering Materials (Chinese edition), No.1: 1-5, 1988.

(6) Gladman, T. Dual-phase and other formable steels, Metals Technology 10: 274-281, 1983.

(7) Owen, W. S. Can a simple heat treatment help to save Detroit, Metals Technology 7: 1-13, 1980.

(8) Matsuoka, T. and Yamamori, K. Metallurgical aspects in cold rolled high strength steel sheet, Metall. Trans. 6A: 1613-1621, 1975.

(9) Rashid, M. S. Manufacture of automotive components from dual phase steel. In Dual Phase and Cold Pressing Vanadium Steels in The Automobile Industry-Proceedings of Seminar in Berlin, Oct. 1978, p.32-41.

(10) Davies, R. G. and Magee, G. L. High strength steel technology development at Ford. In Dual Phase and Cold Pressing Vanadium Steels in The Automobile Industry-Proceedings of Seminar in Berlin, Oct. 1978, p.25-30.

(11) Erasmus, L. A. Project report 928-475, Stelco R & D, Canada, July, 1979, p1-28.

(12) Speich, G. R., Demarest, V. A. and Miller, R. L. Formation of austenite during intercritical annealing dual phase steels, Metall. Trans. 12A: 1419-1428, 1981.

(13) Garcial, C. I. and Deardo, A. J. Formation of austenite in 1.5pct Mn steels, Metall. Trans. 12A: 521-530, 1981.

(14) Garcial, C. I. and Deardo, A. J. The formation of austenite in low alloy steels. In Kot, R. A. and Morris, J. W. Structure and Properties of Dual Phase Steels. TMS-AIME, Warrendale PA, 1979. P.40-61.

(15) Demeri, M. Y. The formability of dual phase steels, Metall. Trans. 12A: 1187-1196, 1981.

(16) Sakams, Y., Matlock, D. K. and Krauss, G. Intercritically annealed and isothermally transformed 0,15pct C steels containing 1.2 pct Si-1.5 pct Mn and 4 pct Ni, Part I Transformation, microstructure and room-temperature mechanical properties, Metall. Trans. 23A: 1221-1232, 1992.

(17) Okita, T. and others. Production and quality of hot rolled dual phase steel, Nippon Kokan Technical Report, Overseas No.43, 1985, P.25-32.

(18) Marder, A. R. and Bramfitt, B. L. Processing of a molybdenum-bearing dual-phase steel. In Kot, R. A. and Morris, J. W. Structure and Properties of Dual Phase Steels. TMS-AIME, Warrendale PA, 1979. P.242-259.

(19) Marder, A. R. The effect of heat treatment on the properties and structure of molybdenum and vanadium dual phase steels, Metall. Trans. 12A:,1569-1579, 1981.

(20) T. Tanaka, M. Nishida, K.Hashiguchi, and T. Kato, Formation and properties of ferrite plus martensite dual-phase structures. In Kot, R. A. and Morris, J. W. Structure and Properties of Dual Phase Steels. TMS-AIME, Warrendale PA, 1979. P.221-241.

(21) Nakagawa, A., Koo, J. Y. and Thomas, G. Effect of vanadium on structure-properties relations of dual phase Fe/Mn/Si/0.1C steels, Metall. Trans. 12A: 1965-1972, 1981.

(22) Shen, X. P. and Priestner, R. Effect of boron on the microstructure and tensile properties of dual-phase steel, Metall. Trans 21A: 2547-2553, 1990.

(23) Kim, N. J. and Thomas, G. Effect of morphology on the mechanical behavior of a dual phase Fe/2Si/0.1C steel, Metall. Trans. 12A: 483-489, 1981.

(24) Kim, N. J. and Nakagawa, A. H. Effective grain size of dual phase steel, Material Science and Engineering, 83:145-149, 1986.

(25) Cai, Xue-Ling, Garratt-reed, A. J. and Owen, W. S. The development of some dual phase steel structure from different starting microstructure, Metall. Trans. 16A: 543-557, 1985.

(26) Coates, D. E. Diffusion-controlled precipitate growth in ternary systems I, Metall. Trans. 3A: 1203-1212, 1972.

(27) E. Randich and J. I. Goldstein, Non-isothermal finite diffusion-controlled growth in ternary systems, Metall. Trans. 6A: 1553-1560, 1975.

(28) Van Der Ven, A. and Delaey, L. Model for precipitate growth during the $\gamma \rightarrow \alpha + \gamma$ transformation in Fe-C and Fe-C-M alloys, Progress in Materials Science 40: 181-246, 1986.

(29) Pussegoda, N., Tyson, W. R., Wycliffe, P. and Purdy, G. R. Segregation of manganese during intercritical annealing of dual phase steels, Metall. Trans. 15A: 1499-1520, 1984.

(30) Yang, D. Z., Brown, E. L., Matlock, D. K. and Krauss, G. The formation of austenite at low intercritical annealing temperature in a normalized 0.08C-1.45Mn-0.21Si steel, Metall. Trans. 16A: 1523-1526, 1985.

(31) Davies, R. G. Influence of silicon and phosphorous on the mechanical properties of both ferrite and dual phase steels, Metall. Trans. 10A: 113-118, 1979.

(32) Erasmus, L. A. and Ratnaraj, R. The partitioning of manganese & nitrogen in dual phase steels, Technical Report, University of Canterbury.

(33) Ratnaraj, R. Nitrogen in HSLA and dual phase steels Christchurch, University of Canterbury, 1989. 256p (Thesis: PhD: Mechanical Engineering).

(34) Laukois, J. V. and Wagoner, R. H. Plastic behavior of dual phase steel following plane-strain deformation, Metall. Trans. 16A: 421-425, 1985.

(35) Korzekwa, D. A., Matlock, D. K. and Krauss, G. Dislocation substructure as a function of strain in a dual phase steel, Metall. Trans. 15A: 1221-1228, 1984.

(36) D. K. Matlock, G. Krauss, L. F. Ramos, and G. S. Huppi, A correlation of processing variables with deformation behavior of dual-phase steels. In Kot, R. A. and Morris, J. W. Structure and Properties of Dual Phase Steels. TMS-AIME, Warrendale PA, 1979. P.62-90.

(37) Ballinger, N. K. and Gladman, T. Work hardening of dual-phase steels, Metal Science 15: 95-108, 1981.

(38) Chang, Peng-Heng Temper-aging of continuously annealed low carbon dual phase steel, Metall. Trans. 15A: 73-86, 1984.

(39) Dutta, V. B., Suresh, S. and Ritchie, R. O. Fatigue crack propagation in dual phase steels: effect of ferritic-martensite microstructure on crack path morphology, Metall. Trans. 15A: 1193-1207, 1984.

(40) Ramesh, R., Kim, N. J. and Thomas, G. Improvement in toughness of Fe-Cr-Mn-C steels by thermal-mechanical treatment, Metall. Trans. 21A: 683-695, 1990.

(41) Chang, Peng-Heng and Preban, A. G. The effect of ferrite grain size and martensite volume fraction on the tensile properties of dual phase steel, Acta. Metall. 33: 897-903, 1985.

(42) Cuddy, L. J. Grain refinement of Nb steels by control of recrystallization during hot rolling, Metall. Trans. 15A: 87-98, 1984.

(43) Pipak Kumar Mondal and Ranjit Kumar Ray, Development of {111} texture during cold rolling and recrystallization of C-Mn-V dual phase steel, Material Science and Engineering 158A: 147-156, 1992.

(44) Chang, Peng-Heng Effect of prior cold rolling and post temper rolling on the properties of continuously annealed low carbon dual phase steel, Metall. Trans. 15A: 671-678, 1984.

(45) Jingke Liu, Zhonghao Jiang, and Jianshe Lian, Influence of predeformation on microstructure and mechanical properties of 1020 dual phase steel, Material Science and Technology 7: 527-532, 1991.

(46) Yang, D. Z., Brown, E. L., Matlock, D. K. and Krauss, G. Ferrite recrystallization and austenite formation in cold-rolled intercritically annealed steel, Metall. Trans. 16A: 1385-1392, 1985.

(47) Lagnebory, R. Structure-properties relationships in dual phase steels. In Dual Phase and Cold Pressing Vanadium Steels in The Automobile Industry - Proceedings of Seminar in Berlin, Oct., 1978, p.43-51.

(48) Jena, A. K. and Chaturvedi, M. C. On the effect of the volume fraction of martensite on the tensile strength of dual phase steel, Materials Science and Engineering 100: 1-6, 1988.

(49) Davies, R. G. Influence of martensite composition and content on the properties of dual phase steels, Metall. Trans. 9A: 671-679, 1978.

(50) Mileiko, S. T. The tensile strength and ductility of continuous fibre composites, J. Mater. Sci. 4: 974-977, 1969.

(51) Davies, R. G. The mechanical properties of zero-carbon ferrite-plus-martensite structure, Metall. Trans. 9A 451-455, 1978.

(52) Jiang, Z., Lian, J. and Chen, J. Strain hardening behavior and its relationship to tensile mechanical properties of dual phase steel, Material Sciences and Technology 8: 1075-1081, 1992.

(53) Laukonis, J. V. and Wagoner, R. H. Plastic behavior of dual phase steel following plane-strain deformation, Metall. Trans. 16A: 421-425, 1985.

(54) Y. Sakams, D. K. Matlock, and G. Krauss, Intercritically annealed and isothermally transformed 0,15pct C steels containing 1.2 pct Si-1.5 pct Mn and 4 pct Ni, Part II, Effect of testing temperature on stress-strain behavior and deformation-induced austenite transformation, Metall. Trans. 23A: 1233-1241, 1992.

(55) Tomita, Y. and Okabayashi, K. Tensile stress-strain anylysis of cold worked metals and dual phase steels, Metall. Trans. 16A: 865-872, 1985.

(56) Jiang, Z., Guan, A. and Lian, J. The relationship between ductility and material parameters for dual phase steel, J. Mater. Sci. 28: 1814-1818, 1993.

(57) Ramos, L. F., Matlock, D. K. and Krauss, G. On the deformation behavior of dual-phase steels, Metall. Trans. 10A: 159-261, 1979.

(58) Grujicic, M., Erturk, T. and Owen, W. S. A finite element analysis of the accommodation strains in the ferrite phase on the work hardening of a dual-phase steel, Materials Science and Engineering 82: 151-159, 1986.

(59) Nagorka, M. S., Krauss, G. and Matlock, D. K. The Effect of microstructure and strain rate on the stage III strain hardening and ductility of dual-phase steels, Materials Science and Engineering 94: 183-193, 1987.

(60) Su, Y. L., Gurland, J. Strain partitioning, uniform elongation and fracture strain in dual-phase steels, Materials Science and Engineering 95: 151-165, 1987.

(61) Lian, J., Jiang, Z. and Liu, J. Theoretical model for the tensile work hardening behavior of dual-phase steel, Materials Science and Engineering 147A: 55-65, 1991.

(62) Sarwar, M. and Priestner, R. Influence of ferrite-martensite microstructure morphology on tensile strength of dual-phase steel, J. Mater. Sci. 31: 2091-2095, 1996.

(63) Nakagawa, A. H. and Thomas, G. Microstructure-mechanical properties relationship of dual-phase steel wire, Metall., Trans. 16A: 831-840, 1985.

(64) Li, Chengji, Sheng, Huasen, Dou, Guangju and Cao, Fengyu Investigation of Non-patenting process for cold drawing dual phase steel wires, Jin Shu Re Chu Li (Heat-Treatment of Metals, in Chinese) No.1: 19-23, 1992.

(65) Donald, I. W. and Metcalfe, B. L. The preparation, properties and applications of some glass-coated metal filaments prepared by the Tylor-wire process, J. Mater. Sci. 31: 1139-1149, 1996.

(66) Gilbert, S. M. and Gillam, E. Deformation of cold-rolled wire-reinforced copper composites, Composites 14: 41-51, 1983.

(67) Moore, J. T., Wilson, D. V. and Roberts, W. T. Fabrication of formable metal-metal composites, Materials Science and Engineering 48: 113-121, 1981.

(68) Moore, J. T., Wilson, D. V. and Roberts, W. T. Evaluation of formable light metal-alloy steel composites, Materials Science and Engineering 48: 123-136, 1981.

(69) Dragone, T. L., Schlautmann, J. J. and Nix, W. D. Processing and creep characterization of a model metal matrix composites: lead reinforced with nickel fibers, Metall. Trans. 22A: 1029-1036, 1991.

(70) Toribio, J. and Lancha, A. M. Effect of cold drawing on environmentally assisted cracking of cold-drawn steel, J. Mater. Sci. 31: 6015-6024, 1996.

(71) Evans, A. G. and Marshall, B. The mechanical behavior of ceramic matrix composites, Acat Metall. 37: 2567-2583, 1989.

(72) Hsueh, Chun-Hway Crack-wake interfacial debonding criteria for fiber-reinforced ceramic composites, Acta Mater. 44: 2211-2216, 1996.

(73) Zhang, G. D. and Chen, R. Effect of the interfacial bonding strength on the mechanical properties of metal matrix composites, Composite Interfaces 1: 337-355, 1993.

(74) Guo, Z. X. and Derby, B. Solid-state fabrication and interfaces of fibre reinforced metal matrix composites, Progress in Material Science 39: 411-495, 1995.

(75) Rajesh, G., Sinharoy, A. and Bhagat, R. B. A fracture mechanics based numerical analysis for predicting optimum interface properties in a metal matrix composites, Composites Engineering 5(6): 583-596, 1995.

(76) Ibrahim, I. A., Mohamed, F. A. and Lavernia, E. J. Particulate reinforced metal matrix composites-a review, J. Mater. Sci. 26: 1137-1156, 1991.

(77) Gupta, M., Ibrahim, I. A., Mohamed, F. A. and Lavernia, E. J. Wetting and interfacial reactions in Al-Li-SiCp metal matrix composites processed by spray atomization and deposition, J. Mater. Sci. 26: 6673-6684, 1991.

(78) Laurent, V., Chatain, D. and Eustathopoulos, N. Wetatability of SiC by aluminium and Al-SiC alloys, J. Mater. Sci. 22: 244-250, 1987.

(79) Warren, R. and Andersson, C-H. Silicon carbide fibres and their potential for use in composite materials, part II, Composites 15: 101-111, 1984.

(80) Johnson, R. E. Conflict between Gibbsian thermodynamics and recent treatments of interfacial energies in solid-liquid-vapor systems, J. Phys. Chem. 63: 1655-1658, 1959.

(81) Vennet, R. M., Wolf, S. M. and Levett, A. P. Multiply necking of tungsten fibers in a brass-tungsten composite, Metall. Trans. 1: 1569-1575, 1970.

(82) Schoene, C. and Scala, E. Multiply necking phenomena in metal composites, Metall. Trans. 1: 3466-3469, 1970.

(83) Sun, S. J. and Zhang, M. D. Interface characteristics and mechanical properties of carbon fibre reinforced copper composites, J. Mater. Sci. 26: 5762-5766, 1991.

(84) Wang, C. Fracture mechanics of single-fibre pull-out test, J. Mater. Sci. 32: 483-490, 1997.

(85) DiFrancia, C., Ward, T. C. and Claus, R. O. The single-fibre pull-out test. 1: Review and interpretation, Composites 27A: 597-612, 1996.

(86) Geng, Y. and Leung, C. Y. A microstructure study of fibre/mortar interfaces during fibre debonding and pull-out, J. Mater. Sci. 31: 1285-1294, 1996.

(87) Lawrence, P. Some theoretical considerations of fibre pullout from elastic matrix, J. Mater. Sci. 7: 1-6, 1972.

(88) Chua, P. S. and Piggott, M. R. The Glass fibre-polymer interface: I. Theoretical considerations for single fibre pullout test, Comp. Sci. & Tech. 22: 33-42, 1985.

(89) Zhou, L.-M., Mai, Y.-W., Ye, L. and Kim, J.-K. Techniques for evaluating interfacial properties of fibre-matrix composites. In Newaz, G. M., Neber-Aeschbacher, H. and Wöhlbier, F. H. Metal Matrix Composites Trans. Tech. Publications Ltd, 1995. P.549-600.

(90) Singh, R. N. and Sutcu, M. Determination of Fibre-matrix interfacial properties in ceramic matrix composites by a fibre push-out test, J. Mater. Sci. 26: 2547-2556, 1991.

(91) Eldridge, J. I. and Brindley, P. K. Investigation of interfacial shear strength in a SiC fibre/Ti-24Al-11Nb composite by a fibre push-out technique, J. Mater. Sci. letts. 8: 1451-1454, 1989.

(92) Honda, K. and Kagawa, Y. Debonding criterion in the pushout process of fibre-reinforced ceramics, Acta Mater. 44: 3267-3277, 1996.

(93) Clyne, T. W. and Withers, P. J. An introduction to metal matrix composites. Cambridge University Press, 1993.

(94) Ochiai, S. Strength of unnotched composites. In Ochiai, S. Mechanical Properties if Metallic Composites. Marcel Dekker, Inc., 1994. P.473-510.

(95) H. Lilholt, Strengthening and its mechanisms. In Ochiai, S. Mechanical Properties if Metallic Composites. Marcel Dekker, Inc., 1994. P.389-471.

(96) Shaw, L. L. and Miracle, D. B. Effect of an interfacial region on the transverse behavior of metal-matrix composites-a finite element analysis, Acta Mater. 44: 2043-2055, 1996.

(97) Weber, C. H., Chen, X., Connell, S. J. and Zok, F. W. On the tensile properties of a fiber reinforced titanium matrix composite - I unnotched behaviour, Acta Metall. Mater. 42: 3443-3450, 1994.

(98) Cox, B. N., James, M. R., Marshall, D. B. and Addison, R. C. Jr., Determination of residual stresses in thin sheet titanium aluminide composites, Metall. Trans. 21A: 2701-2707, 1990.

(99) Wang, Z. G., Li, S. and Sun, L. Fatigue and fracture behavior of discontinuously reinforced aluminum matrix composites. In Newaz, G. M., Neber-Aeschbacher, H. and Wöhlbier, F. H. Metal Matrix Composites. Trans. Tech. Publications Ltd, 1995. P.729-748.

(100) Wilson, D. V. and Bate, P. S. Internal elastic strains in an IF steel following changes in strain path, Acta Mater. 44: 3371-3383, 1996.

(101) Tsai, S. D., Mahulikar, D., Marcus, H. L., Noyan, I. C. and Cohen, J. B. Residual stress measurements on Al-graphite composites using X-ray diffraction, Materials Science and Engineering 47: 145-149, 1981.

(102) Ledbetter, H. M. and Austin, M. W. Internal strain (stress) in an SiCp-Al reinforced composites: an X-ray diffraction study, Materials Science and Engineering 89: 53-61, 1987.

(103) Saigal, A., Kupperman, D. S. and Majumdar, S. Residual strains in titanium matrix high-temperature composites, Materials Science and Engineering 105A: 59-65, 1992.

(104) Majumdar, S., Singh, J. P., Kupperman, D. and Krawitz, A. D. Application of neutron diffraction to measure residual strains in various engineering composite materials, J. Eng. Mat. & Tech. 113: 51-59, 1991.

(105) Allen, A. J., Bourke, M., Dawes, S., Hutchings, M. T. and Withers, P. J. The analysis of internal strains measured by neutron diffraction in Al/SiC MMCs, Acta Metall. Et Mater. 40: 2361-2373, 1992.

(106) Ramamurty, U., Dary, F.-C. and Zok, F. W. A method for measuring residual strains in fibre-reinforced titanium matrix composites, Acta Mater. 44: 3397-3406, 1996.

(107) Kelly, A. and Nicholson, R. B. Precipitation hardening, Progress in Materials Science 10:, 149-391, 1969.

(108) Wang, S. R. and Tseng, A. A. Macro- and micro-modeling of hot rolling of steel coupled by a micro-constitutive relationship, Mater. & Des. 16 (6): 315-336, 1995.

(109) Melloy, G. F. and Dennision, J. D. Continuum rolling- a unique thermomechanical treatment for plain-carbon and low alloy steels, In The Microstructure and Design of Alloy, Vol.1. Institute of metal and iron and steel institute, Cambridge, 1973. P.60-64

(110) Tanaka, T. Controlled rolling of steel plate and strip, International Metals Reviews No.4: 185-212, 1981.

(111) Ginzburg, Vladimir B. Steel-Rolling Technology, Theory and Practice. Macel Bekker, Inc., 1989.

(112) Kalpakjian, S. Manufacturing Processes for Engineering Materials. 1984. P.344.

(113) Diffusion welding and brazing. In O'Brien, R. L. Welding Handbook, Vo1.2, Welding Processes. American Welding Society, 1991. P.814-837

(114) Chou, T. W., Kelly, A. and Okura, A. Fibre-reinforced metal-matrix composites, Composites 16: 187-206, 1985.

(115) Moore, J. T., Wilson, D. V. and Roberts, W. T. Formability limits of metal-metal composites on rolling in the direction of fiber alignment, Materials Science and Engineering 48: 107-112, 1981.

(116) Shota, I. and Watanable, O. The strength of carbon fibre-reinforced nickel composites produced by electro-deposition and hot-pressing, J. Mater. Sci. 14: 699-704, 1979.

(117) Chang, M. and Scala, E. Plastic deformation processing compressive failure mechanism in Al composite materials. In Composite Materials: Testing and Design. ASTM STP 546, p.561-579.

(118) Linnert, G. E. Welding Metallurgy, Carbon and Alloy Steels, Vol. 1, Fundamentals. American Welding Society, 1965.

(119) Abrahamson, G. R. Permanent periodic surface deformation due to a travelling jet, J. Appl. Mech. 519-528, 1961.

(120) Öberg, Å., Mårtensson, N. and Schweitz, J-Å. Fundamental aspects of formation and stability of explosive weld, Metall. Trans. 16A: 841-852, 1985.

(121) Kowalick, J. F. and Hay, D. R. A mechanism of explosive bonding, Metall. Trans. 2: 1953-1958, 1971.

(122) Jarvis, C. V. and Slate, P. M. B. Explosive fabrication of composite materials, Nature 220: 782-783, 1968.

(123) Fleck, J., Laber, D. and Leonard, L. Explosive welding of composite materials, J. Composite Materials 3: 699-701, 1969.

(124) Bhalla, A. K., Williams, J. D. Production of stainless steel wire-reinforced aluminum alloy sheet by explosive compaction, J. Mater. Sci. 12: 523-530, 1977.

(125) Chadwick, M. D. and Jackson, P. W. Explosive welding in planar geometries. In Blazynski, T. Z. Explosive Welding, Forming and Compaction. Applied Science Publisher Ltd., 1983. P.219-287.

(126) Reed-Hill, R. E. Physical Metallurgy Principles. D. Van Nostrand Company, 1973. P.688.

(127) Andrews, K. W. The calculation of transformation temperatures and austenite-ferrite equibria in steels, J. Iron & Steel Inst. 184: 414-427, 1956.

(128) Deb, P. and Chaturvedi, M. C. Influence of thermomechanical treatment on the structure-properties relationship of microalloyed dual-phase high strength low alloy steel, Materials Science and Engineering 78: L7-L13, 1986.

(129) Karlsson, B. and Sundstrom, B. O. Inhomogeneity in plastic deformation of two-phase steels, Materials Science and Engineering 16: 161-168, 1974.

(130) Szewczyk, A. F. and Gurland, J. A study of the deformation and fracture of dual-phase steel, Metall. Trans. 13A: 1821-1826, 1982.

(131) Reed-Hill, R. E. Physical Metallurgy Principles. D. Van Nostrand Company, 1973. P.309.

(132) Courtney, T. H. Mechanical Behavior of Materials. McGraw-Hill Publishing Company, 1990. P.204.

(133) Heat treating, ASM Metals Handbook, Vol.4. ASM, Metals Park, OH, 1991. P.78.

(134) Sinha, A. K. Ferrous Physical Metallurgy. Butterworths, 1989.

(135) Ochiai, S. and Murakami, Y. Theoretical prediction of tensile strength of fibers as a function of thickness of brittle zone on fiber surfaces, Metall. Trans. 12A: 1155-1161, 1981.

(136) Ochiai, S. and Murakami, Y. Tensile strength of composites with brittle reaction zone at interfaces, J. Mater. Sci. 14: 831-840, 1979.

(137) Withers, P. J., Stobbs, W. M. and Pedersen, O. B. The application of the Eshelby method of internal stress determination to short fibre metal matrix composites, Acta Metall. 37: 3061-3084, 1989.

(138) Reed-Hill, R. E. Physical Metallurgy Principles. D. Van Nostrand Company, 1973. P.550.

(139) Brandes, E. A. and Brook, G. B. Smithell Metals Reference Book. Seventh ed. Butterworth-Heinemaan Ltd., 1992.

(140) Lynch, C. T. CRC Handbook of Materials Science. CRC Press, 1975.

(141) Smith, W. F. Foundations of Materials Science and Engineering. McGraw-Hill Inc., 1993.

(142) Cahn, J. W. and Hilliary, J. E. Free energy of a nonuniform system. I. Interfacial free energy, J. Chem. Phys. 28: 258-267, 1958.

(143) Lee, Y. W. and Aaronson, H. I. Anisotropy of coherent interphase boundary energy, Acta Metall. 28: 539-548, 1980.

(144) Ramanujan, R. V., Lee, J. K., Le Goues, F. K. and Aaronson, H. I. A Discrete lattice plane analysis of the energy of coherent $\{0001\}_{h.c.p.} // \{111\}_{f.c.c.}$, $\langle 11\bar{2}0\rangle_{h.c.p.} // \langle 1\bar{1}0\rangle_{f.c.c.}$ interfaces, Acta Metall 37: 3051-3059, 1989.

(145) Ankem, S. and Margolin, H. A rationalization of stress-strain behavior of two-ductile phase alloys, Metall. Trans. 17A: 2209-2226, 1986.

(146) Cribb, W. R. and Rigsbee, J. M. Work-hardening behavior and its relationship to the microstructure and mechanical properties of dual-phase steels. In Kot, R. A. and Morris, J. W. Structure and Properties of Dual Phase Steels. TMS-AIME, Warrendale PA, 1979. P.91-117.

(147) Reed-Hill, R. E. Physical Metallurgy Principles. D. Van Nostrand Company, 1973. P.759-760.

Appendix A*

The Microstructure and Mechanical Properties of As-Rolled Dual Phase Steel

Part I: Manganese Partitioning and Microstructure

Sun Shoujin* Martin Pugh* and Les Erasmus*
*Department of Mechanical Engineering, University of Canterbury, New Zealand

Abstract

A systematic study on the influence of pre-annealing and post-annealing heat-treatments on the microstructure and the manganese partitioning between martensite and ferrite phases of dual phase steel has been made. The partitioning coefficient decreases with increasing annealing temperature and increases with annealing time until reaching the final equilibrium value.

Key Words: as-rolled dual phase steel, pre-annealing, post-annealing, hot-rolling, microstructure, partitioning.

1. Introduction

Dual phase steel, which is essentially a composite material comprising hard martensitic islands reinforcing a ductile ferrite matrix, has a high tensile strength combined with good ductility (shown in figure 1). Its large commercial potential, based on these properties, has resulted in considerable research efforts around the world[1,2,3].

The desirable microstructure of dual phase steel is generally achieved by heating the low carbon steel between the AC_1 and the AC_3 temperatures, i.e., in the $\alpha + \gamma$ region of the Fe-Fe_3C equilibrium diagram, followed by air-cooling or water- quenching according to the chemical composition of the steel, to transform the austenite to martensite[4].

Another method to produce "ferrite plus martensite" steel is to hot-roll the steel in the austenitic region: the ferrite will form during the cooling period between hot rolling and coiling while the austenite transforms to martensite during coiling. In this case

* Published in IPENZ'96 conference, Feb. 1996, Dunedin.

however, *CCT* curves, which are dependent on the chemical composition of steel[5], must be closely followed.

The partitioning of manganese during intercritical annealing will increase the manganese content and lower the carbon content in the austenite, although it must be remembered that the partitioning of carbon during heat-treatment results in the carbon content of the austenite (max 2%) being higher than that in the ferrite (max 0.02%).The high manganese content and relatively high carbon content of the austenite will suppress the martensite transformation temperature, increase the strength and hardness of the martensite phase and prevent the formation of carbides. The shape and preferred orientation of the martensite phase is determined by the thermo-mechanical treatment[6] and the following post-annealing treatment.

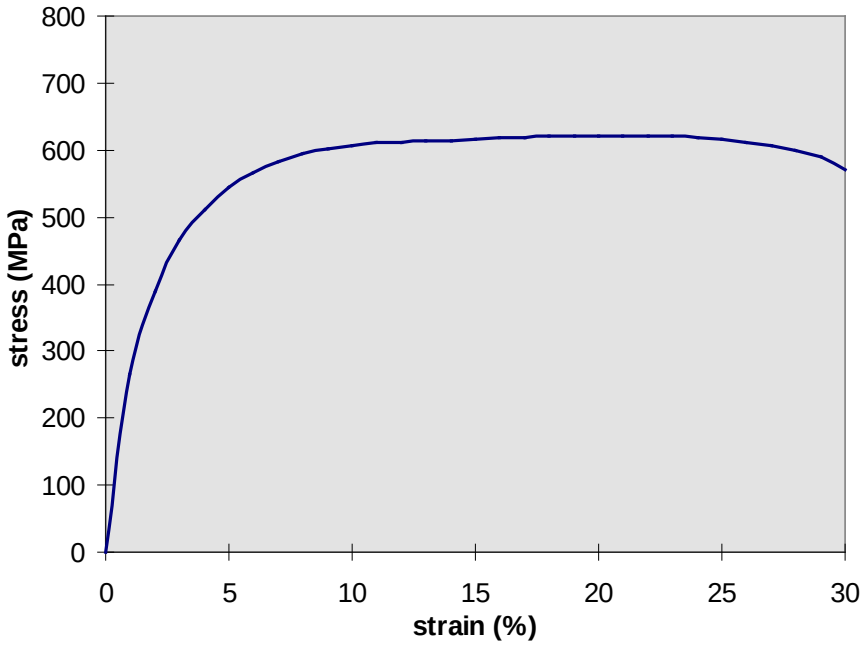

Fig.1 Typical stress-strain curve of dual phase steel

Although dual phase steels have been studied for over two decades, the previous work has concentrated on its formability, microstructure, properties and the influence of alloying elements and pre-deformation on the formation and properties of dual phase steel[7,8]. Temper-aging[9] and grain refinement by controlled rolling[6,10] have also been investigated. However, a systematic study of the effect of distribution and shape of the martensite phase on the mechanical properties of dual phase steel has not been made.

The purpose of the current research was to obtain fibrous martensite of a preferred orientation in the microstructure of dual phase steel and ascertain whether this material has a superior reinforcing effect compared to other martensite distributions and morphologies.

2. Materials and Experimental Procedure.

2.1 Experimental materials.

The steel used in this experiment was in the form of 40x40 mm^2 billets and in the as-forged condition. Its chemical composition is given in Table 1.

Table 1 Chemical Composition of Experimental Steels

C	Mn	Si	S	P	Al	Ni	Cr	Mo	Cu	Sn	V	Ti
0.11	2.67	0.020	0.015	0.016	0.003	0.046	0.046	0.013	0.034	0.003	0.008	0.003

2.2 Heat-treatment and Rolling

The heat-treatment for the forged steel before rolling is hereafter referred to as pre-annealing; the temperature of this treatment determines the volume fraction of martensite in the steel (20-30%). The optimum pre-annealing temperature for samples was found to be 680°C. In order to obtain high partitioning of carbon and manganese in the martensite and ferrite, the steels were heated at these temperatures for 48 hours and 96 hours under a flowing argon atmosphere in order to avoid oxidation. Immediately after this heat treatment, the steels were hot-rolled, the final thickness of the rolled plate being approximately 2.0 mm.

The effect of post-roll-annealing on the microstructure was determined by annealing steel at the following temperature, 670, 680 and 690°C and for various times(1,4 and 48 hours).

2.3. Metallography

Scanning Electron Microscopy (SEM) was used to observe the microstructure of the steel after polishing and etching. Elemental analysis in the martensite and ferrite was determined with an energy dispersive X-ray analyzer attached to the SEM. The volume fraction of martensite was measured using the point-counting method on selected micrographs.

Figure 2 shows the experimental process and the phase compositions in individual stage.

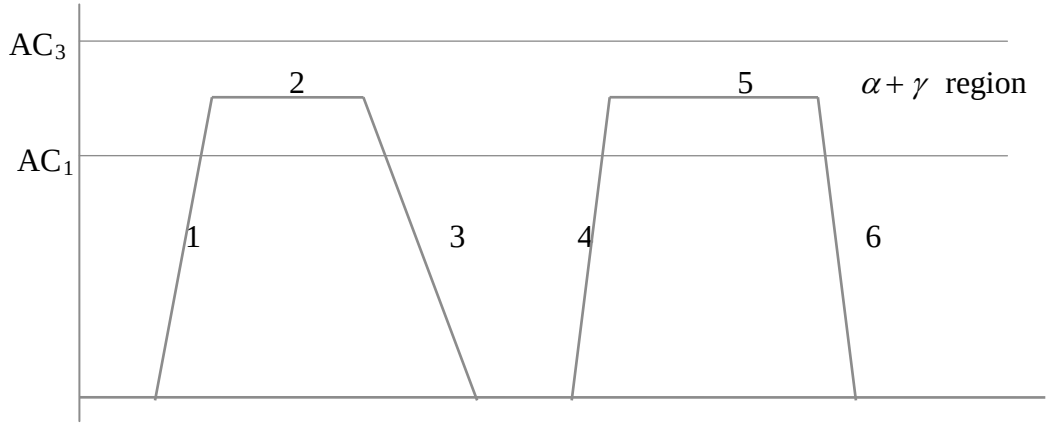

Fig.2 Schematically illustration of experimental process
1 and 4: heating, 2:pre-annealing, 3:rolling and air cooling,
5:post-annealing, 6:water quenching.

3. Results and Discussion

Figure 3 shows the typical microstructure (SEM) developed in a sample after heat-treatment for 48 hrs at 680°C. The influence of pre-annealing temperature on the volume fraction of martensite and the extent of manganese partitioning in the martensite and ferrite are shown in Figures 4 and 5 respectively. It can be clearly seen that the volume fraction of martensite increases with higher heat-treatment temperatures and the degree of manganese partitioning reaches a maximum at 680°C. In order to obtain approximately 30% martensite and a high degree of manganese partitioning in the martensite, 680°C was chosen as the final heat-treatment temperature for the steel.

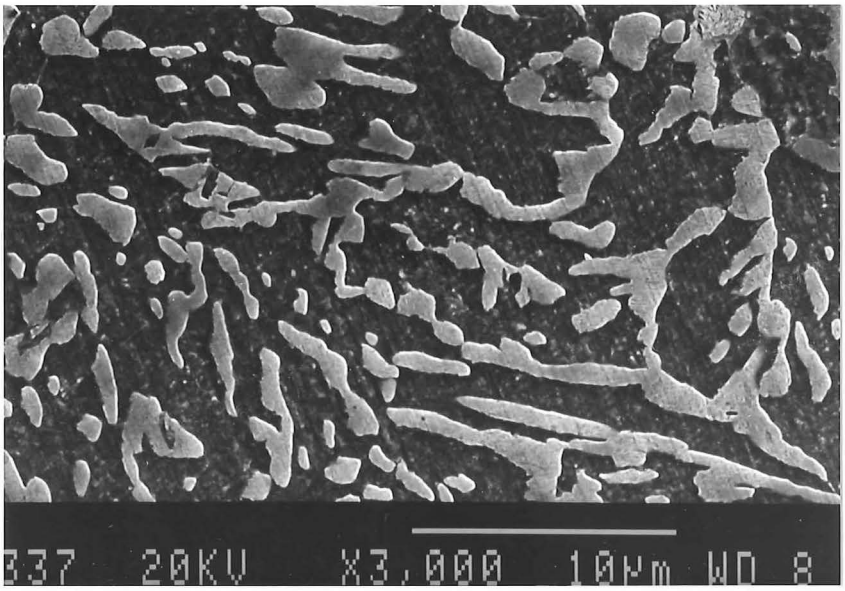

Fig.3 SEM Photos of steel after pre-annealing at 680°C
(the white islands are martensite, the dark matrices are ferrite)

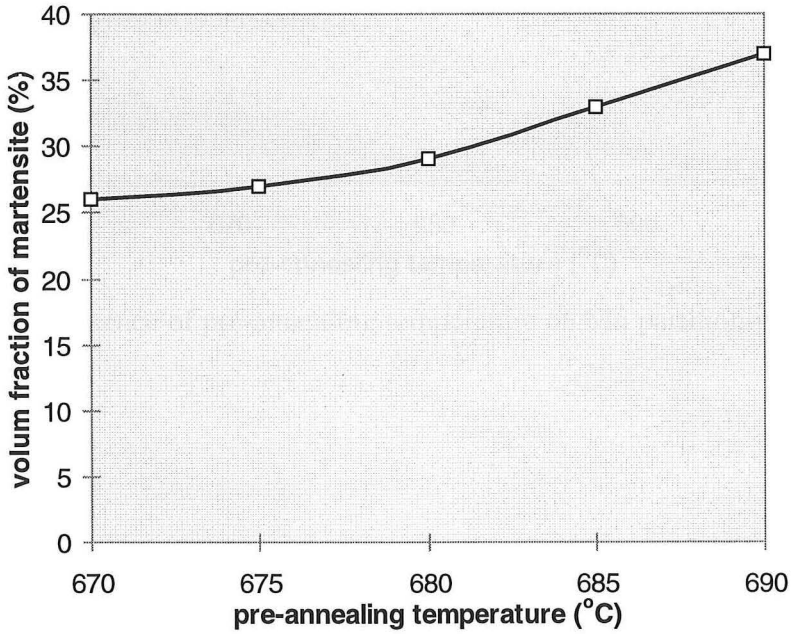

Fig.4 The influence of pre-annealing temperature on the martensite content(48 hrs)

Fig.4 The influence of pre-annealing temperature on the martensite content(48 hrs)

The influence of pre-annealing time on the above factors is shown in Figures 6 and 7; the partitioning coefficient, which is defined as the ratio of average manganese content in martensite grains to that in the adjacent ferrite matrix, and the resulting volume fraction of martensite both increase with intercritical annealing time. This effect diminishes at longer pre-annealing times and finally, the growth of austenite into the ferrite and the volume fraction of the martensite phases will both reach the equilibrium values.

During heat-treatment, the manganese will redistribute in the austenite and ferrite because of the difference in heats of solution of manganese in these phases (ΔH). according to Andrews[11], the final equilibrium value of the partitioning coefficient is:

$$\frac{C_{Mn}^{\gamma}}{C_{Mn}^{\alpha}} = \exp(-\frac{\Delta H}{R \cdot T}) \qquad (1)$$

The partitioning coefficient will increase with annealing time and eventually reach the equilibrium level, the value of which will decrease with increasing annealing temperature.

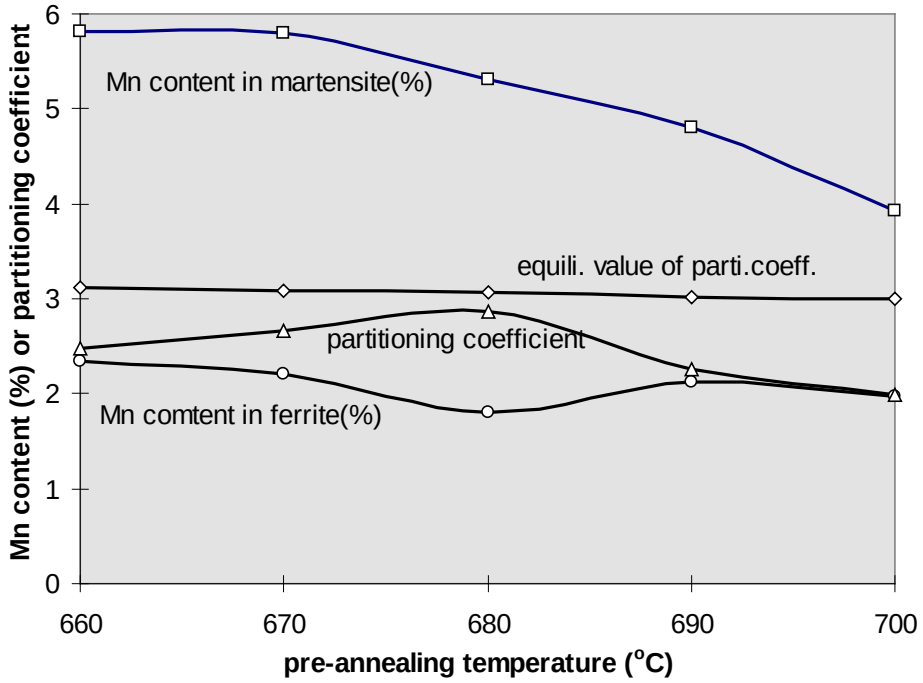

Fig.5 The influence of pre-annealing temperature on Mn partitioning (48 hrs)

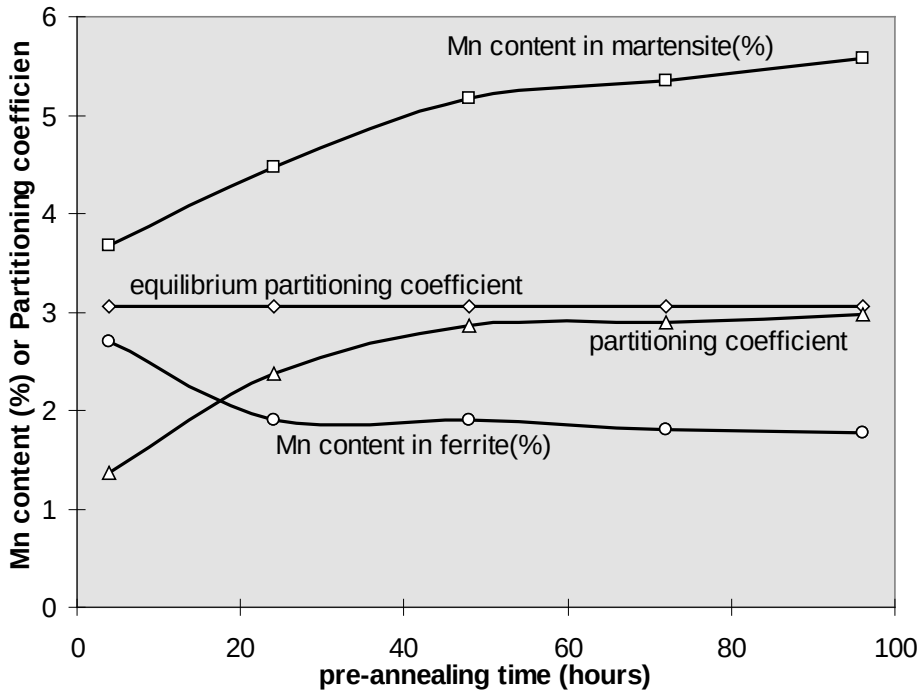

Fig.6 The effect of pre-annealing time on Mn partitioning in steel (at 680°C)

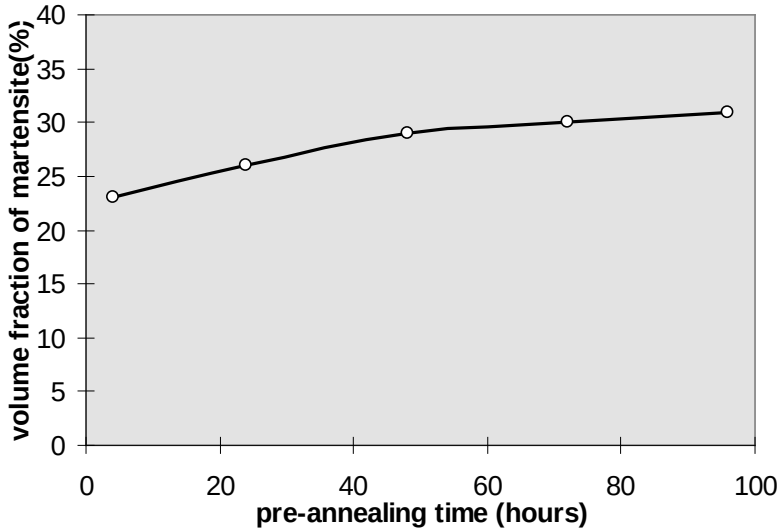

Fig.7 The influence of pre-annealing time on the martensite content (680°C)

3.2 Hot rolling

The hot rolling involves mechanical processing in the $\alpha + \gamma$ region, which changes the morphology of both ferrite and austenite (which will transform to martensite after cooling), the rolling process is illustrated in Figure 8. Thermomechanical treatment has little effect on the volume fraction of martensite and the manganese partitioning at any given temperature.

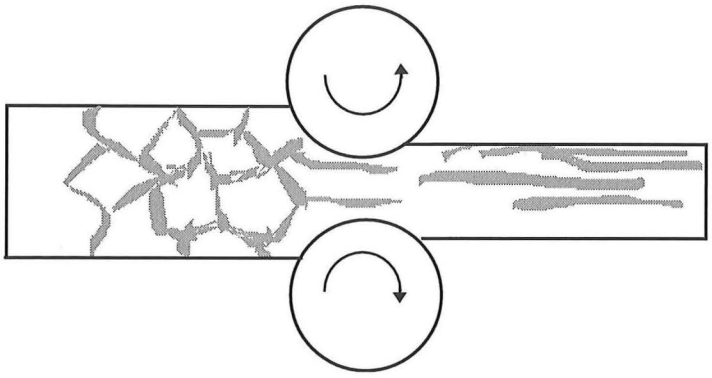

Fig.8 Schematically illustration of microstructure of dual phase steel due to hot rolling (the white is ferrite matrix, and the dark austenite)

During hot rolling, the austenite grain islands are flattened and elongated. In addition, with rolling, the temperature of the sample decreases into the alpha-region, which will produce a desirable combination of increased strength and toughness in extra-low-carbon steel because of:
(1) grain refinement of both gamma and alpha structure by repeated heavy deformation,
(2) dynamic recovery that produces a fine polygonal substructure, and
(3) cube-on-corner crystallographic texturing that results from the deformation process.

Manganese also exists in the steel in the form of manganese sulphide inclusion which can produce cracks after hot-rolling as shown in Figure 9, these cracks will, of course, be detrimental to the tensile properties of the steel.

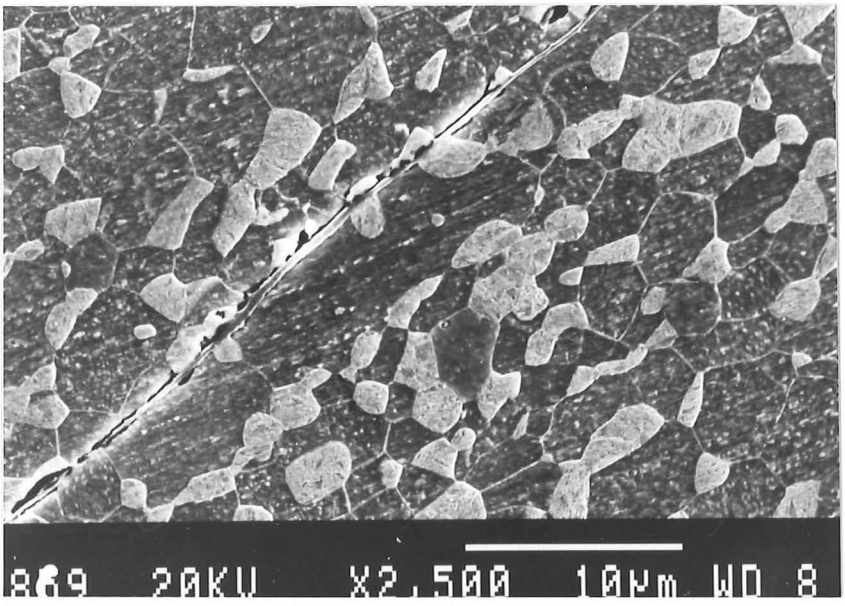

Fig.9 Crack formed by manganese sulphide during hot-rolling

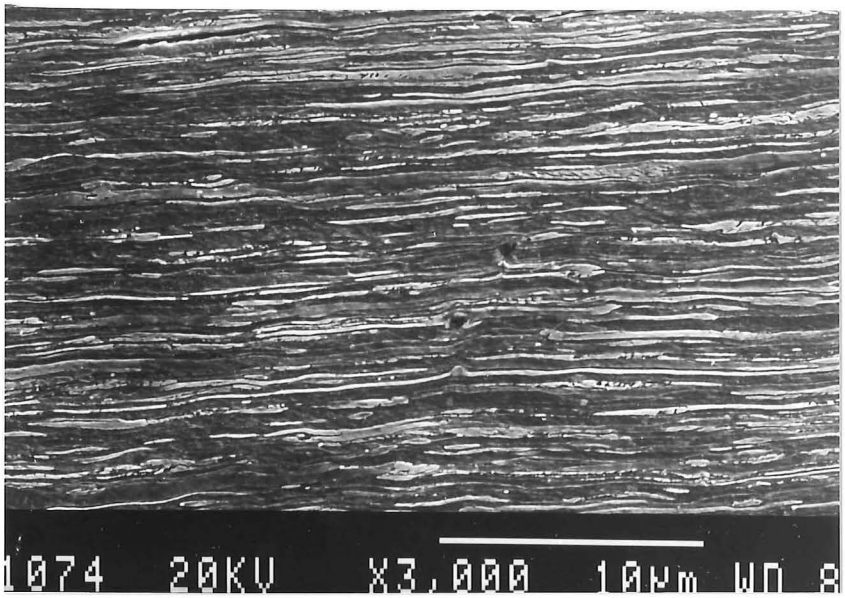

(a) parallel to rolling direction

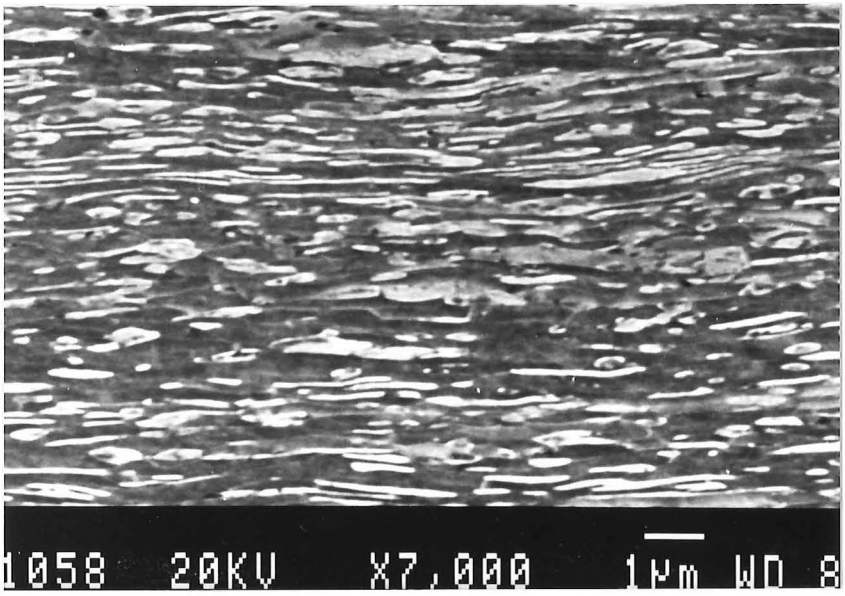

(b) perpendicular to rolling direction

Fig.10 The microstructure of steel after pre-annealing and rolling

The final microstructures both parallel and vertical to the rolling direction for steels after pre-annealing for 48 hours and rolling at 680°C are shown in Figure 10. The martensite phase exists in the form of fibres and ribbons instead of islands, as in normally the case, the higher aspect ratio of martensite phase leads to a reinforcing effect (in the fibre/rolling direction) as would be expected from composite theory.

3.3 The effect of post-annealing

Post-annealing effects the microstructure of the as-rolled dual phase steel. After post-annealing, the release of the high energy imported by the rolling tends to shorten the long fibrous martensite with a resultant decrease in aspect ratio, as would be expected, the more equiaxed structure being more thermodynamically stable under these conditions. This change in morphology with post-annealing time is shown in Figure 11(a, b, c and d).

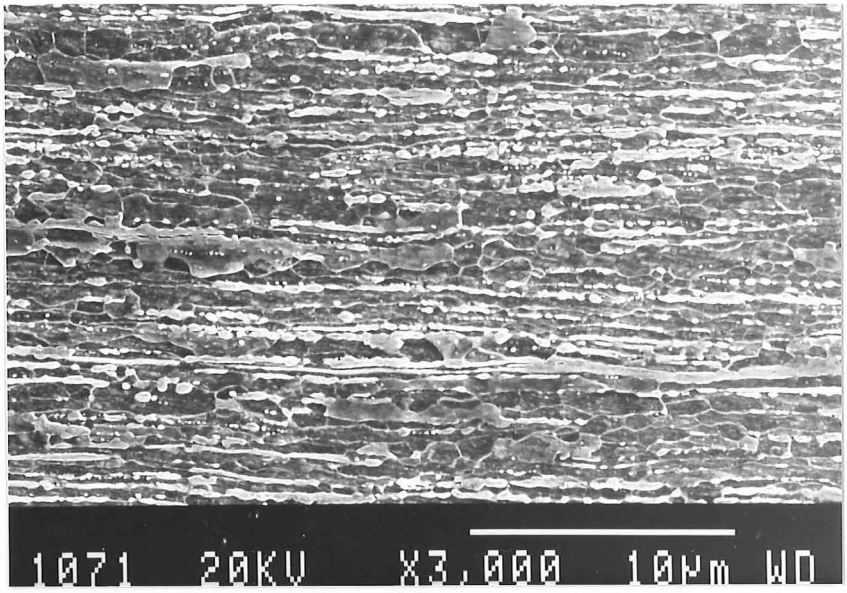
1071 20KV X3,000 10µm WD

(a)

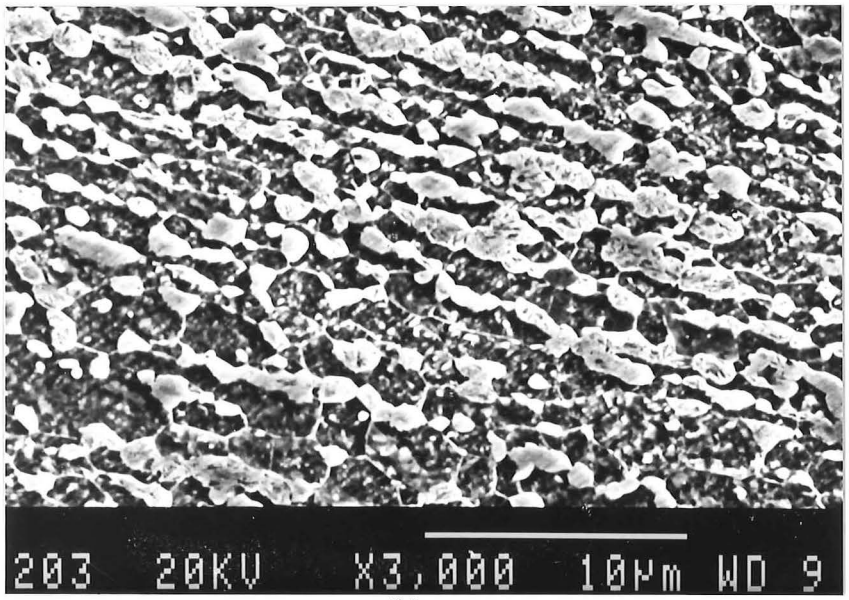
203 20KV X3,000 10µm WD 9

(b)

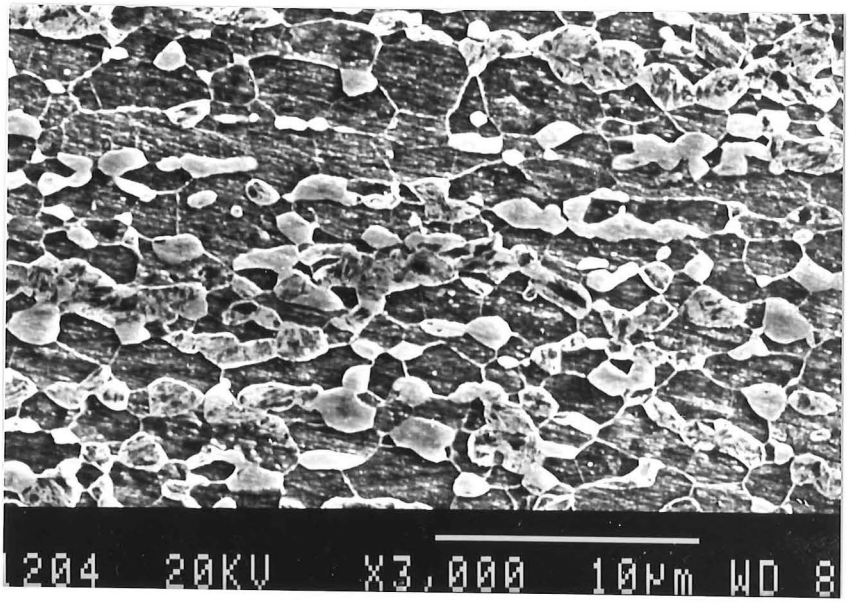
204 20KV X3,000 10µm WD 8

(c)

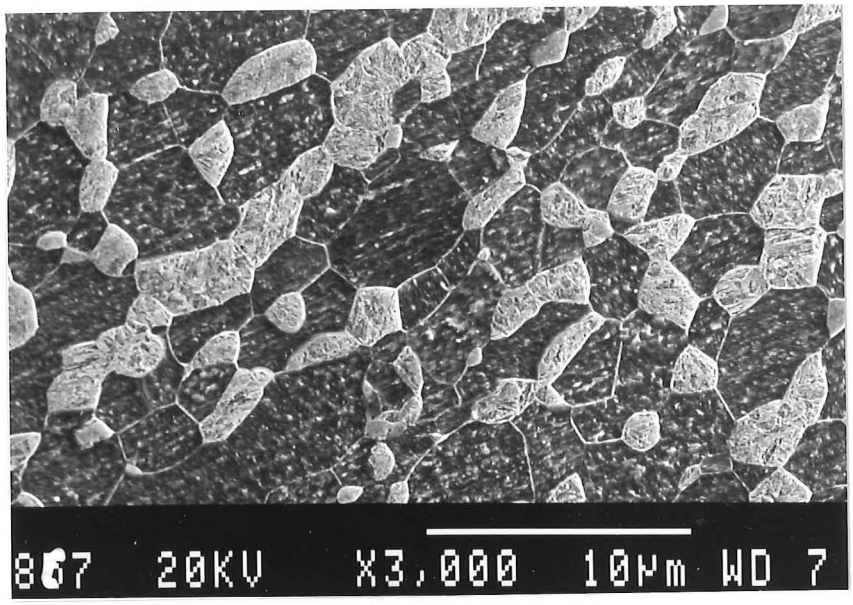

(d)

Fig.11 The change of martensite morphology after post-annealing at 680°C for (a)10 min., (b)60 min., (c)240 min. and (d)48hrs

During post-annealing at 690°C, the Mn content in the martensite and the degree of partitioning in steel (pre-annealed at 680°C for 48hrs) both decrease initially then increase and reach a constant level after 4 hrs (see Figure 12). The final partitioning coefficient of the steel after post-annealing is still less than in the as-rolled condition because the post-annealing temperature is higher than that of pre-annealing and hot-rolling. The difference in temperature between pre- and post-annealing causes the redistribution of manganese in the martensite and ferrite. The decrease in the martensite fraction, which is shown in Figure 13, is most likely caused by the decarburization of the thin rolled steel plate during post-annealing for 48hrs.

There is no significant variation of martensite volume fraction with increasing post-annealing temperature (shown in Figure 14), unlike compared the variation seen with increasing pre-annealing temperature. However, a lowering of the carbon content through decarburization will reduce the volume fraction of martensite obtained.

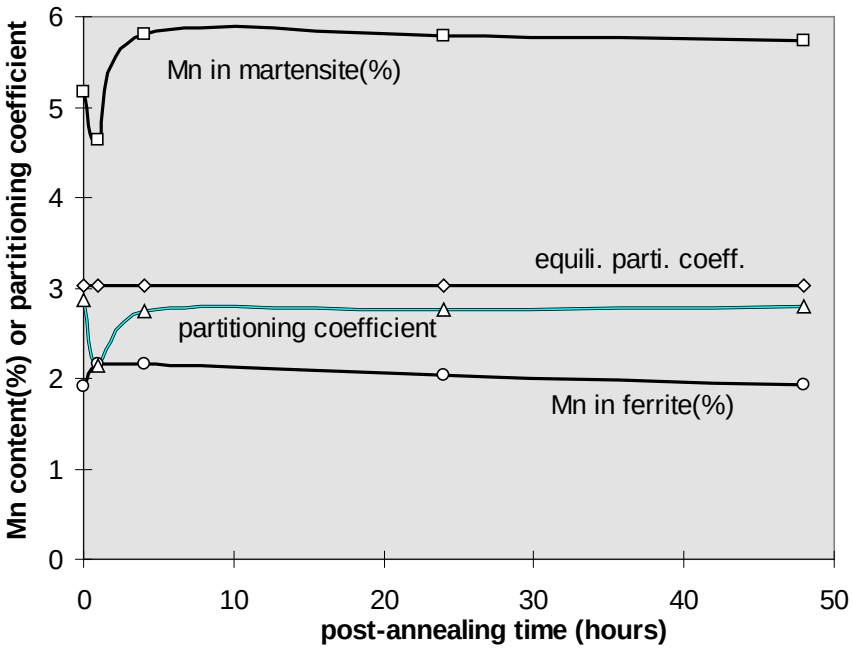

Fig.12 The influence of post-annealing time on the Mn partitioning at 690°C

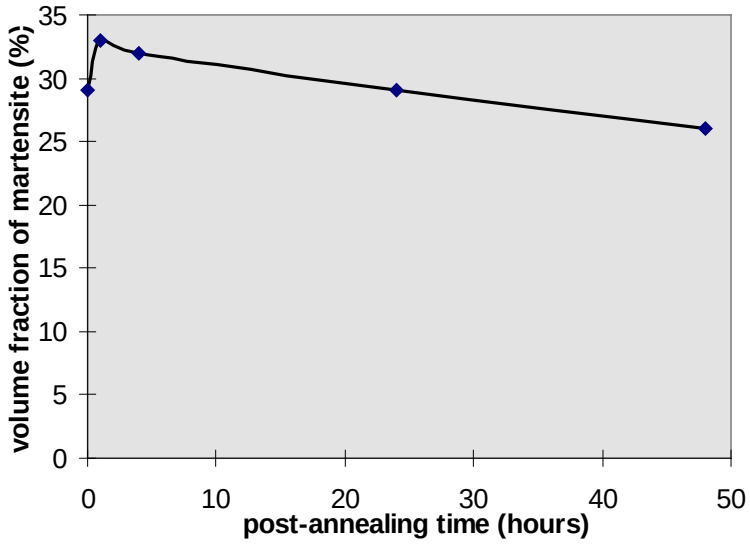

Fig.13 The effect of post-annealing time on martensite volume fraction at 690°C

Since in theory, we have

$$C_{Mn} = C_{Mn}^{\alpha} \cdot V_{\alpha} + C_{Mn}^{MA} \cdot V_{MA}$$

Where, C_{Mn} is the total manganese content(2.71%), C_{Mn}^{α} and C_{Mn}^{MA} are the manganese contents in the ferrite and martensite respectively, and V_{α} and V_{MA} are the volume fractions of ferrite and martensite respectively ($V_{\alpha} + V_{MA} = 1$).

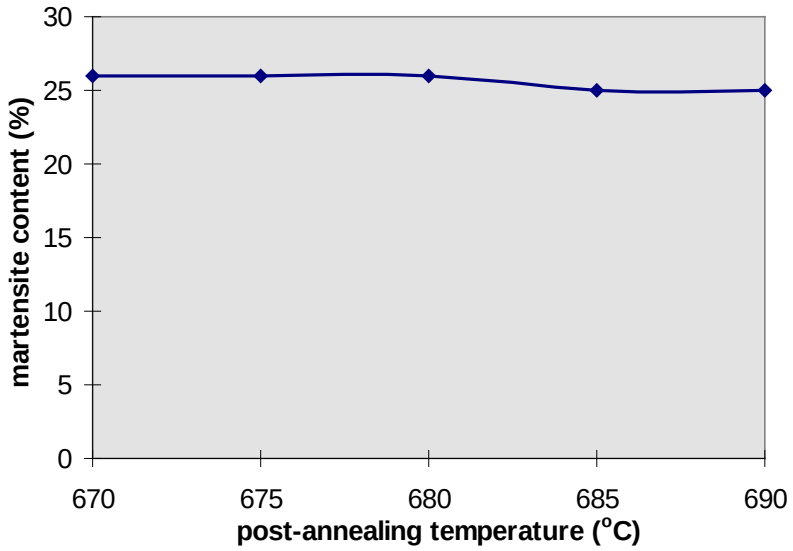

Fig.14 The influence of post-annealing temperature on martensite fraction (48 hrs)

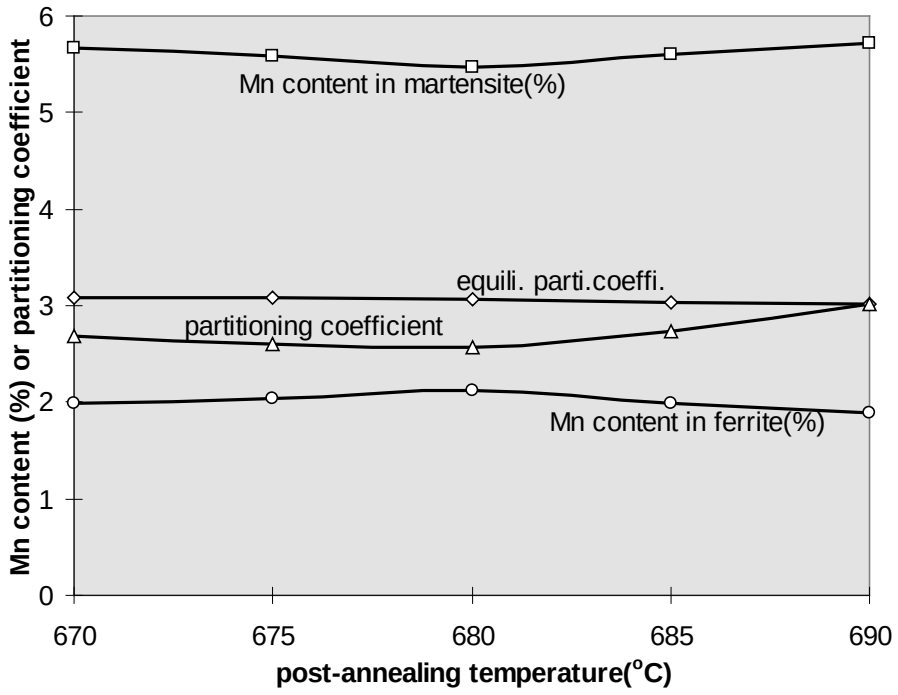

Fig.15 The influence of post-annealing temperature on the Mn partitioning of steel (48 Hrs)

If the volume of martensite decreases (and thus the volume of ferrite increases), the level of manganese in the martensite will increase whilst decreasing in the ferrite (as the overall manganese content is constant), and the results in an increase in the manganese partitioning at the high temperatures (as shown in Figure 15).

4. Conclusion

The following conclusion are drawn from the current study:

1. In contrast to the volume fraction of martensite, the Mn-partitioning coefficient decreases with increasing pre-annealing temperature, but both the martensite volume fraction and Mn-partitioning increase with pre-annealing time until they reach an equilibrium value.

2. Hot rolling, starting in the two phases ($\alpha + \gamma$) region elongates the martensite into a fibrous form.

3. Post-annealing decreases the aspect ratio of this fibrous martensite. Decarburization during post-annealing reduces the martensite volume fraction.

5. Reference

1. V. B. Dutta, S. Suresh, and R. O. Ritchie, *Fatigue Crack Propagation in Dual Phase Steels: Effect of Ferritic-Martensite Microstructures on Crack Path Morphology*, Metall. Trans., 15A(1984), 1193-1207.
2. Xue-Ling Cai, A.J. Garratt-reed, and W.S. Owen, *The Development of Some Dual Phase Steel Structure from Different Starting Microstructures*, ibid., 16A(1985), 543-557.
3.Peng-Heng Chang, *Effects of Prior Cold Rolling and Post Temper Rolling on the Properties of Continuously Annealed Low Carbon Dual Phase Steel*, ibid., 15A(1984), 671-678.
4. R. G. Davies, *Deformation Behavior of a Vanadium Strengthened Dual Phase Steel*, ibid., 9A(1978), 41-52.
5. R. Ratnaraj, *Nitrogen in HSLA and Dual Phase Steels* (Ph.D. thesis, University of Canterbury, New Zealand, 1989).
6. R.Ramesh, N. J. Kim, and G. Thomas, *Improvement in Toughness of Fe-Cr-Mn-C Stells by Thermal-Mechanical Treatment*, Metall. Trans., 21A(1990), 683-695.
7. R. G. Davies, *Influence of Silicon and Phosphorus on the Mechanical Properties of Both Ferrite and Dual Phase Steels*, ibid., 10A(1979), 113-118.
8. C. I. Garcial and A. J. DeArdo, *The Formation of Austenite in Low Alloy Steels* in "Structure and Properties of Dual Phase Steels (Edited by R. A. Kot and J. W. Morris), AIME, New York, 1979, pp40-61.
9. Peng-Heng Chang, *Temper-Aging of Continuously Annealed Low Carbon Dual Phase Steel*, Metall. Trans., 15A(1984), 73-86
10. L. J. Cuddy, *Grain Refinement of Nb Steels by Control of Recrystallization during Hot Rolling*, ibid., 15A(1984), 87-98.
11. K. W. Andrews, *The calculation of transformation temperature and austenite-ferrite equilibria in steels*, Journ. of Iron & Steel Inst. v184, December,1956, pp414-27.

Appendix B*

The Microstructure and Mechanical Properties of As-Rolled Dual Phase Steel

Part Ⅱ: Mechanical Properties

Shoujin Sun, Martin Pugh and Les Erasmus
Department of Mechanical Engineering, University of Canterbury, New Zealand

Abstract

The influence of pre-annealing and post-annealing heat treatments on the tensile properties of dual phase steel has been investigated. Post-annealing lowers the tensile strength and increases the % elongation by decreasing the aspect ratio of the fibrous martensite. The as-rolled steel shows a “delamination-type” fracture whereas the post-annealed steel does not. The tensile strength of these partitioned and fibrous steels are compared with Mileiko's theory for plastic instability in ductile composites.

1.Introduction

Dual phase steel developed from high strength, low alloy (HSLA) steel consisting of martensite and ferrite phases, in which the martensite imparts high strength and the ferrite matrix supplies good elongation, can produce a very desirable combination of strength and ductility.

It is well known that the tensile strength and ductility of dual phase steel depend not only on the grain size and properties of the constituent phases, but also on the volume fraction, distribution, shape and carbon content of the martensite phase[1,2,3], and the carbide precipitation in the ferrite[4]. Fine grain size[3,5,6], high strength and a high volume fraction of martensite will increase the tensile strength of a dual phase steel, but a high volume fraction of martensite combined with carbide precipitation reduces ductility. The amount and carbon content of the martensite phase are primarily dependent on the intercritical annealing temperature and the overall carbon content of the steel[1,7,8,9], but are also affected by manganese partitioning.

Davies et al[6,10] has concluded that the strength of dual phase steel is dependent only on the volume fraction of martensite, and is not dependent on the carbon content of the martensite phase. This appears simplistic as the strength of composite material is a

* Published in IPENZ’96 conference, Feb. 1996, Dunedin.

function of the constituent phases' strengths; in this case, the martensite strength is primarily dependent on its carbon content.
The significant mechanical characteristics of dual phase steel is a low yield strength followed by continuous yielding behaviour with a high initial work-hardening rate, which is attributed to the austenite-to-martensite transformation within the constraints of the ferrite matrix. Micrographs of high dislocation densities adjacent to martensite areas have been presented[11] to support this theory.

Mileiko's theory[12] which derives the tensile strength parallel to the fibre direction of fibre composites consisting of two ductile phases, has been found to be applicable to dual phase steel even though the martensite is not exactly in a continuous fibre form[13,14].

The purpose of the current research was to obtain preferred orientation of fibrous martensite in the microstructure of dual phase steel and ascertain whether this material has a superior reinforcing effect compared to other martensite distributions and morphologies. The work-hardening rates were calculated and compared with Mileiko's theory.

2. Material and Experimental Procedure.

The material and heat treatments employed can be found in part I of this study[15].

Tensile testing samples were machined from the rolled strips as shown in Figure 1. The tests were carried out at ambient temperature with a crosshead speed of 0.2mm/s. The fracture surfaces obtained were examined by SEM.

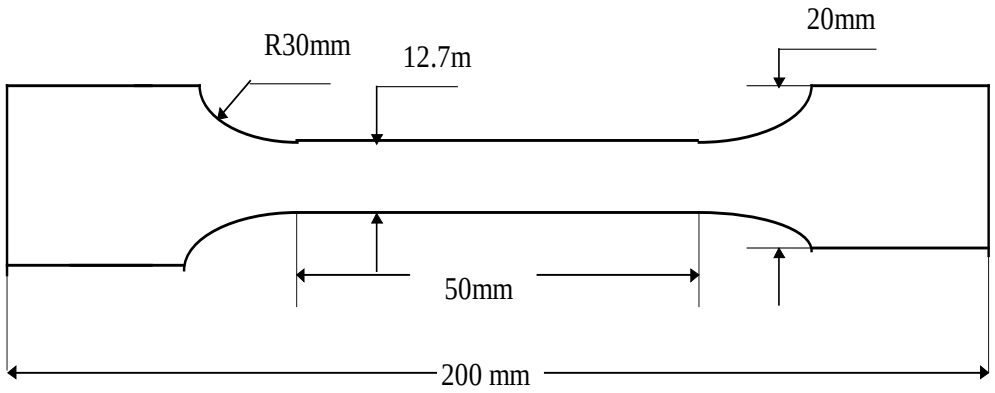

Fig.1 Illustration of test sample

3. Results and Discussion

3.1 The influence of pre-annealing

The influence of pre-annealing on the mechanical properties of as-rolled dual phase steel is shown in Tables 1 and 2. All tensile tests were carried out on samples cut parallel to the rolling direction. The tensile strength after pre-annealing at 680°C is lower than after pre-annealing at either 670°C and 690°C, and the % elongation is

correspondingly higher. This is due to carbide precipitation at the lower annealing temperature (670°C) and a higher volume fraction of martensite at the higher temperature (690°C). Both of the factors lead to an increase in the tensile strength and a decrease in the elongation to fracture. The best combination of high tensile strength (1312MPa) and high elongation (19.3%) was thus obtained by pre-annealing at 680°C for 96 hrs and rolling at 680°C. The true stress-true strain curves for steel both in the as-rolled and post-annealed states, are shown in Figure 2. Also shown is the stress-strain curve based on Mileiko's theory. This has been generated using values for the strength, and true uniform strain for the martensite and ferrite phases from the literature[13].

Table 1 The influence of pre-annealing temperature on mechanical properties (48 hour)

Annealing temperature (°C)	670	680	690
Tensile strength (MPa)	1218	968	1392
0.2%YLD stress (MPa)	676	913	847
Elongation (%)	6.5	24.0	4.4

Table 2 The effect of pre-annealing time on the tensile properties of steel at 680°C

Annealing time (hours)	4	48	96
Tensile strength (MPa)	1327	968	1312
0.2%YLD stress (MPa)	1069	913	726
Elongation (%)	4.6	24.0	19.3

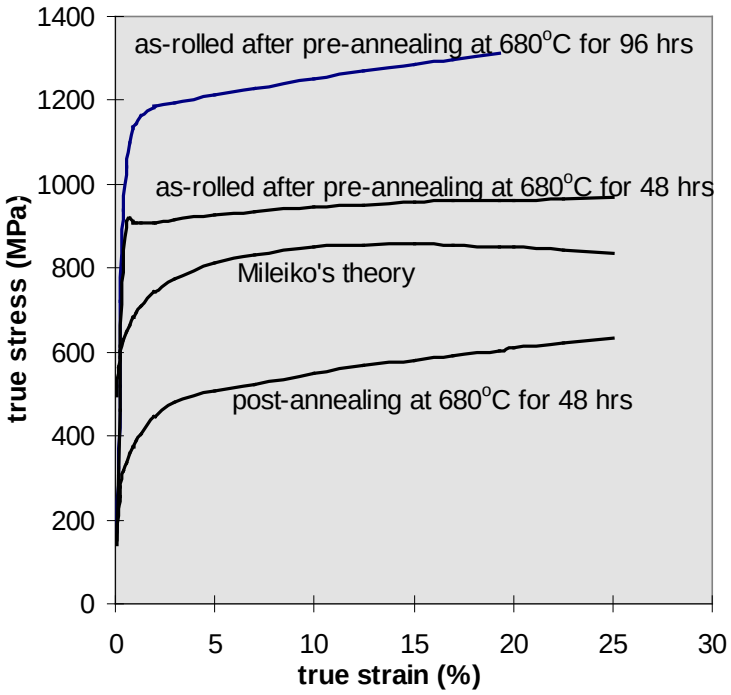

Fig.2 True stress-true strain curves for steel

3.2 The influence of post-annealing

The variations of the tensile properties of the dual phase steel with post-annealing time and temperature are shown in Figures 3 and 4. With increasing post-annealing time, the tensile strength and 0.2% yield stress decrease (and percent elongation increases) due to both the decreasing aspect ratio and volume % of the martensite phase (as shown in part I)[15], thus reducing the reinforcing effect of the fibrous martensite. An important conclusion can thus be drawn that the increased hot-rolled tensile strength is due in part to the martensite morphology.

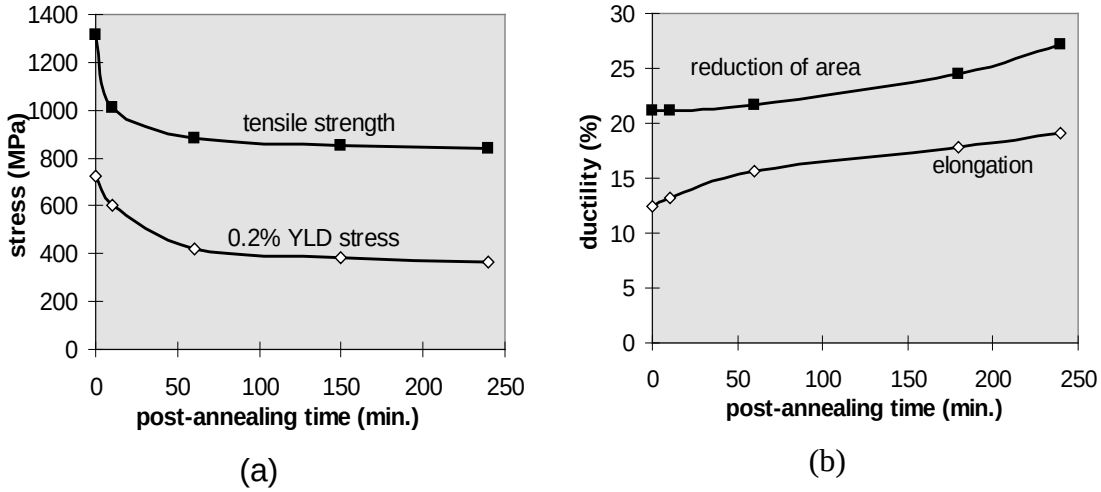

(a) (b)

Fig.3 The effect of post-annealing time on (a) tensile strength and (b) ductility (690°C)

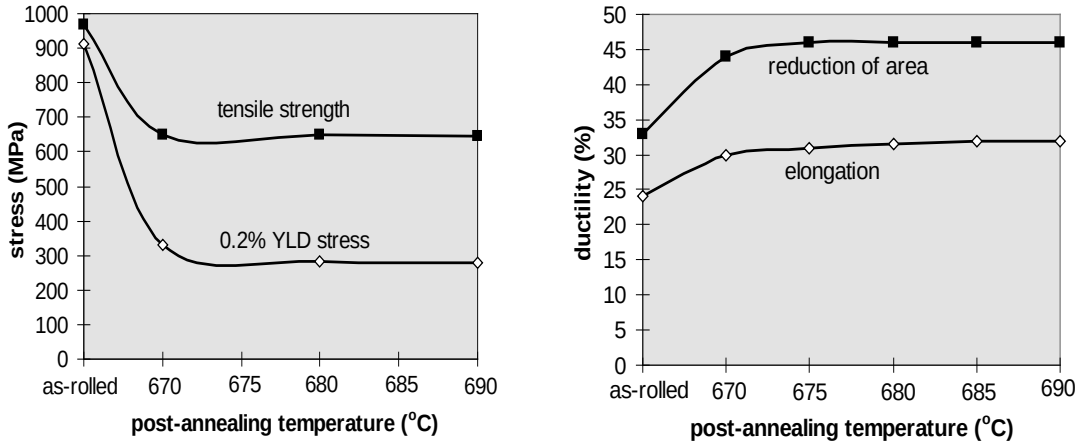

Fig.4 The influence of post-annealing temperature on the tensile properties (48 hrs)

3.3 Mechanical properties as a function of martensite volume

The variation of tensile strength with volume fraction of martensite for both as-rolled and post-annealed conditions is shown in Figure 5; the tensile strengths increase with increasing volume fraction of martensite for both conditions. The tensile strengths of the as-rolled steel are superior to those of the post-annealed steel for the same vol.% martensite. The difference in tensile strength between the as-rolled and post-annealed steels is attributed mainly to the difference in aspect ratio of the martensite "fibres".

The influence of the martensite volume fraction on the total elongation and reduction of area for these steels is shown in Figure 6 and 7, respectively. Both the elongation and reduction of area decrease sharply with increasing martensite, which means that the high ductility of dual phase steel can only be achieved with lower volume fractions of martensite, ie <30%.

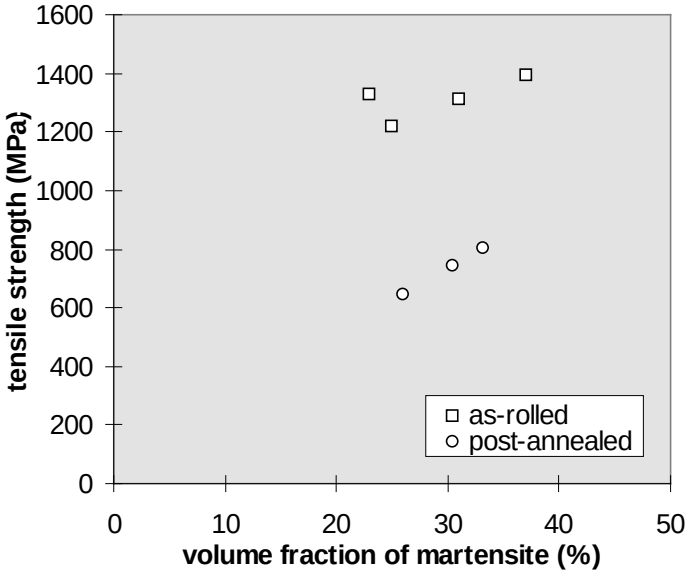

Fig.5 Tensile strength of steel as a function of vol.% martensite

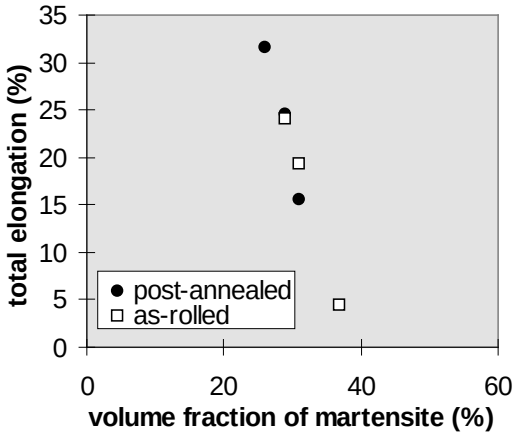

Fig.6 Elongation as a function of volume fraction of martensite

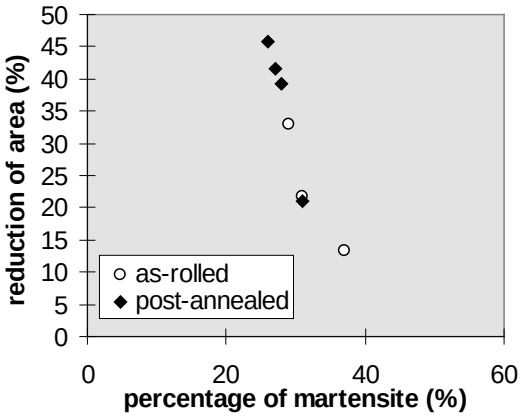

Fig.7 Reduction of area as a function of martensite volume fraction

3.4 Fractography

The fracture of the as-rolled steel has the appearance of delamination (Fig.8). Whilst the material is not fabricated from individual laminae, the hot-rolling process has produced ribbons of martensite oriented in the rolling plane of the steel sheet. Due to the combination of these very strong aligned ribbons and the ductile ferrite matrix the fracture has occurred preferentially along the axis of the ribbon orientation. The fracture in fibrous dual phase steels has been shown to be by void nucleation at the martensite-ferrite interface[16] and in this case, the majority of this interface is in the plane of rolling and hence the jagged fracture surface.

As the strength of the dual phase steel decreases (due to a decrease in the aspect ratio), this "laminar type" failure decreases. For example, the tensile strength and elongation of steel with pre-annealing at 680°C for 96hours are 1312MPa and 19.3% respectively, and eight "layers" can be seen in the fracture surface (see Fig.8a). In contrast, for the same steel and conditions but with only 48 hrs pre-annealing, the tensile strength was 968MPa with an elongation of 19.3%, and the laminar nature of the fracture is reduced showing 5 apparent layers (Fig.8b). Figures 8(c) and (d) show the ductile failure in the ferrite regions of these layers.

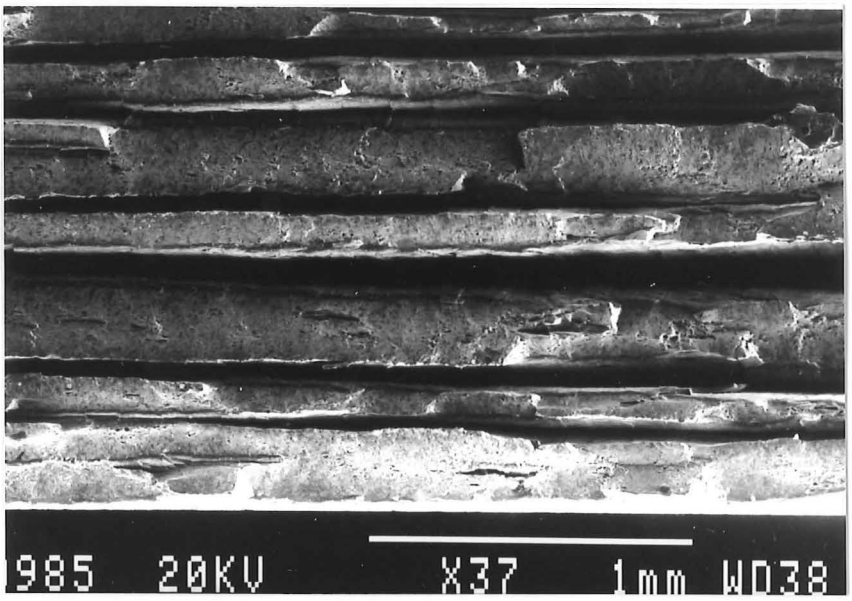

(a)

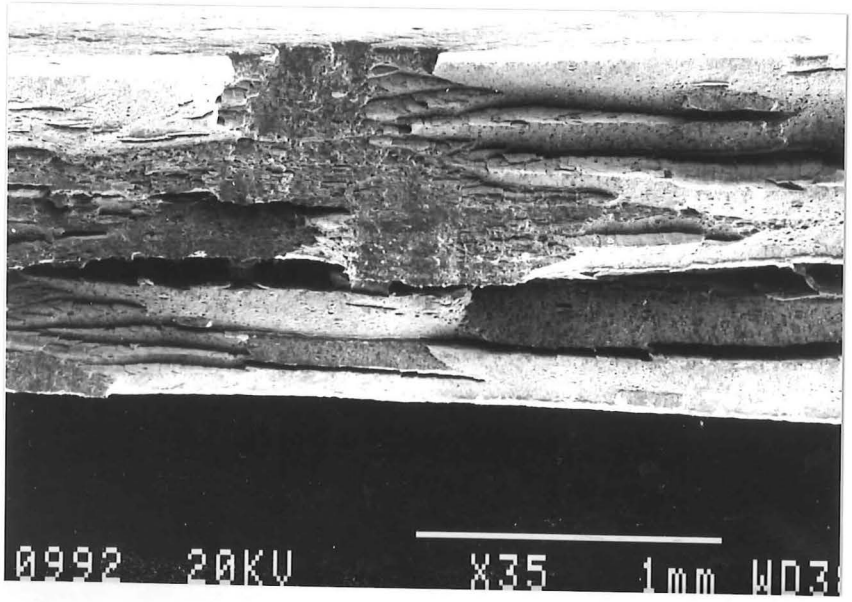

(b)

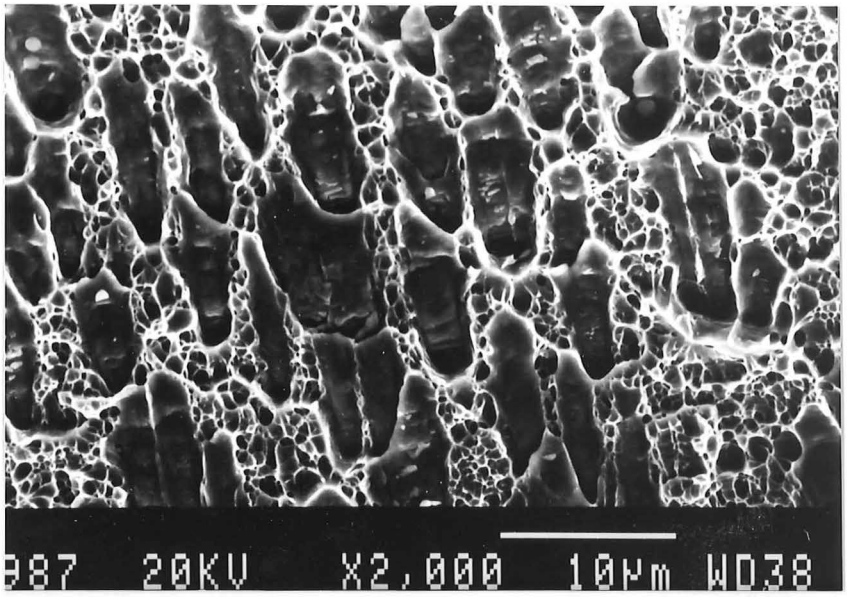

(c)

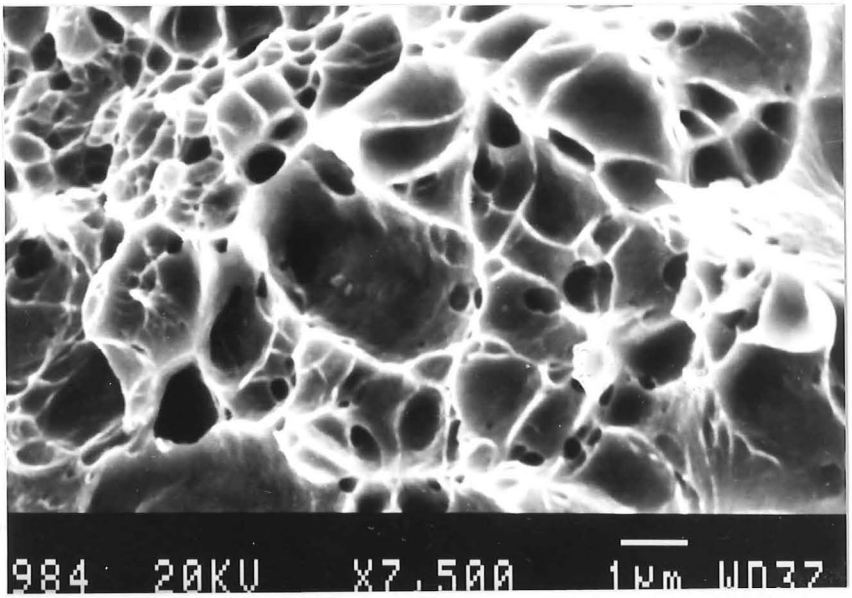

(d)

Figure 8 Fracture surface of as-rolled steel

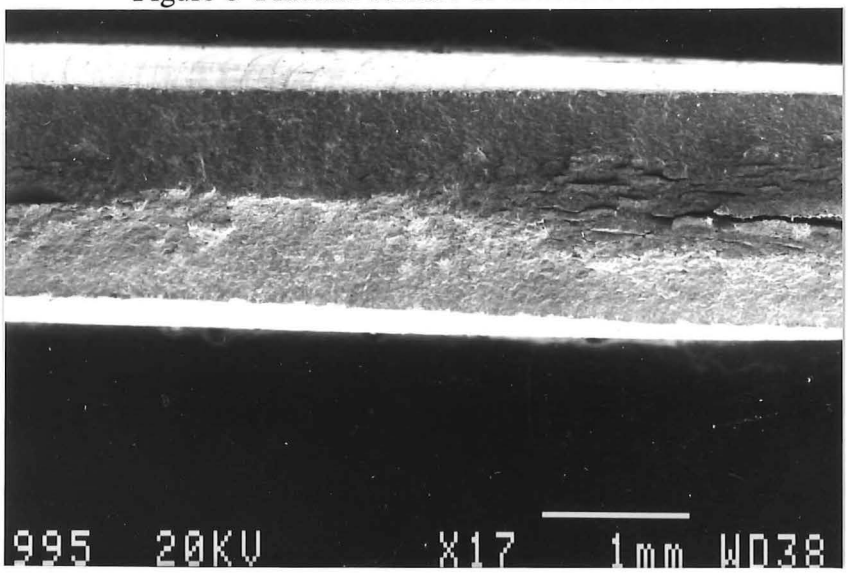

(a)

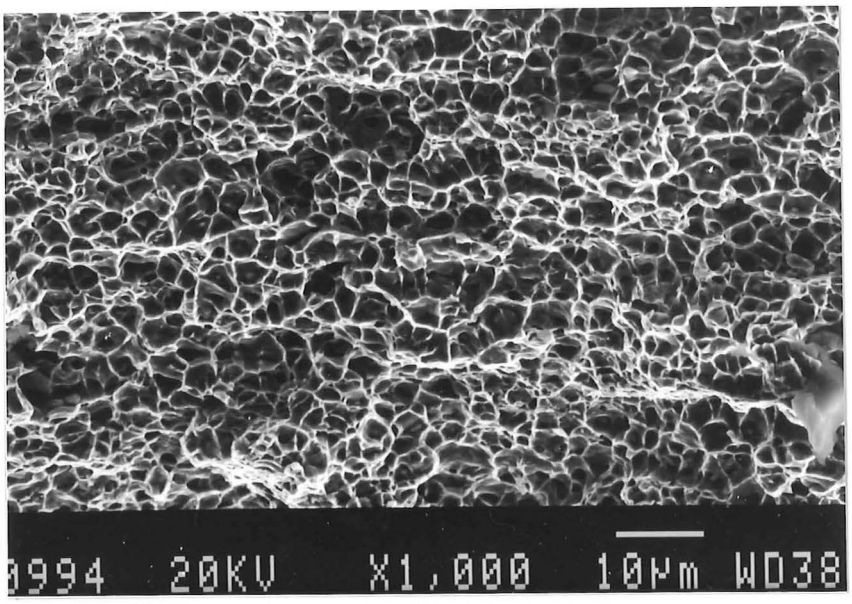

(b)

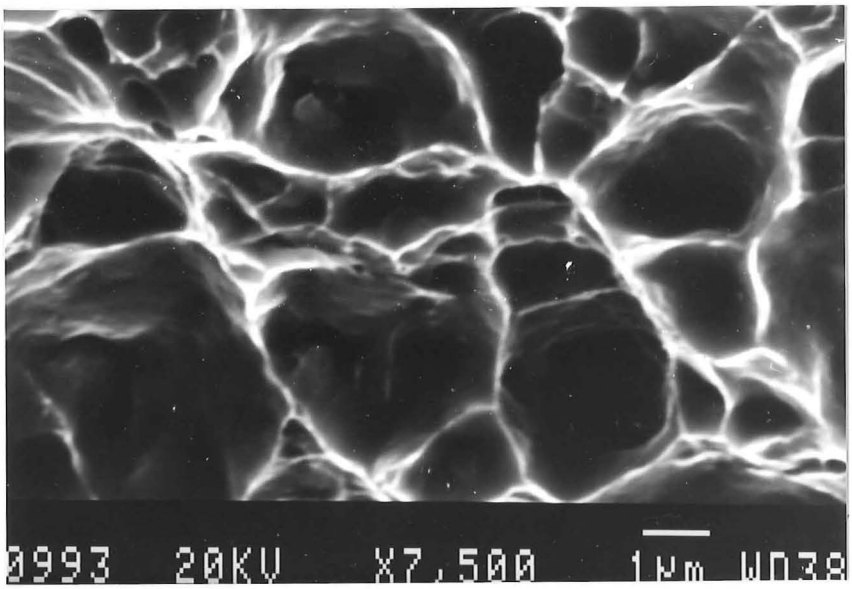

(c)

Figure 9 The fracture surface of steel after post-annealing

The fracture surface of steel after post-annealing at 680°C for 48 hours is different from that in the as-rolled state. From Figure 9, it can be seen that there is no "delamination" taking place and no martensite pull-out, the plastic deformation takes place on the whole fracture surface, and the ductility is higher than that of the as-rolled steel. This is due to the change in the martensite morphology and volume fraction.

3.5 Work-hardening behaviour

The strain hardening behavior of dual phase steel has been related to the dislocation density in the ferrite phase[17]. The distribution of dislocation tends to be non-uniform with regions of high dislocation density in the ferrite adjacent to the transformed martensite grains and a low density in the interior of the ferrite grains. The plastic strain behaviour of dual phase steel consists of several processes[18-22], and cannot always be described by a single n value over the whole plastic strain range.

The following stress-strain equation is often used to analyse the deformation behavior of steel: $\sigma = k \cdot \varepsilon^n$ (1)

where, σ is the true stress, ε is the true plastic strain, k and n are constants, in which n is the work-hardening parameter of the steel.

Thus, the work-hardening parameter, n, can be calculated from the plot of $\lg\sigma$ versus $\lg\varepsilon$,

$$n = \frac{\Delta \lg \sigma}{\Delta \lg \varepsilon} \quad (2)$$

or $$n = \varepsilon_c \quad (3)$$

where, ε_c is the true uniform strain, The plot of σ *vs* ε on a logarithmic scale is shown in Figure 10 for the different steels and it is apparent that the as-rolled steel contains two distinct work-hardening processes, with the exponent, n, for the initial strain-hardening process being much higher than for the second process. The first work-hardening stage occurs at low plastic strain where the ferrite phase deforms plastically and the martensite elastically; the work hardening in this stage is primarily controlled by the dislocation distribution and density in the ferrite[21]. The second stage (in the high strain range) is associated with the plastic deformation of both ferrite and martensite. Because of the high degree of "fibering" induced by the rolling process, not only is the martensite phase in the form of this ribbons, but the ferrite matrix is sandwiched between these ribbons in a similar way to the ferrite in pearlite colonies. This could explain the rapid work-hardening seen in the early stages in the as-rolled material (a similar behavior is also observed in pearlite).

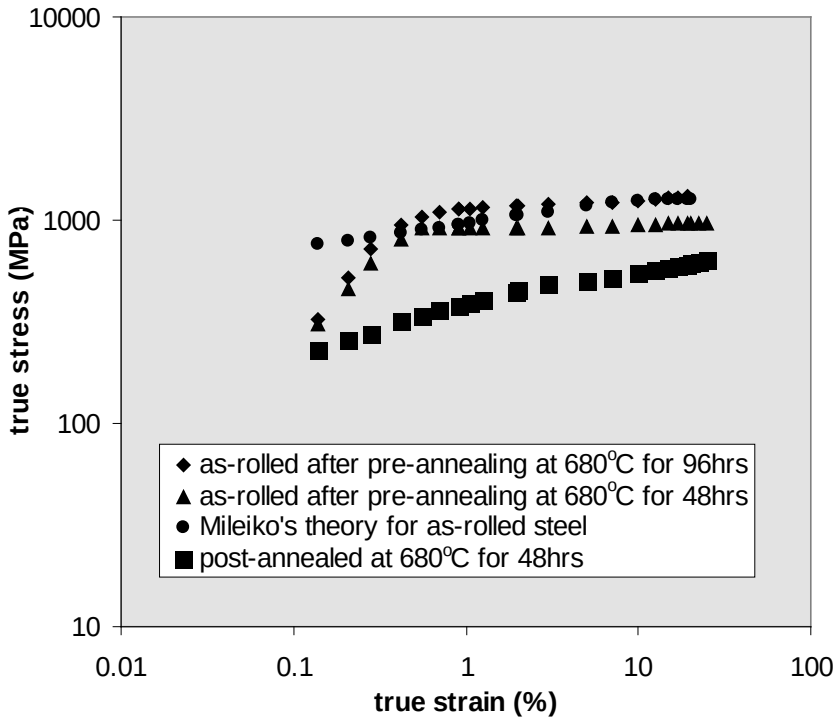

Fig.10 The log-log plot of $\sigma \# \varepsilon$ curves for dual phase steels (from Fig.2)

In contrast with as-rolled steel, the post-annealed material's behavior shows a similar trend to that predicted by Mileiko's theory although there is a slight indication of a

bimodal distribution but the magnitude is considerably lower than in the case of the as-rolled steel and the transition is more gradual.

3.6 Comparison with Mileiko's theory

Because the dual phase steel can be viewed as a composite made of two ductile components, the composite mechanics derived from the usual model of brittle fibre/ductile matrix composites may be invalid for dual phase steel. By using the following assumptions:
(1) the strength of the interface between fibre and matrix is high enough to resist the necking of any one component without necking of the composite as a whole;
(2) the stress and strain relationships for the composite and each component obey the equation (1);
Mileiko developed a theory which related the strength and ductility of two ductile components to the mechanical properties of such a composite by application of the plastic instability criteria to the composite. The suggestion in the present work is that each component of the dual phase steel can meet the above assumptions (although the martensite is not in the form of continuous fibres) and Mileiko's theory is applicable to dual phase steel.

For dual phase steel, Mileiko's theory can be written as:

$$V = \frac{1}{1+\beta\frac{\varepsilon_c-\varepsilon_m}{\varepsilon_f-\varepsilon_c}\varepsilon_c^{\varepsilon_m-\varepsilon_f}} \tag{6}$$

where

$$\beta = \frac{\sigma_m\cdot\varepsilon_f^{\varepsilon_f}\cdot\exp\varepsilon_m}{\sigma_f\cdot\varepsilon_m^{\varepsilon_m}\cdot\exp\varepsilon_f} \tag{7}$$

and for the tensile stress at ε:

$$\sigma = V\cdot\lambda'\cdot\sigma_m + (1-V)\cdot\lambda''\cdot\sigma_f \tag{8}$$

where

$$\lambda' = (\frac{\varepsilon}{\varepsilon_m})^{\varepsilon_m}\cdot\exp(\varepsilon_m-\varepsilon) \tag{9}$$

and

$$\lambda'' = (\frac{\varepsilon}{\varepsilon_f})^{\varepsilon_f}\cdot\exp(\varepsilon_f-\varepsilon) \tag{10}$$

where, σ_c and ε_c are the tensile strength and the true uniform strain, respectively, of dual phase steel.
σ_m and ε_m are the tensile strength and the true uniform strain, respectively, of martensite.

σ_f and ε_f are the tensile strength and the true uniform strain, respectively, of ferrite.

V is the volume fraction of martensite in steel.

The ultimate tensile strength (σ_c) and the flow stress ($\sigma_{0.2\%}$) are the stresses at which $\varepsilon = \varepsilon_c$ and $\varepsilon = 0.002$, respectively. The tensile strength and flow stress can thus be predicted by replacing ε with ε_c and 0.002, respectively in equation (16), giving:

$$\sigma_c = V \cdot \sigma_m \cdot (\frac{\varepsilon_c}{\varepsilon_m})^{\varepsilon_m} \cdot \exp(\varepsilon_m - \varepsilon_c) + (1-V) \cdot \sigma_f \cdot (\frac{\varepsilon_c}{\varepsilon_f})^{\varepsilon_f} \cdot \exp(\varepsilon_f - \varepsilon_c) \quad (11)$$

and

$$\sigma_{0.2\%} = V \cdot \sigma_m \cdot (\frac{0.002}{\varepsilon_m})^{\varepsilon_m} \cdot \exp(\varepsilon_m - 0.002) + (1-V) \cdot \sigma_f \cdot (\frac{0.002}{\varepsilon_f})^{\varepsilon_f} \cdot \exp(\varepsilon_f - 0.002) \quad (12)$$

The tensile strength and flow stress can then be calculated according to Mileiko's theory. The tensile strength and flow stress at 0.2% offset for the steel, predicted by substituting 2000MPa, 415MPa, 0.07 and 0.31 for σ_m, σ_f, ε_m and ε_f respectively in Equations (11) and (12) (these are values that have been put forward and used by Davies and other workers for dual phase steels[13,14]) are compared with the experimental data for the as-rolled and post-annealed steels in Figures 11 and 12. It can be seen that the experimental values for the as-rolled steel are considerably higher than those predicted by Mileiko's theory whereas those for the post-annealed steel are much closer to the predicted values and are in fact slightly lower. This difference between the theoretical and experimental values are most likely due to the effect of (a) the martensite aspect ratio and also (b) the variation of the tensile strength of the martensite owing to its varying contents of carbon and manganese.

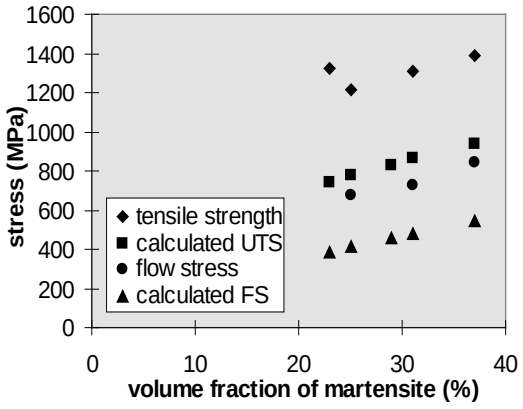

Figure 11 Variation of tensile strength and flow stress with volume fraction of martensite for as-rolled steel

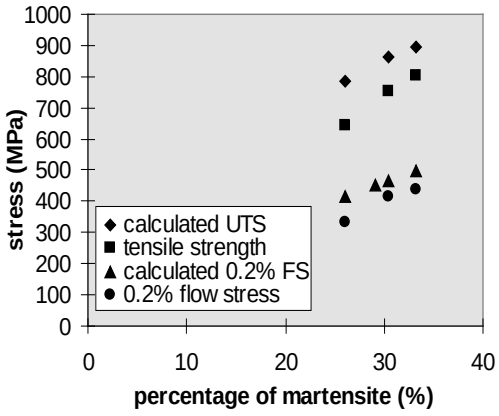

Figure 12 Tensile strength and flow stress as a function of volume fraction martensite for post-annealed steel

The relationship of work-hardening exponent, n, and martensite volume fraction can also be predicted by Equation (6). The comparison between theoretical and measured data is shown in Figure 13; the calculated work-hardening exponents are higher than those of post-annealed steel and lower than those of as-rolled steel at the same volume fraction of martensite.

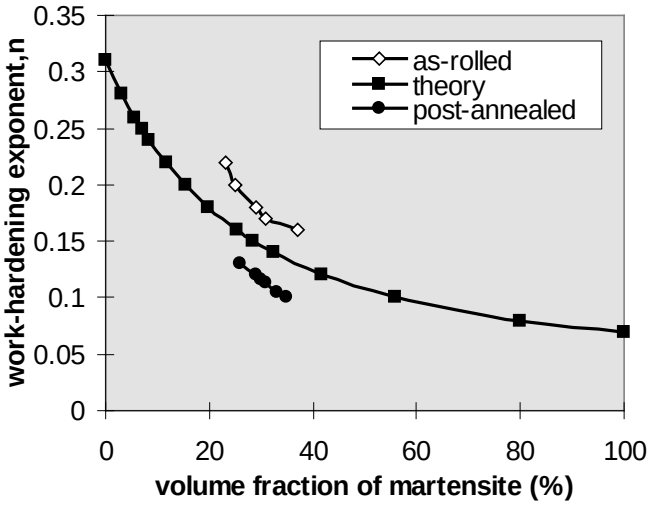

Fig. 13 Plot of work-hardening exponent, n, *vs* volume fraction of martensite

The measured values of tensile strength, flow stress and work-hardening exponent do not closely match the predicted values: the data set for the as-rolled steels are higher than those predicted whilst the post-annealed are lower. This is thought to be due in large part to the fibrous structure of the as-rolled material increasing the apparent strength of the ferrite matrix and increasing the aspect ratio of the stronger martensitic reinforcing phase. The post-annealed structure has a nearly equi-axed structure in comparison and the annealing treatment will have also led to a drop in the carbon content of the martensite and thus lessen the strength of the reinforcing phase.

Using more realistic value for the tensile strengths of the constituent phases in the as-rolled and post-annealed steels by extrapolating from Figure 5, a better comparison can be made with Mileiko's equation. This relationship between experiment (points and broken lines) and theory (bold lines) is shown in Figures 14 and 15 (σ_m=2400MPa, σ_f=830MPa for as-rolled steel, σ_m=2080MPa, σ_f=200MPa for post-annealed steel). It is found that the revised "Mileiko predictions" are a closer fit to the experimental values except for the 0.2 % flow stress of post-annealed steel.

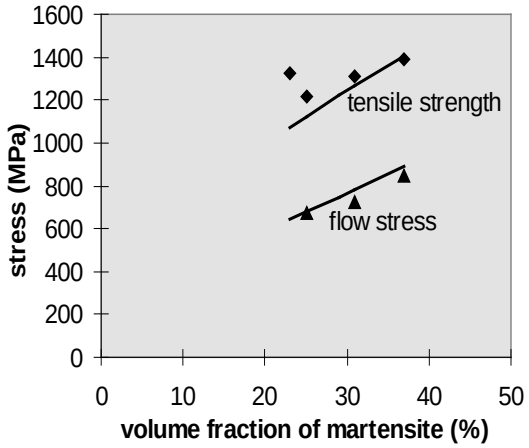

Fig.14 Variation of tensile strength and flow stress with volume fraction of martensite for as-rolled steel

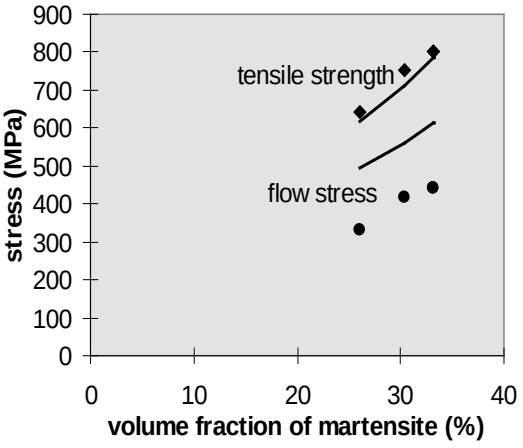

Fig.15 Tensile strength and flow stress as a function of volume fraction martensite for post-annealed steel

4. Conclusion

1. The optimum combination of tensile strength and elongation of as-rolled Fe-2.7Mn-0.1C steel can be achieved by pre-annealing at 680°C for 96 hours; lower and higher temperatures will respectively, promote carbide precipitation and increase the volume fraction of martensite, both of which will degrade the ductility of the steel.

2. With increasing post-annealing time, the strength decreases to a constant value, independent of post-annealing temperature. The ductility increases with increasing annealing time and increases at higher post-annealing temperatures.

3. The strength of dual phase steels is strongly dependent not only on the volume fraction of martensite but on the morphology of the second phase; a high aspect ratio martensitic phase increases the strength of the material.

4. With heavily rolled dual phase steel, the constituent components strengths used in Mileiko's theory need to be re-evaluated.

5. Reference

1. G. R. Speich, V. A. Demarest, and R. L. Miller, "Formation of Austenite During Intercritical Annealing of Dual Phase Steels", *Metall. Trans.*, 12A(1981). 1419-1428.
2. G. R. Speich, R. L. Miller, "Mechanical Properties of Ferrite-Martensite Steels" *in* "Structure and Properties of Dual Phase Steels" (Edited by R. A. Kot and J. W. Morris), AIME, New York, 1979, pp145-182.
3. Peng-Heng Chang and A. G. Preban, "The Effect of Ferrite Grain Size and Martensite Volume Fraction on the Tensile Properties of Dual Phase Steel", *Acta Metall.*, 33(1985), 897-903.
4. A. Nakagawa, J. Y. Koo, and G. Thomas, "Effect of Vanadium on Structure-Properties Relations of Dual Phase Fe/Si/0.1C Steels", *Metall. Trans.*, 12A (1981), 1965-1972.
5. R. G. Davies, "Influence of Silicon and Phosphorus on the Mechanical Properties of Both Ferrite and Dual Phase Steels", *ibid.*, 10A(1979), 113-118.
6. R. G. Davies, "Influence of Martensite Composition and Content on the properties of Dual Phase Steels", *Metall. Trans*., 9A (1978),671-679.
7. R. Ratnaraj, "Nitrogen in HSLA and Dual Phase Steels" (Ph.D. thesis, University of Canterbury, New Zealand, 1989).
8. N. Pussegoda, W. R. Tyson, P. Wycliffe, and G. R. Purdy, "Segregation of Manganese during Intercritical Annealing of Dual Phase Steels", *Metall. Trans.*, 15A(1984), 1499-1520.
9. L. A. Erasmus, R. Ratnaraj, "The Partitioning of Manganese and Nitrogen in Dual Phase Steels", (Report in University of Canterbury, New Zealand).
10. J. Y. Koo, and G. Thomas, "Thermal Cycling and Microstructure for Improved Properties of Fe-0.12%C-0.5%Mn Steels", *Mater. Sci. Eng*., 24(1976), 187-198.
11. G. Tither and M. Lavite, "Beneficial stress-strain behavior of moly-columbium steel line pipe" *Journal of Metals*, No.9, 27(1975), 15-23.
12. S. T. Mileiko, "The Tensile Strength and Ductility of Continuous Fibre Composites", *J. Mater. Sci.*, 4(1969), 974-977.

13. R. G. Davies, "The Mechanical Properties of Zero-Carbon Ferrite-Plus-Martensite Structure". *Metall. Trans.*, 9A(1978), 451-455.
14. L. A. Erasmus, "The Relationship between Tensile Strength and Ductility of 3% Manganese Dual Phase Steels", (Report in University of Canterbury, New Zealand).
15. Sun shoujin, M.D.Pugh and L.A.Erasmus, “The Microstructure and Mechanical properties of As-Rolled Dual Phase Steel, Part I: Manganese partitioning and microstructure”, paper for 1996 IPENZ Conference in Dunedin.
16. K. J. Kim and G. Thomas, “Effect of Morphology on the Mechanical Behavior of Dual Phase Fe/2Si/0.1C steel”, *Metall. Trans.*, 12A(1981), 483-489.
17. D. A. Korzekwa, D. K. Matlock, and G. Krauss, "Dislocation Substructure as a Function of Strain in Dual-Phase Steel", *Metall. Trans.*, 15A(1984), 1221-1228.
18. Z. Jiang, J. Lian, and J. Chen, "Strain Hardening Behaviour and Its Relationship to Tensile Mechanical Properties of Dual Phase Steel", *Materials Sciences and Technology*, 8(1992), 1075-1081.
19. J. V. Laukonis and R. H. Wagoner, "PLastic Behavior of Dual Phase Steel Following Plane-Strain Deformation", *Metall. Trans.*, 16A(1985), 421-425.
20. Y. Sakams, D. K. Matlock, and G. Krauss, "Intercritically Annealed and Isothermally Transformed 0.15pct C Steels Containing1.2 pct Si-1.5 pct Mn and 4 pct Ni, Part 2, Effect of Testing Temperature on Strass-Strain Behaviour and Deformation-Induced Austenite Transformation. *ibid.*, 23A(1992), 1233-1241.
21. Y. Tomita and K. Okabayashi, "Tensile Strass-Strain Analysis of Cold Worked Metals and Dual Phase Steels", *ibid.*, 16A(1985), 865-872.
22. Z. Jiang, Z. Guan, and J. Lian, "The Relationship Between Ductility and Material Parameters for Dual Phase Steel", *J. Mater. Sci.*, 28(1993), 1814-1818.

Appendix C*

Modelling analysis of manganese partitioning of dual phase steel during annealing

Shoujin Sun, Les Erasmus and Martin Pugh,
Department of Mechanical Engineering, University of Canterbury

Abstract

A model is developed to analyse the manganese partitioning in austenite and ferrite during annealing of dual phase steel. This model is based on manganese diffusion, austenite growth and mass balance principal. The effect of austenite grain size and annealing time on manganese partitioning is predicted by the modelling analysis and compared with experiments.

1. Introduction

Manganese is an austenite stabilizer, which has a higher solubility in austenite than in ferrite (shown in Figure 1). When an alloy, A, is annealed in the two-phase region, manganese partitioning between the austenite and the ferrite will take place: the ratio of manganese in austenite to that in ferrite is defined as the manganese partitioning coefficient, which will vary with annealing temperature and isothermal holding time.

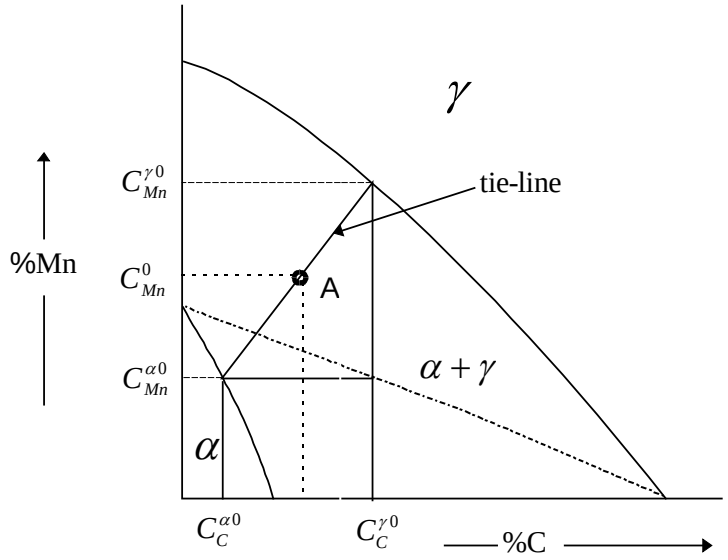

Figure 1 Manganese contents in austenite and ferrite of alloy A in the iron-rich corner of Fe-Mn-C ternary phase diagram

* Published in IPENZ'98 conference, Feb. 1998, Auckland.

The manganese partitioning during intercritical annealing has drawn a lot of attention[1, 2] because it is important in austenite → martensite transformation and strengthening austenite in dual phase steel. Both experimental[1, 2, 3] and theoretical analysis[1, 4] have been carried out but the details for theoretical modelling have not been released.

The present study develops a model to analyse manganese partitioning based on thermodynamics and austenite growth. The theoretical prediction will be compared with experimental data.

2. Formation of dual phase steel

Manganese partitioning occurs during formation of dual phase steel, so the review of formation process of dual phase steel is necessary, and as follows[1, 4]:

(a) Transformation of pearlite to austenite (or dissolution of pearlite). This is controlled by carbon diffusion within the interlamellar spacing of pearlite (~0.2 um), and is very rapid occurring in a few second or less.

(b) The nearly-formed austenite grains grow both into the ferrite and along the ferrite grain boundaries (in order to achieve partial equilibrium given by the lever rule in the two-phase region). This step is controlled by both carbon and manganese diffusion.

(c) Final equilibration within the austenite. The concentration gradients of the substitutional elements such as manganese will be eliminated by their diffusion through the austenite grains.

The manganese diffusion takes place during the growth of austenite (ie after the completion of stage (a) - nucleation). Analysis of manganese partitioning will start after the completion of stage (a) - a few seconds after annealing.

3 Modelling

Consider the intermediate quenched dual phase steel[5]; the ferrite is presented as a polygon and the austenite as a needle, but the austenite will be a granule in the cross-section (shown in Figure 2a). A polygonal unit with the austenite needle in its centre is selected as an analysis unit (shown in Figure 2b).

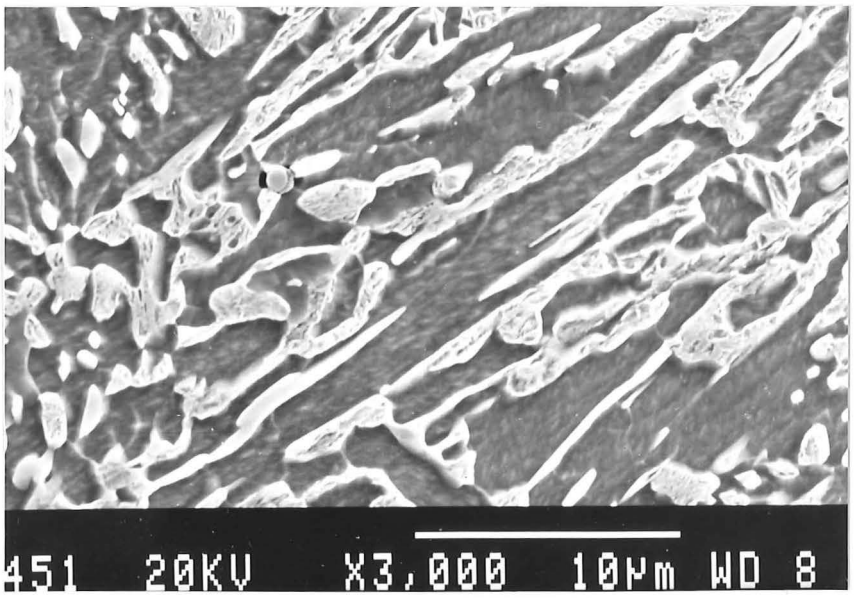

(a) Microstructure

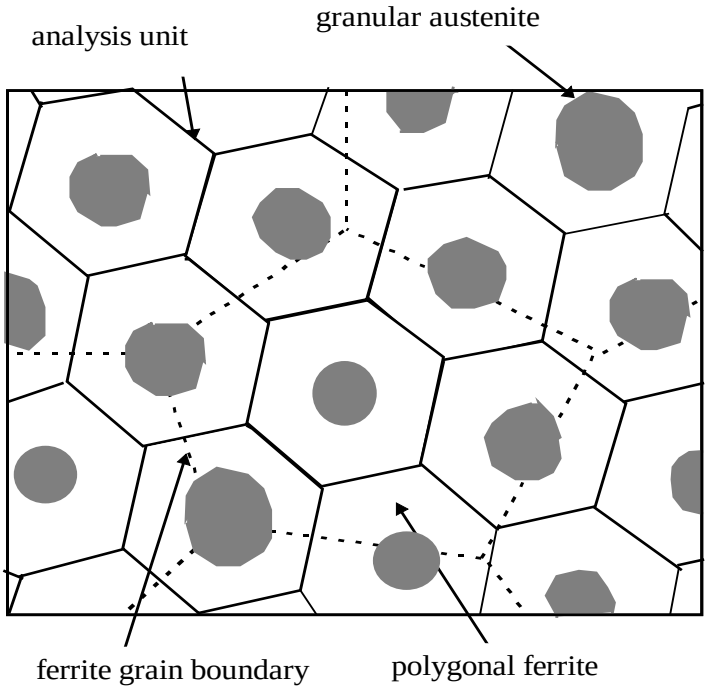

(b) Illustration

Figure 2 Intermediate quenched dual phase steel microstructure (a) and illustration

For the simplification of analysis, both the unit and austenite are considered as concentric cylinders (as shown in Figure 3).Owing to the high aspect ratio of the needle austenite, the manganese diffusion between austenite and ferrite in axial direction of austenite "fibre" can be ignored comparing with the diffusion in radial direction of austenite "fibre. The analysis of manganese diffusion in this section is based on the diffusion in radial direction.

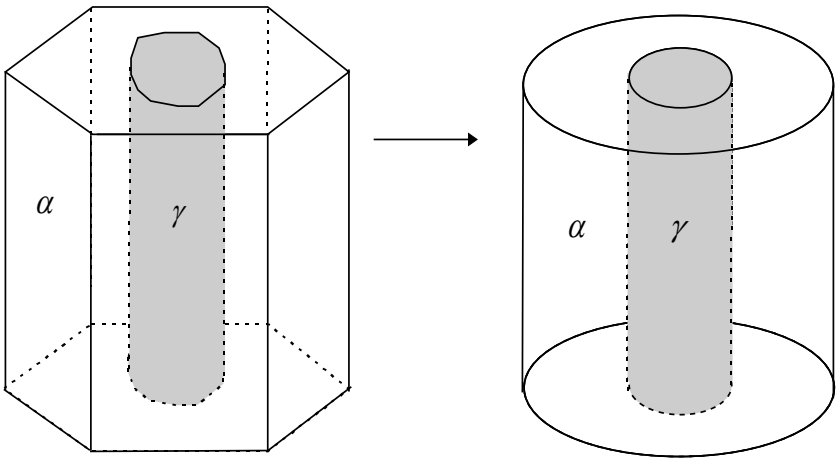

Figure 3 The simplification of analysis unit for dual phase steel

Take the axis x as the distance from the centre of austenite cylinder in redial direction, and axis y as the concentration of manganese, the coordinate set-up is shown in Figure 4.

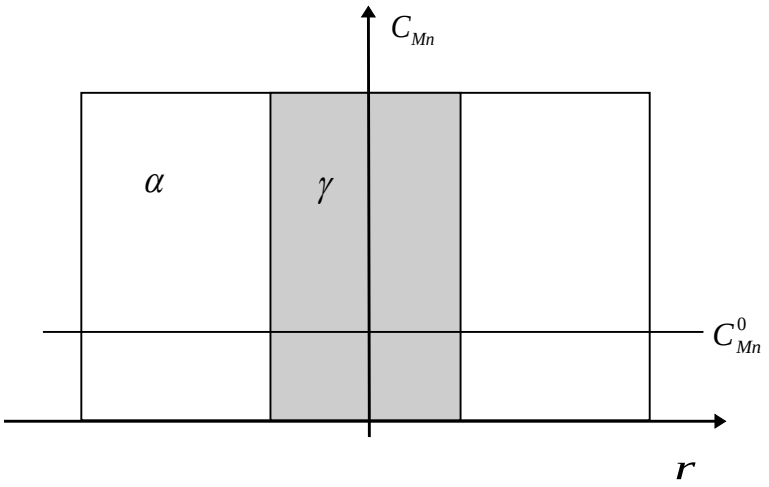

Figure 4. Set-up of the coordinate for analysis of manganese between austenite and ferrite during intercritical annealing

After nucleation of austenite, the manganese diffusion occurs. At the beginning of the manganese diffusion, the ferrite is supersaturated with manganese. The supersaturated manganese will precipitate in the boundary between austenite and ferrite and form a low manganese rim in the edge of ferrite grain (manganese content is $C_{Mn}^{\alpha 0}$, the equilibrium manganese solubility in ferrite at temperature T), the precipitated manganese will dissolve in austenite and form a high manganese rim in the boundary of austenite side (manganese content is $C_{Mn}^{\gamma 0}$, the maximum manganese solubility in austenite at temperature T).

Because the diffusion rate of manganese in ferrite is three orders higher than in austenite, the precipitated manganese from the ferrite will form a manganese-rich rim (the manganese concentration is C_{Mn}^{i}, which is variable) in the interface between ferrite and austenite in addition to dissolve in austenite, the inner dimension of manganese-rich rim is the grain size of austenite, and outer dimension of the manganese-rich rim is the inner size of ferrite, and manganese gradient exists in the region within the austenite ($< r_\gamma$) and ferrite ($> r_\alpha$). The dimension relationship is shown in Figure 5 as:

$$r_\gamma + \Delta r = r_\alpha \tag{1}$$

where Δr is the thickness of manganese-rich rim in the interface, which is at the scale of grain boundary, and the manganese-rich rim is thought as a interphase, which is not either austenite or ferrite. Both r_γ and r_α increase with annealing time at a given temperature, which means that the boundary between austenite and ferrite is moving.

According to the growth kinetics of austenite, the grain size of austenite at a given temperature T is:

$$r_\gamma = k_0 t^n \cdot \exp(-\frac{Q}{2RT}) \tag{2}$$

where, Q is the empirical heat of activation for the austenite growth process, k_0 and n are the constants for a given alloy at the given temperature, generally the exponent n

increases with increasing temperature and reaches the value of $1/2$ [6]. The equation (2) differentiated with respect to t gives the mowing velocity of austenite-ferrite boundary.

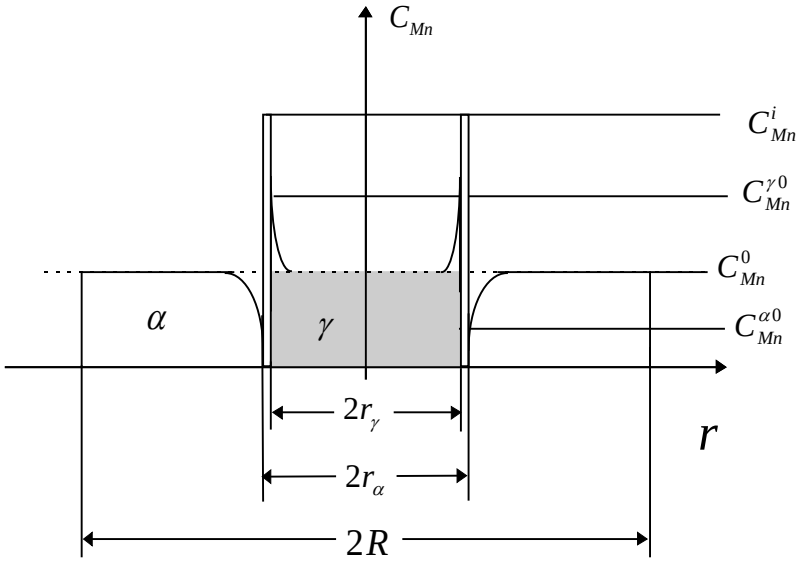

Figure 5 The illustration of manganese distribution in austenite and ferrite during intercritical annealing

With the annealing going, the supersaturated manganese in the ferrite will transport to the boundary to form a manganese-rich rim in the boundary, which is the manganese source for manganese diffusion in the austenite. The manganese in manganese-rich rim in the boundary will diffuse into austenite until the manganese gradient in austenite is eliminated. The diffusion of manganese in the ferrite and austenite can be obtained by solving Fick's second law at the proper boundary conditions.

Fick's second law for manganese diffusion is written as:

$$\frac{\partial C_{Mn}}{\partial t} = -\nabla J_{Mn} \tag{3}$$

where, ∇ is the grad operation. In ternary system, the manganese diffusion flux J_{Mn} depends on concentration gradient of both carbon and manganese, it is expressed phenomenologically with self-diffusion and inter-diffusion coefficient as:

$$J_{Mn} = -D^{inter}_{Mn}\nabla C_C - D_{Mn}\nabla C_{Mn} \tag{4}$$

where D^{inter}_{Mn} is the inter-diffusion coefficient, and D_{Mn} is the self-diffusion coefficient. The inter-diffusion coefficient, D^{inter}_{Mn}, gives a quantitative measure of the effect of a concentration gradient of carbon on the flux of the manganese. In Fe-C-Mn ternary alloys, the effect of carbon gradient on the flux of Mn is general negligible, so the Fick's second law on Mn diffusion is written as follow when D_{Mn} is independent of manganese content:

$$\frac{\partial C_{Mn}}{\partial t} = -D_{Mn}\nabla^2 C_{Mn} \tag{5}$$

The boundary conditions for Mn diffusion in ferrite are:

$$\begin{cases} C_{Mn}^{\alpha} = C_{Mn}^{0} & when \quad t = 0 \\ C_{Mn}^{\alpha} = C_{Mn}^{\alpha 0} & when \quad r = r_{\alpha} \end{cases} \tag{6}$$

The solution to Fick's second law in ferrite can be written as:

$$C_{Mn}^{\alpha} = C_{Mn}^{0} - \left(C_{Mn}^{0} - C_{Mn}^{\alpha 0}\right) \cdot \left[1 - erf\left(\frac{r - r_{\alpha}}{2\sqrt{D_{Mn}^{\alpha} t}}\right)\right] \text{ when } r_{\alpha} \le r \le R \tag{7}$$

$$\text{and } D_{Mn}^{\alpha} = D_{Mn}^{\alpha 0} \exp\left(-\frac{Q_{Mn}^{\alpha}}{R \cdot T}\right) \tag{8}$$

The boundary conditions for manganese diffusion from the rich rim in austenite are set as:

$$\begin{cases} C_{Mn}^{\gamma} = C_{Mn}^{0} & when \quad t = 0 \\ C_{Mn}^{\gamma} = C_{Mn}^{\gamma 0} & when \quad r = r_{\gamma} \end{cases} \tag{9}$$

The equation for manganese distribution in austenite is:

$$C_{Mn}^{\gamma} = C_{Mn}^{0} - \left(C_{Mn}^{0} - C_{Mn}^{\gamma 0}\right) \cdot \left(1 - erf\left(\frac{r_{\gamma} - r}{2\sqrt{D_{Mn}^{\gamma} t}}\right)\right) \text{ when } 0 \le r \le r_{\gamma} \tag{10}$$

$$\text{and } D_{Mn}^{\gamma} = D_{Mn}^{\gamma 0} \exp\left(-\frac{Q_{Mn}^{\gamma}}{R \cdot T}\right) \tag{11}$$

Regardless of the manganese compound, the manganese is still thought to dissolve as a solute, mass balance equation should be applicable:

$$\frac{\int_{S_{\alpha}} C_{Mn}^{\alpha} dS_{\alpha}}{S_{\alpha} + S_{\gamma} + S^{i}} + \frac{\int_{S_{\gamma}^{'}} C_{Mn}^{\gamma} dS_{\gamma}}{S_{\alpha} + S_{\gamma} + S^{i}} + \frac{S^{i} C_{Mn}^{i}}{S_{\alpha} + S_{\gamma} + S^{i}} = C_{Mn}^{0} \tag{12}$$

where S_{α}, S_{γ} and S^{i} are the areas occupied by ferrite, austenite and the manganese-rich rim (interphase), their relationships meet:

$\frac{S_{\gamma}^{'}}{S_{\alpha} + S_{\gamma}^{'} + S^{i}} = V_{\gamma}$, the volume fraction of austenite, increasing with annealing;

$S_{\gamma} = \pi \cdot r_{\gamma}^{2}$, the area of austenite, increasing with annealing;

$S_{\alpha} = \pi \cdot \left(R^{2} - r_{\alpha}^{2}\right)$, the area of ferrite, decreasing with annealing;

$S^{i} = \pi \cdot \left(r_{\alpha}^{2} - r_{\gamma}^{2}\right)$, the area of manganese-rich rim in interface, it final value is 0.

The equilibrium manganese contents in ferrite and austenite at temperature T, $C_{Mn}^{\alpha 0}$ and $C_{Mn}^{\gamma 0}$ also meet the balance requirement:

$$C_{Mn}^{\alpha 0} \cdot (1 - V_{\gamma}^{final}) + C_{Mn}^{\gamma 0} \cdot V_{\gamma}^{final} = C_{Mn}^{0} \tag{13}$$

where, V_{γ}^{final} is the equilibrium volume fraction of austenite.

The equilibrium manganese contents in ferrite and austenite, $C_{Mn}^{\alpha 0}$, $C_{Mn}^{\gamma 0}$, can be found from:

(a) thermodynamics: the following equation (14)[7] can decide the equilibrium concentration of manganese in ferrite and martensite, associated with equation (13).

$$\frac{C_{Mn}^{\gamma 0}}{C_{Mn}^{\alpha 0}} = \exp(-\frac{\Delta H}{R \cdot T}) \tag{14}$$

where ΔH is the difference in heats of solution of manganese in austenite and ferrite phases; or:

(b) the Fe-C-Mn ternary phase diagram (Figure 1).

When dual phase steel is annealed at temperature T for annealing time t, the variation of manganese contents in ferrite and austenite can be obtained through solving the equation (7) and (10), the mean manganese contents in ferrite and austenite can be obtained by integrating equation (7) and (10) with the ferrite and austenite areas respectively, and the partitioning coefficient can be written as:

$$\frac{\dfrac{\int_{S_\gamma} C_{Mn}^{\gamma} dS_{\gamma}}{S_{\gamma}}}{\dfrac{\int_{S_\alpha} C_{Mn}^{\alpha} dS_{\alpha}}{S_{\alpha}}} = \frac{S_{\alpha}}{S_{\gamma}} \cdot \frac{\int_{S_\gamma} C_{Mn}^{\gamma} dS_{\gamma}}{\int_{S_\alpha^0} C_{Mn}^{\alpha} dS_{\alpha}} \tag{15}$$

4. Example

Take a steel with $C_{Mn}^{0} = 2.67\%$ as an example, the annealing temperature is 680°C, the parameters are set as:

the final grain size of austenite/martensite $r_f = 0.56\mu m$;

the grain size of unit $R = 1.0\mu m$;

the final volume fraction of austenite/martensite $V_{\gamma}^{final} = 31.5\%$;

the dimension of manganese-rich rim is at the boundary scale as $\Delta r = 0.001\mu m$

the maximum solubility of manganese in austenite at 680°C is taken $C_{Mn}^{\gamma 0} = 5.0\%$;

and the maximum content of manganese in ferrite is as $C_{Mn}^{\alpha 0} = 1.6\%$.

The distribution of manganese in ferrite is:

$$C_{Mn}^{\alpha} = 2.67 - 1.07\left(1 - erf\left(\frac{r - r_{\gamma} - \Delta r}{2\sqrt{D_{Mn}^{\alpha} t}}\right)\right) = 1.6 + 1.07 erf\left(\frac{r - r_{\gamma} - \Delta r}{2\sqrt{D_{Mn}^{\alpha} t}}\right)$$

when $r_{\gamma} + \Delta r \le r \le 1 \times 10^{-4}$

$$D_{Mn}^{\alpha} = 1.49 \exp\left(-\frac{233600}{8.31 \times 953}\right) = 2.31 \times 10^{-13}\ cm^2/s$$

The variation of manganese in austenite is:

$$C_{Mn}^{\gamma} = 2.67 + 2.33\left(1 - erf\left(\frac{r_{\gamma} - r}{2\sqrt{D_{Mn}^{\gamma} t}}\right)\right) = 5.0 - 2.33 erf\left(\frac{r_{\gamma} - r}{2\sqrt{D_{Mn}^{\gamma} t}}\right) \quad \text{when } 0 \le r \le r_{\gamma}.$$

$$D_{Mn}^{\gamma} = 0.16 \exp\left(-\frac{261700}{8.31 \times 953}\right) = 7.12 \times 10^{-16}\ cm^2/s$$

but Pussegoda[1] suggested that the diffusion rate of manganese in austenite may increase with increasing Mn levels to a maximum at ~3 pct Mn, so the diffusion rete of manganese in austenite at 680°C is set by increasing 10 times, as:

$$D_{Mn}^{\gamma} = 7.12 \times 10^{-15}\ cm^2/s$$

And the partitioning coefficient is:

$$\frac{\frac{1}{\pi \cdot r_{\gamma}^2}}{\frac{1}{\pi \cdot \left((1 \times 10^{-4})^2 - (r_{\gamma} + \Delta r)^2\right)}} \cdot \frac{\int_0^{r_{\gamma}} \left(5.0 - 2.33 erf\left(\frac{r_{\gamma} - r}{2\sqrt{7.12 \times 10^{-15} t}}\right)\right) \cdot r dr}{\int_{r_{\gamma} + \Delta r}^{1 \times 10^{-4}} \left(1.6 + 1.07 erf\left(\frac{r - r_{\gamma} - \Delta r}{2\sqrt{2.13 \times 10^{-13} t}}\right)\right) \cdot r dr}$$

The manganese distribution across austenite and ferrite and partitioning are shown in Figures 6 and 7.

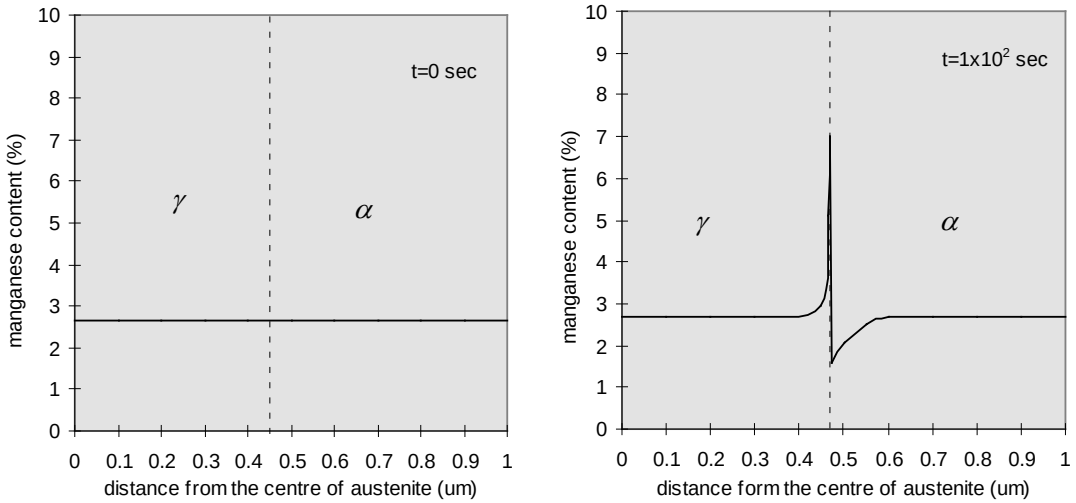

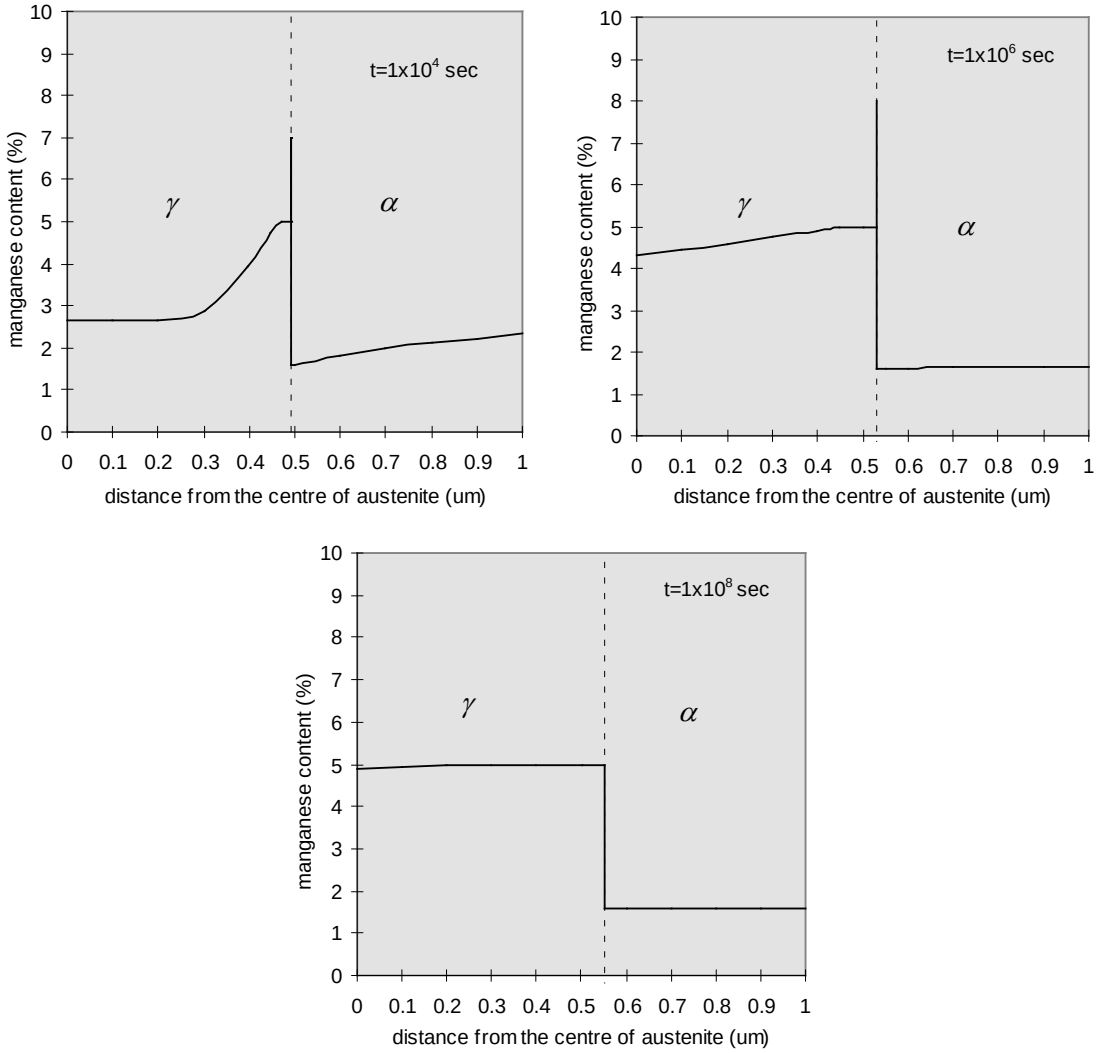

Figure 6 Prediction of manganese distribution as a function of annealing time at 680℃ for 0.11%C-2.67% Mn steel

The effect of austenite grain size (diameter of fibre) on the partitioning is sown in Figure 8, the smaller the austenite grain size, the less the time is needed to reach final equilibrium partitioning, the partitioning coefficient of small austenite grain is higher that that of large grain before reaching equilibrium.

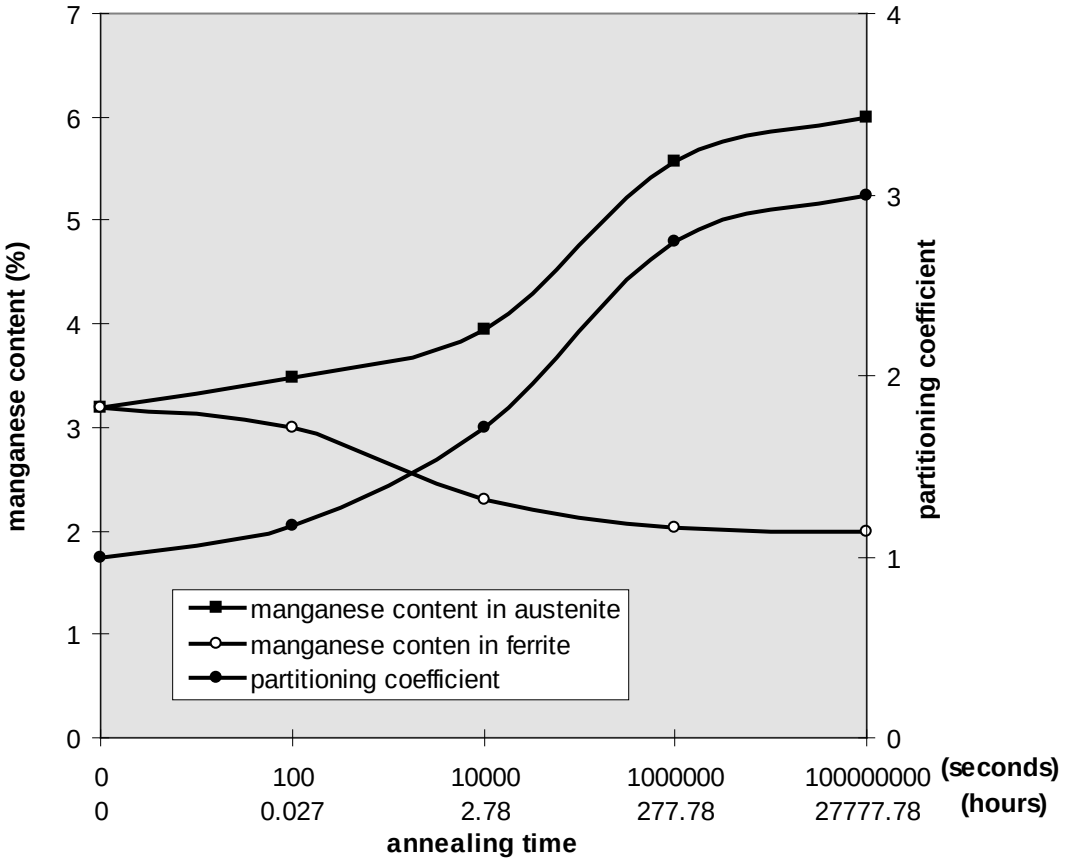

Figure 7 The predicted variation of manganese contents in austenite and ferrite and partitioning coefficient with annealing time (0.11% C-2.67% Mn steel)

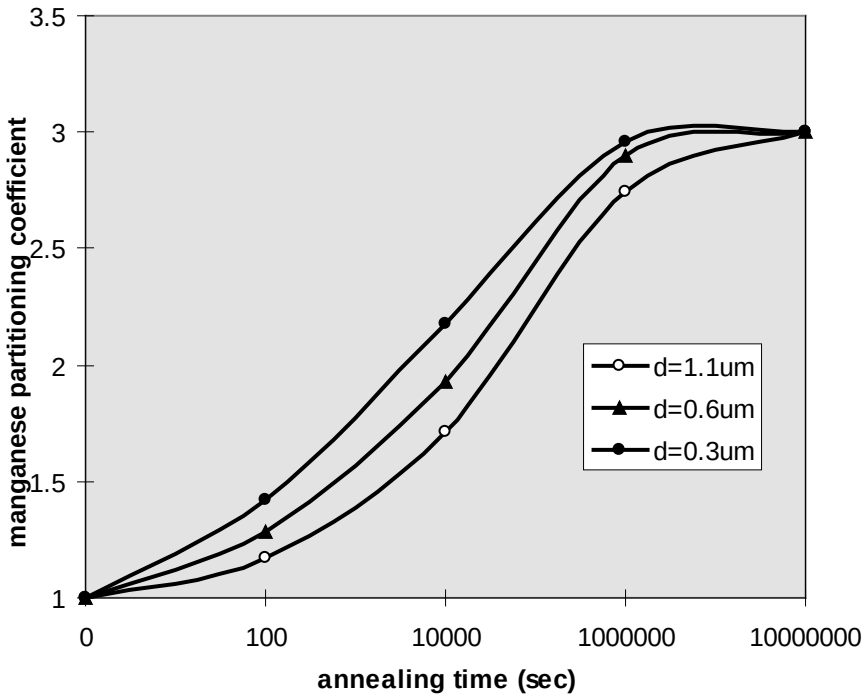

Figure 8 Predicted effect of diameter of austenite "fibre" on the Mn partitioning

5. Comparison with experiments

The comparison between theory and experimental data of steel[3] is shown in Figure 9, the theoretical data with $D_{Mn}^{\gamma} = 7.12 \times 10^{-15}\ cm^2/s$ is lower than the experimental, that is may because that the diffusion rate of Mn in austenite we set is lower than true one. The difference between theory and experimental data verifies that the diffusion rate of Mn in austenite increased with Mn content. If $D_{Mn}^{\gamma} = 7.12 \times 10^{-14}\ cm^2/s$, the theoretical prediction of manganese partitioning is much close with experimental.

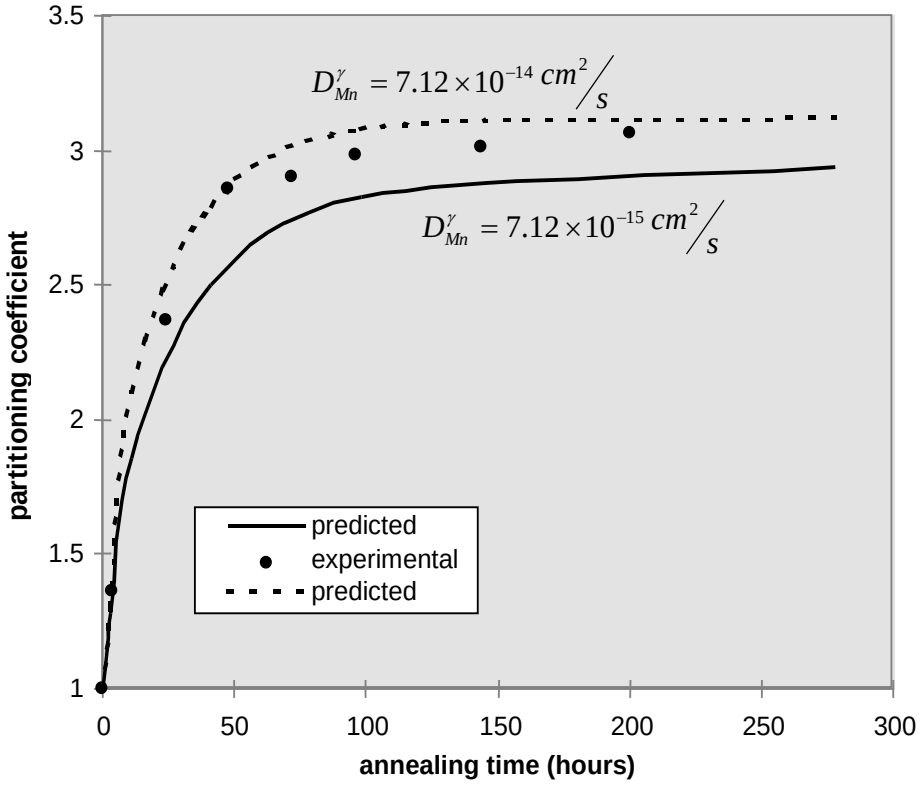

Figure 9 The comparison of partitioning coefficient between theoretical prediction and experimental data for 2.62% Mn steel 680℃

6. Conclusion

Manganese partitioning during annealing of dual phase steel takes place because of the manganese solubility difference in ferrite and austenite, the driving force for manganese partitioning is the difference in heat of solution of manganese in these two phases.

The analysis of manganese redistribution in ferrite and austenite during annealing is based on the following two processes:

(1) Manganese moves from ferrite to ferrite-austenite boundary and forms a manganese-rich rim; the manganese distribution in ferrite is given by:

$$C_{Mn}^{\alpha} = C_{Mn}^{0} - \left(C_{Mn}^{0} - C_{Mn}^{\alpha 0}\right) \cdot \left(1 - erf\left(\frac{r - r_{\alpha}}{2\sqrt{D_{Mn}^{\alpha} t}}\right)\right) \quad \text{when } r_{\alpha} \le r \le R$$

$$D_{Mn}^{\alpha} = D_{Mn}^{\alpha 0} \exp\left(-\frac{Q_{Mn}^{\alpha}}{R \cdot T}\right)$$

(2) The manganese of manganese-rich rim in ferrite-austenite boundary diffuses into austenite until final equilibration is reached and manganese gradient in the austenite is eliminated. The following equations describe the manganese distribution in austenite:

$$C_{Mn}^{\gamma} = C_{Mn}^{0} - \left(C_{Mn}^{0} - C_{Mn}^{\gamma 0}\right) \cdot \left(1 - erf\left(\frac{r_{\gamma} - r}{2\sqrt{D_{Mn}^{\gamma} t}}\right)\right) \quad \text{when } 0 \le r \le r_{\gamma}$$

$$D_{Mn}^{\gamma} = D_{Mn}^{\gamma 0} \exp\left(-\frac{Q_{Mn}^{\gamma}}{R \cdot T}\right)$$

The diffusion analysis for the above two processes combined with the mass balance

$$\frac{\int_{S_{\alpha}} C_{Mn}^{\alpha} dS_{\alpha}}{S_{\alpha} + S_{\gamma} + S^{i}} + \frac{\int_{S_{\gamma}} C_{Mn}^{\gamma} dS_{\gamma}}{S_{\alpha} + S_{\gamma} + S^{i}} + \frac{S^{i} C_{Mn}^{i}}{S_{\alpha} + S_{\gamma} + S^{i}} = C_{Mn}^{0}$$

and austenite grain growth can give the manganese distribution and partitioning coefficient at any time during annealing. The predicted coefficient shows the same trend as the experimental data with isothermal holding time but is displaced to lower values than the experimental dada which may be due to using a lower manganese diffusion coefficient than is actually present.

7. Reference

(1) N. Pussegoda, W. R. Tyson, P. Wycliffe and G. R. Purdy, Segregation of manganese during intercritical annealing of dual phase steels, Metall. Trans., 15A(1984)1499-1520.

(2) L. A. Erasmus and R. Ratnaraj, The partitioning of manganese & nitrogen in dual phase steels, Technical Report, University of Canterbury.

(3) Shoujin Sun, Martin Pugh, and Les Erasmus, The microstructure and mechanical properties of as-rolled dual phase steel, proceddings of IPENZ annual conference (Feb. 1996, Dunedin), Part I, Manganese partitioning and microstructure, pp380-385.

(4) G. R. Speich, V. A. Demarest, and R. L. Miller, Formation of austenite during intercritical annealing dual phase steels, Metall. Trans., 12A(1981) 1419-1428.

(5) N. J. Kim and G. Thomas, Effect of morphology on the mechanical behavior of a dual phase Fe/2Si/0.1C steel, Metall. Trans., 12A(1981) 483-489.

(6) Robert E Reed-Hill, Physical Metallurgy Principles (D. Van Nostrand Company, 1973), pp309.

(7) K W Andrews, J. Iron & Steel Inst., 184(1956) 414-427.